Quaternary Tephrochronology in Iceland
Dating Principles & Applications

Stephen J. Roberts



PhD Thesis
Department of Geography
University of Edinburgh

2001

EX BIBL. UNIV. EDINBURGI

Declaration

In accordance with the University of Edinburgh regulations, I declare this thesis is my own work except where stated.

Stephen J. Roberts

20th September 2001

Title page photograph: The town of Ísafjörður, the capital of the Vestfirðir Peninsula, NW Iceland, looking NE across Skutulsfjörður towards the Tertiary basalt strata of Kirkjubólshlíð. The foundations of Ísafjörður are thought to be part of a terminal moraine related to a last deglaciation ice readvance of uncertain age. The photograph was taken at 2 a.m. in mid-June 1998.

Quaternary Tephrochronology in Iceland: Dating Principles & Applications

Stephen J. Roberts
PhD Thesis Abstract
Department of Geography, University of Edinburgh, Drummond Street, Edinburgh

This thesis presents multi-method numerical ages and age estimates obtained from the previously undated Óþoli Tephra of the Vestfírðir Peninsula, NW Iceland and the Þórsmörk Ignimbrite (ÞIG), Eastern Volcanic Zone, S Iceland. These provide unique chronological constraints for Quaternary landscape evolution, ice sheet extent and ice-sheet thickness. In addition, they allow ice-free area hypotheses in Iceland to be tested and terrestrial and marine records of palaeoenvironmental change in the North Atlantic region to be linked more securely. The 2.26±0.11 Ma fission-track age of the Óþoli Tephra is particularly important because it places a major new age restriction on glacially driven, macroscale landscape evolution processes of fjord network formation on the Vestfírðir Peninsula.

The pre-radiocarbon, Quaternary era is a vital period in which current glacial/interglacial cycles developed and caused widespread environmental change. Dating controls for this era are limited because of widespread glacial erosion, but in Iceland certain tephra deposits have survived glacial overriding and can provide accurate age constraints and precise spatial correlation for stratigraphic sequences. The two tephra deposits chosen for this study are of great palaeoenvironmental significance. The Óþoli Tephra rests unconformably 580-600 m.a.s.l. near the plateau surface of Skagafjall (NW Iceland). The 100-160 m thick sequence of ice-dammed lake deposits beneath it were thought to have formed '20-17,000' years ago. The ÞIG (Eastern Volcanic Zone, EVZ, S. Iceland) is the largest Quaternary-age ignimbrite deposit in Iceland and glass compositions have been geochemically linked with the highly silicic (SiO_2 >68 wt %) component of North Atlantic Ash Zone-2 (NAAZ-2), 48-58 ka.

Correlation, fission-track (FT) and thermoluminescence (TL) methods were used to produce ages from the glass shards that overwhelmingly dominate the highly silicic airfall and/or pyroclastic flow ash components of these deposits. Dating glass shards is advantageous because they form during the magma-quenching phase of an eruption and nearly always reflect the 'true' eruption age. They are also the most far-travelled and geochemically diagnostic phase of Icelandic tephra. Geochemical correlation age estimates were obtained for the Óþoli Tephra and ÞIG by applying multivariate statistical methods to new and published glass-shard data from 104 highly silicic tephra layers/microtephra horizons of Tertiary-Quaternary age from various marine/terrestrial repositories in and around the northern North Atlantic. The isothermal plateau and diameter corrected fission-track (ITPFT & DCFT) methods used are well-established, grain specific, glass-phase dating techniques that produce accurate ages from tephra deposits older than *ca.* 70 ka. A new coarse-grain (90-150 μm), glass-phase (2.3-2.4 gcm^{-3}/<2.4 gcm^{-3}) TL dating method was developed to take advantage of the glass-rich, phenocryst and micro-inclusion poor nature of the selected deposits. To reconstruct palaeodose values, the established multiple aliquot additive dose TL (MAAD-TL) procedure and an adaptation of a single aliquot regeneration (SAR) luminescence dating procedure, (SAR-TL), that allows continuous assessment of, and correction for, changes in sample TL sensitivity, were used on the Óþoli Tephra. The ÞIG, with a *ca.* 50 ka correlation age estimate, was used as a pseudo-age control for the SAR-TL experiment.

Seven correlation age matches ranging from *ca.* 100 ka-13 Ma were found for the Óþoli Tephra. Composite correlation age matches for the ÞIG are all in the 48.5-58 ka age range with 48.5 ka the best correlative. Chemical correlation dating is therefore useful in constraining the age of distinctive tephra deposits in the late Pleistocene, but is not always effective over longer timescales. The weighted mean ITPFT/DCFT age of the Óþoli Tephra is 2.26±0.11 Ma and considered accurate. No spontaneous fission tracks were observed for the Þörsmórk Ignimbrite, consistent with *ca.* 50 ka age and glass shard uranium content of 3-4 ppm. The natural SAR-TL signal is located in a second phase of approximately linear dose response growth of the TL signal beyond the first main phase of signal saturation. This meant age estimates greater than the generally quoted 0.8 Ma upper limit of luminescence dating could be calculated. Eight out of eleven TL dating attempts were successful with an age range of 0.6-4.8 Ma. The weighted mean age from the three successful MAAD-TL runs with a 5 hour, 155°C pre-heat was 2.06±0.27 Ma. Longer, low temperature pre-heats (16 hrs, 135°C) reduced

age estimates by approximately half. Changes in TL sensitivity were observed during all SAR-TL experiments restricting age estimates to minimum-maximum age ranges. Nevertheless, the Óþoli Tephra SAR-TL age range of 1.74±0.37-4.69±0.74 Ma (pre-heat: 2 minutes, 220°C) encompasses the fission-track age. The natural, glass-phase TL signal of the ÞIG ash is located in the first phase of linear dose response growth before first phase saturation. The minimum-maximum SAR-TL age range is 29±7-40±10 ka. The *ca.* 40 ka maximum SAR-TL age estimate is significantly less than the minimum correlation age estimate, but considered most representative of the geological age because changes in TL sensitivity were greater than for the Óþoli Tephra. The TL methods used need refining, but these results are highly encouraging for developing and applying glass-phase dating procedures across a broader than expected chronological range.

The new numerical ages and context of the Óþoli Tephra suggest a proto-fjord network of similar configuration to the current fjord system had formed early in the Quaternary in NW Iceland and that Iceland-wide glacial activity in the first part of the early Pleistocene (2.5-2.0 Ma) was more extensive and/or more widely distributed than previously thought. The Óþoli eruption is tentatively linked to the Húsafell volcanic complex on the western mainland and is thought to be one of the first deglaciation induced, massive eruption events of the Pleistocene. The Skagafjall deposits were preserved beneath cold-based non-erosive parts of overriding mid-late Pleistocene ice-sheets. Large TL age errors, caused by uncertain palaeowater content estimates, currently prevent the use of TL dating to establish if the Þörsmórk Ignimbrite was deposited by single or multiple eruption events 60-30 ka. Nevertheless, new *ca.* 40 ka SAR-TL and 48.5 ka correlation ages of the ÞIG provide a critical 40-50 ka age constraint on glacial and volcanic processes in the EVZ of southern Iceland. They suggest that volcanic activity in this region was responsible for at least one component of NAAZ-2. The *ca.* 40 ka SAR-TL dated deposit is an age underestimate or could be the second of at least two discrete 60-30 ka eruptions in the EVZ of similar magnitude and geochemistry. These eruptions were massive events, possibly triggered by abrupt climatic upturns between 60-30 ka during the rapidly fluctuating, but generally downward climatic trend towards the LGM.

For Mum, Dad & Emma
with love, and thanks for your unquestioning support

Contents

Acknowledgements (i)

List of Figures (ii)

List of Tables (vii)

Chapter 1: Introduction 1

1.1 Overall Aim & Importance 2
1.1.1 Overall aim 2
1.1.2 Overall importance 2

1.2 Specific Aims 9

1.3 Site Selection 11

1.4 The Vestfírðir Peninsula (Principal study area) 13
1.4.1 Geographical Location 13
1.4.2 Geology 13
1.4.3 Hypotheses for Vestfírðir Peninsula glaciations & landscape evolution processes 27
1.4.4 Tephra deposits & the Vestfírðir Peninsula 31
1.4.5 Principal Vestfírðir study site: Skagafjall 33
1.4.6 Secondary Vestfírðir study sites: Sauðanes, Tóarfjall, Lækjarfjall 35

1.5 The Þörsmórk Ignimbrite (Secondary study area) 36
1.5.1 Geographical location 36
1.5.2 Geology 37
1.5.3 Þörsmórk Ignimbrite: eruption age 39

1.6 Holocene Age Control Eruptions 44
1.6.1 Öræfajökull 1362 AD, SE Iceland 44
1.6.2 Ódáðahraun-Askja (Dyngjufjöll), N. Iceland & Askja 1875 AD eruption 45

Chapter 1: Summary 48

Chapter 2: Tephrochronology: Context & Approach 49

2.1 Principles of tephrochronology 50
2.1.1 Historical development & definitions 50
2.1.2 Tephra production, transport & deposition 51

2.2 The Icelandic Tephra Record: Strengths, Uses & Limitations 56
2.2.1 Strengths & Uses of the Icelandic Tephra Record 56
2.2.2 Limitations of the Icelandic tephra record: the pre-Lateglacial era 64

2.3 Dating of distal tephra deposits in Iceland 68
2.3.1 Current State of Play 68
2.3.2 Dateable phases in Icelandic Tephra 68

2.4 Tephra Dating Methods in the pre-^{14}C era 70
2.4.1 Tephra Dating Methods I: Correlation Dating Methods 76
2.4.2 Tephra Dating Methods II: Radiogenic Fission-track Dating 79
2.4.3 Tephra Dating Methods III: Radiogenic Luminescence Dating 87
2.4.4 Tephra Dating Methods IV: 104
Isotopic Potassium-argon (^{40}K-^{40}Ar) & Argon-argon (^{40}Ar-^{39}Ar) Dating 104

2.5 Global Examples of Multi-method Tephra Dating 105

Chapter 2: Summary 112

Chapter 3: Sampling & Analytical Techniques 113

3.1 Sampling & Identification **114**
3.1.1 Vestfírðir Peninsula: Skagafjall, Sauðanes, Tóarfjall & Lækjarfjall 114
3.1.2 Þörsmórk Ignimbrite 117
3.1.3 Source correlation samples 117
3.1.4 Holocene TL age-control eruptions 117

3.2 Geochemical & Correlation Dating Methods **119**
3.2.1 Introduction 119
3.2.2 Geochemical Methods 119
3.2.3 Correlation Dating Methods: Statistical theory 125
3.2.4 Correlation dating: Application of statistical methods 131

3.3 Fission-track Dating of Icelandic Tephra Deposits **133**

3.4 Thermoluminescence (TL) Dating of Icelandic Tephra deposits **137**
3.4.1 Dose rate determination 137
3.4.2 TL characterisation & palaeodose reconstruction experiments 138
3.4.3 Testing which phase is responsible for the TL signal 147

3.5 Testing FT & TL Ages of the Óþoli Tephra:
Palaeomagnetic Polarity Reversal Dating Analysis 149

Chapter 4: Results 150

4.1 Identification of tephra deposits **151**
4.1.1 Vestfírðir Peninsula 151
4.1.2 Þörsmórk Ignimbrite 158
4.1.3 Holocene age control, highly silicic tephra deposits 160

4.2 Chemistry & Correlation Dating **162**
4.2.1 Classification 162
4.2.2 Geochemical Correlation Dating Results 176
4.2.3 Palaeomagnetic reversal correlation dating of Skagafjall sediments 183

4.3 Fission-track Dating **191**
4.3.1 ITPFT & DCFT of the Óþoli Tephra 191
4.3.2 Hjallanes Tephra 192
4.3.3 Þörsmórk Ignimbrite 192

4.4 Thermoluminescence (TL) Dating **199**
4.4.1 Dose Rate Determination 199
4.4.2 TL Characterisation & Palaeodose Evaluation Experiments 212
4.4.3 Quantitative TL Dating Experiments 4 & 5 219
4.4.4 Testing phase-TL signal relationship 231

Chapter 4: Summary **235**

Chapter 5: Discussion 237

Section A: Final assessment of Tephra Ages 238

5.1 Evaluation of TL age estimates & age ranges **238**
5.1.1 Evaluation of factors affecting dose rate values 239
5.1.2 Factors affecting palaeodose values 245
5.1.3 Final TL Age Assessment 252

5.1.4 Final Tephra Age Assessment 254

Section B: Palaeoenvironmental Implications 257

5.2 Source volcanoes **257**

5.3 Formation of Skagafjall Sedimentary Sequence **264**
5.3.1 New Skagafjall Sedimentary Evolution Models 270
5.3.2 The Plio-Pleistocene transition in Iceland:
Implications of the *ca.* 2.26 Ma age of the Óþoli Tephra 276

5.4 Preservation of the Skagafjall Sedimentary Sequence **286**
5.4.1 Modes of Pleistocene Glaciation 286
5.4.2 Preservation of the Skagafjall Sedimentary Sequence 292

5.5 Þörsmórk, S Iceland **297**
5.5.1 Landscape evolution models 297
5.5.2 Eruption Models for the 60-40 ka 305

Chapter 6: Conclusions 309

6.1 Tephra Ages **310**
6.1.1 Óþoli Tephra 310
6.1.2 Þörsmórk Ignimbrite 311

6.2 Tephra Dating Methods **312**
6.2.1 Correlation Dating 312
6.2.2 Fission-track Dating 312
6.2.3 Luminescence Dating 313

6.3 Palaeoenvironmental Applications **315**
6.3.1 Skagafjall & the Vestfírðir Peninsula 315
6.3.2 Þörsmórk & Southern Iceland 315

6.4 Future Work **316**
6.4.1 Dating techniques 316
6.4.2 Palaeoenvironmental applications 317
6.4.3 Other 318

Appendix A: Definitions & Isotopic Dating of Tephras 319

A1: Definitions & Classification of Volcanic Terms **321**
A1.1 Pyroclastic deposits 321
A1.2 Common Icelandic Rock Types 324
A1.3 Type of eruptions mentioned in text 324

A2: Quaternary Dating Techniques **325**

A3: Brief Review of K-Ar & Ar-Ar Dating of Tephra Deposits **328**

Appendix B: Experimental Theory & Preliminary Methods 330

B1: Experimental Theory for Elemental Analysis **330**
B1.1 Electron-probe microanalysis (EPMA) 330
B1.2 Scanning Electron Microscopy (SEM) 330
B1.3 X-Ray Fluorescence (XRF) 331
B1.4 Inductively Coupled Plasma – Mass Spectrometry (ICP-MS) 331

B2: Preliminary Experiments **333**
B2.1 Density Separation Profiling of Selected Tephra Deposits 333

B2.2 Working Calibration of SUERC Irradiator 2 336

Appendix C: Experimental Data 343

Appendix D: Background to Discussion 389

D1: Glaciolacustrine Environments: Review & Case Studies **389**
D1.1 Contemporary glaciolacustrine environments 389
D1.2 Palaeo-glaciolacustrine environments 389
D1.3 Characteristic deposits of ice-dammed lakes I: Rhythmites 390
D1.4 Characteristic deposits of ice-dammed lakes II: Diamictons 392
D1.5 Pertinent Case Studies 393

References 395-427

Acknowledgements

This project was principally supported by a NERC Studentship Grant no. GT 04/97/85/ES. The initial fission-track analysis was partly funded by a grant from the Moray Endowment Fund, Edinburgh and the trip to Toronto to undertake fission-track analysis was partly funded by a Small Projects Grant from the University of Edinburgh. For all of these, I am very grateful.

My greatest thanks go to my supervisors Dr. Andrew Dugmore and Professor David Sugden for their constant encouragement, enthusiasm and helpful advice.

In addition, I'd like to make a special note of thanks to:
Jon Sigurvinsson – for introducing us to the Skagafjall sections, other aspects of Vestfírðir geology, fieldwork transportation, loan of vital pieces of field equipment (especially the scoop!) and help with all things Icelandic. Without his invaluable assistance none of this study would have been possible. On top of all that, the Sigurvinsson families' hospitality for myself and my co-fieldworkers was very much appreciated and we would all like to extend out most sincere thanks, especially for the fantastic fish suppers!
Dr. David Sanderson – for his initial and continuing enthusiasm and consistently helpful advice in all luminescence related matters and, above all, for allowing me extended access to the SUERC luminescence and other laboratory facilities at East Kilbride.
Professor John Westgate, Dr. Amanjit Sandhu and Dr. Shari Preece – for the initial fission-track analysis and for their excellent fission-track tuition. Their and their respective families' hospitality was very much appreciated and made my a trip to Toronto one I'll remember for a long time!

Many thanks, in alphabetical order, to: Tom Amorosi, Rob Austin-Smith, Tom Bradwell, Tom De-Winton, Andy Dugmore, Jez Everest and Sara Strachan for making Icelandic fieldwork a highly productive and enjoyable experience. I am also grateful to Ragnar Edvardsson and his archaeological and botanical colleagues, for allowing me to tag along on a short trip to Hornstranðir in July 1999. Their hospitality in Bolungarvík and post-trip transportation around Iceland was greatly appreciated, as was their good humour throughout. I'd like to express my gratitude to Peter Hill, Paula McDade and John Craven (all Department of Geology, University of Edinbrugh) for assistance with, and discussions about, various things, but mostly SEM and EPMA matters. Many thanks to: Iona Antony, Lorna Carmicheal, Alan Creswell, Iain Houston, Simon Murphy, Valerie Olive, Anne Sommerville and Fin Stuart at SUERC for laboratory and other assistance, discussions and games of snooker during my visits to East Kilbride. Thanks also to Águst Gudmunðsson, Björn Hardarsson, Guthren Larsen, Jan Mangerud, Kristian Sæmundsson and Stefan Wastegård for helpful discussions about tephra and other aspects of Icelandic and Vestfírðir geology; to Alastair Gemmell at Aberdeen University for the loan of various bits of luminescence kit and to Dr Bob Galloway, Physics Department, University of Edinburgh, for useful discussions about the luminescence side of things. Thanks also to Kevin Hicks for showing me lots of Adobe Illustrator 'tricks'.

Many thanks to following people in the Geography Department who have helped me out in a variety of ways and/or made the last few years enjoyable (again in alphabetical order): Isobel Anderson, Hannah Avis, Anne Breen, Tom Bradwell, Sarah Davies, Steve Dowers, Donna Easterlow, Simon Evans, Jez Everest, Alastair Fleming, Chris Fogwill, Sarah Gilchrest, Darcy Gilley, Lorraine Gormley, Nick Hardy, Ray Harris, Anona Lyons, Anja Maaike-Green, Sue Maclachlan, Bob McCulloch, Shonagh McGowan, Clare Muller, Malcolm Murray, Antony Newton, Gavin Park, Chris Place, Bill Phillips, Josie Preistley, Ross Purves, Kate Smith, Sara Strachan, Leslie Sutherland, Fran Taylor, Keith Turner, Raphael Villegas-Patraca, Zheng Wang, Nicola Wood, Kerry Watt, Marica, Shelia, Winnie, Pat and Gus (with apologies to anyone I missed out!).

Finally, a special mention for Mel and Ailsa for being the best flatmates in the world.

List of **Figures**

Chapters 1-6 1

Figure 1.1 Thesis structure 5

Figure 1.2 Time-space diagram summarising the dating approach adopted 6

Figure 1.3 (**a**) Iceland in the North Atlantic & present day oceanography (**b**) Summary geological map of Iceland and the location of active central volcanoes 7-8

Figure 1.4 (**a**) Reconstruction fo the North Atlantic in the early late Palaeocene (from Chalmers *et al.*, 1995) (**b**) Stationary deep mantle plume hypothesis in the North Atlantic 70-15 Ma (drawn from Gudmunðsson, A. T., 1996) (**c**) Formation of Iceland, general (after Gudmunðsson A. T., 1996) and 8 Ma – present day (from Stecher *et al.*, 1999) (**d**) Variations in Moho depth beneath Iceland and current location of Icelandic hotspot (from Ito *et al.*, 1999) 16-17

Figure 1.5 Summary geological map of the Vestfírðir Peninsula of Iceland. 18

Figure 1.6 (**a**) Summary map of major glacial limits in Iceland (modified from Gudmunðsson, 1997; Ingólfsson and Norðdahl, 2001) (**b**) Multiple Advance Deglaciation (MAD) model (adapted from Ingólfsson *et al.*, 1995; Gudmunðsson, 1997) 21

Figure 1.7 (**a**) Summary of main glacial features of the Vestfírðir Peninsula (**b**) Landscapes of glacial erosion and main outlet routes for glaciation on the Vestfírðir Peninsula (**c**) Landsat 5 remote sensing image of the Vestfírðir and Snæfellsnes Peninsulas 24-26

Figure 1.8 (**a**) Putative LGM ice-free areas in Iceland (**b**) the Vestfírðir Peninsula 29

Figure 1.9 (**a**) Geomorphological features of Skagafjall, western Vestfírðir.(**b**) Stratigraphic profiles of Skagafjall, NW Iceland (from and adapted from Sigurvinsson, 1983). 32

Figure 1.10 (**a**) Location of Þörsmórk in Iceland (**b**) Active volcanoes, volcanic systems and glacial limits of the Eastern Volcanic Zone (**c**) Postglacial eruption sites in the EVZ (adapted from Jakobsson, 1979) (**d**) Distribution and classification of the Þörsmórk Ignimbrite in and around Þörsmórk, S. Iceland and 1998-1999 sampling location references. 41-43

Figure 1.11 Eruption plume dispersal maps for Askja 1875 and Öræfi 1362 eruptions. 47

2

Figure 2.1 (**a**) Classification of pyroclastic fall deposits (Walker, 1973) (**b**) Summary of the processes by which sub-aerial pyroclastic flow and fallout deposits originate (both from Fisher and Schmincke, 1984). 53

Figure 2.2 (**a**) Dispersal patterns of selected tephra deposits for Settlement to present day in Iceland; (**b**) Dispersal patterns of the major silicic eruptions of the Holocene era; (**c**) Prevailing wind directions in present-day Iceland (after Donn and Ninkovich, 1980). 54-55

Figure 2.3 Bi-modal composition of Torfajökull volcanic products (Stecher *et al.*, 1999). 57

Figure 2.4 (**a**) Active volcanic systems and central volcanoes and extinct central volcanoes of Iceland (from Haflidason *et al.*, 2000); (**b**) Total alkali-silica (TAS) evolution trend diagram illustrating the relationship between hard rock TAS composition and it relationship to volcanic system in Iceland. 58

Figure 2.5 Mid-late Pleistocene tephrochronological record of Iceland (from Halflidason *et al.*, 2000).. 59

Figure 2.6 Dispersal pattern of ice-rafted volcanic ash from North Atlantic Ash Zone-1 (NAAZ1). 66

Figure 2.7 Classification scheme for Quaternary dating techniques. 71

Figure 2.8 Palaeomagnetic timescale for the Pliocene and Pleistocene 78

Figure 2.9 (**a**) Schematic illustration of the formation process of a fission-track in a crystalline insulating solid (from Fleischer *et al.*, 1975; Naeser and Naeser, 1988) (**b**) Uncorrected and plateau-corrected ages of volcanic glasses compared to zircon fission-track and/or K-Ar ages (from Naeser *et al.*, 1980). 84-85

Figure 2.10 Schematic 'electron-hole' energy-level diagram illustrating the production mechanism in a semi-conducting crystalline solid (drawn from diagram and text in Aitken, 1985, 1999; Mckeever, 1985; Gibbons, 1997; Duller, 1996). 90-91

Figure 2.11 TL reader apparatus and example of typical output. 92

Figure 2.12 (**a**) Spheres of influence of relative nuclear radiations (after Aitken, 1999); (**b**) Schematic representation of relevant aspects of natural radioactivity in sediment dating (from Aitken, 1999) 97

Figure 2.13 Underlying principle, advantages and disadvantages of traditional multiple aliquot dating methods used. 103

Figure 2.14 Summary of numerical age determinations on the Rangitawa Tephra (from Pillans *et al.*, 1996) 111

3

Figure 3.1 Field sampling technique for ash layers and pumice clasts: (**a**) Example of ash deposit sampling technique from co-ignimbrite ash deposit at site ÞIG 1b of the Þörsmórk Ignimbrite; (**b**) & (**c**) Example of sampling technique for rounded pumice clasts in welded ignimbrite matrix (**d**) Palaeomagnetic reversal dating sampling technique illustrated using samples from the airfall Óþoli Tephra (photo courtesy of Jón Sigurvinsson) 115-116

Figure 3.2 Experimental methods – sample matrix for samples used in this thesis. 120

Figure 3.3 Correlation dating methods and their relationship to other dating methods in this thesis 121

Figure 3.4 Examples of typical electron microprobe EDS spectra 122

Figure 3.5 Relationships between samples and radiogenic dating techniques used 135

Figure 3.6 Flow diagram illustrating the stages undertaken in producing a fission-track age from volcanic glass 136

Figure 3.7 Preliminary multiple aliquot regeneration and additive dose experiment results. 141

Figure 3.8 Sample preparation technique used in this study to produce purified glass separates from glass-rich, non-organic tephra deposits 142

4

Figure 4.1 (**a**)-(**o**) The Óþoli Tephra, Skagafjall, NW Iceland: Summary geomorphology, stratigraphic logs and other features of interest (based, in part, on Sigurvinsson, 1982, 1983) 153

Figure 4.2 Detailed stratigraphic log of Skagafjall section B, units 10-12 157

Figure 4.3 (**a**)-(**t**) The Þörsmórk Ignimbrite, S Iceland: Composite stratigraphic logs of principal sites, main lithofacies units, sampling strategy and schematic cross sections 159

Figure 4.4 (**a**)-(**g**) Askja 1875 and Öræfi 1632 sampling locations and sampling strategy for the A1875 tephra 169

Figure 4.5-1 (a)-(j) Morphological classification of typical glass shards examined **165**

4.5-2 (a)-(h) SEM images of glass shards from the Óþoli Tephra **166**

4.5-3 (a)-(f) SEM images of the Askja 1875, Öræfi 1362 and Þörsmórk Ignimbrite **167**

Figure 4.6 (a) Bulk grain size data for Askja 1875 and Öræfi 1362 tephra samples **(b)** Þörsmórk Ignimbrite (ÞIG 1b, ÞIG 7) and Skagafjall Tephras **168-169**

Figure 4.7 (a)-(b) Total alkali-silica (TAS) classification bi-plots of new grain specific EPMA of glass shards from Icelandic Tephra deposits in this thesis **172**

Figure 4.8 (a) K_2O vs SiO_2 classification bi-plot of new grain specific EMPA of glass shards from Icelandic Tephra deposits presented in this thesis **(b)** AFM diagram for new datapoints **173**

Figure 4.9 (a)-(d) Discrimination binary plots for new EMPA of glass shards from Icelandic tephra deposits in this thesis **174**

Figure 4.10 (a)-(b) Major element PCA diagram for new EPMA of glass shards from Icelandic tephra deposits in this thesis **175**

Figure 4.11 Map of the North Atlantic region showing the location of tephra deposits used in correlation dating analysis. **177**

Figure 4.12 Visual major element correlation dating matches for the Óþoli Tephra **179**

Figure 4.13 Non-mobile major element ternary discrimination plots of EPMA of glass shards from tephra deposits used in direct dating analysis **180**

Figure 4.14-1 0-0.78 Ma multivariate correlation dating analysis of 'as analysed' data from highly silicic tephra deposits in the North Atlantic region **184**

4.14-2 0-0.78 Ma multivariate correlation dating analysis of normalised data from highly silicic tephra deposits in the North Atlantic region **185**

4.14-3 0.01-65 Ma multivariate correlation dating analysis of 'as analysed' data from highly silicic tephra deposits in the North Atlantic region **186**

4.14-4 0.01-65 Ma multivariate correlation dating analysis of normalised data from highly silicic tephra deposits in the North Atlantic region **187**

Figure 4.15 Micro-photographs of spontaneous and induced fission-tracks formed in glass shards of the Óþoli Tephra **195**

Figure 4.16 Induced and spontaneous track size distribution histograms for Óþoli Tephra samples used in fission-track dating **196**

Figure 4.17 Variation and track density ratio with number of tracks counted for spontaneous and induced sub-samples **197**

Figure 4.18 Selected element and water by difference (H_2O_d) vs silica bi-plot illustrating the homogeneous nature of the glass-phase major element composition of the Óþoli Tephra **198**

Figure 4.19 Schematic representation of aspects of natural radioactivity in quartz and feldspar grains compared to volcanic glass shards **201**

Figure 4.20 Flow diagram to illustrate the stage of refinement leading to final dose rate values **202**

Figure 4.21 Natural and 50 Gy thermoluminescence response glow curves for the glass-phase of selected highly silicic Icelandic tephra deposits **214-215**

Figure 4.22 (a)-(c) Natural and 50 Gy thermoluminescence response glow curves for bulk fractions of sediments from Skagafjall (Hjallanes Tephra, rhythmite bed RB4 and rhythmite bed RB10) 216

Figure 4.23 (a)-(b) Optical bleaching and inducement tests on the Óþoli Tephra 217

Figure 4.24 Glass-phase, multiple aliquot additive dose results for the airfall component of the Óþoli Tephra, Skagafjall, NW Iceland: **(a)** Natural + added dose and normalisation dose glow curves **(b)** G1/G2 and G2/G3 data plots and regression analysis **(c)** Palaeodose plateau plots 225

Figure 4.25 Glass-phase, single aliquot thermoluminescence (SAR-TL) regeneration experiment for airfall component of the Óþoli Tephra, Skagafjall, NW Iceland 226

Figure 4.26 Glass-phase, single aliquot thermoluminescence (SAR-TL) regeneration experiment for ash component of inter-bedded ash/lithic/pumice surge-deposit from of the Þörsmórk Ignimbrite, S Iceland 227

Figure 4.27 Examples of SEM chemical maps from discs used in thermoluminescence dating experiments: **(a)** SUTL 551-Óþoli Tephra **(b)** ÞIG 1b-Þörsmórk Ignimbrite **(c)** ÞIG 7-Þörsmórk Ignimbrite. 233

Figure 4.28 Rare earth element chondrite normalised spider diagrams for bulk and separates of the Óþoli Tephra 234

5

Figure 5.1 Variations in water content of Skagafjall sedimentary deposits between 1998 and 1999 244

Figure 5.2 Relationship between rate of cooling and anomalous fading for volcanic products. 250

Figure 5.3 Highly simplified multi-phase thermoluminescence dose response growth model for volcanic glass 251

Figure 5.4 Óþoli Tephra: Summary of new age estimates 256

Figure 5.5 (a) Total-alkali (Na_2O + K_2O) – silica (TAS) diagram showing the geochemical evolution trends of the most active Icelandic volcanic systems and new data **(b)** Median grain size vs distance from source plot used to identify a source range for the Óþoli Tephra 258

Figure 5.6 (a) Source range map for the Óþoli Tephra **(b)** Húsafell, western Iceland 262

Figure 5.7 Superimposition of tephra dispersal patterns and isopachs for the **(a)** Hekla-1104 and **(b)** Hekla-3 eruptions on to the **(c)** Húsafell-Skagafjall axis 263

Figure 5.8 (a)-(f) Schematic 10-2.2 Ma landscape evolution model for Dýrafjörður and Önundarfjörður and its relationship to the formation of the Skagafjall sedimentary sequence. 274

Figure 5.9 Comparison of Skagafjall sedimentary evolution models SSM-1 and SSM-2 275

Figure 5.10 Development of late Pliocene - early Pleistocene ice-sheets in Iceland and their relationship to the Óþoli eruption event (based on an original diagram by Geirsdóttir and Eiríksson, 1994). 278

Figure 5.11 Revision of late Pliocene – early Pleistocene glaciations of mainland Iceland (based on an original from Geirsdóttir and Eiríksson, 1994 with results of this study) 281

Figure 5.12 (a) Comparison of modern and putative Pliocene circulation in the North Atlantic (from Edwards *et al.*, 1991) **(b)** Late Pliocene and early Pleistocene portion of the DSDP Site 607 benthic $\delta^{18}O$ record from the central North Atlantic. 282

Figure 5.13 Summary of major LGM ice flow directions on the Vestfírðir Peninsula in relation to study sites 288

Figure 5.14 **(a)** Cross-section A-B from Fig. 5.13 (adapted and translated from Gudmundsson, 1989) **(b) & (c)** Tertiary basalt bedrock is exposed at study sites with plateaux remnants that are orientated perpendicular to the LGM ice flow models 289

Figure 5.15 **(a)** Formation and **(b)-(c)** Preservation of the Skagafjall sedimentary sequence as an example of macroscale landscape development of the Western Trough network of the Vestfírðir Peninsula 294

Figure 5.16 Timescale for the Weichselian and Holocene periods and the GRIP and GISP $\delta^{18}O$ records and GISP2 volcanic sulphate record of palaeovolcanic activity 298

Appendices A-D A

Figure A1.1 Lithological classification scheme for volcanic rocks 322

B

Figure B2.1 Density profiles for representative bulk fractions of the Hjallanes (Hj-2b) and Óþoli (airfall) Tephras and slope ash deposits from the Þörsmórk Ignimbrite 333

Figure B2.2 Density separation profiling experiment for selected tephra deposits 335

Figure B2.3 Working calibration of SUERC Irradiator 2 against SUERC Irradiator 1 using IEA-F1 standard feldspar. 336

List of **Tables**

Chapters 1-6 1

Table 1.1 Summary criteria for selection of dating samples **11**

Table 1.2 Pre-Pliocene-Pleistocene transition glaciations of Iceland **19**

Table 1.3 Age hypotheses for the Óþoli Tephra **34-35**

2

Table 2.1 **(a)** Components and ^{14}C ages of North Atlantic Ash Zone 1 (NAAZ1); **(b)** Locations and down-core distribution of Scottish late-glacial tephra deposits (both Roberts *et al.*, 1998) **65**

Table 2.2 **(a)** Assumptions for the main dating methods used in this study **(b)** Applicability, limitations and summary information for methods commonly used to date tephra deposits **72-75**

Table 2.3 Example of glass-phase ITPFT fission-track dating data table illustrating typical values than can be expected from tephra deposits of known age and relationship between pre-heating and age estimate variation **86**

Table 2.4 Relationship between natural trap residence time and TL glow curve peak temperature **93**

Table 2.5 Conversion values for elemental concentration method of calculating environmental dose rates **98**

Table 2.6 Summary of main findings of selected tephrochronologically based studies of regional palaeoenvironmental change in North America **108**

Table 2.7 Comparison of ages obtained from North American tephra deposits **109-110**

4

Table 4.1 **(a)** Major element summary data of glass-phase major element chemistry of highly silicic Holocene age samples (A1875, Ö1362) used in correlation and luminescence dating experiments and **(b)** pre-Holocene age samples (ÞIG 1b, ÞIG 7, Óþoli Tephra) **170-171**

Table 4.2 Correlation dating of mid-late Pleistocene highly silicic tephra deposits of Icelandic origin: Visual identification of Óþoli Tephra matches **178**

Table 4.3 **(a)** Multivariate statistical correlation matches for the Óþoli Tephra and Þörsmórk Ignimbrite in the 0-0.78 Ma age range and **(b)** in the 0.01-65 Ma age range **188-189**

Table 4.4 Preliminary palaeomagnetic polarity data for Skagafjall sediments **190**

Table 4.5 Glass-phase fission-track age estimates for the Óþoli Tephra **193-194**

Table 4.6 Fractional water contents for highly silicic Icelandic tephra deposits examined in this thesis **206-207**

Table 4.7 Thermoluminescence luminescence dating homogeneous matrix model dose rate summary data table for ash samples of the Óþoli Tephra and Þörsmórk Ignimbrite **208-209**

Table 4.8 Comparisons of dose rates obtained using homogeneous- and heterogeneous-matrix dose rate models for the Óþoli Tephra and Þörsmórk Ignimbrite **210**

Table 4.9 Summary of chosen dose rate parameters, reasons and most representative dose rate values for the Óþoli Tephra and the Þörsmórk Ignimbrite **211**

Table 4.10 Thermoluminescence dating equivalent dose summary data table **228-229**

Table 4.11 Final TL age estimates for the Óþoli Tephra and Þörsmórk Ignimbrite **230**

5

Table 5.1 Recommendations and criteria for successful TL dating applied to TL dating procedures used in this study. **239-240**

Table 5.2 Common factors affecting the accuracy and precision if luminescence dating and detailed assessment of their impact on TL age estimates for the Óþoli Tephra and Þörsmórk Ignimbrite. **242-243**

Table 5.3 Final ages for the Óþoli Tephra and Þörsmórk Ignimbrite **255**

Table 5.4 Summary descriptions, interpretation, significance and sedimentary evolution model SSM-1 for Skagafjall, Vestfírðir Iceland **265-269**

Table 5.5 Summary of the main global palaeoenvironmental changes 10-1.6 Ma and their influence on landscape development in Iceland and the Vestfírðir Peninsula. **285**

Table 5.6 Modes of glaciation and length of time spent in those modes for Fennoscandian glaciations in the late Pliocene-Pleistocene era (adapted from information in Kleman & Storeven, 1997). **286**

Table 5.7 Comparisons between landscapes identified by Kleman and Storeven (1997) in northern Scandinavia and their equivalents defined by Lárusson (1983). **287**

Table 5.8 Summary descriptions of lithofacies units of in the Þörsmórk region and their significance for constraining landscape development in the Þörsmórk region **301-304**

Table 5.9 Summary of evidence and models for single (SEM) or dual/multiple eruptions (DEM) from the EVZ in the 60-40 ka era. **306**

Appendices A-D

A

Table A1.1 Principal terminology, abbreviations, symbols and units used in this thesis **320**

Table A1.2 Classification schemes for pyroclastic rocks **321**

Table A1.3 Granulometric classification of the end members for pyroclastic fragments **322**

Table A2.1 General effective range of application of dating techniques classified in Figure 2.7 **326**

B

Table B2.1 Summary of density separation profiling experiment results **334**

Table B2.2 Summary density characteristics of selected tephra deposits **334**

Table B2.3 Summary of working calibration effective dose rates **336**

Table B2.4 SUERC Irradiator 2: Working calibration data **337-339**

Table B2.5 TL Expt. 1: Natural vs 50 Gy dose response experimental set up **341**

Table B2.6 TL Expt. 4: Multiple aliquot additive TL dose runs 1-5: experimental conditions and doses applied to discs in runs 1-5 **341**

Table B2.7 TL Expt. 5: Single aliquot regeneration TL experiment: experimental conditions and doses applied to discs in regeneration cycles **342**

C

Table C1.1 New shard specific EPMA data presented in this thesis undertaken in the University of Edinburgh Tephrochronological Unit **344-357**

Table C1.2 Andradite (garnet) standard data for EPMA analyses undertaken in the University of Edinburgh, Tephrochronological Unit. **358-362**

Table C1.3 Summary mean±1σ major element EPMA data from unaltered silicic glass fractions from sites ÞIG 1-23 of the Þörsmórk Ignimbrite. **363**

Table C1.4 Pearson Product Moment Correlation Coefficients (PPMCC) for selected combinations of EPMA data. **364**

Table C1.5 Rare earth element ICP-MS data for the Óþoli Tephra and Þörsmórk Ignimbrite **365**

Table C1.6 Summary of XRF data **366**

Table C2.1 65-0 Ma correlation dating dataset **367-372**

Table C3.1 Track size diameter data for sample UT1656 as an example of the precise measurement of track sizes available **373**

Table C3.2 (**a**) Track size summary statistics and Ds/Di ratios (**b**) Track size distributions used to construct Figure 4.16 **374**

Table C3.3 Track count data for sample UT1656 analysed by SJR **375**

Table C4.1 Equivalent dose and TL age estimate summary data for MAAD-TL and SAR-TL experiments on volcanic glass fractions of the Óþoli Tephra and Þörsmórk Ignimbrite. This table is the same as Table 4.10 except homogeneous matrix model dose rates have been used to calculate ages rather than weighted mean homogenous/heterogeneous matrix model dose rates **376**

Table C4.2 Alpha efficiency data for the Óþoli Tephra and the Þörsmórk Ignimbrite samples used in SAR-TL dating experiment. **377**

Table C4.3 Thick source beta counting (TSBC) data for the Óþoli Tephra and the Þörsmórk Ignimbrite samples used in TL dating experiments **378**

Table C4.4 *In-situ* gamma spectrometry measurements for the Skagafjall sedimentary sequence **379**

Table C4.5 Palaeowater variation content scenarios for the Óþoli Tephra **380-381**

Table C4.5 (**a**)-(**c**) MAAD-TL runs 1-3: 10°C ratio data (**d**)-(**e**) MAAD-TL runs 4-5: 10°C data **382-383**

Table 4.7 (**a**) Uncorrected SAR-TL 200-400°C, 10°C data for the Óþoli Tephra (SUTL 551) used to construct Figure 4.25 (**b**) Test dose corrected SAR-TL 200-400°C, 10°C data for the Óþoli Tephra (SUTL 551) **384-385**

Table 4.8 (**a**) Uncorrected SAR-tl 200-400°C 10°C data for the Þörsmórk Ignimbrite (ÞIG 7) (**b**) Test dose corrected SAR-TL 200-400°C, 10°C data for the Þörsmórk Ignimbrite (ÞIG 7) **386-387**

Table C5.1 Grain size statistical data for airfall tephra deposits examined in this thesis. **388**

D

Table D1.1 Criteria for differentiating between glaciolacustrine and glaciomarine rhythmites (modified from Ó Cofaigh and Dowdeswell, 2001). **392**

Chapter 1
Introduction

'[Tephras from Iceland] are proving increasingly critical in a number of respects: climate-volcanism interactions, stratigraphy, calibration of the marine reservoir effect in radiocarbon dating (with implications for palaeocirculation), impact on human communities - indeed it would be difficult to find another single theme that so exemplifies the multi-disciplinary nature of Quaternary Science'.

Scourse (2000; p.1)

1.1 Overall Aim & Importance

1.1.1 Overall aim

To obtain age estimates for previously undated Icelandic tephra deposits older than the limit of ^{14}C dating (*ca.* 50 ka) using a multi-method approach and to examine the implications of those ages for regional/global palaeoenvironmental change and landscape evolution processes. In particular, this study develops new glass-phase thermoluminescence dating techniques, taking advantage of the glass-rich, phenocryst-poor nature of highly silicic Icelandic tephra deposits.

1.1.2 Overall importance

Understanding past variations in global climate during the Quaternary is important for two reasons:

1) The last 2.5 Ma[1] overlaps with the time frame of human experience (Lowe and Walker, 1997).
2) The mechanisms that drive natural periodic change in the present day climate were established during the Quaternary period. In the last decade our potentially detrimental influence on these natural processes has become an important global issue (Alley and Koci, 1990; Howard, 1997; Dahl-Jensen *et al*, 1998; IPCC, 1995, 2001). A better understanding of the mechanisms that control long term variations in past climate is required to produce accurate reconstructions of future climate change, allowing the separation of natural and anthroprogenically induced effects (IPCC, 1995). Establishing the extent and timing of major continental ice sheet advances is a fundamental component of models that predict the direction of future climate change (IPCC 1995; Saltzman, 1995; Maslin and Berger, 1997). Relatively little is known, however, about the landscape impact of the major pre-LGM Quaternary glaciations around the world because, firstly, few chronologically well-constrained sequences have been found to delimit these events (cf. Kleman and Stroeven, 1997) and, secondly, it is difficult to date unconsolidated sedimentary deposits older than 0.8 Ma accurately (Boellstorf, 1978; Berger, 1994; Westgate *et al.*, 1997). Although the terrestrial glacial record in Iceland is fragmentary with most of the mid-late Pleistocene record missing or currently undated, the Miocene-early Pleistocene record is one of the most detailed and continuous record of glaciation in the Northern Hemisphere (Geirsdóttir and Eiríksson, 1994). Good age constraints for the Miocene-early Pleistocene are provided by radiometric dating of bracketing or *in-situ* volcanic deposits. Unique and critical constraints on the length and severity of the early-mid Pleistocene glacial cycles have therefore been established and Milankovitch-scale, 100,000 year glacial-interglacial cyclicity identified in the late Pliocene

[1] See abbreviations list in Appendix A: Table A1.1; The 'long' Quaternary time scale has been adopted in this thesis. A full discussion can be found in Lowe and Walker (1997; p. 2) and Suc *et al.* (1997). In summary, a globally synchronous downturn in climate has been recognised in proxy climate records *ca.* 2.5 Ma (de Jong, 1988; Kukla, 1989; Kukla, *et al.*, 1996). This is also true of the 'shorter' time scale, 1.64-1.81 Ma (Selli *et al.*, 1977; Hilgen, 1991), but the start of the longer time scale coincides with the Matayama-Gauss geomagnetic polarity epoch reversal boundary at 2.43-2.47 Ma (Thompson, 1991). The 2.5 Ma boundary marks the end of a well-defined era rather than a palaeomagentic event. It has proved easier to identify and correlate than shorter, less well defined polarity events such as the Olduvai geomagnetic event that coincides with the start of the shorter Quaternary time scale (Suc *et al.*, 1997).

and early-mid Pleistocene periods (Sæmundsson and Noll, 1974; Eiríksson, 1985; Geirsdóttir and Eiríksson, 1994). In addition, fluctuations in the extent and thickness of the main Pleistocene Icelandic ice sheets are an imprint of oceanographic processes in the North Atlantic, which are thought to be the principal driving mechanism of rapid global climate change (Broecker and Denton, 1989; Burton *et al.*, 1997; Geirsdóttir and Eiríksson, 1994; Adkins *et al.*, 1997; Boyle, 2000; Pflaumann and Voelker, 2000). Hence, the glacial record in Iceland is globally significant record, but a lack of direct chronological data to constrain the extent of the main Icelandic ice sheets at other critical points in the pre-LGM, Quaternary era remains.

Williams *et al.* (1998; p. 7) concluded that 'we still have a very long way to go to gain the spatial and temporal resolution necessary to test existing models of global atmospheric circulation in the Quaternary'. Significant progress has been made towards this goal since the 1950s through radiocarbon dating (^{14}C) of organic material for the 50-0 ka time period and, more recently, by the retrieval and correlation of incrementally dated ice-core, dendrochronological and other high resolution palaeoclimate records (Oeschger and Langway, 1989; Bond *et al.*, 1993; Dansgaard *et al.*, 1993; Porter and An, 1995; Bard *et al.*, 1996; Kukla and Cilek, 1996; Barlow *et al.*, 1997; Rasmussen *et al.*, 1997; Hughen *et al.*, 1997).

Identifying and dating terrestrial palaeoenvironmental records older than 50 ka (*i.e.* of pre-^{14}C, Quaternary age) is a critical step in improving our overall understanding of Quaternary palaeoclimatic change. Stocker (2000) considers such evidence important because it complements existing physical and biochemical models and high-resolution palaeoclimate records of late Pleistocene climate change. Recent recommendations for research suggest concentrating on high-resolution records of terrestrial climate change in this time period and correlating them to specific periods of the more complete oceanic record (Broecker, 1997; Maslin and Berger, 1997). In this respect, tephra is a powerful tool for establishing stratigraphic ages and correlating records of palaeoenvironmental change (Thórarinsson, 1981; Dugmore and Sugden, 1991; Larsen *et al.*, 2001; section 2.1). There are two main reasons for this:

1) Tephra deposits or their bracketing deposits can be dated directly using radiogenic and isotopic methods (Westgate *et al.*, 1992; Haflidason *et al.*, 2000; Sarna-Wojcicki, 2000).
2) Eruption plumes disperse volcanic material over a wide area, forming age equivalent time-parallel marker horizons. These can be used to link marine and terrestrial records of palaeoenvironmental change, allowing spatial and temporal dimensions of climate change to be compared (Lowe *et al.*, 2001; Turney *et al.*, 2001).

The latter is one of tephrochronology's most valuable assets because direct correlation is 'normally ... impossible over most of the [Quaternary] record and in most geographical areas' (Gibbard and West,

2000). Furthermore, Sejrup *et al.* (2000, p. 668) stated that the biggest problem with studies of pre-LGM Quaternary glaciations is that 'precise absolute age control is lacking and thus the correlation has been based on linkages ... which might not be valid'. Consequently, some of the most chronologically well-constrained terrestrial records of glaciation and other aspects of palaeoenvironmental change in the pre-^{14}C, Quaternary era are found in and around volcanic areas, *e.g.* Westgate *et al.* (1987, 1992, 1997) and Shane (2000). In many parts of the world, however, the full potential of tephra deposits often remains unrealised because of poor age definition (Berger, 1992). Icelandic tephra layers of Holocene age are well-dated and this record has been used in a variety of ways. The pre-Lateglacial (<15 ^{14}C ka BP), Pleistocene terrestrial tephra record in Iceland is, however, poorly constrained. This study aims therefore to build on long-established principles of tephrochronogically-based studies in Iceland (*e.g.* Thórarinsson, 1963, 1981; Sigurdsson and Sparks, 1981; Dugmore, *et al.*, 1999; 2000; Larsen *et al.*, 1999; 2001), and the North Atlantic region (*e.g.* Mangerud *et al.*, 1984; Lacasse *et al.*, 1995; 1996; Birks *et al.*, 1996; Zielinski *et al.*, 1995; 1997; Turney *et al.*, 1998; 2001) in the historical and ^{14}C era, by incorporating the principles and methods from pre-^{14}C era tephra studies from outside Iceland (*e.g.* Westgate and Gorton, 1981; Westgate *et al.*, 1997; Shane, 2000) (Figs. 1.1, 1.2).

Multi-method, glass phase correlation, fission-track (FT) and thermoluminescence (TL) dating of the airfall/fallout component of the Óþoli Tephra (Skagafjall, NW Iceland; Fig. 1.3) and the Þörsmórk Ignimbrite (S Iceland; Fig. 1.3) provides an opportunity to address many of the issues outlined above. These deposits were selected for the following reasons:

1) the possibility that pre-LGM ages might be obtained
2) the large quantities of undisturbed tephra available that allowed a multi-method dating approach to be adopted
3) deposits that are overwhelming dominated (>95-98 %) by diagnostic and uncontaminated unaltered glassy volcanic products that probably reflect the true eruption age
4) the ability to obtain pure glass-phase separates from the bulk material rapidly and relatively easily allows new glass-phase luminescence dating techniques to be developed

Hence, in summary, the general twin aims of this thesis are

1) To date important tephra deposits using existing and newly developed glass-phase tephra dating methods
2) To use the ages obtained to constrain processes of regional landscape development.

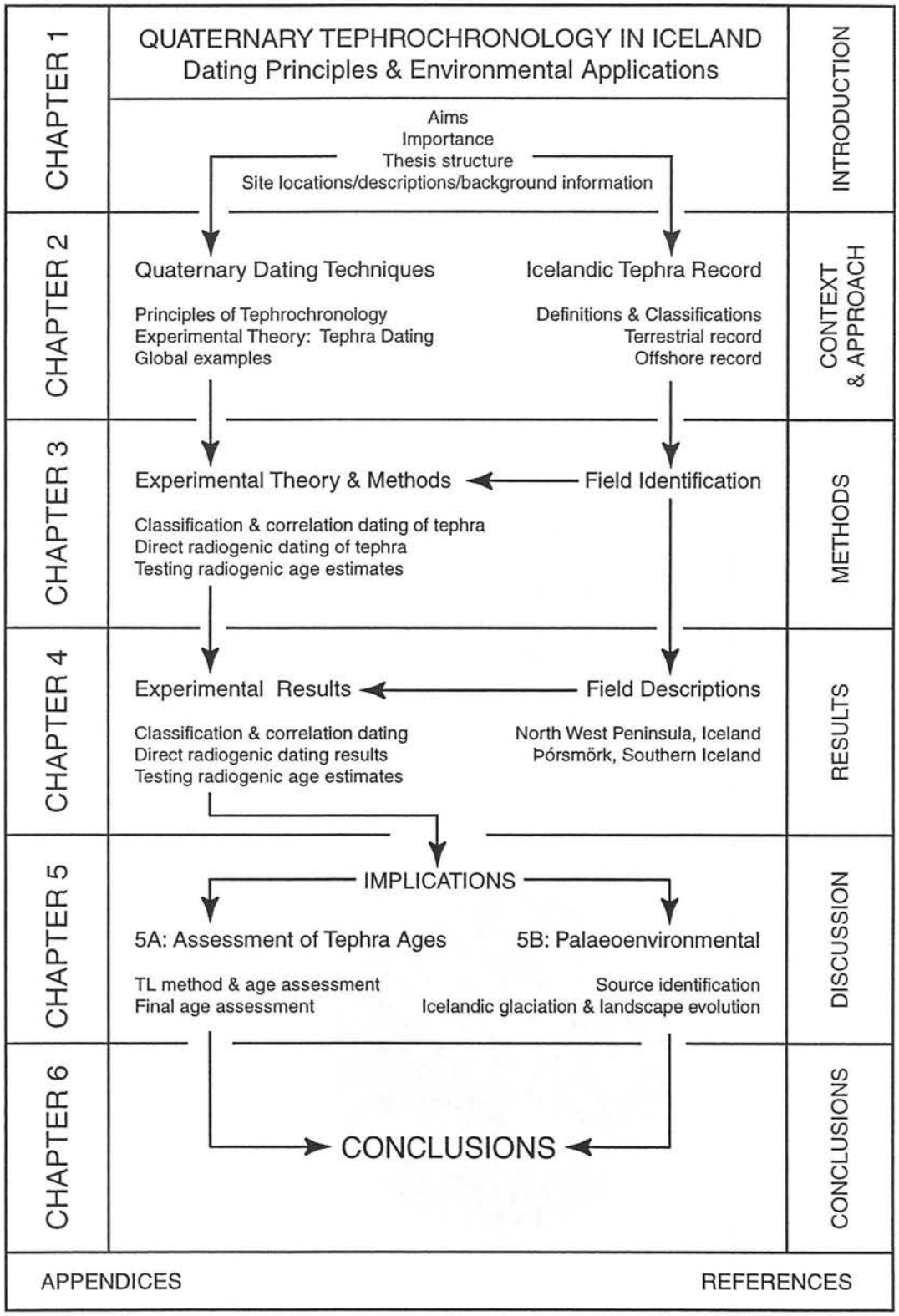


Figure 1.1 Thesis structure

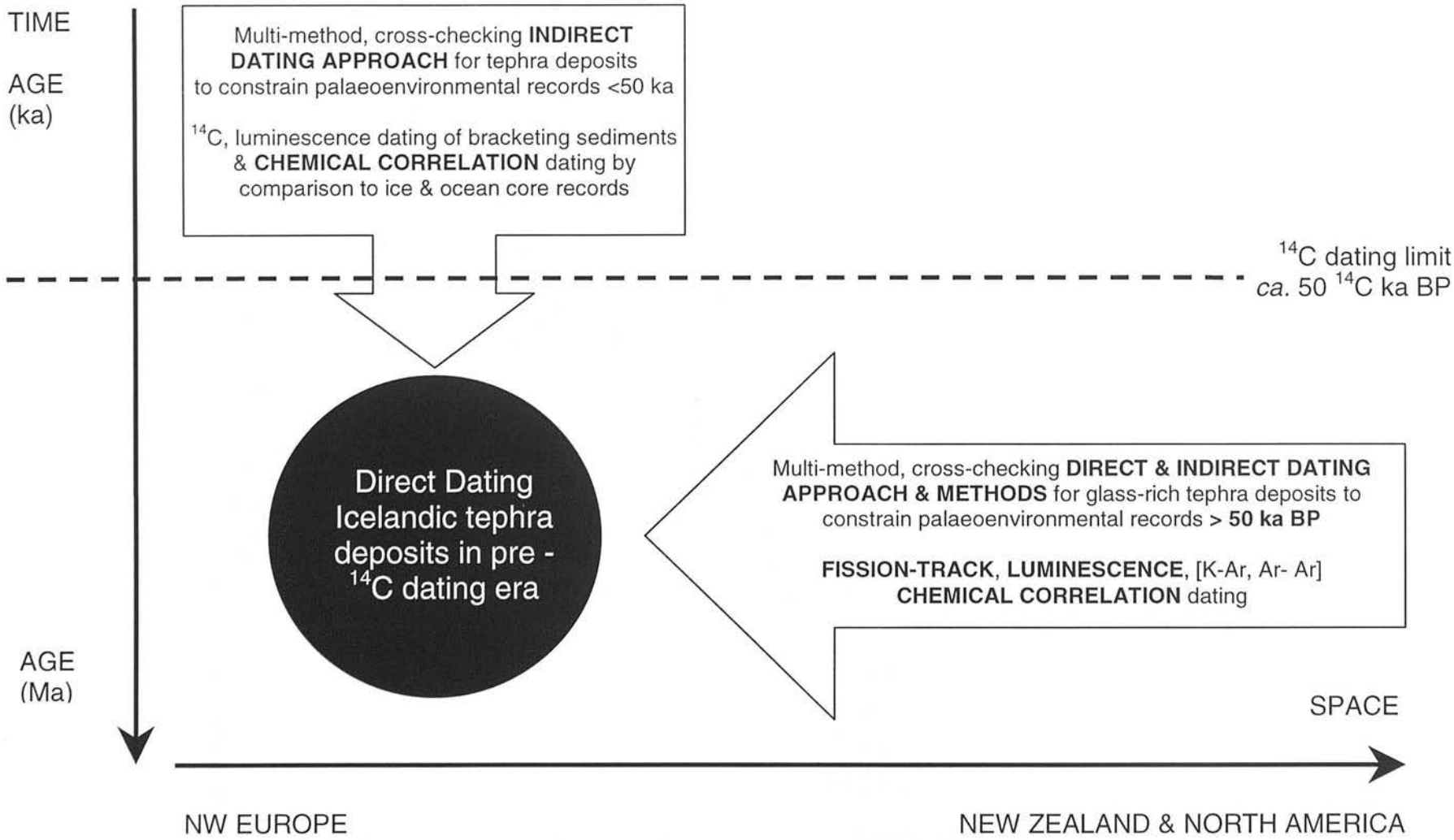


Figure 1.2 Time-space diagram summarising the dating approach adopted in this thesis. Methods used are in capitals.

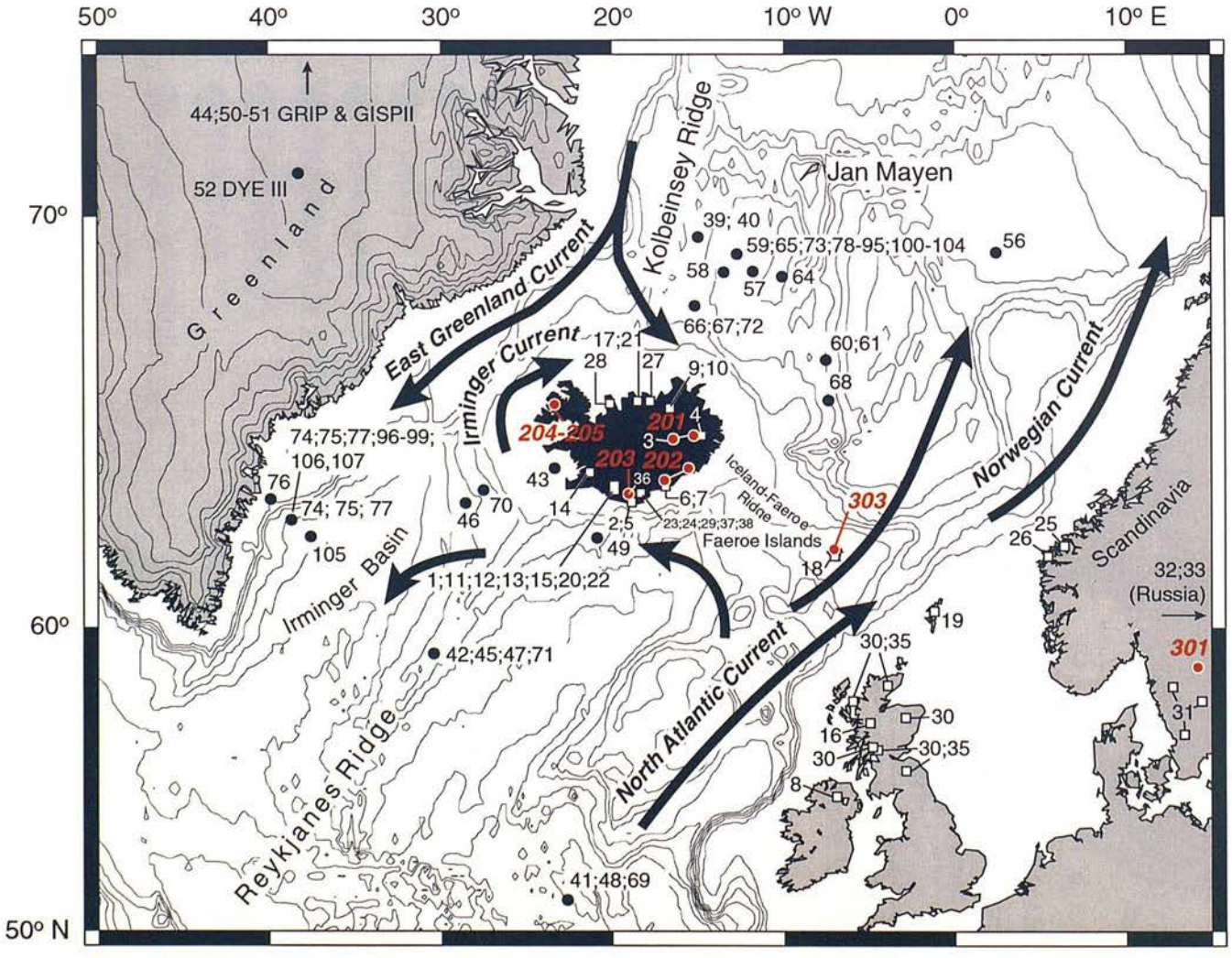


Figure 1.3 (a) Location map of the North Atlantic region showing the major present-day surface oceanographic features and locations of tephra deposits used in correlation dating analysis (see chapters 3 & 4 for more details). Based on the GEBCO (1994) Digital Atlas (British Oceanographic Data Centre for IOC and IHO) and Eíriksson *et al.*, 2000b).
Numbers are ID numbers on cluster and PCA diagrams. A full list of deposits, ID numbers & chemical data can be found in Appendix C2.

(*contd.*)

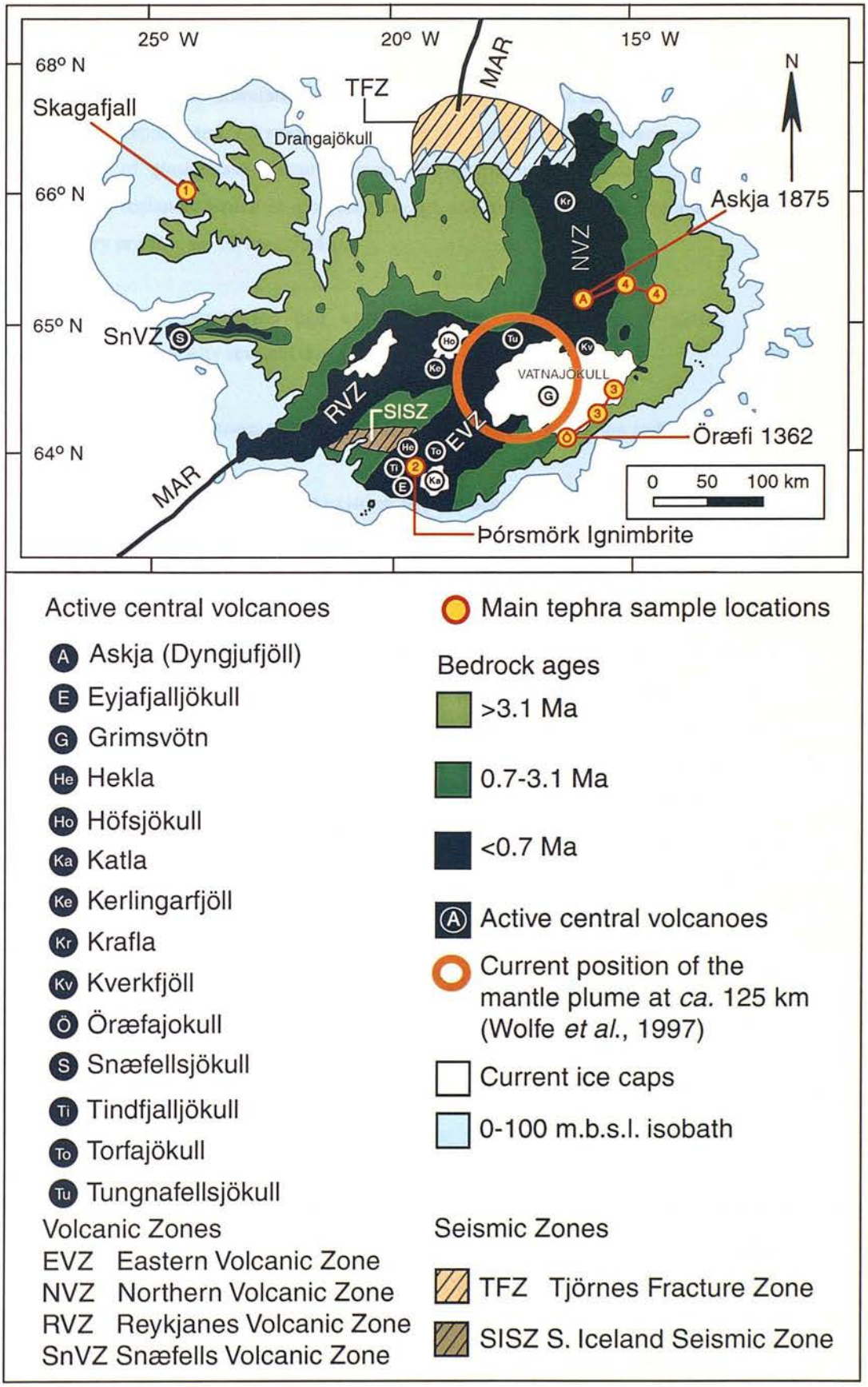


Figure 1.3 (b) Summary geological map of Iceland, active central volcanoes and main tephra sampling locations (drawn from information in Jóhanneson and Sæmundsson, 1989; Wolfe *et al.*, 1997; Larsen *et al.*, 1999)

1.2 Specific Aims

1) To establish accurate 'correlation'[2] and/or 'numerical' ages for the unaltered ash components of the Óþoli Tephra and Þörsmórk Ignimbrite. In particular, to investigate and develop the application of glass-phase thermoluminescence techniques, and critically evaluate the use of glass-phase Icelandic tephra as a correlation-age and numerical-age chronometer for the pre-^{14}C, Quaternary era (*i.e. ca.* 50 ka-2.5 Ma).

2) To corroborate tephra-based age estimates using non-tephra-based dating methods, *e.g.* palaeomagnetic polarity reversal dating.

3) To identify source volcanoes or volcanic systems for the Óþoli Tephra and Þörsmórk Ignimbrite.

4) To provide constraints for and test existing hypotheses of former ice sheet extent, thickness and landscape impact in Iceland by developing new models of macroscale landscape evolution for the North West (Vestfírðir) Peninsula and Þörsmórk regions of Iceland.

To achieve these aims a multi-method, glass-phase dating strategy was chosen. The Óþoli Tephra was examined as an 'unknown' age sample. Following successful preliminary luminescence test experiments on the Óþoli Tephra (Fig. 3.7) new glass-phase luminescence methods were developed using the highly silicic unaltered glass fractions of the Þörsmórk Ignimbrite as a pre-LGM correlation-age control and similar fractions of tephra from the Öræfi 1362 AD (Ö1362) and the Askja 1875 AD (A1875) eruptions as *ca.* 1000 year and 'zero' historical (numerical) age controls, respectively. Tephra from the Ö1362 and A1875 eruptions were also used as altitude control samples to examine the effect on luminescence properties of Holocene age glass-shards that have been injected into the stratosphere.

The significance of the ages obtained from the Óþoli Tephra for landscape evolution processes in the Vestfírðir Peninsula are evaluated and new models of macroscale landscape evolution proposed. In doing so, this study builds on the pioneering work and comprehensive and detailed descriptions by Sigurvinsson (1982; 1983) of the sedimentary sequence preserved on Skagafjall and Lárusson (1983) of the geomorphology of the Dýrafjörður region.

Figure 1.1 shows how this thesis is structured to achieve the stated aims. The rest of this chapter introduces the sites chosen and relevant background information. Chapters 2-4 are split into two broad sections. The first part of each of these chapters (and the right hand-side of Fig. 1.1) examines issues surrounding the Icelandic tephra record and its identification in the field. The second half of each chapter (and the left-hand side of Fig. 1.1) deals with tephra dating methods. Chapter 5 examines

[2] See Figure 2.7 for definitions of these terms

issues raised by the methods used and the ages obtained. It also examines the validity of the broad assumptions used to calculate the luminescence age estimates presented in chapter 4 and determines if different calculation methods have a significant impact on the ages obtained. Final luminescence ages can be found at the end of this chapter with a summary of the reasons for using the chosen parameters. Part A of chapter 5 discusses issues relating to the luminescence methods and results, while chapter 5B examines the implications of the direct ages obtained for the Óþoli Tephra and the Þörsmórk Ignimbrite. Landscape evolution models are developed and used to explain the contrasting pre-, syn- and post-formation and preservation processes that occur in these two regions.

1.3 Site Selection

The criteria in Table 1.1 were used to select individual study sites.

Numerical-age dating samples	**Correlation/numerical age & altitude control samples**
1. Tephra deposits should be potentially pre-Lateglacial[3] in age *i.e.* > 15 ^{14}C ka BP	1. Independent age estimates or actual dates should exist for the tephra deposits or the sites they come from
2. Sufficient quantity of material should be available to allow multi-method age analysis	2. At least one sample should be a 'zero' or 'near zero-age' control
3. Sites should be accessible for transporting equipment and samples	3. Significant major elements should be similar to that of the direct dating sample
	4. Eruption style and mechanisms should be similar
	5. Post-eruption atmospheric transport pathways of tephra should be reasonably similar
	6. Sites should be accessible for transporting equipment and samples
Sites/Tephra deposits selected	**Tephra deposits selected**
Vestfírðir Peninsula	*Vestfírðir Peninsula*
Skagafjall/Óþoli Tephra	-
Southern Iceland	*Southern Iceland:*
Þörsmórk/Þörsmórk Ignimbrite	Þörsmórk Ignimbrite
	Öræfi 1362 AD Tephra
	Askja 1875 AD Tephra

Table 1.1 Summary criteria for selection of dating samples. Sample collection methods are described in section 3.2.

The principal study area is the Vestfírðir Peninsula, which has not been volcanically active for over 7 Ma and has only one permanent ice cap on the northern plateau of Drangajökull (Fig. 1.3). Using the criteria in Table 1.1 a single site, Skagafjall, was pre-selected in the Vestfírðir Peninsula. Three additional elongate SE-NW trending plateaux areas, Tóarfjall, Sauðanes and Lækjarfjall experienced similar formation processes as Skagafjall and these were also investigated (Figs. 1.3 & 1.7).

The secondary study area is the Þörsmórk region and in particular the Þörsmórk Ignimbrite formation of southern Iceland. Þörsmórk is located near the southern tip of the active Eastern Volcanic Zone,

[3]The late-glacial period is defined as the period of deglaciation from the LGM to the start of early Holocene 'warm' conditions similar to today *i.e.* 15-10 ^{14}C ka BP (Walker *et al.*, 1999). It incorporates several glacial re-advances of 1000-2000 year duration that have been identified in late Quaternary stratigraphy of NW Europe and the Greenland Ice cores.

surrounded by five ice-capped active (or currently dormant) central volcanoes (Fig. 1.3). The Þörsmórk Ignimbrite was chosen primarily because its pre-^{14}C age would make a good methodological control for the Óþoli Tephra. Seventeen outcrops of the Þörsmórk Ignimbrite (ÞIG) and bracketing deposits were investigated in the Þörsmórk region with the intention of linking local stratigraphies to investigate broad pre- and post- ÞIG climate transitions. The wide range of accessible glassy material, from large pumice clasts, *ca.* 50 cm in diameter, to co-ignimbrite and interbedded ash deposits was also advantageous. Correlation dating results suggested that the Þörsmórk Ignimbrite (often referred to as ÞIG from this point) might be suitable as a TL age control. In addition, correlation, fission-track and thermoluminescence dating provided an opportunity to:

1) Resolve the debate surrounding the age of the ÞIG.
2) Examine broad changes in the pre- and post-ÞIG environment and develop regional landscape evolution models based on these changes.
3) Investigate linkages between local terrestrial stratigraphies and marine and ice core proxy record of regional and global change in the North Atlantic region using the diagnostic chemical characteristics of the ÞIG as a marker horizon.
4) The Þórsmörk Ignimbrite was also considered as a potential source correlation sample for the Óþoli Tephra.

These aims are relevant to the principle aims of this thesis, hence the inclusion of the ÞIG as a second case study.

Other highly silicic tephra deposits with broadly similar major element composition to the Óþoli Tephra and the silicic fraction of the Þörsmórk Ignimbrite were selected as Holocene/zero-age and altitude control samples for luminescence dating experiments. Prescott and Robertson (1997) recommend the inclusion of 'zero-age' samples in luminescence studies. The Öræfi 1362 AD and Askja 1875 AD eruptions are the most recent highly silicic Plinian eruptions in Iceland. They were chosen primarily as near-zero and zero age controls for luminescence dating, but the chemical characteristics also provided interesting on and off rift comparisons for the Óþoli Tephra. Similarities between the mode of formation and composition of their tephra deposits to the Óþoli Tephra is particularly advantageous. In addition, the widespread dispersal of ash in Iceland provides an opportunity to examine volcanic glass-phase thermoluminescence properties. Ten sampling locations at six sites associated with the Öræfi 1362 AD (Ö1362) and Askja 1875 AD (A1875) eruptions were investigated. The next section describes the two major study areas and the Holocene control eruptions in the context of wider Icelandic glacial and volcanic activity.

1.4 The Vestfírðir Peninsula (Principal study area)

1.4.1 Geographical Location

The Vestfírðir Peninsula of Iceland covers an extensive land area about 104 km^2. It is joined to the mainland by a narrow 10 km wide, land bridge. The Glama plateau rises 600-900 m.a.s.l, dominating the central region of the Vestfírðir Peninsula and was ice-capped as recently as 1840 AD (Thórarinsson, 1943). The only remaining ice cap, Drangajökull[4], is located on the Hornstranðir Peninsula, the north-eastern arm of Vestfírðir *ca.* 400 km from Greenland (Figs. 1.3-b & 1.5). The Western Fjords between Breiðafjörður and Ísafjarðurjúp, bracket NW-SE trending peninsulas that are characterised by alpine summits and flat-topped plateaux of the Vestfírðir Highlands rise to. 800 m.a.s.l. (Fig. 1.5).

1.4.2 Geology

(a) Formation of the Iceland & the Vestfírðir Peninsula: 60 Ma – present day

Iceland, the youngest island mass in the world, lies at the intersection of the Mid Atlantic Ridge (MAR) and the aseismic Icelandic transverse ridge. Pre-Tertiary volcanism associated with Greenland rifting from Europe *ca.* 70 Ma (Bott, 1985; Morton *et al.*, 1995) and increased upwelling from a newly formed deep-mantle plume, the Iceland plume, *ca.* 65-55 Ma, created the Tertiary igneous provinces of the North Atlantic (Richards *et al.*, 1989; Nadin *et al.*, 1995). Vigorous magmatism occurred along a 2000 km long rift section of the present day Atlantic Ocean for about 10 Ma *ca.* 60-50 Ma (Morgan, 1981; Mutter and Zehnder, 1988). The principle spreading axis of the northern North Atlantic MAR shifted westwards about 35-30 Ma from the now extinct Aegir Ridge, opening up a new rift system closer to the eastern continental margin of Greenland (Fig. 1.4-a, b). At this time, as a result of 30-20 million years of north-westward sea-floor spreading, the stationary deep mantle Iceland plume (previously located beneath Greenland) had shifted to the eastern continental shelf of Greenland. An embryonic landmass was created *ca.* 16-13 Ma when the new rift system and the mantle plume nearly coalesced (Gudmundsson, A. T., 1996). The remains of this original Icelandic land mass can be found in the oldest rock formations of present-day north-western, northern and eastern Iceland (Fig. 1.3) (McDougall *et al.*, 1984).

The present-day thick crust beneath Iceland and high level of volcanic and tectonic activity has been attributed to the interaction between the MAR spreading centre and the Iceland mantle plume (Korenaga and Kelemen, 2000). Three volcanic rift zones, the sub-parallel Western Volcanic Zone (WVZ) and the Eastern Volcanic Zone (EVZ) in the south and the Northern Volcanic Zone (NVZ), are the surface manifestation of the MAR in Iceland. The EVZ and the WVZ are separated by the South Iceland Seismic Zone (SISZ) transform fault system. The NVZ extends northwards from

[4] In Icelandic –jökull means glacier/ice cap, –dalur means valley, and -fjörður means fjord

beneath Vatnajökull to the offshore Tjörnes Fracture Zone (TFZ). The TFZ links northern Iceland with the Kolbeinsey Ridge section of the MAR (Fig. 1.3). The volcanic rift zones, collectively known as the neovolcanic zone, are composed of central volcanoes transected by rifts and fissures swarms. These erupt frequently producing a wide variety of chemically complex eruptive products that reflect the extent and / or number of stages of melting at their source (McGarvie *et al.*, 1990; Eiler *et al.*, 2000).

Simple eastward migration of the mantle plume to its present position beneath the Vatnajökull ice cap in Southeast Iceland does not adequately explain the complex manifestation of the MAR in Iceland. The development of areas of enhanced seismicity and petrologically distinct volcanic zones with rhyolite producing central volcanoes is generally thought to be the result of a combination of the following additional factors:

1) Normal symmetric oceanic plate spreading processes,
2) Two major south-eastward positional jumps of the main rift axis in the last 15 Ma
3) The dislocation the of eastern rift-limb
4) Evolutionary processes along aseismic transverse ridges

(Jakobsson, 1979; Sæmundsson, 1979; Bott, 1985; Gudmunðsson, A. 1995; Darbyshire *et al.*, 2000).

The Vestfírðir Peninsula is the furthest landmass from the neovolcanic zone in Iceland. It has been volcanically inactive for about 6-7 million years, when the last major eastward jump in the position of the rift axis occurred (Du and Fougler, 1999; Fig. 1.4-a-c). The oldest rocks in Iceland (16.0±0.3 Ma) are found on this peninsula (Moorbath, 1968; Jóhannesson and Sæmundsson, 1998).

The north-western part of Vestfírðir drifted out of the active rift zone *ca.* 14-12 Ma, followed at *ca.* 8 Ma (Gudmunðsson, A. *et al.*, 1996) by the south-eastern corner. Featureless basalt lava plains with rows of low tephra cones, occasional lava shields and central volcanoes, possibly capped by small glaciers, were the characteristic topographic features of the late Tertiary period in the north-western, northern and eastern fringes of Iceland (Lárusson, 1983). Today the landscape of the Vestfírðir Peninsula consists almost entirely of sub-aerial tholeiitic and porphyritic basalt lava layers separated by relatively minor outcrops of olivine basalt layers and volcaniclastic and sedimentary horizons (Sæmundsson, 1979).

Gudmunðsson (1989) divided the composition of the bedrock of Vestfírðir in the following manner: 85-95% - basaltic lava flows; 3-5 % acidic and intermediate rocks; 5-10 % sedimentary inter-beds, *i.e.* consolidated tuffs, aeolian soil, sandstones and conglomerates. In general, the acid rocks and tuffs are associated with extinct volcanoes and the lava layers are about 5-15 m thick with a dip of between 4-8° towards the Southeast (McDougall *et al.*, 1984; Gudmunðsson, *et al.*, 1996). Based on the more

detailed lithological classifications, Gudmunðsson (1989) identified five broad layer types in the highlands of the western fjords between Arnarfjörður and Ísafjarðardjúp.

(b) Glaciation of Iceland and the Vestfírðir Peninsula

Iceland is now only partially glaciated. Vatnajökull, in the south-eastern corner is the largest ice cap in Europe covering *ca.* 11% (11,200 km^2) of the country (Geirsdóttir and Eiríksson, 1994). Most of the smaller ice caps are located in the neovolcanic zones covering many of the central volcanoes (Fig. 1.3-b). Outside the neovolcanic zone Drangajökull, on the Vestfírðir Peninsula is the largest ice mass. Other smaller ice caps can be found in the alpine-style mountains of Northern Iceland.

(i) Tertiary – early Pleistocene

Evidence for early Pliocene glacial activity in Iceland comes from inter-bedded lava and 'tillite' deposits in northern and eastern Iceland (Sæmundsson, 2000). These were first described by Pjetruss (1900), who suggested a Pleistocene age based on floral evidence. This view prevailed until McDougall and Wesink (1966) and Vilmundardottir (1972) produced the first Tertiary age potassium-argon ages from lava inter-bedded between 'tillites'. The glacial origin of some of these 'tillites' has been questioned (McDougall *et al.*, 1976), but the oldest undisputed basalt lava flows beneath tillite deposits are the *ca.* 6.6-4.8 Ma layers from Bessastaðaa, East Iceland (Table 1.2; McDougall *et al.*, 1976; Watkins and Walker, 1977). Other lava/tillite sequences in northern and eastern Iceland indicate that the first ice sheets had extended across large parts of the Icelandic landscape *ca.* 3.5-3 Ma (Wesink, 1964; Einarsson *et al.*, 1967; Albertsson, 1976; 1981; Geirsdóttir and Eiríksson, 1994).

The whole of the Vestfírðir Peninsula is characterised by landscapes of glacial erosion (Sugden & John 1976; Fig. 1.7-b), but only relative chronologies have been established for most of these features (Lárusson 1983). Consequently, post-Tertiary landscape evolution of this area remains largely unexplained due to the lack of dateable deposits (Sæmundsson, 1979). The lava plains of the Vestfírðir Peninsula are of Miocene age and were deposited before the onset of glacial conditions in Iceland, hence the lack of lava and tillite interbeds. The expansion of early Pleistocene ice sheets is currently thought to have been restricted to the main central area of Iceland *e.g.* Geirsdóttir and Eiríksson (1994). There is, however, abundant geomorphological evidence that the repeated advance of major ice sheets across the Vestfírðir Peninsula has significantly modified the classical flat-topped plateau lava pile since the mid-Pliocene, creating glacially incised fjord landscapes.

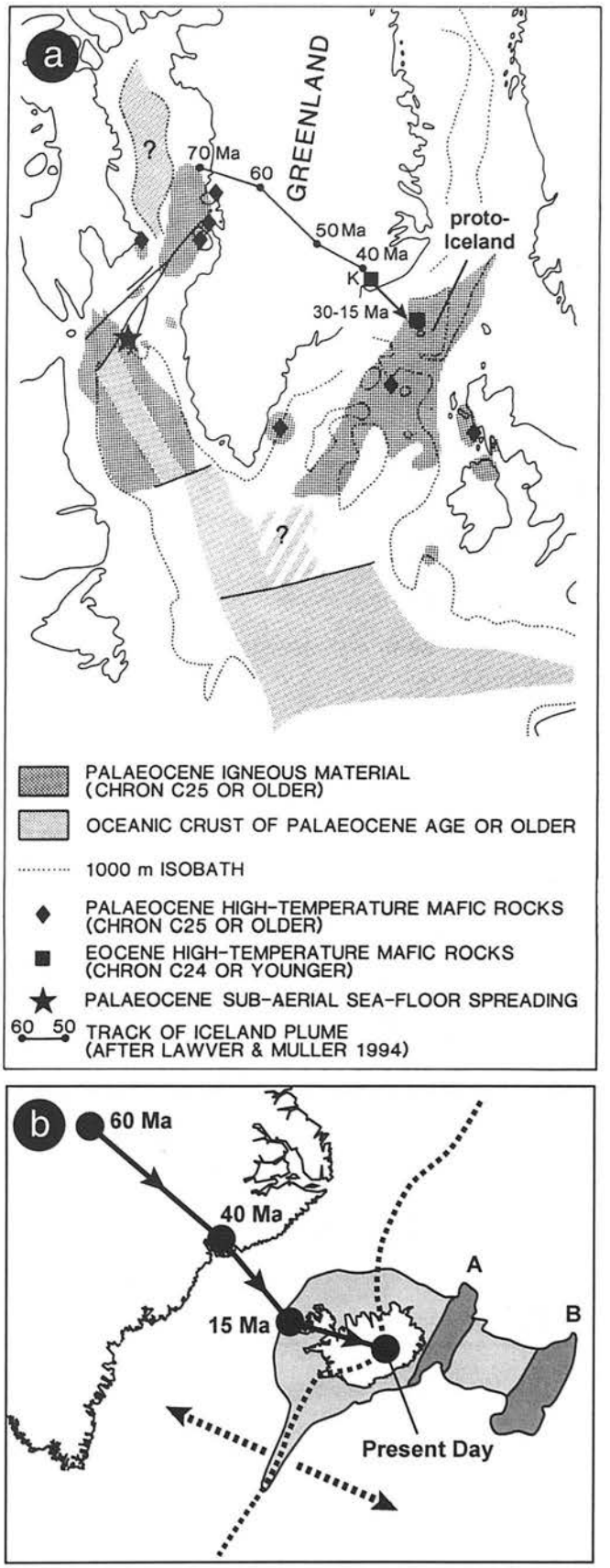


Figure 1.4 (a) Reconstruction of the northern North Atlantic in the early late Palaeocene to early Eocene showing the early formation of Iceland, incipient sea-floor spreading and the eastwards migration of the mantle plume beneath Greenland 70-15 Ma (modified from Chalmers *et al.*, 1995) **(b)** Stationary deep mantle plume hypothesis in the North Atlantic. A & B are locations of the former rift system between 60-35 Ma. At 35 Ma a new rift system opened off the east coast of Greenland and nearly coalesced with the deep mantle plume. The Icelandic landmass was formed as a result of increased magma production and eastwards migration of the new rift system (see overpage) (modified from Gudmunðsson, A. T., 1996).

Refs: Chalmers, J. A., Larsen, L. M., Pedersen, A. K. (1995). Widespread Palaeocene volcanism around the northern North Atlantic and Labrador Sea: evidence for a large, hot, early plume head. *Journal of the Geological Society, London*, **152**, 965-969.
Lawver, L. A., & Miller, R. D. (1994). Iceland hotspot track. *Geology*, **22**, 311-314.

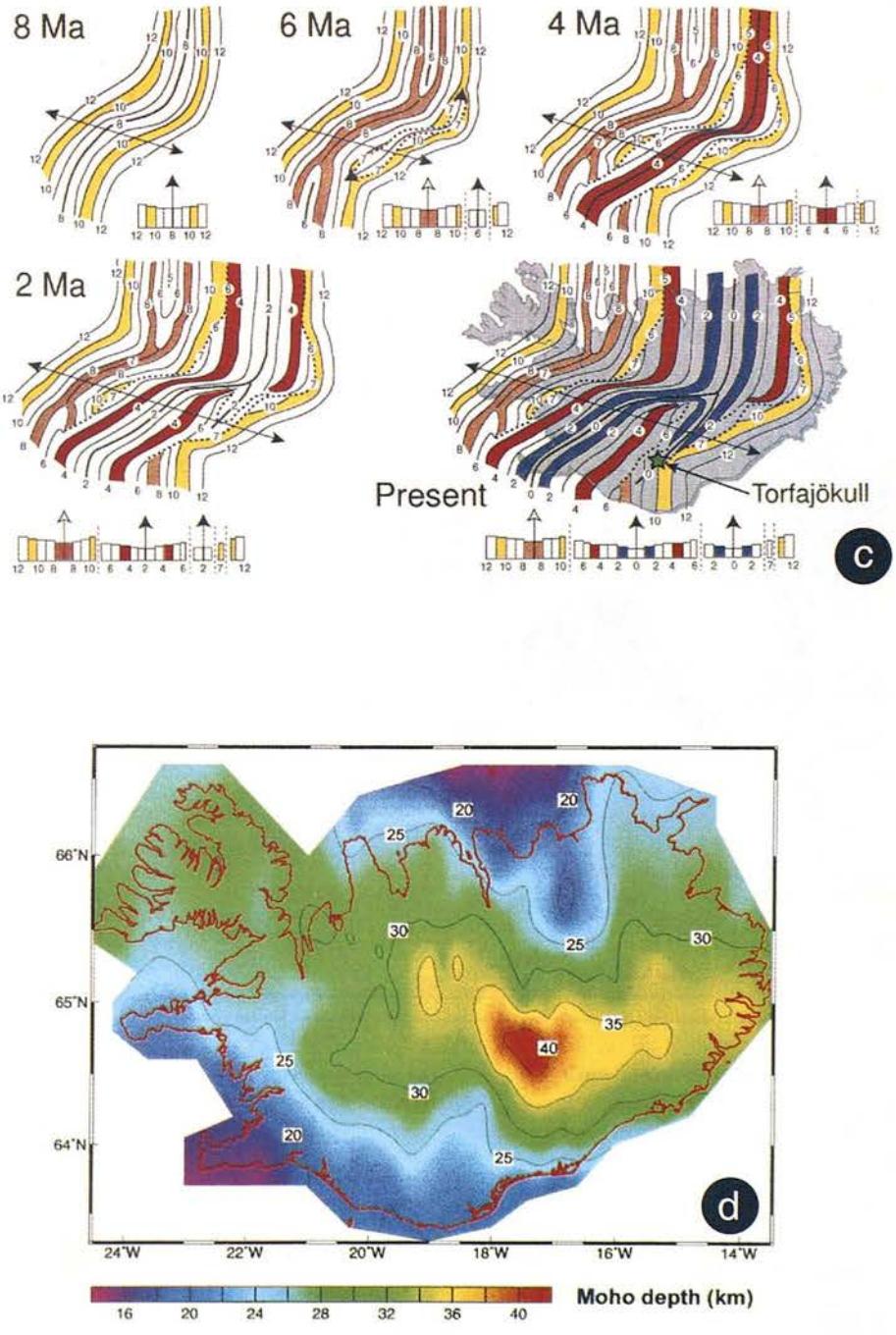


Figure 1.4 (c) Formation of Iceland and evolution of the Icelandic rift zones from 8 Ma to present day (from Stecher *et al.*, 1999) **(d)** Gravity anomaly map of Iceland showing the depth of the Moho beneath Iceland and the location of the deep mantle plume beneath central Iceland (from Wolfe *et al.*, 1997).

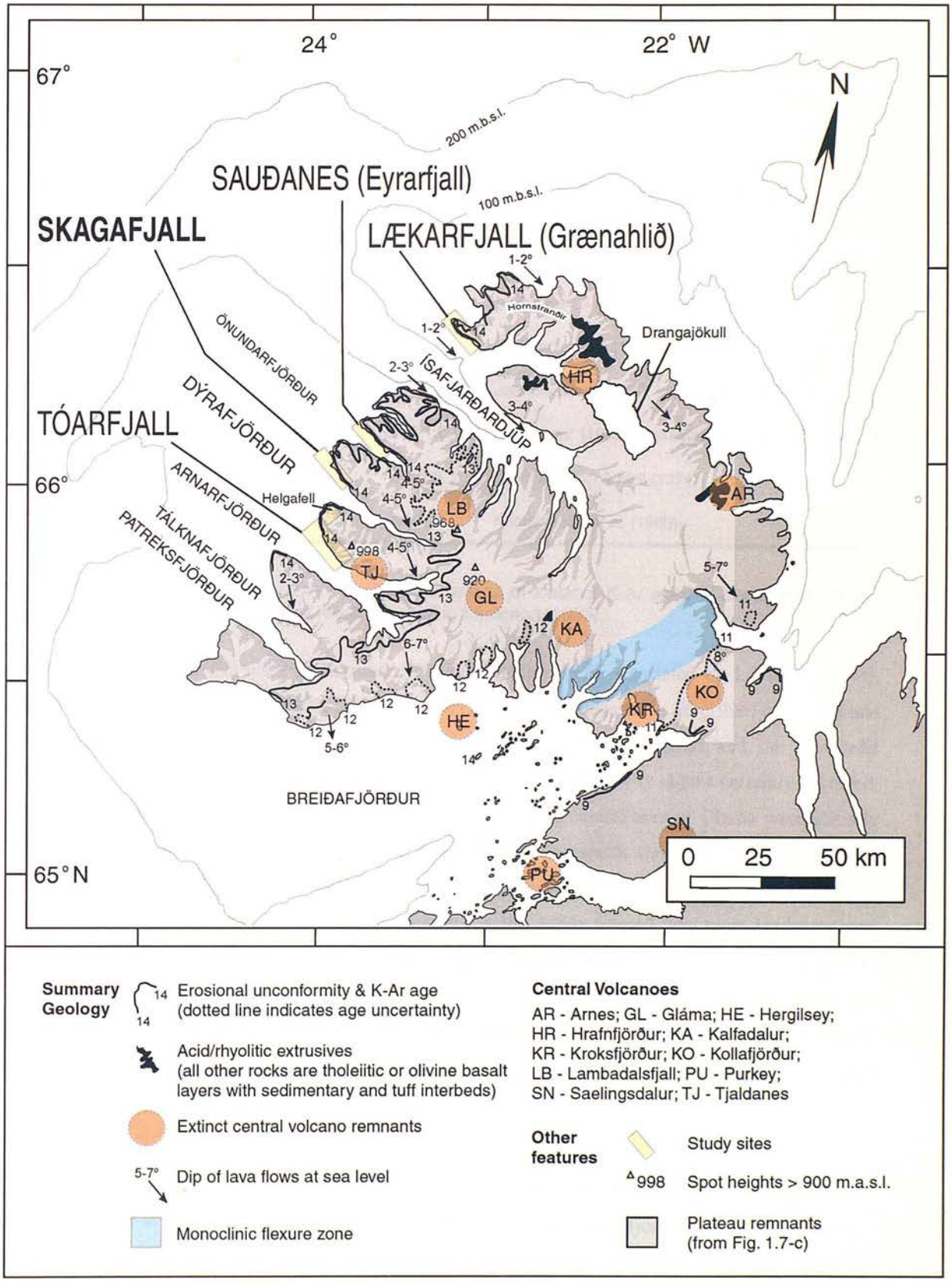


Figure 1.5 Compilation summary map of the main geological features of the Western Troughs of the Vestfirðir Peninsula (drawn from information in Gudmundsson A., 1986, 1989; McDougall *et al.*, 1984; Gudmundsson *et al.*, 1996; Jóhanesson and Sæmundsson, 1998).

LOCATION	TILLITE HORIZONS (number)	AGE RANGE (Ma)	REFERENCES & LOCATION MAP
1) Hornafjörður, E Iceland	3#	7-5 Ma	Fridleifsson (1995)
2) Skaftafell, S Iceland	2	4-3.2 Ma	Sæmundsson (1979); Helgason & Duncan (1992)
3) Bessastaðaa, E Iceland	2	6.6-6.3; 4.8	McDougall *et al.* (1977); Watkins & Walker (1977); Hjartsson and Hafstað (1997)
	7-9	3.1-1.6	McDougall & Wensink (1966)
	2	3.1	Vilmundardóttir (1972)
4) Mid-West Iceland	1	4.4-4.3	Jóhannesson (1975); McDougall *et al.* (1977)
5) Tjörnes, N Iceland	10	3.32-1.8	Einarsson* (1968); Geirsdóttir & Eiríksson (1996)
6) Húsafell, SW Iceland	11	3.1-1.5	Sæmundsson & Noll (1974)
7) Esja-Akrafjall	11-16	3.1-1.8	Kristjánsson *et al.* (1980)

Table 1.2 Pre-Pliocene-Pleistocene transition glaciations of Iceland: K-Ar ages of basalt lavas below 'tillites' glaciations of Iceland (# = at least; * = cited in Lárusson, 1983).

Thoroddsen (1901, 1902; cited in Lárusson, 1983), Winkler (1938; translated by Lárusson, 1983), Sigurdsson (1967), Lárusson (1983), Gudmundsson (1989), Gudmundsson *et al.* (1996) examined and mapped tectonic and present day hydrographic features of western Iceland and the Vestfirðir Peninsula. All concluded that Tertiary and early Pleistocene glacial activity almost certainly occurred. Lárusson (1983) proposed that ice streams emanating from the central area of Glama were initially concentrated in sizeable fluvial valleys that drained north-westwards through the oldest bedrock formations between Patreksfjörður-Ísafjarðardjúp-Hornstranðir. The fluvial valleys originated by exploiting tectonic fractures, *e.g.* dykes, that existed in the newly formed lava plain landscape and drainage was guided north-westwards by the dip of plateau lavas that existed between *ca.* 10-16 Ma (Kristjánsson *et al.*, 1975). Lárusson (1983; p. 27) concluded that 'the orientation of fractures and fjord valleys in Vestfirðir shows that in some areas (*i.e.* primarily around Drangajökull, the land-bridge connecting Vestfirðir to the mainland and in the SW tip of the Peninsula) there exists such a distinct relationship between the two that it must be causative'.

(ii) Mid-late Pleistocene

Terrestrial evidence of glacial activity during the mid Pleistocene in Iceland is sparse in comparison to the well-dated sections from the Late Pliocene and Early Pleistocene (Hjort *et al.*, 1986; Geirsdóttir and Eríksson, 1994). Thoroddsen (1892a, b) first suggested that an 'Ice Age' ice cap terminated not far offshore of Vestfirðir and covered the whole of the country except for a few mountain peaks close to the ice margin. The thickness and extent of the major mid-late Pleistocene ice sheets has been

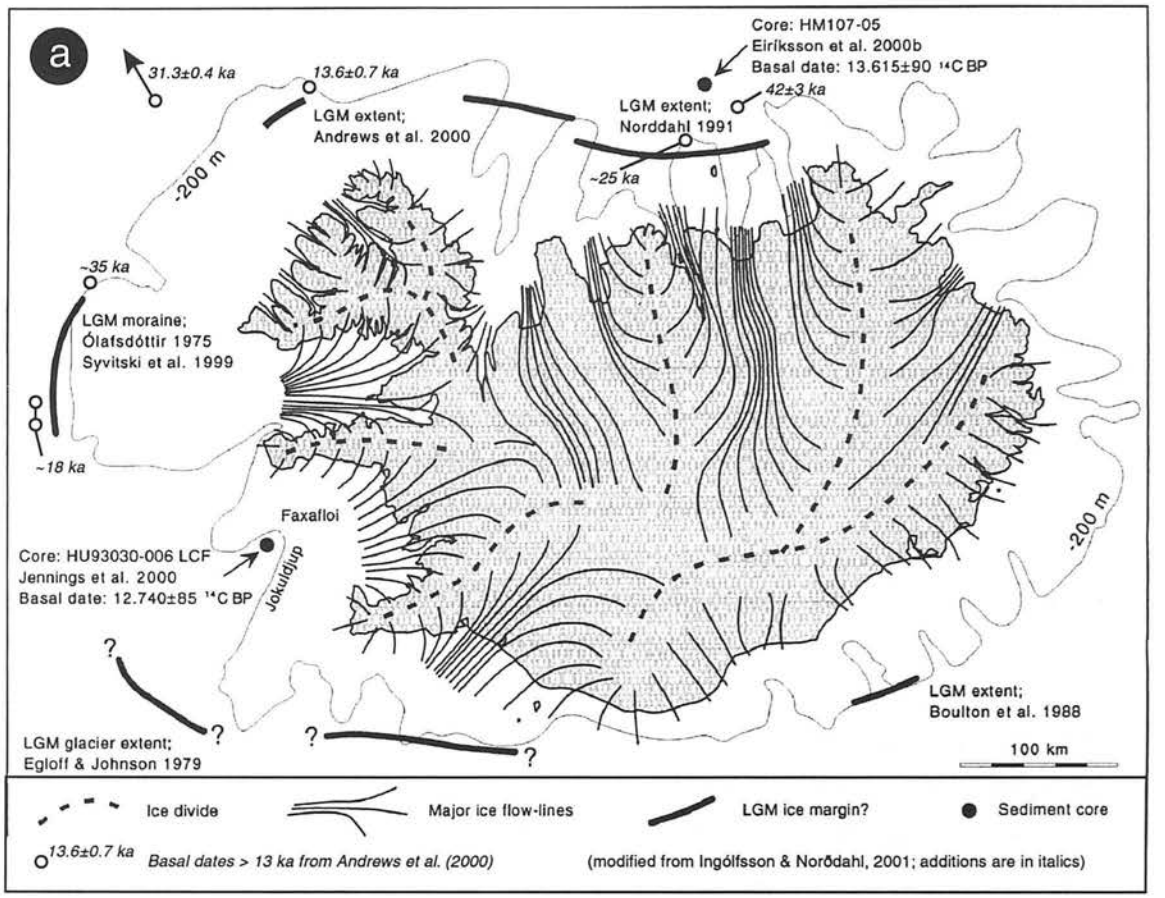
estimated from the heights of sub-glacial table mountains in central Iceland (*e.g.* Rundgren *et al.*, 1997). A 25-30m high, 800 m wide submarine ridge, situated at a depth of 250m, 140km west of Snæfellsnes, known as the Látragunn end moraine, is thought to represent the maximum extent of the last glacial cycle or that of the penultimate, Saalian, glaciation (Fig. 1.6-a) (Olafsdóttir, 1975). Syvitski *et al.* (1999) obtained a basal marine core age of 35.56±0.56 ^{14}C ka BP from the base of a diamicton deposit to the north of this moraine. However, the stratigraphic relationship between the two deposits described above has yet to be established (Andrews, *manuscript*).

(iii) Last Glacial Maximum (LGM) and Post LGM glacial activity

Other evidence of glacial activity during the late Pleistocene period is restricted to the last, Weichselian, glaciation and subsequent re-advance stages during the last deglaciation. The extent of the Icelandic ice sheets at the Last Glacial Maximum (LGM; 22-18 ka BP in Iceland; Hjort *et al.*, 1986) remains uncertain. Near-encompassing terminal moraine limits have been identified offshore, but the relationship between ^{14}C ages from sediment cores and geomorphological evidence has not been securely established (Syvitski *et al.*, 1999; Andrews *et al.*, 2000; Andrews, *submitted*) (Fig. 1.6a).

Deglaciation of the mainland LGM ice-sheet to present day ice limits was interrupted by numerous readvances (Ingólfsson, 1991, Petursson, 1991). Although there is continuing debate over the timing and extent of these readvance stages the Multi-Advance Deglaciation (MAD) model (Norðdahl, 1991; Ingólfsson and Norðdahl, 1994) is now widely accepted (Gudmunðsson, 1997). Two readvance stages, the Álftanes and Buði, and their timing are the key. The Álftanes readvance stage was originally thought to have occurred between 13-12 ^{14}C ka BP ('Older Dryas') and is named after a site on the Reykjavik peninsula where terminal moraines were first discovered (Tryggvasson and Jónsson, 1958). The Buði readvance stage was originally linked to the 'Younger Dryas' readvance stage. It is named after a waterfall on the river Þjórsá in southern Iceland where marine sediments *ca.* 100 m.a.s.l. beneath a prominent terminal moraine were dated to *ca.* 11-10 ^{14}C ka BP (Kjartansson, 1943; translated in Lárusson, 1983). Based on ^{14}C dating of marine shells, sediments and organic material in or beneath moraine complexes in the Borgarfjörður region of western Iceland, Ingólfsson (1987) suggested that up to nine chronologically distinct readvances could have occurred. This contradicted existing dual-advance deglaciation models (Einarsson, 1968, 1991). Recent ^{14}C dating of moraine deposits of 'mainland'[5] Iceland has revealed that the Álftanes Stage is most likely associated with the 'Younger Dryas' readvance and the Buði Stage with a early Holocene 'Preboreal' oscillation (Norðdahl and Einarsson, T., 1988; Hjartsson and Ingólfsson, 1988; Hjartsson, 1989; Norðdahl, 1991; Sæmundsson, Þ., 1994, 1995; Björck *et al.*, 1997; Richardson, 1998). Recently, evidence for a more extensive Preboreal ice sheet (the Svalbard Glacial Event) has been found on the Digranes peninsula in the far north-east corner of Iceland (Richardson, 2000).

[5] Mainland Iceland is defined in this context as all parts of Iceland excluding the North West Peninsula



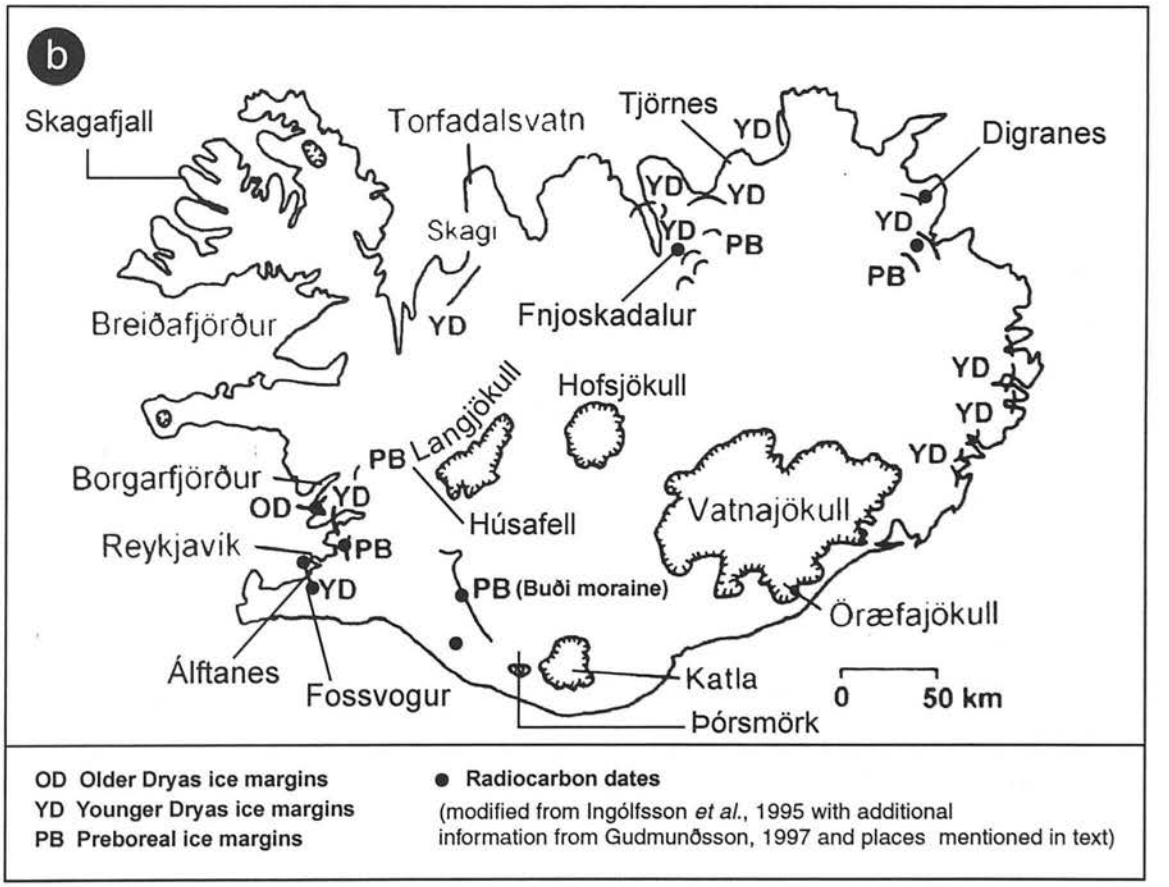


Figure 1.6 (a) The concept of an all encompassing LGM ice-sheet in Iceland extending approximately to the 200 m.b.s.l. isobath (modified from Ingólfsson and Norðdahl, 2001 **(b)** The Multiple Advance Deglaciation (MAD) model (modified from Ingólfsson *et al.*, 1995; Gudmundsson, 1997; Richardson, 1999).

In conclusion, the MAD model suggests the last mainland ice-sheets were particularly sensitive to rapid late-glacial and early Holocene climate change that have been identified in the Greenland ice cores and proxy records of the northern North Atlantic (Bond *et al.*, 1992; 1993; Ingólfsson and Norðdahl, 1994; Koç *et al.*, 1993, 1996).

The extensive mainland ice-sheet disappeared by 7.8 ^{14}C ka (Kaldal and Víkingsson, 1991). Since 7.8 ^{14}C ka, glacial activity has been confined to and around volcanic edifices predominantly in the southern half of Iceland. Certain outlet glaciers (*e.g.* Sólheimajökull, a southern outlet of Mýrdalsjökull and Lambutungajökull, a confined eastern outlet of Vatnajökull) are highly sensitive to, and fluctuate in phase with, decadal-annual variations (*e.g.* NAO) in the position of the oceanic and atmospheric Polar Fronts the North Atlantic around Iceland (*e.g.* Sharp, 1984; Dugmore and Sugden, 1991; Koç *et al.*, 1996; Bradwell, 2000, 2001). Detailed reviews of post-LGM environmental change in Iceland can be found in Ingólfsson and Norðdahl (1994) and Gudmunðsson (1997).

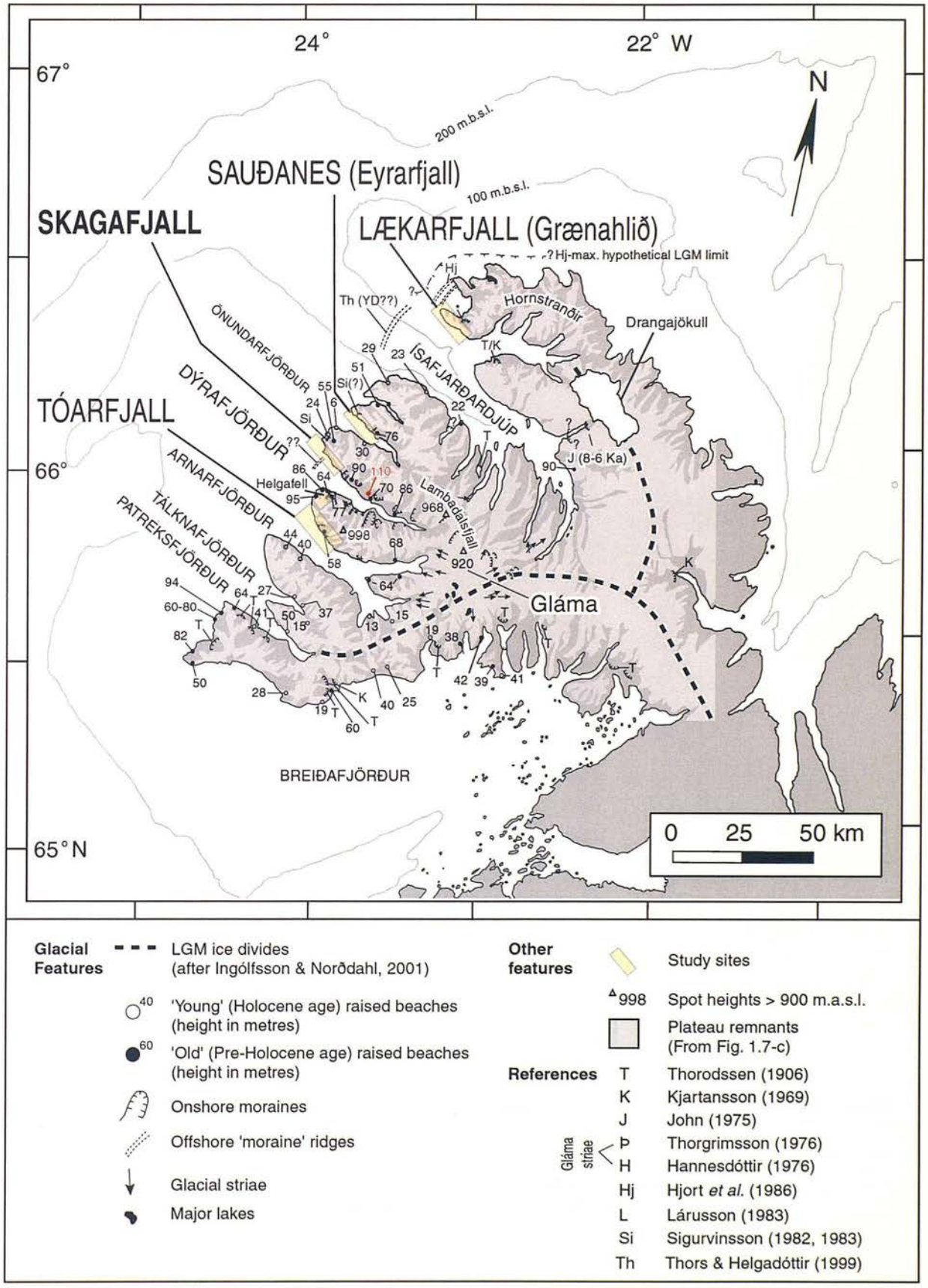
Significant clues for the extent of the LGM and post-LGM ice sheets can be found on and around the Vestfírðir Peninsula. Larusson (1983) identified abundant geomorphological evidence for post-LGM episodes of glacial incision, but no pre-Holocene ages have been obtained (John and Sugden, 1962; John, 1975; Hansom and Briggs, 1991). It has been suggested that some high altitude glacial features, *e.g.* cirques, could be relics, possibly up to 1-3 million years old (Lárusson, 1983; Gudmunðsson, *pers. comm.*). 'Small, inconspicuous moraines'...'found at the head of Dýrafjörður [location unspecified] at a height of 600-700 m [that were] formed during a glacial readvance' have been found by Þorgrímson (1976, p. 267) and Sigurvinsson (1982 & *pers. comm.*) found similar features *ca.* 500-600 m.a.s.l. on Sauðanes (Fig.1.7-a).

Large lateral and end moraines and raised beach platforms can be found along the coastline of many fjords and numerous well-developed cirques are common in the steep plateau cliff faces (Fig. 1.7-a) (John, 1974; Larusson, 1983; Hjort *et al*, 1986). Raised beaches are common across the Vestfírðir Peninsula. They provide evidence for rapid rise and equally rapid fall in post glacial sea-level (John, 1975) and can be used as a proxy measure of former extent, thickness and distribution of the last ice-sheet on Vestfírðir. Marine limits up to 111±1 m.a.s.l. have been found near Núpur on the northern shore of Dýrafjörður (Lárusson, 1983). In contrast, the maximum height of raised beaches on Hornstranðir is 26 m.a.s.l. (Hjort *et al.*, 1986). Radiocarbon dating of raised beaches in the western troughs and eastern coast of Hornstranðir showed that sea level returned to 1 m.a.s.l. *ca.* 9000-9930 ^{14}C BP, fluctuated up to 8.5 m before slow regression to present sea-level 8,830 ^{14}C BP (John, 1975; Hansom and Briggs, 1991). It is interesting to note that the timing of this minor fluctuation is similar to the 8,521±69 ^{14}C maximum age of the Svalbard Glacial Event in NE Iceland (Richardson, 2000).

Lárusson (1983) suggested that the configuration and height of the Vestfírðir raised beaches is due to rapid and significant postglacial crustal rebound. Furthermore, ice retreat caused crustal deformation in the Dýrafjörður and Arnarfjörður district along a line parallel to Dýrafjörður in the direction of Glama, suggesting Glama was an independent centre of postglacial uplift (Lárusson, 1983).

Lárusson (1983) also constructed the only known relative chronology of deglaciation events for the Vestfírðir Peninsula based on the relationship between marine terraces and end moraines and/or ice marginal deposits on the peninsulas between the western fjords of Arnarfjörður and Dýrafjörður. The height of the highest marine limit and large open ended lateral moraines in Dýrafjörður and Önundarfjörður, in particular, are thought to be related to a single Lateglacial deglaciation re-advance phase of stadial proportions. Lárusson (1983) called this stage the Tjaldanes Stage after Tjaldanesdalur on the northern Arnarfjörður shore where the relationship between raised beach and moraine deposits is best displayed. Glacial activity in the Tjaldanes Stage led to renewed crustal downwarping and retardation of post-LGM uplift. The Tjaldanes readvance was linked to the Buði stadial, but a lack of suitable organic material (*e.g.* marine shells) meant it could not be directly dated. This 'tentative' correlation might have to be revised in the light of new evidence from elsewhere in Iceland (above). In conclusion, John (1975), Lárusson (1983) and Hansom and Briggs (1991) suggested thick ice cover existed on the Vestfírðir Peninsula at the LGM, boosted by a secondary ice accumulation centre over Glama in addition to Drangajökull. During post-LGM readvances independent ice caps, again centred on Glama and Drangajökull, most probably developed on Vestfírðir (Lárusson, 1983; Hansom and Briggs, 1991).

Lárusson (1983) grouped all Holocene glacial activity into a single 'post-Tjaldanes stage' reflecting a general lack of age control in this period and the relatively minor nature of fluctuations in ice extent compared to the magnitude of pre-Holocene activity. Post-Tjaldanes activity did not advance beyond Tjaldanes limits. John and Sugden (1962) mapped the glacial features of Kaldalon. Radiocarbon ages suggest the moraine limits in this valley are Holocene or at most Younger Dryas in age (Sugden and John, 1962; Hjort *et al.*, 1986). During the 'Little Ice-Age' maximum, *ca.* 1756-1860 AD, sea-ice off the Vestfírðir coast was extensive, Glama supported a permanent plateau ice-cap creating a radiating pattern of bedrock striations and local end moraines (Fig. 1.7-a). In addition, the outlet glaciers from Drangajökull advanced significantly and glaciers filled several cirques in Hornstranðir and the plateaux between the Western Troughs of Arnarfjörður and Ísafjarðardjúp (Eythorsson, 1935; Thórarinsson, 1943; John and Sugden, 1962; John, 1973; Sugden and John, 1976; Lárusson, 1983; Hjort *et al.*, 1986). Current glacial activity is restricted to the Drangajökull area on the Hornstranðir Peninsula. Drangajökull is the fifth largest ice cap in Iceland. The other four are located in the southern half of mainland Iceland and are (in order of largest to smallest) Vatnajökull, Langjökull, Hofsjökull and Mýrdalsjökull.



Glacial Features

- LGM ice divides (after Ingólfsson & Norðdahl, 2001)
- 40 'Young' (Holocene age) raised beaches (height in metres)
- 60 'Old' (Pre-Holocene age) raised beaches (height in metres)
- Onshore moraines
- Offshore 'moraine' ridges
- Glacial striae
- Major lakes

Other features

- Study sites
- 998 Spot heights > 900 m.a.s.l.
- Plateau remnants (From Fig. 1.7-c)

References

- T Thorodssen (1906)
- K Kjartansson (1969)
- J John (1975)
- Gláma striae: Þ Thorgrimsson (1976)
- Gláma striae: H Hannesdóttir (1976)
- Hj Hjort *et al.* (1986)
- L Lárusson (1983)
- Si Sigurvinsson (1982, 1983)
- Th Thors & Helgadóttir (1999)

Figure 1.7 (a) Compilation summary map of the main glacial features of the Western Troughs of the Vestfirðir Peninsula.

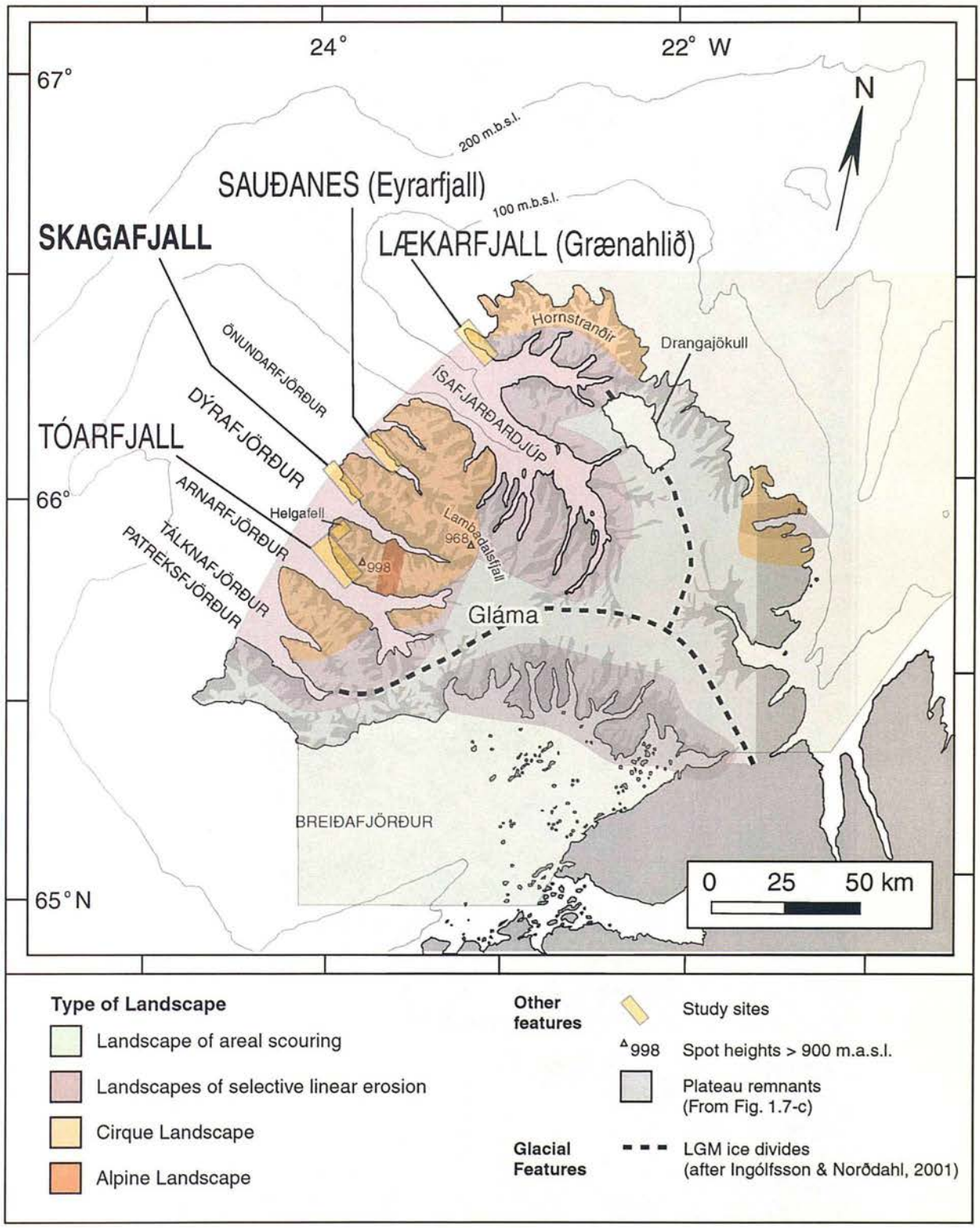


Figure 1.7 (b) Landscapes of glacial erosion on the Vestfirðir Peninsula (drawn from information in Lárusson, 1983). Landscapes of glacial erosion are as defined in Sugden and John (1976).

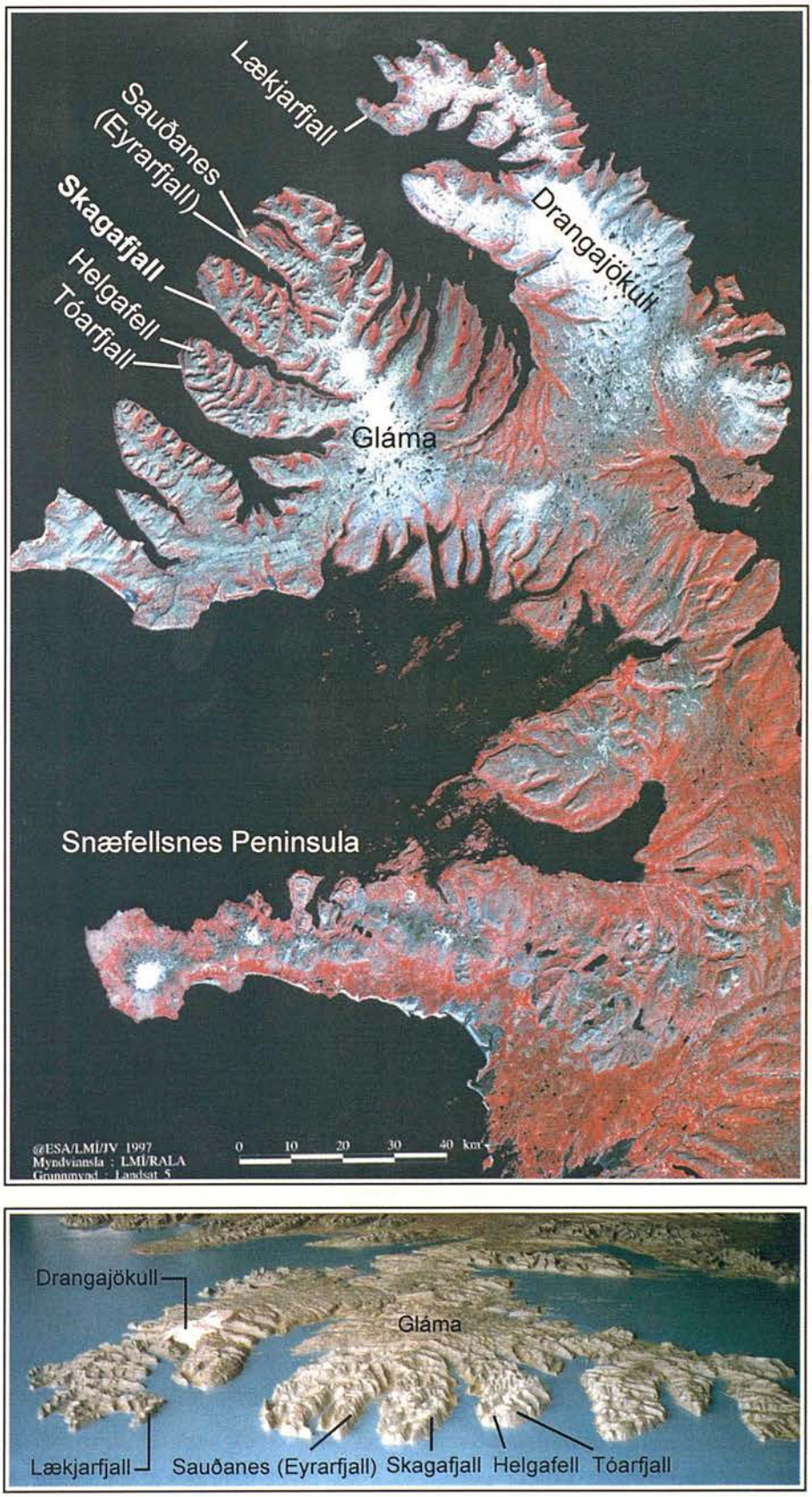


Figure 1.7 (c) False colour Landsat 5 image of the Vestfirðir and Snæfellsnes Peninsulas. The high altitude plateaux and glacial landscapes of selective linear erosion in the Western Troughs are clearly visible as are the numerous lakes in the central Gláma and Drangajökull. The latter are characteristic features of glacial landscapes of areal scouring and were classified as such by Larússon (1983) (Fig. 1.7b) (from ESA/LMÍ/JV, Iceland Geodetic Survey, 1997) **(d)** The Western Troughs of the Vestfirðir Peninsula looking approximately SE towards mainland Iceland. Again, the glacial landscapes of areal scouring are clearly distinguishable from those of selective linear erosion (photograph of the LMI 3-D Map of Iceland, Reykjavik Town Hall).

1.4.3 Hypotheses for Vestfírðir Peninsula glaciations & landscape evolution processes

Four closely linked hypotheses have been advanced to explain topographic and glacial features of the Vestfírðir Peninsula. They remain largely unresolved due to the lack of chronological evidence.

Hypotheses 1: Pre-LGM glacial activity on Vestfírðir

The principal limitation in investigating this hypothesis is the lack of chronological constraints. Lárusson (1983; p. 29 and 31) stated that 'no tillites have been discovered in Vestfírðir – the rocks of Miocene age being too old' and 'no evidence has been found for glaciations in Vestfírðir earlier than the last glacial, but there is no reason to suggest that glaciations are less frequent than elsewhere. Indeed, the present day glaciation limit is lower than Vatnajökull (Ahlman, 1937)'.

Hypothesis 2: LGM ice-sheets were restricted to the inner shelf of Iceland

If the restricted LGM ice sheet hypothesis is correct, ice advancing through Ísafjarðurjúp from the plateaux of the Vestfírðir Peninsula did not reach the continental shelf edge. Several lines of evidence suggest that the western half of the LGM ice sheet was restricted to the current continental shelf. At the LGM, global sea level was about 120 m lower than today (Bard *et al.*, 1989; Fairbanks, 1989). Hjort *et al.* (1986) used palaeo-ice thickness estimations to calculate that the LGM ice extended only half way to the edge of the current continental shelf and 6-10 km from the present shoreline of Hornstranðir in the Vestfírðir Peninsula. Hjort *et al.*, (1986) cited modern day analogues to suggest that a dramatic and rapid reduction in ice thickness occurs in areas where previously restricted valley glaciers are allowed to spread onto an unconfined oceanic shelf.

Further evidence in support of this 'restricted ice-cap' hypothesis can be found in bathymetric profiles of the main fjords in Vestfírðir. Apart from the entrance to Ísafjarðardjúp, the continental shelf of the Vestfírðir Peninsula is undissected and <100 m deep. This is in contrast to deeply incised submarine canyons that characterise the coastal margins of active ice centres in southern and south-east Iceland (Boulton *et al.*, 1988; Fig. 1.6). In places, the fjords of Dýrafjörður and Önundarfjörður are less than 20 m deep. Recently, a large diamicton ridge looping the end of Ísafjarðurjúp has been identified (Thors and Helgadóttir, 1999). A basal core date of 34.2±0.64[6] ^{14}C ka BP from a site in Djupall at the entrance to Ísafjarðurjúp has been obtained (Fig 1.7-a). Jennings *et al.* (2000) and Andrews (*submitted*) suggested that this is the maximum limit of the LGM ice sheet. Coarse gravels on the proximal oceanic shelf off Vestfírðir were thought to be glacially derived (Thors, 1974). Hjort *et al.* (1986) suggested two shallow offshore banks in Aðalvík, Hornstranðir, may represent LGM limits. Although numerous basal ^{14}C ages from marine cores from the northwestern continental shelf now exist, secure evidence for a restricted LGM ice advance has proved elusive. This is principally

[6] Age includes a marine reservoir correction of 600 years (Andrews *et al.*, 2000)

because the relationships between physical manifestation of ice limits and core data remain uncertain (Andrews *et al.*, 2000; Jennings *et al.*, 2000).

Hypothesis 3: Ice-free areas existed at the LGM – the nunatak theory & Vestfirðir

Closely linked to the second hypothesis is the theory that isolated high altitude ice-free areas were widespread in remote northern and north-western parts of Iceland at the LGM (*i.e.* the nunatak hypothesis[7]). Thoroddsen (1892a; 1892b, 1906) suggested that nunataks might have existed between outlet glaciers, restricted to small areas close to the edge of the ice cap (cited in Hjort *et al.*, 1986). The widespread presence of such areas across Iceland was first postulated by Lindroth (1931) to provide support for his 'plant-refugia' hypothesis. Since then, strong biological evidence for and against the existence of ice-free areas in Iceland has been presented but no consensus has been reached (Gelting, 1934; Friðriksson, 1962*; Steindorsson, 1962*; 1964*; Hjort *et al.*, 1986; Einarsson and Albertsson, 1988; Buckland and Dugmore, 1991; Rundgren and Ingólfsson, 1997; Fig. 1.8).

The physical evidence in support of ice-free areas is also controversial (Sugden and John, 1976; Miller, 1982; Forman and Miller, 1984; Dahl, 1992; Kleman and Storeven, 1997). In summary, the absence of physical evidence for ice activity does not mean ice-free conditions existed or that glacial overriding has not occurred (Hoppe, 1982; Nesje and Dahl, 1990; Kleman, 1994). In Vestfirðir, Thórarinsson (1937), Einarsson (1968), John (1975) and Hjort *et al.* (1986) have argued for the existence nunataks and/or more extensive ice free areas on the Vestfirðir Peninsula during the LGM while Thoroddsen (1906), Lárusson (1983) have advanced the opposing viewpoint. Lárusson (1983) believed that most of the 300 high altitude cirques he mapped in the coastal cliffs in between the major fjords of NW and E Vestfirðir are relic features formed between 3-1 Ma. Some have, therefore, survived being overridden by thick, non-erosive ice sheets at least ten times since their formation. Hjort *et al.* (1986; p.14) were unable to find any signs of active glacial erosion on the plateaux of Hornstranðir, but believed that at the LGM 'thin inactive and/or cold based icefields' covered all but the highest plateaux. Even apparently clear-cut geomorphological evidence for glacial activity can be ambiguous. For example, Hoppe (1968) found abundant meltwater channels, glacial striae, roche moutonnées and thin till sheets covering the island of Grimsey off the North coast of Iceland. Although he concluded that LGM ice was probably tens of kilometres thick out to the 200 m isobath '[the presence of LGM] nunataks cannot be excluded' (Hoppe, 1968; p. 22). Further, coastal nunataks and cirque topographies can survive glacial over-riding, especially when the glaciers are cold-based and non-eroding.

[7] Nunataks are defined as mountain peaks that remain above the ice.
* = cited or translated in Lárusson (1983)

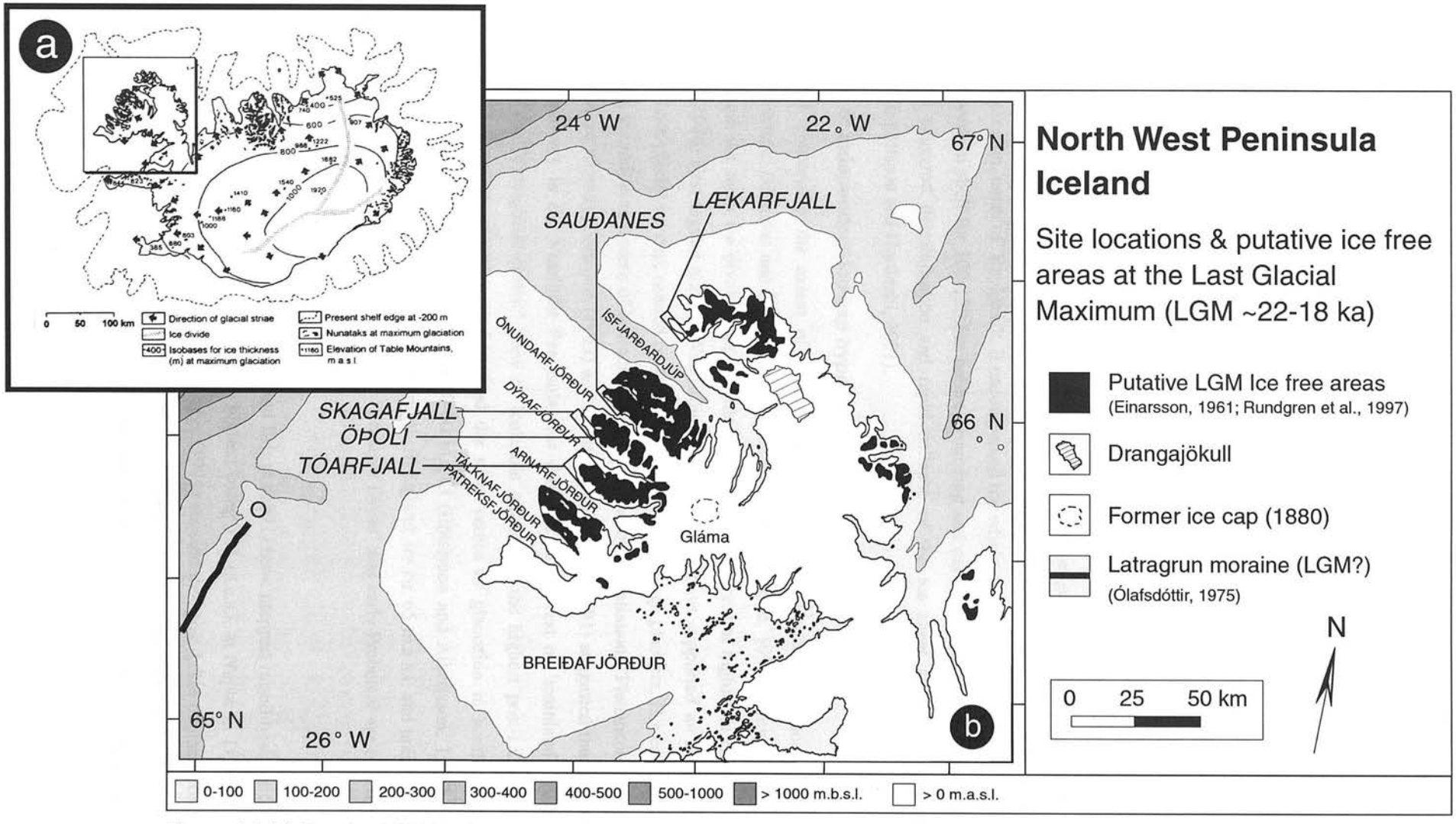


Figure 1.8 (a) Putative LGM ice-free areas in Iceland (from Rundgren *et al.*, 1997 and associated references) **(b)** The Vestfírðir Highlands of the North West Peninsula are located between Ísafjörðardjúp and Arnarfjörður. Sections A-C are 1-2 km NW of Óþoli. Figure drawn from information in Olafsdóttir (1975); Hjort *et al.* (1986); Rundgren *et al.* (1997).

Hypothesis 4: LGM ice sheets covered the whole of Iceland and its offshore shelf

Alternatively, the LGM and early deglaciation ice sheets extending onto the outer continental shelf and covered an area delimited by the current 200 m bathymetric contour (Syvitski *et al.*, 1999). Thoroddsen (1906) first suggested that the whole Icelandic landmass was ice-covered during the 'Pleistocene' glaciation. Lárusson (1983) argued that this scenario probably occurred at least at the LGM (Weichselian) and also at the height of penultimate (Saalian) glacial maximum *ca.* 130 ka. By fitting theoretical ice sheet profiles to reach Olafsdóttir's (1975) Látragunn end moraine Lárusson (1983), argued that at the LGM the whole of the Vestfírðir Peninsula was buried in an ice sheet that was at least 120 m higher than Kaldbakur, at 998 m.a.s.l., the highest point of the Vestfírðir peninsula. The main limitation of this approach is that the age of the Látragunn end moraine has yet to be established securely (Andrews *et al.*, 2000). Recently, Ingólfsson *et al.*, (1995) and Ingólfsson and Norðdahl (2001) suggested that the LGM ice sheet in Iceland was thick, up to 840±150 m in the Borgarfjörður region, north of Reykjavík. It encompassed the whole of Iceland and ice extended onto the exposed western shelf for 100-150 km before grounding and calving at *ca.* 350 m.b.s.l. Eustatic sea-level rise triggered destabilisation and rapid collapse of the ice sheet at the start the last deglaciation (Ingólfsson and Norðdahl, 2001).

Hypothesis 5: Independent ice-cap hypothesis

Most theories concerning the extent of former glacial activity in Iceland have tended to be 'Vatnajökull-centric' (Hansom and Briggs, 1991; Geirsdóttir and Eiríksson, 1994). They assume that ice flowed from the main ice divides that extended along the south central highlands (Fig. 1.6-a). Thoroddsen (1906) first argued that the Vestfírðir Peninsula could have supported an independent LGM and/or Late-glacial ice cap, centred on the Glama and/or the Dranga plateaux. His early studies were based on the radiating pattern of bedrock striations created by a continuous 'Pleistocene' ice cap (Fig. 1.7-a). More recently, Lárusson (1983) and Hansom and Briggs (1991) suggested that the style of isostatic recovery in the Vestfírðir Peninsula was different to the rest of 'mainland' Iceland. According to the 'Vatnajökull-centric' view of Icelandic glaciation, the highest post-LGM raised beaches should occur about 100 m.a.s.l. around the main centre of glaciation in south Iceland. Elsewhere raised beaches should be between 30-60 m.a.s.l (Einarsson and Albertsson, 1988). The highest raised beaches on the Skagi Peninsula in northern Iceland are *ca.* 65 m.a.s.l. and uplift rates in the interval between readvances between the late 'Younger Dryas' and early Preboreal are on average 11-12 $cmyr^{-1}$ (Rundgren *et al.*, 1997).

Lárusson (1983), Sigurvinsson (1982), Hansom and Briggs (1991) have mapped raised beach profiles around the Vestfírðir Peninsula above 60 m, the highest being 111 m.a.s.l. at Núpur in Dýrafjörður (Fig. 1.7-a). As discussed earlier, Hansom and Briggs (1991) showed that post-LGM deglaciation sea level in Vestfírðir fell rapidly from *ca.* 136 m.a.s.l. to at least -2 m.a.s.l. between 12-9 ^{14}C ka BP. Raised beaches up to *ca.* 100 m.a.s.l. on Vestfírðir are formed by rapid post glacial uplift and suggest

LGM and Tjaldanes Stage ice caused significant regional crustal downwarping. Lárusson (1983) used these 'marine limits' to validate his hypothesis that the Vestfirðir Peninsula must have been covered by a substantial LGM ice cap that was at least 500 m thick. Hansom and Briggs (1991) concurred and questioned the Vatnajökull-centric view of Icelandic glaciation. They also concluded that Vestfirðir must have supported a substantial LGM and/or an independent 'Younger Dryas' ice cap.

1.4.4 Tephra deposits & the Vestfirðir Peninsula

The Vestfirðir Peninsula is the furthest part of mainland Iceland from the neovolcanic zone. Visible macrotephra layers are uncommon because of the unfavourable direction of the prevailing winds across Iceland (section 2.1.2). The white silicic Sn-1, Sn-2, Sn-3 layers from Snæfellsnes (Jóhannesson *et al.*, 1981) are sporadically distributed. Two of these were identified in Holocene peat and soil deposits in Ingaldsandur and one on Hornstranðir during preliminary investigations. The basaltic Hælavík Tephra (*ca.* 9 ^{14}C ka BP - Hjort *et al.*, 1986) found on the eastern coast of Hornstranðir has been geochemically linked to the eruption that produced the Saksunarvatn Ash (Hjort *et al.*, 1986). In contrast, while all the major mid-Holocene silicic eruptions of Hekla (H3, H4, H5; Fig. 2.2-d) and numerous basaltic eruptions are represented in soil sections of northern Iceland, no visible other visible tephra deposits of Holocene age have been found on Vestfirðir.

The only other known tephra deposit in the Vestfirðir Peninsula, assumed to be of Quaternary age, is a silicic tephra deposit that overlies a glacio-lacustrine sedimentary sequence near the plateau surface of Skagafjall. The Skagafjall sedimentary sequence is unique in this part of Iceland (Sigurvinsson, pers. comm.). Sigurvinsson (1982, 1983, p.104) discovered a stratigraphically well-constrained rhyolitic tephra deposit that is 'up to 10 m thick' in places. Although most of this is a result of post-depositional reworking, such a thickness is highly unusual compared to the thickness of tephra layers in Holocene peats of the Vestfirðir Peninsula.

This tephra deposit is now referred to as the Óþoli Tephra. It is recommended that tephra deposits should be named after a distinctive geographic location that relates to where it was first found to avoid confusion with chemically similar deposits that might not be from the same eruption event (Westgate *et al.*, 1992). Óþoli is the name of the highest plateau area on Skagafjall (Figs. 1.8-a, 1.9-a). Jon Sigurvinsson chose the name Óþoli Tephra when we visited the site in June 1998. The name Óþoli means 'something that cannot last or continue for a long time' and is an ancient-Icelandic word that is not used to describe a geographical location anywhere else in Iceland (Sigurvinsson, *pers. comm.*). Sigurvinsson (1983) described the Óþoli Tephra as a glass-rich rhyolitic deposit. Unaltered glass shards make up greater than 95% of the bulk composition of this tephra deposit. Other phases include altered glass, feldspar grains of uncertain origin, iron ore and traces of pyroxene.

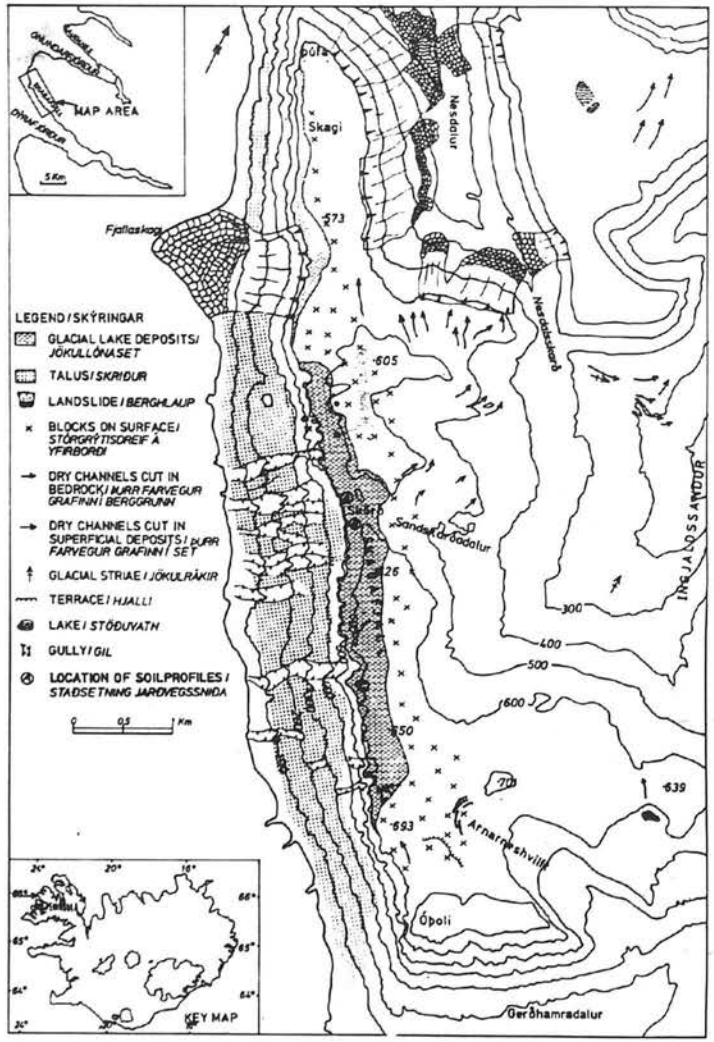


Fig. 1. Map of Skagafjall showing the glacial lake deposits. Location of sections shown on map.
Mynd 1. Kort af Skagafjalli sem sýnir jökullónasetið. Lega sniðanna er sýnd á kortinu.

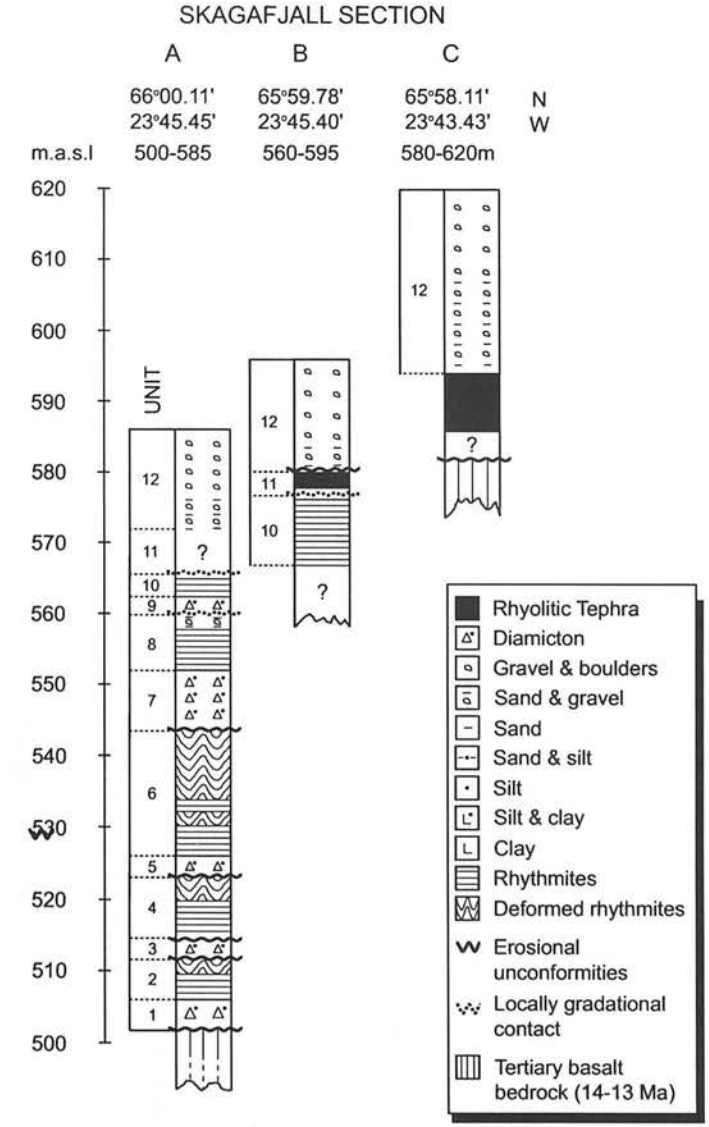


Figure 1.9 (a) The original geomorphological map of Skagafjall from Sigurvinsson (1983) **(b)** Sedimentary sections on Skagafjall, Vestfirðir peninsula, Iceland (modified from Sigurvinsson, 1983).

1.4.5 Principal Vestfírðir study site: Skagafjall

The main purpose of this thesis is establishing the age and origin of the Óþoli Tephra and its bracketing sediments. Skagafjall, on the northern side of Dýrafjörður, is a 9-km elongate plateau ridge with a maximum altitude of 720 m.a.s.l. Sigurvinsson (1982) discovered 7-km long sedimentary lake terrace 500-620 m.a.s.l., in a depression near the surface of this dissected plateau. These deposits were assumed to be significantly younger than the 16-13 Ma Tertiary basalt bedrock (Gudmundsson, 1989; Fig. 1.5). Sigurvinsson (1983) considered lake to be a lateral ice-dam feature formed at the lateral margins of an ice stream that once occupied Dýrafjörður. He suggested they were similar in age and form to ice-dammed lake deposits in Fnjóskadalur North Iceland that were thought to have been formed shortly after the LGM (Norðdahl, 1981) and that the whole sequence was probably deposited *ca.* '20-17 ka BP', at the height of the Weichselian glaciation. However, Norðdahl and Haflidason (1992) later discovered the Skógar Tephra in the Fnjóskadalur lake sequence and linked it to the Vedde Ash from Norway (Mangerud *et al.*, 1984). The age of the ice dammed-lake sediments was revised and this 'ice-lake' formation stage in this part of North Iceland is now associated with the Álftanes (Younger Dryas) glacial readvance stage (Norðdahl and Haflidason, 1992).

Three principal sedimentary sections (A-C) are exposed on Skagafjall by snow patch meltwater between July and September (Fig. 1.8-b). Sigurvinsson (1982; 1983) describes the deposits and their genesis in detail. In summary, they are a thick sequence of inter-bedded tephra, rhythmites and diamictons deposited into a large ice dammed lake of variable size and depth. If the rhythmites record annual variations in sediment input then the ice dammed lake existed for at least 2000 years (Sigurvinsson, 1983).

The age hypotheses for the Óþoli Tephra are shown in Table 1.3. They were developed before undertaking dating analysis. The basis of all the models is the presence of several erosional contacts and repeated units of thick diamicton deposits. The unit numbers relate to those originally defined by Sigurvinsson (1983) (Fig. 1.9-b) with odd numbered diamicton units representing stages of glacial advance and even numbered rhythmite units representing ice-stagnation phases with the formation of a substantial topographically ice-dammed lake on the Dýrafjörður margin of Skagafjall. The first hypothesis was developed with reference to the ice-free areas hypothesis (no. 3). Sigurvinsson's (1983) 20-17 ka age estimate is the basis for hypotheses (b) and (c).

Table 1.3 (a)-(c) (below) Age hypotheses for the Skagafjall section, established before undertaking dating analysis. Ages marked with an asterisk in are ka ^{14}C BP.

(a) Glacial-Interglacial Diamictons of the Pleistocene (Óþoli Tephra = 24*-128 ka)

Milankovitch Timescale Hypothesis

Skagafjall could be a terrestrial record of severe Pleistocene glaciation in Iceland, hence several erosional contacts and thick diamicton deposits. The ages of the Óþoli Tephra are as if the diamictons represent deposition during full glacial cycles.

Unit	$\delta^{18}O$ Stage	Age (ka BP) ($\delta^{18}O$ years)	Tephra	Age (ka BP)
1	?			
3	22	~900		
5	16	630 - 690		
7	12	430 - 480		
9	6	128 - 190		
			Óþoli Tephra	**128-24***
11	2	10*- 24*		

(b) Stadial Diamictons of the last glaciation (70 - 11.5 k GRIP yrs BP[8]; Óþoli Tephra = 16.5-21. 5 ka)

Sub-Milankovitch Timescale Hypothesis

This model assumes that palaeoclimatic synchroneity across the whole North Atlantic region on such a scale might be evident in the deposits of Skagafjall. The diamictons could be a terrestrial record of the last six Weichselian Heinrich events (HE) at 53-51, 44.5-43.5, 36.5-35, 28.0-26.5, 22.0-21.5, 16.5-15.0 ka and the 'Younger Dryas' event 12.0-11.5. Heinrich Events mark the end of millennial scale cooling cycles (Bond cycles) and occur in the last and/or coldest stadial immediately prior to a period of rapid warming. They are associated with massive iceberg rafting from the Laurentide Ice Sheet (LIS) and subsequent deposition of significant layers of Ice Rafted Detritus (IRD) in marine sediments of the North Atlantic. (Bond *et al.*, 1992, 1993; Bond and Lotti, 1995; Porter and An, 1995; Willliams *et al.*, 1998). Evidence for Heinrich Events exists in a number of marine cores, the Greenland ice cores and the loess deposits of China (*e.g.* Bond *et al.*, 1992, 1993; Porter and An, 1995; Thunnell and Morton, 1995). They suggests the oceans and the atmosphere behaved as an intimately linked system during the last glacial cycle. In addition, the timing of cooling events and iceberg discharges from the Fennoscandian Ice Sheet (FIS) identified in cores from the Norwegian Sea indicate that the LIS and FIS responded in phase to the climatic changes of the last ~70 ka (Fronval *et al.*, 1995; Grousset *et al.*, 2000; Scourse *et al.*, 2000). The age of the Óþoli Tephra in this hypothesis matches Sigurvinsson's (1983) estimate.

Unit	Heinrich Event	Age (ka BP) (GRIP years)	Tephra	Age Range (ka BP)
1	6	51.0-53.0		
3	5	43.5-44.5		
5	4	35.0-36.5		
7	3	26.5-28.0		
9	2	21.5-22.0		
			Óþoli Tephra	**16.5-21.5**
11	1	15.0-16.5		

contd. overpage

[8] GRIP years BP are ice core years BP using the GRIP incremental chronology (Björck *et al.*, 1998). These correspond to calendar years BP (1950) for the younger levels in the GRIP ice core.

(c) Late Weichselian Stadial Diamictons (Óþoli Tephra = 10.5-38 ka)

Fluctuating LGM ice sheet hypothesis - All deposits in the 38-10.5 k GRIP yrs BP age range

Deposits are related to fluctuations at the margins of an encompassing LGM Iceland ice sheet. If it existed (see section 1.4.5), the LGM Icelandic sheet was potentially highly unstable and sensitive to rapid climate changes during the last glacial period (Gudmundsson, 1997). Bond and Lotti (1995) argue that the cyclic discharge of ice every 2000 -3000 years from the LGM Greenland and Icelandic ice sheets was primarily responsible for the deposition of 13 IRD layers in the North Atlantic between 38-10 ^{14}C ka BP. This period incorporates the transition from the Last Glacial Maximum (LGM - 22.0 k GRIP yr BP) to the start of the Holocene epoch (*ca.* 11.5 GRIP k yr BP). There are two main stadial events during this period and two further episodes of noticeable cooling (Björck *et al.*, 1998). Between 38-22 ^{14}C ka BP there are at least three more stadial events. The age of the Óþoli Tephra could be similar to or younger than Sigurvinsson's (1983) estimate.

1.4.6 Secondary Vestfirðir study sites: Sauðanes, Tóarfjall, Lækjarfjall

A secondary aim of this study area was searching neighbouring plateaux (with NW-SE trending plateau margins) for similar sedimentary deposits to those found on Skagafjall. The ice-free areas of the Vestfirðir Peninsula proposed by Einarsson (1968) (Fig. 1.8-a) are amongst the most likely places to find terrestrial evidence of pre-Weichselian glacial activity in Iceland. The main topographic features of the Arnafjörður and Ísafjarðardjúp region are four parallel NW-SE trending fjords delimited by elevated flat-topped plateaux that have been incised to form alpine-style glacial valleys (Fig. 1.7-b). At glacial maxima these fjords are thought to be the main outlet routes for major ice streams from the interior highlands of the Glama (Fig. 1.7-a) (Larusson, 1983).

The other three sites chosen[9] are approximately NW-SE trending high altitude plateaux remnants. From south to north, Tóarfjall and Sauðanes are located between Arnafjörður and Ísafjarðardjúp to the south and north of Skagafjall respectively. Lækjarfjall is the outermost Ísafjarðardjúp facing plateau remnant on the western limb of Hornstranðir. No similar sedimentary deposits have been found on the plateaux adjacent to Skagafjall, although weathered fragments of rhythmite beds can be found scattered across the top of Sauðanes (Sigurvinsson, *pers. comm.*). This suggests that similar palaeoenvironments might have once existed at least in Önundarfjörður and Dýrafjörður. Jon Sigurvinsson[10] had already visited Tóarfjall, but has not found any sedimentary deposits of a similar nature to the Skagafjall deposits. Lækjarfjall had not been visited for this purpose and its last use was as a military gun-post during World War II.

[9] These sites were chosen as study locations after a visit with Jon Sigurvinsson to the area in June 1998.
[10] Contact address: Framhalddsskóli Vestfjarðs, Torfnesi, Pósthólf 97, 400 Ísafjörður.

1.5 The Þörsmórk Ignimbrite (Secondary study area)

A substantial amount of work has been undertaken investigating the glassy products of the Þörsmórk Ignimbrite. The completed work presented in this thesis forms part of an ongoing logging, dating and modelling project that aims to investigate Weichselian landscape development in the Þörsmórk region. It is self contained and especially relevant to the overall aims of this thesis. The inclusion of the Þörsmórk Ignimbrite data is justified because the correlation ages obtained from the fallout ash components of the Þörsmórk Ignimbrite provided a particularly useful age comparison (and robust correlation-age control) for new glass-phase thermoluminescence methods used to date the Óþoli Tephra (section 3.5.5). In addition, the eruption magnitude and/or explosivity was thought to be analogous to the Óþoli Tephra eruption.

In summary, the specific aims of the Þörsmórk Ignimbrite case study are (in order of precedence):

1) To provide a pre-Holocene age control sample for glass-phase TL dating of the Óþoli Tephra and characterise a range of glassy volcanic products for TL analysis.
2) To identify if any deposits in the Þörsmórk region were chemical correlatives of the Óþoli Tephra.
3) To determine if the ignimbrite deposits in the Þörsmórk region are from the same or multiple eruption events using Electron Probe Microanalysis (EPMA)

1.5.1 Geographical location

The Þörsmórk Ignimbrite was first described in the scientific literature by Thórarinsson in 1961 and formally named by Jørgensen (1981). It is one of the largest eruptive bodies in Iceland covering an area of about 80 km^2 in the heart of the transitional-alkalic province of the Eastern Volcanic Zone (EVZ). The only deposits in the Icelandic terrestrial tephra record that definitely relate to this eruption are those from the area surrounding the former farmstead (and now major tourist centre) of Þörsmórk. Intermittent volcanic aggradation and glacial erosion along the Krossa and Markarfljót valleys has created stratigraphic sections with dateable volcanic deposits (Thórarinsson, 1969). The Þörsmórk Ignimbrite has not been directly dated at its type site, but recent studies have suggested that its major element chemistry is sufficiently distinctive to provide an excellent correlation age estimate (Lacasse *et al.*, 1996; Zielinski *et al.*, 1997).

Jørgensen (1980) mapped the spatial distribution of the ignimbrite. The main outcrops are almost enclosed by three ice-capped, active central volcanoes, Eyjafjalljökull to the south, Katla to the east, Tindfjalljökull to the north. Torfajökull, is located further to the NE and Hekla is further north beyond Tindfjalljökull (Fig. 1.10). The best exposures are located on a 4-5 km stretch along the northern border of the Krossa river (Fig. 1.10-c: sites 3, 5, 7, 8, 15, 16; Fig. 4.3-b to f.). In this area the visible thickness of the ignimbrite is about 30 m (Thórarinsson, 1969). Sections to the north of these are

generally between 10-50 m thick although some profiles are up to 200 m thick (Jørgensen, 1980; Fig. 1.10-c: sites 11, 12, 13, 14, 21, 22, 23; Fig 4.3-g, h, o). Less substantial deposits are located to the south of the Krossa (Jørgensen, 1980; Fig. 1.10-c: sites 1, 2, 6, 19, 20; Fig. 4.3-a). Most of the ignimbrite sections in the main Þörsmórk area are heavily eroded, having been exposed by glacio-fluvial action along the Krossa and Markarfljot valley floors (Fig. 1.10-c; Fig. 4.3-b). Thórarinsson (1969) and Jørgensen (1980) were not able to find a basal contact and, at most sites, only slope deposits are accessible.

1.5.2 Geology

(a) Active volcanism in Southern Iceland

Post-glacial volcanism in Iceland is concentrated in four separate areas (Fig. 1.3). Glacial activity in the EVZ is concentrated on the five main central volcanoes, Eyjafjalljökull, Katla, Hekla, Tindfjalljökull and Torfajökull (Fig. 1.10-b). The EVZ is a highly active volcanic region and most of the highly explosive Holocene eruptions have been linked to silicic magma sources in the area (Larsen, 2000; Larsen *et al.*, 2001).

Regional volcanism is characterised by the transition from high Fe-Ti tholeiites to alkaline basalts (Jakobsson, 1979). The five silicic centres listed above show contrasting geochemical trends, from the almost calc-alkaline Hekla centre to the slightly peralkaline Torfajökull centre (McGarvie *et al.*, 1984). Most of the basaltic ash layers in the Þórsmörk region can be traced to the Hekla and Katla centres. Twenty-five silicic tephra layers of Holocene age have been linked to eruptions from Hekla (Thórarinsson and Sæmundsson, 1979; Larsen, 2000). Tephra from the Hekla-3, -4, -5 eruptions has the widest distribution forming thick layers across northern of Iceland (Boygle, 1998). A further 20 basaltic eruptions are known from the prehistoric, Holocene era. Katla is the source of numerous silicic tephra layers in the Holocene period (SILK layers: *e.g.* Newton, 1999; Larsen *et al.*, 2001). It is also thought to be the source of the Vedde Ash/Skógar Tephra, one of the largest and most widely dispersed (and most studied) highly silicic late Pleistocene eruptions from Iceland (Ruddiman and Glover, 1972; Mangerud *et al.*, 1984; Norðdahl and Haflidason, 1992; Zielinski *et al.*, 1997; Wastegård *et al.*, 2000a, b). The Vedde/Skógar eruption has been dated *ca.* 10.3 ^{14}C ka BP or 11.5 GRIP ice core ka and is the main component of North Atlantic Ash Zone 1 (NAAZ-1) (Björck *et al.*, 1992; Grönvold *et al.*, 1995; Birks *et al.*, 1996). Roberts (1997) and Bond *et al.*, (2001) have recently questioned whether the widespread distribution of the Vedde Ash across the North Atlantic region is the result of a single eruption.

Torfajökull is Iceland's largest active rhyolite volcano and possibly the most active rhyolitic volcano in the world with ten highly silicic (SiO_2>68 %) eruptions in the post-glacial period alone (McGarvie, 2000). The last eruption from Torfajökull was in *ca.* 1480 AD. Tindfjalljökull is the least active central volcano in this region. It is a 'highly differentiated central volcano rich in rhyolite and now

partly ice covered' Thórarinsson, (1969, p. 155[#]). It is classified as a dormant volcano because there have been several eruptions along the margins in post-glacial times (Thórarinsson, 1969; Thórarinsson and Sæmundsson, 1979; Jakobsson, 1979). It is dominated by slightly alkaline basalts and minor intermediate rocks and abundant sub-alkaline to slightly peralkaline rhyolites (Jakobsson, 1972; Imsland, 1978; Jakobsson, 1979; Sæmundsson, 1979; Jørgensen, 1980) and is thought to be the source of the Þörsmórk Ignimbrite.

(b) Ignimbrite forming eruptions & the characteristics of the Þörsmórk Ignimbrite

Ignimbrite[11] forming eruptions commonly have three stages of activity. A Plinian/pumice fall phase, a pyroclastic-flow phase (which produces ignimbrite and pyroclastic-surge deposits), and an effusive phase (Wright and Walker, 1981; Wright *et al.*, 1981a; Druitt, 1997) (Section 2.1.2; Fig. 2.1). The first two phases are often missing because of surging effects, the failure to form a sustainable high-altitude eruption column and/or post-eruption erosion (*e.g.* Francis *et al.*, 1983). Classically defined ignimbrite forming surges occur during the initial phase of eruption column collapse and are the result of tapping from deeper, less gas rich levels of the magma chamber (Cas and Wright, 1980). Vent radius, gas velocity and water content are, in that order, the most important controls on column collapse. Vent radius expansion during eruption is the most common trigger for the ignimbrite forming phase. Ignimbrite phases are often followed by co-ignimbrite breccia formation phase when less evolved eruption products are deposited by pyroclastic fall and less vigorous, but turbulent flow processes (section 2.1.2) (Jørgensen, 1980). Further details of ignimbrite forming eruptions and their products can be found in Cas and Wright (1980), Sparks *et al.* (1997) and Freundt *et al.* (2000)

Thórarinsson (1969) suggested that the Þörsmórk Ignimbrite originated from Tindfjalljökull. The summit of the volcano is thought to be a collapse caldera connected with the formation of the Þörsmórk Ignimbrite (Jørgensen, 1987). There is no evidence for a Plinian phase of activity. This might be because the base of the deposit is not visible in any of the localities visited by Thórarinsson (1969) and Jørgensen (1980; 1981). All the structural and depositional features of the ignimbrite preserved in and around Þörsmórk are associated with emplacement from pyroclastic flows or surges (Jørgensen, 1980; 1981). These were probably explosively generated, created by instabilities in the lower parts of the eruption column (Sparks *et al.*, 1997). The deposit would have mantled the existing topography and been concentrated in valley troughs and sides. Given an average thickness of 20-25 m Thórarinsson (1969) calculated that the volume of the ignimbrite in the Þörsmórk region is 1.5-2.0 km^3. At least 2-3 km^3 of freshly fallen tephra was probably dispersed over a wider area. The eruption is, therefore, the same order of magnitude as those that formed the Tertiary ignimbrites of East Iceland (Walker, 1962) and the thickest rhyolitic tephra layers of the post-glacial and historical era, such as Hekla 3, Hekla 4, Öræfi 1362 AD (Jørgensen, 1980; Larsen *et al.*, 1999).

[#] Cited and translated in Jørgensen (1981)
[11] See Appendix A for definitions

Thórarinsson (1969; p.155[#]) described the deposit east of Tröllabúdir (ÞIG 5: Fig. 4.3-d) in the following manner: 'The upper part of the deposit is a non-welded mixture of greyish ash, light and black pumice. The hybrid character of the layer is the result of a simultaneous eruption of two types of magma. The main part is, however, rhyolitic. The non-welded layer gradually emerges downwards into a typically welded layer which is also mixed'. Jørgensen (1981) noted that deposits of similar composition are relatively uncommon in Iceland and that the degree of welding increases significantly towards the NW (Jørgensen, 1980; 1980; Fig. 1.10-c). Jørgensen (1981, 1987) examined the petrology of the ignimbrite in detail. He described it as a large, extrusive, peralkaline body and classified it petrologically as a comendite with a basic component. The different glass compositions indicate that the main rhyolitic body was formed through fractional crystallisation of a rhyo-dacitic parent magma.

1.5.3 Þörsmórk Ignimbrite: eruption age

Thórarinsson (1969) initially assigned the eruption an age of about 200 ka, placing it in the penultimate interglacial ('Mindel-Riss' - Jørgensen, 1980, *i.e.* Saalian-Drenthe, oxygen isotope stage 7). Jørgensen (1981) agreed with this assessment citing as supporting evidence the ignimbrite's presence in stratigraphic sections of neighbouring silicic centres that had been dated by radiometric methods to about that age.

The recent consensus is, however, that the Þörsmórk Ignimbrite is a highly silicic terrestrial component of North Atlantic Ash Zone 2 (NAAZ-2) and, therefore, significantly younger than the age estimate of Thórarinsson (1969) and Jørgensen (1980). Although originally dated to around 64 ka (Ruddiman and Glover 1972), several recent assessments have produced ages ranging between 48.5-58 ka for NAAZ-2 (Appendix C: Table C2.1). These have been obtained by correlating the chemical composition of the terrestrial glass to tephra layers with similar major element chemistry in marine and ice cores from the North Atlantic region and Greenland, respectively. Ages were obtained by comparison to astronomically calibrated $\delta^{18}O$ time scale of the marine record and the incremental, sidereal, time scale of the ice core record (Sigurdsson, 1982; Lacasse *et al.*, 1995; 1996; Ram *et al*, 1996; Zielinski *et al.*, 1997). Zielinski *et al.* (1997) suggested that the widespread distribution of NAAZ-2 in marine cores is most likely due to ice rafting because, as outlined above, Thórarinsson (1969) and Jørgensen (1980) found no field evidence for an initial Plinian eruption phase.

The eruption that formed the Þörsmórk Ignimbrite is thought to have been a single event. It may have been triggered by a regional tectonic event that caused basic lava to be injected into the silicic magma chamber of the Tindfjalljökull volcanic complex (Jørgensen, 1987; Lacasse *et al.*, 1996). It is interesting to note, however, that two distinct tephra deposits, with similar chemical composition to NAAZ-2 and the Þörsmórk Ignimbrite, have been found in the GRIP and GISP2 Greenland ice cores at 53.5 ka and 55 ka (Ram and Gayley, 1991; Ram *et al.*, 1996; Zielinski *et al.*, 1997). Furthermore, Zielinski *et al.* (1997) suggested that NAAZ-2 was the result of two simultaneous eruptions. Katla and

Torfajökull were put forward as the most likely alternative source volcanoes to Tindfjalljökull (Zielinski *et al.* 1997).

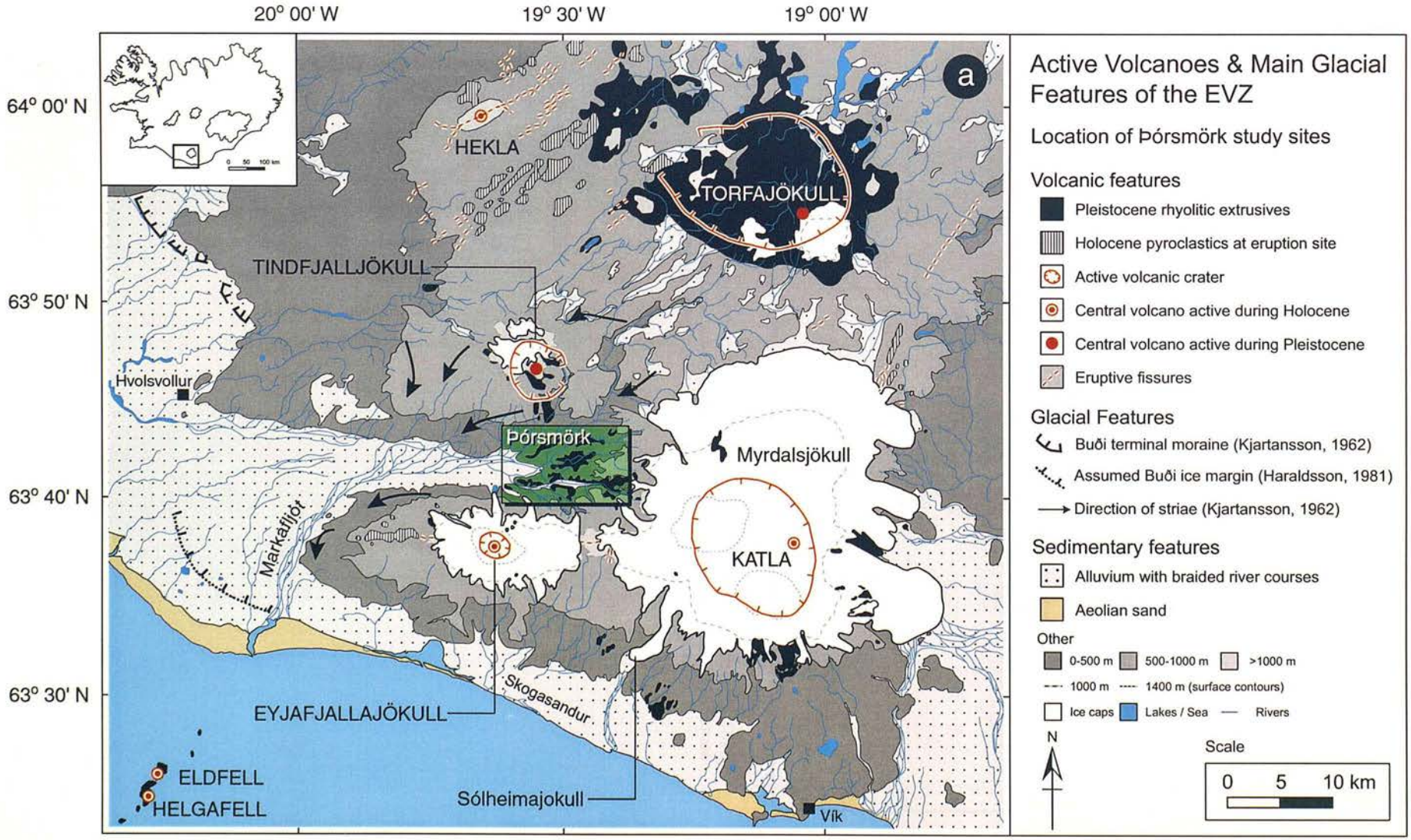


Figure 1.10 (a) Active volcanoes, pyroclastic and extrusive deposits and main glacial features of the Eastern Volcanic Zone (EVZ). Based on the 1:250,000 Geological Map no. 6 of the Iceland Geodetic Survey. The underlying geology of area covered by the Þórsmörk box is all described as 'basic and intermediate hyaloclastites and tuffaceous sediment younger than 0.7 Ma' (*contd. overpage*).

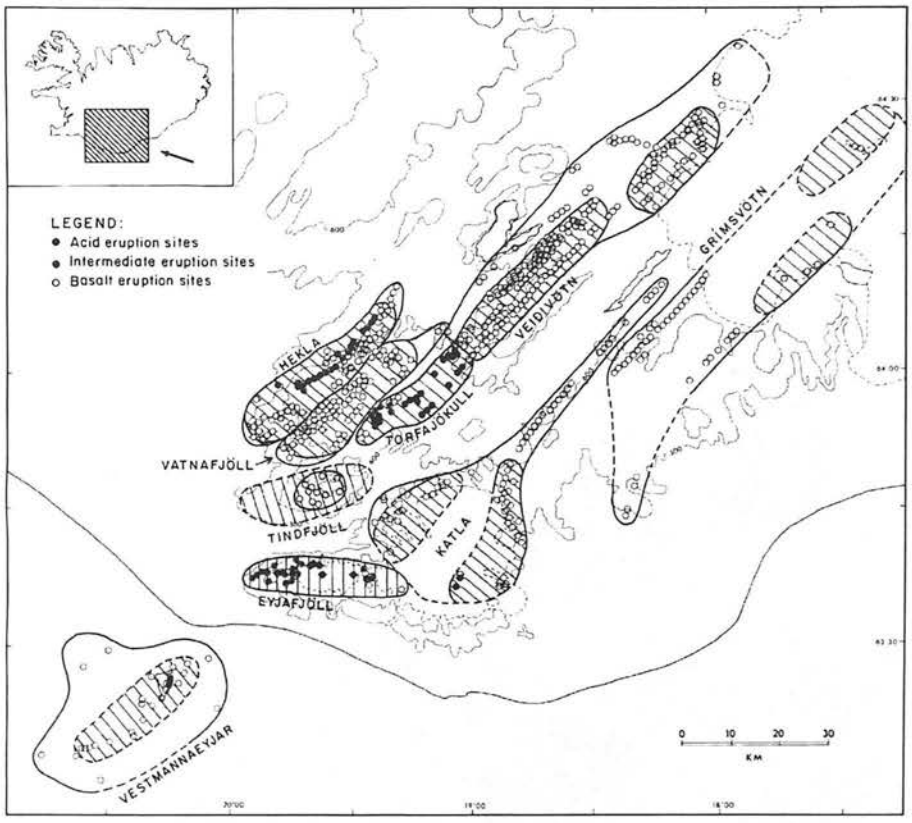


Figure 1.10 (b) The nine volcanic systems of the EVZ (from Jakobsson, 1979). Circles = known postglacial eruption sites; circles with a horizontal bar are approximate eruption sites; diagonal lines = intensely active centres; (*contd. overpage*).

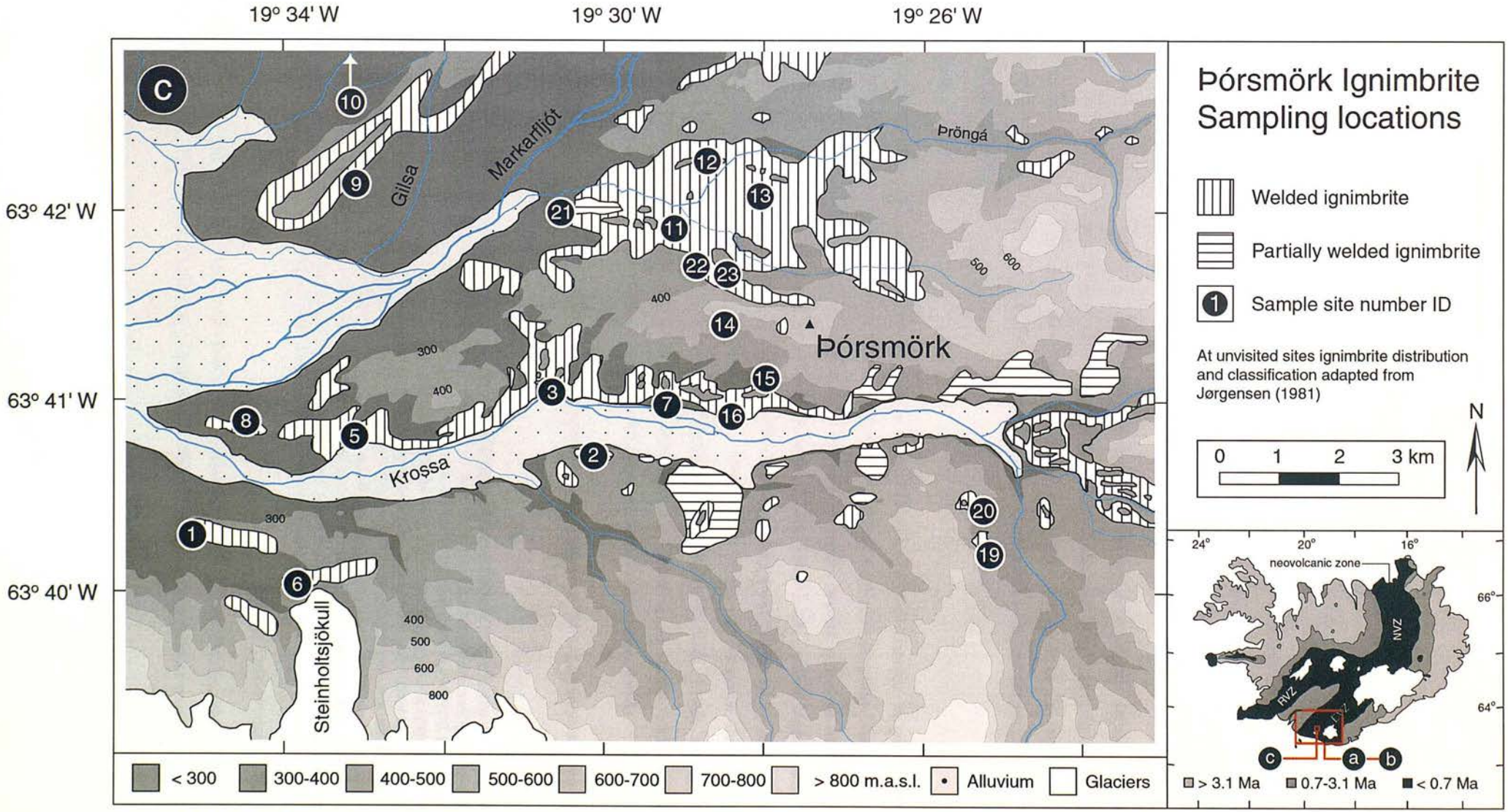


Figure 1.10 (c) Classification of the Þórsmörk Ignimbrite (after Jørgensen, 1980, 1981) with July-August 1998-1999 sampling locations shown

1.6 Holocene Age Control Eruptions

1.6.1 Öræfajökull 1362 AD, SE Iceland

(a) Geographic location

Öræfajökull, at 2119 m, is Iceland's highest peak and also its most active composite stratovolcano during the post-glacial period. It is located to the east of the EVZ on the southern margins of the Vatnajökull ice cap in an intra-plate setting (Fig. 1.3; Larsen *et al.*, 1999).

(b) Geology

The snow-capped volcanic edifice is constructed principally of sub-aerial basalt and andesite lavas and partially of sub-glacial pillow lavas and hyaloclastites. Overall, the rock suite has been classified as calc-alkaline. Reversed magnetic rocks have been found at its base, but most of the structure is normally magnetised indicating an age of < 0.7 Ma. A small caldera exists near the summit, *ca.* 1850 m.a.s.l. (Prestvik, 1979).

(c) Tephra

Historically, there have been two silicic eruptions in 1362 AD and 1727 AD (Larsen *et al.*, 1999). The 1362 AD event took place mainly in the caldera. It was a purely explosive eruption producing > 10 km^3 of freshly fallen tephra and is the second most voluminous tephra deposit in Iceland in historic times after the basaltic Veiðivötn eruption of 1477 (Larsen, 2000). Only 2 km^3 of this highly silicic (>70%) tephra fell on land with prevailing westerly winds transporting most of the ejecta across the North Atlantic (Pilcher *et al.*, 1995; Larsen *et al.*, 1999). The 1362 AD eruption event was accompanied by two massive jökulhlaups from Falljökull and Rótarfjallsjökull. These styles of volcanism reflect a long, 500-year repose period. Today, tephra isopachs up to 10 cm thick can be found in soils covering a 4300 km^2 area surrounding the main edifice (Thórarinsson, 1958).

A detailed description of the Ö1362 eruption can be found in the annals from See of Skáholt written in the monastery at Modruvellir in North Iceland:

'[The] Volcanic eruption in three places in the South kept burning from Flitting Days [early June] until the autumn with such a monstrous fury as to lay waste the whole of the Litlahérað as well as a great deal of Hornafjörður and Lónshverfi districts causing desolation for a distance of some 100 miles. At the same time there was a glacier burst from Knappafellsjökull into the sea carrying such quantities of rocks, gravel and sand as to form a sandur plain where there had previously been 30 fathoms of water. Two parishes, those of Hof and Rauðilækur were entirely wiped out. On even ground one sank in the sand [pumice and ash] up to the middle of the legs and winds swept it into such drifts that buildings were almost obliterated. Ash was carried over the northern country to such a degree that footprints became visible in it. As an accompaniment to this, pumice was seen floating off the North-West Iceland (Vestfirðir) in such masses that ships could hardly make their way through it.'

(cited in Thórarinsson, 1980)

The scale and impact of the eruption is clearly demonstrated by this quote. Further, the name of farmstead directly below the volcano was changed from Hérað, meaning important or extensive rural

settlement to Öræfi, meaning 'wasteland'. In addition, this quote illustrates the accuracy and detail to which eruption events, plume directions, tephra deposition and the after effects of an eruption are recorded in Icelandic historical records.

1.6.2 Ódáðahraun-Askja (Dyngjufjöll), N. Iceland & Askja 1875 AD eruption

(a) Geographic location

The fissure system of the Dyngjufjöll is located approximately 100 km N of Vatnajökull in the Eastern Highlands of the tholeiitic Northern Volcanic Zone (NVZ) of Iceland (Fig. 1.3). The volcanic complex covers *ca.* 400 km^2 (Fig. 4.4). Askja, the main caldera and central volcano, covers an area of *ca.* 45 km^2. It is bounded in the south and east by precipitous cliffs and, to the north and west, by cliffs that cut through the lavas that cover the bottom of the caldera.

(b) Geology

Pleistocene rocks of uncertain age and predominantly basaltic composition form the basement rock type in the Askja crater (NVI, 2000). Post-glacial lavas contain several rhyolitic ash layers, the oldest of which has been dated to *ca.* 9800 BP. Between 9800-4500 BP, during glacial unloading of the area, volcanic productivity was 30 times greater than anytime since (Sigurdsson and Sparks, 1981). A melting anomaly caused by changes in pressure exerted by the loading and unloading of up to 2000 m of ice has been suggested as an explanation (Sigvaldason *et al.*, 1992). Caldera collapse dates back before the Hekla-4 eruption *ca.* 4500 BP (NVI, 2000), although significant and rapid subsidence was noted in SW corner of the caldera following the 1875 eruption. This led to the formation of Öskjuvatn in the years following the 1875 eruptions (Sigurdsson and Sparks, 1981). This lake filled gradually between 1875-1907 rising from 150m below the caldera floor to its current level of 50 m below (MacDonald *et al.*, 1987). Today a circular crater-like depression with a maximum depth of 224 m exists. The secondary phreatic explosion crater Víti is located on north-east crater rim. It was formed at the end of the Plinian phase of the 1875 eruption.

(c) A1875 Eruption: Tephra production & Dispersal

The last Plinian eruption in the Dyngjufjöll volcano took place from within the Askja caldera a few hours before 8 a.m. on 29th March 1875 and lasted about 6-7 hours (NVI, 2000). This eruption is a classic example of how tephra can be rapidly distributed over long distances across the North Atlantic and northern Europe (Einarsson, 1986; Fig. 1.11). The explosive phase of the eruption produced large volumes of fine-grained, grey-white, non-vesicular, rhyolitic tephra. The ash cloud was dispersed across eastern Iceland by strong westerly winds forming visible layers 20-30 cm thick for up to 50 km away during the eruption (Thórarinsson, 1963; Kayhko, 2000). Tephra fall was noted at Seydisfjordur, 80 km away on the east coast of Iceland, at 8 a.m., along the west coast of Norway (*ca.* 1100 km) at 7 p.m. that evening and in Stockholm (1900 km) at 11 a.m. the following morning (Mohn, 1877). Visible layers up to 1 cm thick are still visible in soil profiles up to 70-80 km E-NE of Askja. Microtephra layers, invisible to the naked eye, but with distinct eruption-related shard count peaks,

have been identified in Scandinavia (Sigurdsson and Sparks, 1981; Bergman, *pers. comm.*). The eruption produced 1.8 km^3 or 0.43 km^3 solid rock equivalent (SRE) of ash out of 0.89km^3 SRE of eruptive material (NVI, 2000).

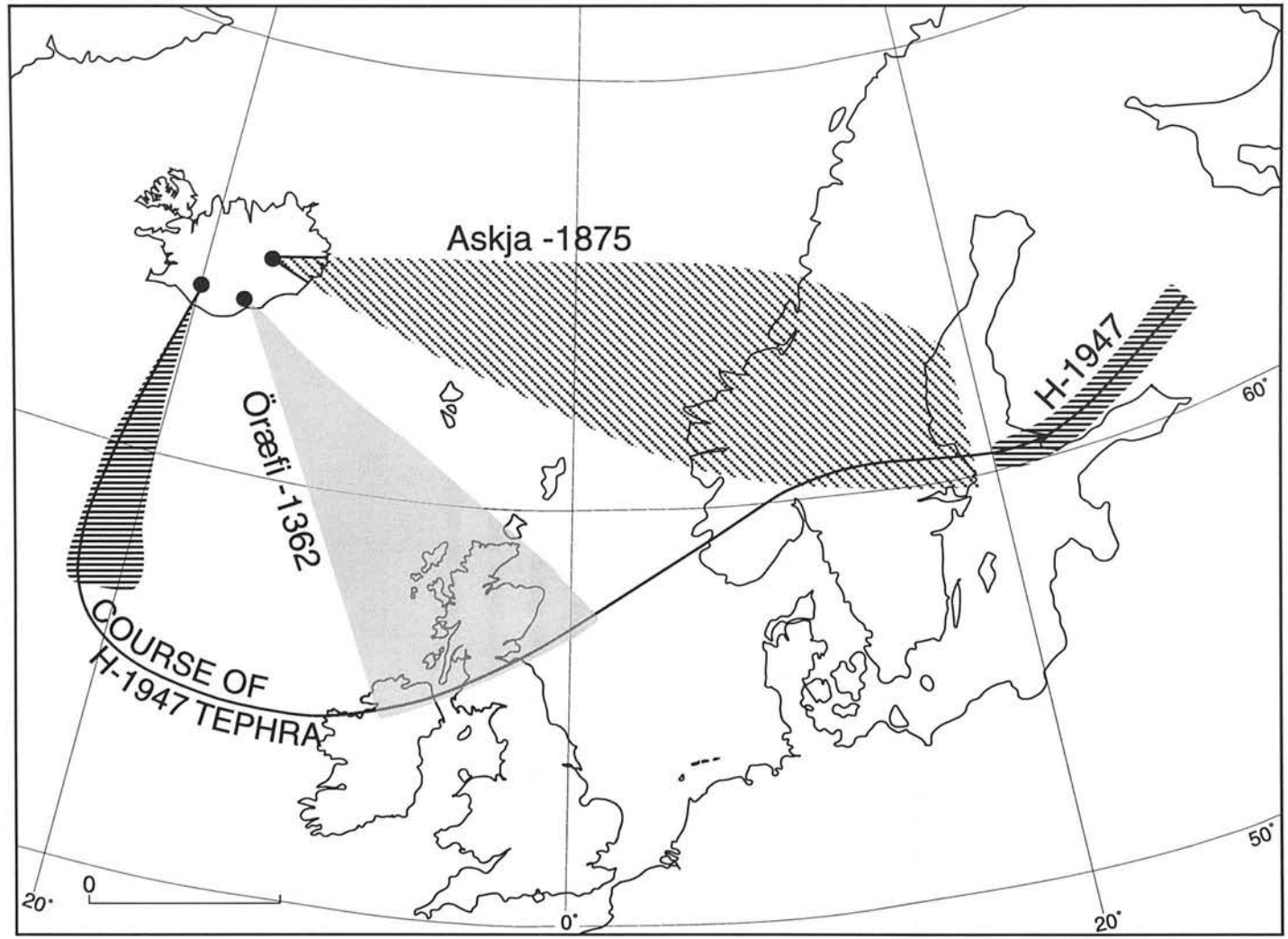


Figure 1.11 Eruption plume dispersal maps for the Öræfi 1362 AD, Askja 1875 AD and the Hekla 1947 AD eruptions. The Hekla 1947 eruption is discussed further in Chapter 2 (modified from Larsen *et al.*, 1999).

Chapter 1 **Summary**

- Icelandic tephrochronology can make further valuable contributions to studies of Quaternary climate change by providing a means to:
    1. Date and evaluate the significance of terrestrial records of glaciation and environmental change in Iceland that lie beyond the radiocarbon limit of *ca.* 50 ka.
    2. Develop further innovative/new applications of thermoluminescence and fission-track dating by taking advantage of the glass-rich, phenocryst poor nature of Icelandic tephra deposits.

- The primary aim of this thesis is to establish the age of the Óþoli Tephra, Skagafjall, Vestfírðir Peninsula, Iceland.

- A secondary aim is to obtain glass-phase ages for the Þörsmórk Ignimbrite, southern Iceland and assess the implications of ages for recent eruption theories.

- Existing and new correlation ages from the Þörsmórk Ignimbrite and historical document ages of the Ö1362 & A1875 are used as 'correlation-age' and 'near zero-age' control samples, respectively, for direct dating experiments on the Óþoli Tephra and the Þörsmórk Ignimbrite.

- Many of the elevated plateaux of the Vestfírðir Highlands could have remained ice-free at the Last Glacial Maximum. The palaeoenvironmental significance of the ice-dammed lake deposits of Skagafjall is to be examined by multi-method dating the Óþoli Tephra. Fieldwork was concentrated on this region. NW-SE trending plateaux areas similar to Skagafjall were examined for sedimentary sequences that might contain tephra deposits.

Chapter 2
Tephrochronology: Context & Approach

This chapter examines the principles of tephrochronology with particular reference to Icelandic tephra studies (Sections 2.1). Section 2.2 examines the strength and limitations of the Icelandic tephra record, and its uses, concentrating in particular on recent exciting developments in tephra studies and their application to palaeoenvironmental change studies in the North Atlantic region. Sections 2.3 and 2.4 evaluate the tephra-dating techniques most applicable to Icelandic tephra deposits in the pre-^{14}C era. Section 2.5 illustrates how pre-^{14}C era tephrochronological studies in other volcanic regions have had a dramatic influence on studies of palaeoenvironmental change using North America and New Zealand as case studies.

2.1 Principles of tephrochronology

2.1.1 Historical development & definitions

Although modern tephra studies are commonly thought to have begun during the inter-war period of the twentieth century, their ancestry can be traced back much further in history (*e.g.* Mohn, 1877; Connell, 1846). In the mid-1940s, after extensive archaeological field-studies in Iceland, Thórarinsson (1944) introduced the term tephra to modern science.

'I also wanted a term in linguistic harmony with magma and lava. In classical Greek there are two words for [volcanic] ash: connis and tephra [τεφρα]. I chose tephra partly because it fitted phonetically with lava and magma and partly because I found that Aristotle had used the word for volcanic ash in his work Meteorologica in an account of an eruption on the island of Hiera, one of the Lipari Islands. That account is ... the oldest description of a tephra fall and transport in European literature'

Thórarinsson (1944; cited in Thórarinsson, 1980; p.19)

Thórarinsson later defined tephra as a non-genetic, collective term for unconsolidated accumulations of airborne pyroclasts of any size and chemical composition (Thórarinsson, 1974). This definition of tephra is used throughout this thesis. It is synonymous with the term 'pyroclastic material' that describes all pyroclastic air-fall and flow deposits, ignimbrites, welded and non-welded tuffs, scoria, blocks and bombs (>64 mm), lapilli (2-64 mm), pumice and volcanic ash (<2 mm) (Fig. 2.1; Appendix A1) (Thórarinsson, 1944; 1974; Le Maitre, 1976; Whitten and Brooks, 1972; Schmid, 1981; Fisher and Schmincke, 1982; Le Bas *et al.*, 1986; Le Maitre *et al.*, 1989). Volcanic and igneous terms used in this thesis follow the IUGS classification system of Le Bas *et al.* (1986). Stratigraphic terms and diagnostic characteristics are as defined in Cas and Wright (1987: Appendix II, p. 479-485). Further definitions and detailed descriptions of the products and styles of explosive volcanism can be found in Le Maitre (1976), Wright *et al.* (1981a, b), Sparks *et al.* (1997).

Thórarinsson (1944) also introduced the term tephrochronology defining it as 'a dating method based on the identification, correlation and dating of tephra layers'. He developed the first tephrochronological system based on historical[12] ash layers in Iceland and described the underlying principles upon which it is based (Table 2.2-a) (Thórarinsson, 1967; 1974; 1981; Thórarinsson and Sæmundsson, 1979). These principles have been applied to numerous tephra studies around the world. Compilations of global examples can be found in Westgate *et al.* (1992), Sarna-Wojcicki (2000), Shane (2000), Hallet *et al.* (2001, p. 284) and, for Icelandic tephra studies, Haflidason *et al.*. (2000) (Appendix C: Table C2.1).

[12] Historical tephra deposits in Iceland are those deposited after Landnám (Settlement) tephra, so called because it coincides with the arrival of the Norse settlers or *landnámsöld*, conventionally put between A. D. 870-930 (1994; Dugmore *et al.*, 2000).

2.1.2 Tephra production, transport & deposition

The largest volume of tephra is produced during the initial phase of an explosive volcanic eruption (Larsen *et al.*, 2001). Immediately after an eruption, tephra deposits blanket the surrounding area in a layer of ash several centimetres thick. These layers thin out along the principal axis of plume transport. Macroscopic tephra layers have been found up to 600 km from the source volcano, sometimes in directions that are perpendicular to the prevailing wind direction (Kohn, 1979; Eden and Froggatt, 1988). Such long-range or 'distal' layers are the products of the most intense and large magnitude eruptions (Shane, 2000).

Silicic-tephra producing Plinian eruptions are far less frequent than the various styles of basaltic-tephra producing eruptions. During the Plinian phase, high altitude eruption plumes are formed and tephra is distributed over a wide area in a short space of time (Thórarinsson, 1963; Sparks *et al.*, 1997; Larsen *et al.*, 1999). Compositional changes in the magma chamber as the eruption progresses can create different regional dispersal patterns for progressively silica-depleted tephra from the same eruption event. The chemical composition of silicic glass shards in particular is often diagnostic, allowing eruption sources, and sometimes individual eruptions to be differentiated. This makes silicic, and more specifically, highly silicic (SiO_2 > 68 %) tephra layers particularly valuable marker horizons. Usually, most of the silicic tephra is produced and ejected during the early phases of the eruption (Sarna-Wojcicki, 2000; Table C2.1 for Icelandic examples).

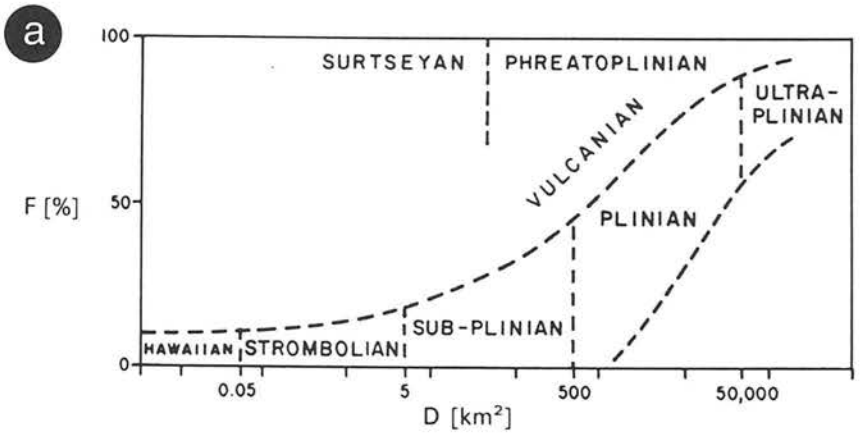
Uniform blankets of tephra are not found in all areas beneath the passage of the plume. Several factors determine where the largest volumes of tephra will be deposited. The explosivity of the eruption, prevailing wind speed and direction, settling characteristics and interactions of tephra grains within the eruption plume are initially important, but changes in post-eruption atmospheric and meteorological conditions soon become more influential (Sparks *et al.*, 1997). Although rapid changes in wind direction are common in Iceland, silicic tephra from the Plinian phase is normally carried in one direction (Fig. 2.2). This forms a sector of tephra, which is relatively narrow close to the source volcano, but fans out with distance (Thórarinsson, 1967; Sigurdsson and Sparks, 1978). Tephra from the major historic and Holocene eruptions deposited tephra across parts of Iceland and the North Atlantic that coincide with the contemporaneous wind directions (Larsen and Thórarinsson, 1977; Kirkbride and Dugmore, 2001) (Fig. 2.2-c).

When eruptions last several days, changes in wind direction can disperse tephra widely. In NW Europe, for example, the deposition of tephra after the eruption of Hekla in 1947 AD did not simply coincide with areas that experienced heavy post-eruption precipitation (Dugmore and McCulloch, *submitted*). Instead, after initial injection to 20-30 km into the upper atmosphere and some localised deposition in parts of south Iceland, the tephra plume fell to an altitude of 10 km (500 mBar) and drifted first south into the North Atlantic and then east across mainland Europe. No known fallout


EX BIBL. UNIV. EDINBURGH

exists from the plume until it reached Finland. Over areas of Finland, the eruption plume coincided with occluding frontal systems that extended upwards into the eruption plume at 5-10 km, promoting tephra deposition. This is an extreme example of 'secondary thickening' within the plume, also noted with the plume passage and fallout from the 1980 eruption of Mount St. Helens.

Primary air-fall deposits can be concentrated into thicker layers by post-depositional geomorphic, fluvial and lacustrine processes. For example, the Saksunarvatn Ash is a black tephra deposit thought to be the product of an eruption from Grimsvötn system beneath Vatnajökull *ca.* 9000 ^{14}C BP (Mangerud *et al*, 1986). It is named after a lake in the Faroe Islands where a 45cm thick deposit of reworked tephra that had been concentrated by lacustrine processes was first described and dated (Jóhansen, 1975; Mangerud *et al.*, 1984). Airfall tephra layers in the surrounding peat deposits are only 0.5-1cm thick.



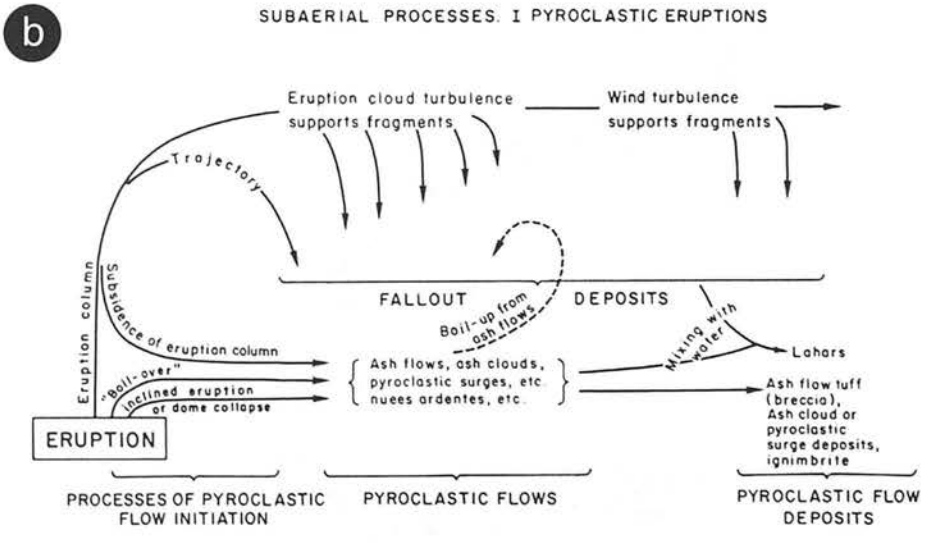


Figure 2.1 (a) Classification of pyroclastic fall deposits of Walker (1973). The terms Phreatoplinian were added by Self and Sparks (1978) and Ultraplinian by Walker (1980). F % is the weight percent of tephra <1 mm where it is crossed by an isopach line which is 10% of the maximum thickness (0.1 T_{max}); D is the area enclosed by the 0.1 T_{max} line (after Wright *et al.*, 1980; from Fisher and Schmincke, 1984). **(b)** Summary of the processes by which subaerial pyroclastic flow and fallout deposits originate (from Fisher and Schmincke, 1984).

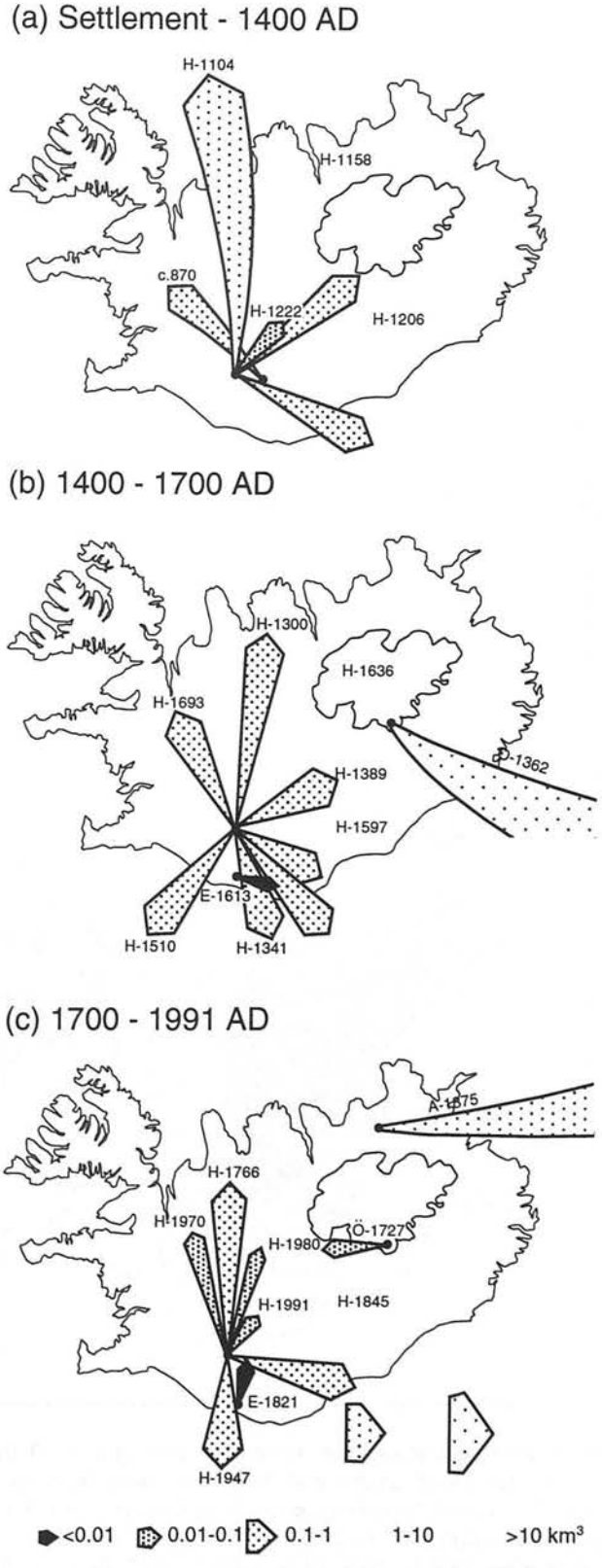
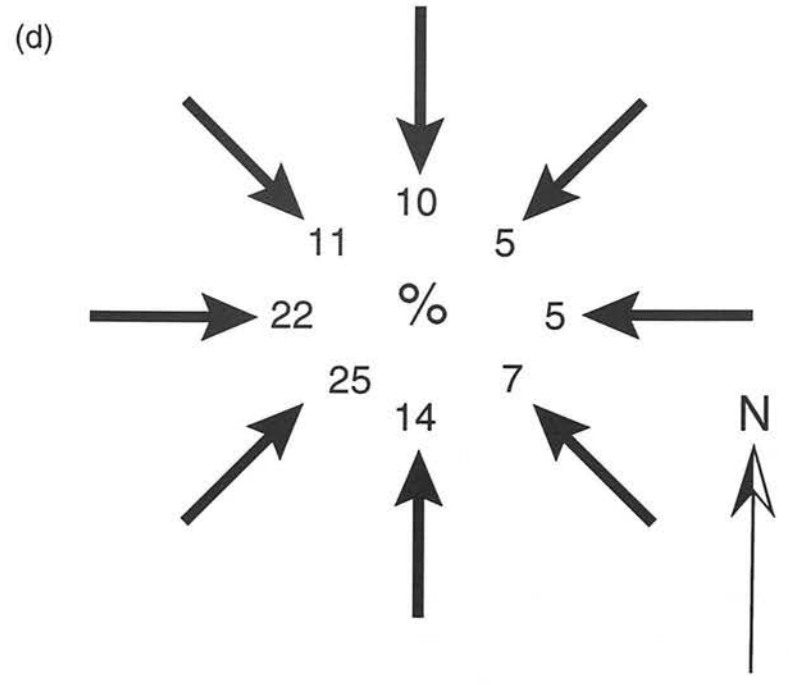


Figure 2.2 (a)-(c) Dispersal plume directions of selected Settlement to present day Icelandic eruptions. Note the narrow nature and the predominantly northerly and easterly direction of initial plume transport (from Larsen *et al.*, 1999; *contd.*)



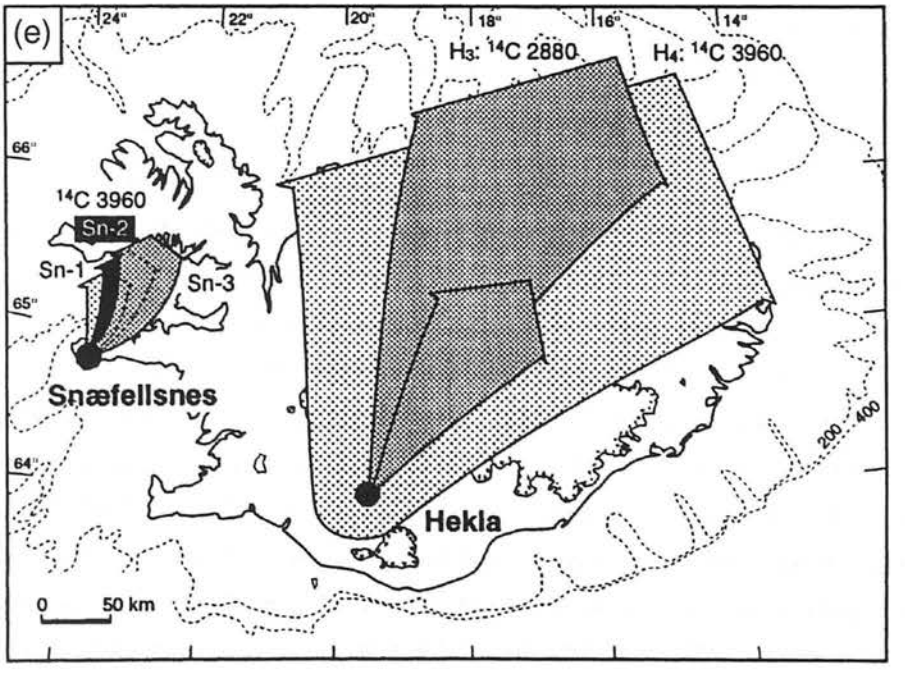


Figure 2.2 (d) Prevailing wind directions in present-day Iceland expressed as percentages (adapted from Donn and Ninkovitch, 1980) **(e)** The main axis of distribution for the mid-Holocene silicic eruptions of Hekla-3 (H3) and Hekla-4 (H4) (Larsen and Thórarinsson, 1977). The Snæfellesnes eruption Sn-1 (1750±150 BP), Sn-2 (3690±100 BP) and Sn-3 (ca. 7-9 ka were at least an order of magnitude smaller than the Hekla eruptions (Jóhannesson *et al.*, 1981). The direction of the main axis of tephra distribution was similar to the Hekla eruptions, but the position of Snæfellsnes directly south of the Western Troughs of Vestfirðir led to the deposition of Sn-1, 2, 3 in Holocene age soils. A tephra deposit with geochemical characteristics of the Snæfellesnes Volcanic Zone was found in Holocene age soils in Ingaldsandur (see p. 6 of Table C1.1 for details).

2.2 The Icelandic Tephra Record: Strengths, Uses & Limitations

Iceland is one of the most geologically active oceanic islands in the world. There are thirty-two active or dormant volcanic systems. These are elongate, *en-echelon* features that often produce bi-modal and/or chemically diagnostic eruptions products (Jakobsson, 1979; Furman *et al.*, 1995; Figs. 2.3 & 2.4). The recent compilation by Haflidason *et al.* (2000) of mid-late Pleistocene tephra deposits of Icelandic origin in the North Atlantic region demonstrates the high resolution of the Icelandic tephra record in the 15-0 ka era (Fig. 2.5). A significant proportion of this valuable volcanological and chronological resource was constructed in the last two decades.

2.2.1 Strengths & Uses of the Icelandic Tephra Record

During the historical period (*ca.* 1100-0 ka) in Iceland there have been 250-300 eruptions, one, on average, every four years (Gudmunðsson, A. T., 1996; Larsen, 2000). Over 200 of these have been confirmed by chemical analysis of tephra layers or lava flows and/or historical records (Larsen, 2000). Over 75 % have produced a visible tephra layer on the Icelandic mainland. Tephra is the only product of over 130 of these eruptions (Larsen *et al.*, 2001). Hence, some tephra deposits in Iceland of Holocene age do not necessarily need the application of multiple dating methods to achieve accurate age constraint suggested by the quote at the start of this chapter. Holocene and late-glacial tephra layers are particularly powerful dating tools for archaeology, studies of natural, and anthroprogenic palaeoenvironmental change, within Iceland (Dugmore and Maizels, 1985; Hallsdóttir, 1987; Dugmore, 1989; Dugmore and Sugden, 1991; Haflidason *et al.*, 1996, 1998; Dugmore *et al.*, 2000). The main reasons for this are:

(a) Distribution & documentation

Over the last fifty years, the stratigraphical position and geochemical identity of numerous Icelandic tephra layers has been well documented (Thórarinsson, 1958, 1963, 1967, 1974; Björck *et al.*, 1992; Haflidason *et al.*, 2000). Detailed isopach maps, showing the distribution of tephra layers of similar thickness, have been constructed for most historical eruptions and for the major pre-historical eruptions of the Holocene era (*e.g.* Haflidason *et al.*, 2000; Larsen *et al.*, 2001). Twelve widely dispersed highly silicic eruptions are of particular value to tephrochronological studies in the post-glacial era, < *ca.* 9300 ^{14}C ka BP (Larsen *et al.*, 1999). They are more diagnostic than the products of non-explosive/effusive and/or basic eruptions and have been used to link palaeoenvironmental archives from the northern North Atlantic, the Nordic Seas and the surrounding terrestrial environments *e.g.* Mangerud *et al.*, (1984), Wastegård *et al.*, (2000a, b; 2001), Turney *et al.* (2001). Numerous black, basaltic and olive-green dacitic tephra layers have been found in Holocene sequences around the main central volcanoes (see *e.g.* Larsen *et al.*, 2001: Fig. 2, p. 121). Away from these areas their distribution is more restricted although some deposits associated with explosive hydromagmatic or latter and more evolved phases of Plinian eruptions have been found in terrestrial

regions of the circum North Atlantic (*e.g.* Mangerud *et al.*, 1986; Dugmore *et al.*, 1996; Davies *et al.*, 2001).

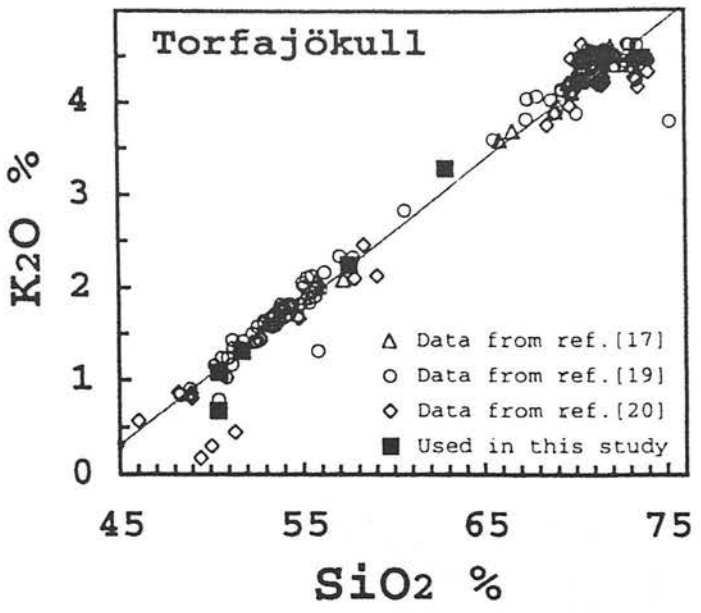


Figure 2.3 Bi-modal composition of Toarfajokull. Intermediate compositions are almost completely absent despite over 200 analyses (from Stecher *et al.*, 1999).

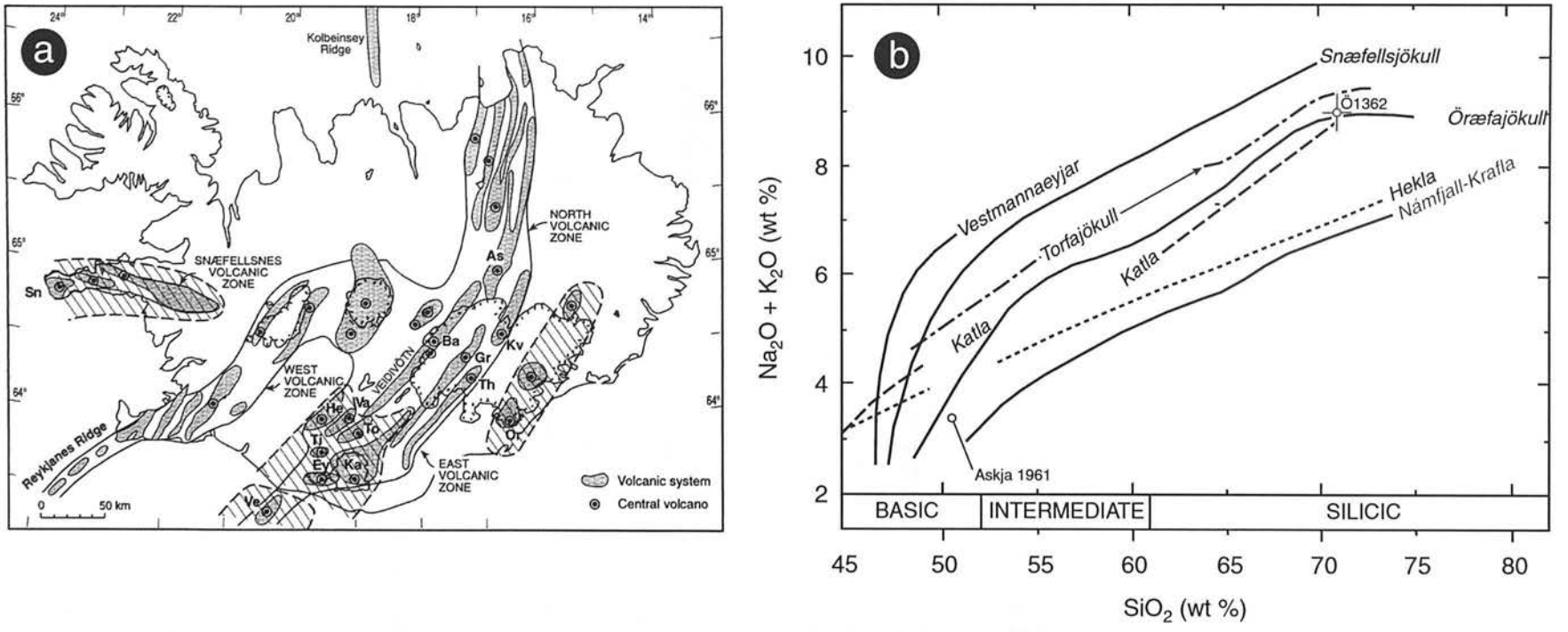


Figure 2.4 (a) The 32 distinct volcanic systems (shaded grey)in the neovolcanic zone of Iceland (from Haflidason *et al.*, 2000). Volcanic systems beneath diagonal lines have alkali olivine basalt affnities. Others are defined as on-axial volcanic zones/central volcanoes and have a tholeiitic affinity. Petrological zones are as defined by Jakobsson (1972, 1979). Central volcanoes are shown as circles. A full list of active central volcanoes can be found in Figure 1.3 **(b)** Total alkali ($Na_2O + K_2O$) - silica (TAS) diagram showing the geochemical evolution trends of the most active Icelandic volcanic systems. Evolution trends are based on hard rock analyses from Jakobsson (1979) & Óskarsson *et al.* (1985) . Data for the Askja 1961 eruption is form Sparks *et al.* (1981). Additional data for Ö1362 (blue circle with 1σ error bars) is from Sigurdsson (1982). Data in (b) has been recalculated to 100% on a volatile-free basis.

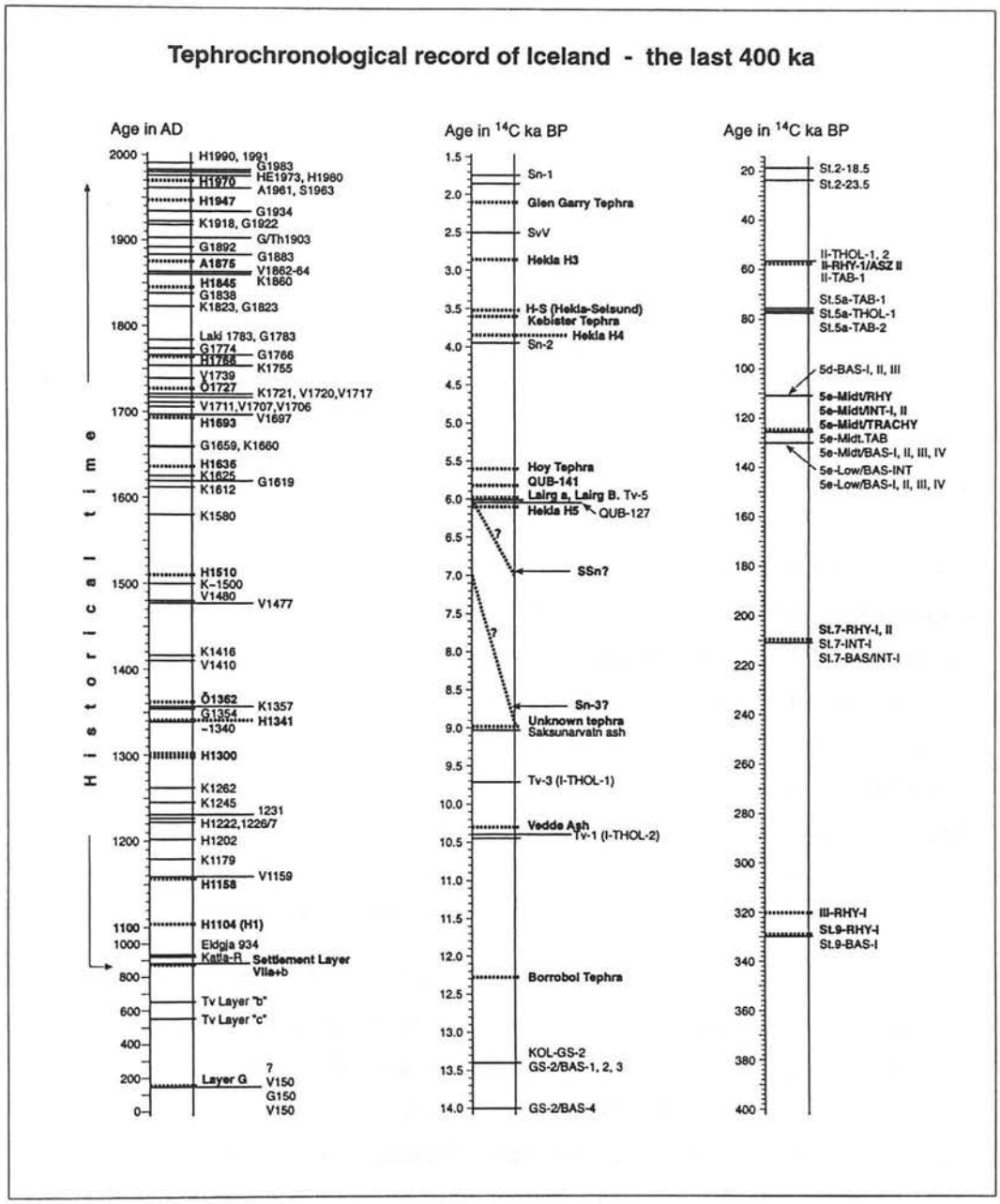


Figure 2.5 Summary diagram of the main features of the Icelandic tephra record for the last 400 ka (from Haflidason *et al.*, 2000). Dashed line = intermediate and silicic/rhyolitic layers; solid line = basaltic layers.

(b) Eruption age

Iceland's volcanic origins and position on the track of the major storm fronts that cross the North Atlantic creates high rates of aeolian-based sedimentation, soil production and peat accumulation that separate tephra layers. The high resolution sequences produced can be accurately radiocarbon dated and are instrumental in understanding mechanisms that control fluctuations in sediment supply and rapid environmental change in Iceland during the Holocene (Dugmore *et al.*, 2000). The timing of historical eruptions is well documented and often highly precise, sometimes to within an hour (Larsen *et al.*, 1999). An accurate and precise radiocarbon-based chronology has been constructed for many pre-historical eruption products (Pilcher *et al.*, 1995; Dugmore *et al.*, 1995a, b; Larsen *et al.*, 2001).

Attempts have been made to establish direct relationships between eruption events in Iceland and climatic change in the North Atlantic region and Europe (*e.g.* Blackford *et al.*, 1992; Lotter and Birks, 1993). Studies of this nature are often hampered by poor resolution of the dating techniques in the climate proxy records employed or by inherent delays in biological systems in response to climate change (Birks and Lotter, 1994; Caseldine *et al.*, 1999). For example, Eiríksson *et al.* (2000a) used the Hekla-3 tephra as a marker horizon to directly compare the timing of mid-Holocene climate changes in the ocean and terrestrial environment. A marked decline of birch forest and increased rates of soil erosion took place in Iceland after the Hekla 3 eruption and had previously been linked to the eruption. A gradual increase in the relative abundance of polar species of planktonic forminifera occurred prior to the eruption and coincided with an episode of glacier expansion in North Iceland 3700-3000 cal. years BP (Stötter *et al.*, 1999). Hence, they suggested that the post-Hekla-3 changes in the terrestrial environment were part of a more general cooling trend.

(c) Chemical characteristics of source volcanoes

The petrology and geochemical characteristics of the active volcanic systems in Iceland are well-defined, enabling source volcanoes to be identified (Fig. 2.4; Jakobsson, 1979; Sigurdsson and Sparks, 1978; Meier *et al.*, 1985; Larsen *et al.*, 2001). The possibility that major eruptions alter the geochemistry in some systems has been suggested. Larsen *et al.* (2001) showed that the twelve silicic tephra layers (SILK layers: SiO_2 = 63-67 %) from explosive dacitic subglacial eruptions of Katla (erupted between *ca.* 6600-1675 years BP) had a distinctive and stable geochemistry that is significantly different to the Plinian style eruption that produced highly silicic NAAZ-1 tephra and the highly effusive tenth century AD Eldgjá eruption.

(d) Ice-core / glacier records

Volcanic glass shards from eruptions produce elevated volcanic-sulphate levels in ice core records. Larger than average sulphate peaks in the Greenland ice cores are most commonly associated with Icelandic eruptions. Proxy records of volcanic eruptions in the last 110,000 year have been obtained from the GRIP and GISP2 Greenland ice cores. In addition, detailed 800 year records of tephra

deposition have been obtained from ice cores extracted from Vatnajökull (Zielinski *et al.*, 1996, 1997; Larsen *et al.*, 1998). Both types of record have been used to identify Holocene eruption events that are not recorded in the terrestrial record of Iceland. In addition, ice core records of this type provide calendar age estimates for Holocene and Lateglacial tephra deposits and allow the relationship between climate change and volcanic activity to be investigated at a previously unobtainable level of temporal resolution (Hammer, 1980; Grönvold *et al.*, 1995; Zielinski, 1995, 2000; Zielinski *et al.*, 1995, 1996, 1997). Zielinski (1995, p. 20,940) quotes dating errors as low as ± 0.5 % for the last 2100 years and ± 1% for the last 30,000 years. These are 'conservative' estimates, however, and incremental ice core ages have a general dating error of ± 2 %, *i.e.* ± 1000 years at 50 ka (Zielinski, *et al.*, 1994). Delayed and/or secondary deposition is not a significant problem for the summit cores (GRIP and GISP2) where the maximum time lag between eruption and deposition is up to only 2 years (Zielinski, 1995). Large age discrepancies have been noted in older sections of pre-^{14}C age between the summit cores and cores from SE Greenland, *e.g.* Dye-3 where ice-flow, basal shearing and breaks in the ice core stratigraphy have been identified (Ram and Gayley, 1991; Clausen *et al.*, 1997; Johnsen *et al.*, 2001). For example, an erosional unconformity separates two ash-rich aggregate layers associated with NAAZ-2 near the base Dye-3 ice core (Ram and Gayley, 1991[13]). Aggregate layers contain a mixture of basic to highly silicic glass-shards. Some glass shards are up to 300 μm long and reflect airfall deposition from exceptionally explosive and large magnitude eruptions from the Icelandic system because it is the only source of explosive volcanism in the North Atlantic region (Werner *et al.*, 1996).

The GISP2 volcanic sulphate aerosol record of global volcanic activity allows the magnitude and timing of volcanic eruptions to be evaluated (Fiacco *et al.*, 1994). It is thought that even relatively small, high sulphate producing-eruptions have a global volatile (aerosol) signature (Rampino and Self, 1982; Zielinski, 2000). Recent eruptions in the tropical regions (El Chichon, 1982 and Mount Pinatubo, 1991) had a significant effect on global climate (Sparks *et al.*, 1997) because volcanic aerosols from eruptions in the tropics are rapidly incorporated into the equator to pole atmospheric circulation system of the upper atmosphere. This processes also aids deposition in high-latitude ice cores (Palais *et al.*, 1992). Volcanic sulphate peaks at *ca.* 70 ka in the GRIP and GISP2 records have been linked to the massive Toba eruption that occurred in Sumatra *ca.*75 ka (Rose and Chesner, 1990; Chesner *et al.*, 1991; Zielinski *et al.*, 1996; Westgate *et al.*, 1998).

Icelandic eruptions are disproportionately represented in the GISP2 volcanic sulphate record because of the proximity of the Icelandic volcanoes to the Greenland Ice Sheet (Fiacco *et al.*, 1994; Zielinski *et al.*, 1995). Zielinski *et al.*, (1994) estimated that 20 % of the eruptions recorded in the last 2000 years were related to eruptions from Iceland even though they constitute between 1-5 % of global

[13] Major element data for the silicic shards analysed in this study is incomplete and no details were given of the analytical method; hence this deposit was not included in the correlation age matching exercise or in Table C2.1.

volcanic eruptions in this period. Matching eruption events to eruption location in the 9000-2000 years BP period proved difficult, but Zielinski *et al.*, (1994, p. 951) concluded that 'the high amount of SO_4^{2-} [volcanic sulphate] deposition for individual eruptions would favour a more proximal source like Iceland.'. Deposition of glass shards is more limited due to the generally eastwards direction of prevailing wind directions across Iceland.

(e) Linking palaeoenvironmental records in the North Atlantic & aiding problems of the ^{14}C timescale

The example below highlights the enormous potential that the Icelandic tephra record holds for correlating proxy indicators of climate change in the North Atlantic region to determine 'leads and lags' between terrestrial, cryogenic and oceanic climate systems.

The discovery of rapid climate reversals of apparently similar age and duration in several climate proxy records has radically altered views concerning the rate and nature of Quaternary climate change (Dansgaard *et al.*, 1993; Hughen *et al.*, 1997). Whether these changes are synchronous, asynchronous or unrelated has major implications for our understanding the underlying mechanisms of climate change (Severinghaus, 1998). Traditional litho- and biostratigraphic correlation methods and dating techniques such as radiocarbon (^{14}C) dating are not suited to resolving age differences to a sufficiently high resolution (Wohlfarth, 1996; Björck *et al*, 1998; Scott and Harkness, 2000). More fundamentally, Stuvier and Suess (1966) first realised that atmospheric concentrations of ^{14}C could vary by as much as 30% producing age anomalies of several thousand years. It is now widely accepted that changes in the production or exchange mechanisms that control atmospheric ^{14}C levels, other than those created by ^{14}C decay, has led to secular variations in the ^{14}C time spectrum (Scott and Harkness, 2000). This means that ^{14}C time is non-linear and not directly equivalent to calendar years (Taylor, *et al.*, 1996).

To overcome this problem, calibration curves have been constructed. These 'convert' ^{14}C ages to 'real', 'calendar', sidereal, or calibrated time by comparison to long ^{14}C-dated dendrochronologies, ^{14}C dating of annually laminated sediments and paired ^{14}C and uranium series ($^{234}U/^{230}Th$) ages from cores drilled into coral formations (Bard *et al.*, 1993; Becker, 1993; Pearson and Stuvier, 1993; Taylor *et al.*, 1996; Hughen *et al.*, 1998). However, these calibrations have a limited time span of about 20 ka over which they are considered accurate. Beyond this, paired varve and coral ages produce divergent calibration curves. Ages obtained are further compromised by other limitations such radiocarbon age-plateaux, hard water errors and marine reservoir effects (Amman and Lotter, 1989; Björck *et al.*, 1998; Kitagawa and van der Plicht, 1998; Turney *et al.*, 2000). Some of these obstacles have been surmounted by matching variations in the stable isotope ratios of oxygen and carbon to existing records *e.g.* Bender *et al.* (1993), Bloemendal *et al.* (1994), Whittington *et al.* (1996), Benson *et al.* (1997a), Turney *et al.* (1998), Voelker *et al.* (1998).

In the North Atlantic region certain widespread and diagnostic Icelandic tephra deposits have been used to correlate sequences (Mangerud *et al.*, 1984; Lowe and Turney, 1997; Wastegård *et al.*, 2000a). For example, the Vedde Ash (VA) is a widespread chronological marker that has been identified in marine cores extracted from the North Atlantic and the Nordic Seas (Ruddiman and Glover, 1972; Sigurdsson and Loebner, 1981; Fillon *et al.*, 1981; Serjup *et al.*, 1989; Long *et al.*, 1986; Kvamme *et al.*, 1989; Bard et *al.*, 1994; Austin *et al.*, 1995; Austin and Kroon, 1996; Eiríksson, *et al.*, 2000b), late-glacial sequences in Iceland (Björck *et al.*, 1992; Norðdahl and Haflidason, 1992), northern Europe (Jóhansen, 1975; Mangerud *et al.*, 1984; Merkt *et al.*, 1993; Lowe and Turney, 1997; Wastegård *et al.*, 1998; Wastegård *et al.*, 2000a; Turney *et al.*, 2001), Russia (Wastegård *et al.*, 2000b) and in the GRIP and GISP2 ice cores from Greenland (Gronvöld *et al.*, 1995; Ram *et al.*, 1996; Zielinski *et al.*, 1997) (Table 2.1). Climate records from these areas can now be directly linked and the accuracy of ^{14}C ages tested by direct comparison to the incremental, calendar time scale of the Greenland ice cores.

The basaltic Saksunarvatn Ash has also been identified in many of these repositories. It is also a useful marker horizon, but its distribution is more restricted and major element geochemistry not as diagnostic as the Vedde Ash. The Vedde Ash eruption has been strongly linked to the Katla volcanic system in southern Iceland (Lacasse *et al.*, 1995; Wastegård *et al.*, 2000a; Larsen *et al.*, 2001) although Öræfajökull was initially suggested as an alternative source (Serjup *et al.*, 1989). The Saksunarvatn Tephra is linked to Grimsvötn or Kverkfjöll volcanic systems beneath Vatnajökull (Mangerud *et al.*, 1984; Ingólfsson, *et al.*, 1995). Organic deposits bracketing the tephra deposits have produced dates of *ca.* 9 ka BP for the Saksunarvatn Tephra and 10.31 ± 0.05 ka BP (Birks *et al.*, 1996) and 10.6 ± 0.06 ka BP (Mangerud *et al.*, 1986) for the Vedde Ash. These ages coincide with radiocarbon plateaux suggesting the accuracy of ^{14}C ages from this period might be compromised even if they have been calibrated. To overcome such problems Wastegård *et al* (1998) used the occurrence of the Vedde Ash in the GRIP ice core at 11.98 ± 0.08 calendar ka (Grönvold *et al.*, 1995) to calibrate radiocarbon dates constraining climate proxy records in Sweden to a calendar time scale.

The position of the Saksunarvatn Tephra and Vedde Ash in marine cores of the North Atlantic enabled Austin *et al.* (1995) and Haflidason *et al.* (1996) to estimate the spatial variability present in marine ^{14}C reservoir age-correction values for the Holocene and Lateglacial. For the Younger Dryas a reservoir-age correction of 800 years is required in the eastern Norwegian Sea, North Sea and the North Atlantic, but this increases to *ca.* 1100 years in the western Nordic Seas. Reservoir correction-ages for the Holocene were reduced to 690-730 years and the correction was also systematically higher in the western Nordic Seas (Haflidason *et al.*, 1998). Eiríksson *et al.* (2000a, b) similarly used a combination of AMS[14] ^{14}C dates and tephra markers from Hekla 4, Hekla 3 and Hekla 1104 AD, to

[14] Accelerator Mass Spectrometry

constrain proxy records of Holocene climate change and estimate the ^{14}C marine reservoir correction values for the North Atlantic for the mid-Holocene.

The distribution of NAAZ-1 has also been used in other ways. Ruddiman and Glover (1972) first used the distribution of NAAZ-1 in marine cores to reconstruct palaeocirculation patterns at the time of its eruption, assuming that the extensive distribution of this ash layer reflected iceberg rafting patterns in the North Atlantic (Fig. 2.6).

2.2.2 Limitations of the Icelandic tephra record: the pre-Lateglacial era

The terrestrial record of tephra deposition in Iceland older than the Hekla-5 eruption of *ca.* 6100 ^{14}C BP is fragmentary. Accurate isopach maps for tephra layers older than this are difficult to construct. The majority of pre-Lateglacial tephra layers of Icelandic origin have all been identified in terrestrial, ice core and marine records from beyond Iceland (Haflidason *et al.*, 2000; Bond *et al.*, 2001; Larsen *et al.*, 2001; Appendix C2: Table C2.1). The only pre-Holocene tephra deposits of Quaternary age found so far in Iceland are the Skógar Tephra in Fnjóskadalur, northern Iceland, and four distinct tephra layers found in a core taken from Lake Torfadalsvatn on the Skagi Peninsula, North Iceland (Fig. 1.6-b) (Norðdahl and Haflidason, 1992; Björck *et al.*, 1992). The Lake Torfadalsvatn sequence possibly contains evidence for as many as twelve sizeable eruptions during the Lateglacial period. The Tv-1 layer at *ca.* 16.5 ^{14}C ka BP is the oldest of these. Another silicic layer has been correlated to the Vedde Ash and its North Atlantic marine core equivalent, 1-THOL-2 (Kvamme *et al.*, 1989; Björck *et al.*, 1992). The Skógar Tephra is bracketed by pro-glacial lake sediments. It has also been linked to the Vedde Ash eruption and, as a result, the age of the ice-dammed lake that it was deposited into was revised from *ca.* 17 ka ^{14}C BP to 10.3 ka ^{14}C BP (Norðdahl and Haflidason, 1992).

All tephra deposits of pre-Lateglacial age have been identified in marine cores extracted from the northern North Atlantic. Early descriptions of the offshore tephra record grouped layers into three main ash zones. These were labelled North Atlantic Ash Zones 1, 2 and 3 (NAAZ-1, -2 and -3) (Bramlette and Bradley, 1941; Ruddiman and Glover, 1972). Various ages of 16-10 ka (Table 2.3), *ca.* 58-48 ka and *ca.* 350-300 ka, respectively, have been reported (Ruddiman and Glover, 1972; Sigurdsson, 1982; Lacasse *et al.*, 1995, 1996). These terms are still appropriate and widely used, *e.g.* Lacasse *et al.* (1995) and Zielinski *et al.* (1997). Recent oceanographic studies have, however, revealed a more detailed and complex record of Pleistocene and Upper Pliocene volcanic activity in the North Atlantic region (Werner *et al.*, 1996; Clift and Fitton, 1998; Bond *et al.*, 2001). Numerous layers have been identified and chemically characterised in records that extend to *ca.* 50 Ma, about the time of the rift initiation in the mid North Atlantic (Sigurdsson and Loebner, 1981; Sigurdsson, 1982; Kvamme *et al.*, 1989; Clift and Fitton, 1998; Lacasse *et al.*, 1996; Andrews *et al.*, 2000; Bond *et al.*, 2001).

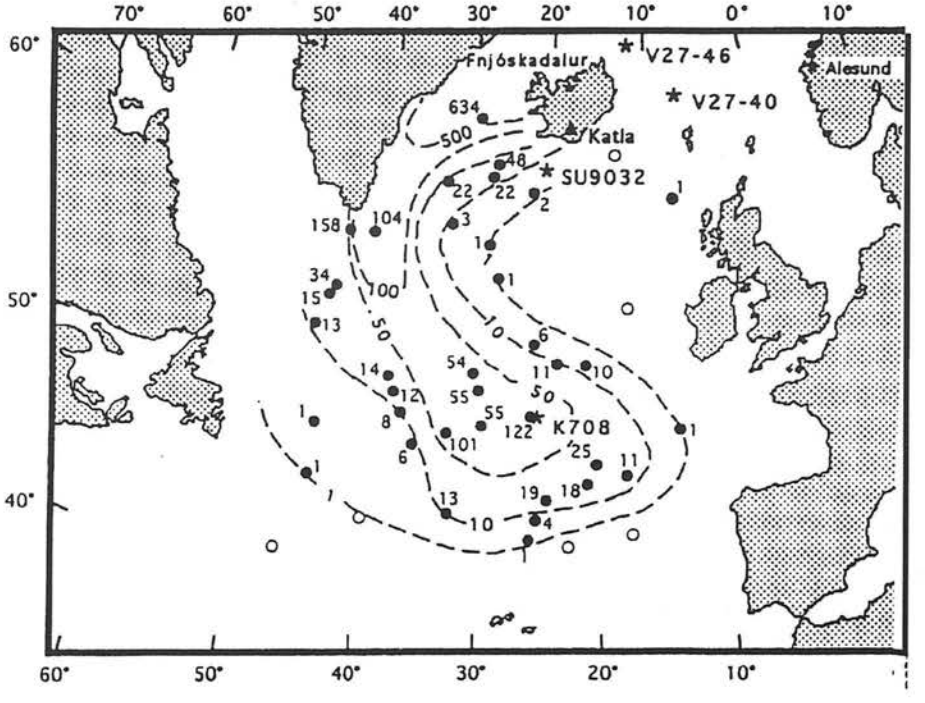
(a) Components of NAAZ1

Tephra Deposit	Locations Discovered	^{14}C age (years BP)
Saksunarvatn Tephra	Iceland[b,e], NAMC[t], Faroe Islands[c, g], Shetland, [u], Orkney[e], [v], Germany[a], Greenland[s]	8700[a], 8900[b], 9000 - 9100[c], 9140[d]
1-Thol-1	Iceland[b]	9200[b]
Vedde Ash	Iceland (Skogar Tephra)[b,c, q], NAMC[h-o], Norway[e,p], Sweden[r],Greenland[s] , Russia[w]	10,300[e], 10,600
1-Thol-2	Iceland[b]	10,800[b]
Borrobol Tephra	Scotland[f], NAMC(?)[j]	12,500[f]

(b) Scottish Lateglacial tephra deposits

Site Name	Lat. (°)	Long. (°)	Depositional Environment	Maximum Depth (m)	Maximum shard concentration no. shards per cm^3 wet sediment (depth cm)	
					Vedde Ash	Borrobol Tephra
1 Borrobol	58° 09.50' N	03° 50'.00' W	infilled lake basin	5	6222 (384)	373 (481)
2 Tanera More	58° 00.40' N	05° 23.60' W	infilled isolation basin	8	259 (526)	17 (565)
3 Tynaspirit West	56° 13.17' N	04° 10.00' W	infilled kettle hole	9.5	128 (752)	9 (925)
4 Whitrig Bog	55° 36.03' N	02° 36.00' W	infilled lake basin in inter drumlin hollow	2.95	743 (114)	65 (239)
5 Muir Park Reservoir	56° 05.18' N	04° 16.97' W	infilled lake basin	8	52 (774)	-
6 Kennethmont	57° 21.05' N	02° 46.42' W	infilled hollow (non-lacustrine)	2.5	22 (210)	-

Table 2.1 Components and radiocarbon ages of North Atlantic Ash Zone-1 (NAAZ-1). NAMC=North Atlantic Marine Cores. Source information: a = Merkt *et al.* (1993); b = Björck *et al.* (1992); c = Mangerud *et al.*, (1986); d = Jóhansen (1975); e = Birks *et al.* (1996); f = Turney *et al.*, (1997); g = Jóhansen (1985); h = Bard *et al.* (1994); i = Sejrup *et al.* (1989); j = Kvamme *et al.* (1989); k = Sigurdsson and Loebner (1981); l = Fillon *et al.* (1981); m = Ruddiman and Glover (1972); n = Long *et al.* (1986); o = Austin *et al.* (1995) and (1996); p = Mangerud *et al.* (1984); q = Norðdahl and Haflidason (1992); r = Wastegård *et al.* (1998) and Wastegård *et al.* (2000a, b); s = Grönvold *et al.* (1995); t = Sjøholm *et al.*(1991); u = Bennett *et al.* (1992); v = Bunting (1994); w = Wastegård *et al.*, (2001).


70°
60°
50°
40°
30°
20°
10°
0°
10°
60°
50°
40°
Fnjóskadalur
V27-46
Alesund
V27-40
Katla
SU9032
K708
634
500
158
104
100
50
10
50
54
55
55
122
101
25
11
10
6
1
1
1

Correlation dating of fragmentary records based on field and/or chemical characteristics in the pre-Holocene era is potentially unreliable for reasons of longer-term major element chemical equifinality between volcanic systems, eruption-deposition delays, post-depositional disturbance in off-shore sediment repositories (Larsen *et al.*, 1999; Bond *et al.*, 2001; Jennings *et al.* 2000; Andrews *et al.*, *manuscript*). Tephra deposition in marine cores does not always reflect the eruption age. Vertical mixing and post-depositional disturbance is common. Moreover, during glacial periods the time between eruption and repository deposition can be significantly extended because tephra deposited on to iceberg rafts or large ice sheets can become trapped, delaying deposition by thousands of years (Andrews *et al.*, 2000; Bond *et al.*, 2001; Andrews, *manuscript*). For example, Roberts (1997) and Bond *et al.*, (2001) questioned whether the all highly silicic fractions of NAAZ-1 are related to the same eruption that produced the Vedde Ash. Bond *et al.*, (2001) suggested that this fraction could be a hybrid of both storage-calving and fallout mechanisms of dispersal. In particular, they noted that the deposition of NAAZ-1 coincided with a rapid, but short-lived increase of ice-rafted debris (IRD) of non-Icelandic origin in ocean cores to the south of Iceland. They associated these IRD layers with carbonate sources of Paleozoic age in eastern Canada (Andrews *et al.*, 1995) and implied that a significantly delayed eruption-deposition, regionally synchronous ice-rafting event was the dominant mechanism of deposition for NAAZ-1 in the northern North Atlantic.

2.3 Dating of distal tephra deposits in Iceland

2.3.1 Current State of Play

Radiometric tephra-dating techniques have not been as widely applied to distal tephra deposits in Iceland as they have been in other volcanic regions for the following reasons:

1) **Historical records and radiocarbon dating** of organic material surrounding tephra layers provide adequate age constraints for tephra deposits of Holocene and Lateglacial age in Iceland and there has been little need to attempt direct dating of tephra deposits. Historical records are limited to 870-950 AD and radiocarbon dating to 40-50 ^{14}C ka.
2) **Terrestrial sequences** of pre-Last Glacial Maximum (LGM) age in Iceland are rare because, apart from some peninsulas and elevated coastal mountains, Iceland was largely ice-covered until *ca.* 7800 yr. BP (Gudmundsson, 1997). The oldest mid-late Pleistocene biogenic records are of Lateglacial age and limited to Skagi Peninsula and other parts of North Iceland (Björck *et al.*, 1992; Norðdahl and Haflidason, 1992; Rundgren *et al.*, 1997). Consequently, most pre-Lateglacial tephra deposits of Pleistocene age and Icelandic origin have been discovered in marine, ice core and terrestrial records from areas surrounding Iceland (*e.g.* Sigurdsson, 1982, Lacasse *et al.*, 1996, Zielinski *et al.*, 1997, Haflidason *et al.*, 2000).
3) **Distal tephra** beds are difficult to date because of their thin and discontinuous nature, fine grains low abundance of phenocrysts and the presence of xenolithic and detrital contamination of non-eruption age (Westgate, 1989). Icelandic tephra deposits, especially distal ones, are dominated by glassy material to the near exclusion of other co-genetic crystal or mineral phases. Hydrated glass shards are the dominant phase of Icelandic tephra. Mineral phenocrysts only constitute about 1-2% of silicic deposits near the eruption vent and even less at distance (Tómasson, 1967). Thus, established isotopic and radiogenic dating techniques are not always applicable to glassy tephras younger than 100 ka and each deposit has to be examined individually to determine which dating technique(s) is most applicable.

2.3.2 Dateable phases in Icelandic Tephra

In order to date any tephra deposit directly the proportions and suitability of datable phases in each sample need to be assessed on a sample-by-sample basis. Developing and applying volcanic glass-dating techniques is particularly beneficial for Icelandic tephra deposits because:

1) **Eruption age:** The age of volcanic glass reflects the 'quench-time' of the eruption when the melt crystallises shortly before ejection of pyroclastic material from the vent. The age of phenocryst assemblages can sometimes reflect pre-eruption crystallisation events and/or extended residence times in the magma chamber or incomplete resetting events (Jørgensen, 1980; 1987; van den Bogaard, 1995; Shane, 2000).

2) **Bulk composition of Icelandic tephra:** Glass is abundant and easily separated from minerogenic fractions in silicic tephra deposits from Iceland because the minerogenic fraction is usually no greater than 4 % and dominated by volcanic feldspars (Tómasson, 1967; Mangerud *et al.*, 1984). Moreover, characteristic crystal and lithic fractions are heavily depleted at distances > 50-100 km due to atmospheric sorting. Potassium-argon dating has been used to date obsidian and lava flows and K-rich feldspars and/or sanidines in proximal ignimbrite and ash flow deposits in Iceland McGarvie (2000). Zircon-grain fission-track dating and quartz phenocryst phase luminescence dating have been used in other volcanic regions (*e.g.* Naeser *et al.* 1973; Pillans *et al.*, 1996). Distal tephra deposits, and especially Icelandic ones, are not well endowed with these minerals and zircon and quartz phenocrysts are normally completely absent. Xenolithic contamination is also a concern.

3) **Chemical correlation of Icelandic tephra:** Glass shards are the diagnostic phase of Icelandic tephras (Larsen *et al.*, 1999). Their major element geochemistry is an important tool that has been used to fingerprint and correlate many tephra deposits from Iceland found in and around the North Atlantic region.

4) **Contamination of proximal deposits:** Xenolithic and detrital contamination by non-eruptive volcanic products is common in volcanically active areas (Kohn *et al.*, 1992). In areas adjacent to the vent, the violent nature of eruption processes introduces lithic fragments and other mineral contaminants of a different age to those ejected from the vent during the eruption being dated (Naeser and Naeser, 1988). Particular problems arise where the underlying bedrock is of similar age and/or composition to the products of the eruption. For example, Seward and Kohn (1997) obtained two distinct zircon fission-track age populations of 1.38 ± 0.11 and 2.15 ± 0.17 Ma from the Mangapipi Ash in the Rangitikei Valley, in southern half of New Zealand's North Island, about 50 km south of the Taupo Volcanic Zone (Shane, 2000). Initially, Seward (1975; 1979) obtained an uncorrected glass fission-track age of 0.88 ± 0.13 suggesting the 1.38 Ma age was possibly correct. Later, Black *et al.* (1996) demonstrated that these early glass fission-track ages were underestimates because the effects of track fading had not been accounted for and that the 1.38 Ma zircon fission-track age was most accurate. The older zircon-fission-track age was due to contamination from older zircons phases in the surrounding bedrock. The use of fading corrected glass-phase fission-track dating avoids this problem.

5) **Contamination of distal deposits:** Post-depositional reworking of thin tephra layers or beds and other erosional processes in remote locations also introduces detrital contaminants of different ages. Seward and Kohn (1997) also used the zircon fission-track technique to date the Rewa Pumice from New Zealand. This deposit shows clear evidence of fluvial reworking. Originally, two distinct age populations of 1.21 and 11.1 Ma were produced, with the younger one considered accurate by comparison to glass-phase fission-track and potassium argon ages. Post depositional mixing and cross-contamination of layers would also apply to glass fractions of

closely spaced layers if there were several layers present, but is less of a problem in areas where tephra layers are unusual and/or widely spaced in stratigraphic profiles.

2.4 Tephra Dating Methods in the pre-^{14}C era

The most suitable methods available for dating Icelandic tephra are evaluated in this section (Fig. 2.7; Tables 2.1, 2.2). Smart (1991b, p. 4) recommended three main criteria for establishing the reliability of ages estimates:

1) For a specific dating technique good agreement between multiple age determinations within a single chronostratigraphic unit.
2) For a specific dating technique there should be an increasing age-depth relationship stratigraphically related samples from a geological sequence.
3) Ages obtained using independent methods should be concordant.

Highly silicic tephra deposits represent temporally well-spaced and well-defined eruptions. Given the lithological nature of the tephra and bracketing deposits examined in this study (Section 4.1), an accurate age is defined as an age that is similar to ages obtained by a well-established and/or independent dating methods (Clarke *et al.*, 1999).

An extensive description of all Quaternary and tephra dating methods can be found in Smart (1991a) and Stratton-Noller (2000). In summary, correlation dating techniques, such as tephrochronology and palaeomagnetism, are valid if numerical ages can be determined at reference or 'type-sites' (Smart, 1991a, b). Radiogenic and isotopic methods have been widely used to produce 'direct-numerical ages' from specific mineral phases and the volcanic glass component of tephras (Table 2.2). Fading corrected fission-track ages are well established and produce accurate ages. The volcanic glass phase is suitable for luminescence dating, but its application has been limited to fine grained (4-11 μm) dating methods in specific regions (Berger and Huntley, 1983; Berger, 1991, 1992). Major uncertainties remain over the effectiveness of purification procedures and the source of luminescence host-emissions for fine-grained volcanic glass-phase dating (Prescott and Robertson, 1997; Berger *et al.*, 1999; Zander *et al.*, 2000). Isotopic dating methods, such as potassium-argon or argon-argon (^{40}K-^{40}Ar or ^{40}Ar-^{39}Ar) and uranium series dating are regarded as generally unsuitable for volcanic-glass phase dating (McDougall and Harrison, 1988; Smart, 1991b; Richards and Smart, 1991; Shane 2000) (Table 2.2; Appendix A3). The accuracy and precision of all these methods is constantly improving as experimental procedures are refined and more sophisticated equipment becomes available. Consequently, the chronological ranges of each technique are continually expanding (Naeser and Naeser, 1988; Pringle *et al.*, 1991; Richards and Smart, 1991; Berger *et al.*, 1992; Berger, 1994).

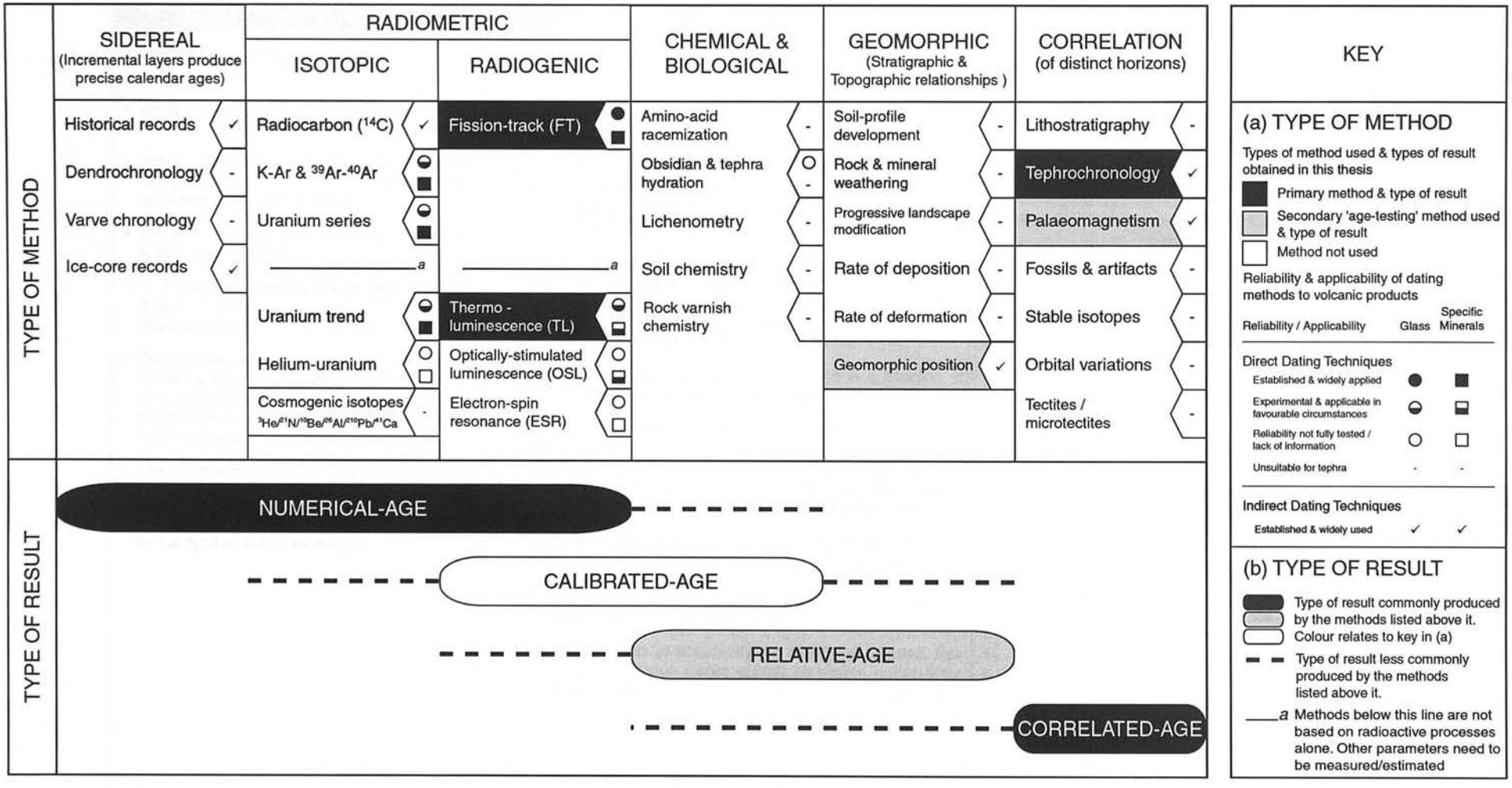


Figure 2.7 Classification scheme for Quaternary dating techniques and their applicability to dating the glass and minerogenic phases of tephra deposits. There are many alternative classification schemes for dating techniques. This scheme is preferred because it groups methods whose underlying principles are the same and provides a broad order of most successful to least successful methods within each grouping. Diagram adapted from information and diagrams in Colman *et al.* (1987), Aitken (1985, 1998), Smart (1991), Prescott & Robertson (1997), Forman *et al.* (2000) and other references in the text.

Correlation Dating Methods	Radiogenic Dating Methods	
Tephrochronology	Fission-track dating	Luminescence dating
• Volcanic eruptions from a single source occur at points in time. • Airfall deposits mantle the existing topography and can be distinguished from reworked deposits in the field • The area of fallout for the eruption covers up to thousands of km^2 • In depositional environments tephra layers display diagnostic and recognisable characteristics that can be correlated • Primary deposits can be dated directly using direct radiogenic and isotopic techniques or their surrounding sediments can be dated using indirect correlation and/or radiometric numerical age techniques • The maximum dateable age is determined by the age of the parent eruption • The minimum age obtainable is determined by the type of dating technique	• The age obtained represents the mineral or glass formation event. If tracks have been completely erased by increases in environmental temperatures the age obtained reflects the last heating event. Where partial track annealing is common, *e.g.* in volcanic glasses, isothermal step or plateau heating procedures or those based on spontaneous vs induced track size variations are required to obtain accurate ages • Spontaneous tracks are fission fragment damage trails left in the lattice structure of certain minerals and glasses from the radioactive decay of ^{238}U in the natural environment. Induced tracks are formed by the same process in the laboratory by the decay of ^{235}U. • The number of spontaneous tracks formed is a function of the ^{238}U content of the sample and its age • When the zeta calibration method is used, the number of tracks induced by laboratory irradiation is a function of neutron flux of the irradiator. The neutron flux can be accurately determined by measuring the number of tracks formed in a muscovite detector covering the glass dosimeter • The decay constants of ^{238}U & ^{235}U are well established: $^{238}U = 1.551 \times 10^{-10}$ yr^{-1} (Jaffey *et al.*, 1971); $^{238}U = 7.03 \times 10^{-17}$ yr^{-1} (Roberts *et al.*, 1968). The $^{235}U/^{238}U$ ratio is constant in nature. Therefore, the ^{235}U track density can be converted to ^{238}U concentration • Fission-tracks can be accurately identified and counted. For volcanic glass, fission tracks should be visible under 500x magnification after etching and, ideally, 5-8 μm in diameter	**1. General assumptions** • For 'normal' sediment dating, the age obtained represents the last 'zeroing' event. *i.e.* the last time a sample was exposed to heat, light or significant pressure. For volcanic glass dating, the geological age, *i.e.* when the formation of the glass from the melt occurred, is of most interest and post formation heat and/or light exposure must not have occurred. • Samples must have been effectively 'zeroed' during the zeroing event. *i.e.* all existing natural TL accumulated has been removed. Samples that are not fully zeroed can retain remnant luminescence signals from a previous zeroing event or even their geological age. For volcanic glass dating undertaken in this study, the zeroing event is defined as its geological formation age • Limited or no post-depositional disturbance since burial **2. Palaeodose assumptions:** • Portions of the luminescence signal must display long term stability • Growth curve characteristics are reproducible, can be statistically modelled and fitted with an appropriate mathematical function *e.g.* single saturating growth curve • No residual signals exist • No dose dependent sensitivity changes in sample • No dose rate dependence in the reconstructed signal • No spurious TL is encountered *i.e.* TL from anything other than the intended phase • No contamination or heat/light exposure **3. Dose rate assumptions** • Dose rate remains constant during burial and radioactive secular equilibrium exists • A water content history can be reconstructed • Overburden history can be reconstructed • Calibrated radioactive sources are used

Table 2.2 (a) Assumptions of the main dating methods used in this thesis. (After - Tephrochronology: Thórarinsson (1974); Steen-McIntyre (1977); Dugmore *et al.* (1995b); Sarna-Wojcicki, (2000) - Fission-track: Price and Walker (1963); Westgate (1989); Sandhu & Westgate (1995); Dumitru (2000) – Luminescence: Aitken (1985); McKeever (1985); Berger *et al.* (1996) Wintle (1997); Prescott & Robertson (1997); Forman *et al.* (2000).

Table 2.2 (b) Evaluation of dating methods commonly used to date tephra deposits

Dating Method; specific glass-phase methods	Age Range (yrs) Lower to Upper *Lower to Upper in favourable conditions* **[Reliable age limits for volcanic glass]**	Theoretical basis; age measurement technique; most reliable dating phases	Applicability to tephra deposits & advantages of glass-phase dating of tephra	General (G) and glass-phase (g) limitations encountered	Recent Relevant Examples & Phases Dated
RADIOGENIC DATING					
FISSION TRACK **Isothermal Plateau Fission-Track (ITPFT)** (Westgate 1988; 1989) **Diameter Corrected Fission-Track (DCFT)** (Sandhu *et al.*, 1993)	30 ka – 5 Ga (Smart, 1991a; Williams *et al.* 1998) **[>100 ka – 10 Ma]**	Damage tracks caused by natural ^{238}U decay Counting ^{238}U tracks on chemically etched slides relative to ^{235}U tracks created by artificially irradiating samples; zircon & (with correction) glass	Applied deposits dominated by large silicic platey glass shards Grain specific minimises Contamination from non-co-genetic phases In undisturbed layers glass-phase dating unequivocally dates eruption event Accurately reproduces co-genetic zircon ages[3]	Relatively low precision (compared to K-Ar & Ar-Ar) of 5-10% at best (G; g) Not suitable for high resolution cyclostratigraphic studies; more suitable for widely spaced eruption event dating (G) 'Young' deposits <100 ka require high U content (*e.g.* >6 ppm) and/or long periods of laboratory counting (g)	**Naeser *et al.* (1980)** comparison of uncorrected and corrected glass-phase ages with zircon phase and isotopic ages **Pillans *et al.* (1996)** glass with examples of zircon phase ages **Westgate *et al.* (1997)** **Westgate *et al.* (1998)** **Preece *et al.* (1999)** All ITPFT glass phase dating
THERMOLUMINESCENCE (TL) & OPTICALLY STIMULATED LUMINESCENCE (OSL) **Multiple Aliquot Regeneration (MAR), Partial Bleach (MA-PB) & Additive Dose Methods (MAAD-TL & OSL)** Various references see Berger (1992), Forman *et al.* (2000) for examples **Single Aliquot Regeneration (SAR-OSL)** Duller (1991), Murray & Roberts 1998)	1000 – 200 ka (Smart, 1991b; Aitken, 1998) *100 – 800 ka* *(Berger et al., 1992)* **[1000-200 ka]**	Accumulation of free electrons from radioactive decay process at 'trapping sites' (impurities) within the lattice Reconstruction of a palaeodose in the laboratory and measurement of environmental dose rate by compositional analysis (*e.g.* XRF, ICP-MS, NAA) and/or spectrometry measurements (*e.g. In-situ* gamma spectrometry, Thick Source Beta Counting TSBC, alpha spectrometry and efficiency measurements) Quartz and non-volcanic feldspars	Can be applied to quartz, & feldspar phenocrysts and glass-phase Successful glass-phase dating procedures established for fine-grained dating Rapid density based purification of the glass phase	Non-co-genetic phenocryst contamination (G) Volcanic feldspars are susceptible to anomalous fading which is difficult to fully correct for in the laboratory (G) Difficulties encountered in producing pure glass-separates using density separation techniques (g) Visually inspection of phase dated is not rapid (g) Relatively long periods of laboratory analysis required	**Berger (1992)** fine-grain glass-phase TL dating procedures and ages **Berger & Neill** (1999) IRSL signals from fine-grained glass-phase **Chen *et al.* (1999); Li & Yin (2000); Bonde *et al.* (2000); Sanzelle *et al.* (2001)** Both TL dating of quartz phenocrysts in pyroclastic deposits

ISOTOPIC DATING					
PRINCIPALLY POTASSIUM-ARGON (^{40}K-^{40}Ar) & ARGON-ARGON (^{39}Ar-^{40}Ar) **None** Also U-series: similar advantages and disadvantages as potassium decay based methods, but less widely applied to tephra deposits than potassium decay based method (Smart, 1991c)	30 ka – 20 Ma (Smart, 1991b) *1000 – 5 Ga* *(Williams et al. 1998)* [50 ka – 5 Ma]	Parent to daughter decay Measurements of isotopic concentrations in a dedicated mass spectrometer and, for Ar-Ar dating, single grain laser fusion followed by mass spectrometric analysis Single grain laser fusion is used to produce age isochrons and detect relict and partially degassed crystals K-rich feldspars and sanidines	Wide range of undisturbed tephra deposits with suitable co-genetic phenocryst phases High precision (*e.g.* 0.5%); rapid measurement; readily reproducible, reliable ages from several co-genetic phases For single grain methods stepwise heating procedures produce a plateau age isochron which is used to identify contaminant grains and those that have retained their original argon	Bulk ages are considered unreliable because of non-eruptive contamination (G) Ages falsified by the retention of original/primordial argon Long decay half life of potassium means the method is not generally applicable to deposits <100 ka that have a low potassium content (*e.g.* < 5 wt %) Loss of Ar from mineral and glass matrix Application of single grain glass-phase techniques is highly experimental – silicic deposits have to be K-rich, >100 ka and must not have experienced post-depositional element exchange (cf. Kaneoka, 1972)	**Hurford and Hammerschmidt (1985)** Accurate ages for the Fish Canyon and Bishop Tuff deposits of western 5North America **Van den Boogard (1995)** Accurate, Lateglacial (*i.e. ca.* 12 ka) ages from single grain Ar-Ar sanidine phenocrysts **Pillans *et al.* (1996)** Multi-method dating of plagioclaise feldspars produced inaccurate and imprecise ages from 400 ka Rangitawa Tephra, North Island, New Zealand **LoBello et al (1987)** **Pringle *et al.* (1992)** **Gansecki *et al.* (1998)** Further examples of single grain /laser fusion identification of contamination and accurate Ar-Ar ages
CORRELATION DATING					
TEPHROCHRONOLOGY **Electron microprobe analysis (EPMA) of glass shards**	0-2 Ma *Potentially unlimited* **[Historical/Holocene *i.e.* < 10 ka]**	Similarity and linkages between bulk compositions and grain-specific glass and phenocryst geochemistry EPMA for major elements and SIMS (secondary ion mass spectrometry) for trace elements Glass shards	Widely applied, underlying technique for characterising tephra deposits Grain-specific analysis avoids non co-genetic contamination Best applied where continuous and well-dated terrestrial record of record exists	Major element analysis is effected by the effects of closure Post-depositional hydration and other elemental substitution processes can lead to spurious correlations Tephra deposited onto ice sheets and/or rafts can experience significant eruption-deposition delays	Recent reviews of tephrochronological studies in Iceland, New Zealand and North America can be found in **Haflidason *et al.* (2000), Sarna-Wojcicki (2000) and Shane (2000)** respectively.

contd.

PALAEOMAGNETIC REVERSAL DATING	Potentially Unlimited	Periodic reversal in Earth's magnetic field in relation to the current normal polarity Solid rock and undisturbed medium-fine grained sediments Lavas	Rapid and easy measurement Works best on continuous records in which several polarity reversals can be identified	Requires numerical dating techniques to tie reversals to specific parts of the palaeomagnetic timescale Self reversal occurs in 1% of volcanic rocks Unsuitable for 1 in 5 sedimentary sequences (Thompson, 1991) where the polarity signal has been realigned by post-depositional disturbance 'Varved' deposits are the most persistently troublesome sedimentary deposits (Thompson, 1991)	**Geirsdóttir and Eiríksson (1994)** palaeomagnetic reversal dating of inter-bedded lava and tillite deposits in Iceland **Preece *et al.*, (1999)** palaeomagnetic reversal dating of Alaskan loess and tephra deposits

Indirect numerical ages have been obtained from the surrounding sediments using ^{14}C and luminescence techniques. The use of these is restricted to the <50 ka and <0.8 Ma age range respectively (*e.g.* Froggatt and Lowe, 1990; Dugmore *et al.*, 1995a; Hadjas *et al.*, 1995; Berger *et al.*, 1992; Birks *et al.*, 1996; Pillans *et al.*, 1996; Benson *et al.*, 1997b; Lowe and Turney, 1997; Shane, 2000).

2.4.1 Tephra Dating Methods I: Correlation Dating Methods

The following criteria are commonly used to characterise and distinguish between tephra deposits: stratigraphical position, phenocryst assemblage and chemistry, glass chemistry, magnetic polarity, and/or palaeoecological/biostratigraphical context. Secure matching of tephra deposits and the source vent requires grain specific major element electron probe microanalysis (EPMA) of glass and quantitative characterisation of mineral components (Froggatt, 1992; Hunt and Hill, 1993; Larsen *et al.*, 1999; Hunt and Hill, 2001). Fe-Ti mineralogy, Fe-oxide compositions, oxygen fugacity and multivariate statistical methods have also been used discriminate between different tephra deposits (Borchardt *et al.*, 1972; Lawson *et al.*, 1987; Stokes and Lowe, 1988; Shane, 2000).

(a) Geochemical Correlation Dating

Electron probe microanalysis (EPMA) has been the foremost analytical technique used in tephrochronological studies since the 1960s (Smith and Westgate, 1969; Westgate and Gorton, 1981; Larsen, 1981; Lowe, 1988; Dugmore *et al.*, 1995a, b; Westgate *et al.*, 1992; Westgate *et al.*, 1998; Haflidason *et al.*, 2000; Sarna-Wojcicki, 2000). Grain specific techniques minimise the effects of cross-phase contamination. They are necessary for tephra deposits because a variety of glass compositions, co-genetic phenocrysts and xenocrystic non-glassy contaminants exist within a single deposit. Major element composition of phenocrysts and glassy eruption products reflects the degree of differentiation within the magma. Eruptive products often follow magma evolution trends that relate to specific volcanic centres (Jakobsson, 1979; Meyer *et al.*, 1985) (Fig. 2.4-b). Explosive eruptions in Iceland usually proceed from a Plinian silicic phase to a less explosive, and sometimes effusive, basic phase. The chemical composition of products from some Icelandic volcanic systems, such as Torfajökull and Snæfell (East Iceland), is bi-modal with no intermediate phase represented (Fig. 2.3; Hards, 1985; Stecher *et al.*, 1999). The degree of hydration is not a reliable dating technique despite early efforts to develop this method (*e.g.* Steen-McIntyre, 1977). This is because the volatile content of magmas and the rate of post-depositional hydration processes in different repositories is highly variable.

While EPMA of glass shards is the single most powerful tool for correlation, it is not always effective. Chemical equifinality is the main limitation as major element composition of the products of central volcanoes within a volcanic system is often similar (Larsen *et al.*, 1999). The Hekla eruptions of 1947 and 1510 AD and the silicic tephras of Katla are good examples (Dugmore *et al.* 1996: Larsen *et al.* 2001). Therefore, Larsen *et al.* (1999) suggested adoption of a balanced approach when attempting

discrimination based on major element analysis alone. Accurate phase-specific trace element compositions are complementary and potentially helpful for discrimination (Bond *et al.*, 2001). This is because trace element composition, and rare earth element composition, is controlled by the overall petrogenic history and composition of source magma (Preece *et al.*, 1999). As such, it is useful for securely fingerprinting source volcanoes or individual eruption events within a volcanic system that cannot be separated by EPMA alone (Westgate *et al.*, 1994; Newton, 1999). Grain specific trace element analysis can be undertaken using laser ablation inductively coupled plasma-mass spectrometry (LA-ICP-MS) and secondary ion mass spectrometry (SIMS) ion-microprobe methods (Bourdon, *et al.*, 1994; Newton, 1999) or by conventional ICP-MS techniques, if different tephra fractions can be effectively separated. Very little trace element work of this type has been undertaken on the glass-phase of Icelandic tephra deposits limiting its use as a correlation-dating tool. Nevertheless, in many cases, the major element chemistry of glass shards is diagnostic, allowing Icelandic tephra layers dispersed over a wide area to be correlated and source volcanic systems to be identified (*e.g.* Mangerud *et al.*, 1984; Zielinski *et al.*, 1997; Wastegård *et al.*, 2000a, b).

(b) Palaeomagnetic polarity reversal correlation dating

At certain times during the Quaternary, the polarity of the Earth's magnetic field has been reversed in relation to its current, normal, configuration (Thompson, 1991; Fig. 2.8). Magnetic minerals in volcanic and sedimentary deposits align themselves with the polarity of the magnetic field at the time of their formation or deposition. Palaeomagnetic polarity reversal dating measures this remanent magnetism, and correlates the local polarity record to palaeomagnetic records of 170 potassium-argon dated lavas from around the world (Mankinen and Dairymple, 1979; McDougall, 1979). Oxygen isotope records have also been used to constrain the palaeomagnetic record. These techniques have identified a sequence of epochs, eras, chrons and subchrons that are the basis of the Geomagnetic Polarity Timescale (Fig. 2.8). There are four major polarity epochs in the Pliocene and Pleistocene epochs. These are the reversely magnetised Gilbert epoch 5.41-3.40 Ma, the normal Gauss epoch, 3.40-2.48 Ma, the reversed Matuyamma epoch, 2.48-0.73 Ma, and the normal Bruhnes (current) epoch. Within these epochs are short-lived polarity reversal events, of the order of thousands to tens of thousands of years. The number, length and relative position of these events aids the identification of epochs and improves confidence in suggested correlations.

Polarity measurements do not yield numerical ages. Where possible absolute dating evidence is preferable because a polarity changes can reflect one of several possible epoch boundaries or polarity excursion events and this can lead to erroneous correlation (Easterbrook, 1988) (Fig. 2.7). Evidence for a certain polarity epoch can be easily eroded from the sedimentary record (Johnson and McGee, 1983). There is also the possibility that 'overprinting' by sediments from a later period with a different polarity may have occurred and a significant time lag may have occurred between formation/consolidation and deposition (Aitken, 1998). Nevertheless, if a continuous and undisturbed

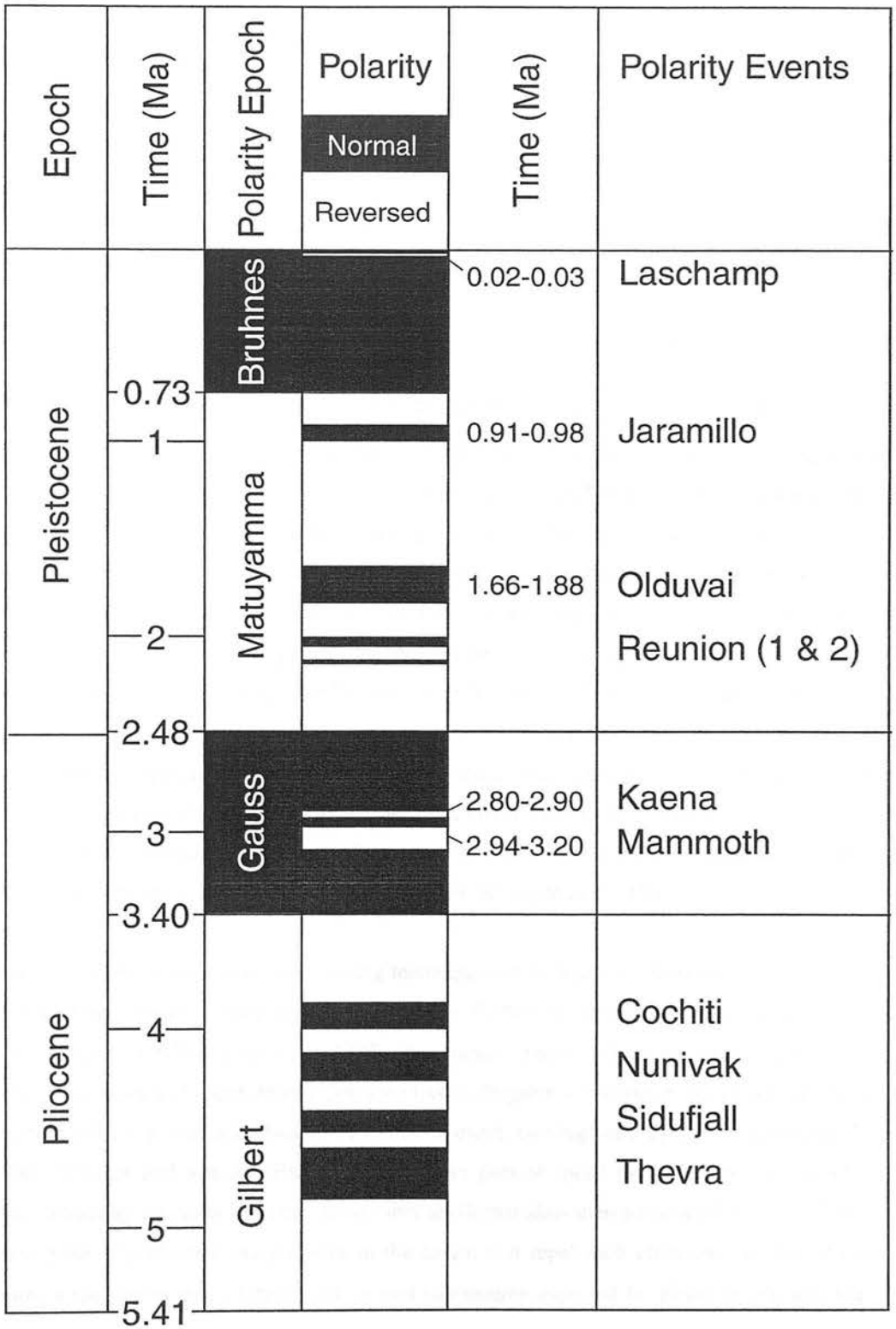


Figure 2.8 The palaeomagnetic timescale for the Pliocene and Pleistocene (drawn from Mankinen and Dalrymple, 1979)

sedimentary or volcanic stratigraphic sequence can be obtained, sampled and analysed palaeomagnetic polarity reversal analysis is a useful correlation dating method.

In summary, to be assigned a correlated-age tephra and/or other sedimentary deposits must share the same diagnostic characteristics as their equivalent at the type-site(s). Several matching criteria are therefore required at distal sites for sound correlation because macroscale features are often similar (Steen-McIntyre, 1977; Thórarinsson, 1980; Hodder *et al.* 1991; Preece *et al.*, 1999; Sarna-Wojcicki, 2000). Closer to the volcanic source, stratigraphic position is often sufficient (Dugmore and Sugden, 1991). Actual 'dates' can be established where historical records exist or tephra deposits have been found in incrementally counted layers of ice cores or varve chronologies (Dugmore, 1989; Smart, 1991a; Grönvold *et al.*, 1995; Noller *et al.*, 2000; Appendix C: Table C2.1). Otherwise, numerical ages need to be obtained from bracketing sediments using ^{14}C and/or luminescence techniques or from phenocryst and/or glass phases within the tephra deposit using radiogenic and/or isotopic techniques.

2.4.2 Tephra Dating Methods II: Radiogenic Fission-track Dating

This section outlines the theoretical basis of fission-track dating introducing aspects that are particularly relevant to dating the volcanic glass-phase. Price and Walker (1963) first used radiation damage tracks (fission-tracks) to date geological events. The most commonly dated phases are zircons, apatites and volcanic glasses. Fission-track dating is a particularly powerful method for dating platey, silicic glass shards since they are often the most abundant and diagnostic eruption-age phase. Moreover, an age from the glass phase alone is guaranteed, because it is a grain specific technique and contaminant grains can be easily avoided when counting tracks (Naeser and Naeser, 1988; Westgate, 1989). Fission-track ages are moderately precise with 1σ errors of 5-10% commonplace (Dumitru, 2000). Standard experimental procedures have been established and followed for the last twenty years by most fission-track laboratories *e.g.* Hurford and Green (1983), Westgate (1989), Hurford (1992; 1999). Technical developments have made accurate fission-track dating of glass-dominated tephras of pre-^{14}C age relatively commonplace (Westgate, 1989; Westgate *et al.*, 1997).

Detailed accounts of the fission-track dating technique can be found in Fleischer *et al.* (1975), Naeser and Naeser and Naeser (1988) and Hurford (1992). Further examples of its applications to volcanic glass are explored in Westgate *et al.* (1997). In summary, fission-tracks are zones of intense damage formed by positively charged, heavily ionising fission fragments of uranium decay passing through an insulating solid, *e.g.* volcanic glass. In each fission event, two high-energy fission fragments fly apart at 180° (Wagner and van den Haute, 1992). These pass at speed through lattice atoms of neutral charge, attracting electrons from the atoms outer shells that slow their passage (Fig. 2.9-a). This leaves narrow zone of positively charged ions in the lattice that repel each other into interstitial positions forming a vacancy or single latent track several nanometres wide and 10-20 μm long (Fleischer *et al.*,

1965; 1975). Fission-tracks do not form in conducting solids because free electrons are attracted to fission fragments leaving the lattice atoms intact.

Uranium has two naturally occurring decay series, ^{238}U and ^{235}U whose parent isotopes are long lived and useful for geological dating (^{238}U: $T_{½}$=4.49 x 10^9 years; ^{235}U: $T_{½}$=7.13 x 10^8 years). ^{235}U is less abundant than ^{238}U comprising only 0.72 atom per cent of natural uranium (Smart, 1991c). Consequently, nearly all natural or spontaneous fission-tracks are formed by the decay of ^{238}U. The method is based on measuring the ratio of spontaneous tracks to laboratory induced tracks. Instead of measuring isotopic abundances directly, radiation damage tracks are used to measure the relative abundance of ^{238}U and ^{235}U. Spontaneous tracks are produced by radioactive fission processes of ^{238}U in the natural environment. Induced tracks are produced artificially by ^{235}U fission processes in the laboratory. Fission-track dating is, therefore, analogous to most other radiometric techniques (Wagner and van den Haute, 1992). The ratio of $^{238}U/^{235}U$ is determined by measuring the density of fission tracks under the microscope after they have been revealed by etching. Track density is a function of the amount of natural uranium present and, for the induced fraction, the neutron dose received in the reactor. The ratio of $^{238}U/^{235}U$ is constant in nature, and, therefore, the fission-track age can be calculated in the following manner:

Eq. 2.1 Fission-track age equation (Price and Walker, 1963)

$$A = \frac{1}{\lambda_D} \ln \left[1 + \frac{\sigma\phi \; g \, I \, \lambda_D \rho_s}{\lambda_F \rho_i} \right]$$

where:

A = *Age in years*
λ_D = Total decay constant for $^{238}U = 1.551 \times 10^{-10} yr^{-1}$ (Jaffey *et al.*, 1971)
λ_F = Decay constant for spontaneous fission of $^{238}U = 7.03 \times 10^{-17} yr^{-1}$ (Roberts *et al.*, 1968)
σ = Cross-section for thermal neutron induced fission of $^{235}U = 580 \times 10^{-24}$ cm^2 (Hanna *et al.*, 1969)
ϕ = *Thermal neutron fluence (neutrons/cm²)*
g =Geometry factor; zircon external detector method = 0.5; glass ITPFT method = 1.0
I = Isotopic ratio $^{235}U/^{238}U = 7.252 \times 10^{-3}$
ρ_s = *Spontaneous track density from ^{238}U (tracks/cm²)*
ρ_i = *Neutron-induced track density from ^{235}U (tracks/cm²)*

Variables in *italics* are determined experimentally.

Inserting all the known variable values above Eq. 2.1 reduces to:

Eq. 2.2 Reduced fission-track dating equation (Price and Walker, 1963)

$$A = 6.45 \times 10^9 \ln \left[1 + \frac{9.28 \times 10^{-18} \phi \; \rho_s}{\rho_i} \right]$$

The only variables that need to be determined to produce fission-track age are the ratio of spontaneous to induced track densities (ρ_s/ρ_i) for the sample and the thermal neutron fluence or flux (ϕ), used to create the artificially induced ^{235}U tracks.

In this study, the neutron flux is calculated using the 'zeta'(ζ) calibration approach (Fleischer and Hart, 1972; Hurford and Green, 1983 for derivations; Naeser and Naeser, 1988). The history, benefits and potential drawbacks of this 'highly effective' technique are explored fully in Hurford (1999; p.30). In summary, the principal advantages are:

- Straightforward determination of the neutron flux.
- Inter-laboratory comparison of ages obtained from different irradiation reactor centres. This has been possible because zeta calibration has been almost exclusively adopted for all mineral and glass fission-track techniques (except population method dating of apatite) since the recommendations of the IUGS Subcommission on Geochronology in 1988 (Hurford, 1999). A glass dosimeter of known age and the muscovite detector that covers it are irradiated at the same time as the glass samples. Track densities are counted for both dosimeter and detector. A 'zeta calibration' factor (Eq. 2.4) is then inserted into a variation of the fission-track age equation (Eq. 2.3).

Eq 2.3 'Zeta' (ζ) calibration fission-track age equation (Hurford and Green, 1983)

$$A = \frac{1}{\lambda_D} \ln \left[1 + \frac{\zeta g \lambda_D \rho_s}{\rho_i} \right]$$

where:
ζ = 'zeta' calibration factor for a given dosimeter, evaluated from standards of known age (A_{std}) as:

Eq 2.4 'Zeta' calibration factor (Hurford and Green, 1983)

$$\zeta = \frac{e^{(\lambda_D A_{std})} - 1}{\lambda_D (\rho_s/\rho_i)_{std} \, g \, \rho_d}$$

where:
ρ_d = fission-track density in the muscovite detector covering the glass dosimeter (tracks/cm^2)

Successful glass fission-track dating depends on the following factors:

1) Thick platey glass shards are required to maximise the surface area for track formation.
2) Pumiceous ash deposits are not suitable because the glass surface area for track formation is substantially reduced.

3) Uranium content of glass. The uranium content of the deposit determines the lower age limit of fission-track analysis. More spontaneous tracks form in glass with a higher uranium content. The glass phase of basaltic tephras is more difficult to date than silicic deposits because the uranium content of basaltic glass is *ca.* 0.1 ppm compared to. 2-20 ppm for silicic glass. Reliable fission-track ages as young as 60-70 ka have been produced from silicic glass with uranium contents of 4-6 ppm (Chesner *et al.*, 1991). Obtaining ages less than 100 ka is dependent on elevated uranium levels and is extremely time consuming taking approximately 6-12 months per sample (Kohn, 1979). Deposits <100 ka must have a high uranium content (*e.g.* >5-6 ppm) to form a statistically significant number of spontaneous tracks (Westgate and Naeser, 1995). In practice, this places an absolute minimum age limit of *ca.* 50 ka for feasible glass-track counting over laboratory time scales.
4) Tracks must be retained once formed and not subject to post-depositional thermal annealing (see below).

All deposits that have experienced post-depositional heating in the environment are likely to exhibit partial or complete loss of spontaneous tracks (fading) by a recyrstallisation process called 'partial track annealing'. Total track annealing removes all tracks and resets the fission-track clock to zero (Dumitru, 2000). Some tracks formed in the glass will have been erased at ambient temperatures (Fleischer and Price, 1964; Fleischer *et al.*, 1965; Naeser *et al.*, 1980; Sandhu *et al.*, 1999). Glass samples with a higher SiO_2 / Al_2O_3 content are more resistant to thermal annealing than those with a low silica content; hence silicic tephra deposits are favoured in fission-track analysis (Sandhu, *et al.*, 1993; Sandhu *et al.*, 1999). Even so, without some kind of stepwise heating or isothermal correction, partial track annealing can cause significant age underestimates (Fig. 2.9-b; Naeser *et al.*, 1980). Consequently, fission-track ages obtained from volcanic glass are often considered to be minimum estimates (Naeser and Naeser, 1988).

Step-heating and isothermal plateau fission-track (ITPFT) procedures were introduced and modified during the 1980s (Table 2.3) (Naeser *et al.*, 1980; Westgate, 1988; 1989). The latter is now firmly established and is a straightforward method. ITPFT and diameter corrected fission-track (DCFT) methods are two independent fading correction techniques currently and widely used in fission-track dating of volcanic glass (Westgate *et al.*, 1997). The ITPFT method incorporates a single thermal pre-treatment of 30 days at 150°C, applied to the spontaneous and induced sample splits after irradiation, to correct for partial fading of fission tracks. It can be applied to tephra beds whose glass shards are larger than 125μm (Burchart *et al.*, 1975; Westgate, 1989; Sandhu *et al.*, 1993). The isothermal plateau is recognised and the effects of fading fully corrected for when track size distributions for spontaneous and induced tracks are concordant (Miller and Wagner, 1981; Sandhu *et al.*, 1993; Shane *et al*, 1995). The DCFT method uses the mean diameter of the spontaneous and induced tracks to

correct for the track-fading effect and can be used for tephra beds whose glass shards are as small as 80μm (Storzer and Wagner, 1969; Sandhu and Westgate, 1995).

The ITPFT method has consistently produced accurate age estimates from volcanic glasses that have experienced a simple thermal history (Naeser *et al.*, 1980; Westgate and Briggs, 1980; Sandhu *et al.*, 1993; Sandhu and Westgate, 1995; Westgate *et al.*, 1997) (Fig 2.9; Table 2.5). If zircon phenocrysts are also present within the tephra deposit, glass ITPFT and isotopic ages can be independently checked. This is desirable because tracks formed in zircon do not anneal at ambient environmental temperatures. Furthermore, single grain dating can be undertaken because zircon grains have uranium concentrations that are an order of magnitude greater than silicic volcanic glass. Many examples of similar glass-ITPFT ages and co-genetic zircon phenocryst fission-track (ZPFT) ages exist (Sandhu *et al.*, 1993; Westgate *et al.*, 1997; Pillans *et al.*, 1996). ITPFT has consistently produced glass fission-track ages that are concordant with those obtained from other co-genetic phases, such as zircon (Pillans *et al.*, 1996). Co-genetic zircon phenocrysts are not always present in all tephra deposits and zircon-phases can also represent non-eruption ages if tracks on xenocrystic or contaminant grains are counted.

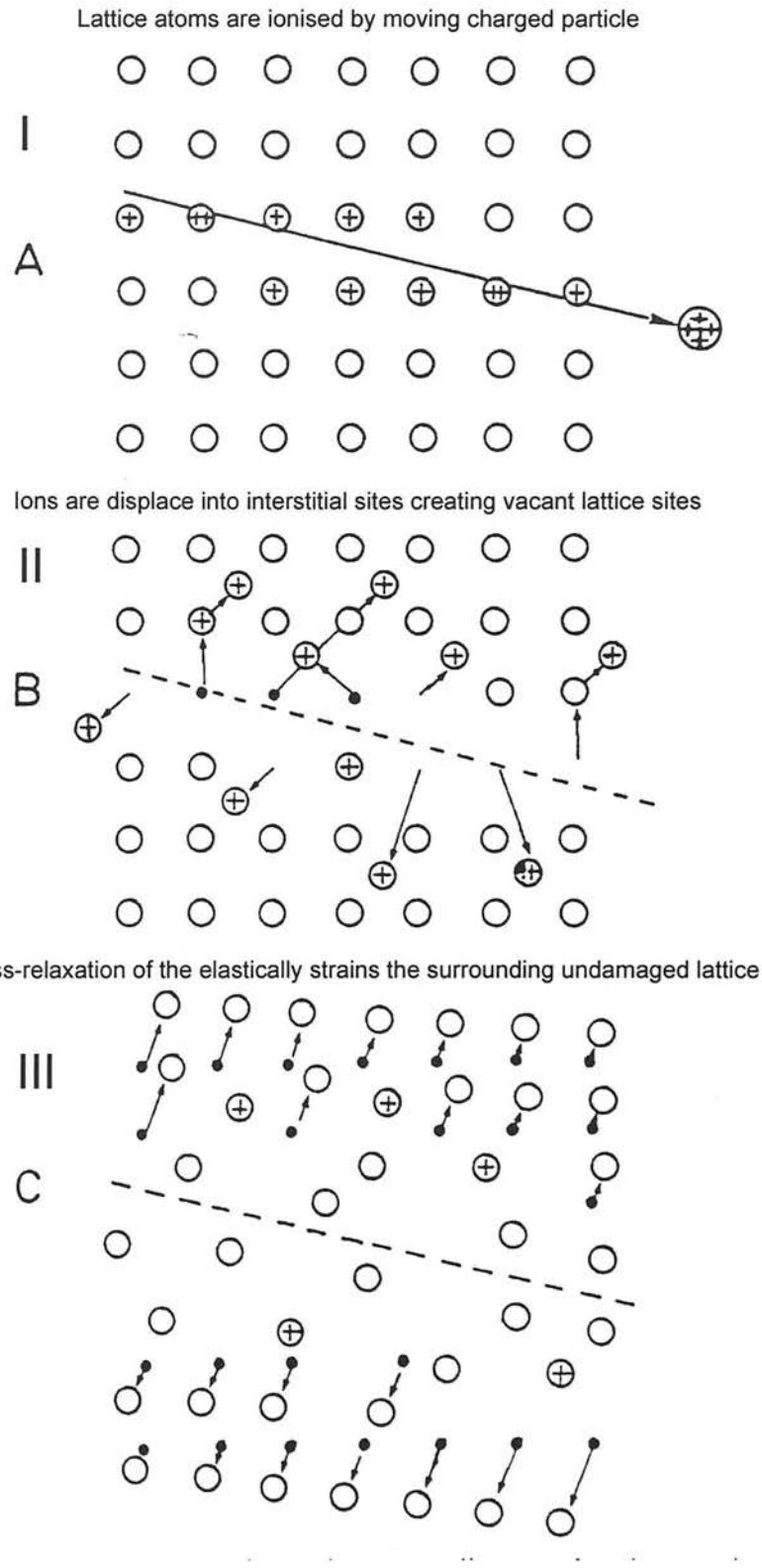


Figure 2.9 (a) The three stage 'ion-explosion spike' model for the production of fission-tracks in covalent solids (adapted from Wagner & van den Haute, 1992; after Fleischer *et al.*, 1975).

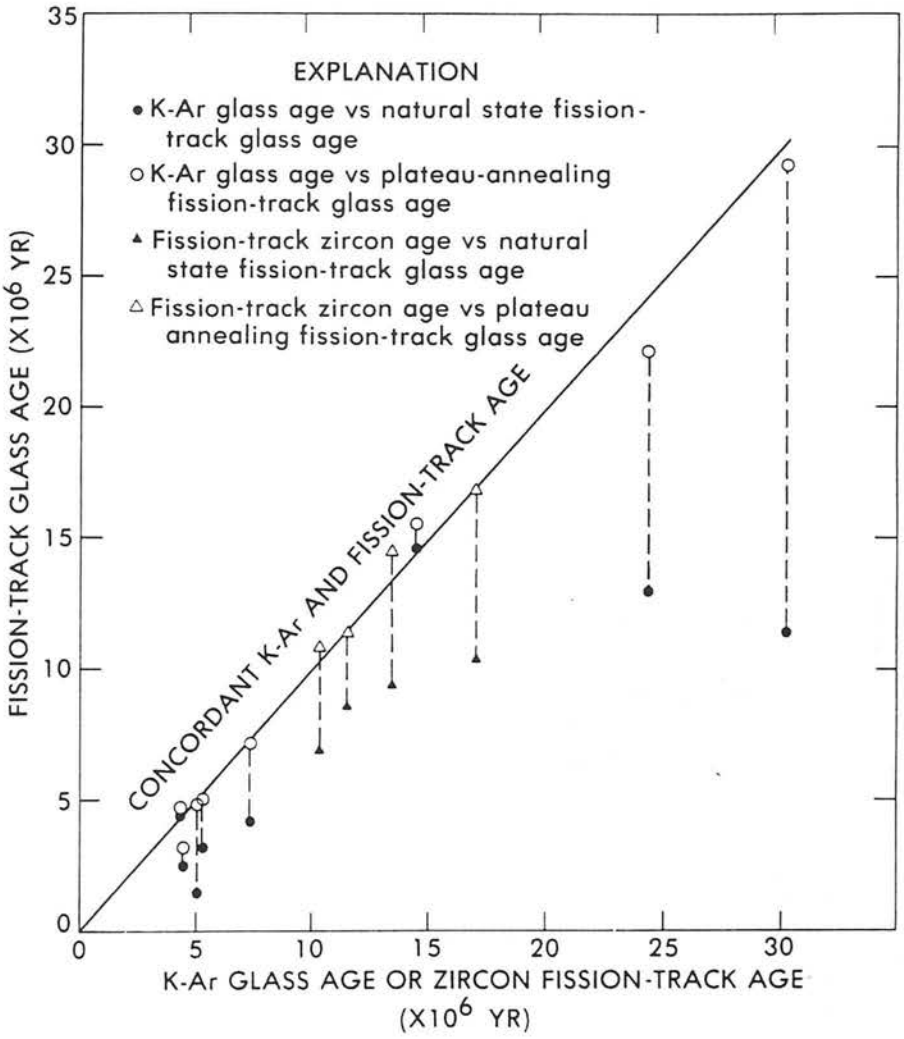


Figure 2.9 (b) Diagram illustrating the benefits of thermal plateau correction techniques (from Naeser and Naeser, 1988).

Table 5.1. Glass ITPFT Age Estimates of Some Quaternary Tephra Beds (Uncorrected Ages Also Given)[a]

Sample name	Days heated at 150°C	Etching conditions HF: (%)	Temp.: (°C)	Time (s)	Spontaneous track density ($x10^2$ t/cm^2)	Induced track density ($x10^4$ t/cm^2)	Neutron fluence ($x10^{15}$ n/cm^2)	D_s / D_i	Age±1σ (Ma)	References
Toba tephra (UT778)	30	26	21.0	145	0.79(50)	26.8(19976)	3.84(14021)	1.07	0.07±0.01	Chesner *et al.* (1991)
Old Crow tephra (UT613)	0	24	20.5	65	1.47(61)	11.25(7000)	1.88(6871)	0.83	0.15±0.02	Westgate *et al.* (1990)
	30	24	23.0	82	0.85(36)	6.62(3748)	1.88(6871)	1.00	0.15±0.02	
Mamaku Ignimbrite (UT1168)	0	25	25.0	90	1.81(57)	19.1(14048)	3.55(16798)	0.86	0.20±0.03	Shane *et al.* (1994)
	30	25	25.0	160	1.59(106)	14.7(11492)	3.55(16798)	1.00	0.23±0.02	
Rockland tephra (RPT(L)15)	30	26	23.6	140	5.60(32)	24.60(10336)	3.45(53493)	0.98	0.47±0.08	Alloway *et al.*(1992)
Ester Ash Bed (UA743)	0	25	21.5	60	3.95(41)	14.55(3244)	3.96(12363)	0.83	0.64±0.10	Westgate *et al.*(1990)
	15	25	22.0	60	3.36(18)	9.59(1902)	3.94(7317)	1.04	0.83±0.20	
	30	25	23.0	50	3.07(21)	9.25(4355)	3.96(12363)	0.98	0.79±0.17	
Lake Tapps tephra (UT462)	0	24	23.0	55	6.53(68)	12.20(5340)	2.02(5720)	0.76	0.65±0.08	Westgate *et al.* (1987)
	30	24	23.0	105	5.08(104)	5.43(2482)	1.89(6871)	0.95	1.06±0.11	
Fort Selkirk tephra (UT82)	0	24	23.0	55	6.33(120)	12.05(7877)	3.79(16842)	0.81	1.19±0.11	Westgate (1989)
	30	24	23.0	105	5.29(32)	8.38(1382)	3.79(16842)	1.09	1.43±0.26	
Pakihikura tephra (BP-303)	0	26	20.0	100	7.11(50)	12.40(3189)	3.42(32050)	0.77	1.17±0.17	Alloway *et al.*(1993)
	15	26	22.0	115	6.81(104)	9.36(3718)	3.42(32050)	0.95	1.49±0.15	
	30	26	22.0	135	5.11(123)	6.41(2804)	3.42(32050)	0.98	1.63±0.15	
Borchers Ash (UA598)	0	26	23.0	55	22.83(301)	28.58(4550)	2.42(9617)	0.78	1.16±0.07	Westgate (1989)
	30	26	23.5	120	20.59(164)	12.46(5924)	2.07(14935)	1.01	2.04±0.16	

[a]Thermal neutron fluence is determined from calibrated muscovite detector covering glass dosimeter (NBS SRM 962:37.38±0.08 ppm) placed at top and bottom of irradiated can. Samples are irradiated at McMaster Nuclear Reactor,Centre, McMaster University, Hamilton, Ontario, Canada. Results on the internal standard (Moldavite tektite glass) compare well with the $^{40}Ar/^{39}Ar$ plateau age of 15.21±0.15 Ma (Staudacher et al.,1982); the weighted mean fission-track age as determined at the University of Toronto is 15.1±0.3 Ma based on eight determinations. Number of tracks counted is indicated in parentheses and error (±1σ) is calculated by combining the Poisson errors in the spontaneous and induced track counts and on the counts in the detector covering the dosimeter. D_s is mean spontaneous track diameter and D_i is mean induced track diameter. See text for information on age estimates of these tephra beds using other methods.

Table 2.3 Example of typical fission-track output values and format of data presentation (from Westgate *et al*, 1997).

2.4.3 Tephra Dating Methods III: Radiogenic Luminescence Dating

'The luminescence techniques are increasingly being incorporated into a wide range of geomorphological studies which seek to establish the nature of landscape changes over the past interglacial-glacial cycle and beyond.'

Stokes (1999, p. 153)

This section outlines the theoretical basis of luminescence dating and describes techniques used to obtain the first luminescence ages from Icelandic tephra deposits.

(a) Experimental theory

Since it was first suggested by Daniels *et al.* (1953), time-dependent luminescence signals produced from ionic crystals, minerals[15] and other types of insulators[16] have been used to date archaeological artefacts, volcanic and non-volcanic sediments, glacial sediments, lavas, obsidians and even meteorite falls, *e.g.* Bettinali and Ferraresso (1968), Singhvi, *et al.* (1982) Sanderson, *et al.* (1983), McKeever (1983), Rendell *et al.* (1985), Berger (1992), Berger and Eyles (1994), Murray (1996), Prescott and Robertson (1997). Several techniques and procedures have been developed to date samples collected from a variety of environmental contexts (Aitken, 1985; 1998; McKeever, 1985; Huntley *et al.*, 1985; Berger, 1988a, b; 1995; Duller, 1991; Wintle, 1973; 1991; 1997; Murray, 1996). A summary table of recent techniques and their application can be found in Berger (1995, p. 96-97). The most commonly dated phases are quartz and feldspar, abundant minerals found in most geological settings. Luminescence ages are moderately precise with 1σ errors of 10-15 % commonplace (Forman *et al.*, 2000).

Most samples that exhibit luminescence phenomena will produce some sort of luminescence age. The best way to determine whether ages are accurate is by comparison with independent ages and calibration of laboratory methods with well-established criteria (Clarke *et al.*, 1999). Some luminescence ages from sediments in the pre-^{14}C, mid-late Pleistocene era have been regarded with suspicion because of the lack of independent dating control available (Gibbons, 1997). Tephra deposits are advantageous, in this respect, because independent dating techniques can be applied to several different phases. This provides an opportunity to develop existing luminescence procedures.

Luminescent minerals and solids that been exposed to alpha, beta or gamma radiation accumulate a luminescence signal that is proportional to the amount of radiation exposure. This signal is directly proportional to the time of exposure since the last zeroing event. If the palaeodose dose (P) can be accurately determined by forming a dose-dependent growth curve from TL signal measurements, and a dose rate can be evaluated from field and laboratory measurement, a luminescence age can be calculated (Eq. 2.5, 2.6). The dose rate represents the rate at which energy is absorbed from the flux of

[15] For example quartz and feldspar

nuclear radiation and several parameters have to be measured (Aitken, 1998). The dose rate can be determined from chemical analysis of the principle radioactive elements K, U, Th, Rb (Bell, 1979) and/or from *in-situ* spectrometry measurements in the field and additional other spectrometry measurements in the laboratory. Some parameters, such as palaeo-water content, need to be estimated. This alone places a major constraint on the precision of luminescence techniques, currently at best about 5% for the most favourable circumstances, but usually between 10-20 % (Forman *et al.*, 2000).

Eq. 2.5 The luminescence dating equation (Aitken, 1985)

$$\text{Age (yrs)} = \frac{\text{Palaeodose (P)}}{\text{Total Dose Rate } (D_T)} \quad \frac{\text{(Gy)}}{\text{(Gya}^{-1}\text{)}}$$

Eq. 2.6 Relationship between palaeodose (P) and equivalent dose (ED) (Aitken, 1985)

$$P = ED + I \quad \text{(Gy)}$$

where: ED = equivalent dose (Gy)
I = sub / supralinearity growth correction (Gy)

Thermoluminescence (TL), Optically-stimulated Luminescence (OSL), Infra-Red-stimulated Luminescence (IRSL) and Photo-stimulated Luminescence (PSL) dating techniques are based on the accumulation of free electrons at 'trapping' sites within the lattice of certain ionic crystals and amorphous solids (Fig. 2.10). Free electrons are produced in abundance during radioactive decay processes in the natural environment. They are attracted to 'electron traps', such as impurity atoms or lattice defects, formed during crystallisation from the melt. When heated or exposed to light, these electrons are ejected from the traps. They then recombine at other lattice defects known as luminescence centres. This 'recombination' process is defined as the 'zeroing event' and results in the emission of a large number of photons and a measurable light signal (Wintle, 1991). The amount of light emitted is dependent on the TL sensitivity of each mineral and the time since the last zeroing event. Sensitivity is defined as the TL signal produced per unit radiation dose. Radiation dose is expressed in Grays (Gy) (Aitken, 1985).

Light and heat sensitive 'trap types' exist within quartz and feldspars and other luminescent solids. Uncertainty over which trap types were responsible for the TL signal in these phases led to the development of the OSL dating method for unheated sediments (Huntley *et al.*, 1985). In OSL dating only luminescence from light sensitive traps is measured. Only one or two electrons can be accommodated at each trapping site, but it takes many to fill all the traps of one type (Aitken, 1998). When all trap types are filled in storage the luminescence of a particular sample is said to have reached 'saturation'. The time taken to reach the first major phase of saturation traditionally

[16] For example covalent solids and glasses

determines the upper age limit of luminescence dating and this varies significantly between mineral phases in different environments on a sample-by-sample basis (Aitken, 1985; Berger, 1988; Huntley *et al.*, 1994; Prescott and Robertson, 1997). Signal saturation is controlled by the quantity of radiation damage that the material can accommodate and the rate at which damage accumulates (Wintle, 1991; Stokes, 1997). The rate at which damage accumulates is dependent on the concentration of radioactive elements (principally K, U and Th) in the surrounding matrix. Dates up to 800 ka have been obtained from feldspars in low dose rate environments (Berger, *et al.*, 1992; Berger, 1994). For single growth to saturation level the growth curve is best fitted using a saturating exponential regression curve (*e.g.* Fig. 2.13), although a saturating-plus-linear regression curve fit is thought to be more suitable for samples near or beyond saturation (Berger, 1990; Wintle, 1997; Huntley and Prescott, 2001). The minimum age range is determined by the degree to which the luminescence signal has been reset, the sample's sensitivity to ionising radiation, charge reorganisation effects that might have occurred during deposition, laboratory pre-treatment procedures and the luminescence technique employed (Stokes, 1997). Currently, the minimum TL age obtainable from all phases of a well-bleached deposit is 1000-2000 years (Wintle, 1997), but advances in single-aliquot and single grain dating techniques are progressively reducing this lower limit. Limitations of the luminescence method are explored in further detail in sections dealing with dose rate and palaeodose evaluation.

Thermoluminescence can be produced in the laboratory and the amount of light emitted measured using the set up illustrated in Figure 2.11. Samples are heated from 0-400° C at a constant rate (*e.g.* 5° $Csec^{-1}$), producing a 'glow curve'. The glow curve for each given electron trap-type is a single peak about 40-50° C in width. The maximum glow-peak temperature (T_{max}) primarily reflects the energy level depth below the conduction band of the trap-type from which eviction has occurred, but is also dependent on the heating rate (Fig. 2.10) (Aitken, 1985). Aitken (1985; p. 41-53 & p. 269-273) provides a more detailed description of the relationship between temperature, T_{max}, electron escape and trap depth summarised in Table 2.4.

Figure 2.10 Simplified 'electron-hole' energy-level representation of luminescence production in a semi-conducting crystalline solid. The production mechanism for luminescence is not fully understood and different mineral and glasses have different mechanisms (Aitken, 1999). A generalised model of current theories is presented below: All luminescence dating techniques are based on the accumulation of trapped electrons from radioactive decay processes in the natural environment (Wintle, 1991). Luminescent materials, such as covalent solids, glasses and ionic crystals, have 'defects' in their otherwise perfectly ordered lattice structure of negative and positive ions. Defects are created by impurity atoms, radiation damage and, for volcanic glasses, rapid cooling from a molten state during formation. They can be positively charged negative-ion vacancy sites or substitutional impurity centres that act as meta-stable trapping sites (traps) for electrons and 'holes'. Traps exist within the 'forbidden energy gap' between the lowest (valence band) and highest (conduction band) energy configuration. Holes can be thought of as atoms from which an electron has been detached during ionisation and in effect they are carriers of positive charge that can diffuse freely within the valence band by gaining an electrons from a neighbouring atom. In some materials they are responsible for the storage of latent luminescence. For simplicity, electrons are the trapped charge carriers in the model below (Aitken, 1985).

(A) Irradiation: Under normal conditions atoms reside within crystalline lattice structures in the lowest possible energy configuration. All electrons are attached to their parent nuclei within the valence band (Duller, 1996). The ionising effects of nuclear radiation provides energy in the form of lattice vibration. This allows electrons to detach themselves from their parent nuclei and escape from the valence band to an 'excited', higher energy state in the conduction band (1-2). In effect, this creates positively charged holes in the valence band (1).

(B) Trapping & Storage: After electron eviction, the energy configuration of the system will be in an unsteady state for an instant. Evicted electrons attempting to return to a lower energy state to restore equilibrium have two possible options. Firstly they can recombine with the holes in the valence band releasing energy acquired from the radiation source and no radiative luminescence production will occur (2-3-4). Alternatively, electrons returning from the higher energy configuration state might become trapped at a positively charged 'electron trapping' sites (2-5-6). An overall gain in energy within the system would occur if evicted electrons did not return to their lowest energy state. Equilibrium is maintained when positively charged holes are attracted to 'hole trapping' sites situated at a characteristic energy levels (E_h) above the valance band (1-7-8). Radioactive decay is an ongoing process and electrons and holes continually accumulate in traps until all available trapping sites become full or 'saturated'.

(C) Heating: The lifetime of electrons in traps is determined by the traps' energy depth level below the conduction band (E_e). Electron eviction occurs at temperatures or after exposure to light of a certain wavelength that reflects this depth. Electrons can escape from 'shallow' energy traps at ambient temperatures in the environment and the lifetime of such traps is short and of little use in geological dating. Luminescence dating utilises electrons evicted from stable 'deep traps' with lifetimes of the order of millions of years. Electrons remain in deep traps until a significant input of non-ionising energy raises the overall energy of the system above its ambient state. Exposure to temperatures or light of certain wavelength in the environment (zeroing event) or during luminescence dating experiments in the laboratory is sufficient to evict electrons from deep traps back into the conduction band (9-10). This process is known as bleaching and can take the form of, for example, kiln firing for pottery or light exposure during aeolian transport for loess and dune sands. In the case of volcanic glass the zero event being dated is its formation from the magmatic melt. Once evicted some electrons recombine at non-luminescent or 'killer' centres where no light is emitted and excess energy is dissipated as heat or at even 'deeper' non-radiative energy traps that retain the electron in the lattice. Other electrons recombine at luminescence centres (11), a particular type of defect usually created by impurities in the lattice (*e.g.* silver, Ag^{2+} or manganese, Mn^{2+} ions). Photon energy is released from the lattice during recombination (or re-trapping) producing a measurable 'luminescence signal' (12). The wavelength of light emitted is characteristic of the impurity (*e.g.* Ag = blue/violet, Mn = orange) (Aitken, 1985). Thermoluminescence is measured by heating the sample at a constant rate using the set up illustrated in Figure 3.9. The intensity of the luminescence signal forms the basis for luminescence dating because it is proportional to the amount of nuclear radiation since the last zeroing event. Therefore, if the radiation dose rate can be measured accurately the time elapsed since the last zeroing event can be determined.

Diagram and text adapted from Aitken (1985; 1998), McKeever (1985), Gibbons (1997), and Duller (1996)

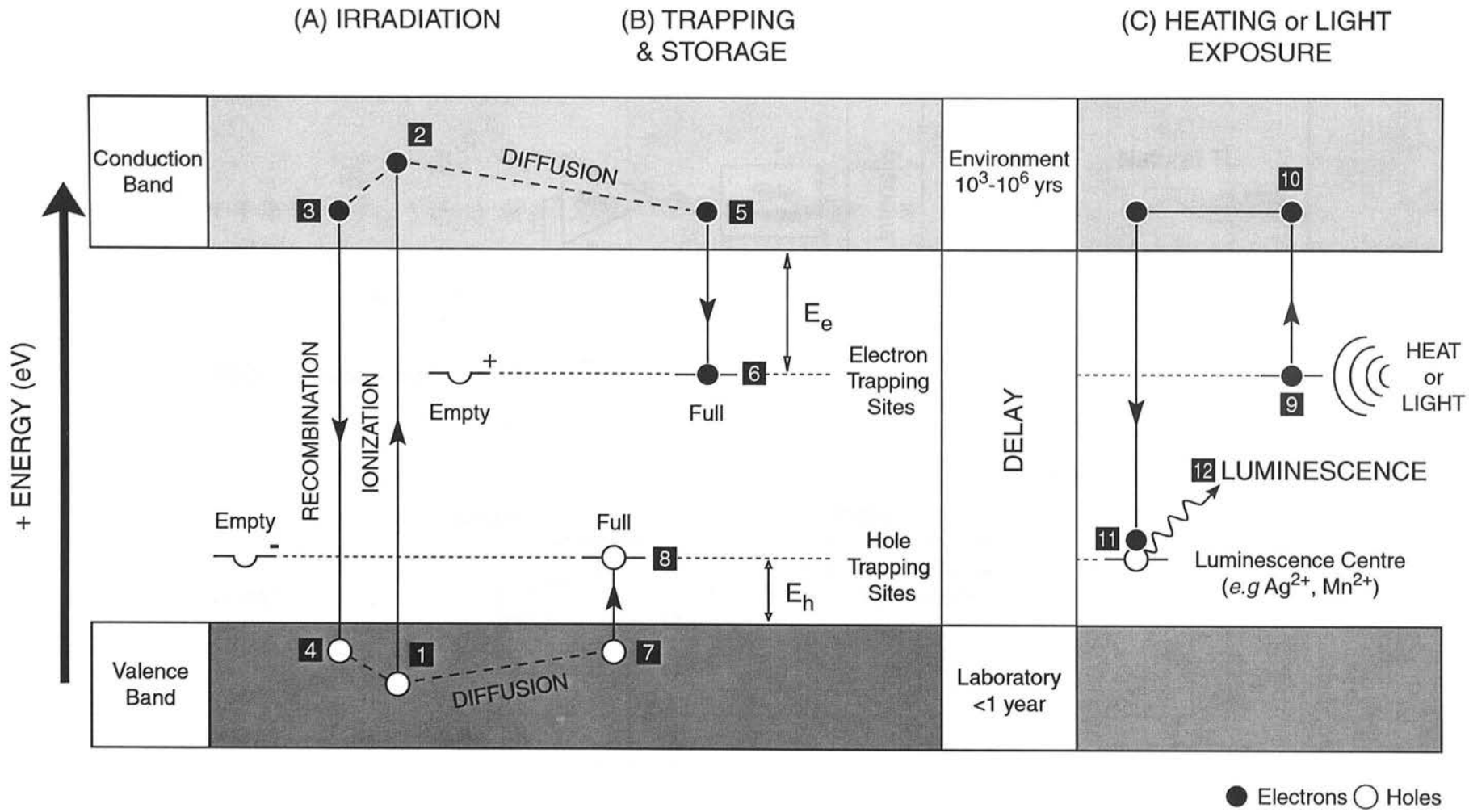


Figure 2.10 Simplified electron-hole energy-level representation of luminescence production in a semi-conducting crystalline solid

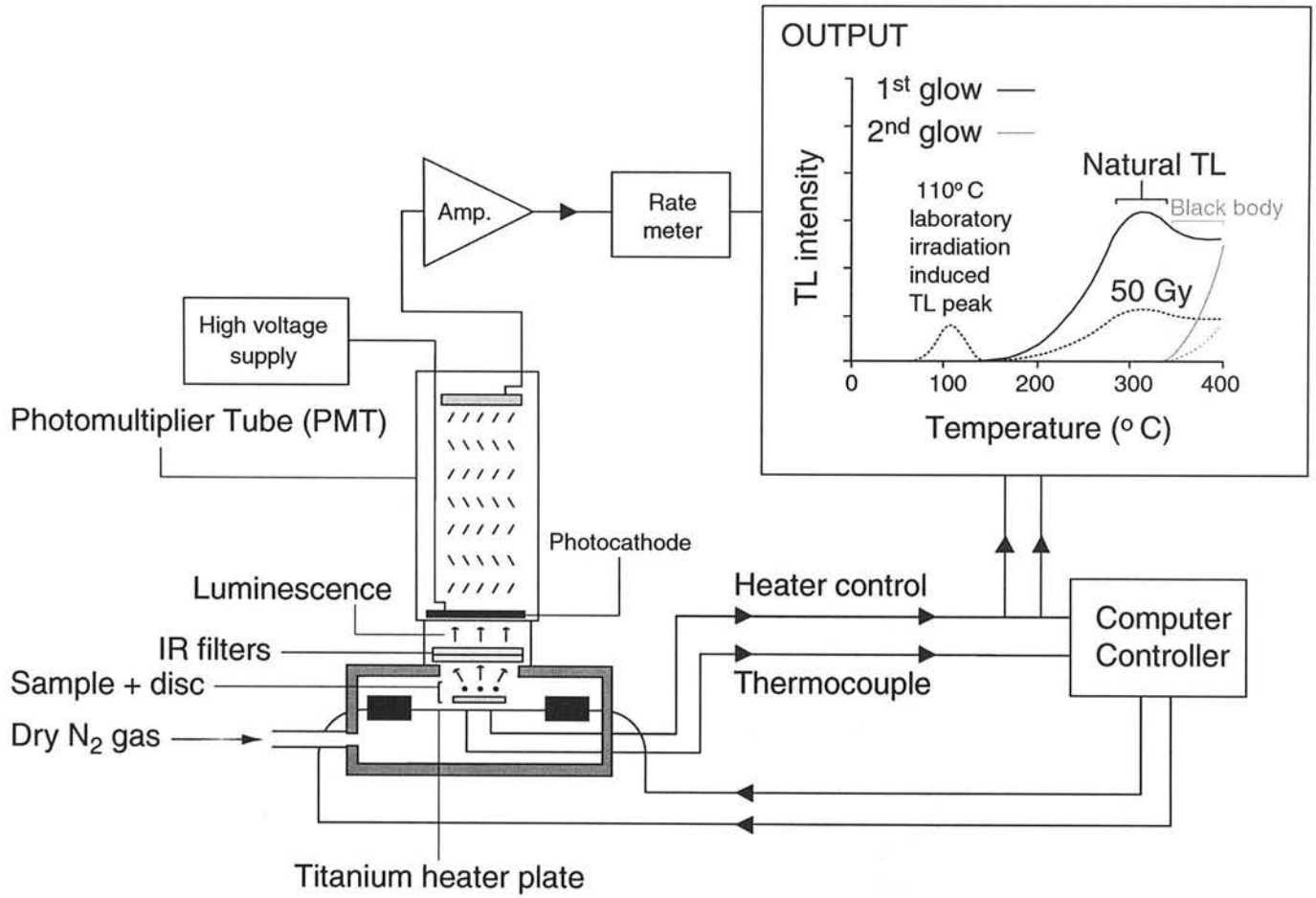


Figure 2.11 SURRC thermoluminescence reader apparatus set-up and typical output from glassy tephra. Diagram drawn and adapted from information and diagrams in Aitken (1985), Ward (1988) and Stokes (1997).

PHASE		QUARTZ		FELDSPAR	
Thermal stability	**Peak temp (T_{max}: °C)**	**Trap lifetime (years)**	**Trap depth (eV)**	**Trap lifetime (years)**	**Trap depth (eV)**
Low	< 100	0.13×10^{-3}	< 0.85	0.16×10^{-3}	0.76
	110	$0.8\text{-}1.2 \times 10^{-3}$	0.98	43×10^{-3}	1.10
Intermediate	190-250	$0.7\text{-}340 \times 10^{3}$	1.42-1.79	3.6×10^{3}	1.40
High	280-400	100×10^{6} - > 10^{8}	1.66-1.69	0.4×10^{6} - 9.2×10^{9}	1.60-1.68

Table 2.4 Relationship between natural trap residence time and TL glow curve peak temperature at ambient temperatures (10-15°C) in the natural environment. The lifetime of an electron in a trap is finite and is determined by the its 'energy depth' below the conduction band (Fig. 2.10). For luminescence dating, electrons evicted from traps in the 250-450°C peak temperature range of the glow curve (~1.5-1.7 eV below the conduction band) are of most interest because they represent a thermally stable reservoir of trapped electrons that do not escape spontaneously at normal temperatures for thousands to millions of years (Fig. 2.10). Correspondingly, the TL signal dissipates rapidly from 'shallow' traps with eviction temperatures around or below the 100° C peak temperature range of the glow curve. Trapped electrons here have short residence lifetimes of approximately 1 hour and the TL signal in this region of the glow curve is highly unstable and not suitable for TL dating. The 110°C peak occurs naturally in quartz and can be induced in all phases when they are subjected to laboratory irradiation. Data from Aitken (1985) and Wintle (1997).

(b) Dateable phases

Crystalline silicates, such as quartz and feldspar are the principal phases used in luminescence dating. Quartz has a well-ordered atomic structure. Complete crystals consist of a rigid, three-dimensional array of SiO_4 tetrahedra linked at each of its four corners (Guinier, 1984). Feldspars are aluminosilicates and crystals form when Al^{3+} ions are substituted for some of the Si^{4+} ions in the silicate framework. The resulting negative charge is balanced by cations such as Na^+, K^+, Ca^{2+}. Luminescence techniques have been successfully applied to quartz and feldspars phenocrysts of pyroclastic material (Takamiya and Nishimura, 1986; Mailler *et al.*, 1992; Spencer, 1999; Chen *et al.*, 1999; Li and Yin, 1999; Berger and Neill, 1999; Bonde *et al*, 2000; Li & Yin, 2000; Sanzelle *et al.*, 2001). Where they are present in sufficient quantities and phenocrystic nature can be firmly established, quartz phenocrysts are preferred because the accuracy of luminescence ages obtained from volcanic feldspars can be compromised by a process called 'anomalous fading' (Wintle, 1973). No luminescence studies on Icelandic tephra deposits have been published. Coarse-grained quartz phenocrysts are uncommon in Iceland tephra and in Icelandic rocks in general.

Non-crystalline, or 'amorphous' materials, such as glass are disordered. No crystals are present and their macroscale atomic structure is effectively the same as the corresponding liquid (melt) from which they crystallised (Guinier, 1984). Luminescence dating of volcanic glass remains a highly experimental, but potentially effective technique. Little is known about the origin of the volcanic glass-host luminescence signal (Berger and Huntley, 1983; Berger, 1991; Horn *et al.*, 1993: Piriou, 1999). Attempts have been made to correlate glass-host luminescence emissions to macroscale physical and chemical properties of man-made and volcanic glass shards. Such studies have been largely unsuccessful (Sanderson, 1982; Muller and Schvoerver, 1990; Berger *et al.*, 1999); but recently Chiavari *et al.* (2000, p. 971) suggested that highest TL sensitivity of ancient mosaic glass *tesserae* 'is shown by glasses with the lowest K_2O content'.

The luminescence production mechanism is still not fully understood for ordered ionic silicates, such as quartz and feldspar. It is thought to be more complex in glassy materials because they are vitreous polymorphs that lack a long-range periodic lattice structure (Sanderson *et al.*, 1983). In addition, glasses are known to have poor long-range charge transport and therefore a low TL sensitivity and a high dose saturation level compared to feldspar or quartz (Ward, 1988). Theoretical glasses are continuously homogenous materials and, as such, are isotropic[17]. Nevertheless, structural order in glasses is not completely random and most have some degree of short-medium range order. Synthetic glasses are doped with certain elements and volcanic glasses contain impurities that can act as luminescence trapping sites (Elliott, 1998). Moreover, atomic movement in amorphous solids is similar to that in crystalline solids, occurring around fixed 'sites' that vibrate continuously while

[17] All directions in an isotropic structure are the same

remaining encaged in a small volume around a fixed point (Guinier, 1984). Consequently, glass-host luminescence phenomena have been observed (Sanderson 1982; Muller and Schvoerver, 1990; Kiyak *et al.*, 1999; Chiavari *et al.*, 2000) and artificial glasses are considered reliable dosimeters and archaeological glasses potentially excellent chronometers (Ward, 1988; Chiavari *et al.*, 2000). For example, Kiyak *et al.* (1999) observed that irradiated samples of commercial glass had dose dependent signals at around 300°C and that the dose response profile grew in a linear manner between 0.5-6 kGy. These results are similar to the work of Ward (1988) who suggested that the dose response profiles of commercial glass are characterised by near linear growth after the first major phase of saturation at *ca.* 10 kGy.

Berger (1988), Wintle (1991), Berger and Huntley (1994) suggested that volcanic glass-based luminescence dating holds much potential provided rigorous purification and well-controlled analytical procedures are established. Further, Berger and Huntley (1983; p. 581) stated that volcanic glass shards are an 'extremely attractive TL sediment clock' for the '30-200 ka time window that is not adequately covered by other dating techniques' such as ^{14}C, ^{40}K-^{40}Ar, ^{40}Ar-^{39}Ar and fission-track. This is principally because the 'zero-event' being dated is the formation of the glass from the melt. As such, the zeroing process is well defined and, unlike other soft sediments, likely to be complete (Berger and Huntley, 1983). Thermoluminescence ages from the purified volcanic glass fraction of tephra deposits in North America have, in some cases, been comparable to those obtained by other dating methods. Berger (1991, 1992) and Berger *et al.* (1996) regarded the fine-grained 4/5-11 μm glass fraction the most desirable for TL dating because, following a series of cleaning and purification processes, this fraction should contain pure glass. Others have questioned the ability to produce 'pure' fine-grained fractions using density separation techniques (Zander *et al.*, 2000). Microphenocrysts or microlites, that could complicate dose rate calculations or produce spurious luminescence signals, could be present in coarser fractions (Berger, 1992). However, both are not always present in all platey silicic glass shards (Newton, 1999) and rarely encountered in platey silicic shards used in glass fission-track dating (Naeser and Naeser, 1988). Where the tephra deposit is glass-rich, microphenocryst and microlite-poor and mineral inclusions absent from the shard matrix, the purified coarse glass fraction (*i.e.* > 100 μm) might be a good TL chronometer. This is principally because detrital feldspar contamination can be identified optically, by SEM analysis and SEM-EDS[18] chemical mapping of discs used in TL analysis (cf. Welton, 1984). The luminescence sensitivity of all potential contaminants is, in most cases, greater than glass resulting in abnormally high luminescence signals and glow curves with different shapes and/or multiple peaks.

Volcanogenic feldspars are particularly susceptible to anomalous fading, a process that can lead to gross age underestimates. This phenomenon was first identified by Wintle (1973) when attempting to date Icelandic lava flows using the thermoluminescence techniques. The luminescence sensitivity of

glass is at least an order of magnitude smaller than that of many other luminescent minerals such as quartz or feldspar (Sanderson, 1982; Sanderson, *et al.*, 1983; Ward, 1988; Berger *et al.*, 1996). Older, pre-Holocene volcanic glass might have a luminescence signal if accessible deposits of sufficient quantity can be found to produce purified glass fractions. Luminescence dating of glassy material requires careful consideration of many factors and new experimental techniques were developed to overcome some unique problems encountered.

(c) Aspects of Dose Rate Evaluation

Of the two main parameters that need to be evaluated to obtain a luminescence age, the total dose rate is the most 'tractable' (Berger, 1995). This is because most of the parameters that contribute to the total environmental radiation dose can be can be measured accurately and by cross-checking methods. That said, where water content history cannot be accurately constrained, dose rates are often a major cause of age uncertainty and imprecision. When calculating the dose rate received by buried sediments, it is assumed that the overall rate of energy absorption is equal to the rate of energy emission, the infinite-matrix assumption (Fig. 2.12) (Aitken, 1985, 1998). Several parameters need to be measured or estimated to calculate the overall dose rate for buried sediment. The total dose rate can be expressed in terms of the contribution from its constituent parts (Eq. 2.6) and can be determined in two ways:

(i) Elemental measurement approach

Bulk, and for tephra, shard-specific chemical compositions can be determined by NAA, XRF, ICP-MS and EPMA methods. The contribution of the radioactive elements, potassium, uranium and thorium, rubidium, to the total dose rate is determined by the use of conversion tables (Table 3.3; Bell, 1979a; Nambi and Aitken, 1986; Adamiec and Aitken, 1998). The existence of radioactive equilibrium in the uranium and thorium decay chains cannot be established using this approach in isolation.

(ii) Spectrometric measurement approach

In-situ and/or laboratory based gamma and/or alpha spectrometry, sample thick-source-alpha and/or beta-counting (TSAC/TSBC, *e.g.* Sanderson, 1988; Forman *et al.*, 2000) can provide cross-checking measurements for (i). They can be used to calculate elemental concentrations (and, therefore, α, β, γ dose rates via conversion factors; Table 2.5), and minimise disequilibrium errors. It is preferable to measure gamma dose rates *in-situ* using portable γ-spectrometers because this incorporates measurements of all gamma radiation within a 30 cm sphere as well as any *in-situ* cosmic dose.

[18] Scanning electron microscope – Energy Dispersive X-Ray System

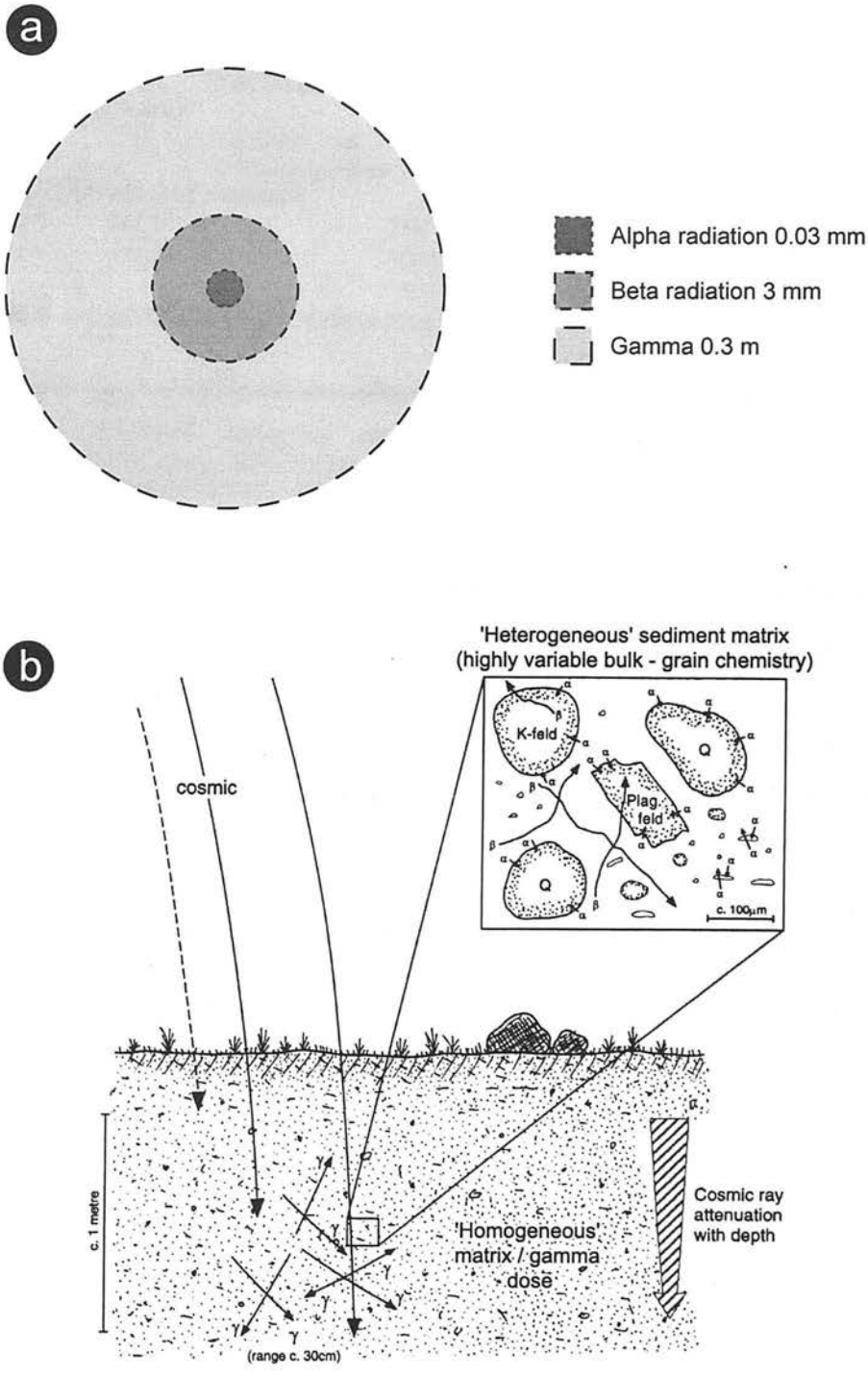


Figure 2.12 (a) Spheres of influence of relevant nuclear radiations (modified from Aitken, 1998). Diagram is not to scale, is schematic and each radius represents the maximum possible distance travelled by each type of radiation. **(b)** Relevant aspects of environmental radioactivity. Alpha, beta, gamma and cosmic radiation penetrates fine-grained silts, hence their common use in dating. Alpha particles only penetrate the outer rim of sand-sized partciles, hence the use of etching to simplify dose rate calculations. See Aitken (1985; 1998, p. 42) and Figure 4.19 for further discussion (from Aitken, 1998).

Radionuclide			Concentration	α	β	γ
Uranium series decay (natural U)						
Uranium	(U)	No thoron loss	1ppm	2.781	0.1470	0.1136
		100% thoron loss		1.261	0.0613	0.0042
Thorium series decay						
Thorium	(Th)	No radon loss	1ppm	0.739	0.0286	0.0521
		100% radon loss		0.310	0.0108	0.0203
Natural potassium and rubidium						
Potassium	(K_2O)		1%	-	0.676	0.202
Rubidium*	(Rb_2O)		1ppm	-	0.00428	-
Superficial cosmic dose rate up to 1000 m.a.s.l, < 50° N/S*				0.18 +attenuation of 14 % per metre		

Table 2.5 Conversion values for elemental concentration method of calculating environmental dose rates. Table adapted from Nambi and Aitken (1986) whose values are not significantly different to Bell (1979) or Adamiec and Aitken (1996).

Notes: Values are infinite matrix dose rates in $mGya^{-1}$. Errors of ± 5 % exist in dose rate data (Bell, 1979). * = Rb and cosmic ray contribution are the least significant factors that need to be incorporated into the dose rate equation. Combined they contribute less than 10% of the total dose rates presented here. For altitudes below 1000 m Prescott and Hutton (1988) calculate a cosmic dose rate $D_c = 0.21 \pm 0.07$ $Gyka^{-1}$ for superficial sites at sea level between 0-50° N/S latitude. According to graphs in Prescott and Hutton (1988), an increase in altitude to *ca.* 65° N does not significantly alter this dose rate. Aitken (1999) considers a superficial cosmic dose rate of 0.18 ± 0.07 $Gyka^{-1}$ to be more generally applicable and this value has been adopted here. The adoption of either value does not alter the total dose rate significantly. Attenuation of cosmic dose at 14 % per metre for rock density of 2 gcm^{-3} has been incorporated into the cosmic dose rate calculation (Prescott and Hutton, 1988; 1994). The full effect of depth and density can be calculated from $D_c = 0.21\exp[-0.07(dr) + 0.0005(dr)^2]$ Gy ka^{-1}, where d = depth of burial and r = density of rock/sediment. However, rock/sediment density is usually between 2-3 gcm^{-3} Rock/sediment densities and dr values can vary greatly, *i.e.* dr = 1.5-50, without affecting the 0.18 $Gyka^{-1}$ value (Aitken, 1999). In other words for depths between 0-10 m variations in the density of the rock away from 2 gcm^{-3} are largely insignificant, especially relative to uncertainties in palaeowater content.

For both techniques, measurement of alpha efficiency measurements is required to compensate for the reduced effectiveness of the alpha radiation. The alpha efficiency factor is expressed as a fraction. It is most easily measured by comparing a samples luminescence response to equal alpha and beta radiation doses. Further details of experimental theory and equipment used in this study for alphaefficiency measurements can be found in Zimmerman (1971), Aitken and Bowman (1975), Varma and Carriveau (1975) and Aitken (1979).

Eq 2.6 Total dose rate equation (Aitken , 1985; 1998)

Fine-grain dating (<10 μm)

$$D_p = kD_\alpha + D_\beta + D_\gamma + D_c$$

Coarse-grain dating (HF etched; ca. 100 μm)

$$D_p = 0.90D_\beta + D_\gamma + D_c$$

where:

D_p = Total dose rate during burial
k = α-efficiency factor (see Aitken, 1985; p.11; 308-317)
D_α = Total alpha dose rate
D_β = Total beta dose rate
Homogeneous matrix & quartz dating: $D_\beta = D_{\beta: Th, U} + D_{\beta: K}$; dose rate contribution from K, U, Th decay
Heterogeneous matrix (feldspar dating): $D_\beta = (D_{\beta: Th, U} + D_{\beta: K})_{INTERNAL} + (D_{\beta: Th, U} + D_{\beta: K})_{EXTERNAL}$
D_γ = Total gamma dose (Internal & external dose rate contribution from K, U, Th)
D_c = Total dose rate due to cosmic radiation.
Usually <10-20% of D_p. Negligible except at high altitude (>1000 m) and/or low radioactivity sites (Munyikwa, 2000). Estimated as 0.18 Gy ka^{-1} at a depth of 1 metre & attenuates at 14% per metre for a rock or sediment of density 2 g cm^{-3} (Prescott and Robertson, 1997; Aitken, 1998). Formulae in Prescott and Hutton (1993) were used to calculate cosmic dose rates in this study.

Notes: No fine-grain dating was undertaken in this thesis. Dose rates calculated are based on the infinite homogeneous matrix assumption (Aitken, 1985) and theoretical radiation dose models that assume the grains are spheres of equal size (Bell, 1980). For coarse-grain dating, this is a good approximation to reality for quartz and feldspar grains in the 90-150 μm fraction, but may not be as appropriate to glass shards that are predominately thin rectangular plates or approximately ellipsoidal grains. HF etching removes the outer alpha irradiated rind to avoid uncertainties associated partial penetration of alpha particles. The numerical factor of 0.90 is included in the coarse-grain equation to account for attenuation due to grain size and the effect of etching process of the beta contribution to the overall dose rate. The factor becomes smaller for grains >100 μm (Aitken, 1998). The effect of HF etching on TL sensitivity needs to be determined for, at least, each sample type. This is often done by comparing ED plateaux from samples that have not been etched with those that have been. For new materials, it is useful, therefore, to examine non-etched ED values before proceeding with ED reconstructions using differentially etched samples, *e.g.* Berger and Huntley (1983).

Full dose rate equations can be found in Aitken (1985). Evaluation of water content is the main source of error in dose-rate calculation. The constituent dose rates are heavily influenced by variations in water content of the material during burial because these can cause substantial attenuation of α, β and γ radiation. Dose rate calculations from samples collected from consistently dry environments use measured water content ($W_{in\text{-}situ}$=WF). In many cases this provides a reasonably accurate of assessment of likely palaeo-water content. Samples from areas with more variable climatic regimes

need to take account of the amount of time samples might spend at or near the maximum (saturation) water content. One way to overcome uncertainties involved in palaeo-water content estimation is to calculate the average water content as the mid-point between measured and saturation water content with error bars that encompass both values ($W_{in\text{-}situ\text{-}sat} = WF_{in\text{-}situ\text{-}sat}$) (*e.g.* Balescu *et al.*, 1997). Further details of methods and equations used to calculate the dose rate and associated errors can be found in Aitken (1985, p. 242-250 & p. 282-288; 1998, p. 38-59 & p.204-215).

(d) Palaeodose Reconstruction

(i) Multiple Aliquot methods

Thermoluminescence dating are commonly described as 'destructive', *e.g.* Stokes (1999). For this reason, multiple aliquot regeneration and additive dose methods, and variations of these, *e.g.* partial-bleach (Prescott and Robertson, 1997), are the most common multiple aliquot techniques used to evaluate the palaeodose. Multiple aliquot methods are summarised and evaluated in Figure 2.13. The principles are equally applicable to OSL and IRSL dating. The disadvantages outlined in Figure 2.13 led to the recent development of single aliquot dating techniques.

(ii) Single Aliquot Methods

Single aliquot OSL and IRSL additive dose and regeneration techniques (*e.g.* SARA and SAA) were recently introduced and have been successfully applied to dune sands (Duller, 1991; 1994) pottery sherds (Mejdahl and Botter-Jensen, 1994) and flood channel deposits (Murray, 1996; Murray and Roberts, 1998). The principal advantage these techniques is that one aliquot is more precise than 30-60 conventionally prepared multiple aliquot samples (Duller, 1991). Single aliquot procedures are widely regarded as unsuitable for TL dating (Wintle, 1997; Stokes, 1999; Clarke, 2000). Additional thermal and dose dependent sensitivity changes occur each time the disc is irradiated and heated in both preheating and during the read-out cycle (Wintle, 1997). Duller (1994) showed that regeneration was not a suitable method for single aliquot IRSL dating of feldspars because optical bleaching changed sample sensitivity. As a result, quartz based single aliquot regeneration OSL dating procedures were developed. Wintle and Murray (1997) showed that the largest change in preheat induced quartz OSL sensitivity occurred in the 230-330°C region of the glow curve. Wintle and Murray (1998) then showed that both preheat and irradiation induced sensitivity changes occur. Using computer modelling McKeever *et al.* (1997) suggested that dose dependent sensitivity changes in single aliquot OSL procedures were small compared to those associated with preheating. These findings led Murray and Roberts (1998) to develop a single aliquot regeneration OSL procedure that corrects for preheating and irradiation induced sensitivity changes by applying a small 'test-dose' after each OSL measurement. The 110°C TL peak was measured for irradiation and test doses by heating the sample up to 160°C. The OSL was then measured. The test dose 110°C TL was used to normalise the OSL signal of the immediately proceeding OSL measurement, hence the term test-dose corrected used in this thesis. Changes in the intensity of the 110°C TL peak relate to changes in sensitivity during the irradiation and read-out cycle. When sensitivity change of the 110°C peak was linear a

post-measurement correction (usually upwards) of the palaeodose could be made and this produced palaeodose values that agreed with those obtained using other methods (*e.g.* Murray and Mejdahl, 1999).

(e) Fading correction & palaeodose evaluation methods

Fading is the most serious limitation to producing accurate luminescence age estimates (Forman *et al.*, 2000). Preheating is used, primarily, to overcome problems associated with fading luminescence signal.

(i) Pre-heating & sensitivity correction

Pre-heating is undertaken between irradiation and TL read-out and usually takes the form of a long, low temperature pre-heat (*e.g.* 50°C for 7 days), intermediate, medium temperature pre-heat (*e.g.* 135° C for 16 hours) or short high temperature pre-heat (*e.g.* 220° C for 2-5 minutes). There is considerable debate over which type of pre-heating regime is most suitable (Roberts *et al.*, 1993, 1994; Stokes, 1996). Berger (1992) and Wintle (1997) suggest longer low temperature pre-heats to guard against anomalous fading in certain feldspars and volcanic glass (see below). There are, however, numerous examples of all of the above and other combinations in quartz and feldspar dating and the only recommendation that Forman *et al.* (2000, p. 169) make is that pre-heating of some description should be undertaken, sufficient to 'isolate the most stable luminescence component'.

In addition, pre-heating is undertaken to counter problems of signal fading during burial which can lead to serious age underestimates (Wintle, 1997; Aitken, 1998; Forman *et al.*, 2000). Decay of the TL signal by normal (thermal) and anomalous fading (athermal) processes leads to age underestimates when compared with ages obtained by independent techniques (Wintle, 1973, 1977). Thermal fading occurs from shallow energy traps that contribute to the overall TL signal of interest. It can be removed by implementing a suitable, experimentally determined, pre-heating regime for each sample (Prescott and Robertson, 1997). Thermal annealing erodes the natural luminescence signal, but the accuracy of the TL age is not compromised provided the pre-heats are applied before measurement of both the natural and laboratory induced TL signal (Aitken, 1985).

Intermediate to long term, or 'anomalous' fading, is more problematic than thermal fading and can lead age underestimates so serious that cannot be overcome by simple pre-heating (Wintle, 1978). Anomalous fading is an athermal process and is so called because it occurs in a part of the glow curve (*i.e.* >200°C) which should be stable. Wintle (1973) first identified anomalous fading while investigating volcanic feldspars. It cannot be removed by any existing laboratory techniques because it is a fundamental physical property of minerals that exhibit it. Therefore, ages obtained from volcanic material, and more specifically volcanic feldspars, are considered to be minimum estimates. Several physical mechanisms have been proposed to explain anomalous fading (Aitken, 1998; p. 219-223), the most commonly accepted is based on a quantum mechanical tunnelling model (Visocekas, 1985;

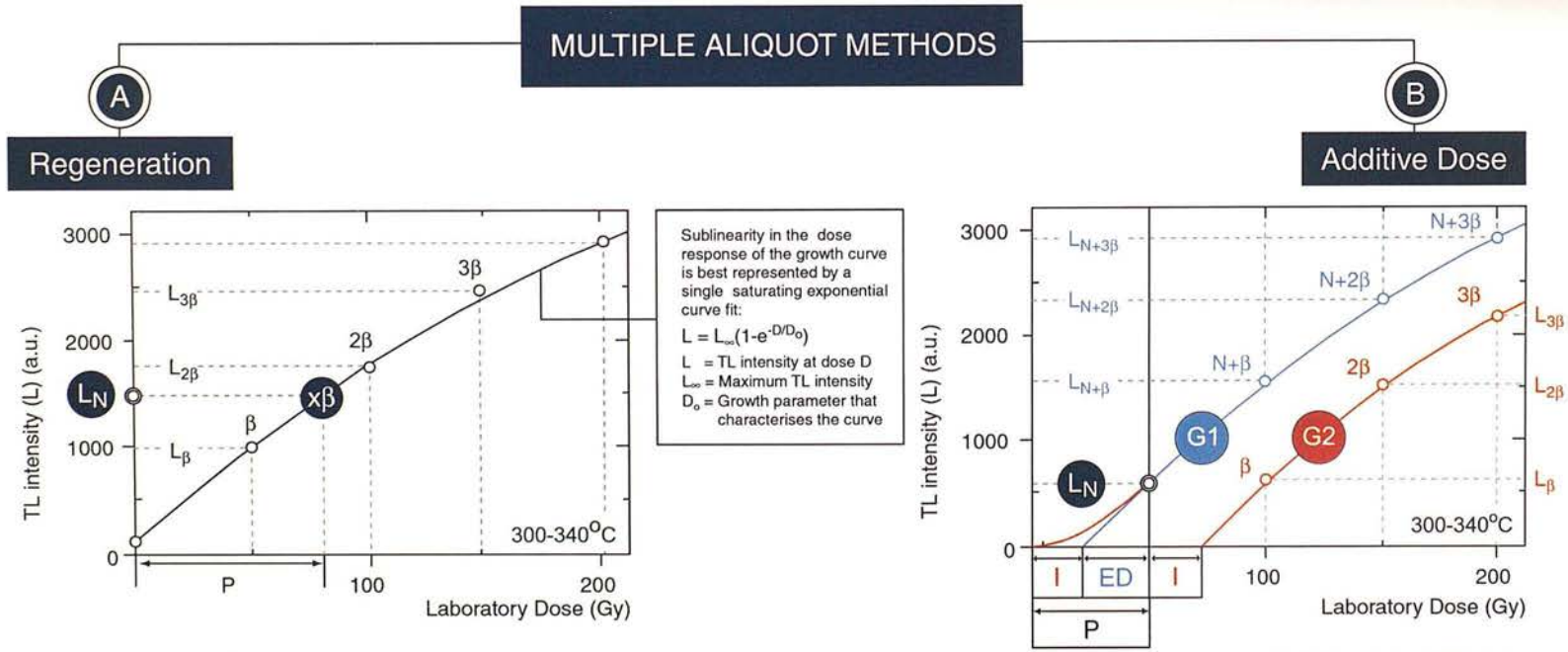
Aitken, 1985; Spooner, 1992; Smith and Sanderson, 1999, *submitted*). The rate of anomalous fading is more rapid at elevated temperatures (Wintle, 1997). For this reason, longer pre-heats at lower temperatures, *e.g.* 100°C for a week, are preferable in phases that are most affected (Mejdahl and Christiansen, 1994). High temperature pre-heats (>250°C) for less than a minute are not recommended because pre-heat changes in feldspar emission spectra have been observed (Clarke and Rendell, 1997; Aitken, 1998). Effective dating is still possible, though, if the fading rate or proportion of the lost signal can be quantified over a 1-2 month storage period (Prescott and Robertson, 1997).

Preheating also equalises sensitivity changes. Sample sensitivity is a measure of 'luminescent recombination probability' (Wintle, 1997) and this varies significantly between samples. Changes in sensitivity can occur in the natural environment, during laboratory heating and by the application of laboratory radiation doses at rates greater than those experienced naturally. Pre-heating both natural and laboratory-irradiated samples can equalise sensitivity changes that might have occurred naturally.

(ii) Plateau plots

In a equivalent dose (ED) and/or palaeodose-temperature plot, an ED/palaeodose plateau represents the thermally stable temperature region of the glow curve where negligible loss of electrons has occurred since the traps were formed or last emptied (*i.e.* the event being dated) (Berger, 1992). An ED/palaeodose plateau is a minimum requirement for accurate TL dating (Aitken, 1985; Prescott and Robertson, 1997). Establishing an ED/palaeodose plateau[19] is the best way of ensuring that the correct ED/palaeodose value is obtained. In addition, it allows error in the reconstructed palaeodose to be evaluated (Wintle, 1997). Its presence also means that no non-uniform sensitivity changes due to heating have occurred and that the pre-heating regime employed was adequate. Low temperature, long duration pre-heats are considered preferable because high temperature, short duration pre-heating schemes can sometimes induce plateau effects that are not related to the true ED/palaeodose value (Berger, 1992).

[19] A plateau is defined as a 40-50°C portion of the glow curve where the palaeodose values are within a single standard deviation of each other (Berger, 1992).



Regeneration Procedure

The natural TL signal (L_N) is determined from one portion of the sample. The natural TL is thermally or optically removed from other portions and the residual TL (L_0) is measured from one of them. Laboratory radiation doses (β, 2β, 3β) are applied to the other portions. Further laboratory doses are applied to additional sets of discs from the second split (2β, 3β etc.). The TL growth characteristic is regenerated for the thermally stable temperature region of the glow curve, determined by the plateau test (*e.g.* 300-340°C). The palaeodose (P) is determined by interpolation (L_N=$L_{x\beta}$)

Advantages

Palaeodose is acquired by interpolation - more statistically valid & precise
Precise form of growth curve & mathematical fit is unimportant

Disadvantages

Inappropriate for samples with poor reproducibility
Dose & heating related sensitivity changes effect palaeodose accuracy

Additive Dose Procedure

For the first glow (G1-blue) each disc in a set of, for example, 8 is given a successively higher laboratory dose that enhances the natural luminescence signal (L_N). The equivalent dose (ED) is evaluated by extrapolating the chosen curve fit to zero. The palaeodose, P = ED + I, where I = dose correction for supralinearity is determined by applying a 2nd series of doses (G2-red). The 2nd dose reverses the order of doses given in the 1st glow so that the total dose received by each disc is equal. A 3rd, normalisation dose (G3) is then applied.

Advantages

Repose to lab. irradiation not altered by lab. zeroing procedure

Disadvantages

ED is acquired by extrapolation - less precise than regeneration
Large errors using SSE fits on samples close to saturation
ED value dependent on the type of curve fitting used
Inappropriate for samples with poor reproducibility

Figure 2.13 Underlying principles, advantages and disadvantages of the two traditional, multiple aliquot methods used to evaluate the palaeodose in luminescence dating (drawn from information in Aitken, 1985; McKeever, 1985; Wintle, 1997 and other references in the main text).

2.4.4 Tephra Dating Methods IV:
Isotopic Potassium-argon (^{40}K-^{40}Ar) & Argon-argon (^{40}Ar-^{39}Ar) Dating

^{40}K-^{40}Ar and ^{40}Ar-^{39}Ar methods were not used in this study for two reasons:

1) The Óþoli Tephra is overwhelmingly dominated by glass shards. Phenocrystic material is rare and possibly xenolithic.
2) At the outset, and for some considerable time during the course of the dating experiments, the Óþoli Tephra was thought to be younger than 250 ka and potassium-rich phenocrysts such as sanidine absent, both of which make isotopic dating difficult.

Isotopic methods have been used in a variety of ways to date tephra deposits. Potassium-argon (^{40}K-^{40}Ar) and argon-argon ($^{40}Ar/^{39}Ar$) dating methods are the most commonly applied tephra dating techniques (Richards and Smart, 1991). Potassium or argon-argon dating of volcanic products utilises samples that are old enough (*i.e.* > 250 ka) or contain abundant potassium-rich feldspar phenocryst phases (K=10-20 wt %) that yield sufficient quantities of radiogenic argon (Pringle *et al.*, 1992; McDougall, 1995). These methods have been used to date basaltic lava flows, obsidians and phenocrysts from near-source tephra deposits in Iceland (Albertsson, 1981; McGarvie, 2000). Pre-^{14}C tephra deposits in the volcanic regions, particularly in the Eastern Volcanic Zone (EVZ) around the Torfajökull complex, have been dated using potassium argon techniques (McGarvie *et al.*, 1998).

Potassium-argon ages can be very precise and reliable and well-dated and reliable deposits provide age standards for other techniques (Pringle *et al.*, 1992; Westgate et al. 1997; Gansecki *et al.*, 1998). Step heating and single crystal laser fusion (SCLF) ^{40}Ar-^{39}Ar dating and isochron age assessment techniques have been developed to identify and minimise contamination problems that were common in ^{40}K-^{40}Ar dating (York *et al.*, 1981; Hurford and Hammerschmidt, 1985; Lo Bello *et al.* 1987; van den Bogaard *et al.*, 1989; Chesner *et al.*, 1991; Pringle *et al.*, 1991; 1992; Gansecki *et al.*, 1998; Renne, 2000). Nevertheless, discrepant ages have often been reported, however, between bulk and single grain analyses or between single-grain analysis of K-rich phases (*e.g.* Fitch *et al.*, 1976; Horn *et al.*, 1993; Mishra *et al.*, 1995; Pillans *et al.*, 1996).

Isotopic methods for dating tephra deposits are not used in this thesis or discussed in further detail in this chapter. A brief review of recent applications of potassium and argon-argon dating of tephra deposits can be found in Appendix A2.

2.5 Global Examples of Multi-method Tephra Dating

Implications for Palaeoenvironmental Change Studies in the pre-radiocarbon, Quaternary era

There are numerous examples of where correlation, radiogenic and isotopic dating techniques have been applied to older tephra deposits of pre-^{14}C Quaternary age around the world, for example in North America (Tables 2.6, 2.7) (Borchardt *et al.*, 1972; Westgate and Fulton, 1975; Perkins *et al*, 1998; Gansecki *et al.*, 1996; Preece *et al.*, 1999; below), New Zealand (Fig. 2.14) (Froggatt and Lowe, 1990; Shane, 2000; below), Europe (van den Bogaard *et al.*, 1989), East Africa (Sarna-Wojcicki *et al.*, 1985), Greenland (Ram *et al.*, 1996), Antarctica (Gow and Williamson, 1971; Marchant *et al.*, 1996). Since this approach has been adopted in this study, it is useful to examine some examples from North America and New Zealand where multi-method direct dating of older tephras is routine.

Isothermal plateau fission-track (ITPFT) analysis of hydrated volcanic glass shards has been an invaluable dating tool in north and western North America. Regional chronological frameworks have been created and existing ones radically modified (Boellstorff, J. D., 1978; Sandhu *et al.*, 1993; Pillans, 1992; Pillans *et al.*, 1994; 1996; Westgate and Naeser, 1995; Shane *et al.*, 1996; Preece *et al.*, 1999) (Table 2.6). Furthermore, procedures for TL dating of volcanic glass were originally developed in North America and later tested in New Zealand (Berger and Huntley, 1983; Pillans *et al.*, 1996).

Continuous tephra records of pre-^{14}C age have not been as well preserved in the formerly glaciated volcanic regions of northern and western North America as parts of the North Island of New Zealand. Like Iceland, both regions have experienced repeated phases of extensive and destructive Pleistocene glacial activity. Sporadic, but substantial tephra deposits of Pleistocene age have been widely dispersed from volcanic regions such as the Wrangell Mountains and Aleutian Arc of Alaska and the Western and mid-Western United States (Perkins *et al.*, 1998). These widespread and well-documented tephra deposits have been invaluable as regional chronostratigraphic markers (Table 2.6). Many have been traced to their source vents and linkages established across wide areas (Preece *et al.*, 1999; Sarna-Wojcicki, 2000). The bulk composition of some proximal tephras is well suited to more than one dating method and comparable ages have been obtained from different phases of the same deposit. This ability to link and cross-check ages across a wide area using a variety of chronometric techniques has been critical in revising timescales of palaeoenvironmental change (Table 2.6). It has allowed the reliability of existing techniques, such as fission-track and in particular ITPFT, to be tested (Westgate, 1989) and aided the development of new glass-phase thermal and optically stimulated luminescence dating techniques (Berger, 1991; 1992; Berger and Huntley, 1994).

A detailed tephrochronological framework has been constructed over the last three decades in areas that surround the volcanically active North Island of New Zealand. This record of continuous

volcanism has been used in a similar manner to its Icelandic counterpart (Moore, 1991; Alloway *et al.*, 1995; Newnham *et al.*, 1998; Lowe *et al.*, 1997) and in different ways (Hodder *et al.*, 1991; Lowe and de Lange, 1998).

The level of detail present in the Holocene terrestrial tephra record is similar to that of Iceland. In addition, palaeoenvironmental records from 64-10 ka exist and these are well constrained by ^{14}C dating and tephrochronology (Lowe, 1988; Eden and Froggatt, 1988; 1996; Alloway *et al.*, 1995). All tephra deposits younger than 64 ka have been assigned to source vents (Shane, 2000). Most of these are located in the Taupo Volcanic Zone (TVZ), one of the world's most frequently active rhyolitic centres (Lowe, 1988; Pillans, 1992; Shane and Froggatt, 1994; Lowe *et al.*, 1997). Widespread and/or stratigraphically important tephra deposits in the pre-64 ka Pliocene and Pleistocene record have been dated by ITPFT, $^{40}Ar/^{39}Ar$ and palaeomagnetic methods. (Froggatt and Lowe, 1990; Houghton *et al.*, 1995; Shane *et al.*, 1995; 1996; 1998; Naish *et al.*, 1996). Some useful, if stratigraphically sporadic, marker horizons have been dated up to about 10 Ma (Shane, 2000). Most tephra deposits of this age have not be assigned to a particular volcanic system (Shane and Froggatt, 1994).

Early glass based fission-track studies from the Taupo Volcanic Zone (TVZ) in New Zealand were not corrected for partial track fading (*e.g.* Seward, 1974). Consequently, significant age underestimates were noted when the original fission-track ages were compared to potassium-argon and more recently ITPFT ages (Westgate, 1988; 1989; Shane *et al.*, 1996; Seward *et al.*, 1997). Recent multi-phase glass-ITPFT ages from TVZ ignimbrites are identical to zircon-phase fission-track ages and, sometimes, as precise as single grain plagioclase feldspar- $^{40}Ar/^{39}Ar$ ages (Houghton *et al.*, 1995; Black *et al.*, 1996; Shane, 2000). In addition, recent ITPFT and DCFT glass-phase ages from various North American tephra deposits (Table 2.7) in the *ca.* 0.1-66 Ma age range are all similar to either zircon-phase fission-track or potassium-argon ages (see notes in Table 5.1 for a list of references).

In New Zealand, there are many specific examples where the ITPFT method has produced some of the most consistent and reliable age estimates for tephra deposits (Shane, 2000). Ages from the Rangitawa (or Mount Curl) Tephra is one of the best examples of multiple dating analysis of a single tephra deposit. This deposit is a widespread mid-Pleistocene marker deposit produced by the largest eruption from the TVZ in the last 500 ka (Milne, 1973; Froggatt *et al.*, 1986). Since Milne (1973) dated it using the early glass fission-track methods, the tephra or its bracketing sediments have been directly dated 51 times (Fig. 2.14). Terrestrial deposits were dated using radiogenic and isotopic using fission-track, TL, IRSL, ^{40}K-^{40}Ar, $^{40}Ar/^{39}Ar$ methods. Pillans *et al.* (1996) collated all known ages and correlated them with chemically similar deposits in the marine record and their associated $\delta^{18}O$ astronomically calibrated age estimates. These marine ages were obtained by EPMA correlation dating of its position in record of two deep seas cores, SO-36-61, *ca.* 1000 km NW of Auckland, and DSDP 594, *ca.* 300 km SE of Canterbury (Froggatt *et al.*, 1986). Thirty-six, or 70%, of the published age estimates were

unreliable, but all nine post-1990 glass-ITPFT and zircon fission-track ages were consistent and considered reliable (Pillans *et al.*, 1996; Shane, 2000). The weighted mean age of glass-ITPFT and zircon FT ages was 345±12 ka, in agreement with the astronomically calibrated age estimate of 340±7 ka. In comparison, single crystal (plagioclase and hornblende) laser fusion ^{40}Ar-^{39}Ar ages from within the tephra produced a wide range of ages, some with excessively large errors (Pillans *et al.*, 1996; p.649, Fig. 2.14). TL and IRSL ages from loess and dunesands that bracket it were considered experimental (Pillans *et al.*, 1996; p. 647; Figure 5.3). The glass-phase ITPFT dating procedure and equipment used in this study was the same as that used by Pillans *et al.* (1996).

Some of the most accurate high resolution records of Pliocene, Pleistocene and Holocene palaeoenvironmental change in the Southern Hemisphere have been constructed around glass-ITPFT dating of pre-64 ka tephra beds (Shane *et al.*, 1996). For example, increased loess production in New Zealand is a proxy record for the intensification of global glaciation. By dating the Te Muna tephras that bracket the first occurrence of loess in the Wairarapa region on the east coast of the North Island, Shane *et al.* (1995) were able to demonstrate that loess production was initiated between 0.87-1.00 Ma. This coincides with the intensification of global glacial activity and the establishment of the full 100,000 year glacial-interglacial Milankovitch cycle. Similarly, Naish *et al.* (1996) used ITPFT and palaeomagnetic dating methods to establish a chronological framework for twenty early Pleistocene (*ca.* 2.5-1.7 Ma) marine depositional units in the Wanganui Basin on the North Island of New Zealand. Palaeomagnetic correlation techniques were used to link this terrestrial record of glacio-eustatically controlled sea level change to changes in the astronomically-tuned global ice-volume or $\delta^{18}O$ record of ODP Pacific Ocean site 846. They concluded that each of the cyclothermic marine units represents a glacial/interglacial isotope stage couplet.

The multi-method, cross-checking approach to dating tephra deposits adopted in North America and New Zealand is, therefore, an excellent way to study older tephra deposits in Iceland. The Icelandic record of volcanism, preserved in the sediments of Pliocene and Pleistocene age in the North Atlantic is comparable in its level of detail to the terrestrial tephra record of New Zealand from the same period. Direct dating of terrestrial tephras of pre-Lateglacial age could be undertaken and compared to well-defined layers from ocean cores. Such a study is critical for assessing the timing of major climatic events in the North Atlantic during the Pleistocene, linking ocean and terrestrial records of climate change, improving in the precision of dating techniques and has a wide range of applications in palaeoceanographic studies.

North America	Description & Methods	Main implications of radiogenic tephra ages	Summary References
Central Alaska & Northern Yukon	33 tephra beds / deposits in loess profiles characterised using major & trace element composition.	These well-dated sequences provide a detailed spatial and temporal record of loess deposition across Alaska. Loess deposition is a proxy indicator of climatic deterioration. It began ca. 3 Ma in interior Alaska. The main source area is the Alaska range created by regional expansion of glaciers. Initiation of loess production in Alaska matches the timing of the start of loess production in other, more continuous Plio-Pleistocene records, such as China.	Westgate *et al.*, (1990) Preece *et al.* (1999) Kukla & Cilek (1996)
	6 glass ITPFT & DCFT ages from constrain the 0.14-2.02 Ma record. Pre-2 Ma record constrained by palaeomagnetic correlation	ITPFT age of the Old Crow Tephra shows that the penultimate Interglacial began in the Yukon and Alaska pre-150 ka, later than previously thought	Westgate *et al.* (1990)
		Using cluster analysis, 19 distinctive tephra deposits were assigned to two chemically distinctive source areas in the Aleutian arc-Alaskan Peninsula and the Wrangell Volcanic Field, SE Alaska.	Preece *et al.* (1999)
Puget Lowland, Washington	Lake Tapps Tephra (LTT) is deposited in silts sands and gravels at 5 localities. In one locality it is overlain by peat. In another the silt and peat are interbedded. The peat has been ^{14}C dated	Dating tephra deposits in this region enables linkages between sediments of the Puget lobe of the Cordilleran Ice Sheet (CIS) and those from the alpine glaciers in the Olympic Mountains. Advances of the CIS into the Puget Lowland are represented by distinctive till deposits. Three advances occurred prior to the deposition of the LTT. Stratigraphic and sedimentological contexts of the LTT suggest that alpine glacier ice might still have existed in the Olympic Mountains and the CIS ice in the Puget Lowlands when the tephra was deposited.	Westgate *et al.* (1987) Easterbrook *et al.* (1981)
	All occurrences of the LTT chemically correlated & dated using glass ITPFT & zircon-FT methods.	LTT age places a lower limit on the deposition of underlying glacial silts. The silts are all reversely magnetised indicating deposition between 2.48 - ca.1 Ma. Valuable, but as yet undated, time-stratigraphic tephras exist in this time period in several sequences described.	Easterbrook (1988) Carson *et al.* (1976)
	Pre-1 Ma record constrained by palaeomagnetic correlation	Earlier correlations between LTT and tephra deposits with similar chemical composition from units with ^{14}C ages of 20 ka are invalid. Normal polarity of silts surrounding younger tephra deposits reinforces the case. Wisconsin age for the drift surrounding the LTT incorrect. ^{14}C ages of 50.1±0.4 ka are invalid or, most probably, infinite ages.	Easterbrook (1988)

Table 2.6 Summary of the main findings of important tephrochronologically based studies and their impact on palaeoenvironmental change studies in North America. Other relevant references can be found in Table 2.7.

LOCATION		TEPHRA CHARACTERISATION Tephra deposit (numbers relate to the age correlation graph)	Principal or type site(s)	Source location & approximate source-furthest deposit distance (km)		DATING METHOD Method → Phase → Age → Error Fission-Track Glass phase-age	Zircon phase-age	Other Methods Luminescence	Isotopic	REFS PM
						Ma		Ma	Ma	
WESTERN CANADA & ALASKA		ALASKA (A), YUKON (Y) & NORTH WEST TERRITORIES (N)								
	(A/Y)	Old Crow Tephra (Oct) (A+Y)	Holitana & Halfway House	E Aleutian Arc-Alaska Peninsula	1500	UC/ITP 0.14 ± 0.01[6]	→ OCt min-max age	TL (g*) 0.17 ± 0.03 TL (I) 0.11-0.14 ± 0.03	N/A	N† 1; 2; 3; 4; 6; 7; 11 N† 65
		Sheep Creek Tephra (SCt) (A+Y)	15 km NW of Fairbanks	Wrangell Volcanic Field (SE A)		N/A		TL (I) 0.19 ± 0.02		N† 195
	(A)	HP Tephra (A)	Fairbanks & Gold Hill	Wrangell Volcanic Field (SE A)	200-250	ITP/DC 0.61 ± 0.05[3]				N† 3
		Ester Ash Bed (A)	tephra & loess deposits	E Aleutian Arc-Alaska Peninsula	150-600	UC 0.64 ± 0.10[1]				R† 1; 3
						ITP 0.81 ± 0.07[6]				1; 2; 3; 7
		SP Tephra (A)		Wrangell Volcanic Field (SE A)	200-250	ITP 0.87 ± 0.06[3]				R† 1; 3; 7
		WP Tephra (A)		Wrangell Volcanic Field (SE A)	200-250	ITP 1.03 ± 0.10[2]				N† 1; 3; 7
		PA Tephra (A)		E Aleutian Arc-Alaska Peninsula	150-600	ITP 2.02 ± 0.14[2]				R† 1; 3; 7
	(Y)	Fort Selkirk Tephra →	Fort Selkirk	Wrangell Volcanic Field (SE A) (?)		UC 1.13 ± 0.09[2]			K-Ar (ba) 1.38 ± 0.06[3]	4
						ITP 1.48 ± 0.19[2]			K-Ar (bb) 1.60 ± 0.08	4
	(N)	Banks Island Tephra (NWT) →	Sachs Harbour & Kanguk Formation	Yellowstone National Park, Wy. (?)	1000	UC 38.50 ± 2.04[1]				4; 22
						ITP 65.67 ± 1.68[1]			K-Ar (g) 66.46 ± 2.21[2]	4; 22
WESTERN UNITED STATES		PEARLETTE' ASH BEDS & YELLOWSTONE SOURCE TUFFS (P), CALIFORNIAN TEPHRAS (C), WASHINGTON (W) & OREGON (W)								
	(P)	Lava Creek Tuff (LCT)	Yellowstone / Wyoming /	Yellowstone National Park, Wy.	1200	→			K-Ar (f) 0.616 ± 0.008	
		Huckleberry Ridge Tuff/Ash Bed (HRT)		Yellowstone National Park, Wy.	1200	UC 1.23 ± 0.07[1]			K-Ar (s) 2.02 ± 0.08	15; 16
						ITP 2.11 ± 0.17[1]			SCAI (s) 2.003 ± 0.014	245; 8; 95;
		Borchers Ash	Meade County, Kansas	≡ HRT (based on chemistry & age)		UC 1.16 ± 0.07[1]				4; 225
						UC 1.30 ± 0.17[1]				15
						ITP 2.04 ± 0.16[1]	EX 1.90 ± 0.10			4; 14; 225
							EX 1.93 ± 0.32			13
	(C)	Bishop Tuff/Ash Bed	California & Mid-West USA	Long Valley Caldera, Ca.	1850		EX 0.74 ± 0.05		K-Ar (s) 0.741 ± 0.014	15
									Ar-Ar (s) 0.733 ± 0.020[2]	18
		Rockland Tephra#	N California & W Nevada	Brokeoff Mtn., Lassen Peak Area	1500		EX 0.40 ± 0.06	TL (g*) 0.49 ± 0.12	K-Ar (p/h) 0.45 ± 0.18[1]-0.31[5]	11; 12; 205; 235
	(W)	Lake Tapps Tephra	Puget Lowland, Washington	Mount St. Helens (?)		UC 0.66 ± 0.04[2]				R‡ 10; 17
		Salmon Springs, Algona & Frigid Creek localities				ITP 1.06 ± 0.11[1]	EX 0.90 ± 0.30			R† 4; 5
						ITP 0.90 ± 0.15[1]	EX 0.85 ± 0.12[2]			R† 4; 5; 17
								ka	ka	
	(O)	Mazama Tephra	Oregon & British Columbia	Crater Lake, Mount Mazama, Or.	1550	N/A	N/A	TL (g*) 7.6 ± 0.2		21
								TL (g*) 8.18 ± 0.53	^{14}C (cal) 7.66 ± 0.1	11
		Trego Hot Springs Ash	Summer Lake, Oregon	Crater Lake (?)	500(?)	N/A	N/A	TL (g*) 24.3 ± 2.7	^{14}C 23.4 ± 2.7	11

Table 2.7 Ages obtained from the glass phase of selected North American tephra deposits compared with ages obtained from other phases and / or their bracketing sediments in North America. Key and references over-page.

Table 2.7: Key & References

General

Upwards arrows indicate that stratigraphic ages are regionally consistent. Numbers in brackets next to the tephra are the key for figure 2. Informal names for tephra deposits are indicated by the hash symbol (#). Dollar sign ($) after a reference indicates the best summary source for reliable ages. Justification for ages used can be found in $ references. Where appropriate ages quoted are taken from the most recent reference.

Dating techniques

FT = Fission-track dating; UC = Uncorrected FT age; Fading correction methods: No fading correction is required for zircon FT ages (-); ITP = Isothermal-plateau fission-track age; DC = Diameter corrected fission-track age. All fission-track ages calculated using zeta method (Hurford and Green, 1983); The population subtraction technique was used for all glass FT dating. Zircon ages obtained principally by the external detector method (EX) (Naeser & Naeser, 1988) - ? = uncertain method; for zircon-FT dating the number in brackets after the age is the number of grains dated; all FT age errors are ± 1σ. TL = Thermoluminescence age; OSL = Optically-stimulated luminescence age; A_d = additive dose method; R_a = Regeneration method; *=fine-grained (4-11 μm) fraction; Luminescence age errors are ± 1σ. K-Ar = ^{40}K-^{40}Ar; Ar-Ar = ^{40}Ar-^{39}Ar (errors ± 1σ for 2 d. p. & ± 2σ for 3 d. p); SCA = single crystal laser fusion ^{40}Ar-^{39}Ar (errors ± 2σ); SCAI = age determined using isochron-method; ^{14}C=radiocarbon age from deposits surrounding tephra; cal = calibrated age. ^{14}C ages are included for completeness & for assessing the reliability of the TL ages obtained from glass. PM = palaeomagnetic dating undertaken. Remanent magnetic polarity: N = Normal; R = Reversed; † = PM profile consistent with other age determinations listed reference; ‡ = PM ages not consistent with other age determinations; †‡ = mixture of consistent and inconsistent ages; ≡ = secure chemical correlation established between tephra layers. Earlier references may quote different ages, especially pre-1985 FT ages where correction for the effects of fading were not undertaken or where the zeta calibration method was not used. Weighted mean ages have been calculate from published data. Where this has been done the superscript number after the age-error (*e.g.* 0.81 ± 0.07[8]) represents number of age determinations used to calculate the weighted mean age.

Phases in tephra or character of bracketing deposit dated

(g) = glass; (f) = feldspar (unspecified); (s) = sanidine; (k) = K-feldspar; (p) = plagioclase feldspar; q = quartz; (a) = apatite; (h) = hornblende; (b) = biotite; (l) = bracketing loess; (ba) = basalt lava above tephra; (bb) = basalt lava below tephra – basalt lava ages are from whole rock samples.

References

1. Westgate, J. A., Stemper, B. A. and Péwé, T. (1990). A 3 m.y. record of Pliocene-Pleistocene loess in interior Alaska. *Geology* **18**, 858-861.
2. Westgate, J. A. (1988). Isothermal plateau fission-track age of the Late Pleistocene Old Crow Tephra, Alaska. *Geophysical Research Letters* **15** (4), 376-379.
3. Preece, S. J., Westgate, J. A., Stemper, B. A., & Péwé, T. L. (1999). Tephrochronology of late Cenozoic loess at Fairbanks, central Alaska. *Geological Society of America Bulletin*, **111**(1), 71-90.
4. Westgate, J. A. (1989). Isothermal plateau fission-track ages of hydrated glass shards from silicic tephra beds. *Earth and Planetary Science Letters*, **95**, 226-234.
5. Easterbrook, D. J., Briggs, N. D., Westgate, J. A., & Gorton, M. P. (1981). Age of the Salmon Springs Glaciation in Washington. *Geology*, **9**, 87-93.
6. Berger, G. W. (1991). The use of glass for dating volcanic ash by thermoluminescence. *Journal of Geophysical Research*, **96**, 19,705-19720.
7. Westgate, J. A., Walter, R. C., Pearce, G. W., & Gorton, M. P. (1985). Distribution, stratigraphy, geochemisttry and palaeomagnetism of the late Pleistocene Old Crow tephra in Alaska and the Yukon. *Canadian Journal of Earth Sciences*, **22**, 893-906.
8. Gansecki, C. A. , Mahood, G. A., and McWilliams, M. O. (1996). ^{40}Ar/^{39}Ar geochronology of rhyolites erupted following the collapse of the Yellowstone caldera, Yellowstone Plateau volcanic field: implications for crustal contamination. *Earth and Planetary Science Letters*, **142**, 91-107.
9. Gansecki, C. A. , Mahood, G. A., and McWilliams, M. O. (1998). New ages for the climatic eruptions at Yellowstone. Single-crystal ^{40}Ar/^{39}Ar dating identifies contamination. *Geology*, **26**, 343-346.
10. Westgate, J. A., Easterbrook, D. J., Naeser, N. D., & Carson, R. J. (1987). Lake Tapps Tephra: An early Pleistocene stratigraphic marker in the Puget Lowland, Washington. *Quaternary Research*, **28**, 340-355.
11. Berger, G. W. (1992). Dating volcanic ash by use of thermoluminescence. *Geology* **20**, 11-14.
12. Sarna-Wojcicki, A. M., Meyer, C. E., Bowman, H. R., Hall, T. M., Russell, P. C., Woodward, M. J., & Slate, J. L. (1985). Correlation of the Rockland ash bed, a 400,000-year-old stratigraphic marker in the northern California and western Nevada, and implications for middle Pleistocene, paleogeography of Central California. *Quaternary Research*, **23**, 236-257.
13. Seward, D. (1979). Comparison of zircon and glass fission-track ages from tephra horizons. *Geology*, **7**, 479-482.
14. Naeser, C. W., Izett, G. A., Wilcox, R. E. (1973). Zircon fission-track ages of Pearlette family ash beds in Meade County, Kansas. *Geology*, **1**, 187-189.
15. Naeser, C. W., Izett, G. A. and Obradovich, J. D. (1980). Fission-track and K-Ar ages of Natural Glasses. *US Geological Survey Bulletin*, **1489**.
16. Naeser, C. W., and Naeser, N. D. (1988). Fission track dating of Quaternary events. *Geological Society of America: Special Paper*, **227**, 1-11.Naeser, C. W., & Naeser, N. D. (1988).
17. Easterbrook, D. J., Roland, J. L., Carson, R. J., Naeser, N. D. (1988). Application of paleomagnetism, fission-track dating, and tephra correlation to Lower Pleistocene sediments in the Puget Lowland, Washington. *Geological Society of America Special Paper*, **227**, 139-165.
18. Hurford, A. J., & Hammerschmidt, K. (1985). ^{40}Ar/^{39}Ar and K-Ar dating of the Bishop and Fish Canyon tuffs: calibration ages for fission-track dating standards. *Chemical Geology*, **58**, 23-32.
19. Berger, G. W., Westgate J.A., and Preece S. J. (1996). Age of Sheep Creek tephra (Pleistocene) in Central Alaska from thermoluminescence dating of bracketing loess. *Quaternary Research* **45**, 263-270.
20. Meyer, C. E., Sarna-Wojcicki, A. M., Hillhouse, J. W., Woodward, M. J., Slate, J. L., & Sorg, D. H. (1991). *Quaternary Research*, **35**, 383-399.
21. Berger, G. W. and Huntley, D. J. (1983). Dating volcanic ash by thermoluminescence. *PACT Journal*, **9**, 581-592.
22. Sandhu, A. S., Westgate, J. A. and Alloway, B. V. (1993). Optimising the isothermal plateau fission track dating method for volcanic glass shards. *Nuclear Tracks and Radiation Measurements* **21** (4), 479-488.
23. Alloway, B. V., Westaget, J. A., Sandhu, A. S, & Bright, R. C. (1992). Isothermal plateau fission-track age and revised distribution of widespread Mid-Pleistocene Rockland tephra in West-Central United States. *Geophysical Research Letters*, **19**, 569-572.
24. Sandhu, A. S. & Westgate, J. A. (1995) The correlation between reduction in fission-track diameter and areal density in volcanic glass shards and its application in dating tephra beds. *Earth and Planetary Science Letters* **131**, 289-299.

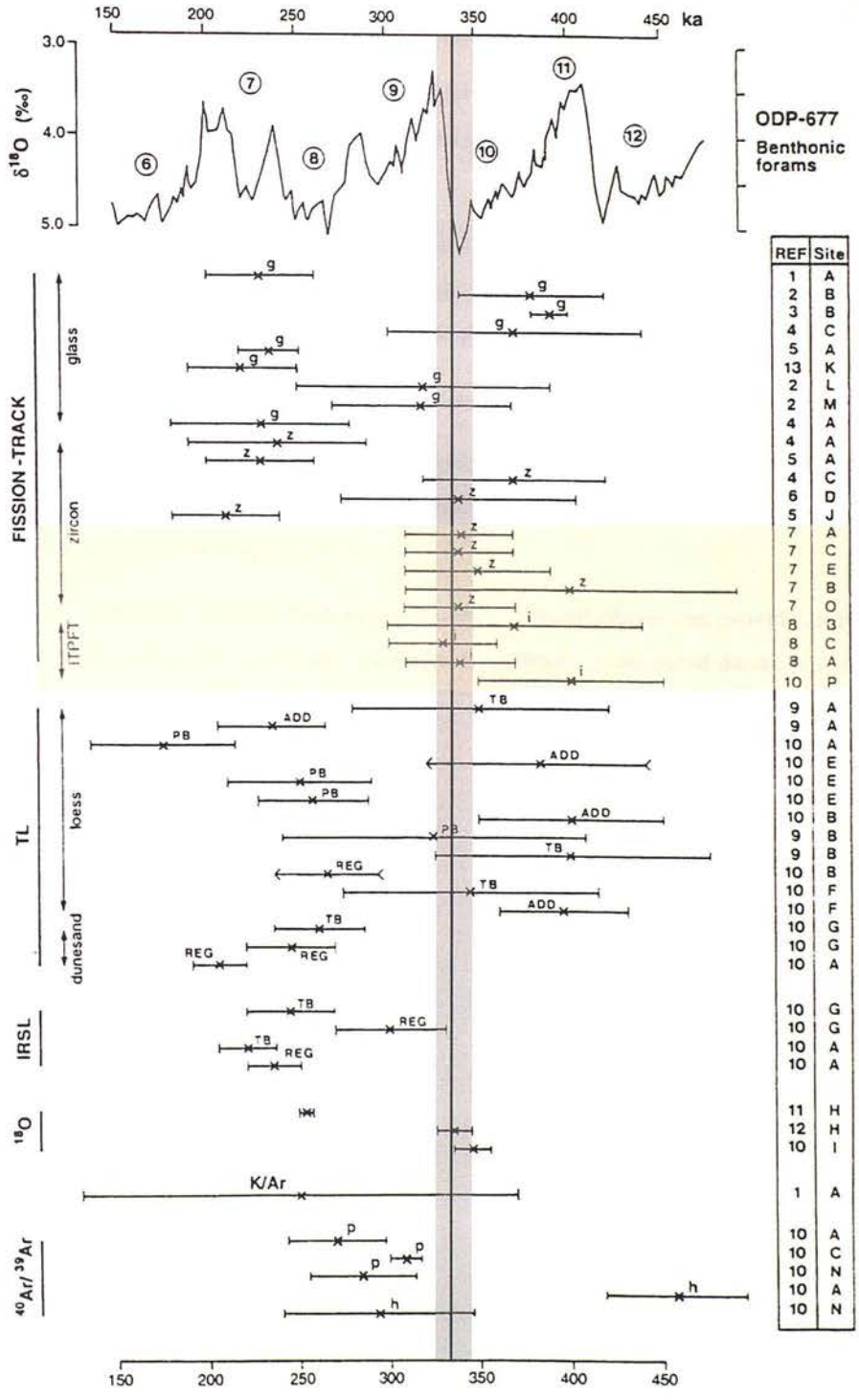


Figure 2.14 Summary of 51 numerical age determinations on the Rangitawa Tephra, New Zealand, undertaken by various authors between 1973-1996 (adapted from Pillans *et al.*, 1996 where a full list of references (1-10) can be found). The important point of this diagram is that the post 1990 zircon and ITPFT ages shaded in yellow are relatively consistent (mean = 345±12 ka) and similar to the astromically calibrated age estimate of 340±7 shaded in grey (Shackleton *et al.*, 1990).

Chapter 2 Summary

- Successful correlation of tephra deposits is best accomplished using several reinforcing criteria.
- Grain specific chemical characterisation and dating techniques are preferable because contamination can be avoided. Rigorous pre-analysis purification procedures are required for non-shard specific techniques such as TL dating.
- It is important to characterise and date hydrated glass shards using chemical methods because they are often the most prevalent and diagnostic phase. Distinctions can often be made between highly silicic eruptions (SiO_2>68%) using major element chemistry.
- Volcanic glass is often the dominant phase in Icelandic tephra and reflects the 'true' eruption age.
- The isothermal plateau fission-track (ITPFT) method for dating volcanic glass complements other grain-specific techniques used for chemical characterisation such as EPMA, laser ablation ICP-MS and ion probe microanalysis (IPMA).
- Where appropriate mineral and glass phases co-exist, mineral phases can provide an independent age assessment and act as precise age standards for volcanic glass-based dating methods such as ITPFT and TL.

Chapter 3
Sampling & Analytical Techniques

This chapter describes the use and development of multiple techniques used to determine the age of the Óþoli Tephra and the Þörsmórk Ignimbrite. Section 3.1 outlines the sampling techniques used. Sections 3.2-3.4 describe the dating methods used and section 3.5 the independent, non-tephra based dating methods included to further constrain the numerical ages obtained from the Óþoli Tephra.

3.1 Sampling & Identification

3.1.1 Vestfírðir Peninsula: Skagafjall, Sauðanes, Tóarfjall & Lækjarfjall

(a) Skagafjall tephra samples

Volcanic and pyroclastic flow units were identified and classified in the field according to Wright *et al.* (1981b) and Thorpe and Brown (1985) and sedimentary units according to Tucker (1982, 1991). Tephra layers/deposits were identified by their colour, thickness, texture and, for thin ash layers, local lateral continuity of the layer. The colour, thickness, structure, degree of consolidation, approximate grain size and the nature of the contact with the surrounding units of each volcanic and sedimentary unit were described or measured on site.

Test samples were collected from the Óþoli Tephra in June 1998. Ten samples for quantitative luminescence dating analysis were collected in June-August 1999 from Skagafjall sections B & C by hammering 22-27 mm diameter, 50 cm long copper and conduit tubes the uncovered, open end into tephra and rhythmite units (Fig. 3.1). *In-situ* gamma spectrometry measurements were made at each sample point. TL samples were stored in light-proof and watertight plastic bags. About 0.5-1 kg of material was collected in watertight plastic sample bags at each TL sample point for further analysis. Major and trace element chemistry and thermoluminescence and fission track dating techniques were undertaken on the tephra deposits of Skagafjall (Fig. 3.2).

(b) Skagafjall palaeomagnetic polarity reversal samples

The ages obtained from the Óþoli Tephra at Skagafjall in the Vestfírðir Peninsula were independently tested by measuring the palaeomagnetic polarity of the tephra and surrounding sediments. Jon Sigurvinsson collected preliminary palaeomagnetic polarity samples in September 2000. Twenty-eight plastic cubes, with an arrow inscribed on one face, were tapped into rhythmite and tephra deposits of section A, B and C. *In-situ* section bearing and dip measurements were made.

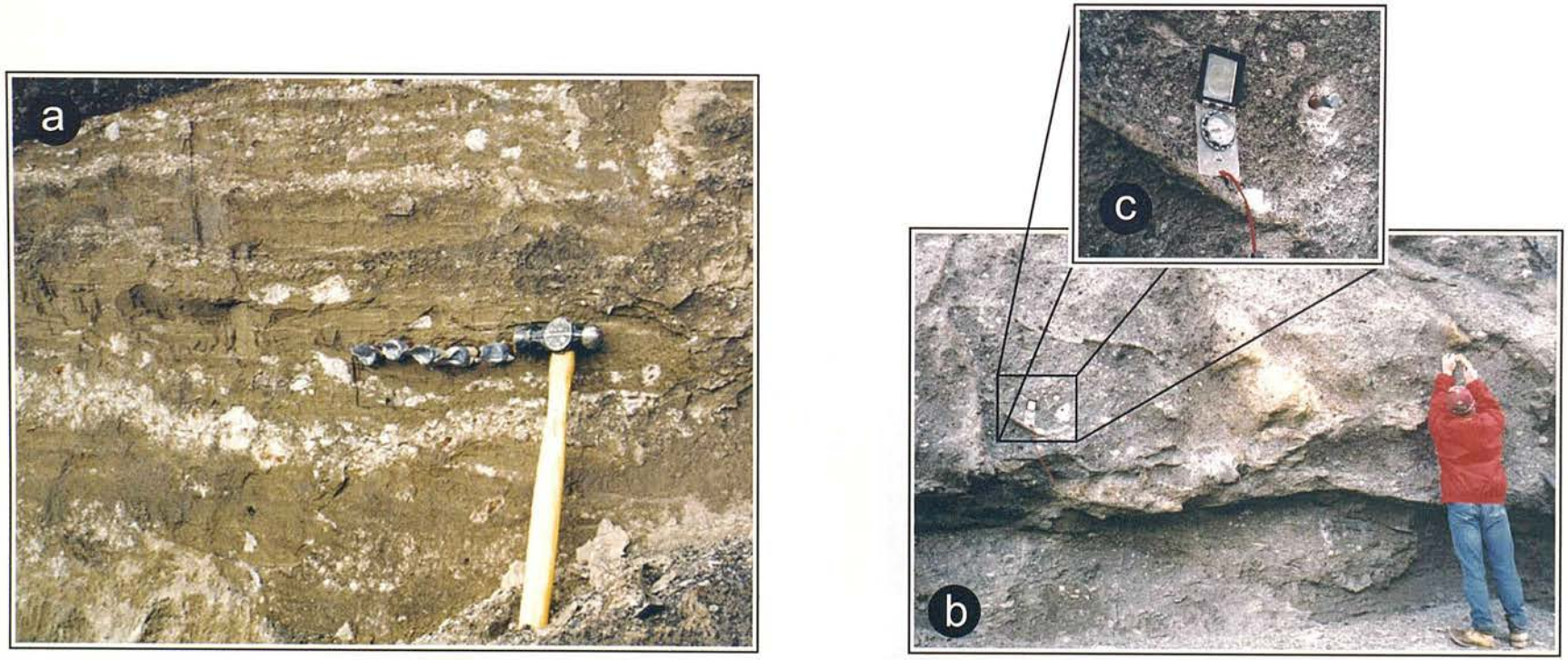


Figure 3.1 (a)-(c) Field sampling technique for ash layers and pumice clasts.
(a) Site ÞIG 1b co-ignimbrite ash layer and 5 x 22 mm diameter copper tubes. In general, sections were cut back 10-50 cm and copper tubes with the outer end covered in duct tape hammered in. White pumice layers, shown in the photograph, were also sampled (ÞIG 1c). For Skagafjall samples, *in-situ* gamma spectrometry measurements were taken once tubes had been excavated **(b)** Sampling pumice clasts embedded in welded ignimbrite deposit at site ÞIG 5 **(c)** 2-5 cm of the exposed surface of white pumice clasts >5 cm diameter were scrapped away and copper tubes hammered in. Tubes that sampled into the welded lithic/ash matrix were discarded on-site.



Figure 3.1 (d) Palaeomagnetic sampling techniques. Pots were tapped into the ash layers and rhythmite beds of the Skagafjall section, labelled and sealed with epoxy glue. Way up and azimuth orientations were determined for each sample.

3.1.2 Þörsmórk Ignimbrite

Samples for chemical and dating analysis were collected from 17 sites (Fig. 1.10). The large volume and wide range of glassy-volcanic material, from pumice clasts to tephra layers dominated by platey ash layers, in such an accessible location was particularly advantageous. Sections were cut back 20-30 cm. Samples were taken using 22 or 27 mm copper tubes. Inter-bedded ash layers and ash deposits overlying the pumiceous rich horizons were sampled (Fig. 3.1-a). In addition, the exposed surface of large white pumice clasts was cleaned back 10-20cm and internal pumice sampled (Fig. 3.1). At most sites the pumice clasts were typically ca. 10-30 cm in diameter (Fig.3.1-b), with the largest sampled *ca.* 50 in diameter. Slope ash deposits were sampled at sites 1, 13, 15. *In-situ* gamma spectrometry measurements were not made because the equipment was not available. EPMA analysis of samples collected from 17 sites and bulk and purified glass-fraction trace element analysis of 6 selected samples was undertaken.

Samples from sites ÞIG 1-8 were collected in 6-7/98 (Fig. 1.10). EPMA was undertaken between 11-12/98. Samples for TL analysis were collected from all sites in 8/99, where applicable from the same sampling points as the previous year. Additional EPMA analysis was undertaken on samples ÞIG 9-22 between 1-2/00.

3.1.3 Source correlation samples

Sigurvinsson (1983) suggested that the Dyngjufjöll volcanic system was the most likely source of the Óþoli Tephra. This was mainly because Askja is the only currently active volcanic system in Iceland that erupts in an explosive manner and produces silicic tephra of tholeiitic composition. Six samples (ASK 4-9) of inter-bedded air-fall ash, tuff or pumice from the eastern flank were collected for source correlation purposes in 7/99 (Fig. 3.2). All locations for the ASK samples were calculated in relation to Víti, the secondary eruption crater on the NE edge of Öskjuvatn.

3.1.4 Holocene TL age-control eruptions

(a) Öræfi 1362 AD (Ö1362)

Samples from the Ö1362 AD eruption were used as TL dating control samples for a recent (638 years BP), explosive, sub-glacial Plinian eruption. The long-distance samples were used to investigate if ejection into the stratosphere was capable of inducing a large TL signal in the glass phase of 'recent' silicic tephra deposits. Samples of tephra from the Ö1362 eruption were collected from sites along the principal Plinian eruption plume axis. The three sites chosen were 9 km (Kvísker), 65 km (Hólmur), 86 km (Fóssdalur), all approximately east of the volcano. The Kvísker and Hólmur samples were collected by Dr. Andrew Dugmore. At each site soil sections that contained the tephra layer were cleaned back *ca.* 50 cm and two 22 mm diameter, 10 or 25 cm long copper tubes were hammered into the tephra layer. Major element analysis was undertaken to check the correct layer had been collected.

(b) Askja 1875 AD (A1875)

Samples were collected from three locations at 0.5 km SE of Víti within the caldera (ASK 5), 55 km to the ENE of Víti at Fiskidalur (ASK 10) and 74 km NNE of Víti at Arnórsstaðamuli (ASK 11). These were used as 'zero age' control samples (125 years BP) for TL dating and again to determine if ejection into the stratosphere was capable of inducing a large TL signal in silicic tephra (see Ö1362 above). Ash rich layers (C & D of Sigurdsson and Sparks, 1978) from sections from inside the caldera, were cleaned back approximately 50-100 cm and sampled using 22 mm diameter copper tubes. At Fiskidalur and Arnórsstaðamuli soil sections were cleaned back approximately 50 cm before 22 mm copper tubes were hammered in. Major element chemistry was undertaken to check the correct layers had been sampled. All samples of this type were collected in 7/99.

3.2 Geochemical & Correlation Dating Methods

3.2.1 Introduction

This section outlines the use of standard analytical techniques used to determine the major and trace element chemistry of the glassy phase of selected tephra deposits. Summaries of the experimental theory that governs the techniques employed can be found in Appendix B1. Comprehensive descriptions of individual techniques can be found in Sweatman and Long (1969), Westgate and Gorton (1981), Potts (1987), Froggatt (1992), Jarvis *et al.* (1992), Hunt and Hill (1993; 1996; 2001) and Rollinson (1993). In summary, grain specific major element data was used to characterise glass composition of the tephra deposit principally for correlation dating. Major and trace element analysis of bulk and purified fractions was used to determine elemental contributions of potassium, uranium, thorium and rubidium radioactive decay to the annual radiation dose in luminescence dating. Figure 3.2 summarises the techniques used on each sample. Figure 3.3 shows their relationship to other dating techniques. Grain size analysis was carried out on selected bulk tephra samples used in TL dating experiments (Appendix C: Table C5.1 for a description of methods used).

Major element chemical data from tephra deposits is most commonly obtained by electron probe microanalysis (EPMA) (Smith and Westgate, 1969; Larsen, 1981). X-ray fluorescence (XRF) can be used to obtain bulk major and trace composition chemical data. Detection limits for XRF are an order of 50 to 100 times lower than EPMA. However, separating the 6-10 g of pure glass or phenocrysts from tephra deposits for XRF analysis is difficult and time-consuming. Trace and rare earth elements can be analysed using ICP-MS techniques. Detection limits are comparable or better than XRF, but only ca. 0.1g of sample is required and purification of samples more efficient.

3.2.2 Geochemical Methods

(a) EPMA

EPMA is used to determine the major element composition of individual glass shards. The procedures that govern the technique were fully established by the work of Sweatman and Long (1969). Smith and Westgate (1969) first applied EPMA techniques to tephra deposits. In addition, EPMA data is required in this thesis for luminescence dating to assess the influence of the internal shard contribution of ^{40}K radioactive decay to the total annual radiation dose received, and for fission-track analysis, to establish the chemical homogeneity of the glass shards. Further details of experimental theory for EPMA can be found in Appendix B1.2. Figure 3.4 shows typical energy dispersive (ED) spectra that were used to identify tephra glass shards before full Wavelength Dispersive analysis was undertaken.

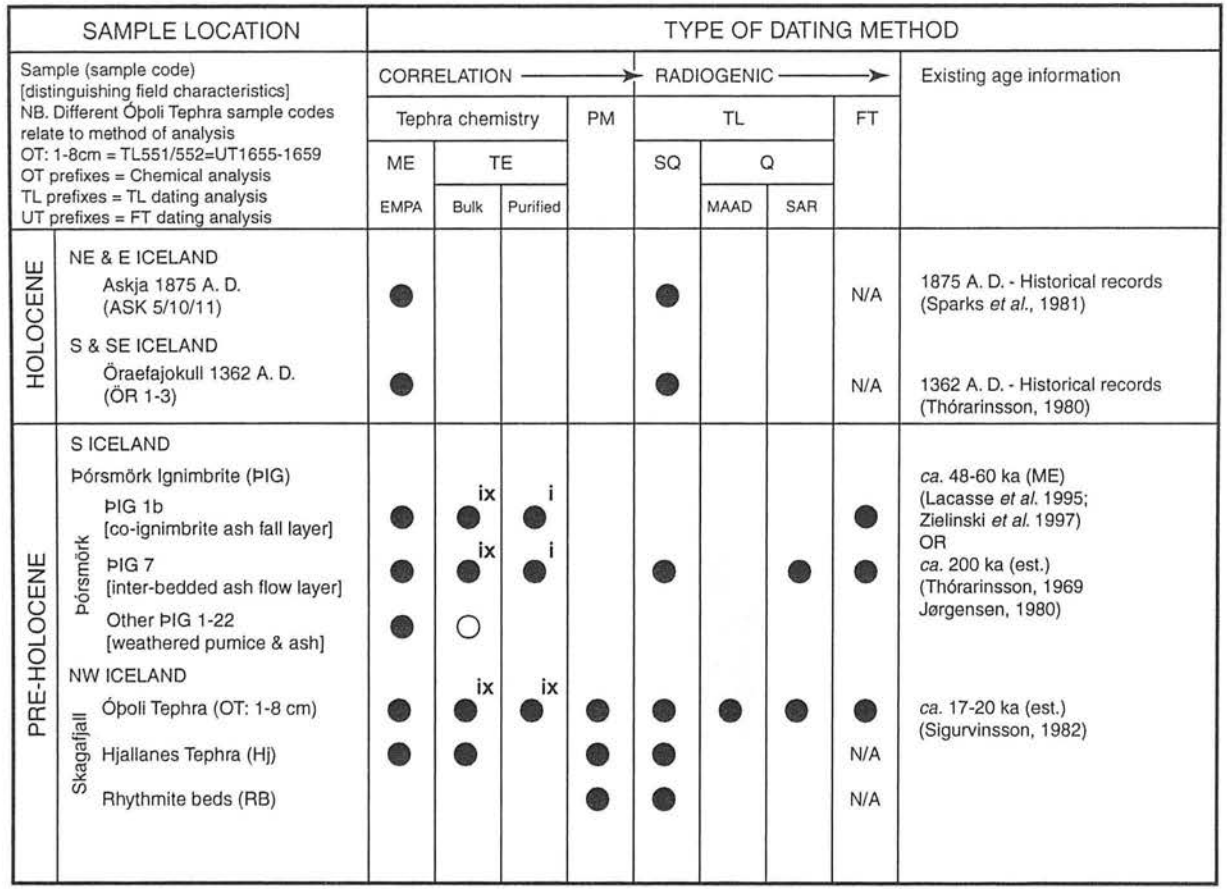


Figure 3.2 Experimental methods applied to samples in this thesis (black circles).

Bulk trace element (TE) analysis was only applied to selected ÞIG 1-22 samples (white circle). The direction of the arrows between the type of dating methods indicates the order in which experiments were undertaken. The only exception is the palaeomagnetic (PM) analysis which was carried out after the fission-track (FT) analysis. Holocene tephra samples were used as zero-age controls. *Methods*: ME=grain specific major element chemical analysis undertaken on the electron microprobe (EMPA); TE= trace element analysis; PM=palaeomagnetism; TL=thermoluminescence dating - SQ=semi-quantitative analysis - Q = quantitative analysis - MAAD=multiple aliquot additive dose technique for palaeodose evaluation; SAR-TL=single aliquot regeneration technique for palaeodose evaluation; FT=fission-track dating; N/A=method not generally applicable to that type of deposit or sample is outside the methods' established time range; (est.)=estimated age, not established quantitatively; i = ICP-MS; x = XRF

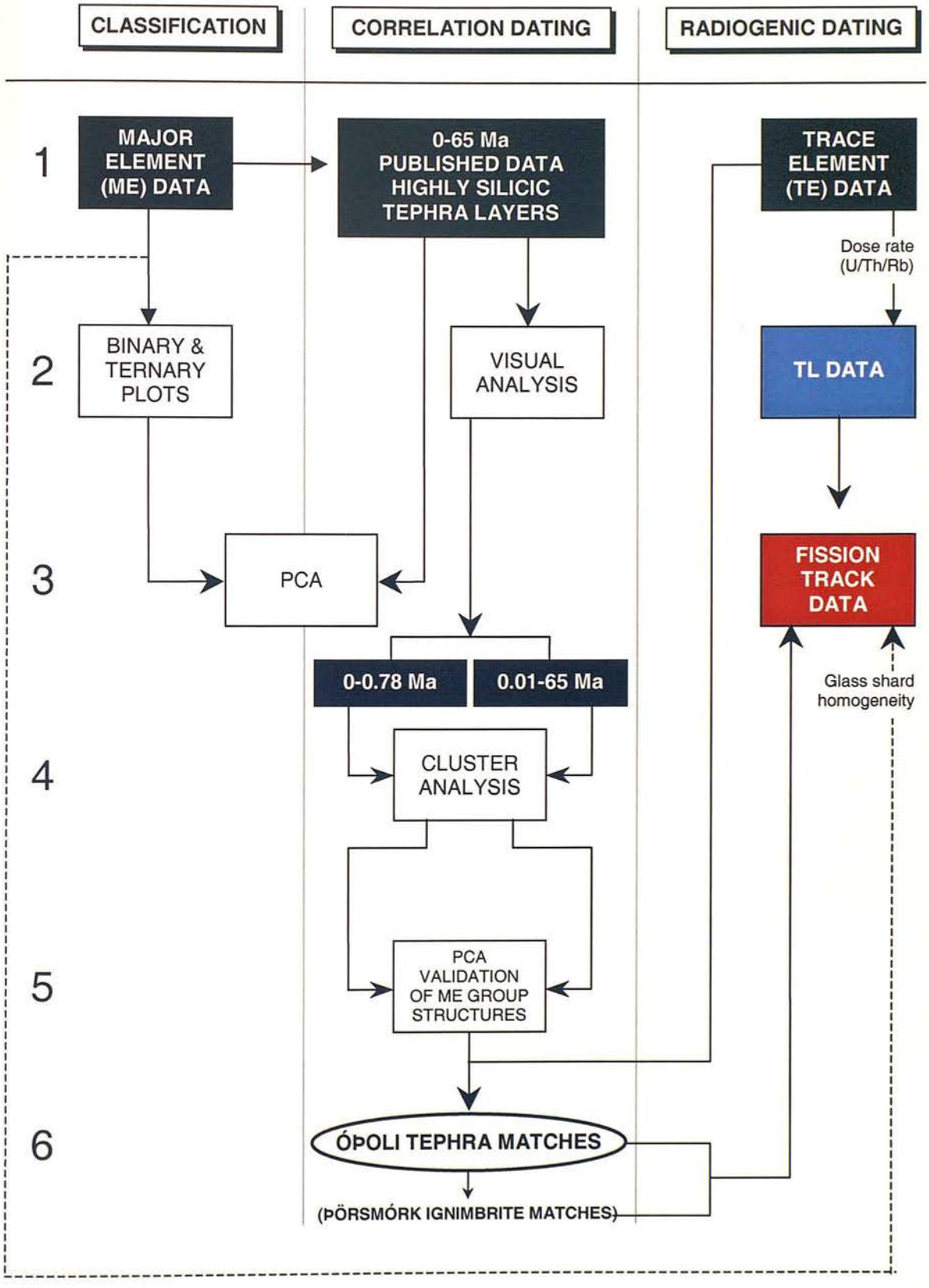


Figure 3.3 Correlation dating methods and their relationship to other dating methods in this thesis. Numbers indicate the order methods were undertaken. Solid lines are main uses of major and trace element data and are essential for dating techniques to which they are linked. Dashed lines are non-essential for the dating techniques, but can improve confidence in the ages obtained. Insufficient shard specific or purified trace element data has been published to undertake trace element based correlation dating, but where it exists it can be used to assess the validity of major element correlations.

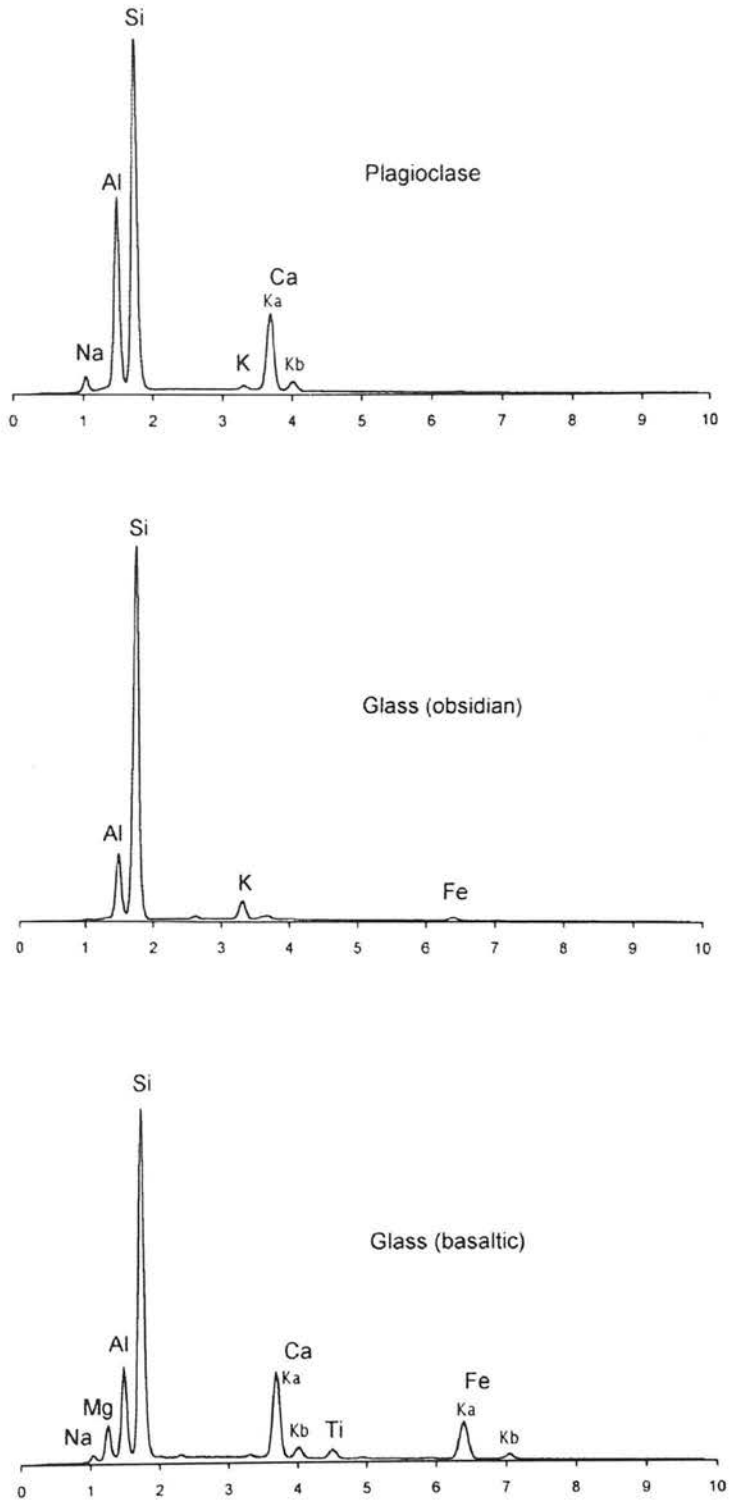


Figure 3.4 Examples of typical ED spectra for plagioclase feldspar, obsidian and basaltic glass. The presence of sodium, iron, magnesium, aluminium and calcium is indicative of tephra glass compositions (both basaltic and rhyolitic) and an easy way to identify grain geochemistry rapidly (from Reed, 1996).

Samples for EPMA were either analysed as found or after being dry sieved between 500-250-150-90 μm nylon meshes and each fraction weighed. The 90-150 μm fraction was then wet sieved through 90 μm nylon meshes. Bulk or 90-150 μm tephra was mounted on glass slides using araldite resin, ground and polished. Grain size and density fractions examined are specified in the appropriate tables. All samples (except those with a UT prefix) were analysed at the University of Edinburgh using a WDS, Cambridge Instruments Microscan V microprobe operating at 20 kV accelerating voltage, focused beam diameter of 5 μm, and a 15 nA beam current. Beam current was determined by the insertion of a Faraday cup into the path of the beam. The beam was centred before each analysis by burning a hole in the araldite resin. Nine major elements were measured from a single point in the thickest part of each shard with a counting time of 10 seconds *per* element. The number of analyses (n) represents the number of individual shards analysed. No more than one analysis per shard was undertaken to reduce the effects of beam induced element mobilisation. In excess of 100 shards were analysed for the Þörsmórk Ignimbrite and Óþoli Tephra to fully determine the chemical characteristics of each phase and identify evolution trends within a particular tephra layer. For other deposits between 10 and 30 shards were analysed, as recommended by Hunt and Hill (1993). Sodium was measured during the first and final counting period to assess the degree of beam induced mobilisation. Calibration to a mixture of pure metals and simple silicate minerals was performed at the start of each day and periodically checked against a synthetic oxide andradite standard. Spectrometer drift was checked and elements re-calibrated if necessary. For analyses undertaken in February 2000, the Lipari Obsidian was included for ad-hoc comparison. Counter dead time was corrected for and a ZAF correction applied to account for the effects of atomic number (Z), absorption (A) and fluorescence (F) (Sweatman and Long, 1969).

New reference datasets of major element EPMA data were constructed by analysing more than 75 shards from the glass fraction of the Óþoli Tephra, the coarse fraction of the Hjallanes Tephra (Hj-2b) and the silicic component of the Þörsmórk Ignimbrite. For other tephra deposits, of established composition such as Ö1362 and A1875, 10-15 glass shards were analysed per sample for comparative purposes.

UT samples were analysed at University of Toronto by Dr. Shari Preece (SP) using a Cameca SX-50 WDS microprobe operating at 15kV accelerating voltage, 10-15 μm beam diameter and 6nA beam current. UT analyses were used to check the chemical homogeneity of samples used in fission-track dating. They also provide a useful inter-laboratory comparison.

All elements are expressed as weight per cent. Shard total conditions are stated with the data tables (Section 4.3; Appendix C: Table C1.2). Shards with a total wt % <90 % were not included to avoid complications not associated with shard characteristics. Those with totals between 90-95 % were only included when no visible electron beam burn marks on the shard surface were observed (Froggatt

1992; Hunt and Hill, 1993). For correlation purposes only shards with wt % > 95% were used for comparison to published results from Icelandic tephra deposits that use similar data (*e.g.* Dugmore *et al.*, 1995b; 1999). Where appropriate analyses have been recast to 100% (normalised) on a water free basis (*e.g.* Froggatt, 1992; Preece *et al.*, 1999).

(b) X-Ray Fluorescence (XRF)

XRF is a technique used to analyse bulk samples. Samples can be prepared as compressed pellets or fused glass disc. XRF techniques are used in this thesis for evaluating the contribution of bulk matrix potassium decay to the total environmental dose rate for thermoluminescence dating techniques and to establish shard water content estimates. Further details are in Appendix B1.3.

XRF data was obtained commercially through XRAL Laboratories in Toronto, Canada. Samples were hand milled using an agate mortar and pestle. Bulk samples were analysed using the fused disc method. A single purified (90-150 μm, <2.3 gcm^{-3}) sample of Óþoli Tephra was analysed using the compressed pellet technique because there was not enough material for a fused disc analysis. Results were obtained by comparison to international standards and independently verified. Corrections were made for absorption-enhancement effects caused by the influence of all other elements in the sample.

(c) Inductively Coupled Plasma – Mass Spectrometry (ICP-MS)

Inductively coupled plasma mass spectrometry (ICP-MS) is used in this study to examine trace elements in bulk tephra and purified glass fractions of tephra (90-150 μm; 2.3-2.4 or <2.4 g cm^{-3}). This data is used primarily to calculate environmental dose rates for thermoluminescence and to test the purity of glass separates of the Óþoli Tephra.

Trace element analysis was undertaken by Dr. Valerie Olive at SUERC[20]. ICP-MS trace element geochemistry was determined using either the bulk or the density separated (<2.4 gcm^{-3} or 2.3-2.4 gcm^{-3}) 90-150μm (purified) highly silicic glass fraction of each tephra (Fig. 3.8). 0.1 g of material was dissolved by a simple tri-acids digestion (HF, HNO_3 and HCl) in a 15 ml screw cap Teflon Savillex beaker and subsequently diluted in 5% HNO_3 for analyses. A VG Elemental PQ2 Plus fitted with a Meinhard nebulizer and a water-cooled glass Scott double pass spray chamber was used. Instrumental sensitivity was set up to 35 million counts per second for 1 ppm ^{115}In. Data acquisition was made in Peak Jumping mode with 3 points per peak and 3 replicates of 90 seconds each and ^{115}In, ^{102}Ru and ^{185}Re were used as internal standards. The quality of the data was controlled by regular analyses of geostandard BCR I. All data are expressed in ppm.

TEX samples were analysed commercially at XRAL laboratories in Toronto using an ICP-MS Na_2O_2 fusion technique (Method code MS90; XRAL, 2001). 1-2 g of each sample was hand milled using an

[20] SUERC is the Scottish Universities Environmental Research Centre formerly known as SURRC – Scottish Universities Research and Reactor Centre

agate mortar and pestle and dissolved in Na_2O_2. Results were obtained by comparison to international standards and independently verified.

3.2.3 Correlation Dating Methods: Statistical theory

(a) Approach adopted

Attempts to correlate major element data collected on different electron probes using different operating conditions and standards can produce misleading and/or spurious correlations. The most fundamental concern is that all chemical analyses are proportional and entirely dependent on the legitimacy of the data collected from pre-existing standard materials. Further, operating conditions and the choice of standard materials vary greatly between individual laboratories. Reasons for low totals (*i.e.* <90-95 wt %) are not always fully explained, making comprehensive comparison between different datasets difficult (Aitchinson, 1986). Rollinson (1993, p. 47) warns that compositional data, and especially major element data is often misused and recommends that 'the approach must be that of "hypothesis testing". Diagrams must be constructed with a clear, testable model in mind so that hypotheses can be refuted or verified'. This approach has been adopted here (Box 3.1). If good analytical procedures are established, followed and reported, chemical data should have a degree of direct comparability. Despite the many potential pitfalls, recent tephra based EPMA inter-laboratory comparison exercises have shown that it is possible to obtain accurate and directly inter-comparable major element data from the glass phase of Icelandic Tephra and that certain highly silicic tephra deposits are distinctive enough for correlation dating purposes (Hunt and Hill, 1996)

(b) Data Transformation

(i) Normalisation

Recalculation of EPMA data to 100% on a volatile (principally H_2O, but also CO_2, S) free basis (normalisation) is the most straightforward way of comparing EPMA data. Totals less than 100% are commonplace in EPMA analysis of volcanic glass shards because the volatile content of each shard is variable and/or subject to post-depositional hydration effects. This difference from 100% is usually expressed as H_2O_d. If strict EPMA analytical procedures are followed and no loss of mobile elements from or superficial marks on glass shards is noted during analysis, it is more than likely that H_2O_d reflects the actual volatile composition of the shard. Since all chemical data is proportional, inter-shard variations in volatile content will affect other element totals. Mobile elements, such as K_2O and Na_2O, and those susceptible to weathering related enrichment or depletion, *e.g.* SiO_2, are particularly affected. Normalised data is required for classification schemes based on alkali content. When used appropriately, normalisation removes the influence of inter-shard volatile variation. It can be a useful discrimination method in itself that can increase confidence in correlation and this is the reason it is commonly used in non-European tephra studies (Frogatt, 1992; Chesner *et al.*, 1991; Westgate *et al.*, 1998; Preece *et al.*, 1999). Data in this study is presented in 'as analysed' (*i.e.* 'unnormalised') and normalised form.

Óþoli Tephra vs 0-65 Ma tephra of the North Atlantic

The major element composition of the Óþoli Tephra is significantly different to the:

0-0.78 Ma hypothesis
Highly silicic glass phase of all tephra deposits of mid-late Pleistocene and Holocene age, in particular, the components of NAAZ1, NAAZ2 or NAAZ3 from terrestrial and marine environments of the northern North Atlantic region.

0.78-65 Ma hypothesis
Highly silicic glass phase of all tephra deposits of early Pleistocene and Tertiary age.

Þörsmórk Ignimbrite hypotheses

ÞIG 1-23 hypothesis
The major element composition of new data from the unaltered glass fraction of the Þörsmórk Ignimbrite sites ÞIG 1-23 is similar.

ÞIG vs NAAZ2 hypothesis
The combined new dataset is indistinguishable from previous analysis of the same fraction from the Þörsmórk area of Jørgensen (1980) and highly silicic tephra deposits of NAAZ2 from marine cores from the northern North Atlantic.

Box 3.1 Null hypotheses (A-D) of major element correlation dating of 0-65 Ma highly silicic (defined as SiO_2>67%, TiO_2 and MgO <1%) tephra deposits in the North Atlantic region was undertaken

Summary of methods & other notes
To test these hypotheses most of the published analyses in the 0-60 Ma age range from terrestrial and offshore repositories were collated (Appendix C: Table C2.1). Nine major elements analysed in this study were selected for cluster analysis. Analyses of highly silicic unaltered glass (*i.e.* SiO_2 >67%, and TiO_2 and MgO <1 %) were selected. These values were chosen because most highly silicic volcanic glass from Iceland with SiO_2 > 67% have TiO_2 and MgO <1 % forming a naturally standardised dataset.

New glass-phase EPMA data from Askja 1875 (A1875) and Öræfajökull 1362 (Ö1362), collected for TL altitude inducement tests, were included as control samples to test how effective each method was in matching data of strong visual similarity. For similarity coefficients (PPM) significance at the 0.01(1%) and 0.05 (5%) level was tested for (Appendix C: CD-R). For cluster analysis the broad division at the *ca.* 66-70% similarity level was applied. Division lines at higher levels of similarity were determined by reference to the level of similarity that existed between new and published data of known similarity (*i.e.* A1875 and published data and analyses of Óþoli Tephra undertaken on the Edinburgh and Toronto microprobes). Division lines for final groupings were drawn at the percentage level that grouped deposits of known similarity and at the division point for known outlier data.

The complete 0-65 Ma dataset of highly silicic glass phase analyses was split according to published ages for each deposit. Potential matches in the 0-0.78 Ma age range were identified by visual inspection before thermoluminescence and fission-track dating was applied to the Óþoli Tephra and the Þörsmórk Ignimbrite. The 0-0.78 Ma dataset is more complete and a larger proportion of analyses undertaken on the Edinburgh microprobe using the same operating conditions than the 0.01-65 Ma dataset. Spurious correlations cannot be completely ruled out from either age dataset for reasons discussed in the text and in the notes beneath Table C2.1.

(ii) Square-root and log ratio transformations

Square root and log-ratio transformations of the original data are two commonly used methods that reduce the effects of 'closure' in continuous or compositional data (Rollinson, 1993; Baxter, 1999). Closure is the term used to describe an increase in one variable that causes the decrease in another variable even if the absolute value of the other variable does not change (Kovach, 1995). Square root transformation is, as its name suggests, a simple square root of the data. Log ratio transformation (Aitchinson, 1986) replaces the original data by the logarithm of the ratio between individual values and the sample mean. Elements affected by closure can be highlighted by Pearson product-moment coefficient of linear correlation (PPM).

(c) Data Classification: Bi-variate & Ternary Diagrams

Bi-variate oxide-oxide major element plots are often the most straightforward way to classify and discriminate between tephra deposits. The silica content classification scheme of Peccerillo and Taylor (1976) and the total alkalis-silica diagram (TAS = Na_2O+K_2O vs SiO_2) originally of Cox *et al.* (1979), but most recently updated by Le Maitre *et al.* (1989), are used widely. Application of the TAS classification scheme to the glass phase of tephra deposits is undertaken with caution in this study, however, because the alkali elements in volcanic glass are mobile. Element mobility occurs during weathering, diagenesis, metamorphism or interaction with a hydrothermal fluid, leading to post-depositional compositional changes. In addition, mobile element concentrations, particularly sodium, can change during the course of EPMA analysis; hence the need to assess and correct for the effects of this loss. Nevertheless, the TAS classification scheme is a useful for initial descriptions and is commonly used in grain-specific studies (Westgate and Gorton, 1981; Preece *et al.*, 1999). Analyses for TAS classification need to be recalculated to 100% (normalised) on a volatile free basis.

Larsen *et al.* (1999) showed that discrimination of silicic Icelandic tephra deposits of Holocene age can often be accomplished using non-mobile element bi-variate and ternary plots without the need for more complex statistical analysis. For major element analysis with 10 oxides there are 45 possible bi-plot permutations and many more three-way combinations. Selected plots are useful for discrimination and certain elements, especially the non-mobile elements TiO_2, MgO, CaO and FeO_{tot}, have proved particularly useful (*e.g.* Newton, 1999).

(d) Correlation Dating: Simple Statistical Description Methods

Methods used in this study have been split into two main types, simple and multivariate. Simple statistical descriptors of, primarily, mean and standard deviation and Pearson product-moment coefficient of linear correlation (PPM) were used in the course of classification, discrimination and correlation analysis.

(i) Mean & standard deviation

All the correlation and discrimination techniques outlined in this section require data to be normally distributed. Published data presented as a mean or as mean and standard deviation values is assumed to be normally distributed. For the mean and single standard deviation values from the 137 analyses of the unaltered, highly silicic glass shards of the Óþoli Tephra and the 218 analyses of the same fraction of the Þörsmórk Ignimbrite analyses this assumption is perhaps valid. It was necessary to assume that some other published data was representative of the whole population even though some of the mean values are based on less than 10 analyses and/or duplicate shard analyses (Appendix C: Table C2.1).

Data in each silicic EPMA dataset (Table C1.1) was tested for normality using the Students' t-test at the 0.05 level. Where normal distributions of data were found, the arithmetic mean and single standard deviations have been presented. Sample points classified as outliers were identified visually and by cluster and principal components analysis. Statistical outliers were removed before calculation of means and standard deviations, but are included in data plots as unfilled points. Data is presented throughout in order of decreasing SiO_2 content.

(ii) Pearson product-moment coefficient of linear correlation (PPM)

Pearson product-moment coefficient of linear correlation matrices are useful as simple statistical descriptors. They are widely used in studies that utilise compositional data and form the basis of more complex linear based ordination techniques, such as .principal components analysis. Correlation is defined by Rollinson (1993; p. 23) as 'a measure of the strength of association between two variables measured on a number of individuals'.

PPM is advantageous because of its simplicity, but is a numerical value with no petrological significance (Rollinson, 1993). Furthermore, when all major elements are included, correlation between datasets is disproportionately influenced by elements, such as silica and aluminium, that constitute a large proportion of the total composition, but contribute little in explaining variance within datasets. This effect can be reduced by square root or log ratio transformation of the data. PPM was used as a preliminary test to identify which elements best describe variance within or between geochemical datasets whose origins might be related.

(e) Correlation Dating: Multivariate Statistical Methods

Multivariate statistical techniques of principal components analysis (PCA), clustering analysis (CA) and discriminant function analysis (DFA) help to identify outliers within datasets and improve confidence in correlations suggested by visual inspection and bi-variate and ternary plots (*e.g.* Stokes and Lowe, 1988; Begét *et al.*, 1992; Shane and Froggatt, 1994; Baxter, 1994). Multivariate techniques reduce complex relationships in multi-dimensional data to relationships that can be more easily studied and interpreted. In all techniques the disproportionate influence of larger elements such as silica and aluminium can introduces bias, but this can be reduced by transforming the dataset.

Normalisation, log-ratio and square root transformations are commonly applied to compositional data (Aitchinson, 1986).

(i) Principal components analysis (PCA)

PCA is described in detail in Jollife (1986), Kovach (1995) and ter Braak and Smilauer (1998). In summary, ordination methods, such as PCA, can highlight trends in data not readily apparent from simple statistical methods or other non-ordination techniques such as cluster analysis. PCA was first developed by Pearson (1901) for use with continuous measurement data across one or more dimensions. It is a simple, but powerful, linear ordination method for multidimensional scaling that uses the PPM correlation or a covariance matrix as a similarity or distance measure. Sample points are simultaneously fitted to straight lines and planes by least-squares regression (Jollife, 1986). This means that complex relationships can be reduced to a single bi-plot that makes similarity relationships and relationships between samples and multiple variables easier to visualise and quantify. PCA is useful in studies that utilise compositional data because it is often difficult to fully assess which variables are important in describing trends in the data. It also allows simultaneously visualisation of similarities between numerous tephra deposits.

There are two key stages in constructing PCA bi-plots:

- **Axis Eigenvalues:** Each sample in PCA is considered as a single dimension or ordination axis. In this case, a sample or a sample point equates to nine major element values from each shard analysis or mean values from each tephra deposit. The power of PCA lies in its ability to summarise each of these dimensions into two or three dimensions that best describe major trends in the whole dataset. This enables large inter-related datasets to be reduced into a more manageable, and hopefully more meaningful, spatial representation. Variation in each dimension is summarised by constructing principal component axes. The eigenvalue for each axis indicates the relative amount of the total variation in the data which is summarised by the axis. Usually, the first two or three axes will describe most of the total variation in the data. If this is the case, patterns of significance can be determined by a set of simple bi-plots, usually axis 2 vs axis 1. Eigenvalues for each axis are expressed as a percentage that indicates the total amount of variance explained by that axis.

- **Sample Eigenvectors:** The eigenvalue for each axis is then used to produce an eigenvector, which is a set of new values for each sample point (Kovach, 1995). When the first two axes describe a large proportion of the variation within the dataset (*e.g.* > 50-60 %) the position of the eigenvectors in two dimensional space can show two things:
  1) **Which variables are important**: The position of variable arrows in relation to the axes on a two dimensional scatterplot reveals which variables are the most important for describing variation in the whole dataset. Variable arrows which are closest to the first axis are most important in describing the variance in the whole dataset, while those closer to the second

axis are less important. Variables (and sample points) in diagonally opposite quarters are negatively correlated. There is no relationship between variables that are perpendicular to each other, but when aligned the correlation is close to unity, *i.e.* a strong correlation exists. Variables with high positive and negative eigenvalues around the first axis account for the largest proportion of variance in the data and the major trends in the data can be explained by these variables (Kovach, 1995).

2) **Similarities between sample points:** The position of each sample point in relation to the origin indicates the rate of change of the regression-fitted variable along each of the axes. Therefore, sample points that are closely spaced are 'similar' to each other and those far apart 'dissimilar'. Further, the variable arrow points in the direction of increasingly fitted values allowing the influence of a particular variable on each sample point to be evaluated. Where a variable(s) arrow passes through a set of sample points this/these variable(s) are responsible for major differences between datasets. Minor differences between datasets that are broadly similar are best described by variables that plot in the opposite quadrant. The position of the unrelated points on the bi-plot relates to the variable that is responsible for that dissimilarity. In this way, outliers within a dataset and differences between datasets can be determined in multidimensional space (Baxter, 1994, 1998, 1999)

Principal components analysis (PCA) has been used on Icelandic tephra deposits to determine those elements that are most important for discrimination and correlation purposes. Using PCA Newton (1999) confirmed that the non-mobile elements, TiO_2, MgO, CaO and FeO, are the best elements for major element glass-phase discrimination and that inter-technique compositional comparisons are not valid (*e.g.* EPMA vs XRF for major elements, ICP-MS vs SIMS for trace elements). Silica and aluminium oxides are the least useful discriminating elements for highly silicic glasses. Potassium can be influential, but rigorous analytical procedures are followed to prevent loss of this element during analysis.

(ii) Cluster Analysis (CA)

Cluster analysis is numerical technique that divide objects into discrete groups (Kovach, 1995). A more detailed discussion of the various techniques and problems associated with different distance measures can be found in Jain and Dubes (1988), Everitt (1993) and Kovach (1995). In summary, cluster analysis is an effective and widely used method for identifying groups and outliers in compositional data (Baxter, 1998). There are two broad types of cluster analysis: agglomerative and divisive methods. The latter are not used in this study. Agglomerative hierarchical methods of cluster analysis group initially separate objects into successively larger groups until a single group has been formed. The degree of similarity of each hierarchy is best expressed as a percentage and presented in the form of a 'dendrogram' that provides rapid visualisation of the group structure. The percentage similarity values are internal references that apply to each dendrogram constructed. Relationships

between different groups are determined on a case by case basis and similarity divisions contain a certain element of subjectivity.

There are seven main agglomerative clustering methods and numerous distance measures that describe the dissimilarity between samples (Kovach, 1995). Of these, average linkage and Ward's minimum variance method, using Euclidean or squared Euclidean distance as a dissimilarity measure, are the simplest and most commonly used methods (Everitt, 1993). Single linkage methods, *e.g.* nearest and farthest neighbour methods, can produce spurious groupings between obviously distinct groups (Baxter, 1999). Ward's method and complete linkage cluster analyses 'over-impose' group structures on data, including outliers that have been identified by other clustering methods and PCA (Baxter, 1994). Euclidean distance is the simplest distance measure because it is the closest analogy of measurements made between two points in the real world, but extended into multi-dimensional space. Euclidean distance based measures tend to favour large data values (Kovach, 1995), but on balance, this is preferable to the creation of spurious correlations. Removing outliers from the original dataset before mean and standard deviation calculations are made or using datasets with low 1σ errors (*i.e.* <10 % of mean) is advantageous because cluster analyses of outlier-free transformed and unaltered datasets then often produce similar results (Baxter, 1994).

3.2.4 Correlation dating: Application of statistical methods

Most of the highly silicic tephra deposits used in tephrochronological and palaeoceanographic studies in the North Atlantic were included in the cluster analysis. A full list of data and references can be found in Appendix C: Table C2.1.

Various linkage methods and standardisation tests (*e.g.* standard deviation normalisation) were undertaken before the final PCA and CA diagrams were selected (Figure 4.14: 1-4). In some cases data have been published without standard deviations, making the value of standardisation based on variance within datasets difficult to assess fully. In test runs various forms of variance-based standardisation of data created unrealistic groupings and was unable to link deposits that were known to be similar. Most of the published data has standard deviation (1σ) errors of 0-10%. Variation about the mean is obviously important, but it was assumed that the data presented is truly representative of the whole population. Outliers were removed from distributed data presented as mean ± 1σ.

Four cluster diagrams were constructed to test the hypotheses outlined in Box 3.1. These were separated by age and normalisation characteristics:

1) 0-0.78 Ma as analysed (*i.e.* mid-late Pleistocene and Holocene deposits)
2) as 1, but data recast to 100% on a water-free basis (normalised)
3) 0.01-65 Ma as analysed (*i.e.* pre-Holocene deposits + A1875 analyses as a control)
4) as 3, but data recast to 100% on a water-free basis (normalised)

To overcome the inherent subjectivity and aid the interpretation of clustering results the published and/or new EPMA of the Askja 1875 (A1875) and Óþoli Tephra were used in this study to provide control limits on acceptable levels of similarity. A1875 makes an effective control sample for Holocene and Lateglacial deposits because, unlike the glass compositions from the Öræfi 1362 AD eruption, its off-axis tholeiitic geochemical signature is distinct from numerous other highly silicic eruptions of transitional alkaline to alkaline compositions of the Eastern Volcanic Zone. There are four sets of highly silicic glass-phase analyses from A1875:

1) New, unpublished data from the Askja crater and eastern Iceland undertaken by SJR during the course of this study
2) Unpublished data from Sweden, analysed by SJR in conjunction with Jonas Bergman of Lund University, Sweden (used here by kind permission)
3) Published data from Larsen *et al.* (1999)
4) Published data from Sparks *et al.*, (1981).

The analyses from 1-3 were undertaken on the Edinburgh Microscan V microprobe under the same operating conditions. Analyses from Sparks *et al.*, (1981) were undertaken on a different microprobe and operating conditions. Analytical sets 1-3 illustrate the good level of similarity that can be expected between analyses undertaken on the same machine and with the broadly similar operating conditions. The comparison between analyses undertaken on the Edinburgh probe and those of Sparks *et al.*, (1981) (1-3 vs 4) illustrates a good level of similarity that might be expected between data from different machines with different operating conditions. In a similar way, the analyses of the Óþoli Tephra undertaken at Edinburgh and Toronto are useful as similarity control samples for deposits of pre-Lateglacial age.

The Mangerud *et al.* (1984) analysis of the Vedde Ash Stratotype is thought to be erroneous because the early EPMA analytical procedure employed did not fully account for the effects of sodium mobilisation. This dataset was used to provide a control limit on acceptable levels of dissimilarity and identify outliers in the correlation dataset (Appendix C: Table C2.1). Further validation of group structures was obtained using PCA .

3.3 Fission-track Dating of Icelandic Tephra Deposits

The overall aim was to produce fission-track ages from glass fractions of the Óþoli Tephra and the Þórsmörk Ignimbrite. The relationship between fission-track dating and other techniques that produce numerical ages is shown in Figure 3.5. Experimental procedures used are summarised in Fig. 3.6.

Óþoli Tephra samples were obtained from the thick air-fall component in Section B, 1-8 cm above the underlying rhythmite bed (no. 10), at Skagafjall. Two separate irradiations were undertaken and two different correction techniques used by three researchers[21]. Þórsmörk Ignimbrite samples were obtained from the co-ignimbrite ash layer, ÞIG 1b, that overlies the partially-welded ignimbrite layers at site 1 (see section 4.2-b)[22]. ÞIG 1b was chosen because large volumes of non-pumiceous, platey ash were available (Fig. 3.1). In addition, ÞIG 1b is not part of the underlying welded ignimbrite and it is also well protected from post-depositional thermal annealing by its basaltic tuff cap.

The population technique was used. This method is only applicable if the glass is from a single source and the uranium concentration is constant. Spontaneous and induced tracks were counted from a number of shards across a known area (point-counting technique) to calculate an overall age rather than calculating an age for each grain (Fig. 3.6) (Naeser and Naeser, 1988; Sandhu *et al.*, 1993). Major element, and, therefore, trace element, chemical homogeneity was established using grain specific electron microprobe major element analysis. For the Óþoli Tephra, 15 shards from each UT sample used for fission-track dating were analysed.

After being split into 'spontaneous' and 'induced' sub-samples (Fig. 3.6), the induced sub-samples were irradiated with the standards at the McMaster Nuclear Reactor, Hamilton, Ontario. For ITPFT dating both sub-samples were annealed at 150°C for 30 days. Spontaneous and induced splits were mounted in epoxy resin on glass slides. Slides were ground using 600 grade silicon carbide papers and 20-30 strokes were sufficient to expose the maximum surface area of the glass shards. Uni-directional scratches were placed on the surface glass shards using 1 μm diamond-paste-polishing. The slides were then etched together in HF (24 %), until the average track diameter was 6-8 μm, washed in de-ionised water, cleaned with an ultrasonic probe and stored in a desiccator.

Tracks were counted in reflected light using a Nikon 275437 microscope at 500x magnification. The area covered was estimated using the point-counting technique (Sandhu *et al.*, 1993). The number of tracks on glass shards that were within a 2x2-grid area in the circular field of view and the number of times the cross-hairs of the grid was located over a glass shard was recorded. Tracks were only

[21] Samples of Óþoli Tephra were collected in June 1998 and August 1999 by Stephen Roberts (SJR), University of Edinburgh and analysed by Dr. Amanjit Sandhu (AS) & Professor John Westgate (JAW), University of Toronto between April and June 2000 and by SJR in June-July 2000. Chemical analyses for UT fission-track dating samples were undertaken by Dr. Shari Preece (SP) at the University of Toronto in April 2000.

counted in glass that is on the surface, as shown by the polishing scratches. Tracks that cut through the edge of a shard or low angle tracks were only counted if a point of light could be brought into focus at the base of the track-cone. A good estimation of the fission-track density occurs when the ratio of tracks to points on glass has stabilised (Sandhu *et al.*, 1993). The point counting technique produces slightly larger age errors, but is robust, simple and more applicable to glass shards that do not cover enough area under the microscope to be effectively counted using the traditional 5x5 grid method (Sandhu *et al.*, 1993; Bigazzi and Galbraith, 1999). Track size distributions were measured for both spontaneous and induced sample splits. This data was used for DCFT age analysis and to establish whether size plateau conditions had been met for ITPFT.

Errors ($\pm 1\sigma$) were calculated according to Bigazzi and Galbraith (1999) by combining Poisson errors in the spontaneous (ρ_s) and induced tracks (ρ_i) and on the number of tracks in the muscovite detector covering the glass dosimeter. Ages were calculated using the zeta approach (Eq. 2.2) (Hurford and Green, 1983). The zeta value is based on six irradiations at the McMaster Nuclear Reactor, Hamilton, Ontario, using the NIST SRM 612 glass dosimeter and the Moldavite tektite glass (Lhenice locality) with an $^{40}Ar/^{39}Ar$ plateau age of 15.21±0.15 Ma (Staudacher *et al.*, 1982). The Huckleberry Ridge Tephra (Borchers Ash, UA 598 - single-crystal (sanidine) laser-fusion $^{40}Ar/^{39}Ar$ age = 2.003 ± 0.014 Ma (2σ) was included as an internal age standard (Gansecki *et al.*, 1998).

[22] Samples of PIG 1b were collected in June 2000 by SJR and analysed in October-November 2000 by JAW.

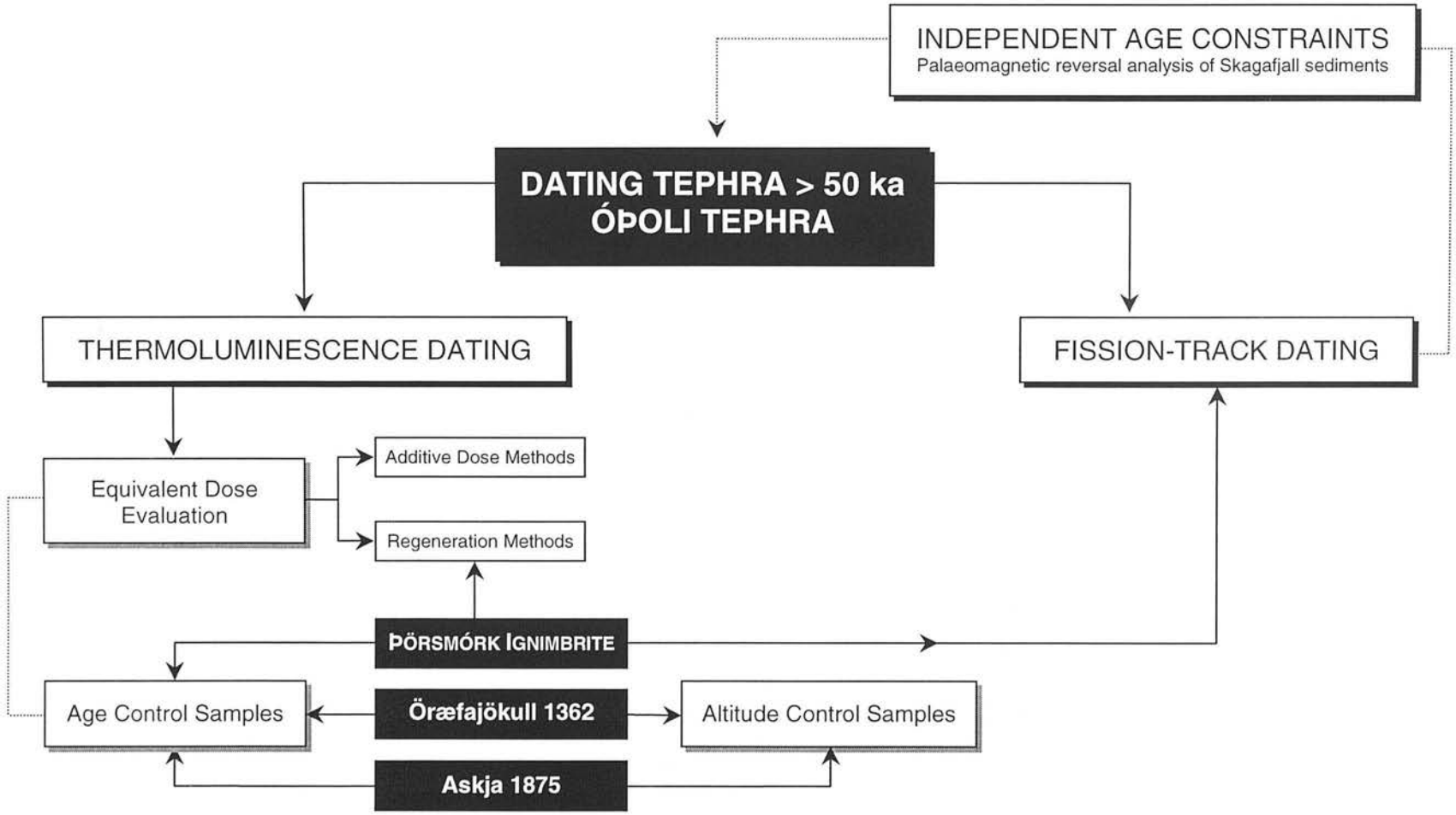


Figure 3.5 Relationships between samples and radiogenic dating techniques that produce a numerical age used in this thesis. Arrows indicate sample-technique relationships. Dotted lines indicate possible linkages between techniques and/or results obtained.

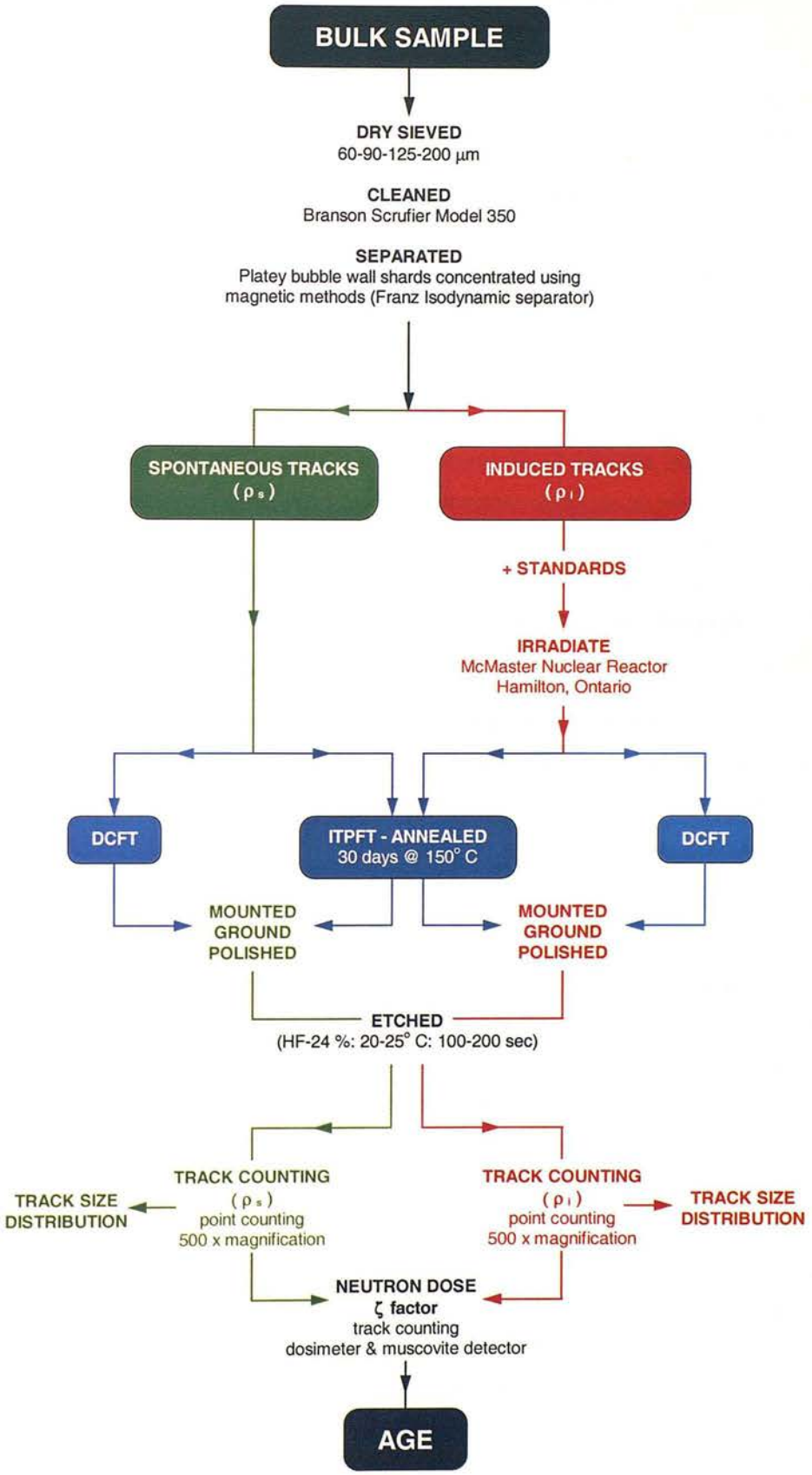


Figure 3.6 Flow diagram illustrating the stages undertaken in producing a fission-track age from volcanic glass.

3.4 Thermoluminescence (TL) Dating of Icelandic Tephra deposits

The overall aim of the luminescence experiments was to obtain a TL age for the Óþoli Tephra. The rhyolitic phase of the Askja 1875 and Öræfajökull 1362 eruptions were used as 'zero-age' samples. The pre-Holocene eruption that formed the Þórsmörk Ignimbrite was used as a pre-Holocene 'known-age' glass control, based on successful geochemical correlation with NAAZ2 deposits in the North Atlantic, with ages between 48-58 ka BP. The relationship between procedures used to produce numerical ages from these deposits is shown in Figure 3.5.

3.4.1 Dose rate determination

The overall aim of the dose rate evaluation experiments was to produce cross-checking dose rate estimates for the Óþoli Tephra. Elemental and spectrometry based dose rate estimates were obtained for the Óþoli Tephra. Spectrometry based field measurements could not be made for samples of the Þörsmórk Ignimbrite because the equipment was not available. A gamma dose rate reduction factor, based on *in-situ* spectrometry of the airfall component of the Óþoli Tephra was included to illustrate an absolute minimum possible dose rate for ÞIG 1b and ÞIG 7 (Table 4.7 for full details).

(a) Concentration (elemental) method

Bulk potassium, uranium and thorium contents were determined by XRF and ICP-MS as described in section 3.2. For pure glass and heterogenous matrix dose rate evaluations internal shard dosimetry was calculated from EPMA of potassium from individual tephra shards and ICP-MS measurements of uranium and thorium on purified fractions of volcanic glass.

(b) Spectrometry method

(i) Gamma spectrometry

Total gamma dose was measured *in-situ* for all samples of Óþoli Tephra from sections B and C at sampling sites TL551-558 (Fig. 4.2). A portable Ortec Micro Nomad spectrometer with a 3 x 3 inch sodium-iodide spectrometer crystal and photo-multiplier assemblage was used. This was initially connected to a Toshiba laptop running Ortec Micro (MCB) program that integrates spectra and calculates the dose rates. Several test runs were undertaken before disconnection from the laptop to ensure correct operation. The spectrometer was then operated in field mode that collects spectra without viewing or computation. Spectra were collected over 512 channels using a preset livetime of 300 seconds. The gamma spectrometer was calibrated at SUERC before fieldwork and count rates were converted gamma dose rates using the following dose rate conversion factors: channel 1 = 0.0060±0.0004, channel 2 = 0.028±0.003, where channel 1 are total counts > 450 KeV and channel 2 total counts > 1350 KeV. Sample geometry was 4π unless stated.

(ii) Thick source beta counting (TSBC)

A SUERC TSBC was used to determine dry infinite beta dose rates. Full details of experimental set-up can be found in Sanderson (1988). About 15 g of dried bulk samples of Óþoli Tephra (TL551/2), ÞIG 1b and ÞIG 7 were placed on a plastic disc inside the TSBC equipment. An equivalent mass of a Shap granite standard was used, β-dose rate = 6.25 $mGya^{-1}$. Standards were measured before and after each set of sample analyses. Background beta rates were collected at the start and end of each measurement session. Count time was 6x100 seconds for the standards and 6x300 seconds for backgrounds and samples.

(c) Alpha efficiency measurements

A six seater Littlemore Scientific alpha irradiation unit with vacuum pump attached was used. During measurement the chamber was evacuated to less than 0.1 mBar. The americium-241 source has a gamma emission of 60 keV and dose applied to a fine-grained sample is *ca.* 135 $Gymin^{-1}$ (16/4/00). Short pillars were attached with a source-sample distance = 15 mm. The dry, 90-150 μm, purified glass fractions of the Óþoli Tephra (TL551/2) and ÞIG7 were crushed. The fine-grained 4-11 μm fraction was suspended from acetone onto two discs per sample. No pre-heats were used. The natural TL was read using and a 15-minute β-dose applied using irradiator one (specifications as above). The induced β-dose TL signal was read out. A 30-minute α-dose was then applied and the TL signal read out. Values for alpha effectiveness were calculated following both the k-value (Zimmerman, 1971) and a-value system (Aitken and Bowman, 1975; Aitken, 1985).

(d) Palaeowater & cosmic dose rate estimates

A full assessment of the likely water content in relation to time spent frozen (*i.e.* at saturation) and/or measured water content was made. Dose rate evaluation was undertaken for the three most commonly used methods of quantifying palaeowater contents: (1) 'as-found'; (2) saturation; (3) mid-point between 'as-found' and saturation water content, placing errors to encompass both the 'as-found' and the saturation contents. Final age estimate dose rates presented in Chapter 4 were calculated in a similar manner to Hansen *et al.* (1999), *i.e.* method (3) above (see Table C4.5). For dose rate estimates calculated using the concentration method, cosmic flux was determined by reference to values in Prescott and Hutton (1993). Further details of method used to calculate the cosmic dose can be found in the notes of Table 2.5.

3.4.2 TL characterisation & palaeodose reconstruction experiments

The overall aim of the palaeodose reconstruction experiments described in Boxes 3.2 and 3.3 was to produce an accurate and reproducible coarse-grain, glass-phase luminescence age for the Óþoli Tephra. To achieve this, the TL characteristics of Icelandic tephra deposits of similar chemical composition and various ages were examined (TL Expts. 1-3). Standard reverse dose, equal total dose multiple aliquot procedures were used in TL Expt. 4 and a new single aliquot TL procedure tested in

TL Expt. 5. Further details of the experimental conditions and procedures can be found in Appendix B2: Tables B2.5, B2.6).

Early visual correlation and preliminary TL dating results indicated that the Óþoli Tephra was of mid-Pleistocene age (Fig. 3.7; Roberts *et al.*, 1999, 2000). Quantitative experimental procedures (TL-Expt. nos. 4 and 5) were developed with a mid-late Pleistocene age in mind. In addition, all luminescence experiments were completed before fission-track analysis was started. Hence, the initial intention was not to reproduce the fission-track age.

Procedures that are common to all experiments are described in sections (b)-(e) below. All luminescence experiments were undertaken in a heuristic manner by at the SUERC Physics Laboratories, East Kilbride[23] between September 1998 and May 2000.

(a) Justification for new Single Aliquot Regeneration-TL (SAR-TL) dating procedure

Single aliquot regeneration TL (SAR-TL) methods developed in this study (Box 3.2) for the Óþoli Tephra are adaptations of the Murray and Roberts (1998) SAR-OSL procedure described in section 2.3.3. They are used in a highly experimental manner with test dose and same-phase age controls (Þörsmórk Ignimbrite) used to assess changes in sensitivity during the laboratory irradiation and pre-heating cycle. Test dose normalisation was undertaken using a 0-400°C TL read out of the test dose. While aware that this could potentially induce irreversible sensitivity changes, a decision was made to proceed with this method for three reasons:

1) In preliminary tests, a natural OSL signal could not be obtained from the Óþoli Tephra. Furthermore, bleaching tests indicated that the stored signal could only be fully removed thermally (see Fig. 4.21).
2) The TL sensitivity of the glass-phase was low. In the experiments on the glass phase of the Óþoli and other tephra deposits, the 50 Gy laboratory induced 110°C radiation peak was not well defined with the intensity of the TL signal low not readily reproducible or reliable. Identifying the 110°C low temperature peak was, therefore, difficult and dose response to low test doses too unreliable to be useful.
3) Substantial disc-disc variation in TL dose response of the glass-matrix of the Óþoli Tephra was observed during preliminary and full quantitative multiple aliquot experiments. Reproducing the palaeodose using the multiple aliquot approach proved difficult and large uncertainties remained over how the magnitude of the natural signal related to that of the added doses (Fig. 3.12).

[23] Experiments 1-3 were undertaken at various times between February 1999 and April 2000. Experiment 4. was undertaken continuously between 10-28th January 2000 and fading tests completed between April 2-5th 2000. Experiment 5 was undertaken continuously between 2-20th April 2000 and fading tests completed between May 22-25th. Dark control samples were kept and contamination discs made for all experiments. Purified glass refers to the 90-150 μm, 2.3-2.4 gcm^{-3} and/or <2.4 gcm^{-3} density separated fraction.

(b) Sample & Disc Preparation

Dating volcanic glass from ash layers is possible provided the glass extracted contains no contaminating quartz or feldspar grains (Berger, 1992). The 90-150 μm fraction was chosen because effective mineral separation of grains less than 100 μm is difficult (Zander *et al.*, 2000). The purification procedure outlined in Figure 3.8 was designed to produce pure glass shard separates (form this point, referred to as the purified glass fraction or glass-phase). It is possible to produce pure-glass separates rapidly and effectively because all contaminant phases that retain a luminescence signal (quartz, feldspar, zircon *etc.*) have densities greater than 2.4 gcm^{-3}. Silicic and dacitic volcanic glass from North America commonly have a density between 2.3-2.4 gcm^{-3} and consistently <2.45 gcm^{-3} (Berger, 1992). Previous studies have taken advantage of this characteristic to effectively separate tephra shards from highly minerogenic, quartz-rich cored-sediment (Lowe and Turney, 1997; Turney *et al.*, 1997; Turney, 1998; Roberts, 1997; Roberts *et al.*, 1998; Wastegård *et al.*, 2000a; Turney *et al.*, 2001). Preliminary density separation experiments with the Óþoli Tephra, Hjallanes Tephra and Þörsmórk Ignimbrite confirmed this to be the case (Fig. B2.1). Densities of 2.3-2.4 and 2.4 gcm^{-3} were used to remove quartz and feldspar grains, which both have densities greater than 2.48 gcm^{-3}. The purification procedure adopted is highly effective principally because the bulk composition of highly silicic tephra deposits from Iceland is glass-rich, microphenocryst- and inclusion-poor.

Photographic dark room conditions with low energy lighting were maintained throughout when handling samples and samples were stored in light tight boxes when not in use. When extracting sediment from the copper tubes 0.5-1 cm of sampled material were discarded from both ends. The rest of the sample was split in two. Sub-sample split A was used for palaeodose evaluation and ICP-MS analysis of purified glass fraction. Sub-sample split B was used for dose rate and bulk geochemical analysis (Fig. 3.8). For experiments 1, 4, and 5 samples were purified using the procedure outlined in Figure 3.11. Mono-layers of purified glass (*ca.* 4-6 mg *per* disc non-centred; *ca.* 2-3 mg *per* disc centred) were mounted on 0.25 mm x 10 mm diameter stainless steel discs that had been cleaned with acetone and sprayed with Electolube SCO200D silicone grease.

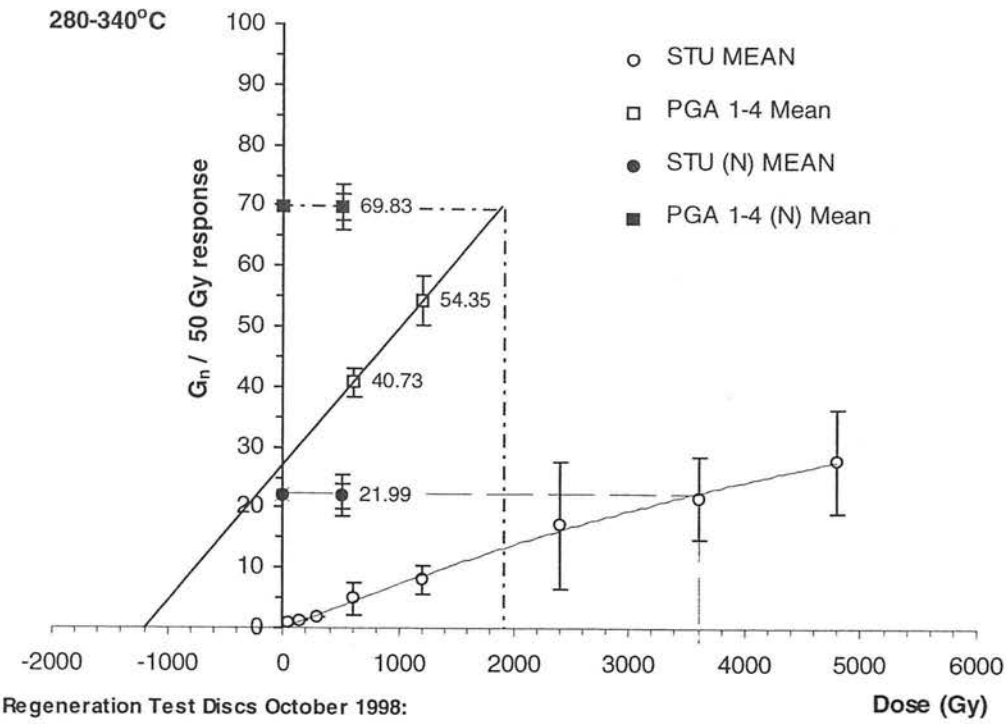


Figure 3.7 Preliminary additive dose and regeneration experiments

Luminescence glow curves were recorded manually from room temperature to 400°C at 5°Cs^{-1} using a SUERC research reader with an Electron Tubes 9883 QB PMT filtered with 7/59 and KG1 filters. Samples were irradiated using an Elsec 9022 irradiator fitted with a 1.85 GBq ^{90}Sr source, giving a silicate dose rate of 55.8 mGys^{-1} (3.27 Gymin^{-1}). Samples for the regeneration test (circles) were treated with 10% HCl, sequentially centrifuged three times in sodium polytungstate solutions of 2.3 gcm^{-3} and 2.4 gcm^{-3}, to produce > 99% glass by volume. Samples were washed five times in de-ionised water, dried from acetone and deposited on 0.25 mm x 10 cm diamter stainless steel discs sprayed with Electrolube SCO200D silicone grease. The natural TL signal (N) of the glass was removed as above and the dose response from 150-4800 Gy was investigated using 90-150 μm, 2.3-2.4 gcm^{-3} Óþoli Tephra. Dose responses for data points < 2400 Gy were normalised to a 50 Gy dose applied after the 1800 Gy dose and, for doses >2400 Gy, to a second 50 Gy dose applied after the 2400 Gy reading. The event being dated is the formation of the glass from the melt and samples are assumed to have no residual TL once the natural TL has been thermally removed.

Samples for the additive dose test were washed in 10% HCl for 20 minutes followed by 30 % H_2O_2 for 1 hour, to dissolve carbonate and organic residues, before 90-150 μm sieving and density separation (as above). The N+600 Gy and N+1200 Gy response was measured using 4 discs for each data point and response to a 50 Gy normalisation dose determined.

There is a gross discrepancy between the gradients of the additive dose and regeneration curve perhaps indicative of a change in sample sensitivity during the course of the experiment. It is noteworthy that the two additive dose values are lower than the natural TL in the additive dose experiment. Assuming no change in sensitivity has occurred the preliminary additive dose ED is 1200 Gy and the regeneration ED is *ca.* 3600 Gy. This equates to a *ca.* 400 ka and 1.2 Ma if the dose rate is about 3 Gya-1

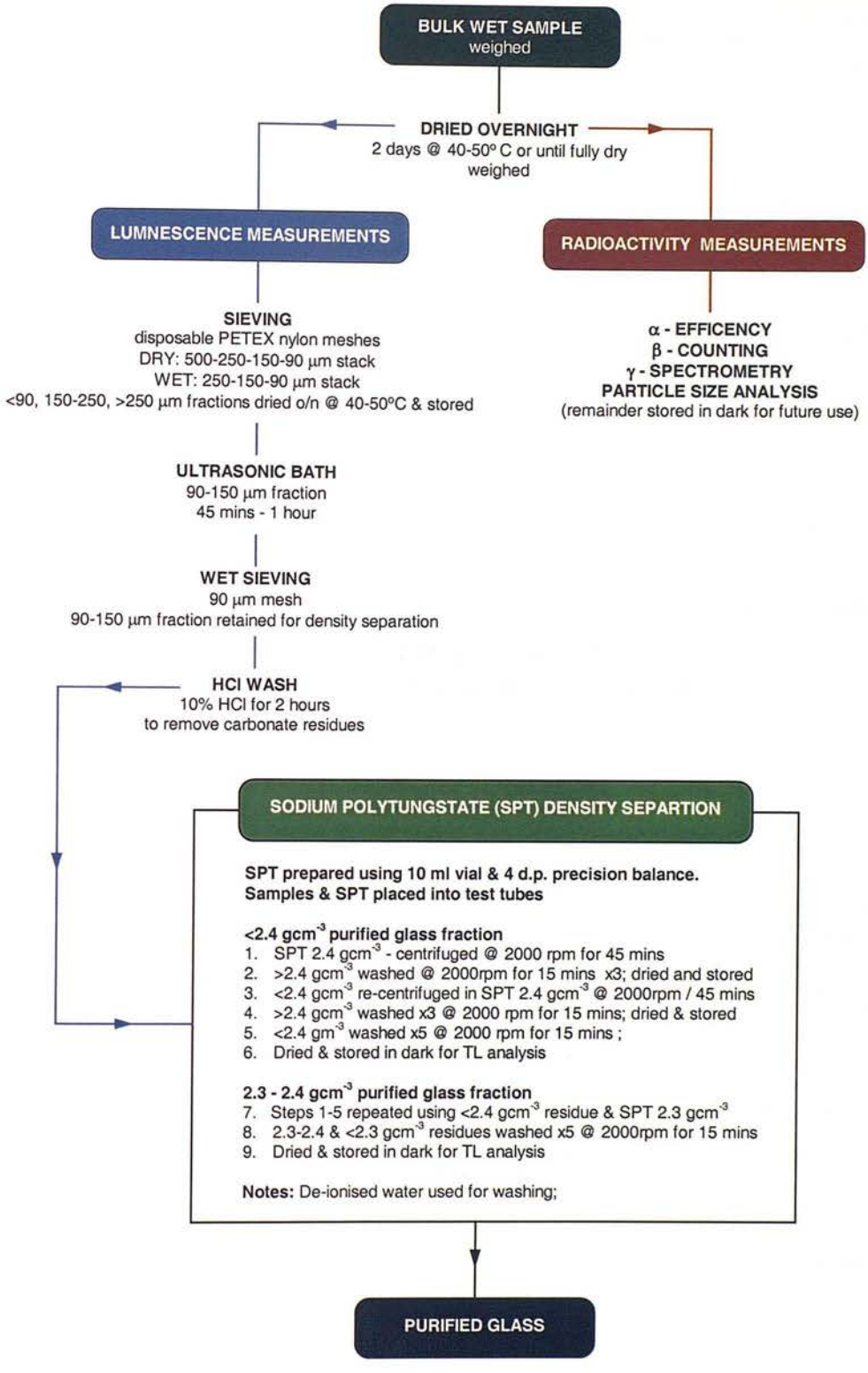


Figure 3.8 Sample preparation technique used in this study to produce purified 90-150μm, 2.3-2.4 gcm^{-3} and <2.4 gcm^{-3} glass separates from glass dominated-non-organic tephra deposits. Plastic equipment was used throughout to avoid contamination from artificial glasses. The use of strong acids (*e.g.* HCl > 10% and HF) and alkalis (*e.g.* H_2O_2) to clean the tephra was avoided to prevent aqueous precipitation on the shard surface or dissolution of the glass matrix. Samples were dried on filter paper except for preliminary regeneration test samples that were dried from acetone. All washes undertaken in de-ionised water.

Box 3.2: TEPHRA TL CHARACTERISATION EXPERIMENTS 1-3

TL Experiment 1
Natural vs 50 Gy response experiments

(a) Natural glass-phase TL and 50 Gy laboratory dose response of Icelandic Tephra

The natural TL and 50 Gy artificial dose response of purified highly silicic glass-phase of tephra from the Holocene eruptions of Askja 1875 AD (A1875: samples ASK 5, 10, 11), Öræfajökull 1362 AD (Ö1362: samples OR 1, 2) were examined. In addition ash and pumice from nine Þórsmörk Ignimbrite (ÞIG 1-21) sites and ash samples of the Óþoli Tephra (SUTL 500, 551, 552) were examined. Askja 1875 acted as a 'zero age' sample in this experiment. Five discs, with approximately equal masses (4-6 mg) of each sample on each, were prepared and irradiated as described in text. Samples from Ö1362: OR3 and Katla *ca.* 1700 BP (Layer Y) was also examined, but these were substantially contaminated by non-glassy phases.

(b) Other relevant samples

The above experiment was repeated using bulk samples from the Hjallanes Tephra (Hj-2b: SUTL 513), rhythmite deposits directly overlying the Hjallanes Tephra (RB-3: SUTL 516) and rhythmite deposits directly below the Óþoli Tephra (RB-10: SUTL 557).

TL Experiment 2
Optical bleaching of TL signals

(a) Field based experiments

Samples of exposed slope ash and pumice were collected from sites ÞIG 1, 13 & 15 to determine if their natural signal was significantly different to buried samples.

(b) Laboratory based

This experiment attempted to bleach the TL signal in the Óþoli Tephra optically using filtered and unfiltered artificial daylight. This observed the effects of exposure to filtered artificial daylight Two sets of six discs (A and B) of 90-150 μm material were prepared. The natural signal was left in set A and thermally removed and measured from set B before exposure to unfiltered and filtered artificial daylight from a 7 $mWcm^{-2}$ Thorn UV lamp within a sealed light box. Set B was used in the TL inducement experiments (TL Experiment 3-b) described below. Exposure time was two hours in all cases. Discs 1-2 of set A were exposed to unfiltered artificial daylight. Discs 3-4 of set A placed in a 'light-tight' petri-dish beneath a Schott UG5 filter that blocks more than 99% of the visible spectrum of light and transmits 70% of energy <400 nm (UV) and 80% of energy >700 nm (IR) to the samples. Discs 5-6 of set A and were exposed to visible and IR parts of the electromagnetic spectrum only. They were placed beneath a Schott GG395 filter that filters out all UV wavelengths <300 nm and 60% <400 nm. All of the energy > 480 nm was transmitted to these samples. At the end of the experiment a radiation dose of 50 Gy was applied to each disc using irradiator 1 and TL response measured.

contd. overpage

TL experiment 3
Optical inducement of TL signal in the Óþoli Tephra

(a) Inducement of TL in the upper atmosphere during plume transport
The hypothesis being tested in this experiment is that eruption and plume transportation processes cannot induce a TL signal into a tephra 'zero-age' tephra deposit. During an eruption glass ejected from the volcano experiences additional heat and intense pressures. In addition distal tephra layers, deposited from Plinian eruption plumes, will have been ejected to greater heights in the atmosphere. A measurable TL signal could have been induced into the glass fraction of 'zero age' tephra deposits by the eruption process or by ejection into the upper atmosphere. The Plinian eruption phase tephra from Askja in 1875 (A1875) and Öræfajökull 1362 (Ö1362) were of similar style, and possibly magnitude, to the eruption event that created the Óþoli Tephra.

Highly silicic tephra layers from A1875 and Ö1362 were sampled at approximately 0-10 km (ASK 5; OR 1), 50-60 km (ASK 10; OR 2) and 70-80 km (ASK 11; OR 3) from the volcano that created them. The natural TL signal was measured from five discs of the 90-150 μm, <2.4 gcm^{-3} fraction using procedures described in section 3.4.2. A radiation dose of 50 Gy was applied to each disc using irradiator 1 and TL response measured.

(b) Laboratory inducement of TL signal I:
Unfiltered natural & artificial daylight inducement of TL signal
This experiment attempted to induce a TL signal equivalent to that found in the Óþoli Tephra by exposing it to artificial and natural daylight. Two sets of four discs were prepared, one covered with mono-layers of bulk material the other with the 90-150 μm fraction. The natural TL signal was thermally removed from all discs using the set up and procedures described in the text. The first disc from each set was exposed to natural daylight for two hours and one week. The TL signal was measured after each exposure. The second disc was kept in the dark as a control sample. This exposure procedure was repeated by placing third disc in a sealed light box fitted with a 7 $mWcm^{-2}$ Thorn UV artificial daylight lamp. The fourth disc was kept as a second control sample.

(c) Laboratory inducement of TL signal II:
Filtered artificial daylight inducement of TL signal
The natural signal was thermally removed and measured from discs 1-6 of set B (from experiment 2-b, above) using the set up described in the text. Discs 1-2 of set B were placed in a 'light-tight' petri-dish beneath a Schott UG5 filter that blocks more than 99% of the visible spectrum of light and transmits 70% of energy <400 nm (UV) and 80% of energy >700 nm (IR) to the samples. Discs 3-4 of set B were placed in a 'light-tight' petri-dish beneath a Schott GG395 filter that filters out UV light. (transmission percentages: 300 nm = 0%; 400 nm = 60%; 500 nm = 100%; 600 nm = 100%). Discs 5-6 of set B were used as dark control samples and a further contamination disc was made. After exposure the TL signal was measured from each disc using the set up and procedure described in the text. At the end of the experiment a radiation dose of 50 Gy was applied to each disc using irradiator 1 and TL response measured.

Box 3.2 Thermoluminescence characterisation experiments of glass-phase of Icelandic tephra.

Notes: No preheats were used during experiments 1-3 to allow glow curve shapes and a preheating regimes for the quantitative dating experiments to be evaluated. Dark control samples were kept and contamination discs made for all experiments. Material distribution and mass for each sample was similar.

Box 3.3: GLASS-PHASE PALAEODOSE RECONSTRUCTION OF THE ÓÞOLI TEPHRA & ÞÖRSMÓRK IGNIMBRITE

TL Experiment 4
Multiple Aliquot Additive Dose TL (MAAD-TL) Experiment
Óþoli Tephra

The results of preliminary TL investigations (Fig. 3.7) led to the adoption of the following multiple aliquot additive dose procedure to determine the age of the Óþoli Tephra. Samples were prepared as in Fig. 3.8. Each TL read-out cycle (G1-G4) consists of disc irradiation on irradiator two (32.0±0.6 $Gymin^{-1}$ + 5.19 Gy transit dose), pre-heating for 135°C for 16 hours or 155°C for 5 hours and TL signal read-out in the form of a 0-400°C glow curve under conditions described above. To test reproducibility, two sets of 8 discs were prepared for each of the five MAAD runs undertaken. Each disc per set was given equal-reverse additive doses (G1 and G2), a normalisation dose (G3) and a fading test dose (G4). For the fading test (G4), half the discs received a dose equal to the normalisation dose (G3) and were stored in the dark for two months. Pre-heats for the fading tests were undertaken after irradiation so that any further loss is due to fading. Experimental conditions, procedures and doses applied for each of the five MAAD runs are summarised in Fig. 4.24. Palaeodose values were determined by integrating across 10°C temperature bands followed by linear and saturating exponential regression analysis of the G1/G3 data points. Corrections for sub- or supra- linearity were made by same style regression of the G2/G3 data points. Normalisation dose sensitisation was evaluated by examining G1/G2 and G2/G3 regression forms for parallel dose-response growth (cf. Scott and Sanderson, 1988). The TL age estimates were calculated from measured total dose rates and palaeodoses reconstructed from the thermally stable region of the glow curve determined by an ED plateau plot.

TL Experiment 5
Single Aliquot Regeneration TL (SAR-TL) Experiment
Óþoli Tephra & Þórsmörk Ignimbrite

The SAR-TL procedure described below is based on the SAR-OSL procedure of Murray and Roberts (1998) (see text for summary and paper for details). The single aliquot regeneration thermoluminescence (SAR-TL) procedure was developed for reasons outlined in the text. It allows monitoring and correction of dose or temperature related sensitivity changes. This can be used to determine whether the fading corrected or the fading and sensitivity corrected age is more likely to be representative of the 'true' age of a given sample. Changes in sample sensitivity were identified in the preliminary TL regeneration experiment (Fig. 3.7).

Samples were prepared as in Fig. 3.8. For the Óþoli Tephra mono-layers of purified glass were concentrated in the centre eight discs. For the Þörsmórk Ignimbrite sample was distributed evenly on the disc. Each TL read-out cycle (G1-G4) consists of disc irradiation on irradiator two (32. 0±0.6 $Gymin^{-1}$ + 5 Gy transit dose), PMT chamber pre-heating for 220°C for two minutes and TL signal read-out (to produce a 0-400°C glow curve as described in text). The natural TL signal from the Óþoli Tephra (SUTL 551) and the Þórsmörk Ignimbrite (ÞIG 7) was thermally removed and measured. The signal was then artificially regenerated beyond its natural TL signal by applying appropriate laboratory radiation doses. The scale of sensitivity change was constantly monitored and corrected for by applying a relatively small test dose (G_{even}) after each regeneration dose (G_{odd}). Test dose G_{even} = 100 Gy for the Óþoli Tephra and 25 Gy for the Þórsmörk Ignimbrite. Fading tests were carried out by irradiating, preheating and storing half the discs in each set in the dark for 60-70 days. Experimental conditions, procedures and doses applied for each sample are summarised in Appendix B2. ED values were determined by integrating over 10°C temperature bands for individual discs followed by weighted mean regression analysis of a form most suited to the data (*e.g.* linear, saturating exponential, saturating exponential + linear). TL age estimates were calculated from measured total dose rates and palaeodoses reconstructed from the thermally stable region of the glow curve determined by an ED plateau plot and the peak area of the glow curve. The SAR-TL procedure and experimental conditions are summarised in Table B2.3.

Box 3.3 Quantitative palaeodose reconstruction experiments.

(c) Pre-heating and fading

Post-irradiation pre-heating was undertaken to remove thermally unstable components. Long term (60-70 day) fading tests were undertaken to test and correct for the effects of anomalous fading. Test samples indicated that manual pre-heats of 220° C for two minutes, 155° C for five hours or 135° C for 16 hours successfully removed the laboratory-induced low temperature *ca.* 110° C TL peak. These temperatures and times were determined from archaeological glass-phase data in Sanderson (1986). Longer, lower temperature pre-heats were preferred when feasible to minimise the effects of fading and to avoid spurious plateau effects. Pre-heats of 220° C were completed on the heater plate within the PMT chamber immediately before read-out, while 135° C and 155° C pre-heats were undertaken in a muffle furnace. For anomalous fading tests, each set of discs was split. The first half-set were irradiated and all discs pre-heated before storage for 60-70 days at ambient temperatures. Any subsequent loss of signal is due to thermal and/or anomalous fading. The second half-set were irradiated after the two-month storage period. All discs were read out together.

(d) TL read-out

All thermoluminescence glow curves were recorded manually using an SUERC TL Research Reader assemblage consisting of an Electron Tubes 9883 QB Photo-multiplier Tube (PMT) fitted with Scott 7/59 and KG1 filters. During operation the PMT was continuously flushed with nitrogen to prevent oxidising reactions that might create spurious luminescence. At the beginning and end of each session the heater plate and surrounding area were cleaned carefully with acetone and the PMT tested using a phosphor of known luminescence intensity. Two or three dummy runs tested whether the temperature module and attached devices were functioning correctly. Blank contamination discs, cleaned with acetone and sprayed with Electolube SCO200D silicone grease, were placed on the work surface and read out at the end of each session. Sample discs were placed in the centre of the heater plate and heated from room temperature to 400° C at 5° Cs^{-1} (Fig. 3.8).

(e) Irradiation

Samples were irradiated together using irradiator 1 or 2 of an ELSEC 9022 irradiator. The irradiator used and dose rate applied is indicated in descriptions of the experimental methods and in data tables of section 4.5.2. Irradiator 1 is fitted with a 1.85 GBq ^{90}Sr β-ray source, giving a silicate dose rate of 55.88 $mGys^{-1}$ or 3.353±0.015 $Gymin^{-1}$ on 1/1/1999 and 54.50 $mGys^{-1}$ or 3.27±0.015 $Gymin^{-1}$ on 1/1/2000. The distance from source to sample for this irradiator is 15 mm. Irradiator 2 is fitted with a 11.1 GBq ^{90}Sr β-ray source, giving a silicate dose rate of 543.33 $mGys^{-1}$ or 32.6±0.6 $Gymin^{-1}$ on 2/9/1997 and 526.67 $mGys^{-1}$ or 31.6±0.6 $Gymin^{-1}$ on 1/1/2000. The distance from source to sample is 5 mm. Irradiator 1 has been calibrated to irradiators at the NPL, Harwell. Irradiator 2 was calibrated to irradiator 1 by SJR in December 1999 before undertaking the multiple aliquot and regeneration experiments (Appendix B2). This gave a working dose rate of 32.00±0.6 $Gymin^{-1}$ and a transit dose of 5.19 Gy. These values were used to calculate exposure times for TL Experiments 4 and 5 (Box 3.3).

3.4.3 Testing which phase is responsible for the TL signal

The following three tests investigated the whether the glass-phase purification procedure was successful and/or whether the TL signal was most likely coming from the glass-phase.

(a) Visual examination of purified sub-samples

Sub-samples of each purified glass fraction were mounted in Canada Balsam and examined on a binocular microscope under normal and cross-polarised light at 100x and where necessary 400x magnification to identify contaminant phases (predominantly feldspars). Samples that were possibly contaminated were not used in quantitative dating experiments. In addition, SEM images of samples chosen for SEM-EDS chemical mapping were systematically scanned at 320x magnification and sometimes examined at 640x magnification.

(b) Energy Dispersive System-Scanning Electron Microscope (EDS-SEM) chemical mapping

The overall aim of this experiment was to identify feldspathic and other non-glass phase contamination. EDS-SEM chemical mapping can is a useful semi-quantitative tool for identifying broad chemical variations in large and/or bulk samples. In theory it should be possible to identify contaminant grains in the purified glass matrix. In practice, contaminant grains could be hidden by shard-shard effects. Nevertheless, EDS-SEM chemical mapping provides a straightforward, if time consuming, semi-quantitative measure of glass-phase purity.

EDS chemical maps were constructed for the following randomly selected discs used in the SAR-TL experiment (Expt. no. 5): (Óþoli Tephra) SUTL 551-D2 (possibly contaminated between G20 and G21 of the SAR-TL experiment); 551-D6; 551-D8; (Þörsmórk Ignimbrite-ÞIG 7): ÞIG 7-D4; ÞIG 7-D5; EDS chemical maps were also constructed for purified glass fractions of the following samples using in the Natural vs 50 Gy experiment (Expt. no. 1): ASK 10-D1; OR 2-D4; ÞIG 1b-D1; ÞIG 1c-D1: ÞIG 5-D1; ÞIG11-D1; PIG16-D2. Discs were attached to SEM stubs and carbon coated. SEM and EDS-SEM chemical mapping images were taken using Philips XL30CP SEM running LINK ISIS software. Beam current was 33 μA, operating voltage 20 kV, filament current 37.1 A, working distance 10 μm, and spot size 6 μm. Images were saved as TIF files. EDS-SEM chemical maps were constructed for eight major elements, as for EPMA, but omitting MnO, using a run time of 30 minutes per disc.

(c) REE composition of separated fractions

An additional ICP-MS trace element experiment was performed on the Óþoli Tephra to evaluate the purity of the glass fractions used in TL dating determine if the trace element chemistry, and in particular the europium (Eu) and/or europium anomaly (Eu*; see section 5.5.1 for a full discussion), of the density separated fractions varied significantly from bulk material. The <90 μm - <2.3, -2.3-2.4, - >2.4 gcm^{-3} and the 90-150 μm - <2.3, -2.3-2.4, - >2.4 gcm^{-3}. It was not possible to repeat this

experiment with ÞIG 1b and ÞIG 7 samples form the Þörsmórk Ignimbrite because there was insufficient quantities of purified material at the end of the dating experiments.

3.5 Testing FT & TL Ages of the Óþoli Tephra: Palaeomagnetic Polarity Reversal Dating Analysis

Palaeomagnetic sample collection procedures are described in section 3.1. Samples were analysed in a MINISPIN high sensitivity, slow speed fluxgate magnetometer. Way-up orientation on all cubes was standardised before spinning. Cubes were spun at 6 Hz about a vertical axis inside a triple shielded cylindrical fluxgate and the output integrated over 6 seconds (24 spins). The magnitude and phases of the signal were extracted calculated automatically by Fourier analysis. Declination measurements were corrected according to the measured section bearing assuming pots were inserted at exactly 90° to this measurement. Inclination was not corrected because dip of the beds could not be measured or was not significant (*i.e.* <20°). Sensitivity of the equipment is better than 0.1×10^{-1} emu Cm^{-3} (10^{-4} A/m) for 24 seconds integration time, but less for 6 second integration time (Molspin, 2001).

Chapter 4
Results

The results obtained during the course of this study are arranged under the following sub-headings:

4.1 Identification of tephra within stratigraphic sections

4.2 Chemical characteristics & correlation dating of tephra deposits

4.3 Radiogenic dating techniques I: Fission-track dating results

4.4 Radiogenic dating techniques II: Thermoluminescence results

4.5 Independent age constraints on fission-track and thermoluminescence ages of the Óþoli Tephra

Full datasets can be found in Appendix C. Lists of chemical data, fission-track count data, dose rate calculations, full 1°C and 10°C palaeodose reconstruction datasets for the TL Experiments 1-5, and full details of regression results not amenable to printing can be found the enclosed CD-R in the appropriate Appendices folder. These datasets are in Word 97, Excel 97 and PDF format and are made available to enable the reader to see how final answers in Chapter 4 were calculated. The copyright of these datasets rests with the author and permission to use them should be sought.

4.1 Identification of tephra deposits

4.1.1 Vestfírðir Peninsula

(a) Skagafjall

Figure 4.1 shows the main sedimentological and geomorphological features of Skagafjall as examined in June-August 1998-99[24] by SJR and Jon Sigurvinsson. Sigurvinsson (1983) labelled the best exposures Sections A-C and his notation is retained here (Fig. 4.1-e, f). Full descriptions of each unit can be found in Table 5.4, alongside detailed interpretation of their significance.

The central area of the Skagafjall sedimentary deposits forms a narrow 5 km ridge, constituting the uppermost stratigraphic unit of Skagafjall. The near surface outcrop of the Óþoli Tephra is visible from aerial photographs (Fig. 4.1-c) and false colour satellite remote sensing images (Fig. 1.7-c) as an area of light grey adjacent to the precipitous Dýrafjörður-facing upper cliff-edge. This effect is clearly visible at Section C in Figure 4.1-a. Similar deposits are visible towards the north-western tip of Skagafjall in and around Fjallskagi, but heavy debris cover prevented identification of further stratigraphic sections in this region. Small and poorly developed cirques are found along this cliff-face, in contrast to Sauðanes which has three well-developed cirque features (Fig. 1.7-c). The lower cliff-face is composed of rock fall debris and gullied slump deposits. A heavily reworked tephra deposit of broadly similar composition to the Óþoli Tephra was found in the two pronged gullied slump deposit approximately below sections A and B in June 1999 while en-route to Fjallskagi (Table C1.1: Skagafjall Basal Tephras). Landslides[25] are confined to the north-western end of Skagafjall. There is one major landslide, Fjallskagi, on the Dýrafjörður-facing cliff face and several smaller apparent cliff-failure slumps on the Nesdalur facing tip of Skagi (Fig. 4.1-c, d). The plateau surface is characterised by zones of large scale (1-2 m diameter) sorted polygons[26] in the central region to the north of Section A and near-parallel large scale (>500 m long) sorted-stripes[27] and soil development (frozen to a depth of *ca.* 1 m) on the north-western tip of Skagi (Fig. 4.1-e). Extensive blockfields[28]

[24] All latitude and longitude measurements in this chapter were taken using a handheld Magellan GPS. The accuracy of this was checked against the GPS reference post at Arnarnes on the north-eastern fjord entrance of Skutlsfjörður (Ísafjörður). Altitude measurements were taken from 1:50, 000 or 1:25, 000 maps obtained from Landmælingar Íslands.

[25] Sigurvinsson's (1983) classification of the Fjallskagi and Nesdalur cliff-edge slump features as landslides is retained here, although Gudmunðsson A. (*pers. comm.*) suggests that all these features are more likely to be rock glaciers. A justifiable case can be made for both scenarios.

[26] Defined as 'a form of patterned ground "whose mesh is dominantly polygonal and has a sorted appearance commonly due to a border of stones surrounding finer material" (Washburn, 1956, p. 831) ... never developed singularly. Diameter a few centimetres to 10 m' (Gary *et al.*, 1976, p. 675). Smaller scale and rock size sorted polygons can be found within the larger scale sorted polygons shown in Figure 4.1-g.

[27] Defined as 'alternating bands of finer and coarser material comprising a form of patterned ground characterised by "a striped pattern and sorted appearance due to parallel lines of stones and intervening strips of dominantly finer material orientated down the steepest slope" (Washburn, 1956, p. 836) ... usually occurring as one of many evenly spaced stripes that often exceed 100 m in length on slopes as high as 30°. An individual stripe may be a few centimetres to 2 m wide with intervening area two to five times wider.' (Gary *et al.*, 1976, p. 675). The large scale stone stripes on Skagafjall can be seen (faintly) on the distant slope in Figure 4.1-m.

[28] Defined as felsenmeer (*translation: 'sea of rocks'*) as 'a flat or gently sloping area covered with a continuous veneer of large angular and subangular blocks of rock derived from well-jointed underlying bedrock by intensive

exist on the highest point of the Skagafjall plateau to the east and south-east of section C towards Óþoli. Numerous medium (0.5-1 m diameter) to large (>1 m) sub-angular-rounded boulders can be found scattered on the surface, although none are as large as the 2-3 m diameter boulders found on Sauðanes. The only large (>0.5 m diameter) erratic with large olivine and pyroxene phenocrysts embedded in a fine-grained basalt matrix (SKAG-1) was sampled for ^{3}He cosmogenic surface exposure dating (Fig. 4.1-h). All other boulders of this size were olivine phenocryst-free.

The best outcrops of the sedimentary deposits are found in narrow (< 1-2 m wide) vertical sections (A-C; Fig. 4.1 a, b) in the central portion of Skagafjall. Section A is the most complete section, but only lower units were partially revealed in mid-late summer 1998 by meltwater from cliff-face snow patches. The Óþoli Tephra was not observed in Section A (Fig. 4.1-f). The lower units 1-3 of Section A remained covered in snow throughout the summer of 1999. The best exposures in sections A and B are 1-2 m wide, at most, and tracing the lateral continuity of stratigraphic units proved difficult for this reason. Sections B and C were fully exposed, but these and the upper units 8-11 of section A were partially buried beneath a veneer of virtually impenetrable slope debris. The direct and unconformable basal contact with the Tertiary basalt lava pile (*ca.* 14 Ma) is partly visible *ca.* 500 m.a.s.l. in Section A and *ca.* 580 m.a.s.l. in Section C.

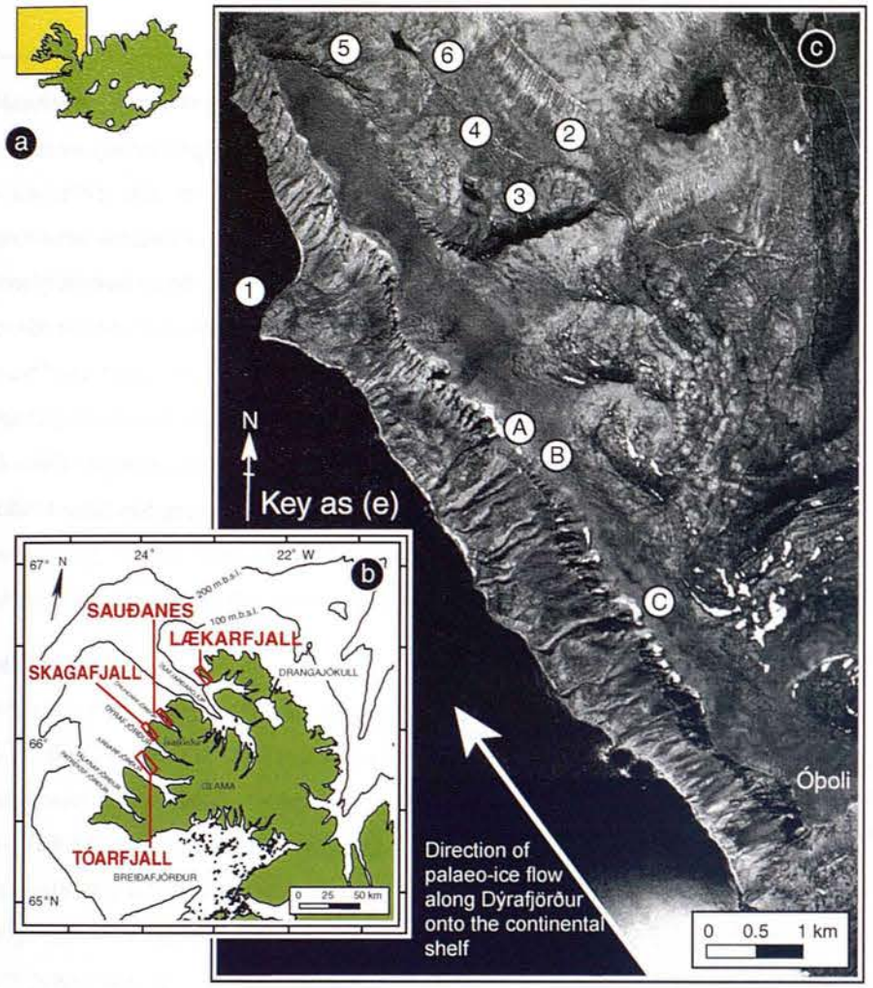
Four distinct sedimentary facies were noted within sections A-C and these are broadly similar to the descriptions in Sigurvinsson (1983):

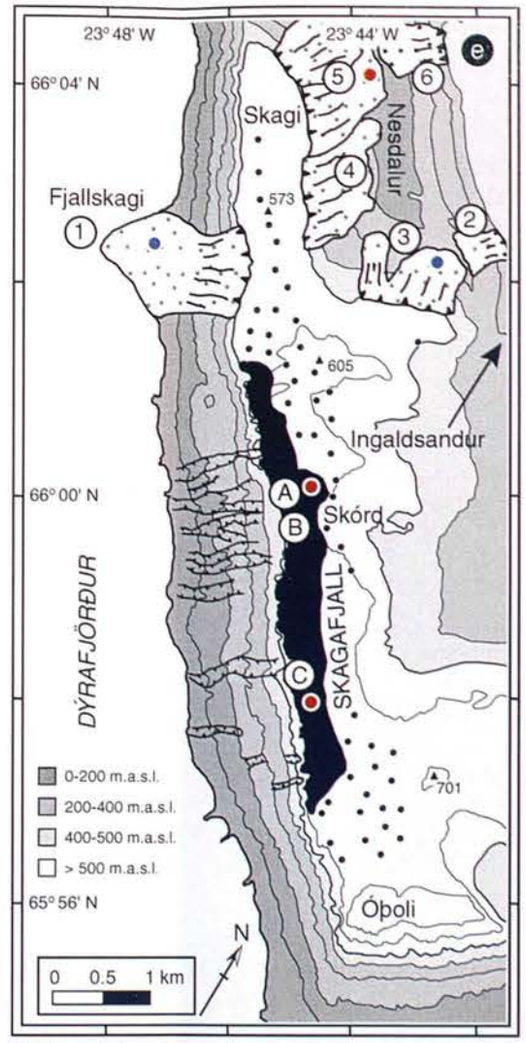
1) **Rhythmic deposits (rhythmite beds)** (RB; after Flint, 1970), on Skagafjall were defined by Sigurvinsson (1983) as 'individual units or couplets of rhythmic strata, without implication as to thickness of pair or period rhythm' (p. 102). Three types were recognised prior to this study. Repetitive interbeds of dark brown clay-silt, usually 3-10 cm thick, and orange clay, usually 2-3 cm thick, are most common (Fig. 4.1-i), but thinner rhythmitic laminations occur throughout the sequence (Fig. 4.1-k). In August 1998, when the sections were well-exposed due to a warmer than average summer, numerous ice-rafted dropstones were found in rhythmite bed 8 (Fig. 4.1-j). Sigurvinsson (1983) concluded that these were formed in a glacial lacustrine environment, most probably in an ice-dammed lake that formed due to increased melt-out at the lateral margins of an ice sheet that flowed north-westwards along Dýrafjörður (Fig. 4.1-a). Sigurvinsson (1983) makes a strong case for each couplet being an annual deposit, *i.e.* a varve, and, if so, the ice-dammed lake existed for at least 2000 years. In addition, the different types of rhythmite bed were thought to reflect different rates of sedimentation associated with the relative location of a nearby glaciolacustrine delta inlet.

---

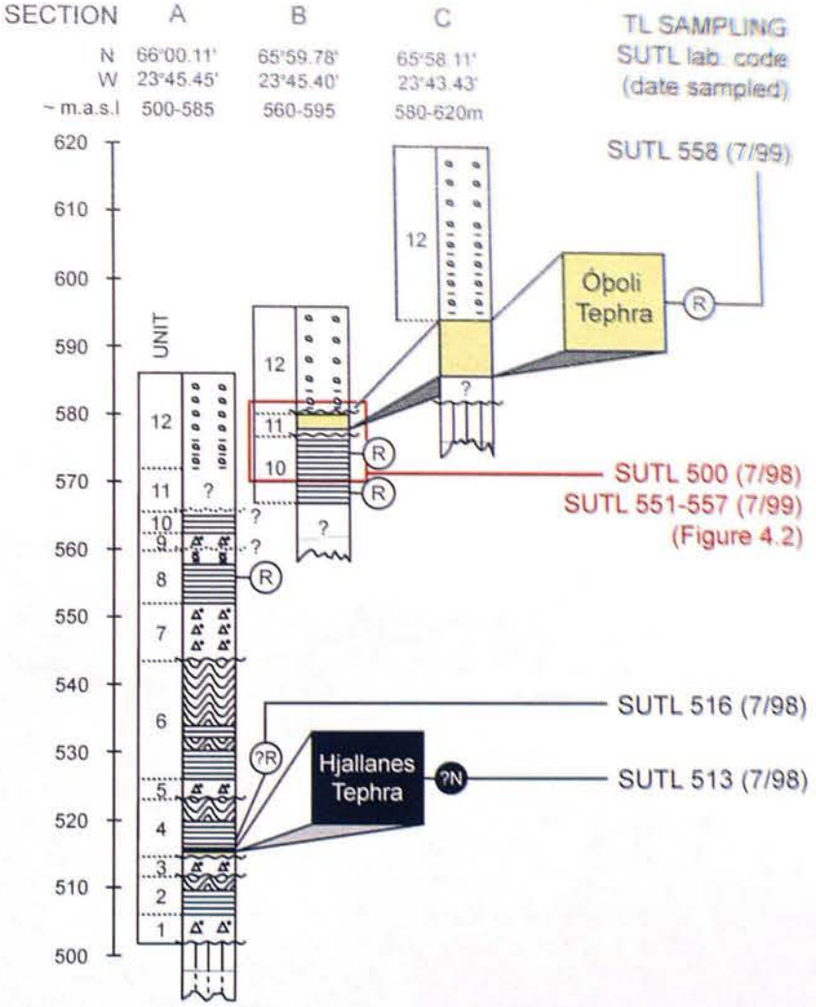
frost action and usually occurring *in-situ* on high, flat-topped mountains or plateaux above the timberline in middle and high latitudes' (Gary *et al.* 1976, p.256).

1) Skagafjall, NW Peninsula, Iceland: Principal sites and summary geomorphological map*





2) Stratigraphic logs of exposed sections & sampling strategy*



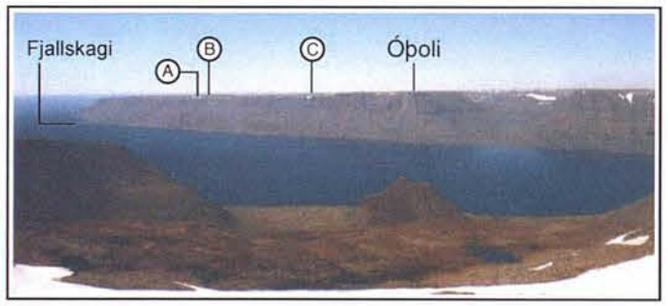
Sedimentary deposits
- Silicic Tephra
- Basic Tephra
- Diamicton
- Silt
- Gravel & boulders
- Silt & clay
- Sand & gravel
- Clay
- Sand
- Rhythmites
- Sand & silt
- Deformed rhythmites

Palaeomagnetic polarity
- N Normal
- ?N Uncertain (probably N)
- R Reversed
- ?R Uncertain (probably R)
- ? Uncertain

(see Table 4.8)

Other
- Tertiary basalt bedrock *ca.* 14 Ma
- Unconformities

d



View from Helgafell, looking approx. N across Dýrafjörður.

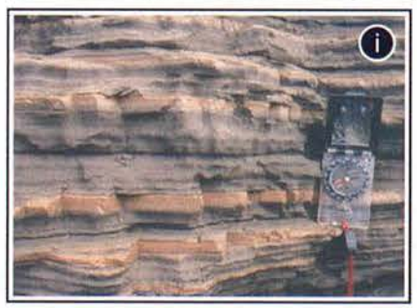
- (A) Exposed sections
- Proposed limit of sedimentary deposits
- Fine grained basalt erratics
- Coarse grained olivine & pyroxene phenocryst-rich basalt erratics sampled for ^{3}He cosmogenic SED
- Zones of medium grained olivine and pyroxene phenocryst-rich basalt erratics sampled for ^{3}He cosmogenic SED
- & (1) Postglacial landslides / rock glaciers
- Cliff scars & associated talus
- 701 Spot heights

3) Plateau surface features

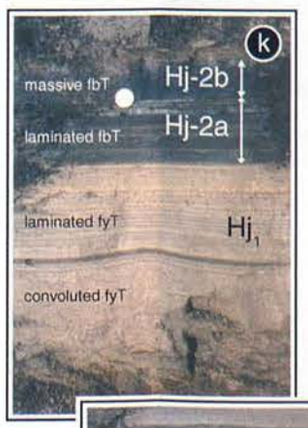




4) Section A: Sedimentary deposits & Hjallanes Tephra

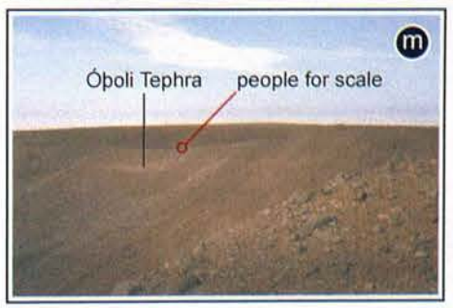








5) Section B & airfall Óþoli Tephra





6) Section C



Figure 4.1 The Óþoli Tephra, Skagafjall, NW Iceland: Summary geomorphology, stratigraphic logs and other features; *redrawn & modified from Sigurvinsson (1983) ***contd.***

Figure 4.1 ***(contd.)*** The Óþoli Tephra, Skagafjall, NW Iceland.

(a) Location map for the North West Peninsula, Iceland.
(b) Location map for Skagafjall, NW Peninsula, Iceland.
(c) Aerial photograph of Skagafjall, taken on 20/7/91. Scale is approximately the same as (e). Location of the exposed sedimentary sections, A-C, and major landslides (or possible rock glaciers (Gudmunðsson, pers. comm.) 1-6, are marked. The broad outline of the limit of the sedimentary deposits can be best seen near C as a light grey area close to the cliff edge. The assumed direction of major palaeo-ice streams emptying onto the continental shelf from source area to the SE of Skagafjall is also shown.
(d) View of Skagafjall from the opposite peninsula, looking approximately north across Dýrafjörður with the location of exposed sedimentary sections A-C, Fjallskagi and Óþoli are marked.
(e) Summary geomorphological map of Skagafjall (re-drawn and modified from Sigurvinsson, 1982, 1983). Exposed section locations, major landslides/rock glaciers are marked. Erratics examined for potential use in ^{3}He cosmogenic surface exposure dating (SED) are classified and locations marked.
(f) Stratigraphic logs of exposed sections, preliminary palaeomagnetic polarity results and thermoluminescence (TL) sampling strategy.
(g) Large scale sorted rock polygon periglacial features on the Skagafjall plateau surface. Each polygon is approximately two metres in diameter. This picture was taken close to the 605 m.a.s.l. spot height in (e). The plateau surface beyond section C and across to the spot height at 701 m.a.s.l. consists entirely of shattered blockfield bedrock debris and with no active soil growth or sorted rock polygons evident.
(h) Cosmogenic sampling of SKAG1 from olivine phenocryst-rich erratic, only one of two such boulders found on Skagafjall. SKAG1 was the most apparently suitable of all boulders sampled for ^{3}He cosmogenic surface exposure dating.
(i) Undeformed and partially lithified rhythmites of rhythmite bed 6 (RB6) of section A.
(j) Dropstones embedded in otherwise undeformed rhythmites of RB8.
(k) Hjallanes Tephra in section A between units 3 & 4 (see text for full description).
(l) Micro-tectonic structures at the base of the Hjallanes Tephra deposit.
(m) Section B taken from section C. Note the people for scale, the visible pale yellow outcrop of the Óþoli Tephra and the poorly sorted debris in the foreground.
(n) Airfall component of the Óþoli Tephra – approximately 8-10 cm of structureless, unconsolidated ash devoid of reworked rhythmite bed material.
(o) Section C from the base of the Óþoli Tephra at this site. Note the poorly sorted debris littering the section.

clay rhythmite couplets and sand partings. This was called Hj-1. Overlying Hj-1 is a black tephra deposit with otherwise similar lithological characteristics. This unit was called Hj-2a. The upper unit is a massive black tephra of sand-silt grade and was called Hj-2b.

Hj-1 is 15-20 cm thick and contains at least 25 finely laminated couplets, each up to 2-3 cm thick, composed of partially lithified yellow tephra of clay-silt grain size that grades upwards into a coarser grey deposit of sand grain size (Fig. 4.1-k). The upper contact of each couplet is distinct. This sub-unit rests unconformably on a convoluted erosional contact of sand and gravel, 20-30 cm thick, that caps the diamicton deposit of unit 3. There are a series of micro-graben structures in the basal 5 cm of Hj-1 (Fig. 4.1-l) possibly created by the convoluted nature of the erosional surface and the subsequent overburden pressure. These micro-faults are capped by 5-6 cm of convoluted yellow tephra and grey sand laminations. A 0.5 cm thick coarse grey sand layer separates the convoluted and horizontal laminations.

Hj-2 is 10-12 cm thick in total. The contact with Hj-1 is sharp. The basal 5-6 cm consists of fine black tephra and brown clay-silt grain size couplets (Hj-2a). The upper contact of each couplet is distinct. Capping these tephra based couplets, 33 cm below RB4, is a 3.8 cm thick layer of massive structureless fine black tephra of sine sand-silt grain size that fines upwards into a more consolidated, structureless, 1 cm thick, olive-green tephra deposit (Hj-2b). The upper and lower contacts of this deposit are distinct. The Hjallanes Tephra unit is capped by a series of non-tephra based sedimentary couplets with a total thickness of 30-40 cm. These are similar in composition to rhythmite bed three (RB3) and other rhythmic deposits in this section, but each couplet is up to 2 cm thick, compared with upwards of 10 cm thick for the other rhythmite deposits (Fig. 4.1-j). A basal erosional contact consisting of coarse orange sand separates this unit from DB3.

The Hjallanes Tephra was only exposed in August 1998. Most of section A, from unit 4 downwards, remained covered by snow throughout June and July 1999. No other tephra deposits were found in the exposed sections.

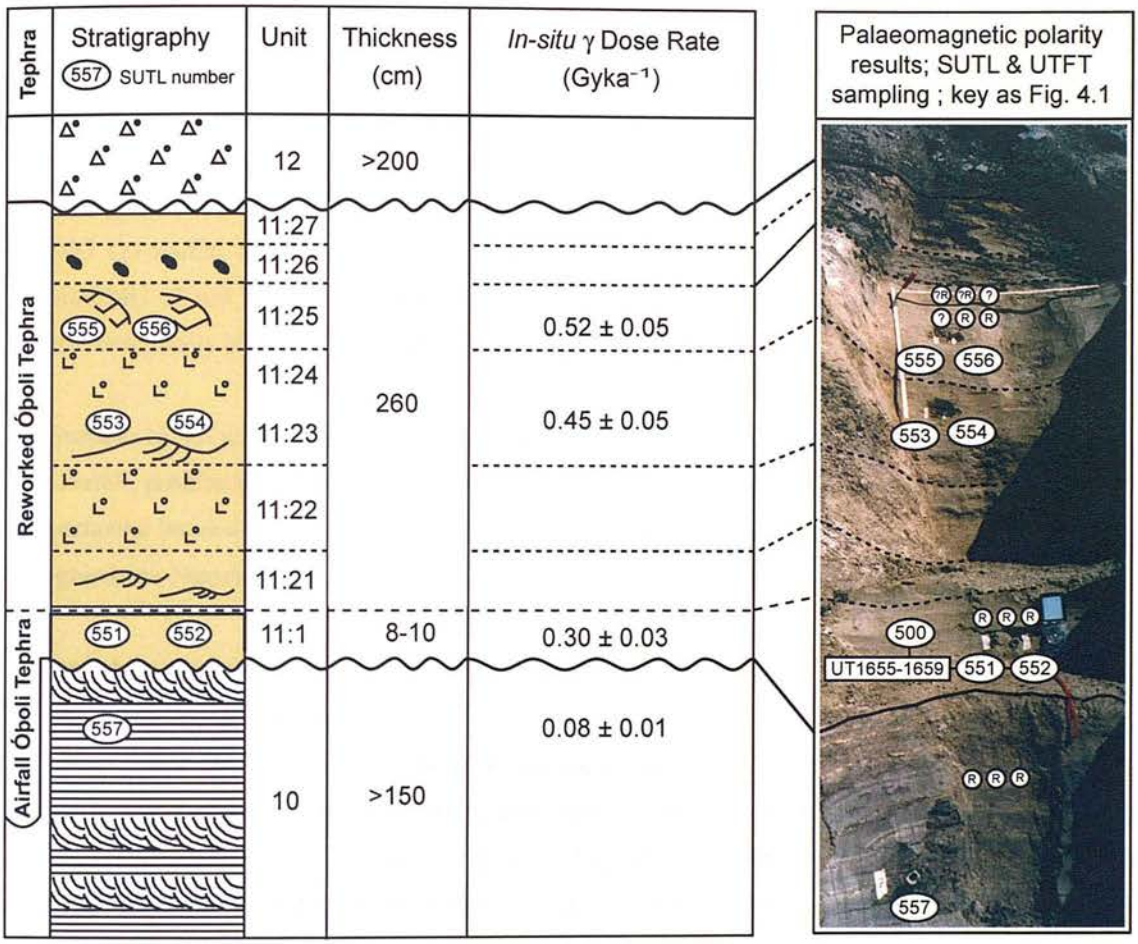
(b) Sauðanes

Traces of material similar to the rhythmite beds of Skagafjall were found at a similar altitude on Sauðanes. No tephra deposits were found. Numerous large erratics litter the plateau surface, some between 2-3 m in diameter, but, as with Skagafjall, the majority are fine-grained basalts with small (<1 mm) feldspar phenocrysts. Four boulders with large olivine/pyroxene phenocrysts suitable for ^{3}He cosmogenic SED were found (SAUD 1-4).

(c) Tóarfjall & Lækjarfjall

No traces of high altitude sedimentary deposits were found on Helgafell and Tóarfjall, on the southern fjord facing side of Dýrafjörður during a reconnaissance visit in June 1998. To date none have been

found on either the northern or southern edge of Súgandafjörður, the next, smaller fjord north of Önundarfjörður (Sigurvinsson, *pers. comm.*). Similarly, no sedimentary deposits were found on the Ísafjarðardjúp fjord facing cliff-edge of Lækjarfjall on Hornstranðir during a brief visit in early July 1999. This plateau surface is predominantly exposed lava pile bedrock littered with small-medium sized boulders none of which were suitable for ^{3}He cosmogenic surface exposure dating.



Sedimentary deposits

- Silicic Tephra
- Diamicton
- Gravel & boulders
- Sand & gravel
- Sand
- Sand & silt
- Basic Tephra
- Silt
- Silt & clay
- Clay
- Rhythmites
- Deformed rhythmites

Palaeomagnetic polarity

- N Normal
- ?N Uncertain (probably N)
- R Reversed
- ?R Uncertain (probably R)
- ? Uncertain

Sedimentary structures

- Small scale cross bedding (10-20 cm height)
- Climbing ripple structures (variable height / amplitude between 0-50 cm)

Other Tertiary basalt bedrock *ca.*14 Ma — Unconformities

Figure 4.2 Detailed stratigraphic log of Skagfjall section B units 10-12 and sampling strategy for luminescence and fission-track dating of the Óþoli Tephra. These units contain the most stratigraphically well-constrained & accessible outcrop of the Óþoli Tephra. Results of *in-situ* gamma (γ) spectrometry readings are shown. The γ-dose rate of the tephra deposit is an order of magnitude greater than that of the underlying rhythmite bed (RB10). The dose rate is higher in the reworked tephra deposit compared to the airfall component and highest in the part of the reworked deposit that contains the smallest proportion of reworked silt and clay deposits.

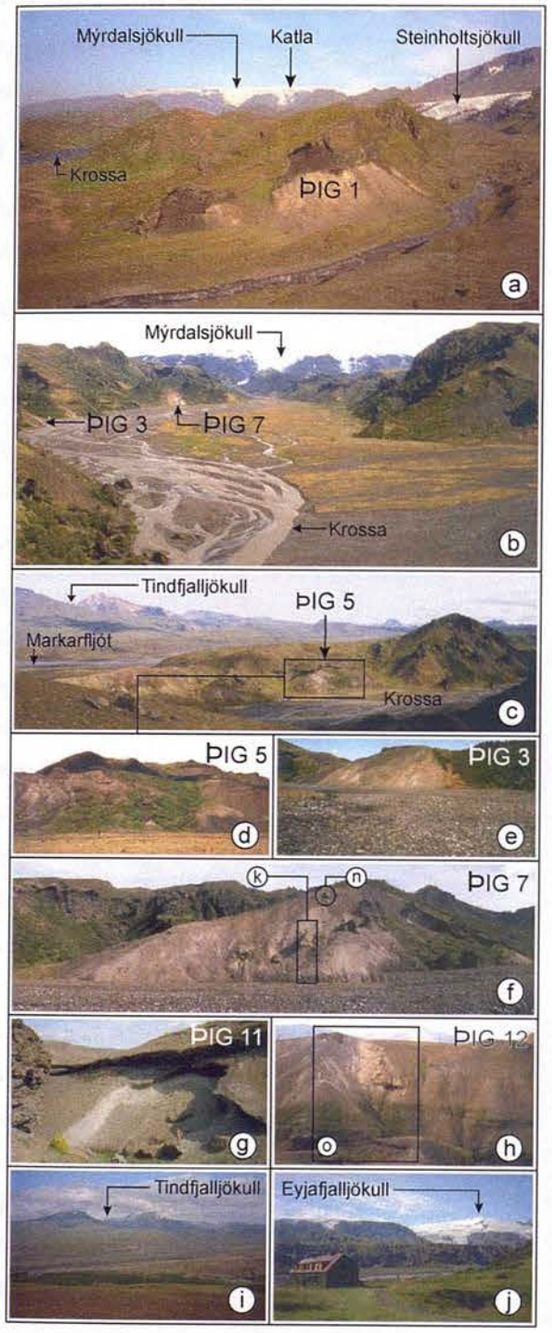
4.1.2 Þörsmórk Ignimbrite

The thickest ignimbrite deposits are along the principal valleys and outlet routes from Mydralsjökull. The most visible and heavily eroded ignimbrite exposures are located along the northern border of the sandur of the Krossa river where the thickness of the ignimbrite is about 10-50 m (Fig. 4.3: b-f, cross-section C-D). Some sections, *e.g.* site ÞIG 7, have been completely exposed along the main outlet routes of the Mydralsjökull ice cap, Markarfljót and the Krossa. At others stratigraphic sections are well-preserved and distinct contacts between lithofacies units are clearly (site ÞIG 1) or partially (site ÞIG 12) visible. Site ÞIG 12 was inaccessible, but mapped from the opposite riverbank. Sections at sites ÞIG 12 and 15 are covered by a veneer of weathered pumice and ash deposits up to 100 m thick that completely obscure the underlying stratigraphy.

Sections to the north of the Krossa are generally between 10-50 m thick (Fig. 4.3: g-h, section A-B). Overall, profiles in this region are up to 150 m thick (*e.g.* site ÞIG 12; Fig. 4.3; o). Site ÞIG 12 is of particular interest because it the only locality where a distinct unit of pillow lava is visible beneath the ignimbrite deposit (Fig. 4.3; o-p). The contacts between all the units at site ÞIG 12 are obscured.

Ignimbrite deposits between 10-20 m thick were found on either side of Steinholtsdalur (Fig. 4.3-a, Section A & B). The deposits that bracket the main ignimbrite body in this area are intriguing. A laterally discontinuous layer of unwelded rhyolitic co-ignimbrite ash, 1-2m thick, with 5-20 cm thick layers dominated by white pumiceous clasts, up to 5 cm in diameter, overlies the main ignimbrite body at a single locality - site ÞIG 1 (Fig. 4.3-a, l, r). This co-ignimbrite ash bed is capped by a black, basaltic tuff unit of similar thickness that is in turn overlain by a 10-15 m unit of fragmented pebble to cobble sized clasts of vesicular and fine grained basalt, 5-10 cm in diameter, some with glassy rinds, set in a welded glass/black tuff dominated matrix (*i.e.* hyaloclastite). The contacts between the ash, tuff and hyaloclastite deposits are pronounced (Figure 4.3-r). Lithic and pumice dominated layers 10-20 cm thick can be found in the area beneath the co-ignimbrite ash deposit and in the direction of the Gigjökull lateral moraine, but the contact between the co-ignimbrite ash and the layered ignimbrite is obscured. On the northern perimeter of Steinholtsjökull, at site ÞIG 6, the ignimbrite outcrops in a highly localised zone as weathered slope-ash that blankets a series of lava flow-beds, each about 5 m thick. These lava beds can be traced east and southwards up Steinholtsdalur to the glacier-bedrock intersection. At site ÞIG 6 the ignimbrite is covered by about 15-20 m of inter-bedded basaltic tuff, hyaloclastite and tillite deposits. The upper and lower contacts of the ignimbrite are obscured by substantial volumes of slope debris.

The Þörsmórk Ignimbrite blanketed the Þörsmórk region of southern Iceland. The thickest units were probably the result of deposition from pyroclastic flows that became concentrated in large topographic depressions that existed at the time of the eruption. The results of this study confirm the findings of



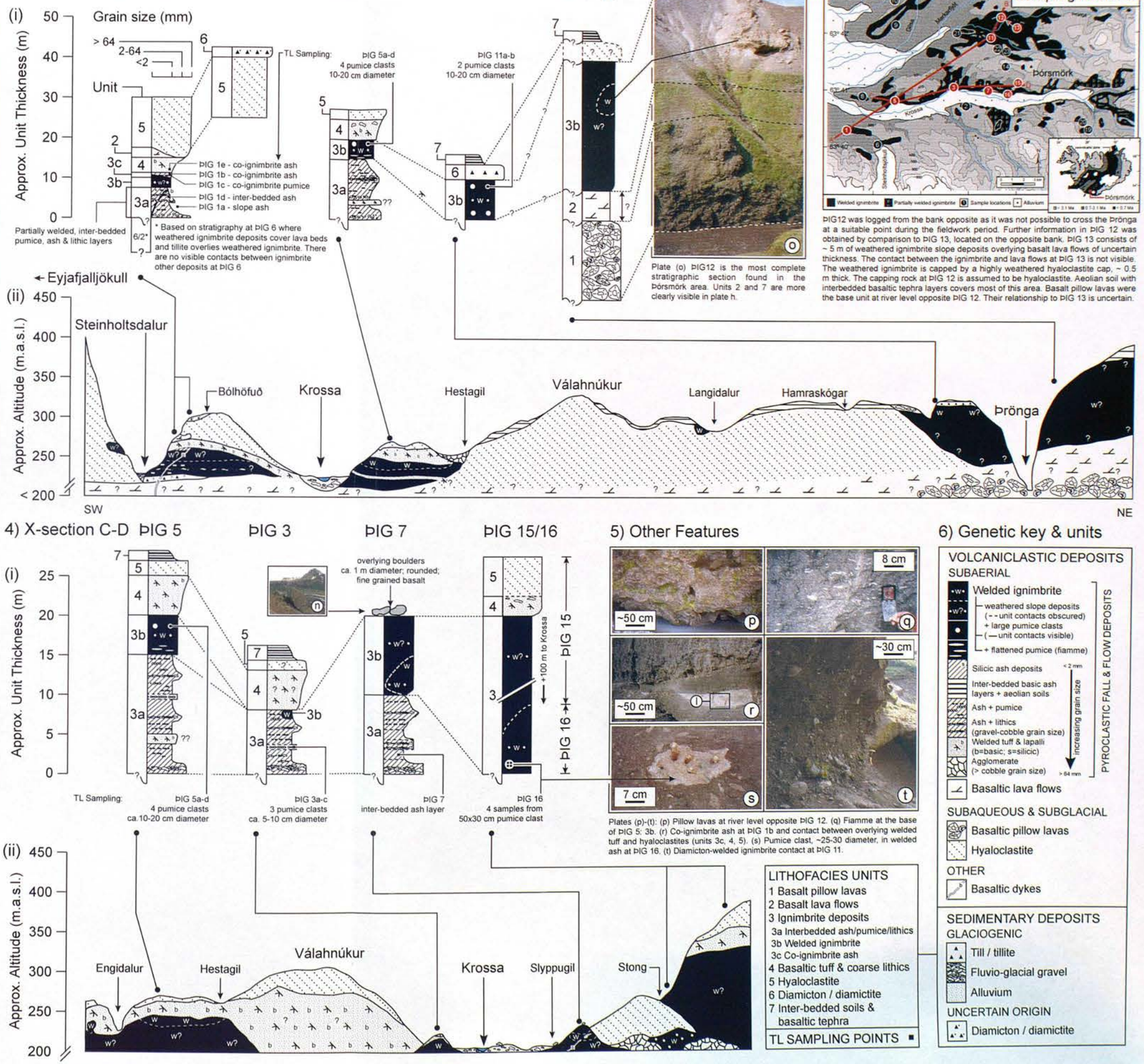


Figure 4.3 The Þórsmörk Ignimbrite (ÞIG): Composite stratigraphic logs of main lithofacies units at principal sites, sampling strategy and schematic cross sections *contd.*

Figure 4.3 ***(contd.)*** The Þörsmórk Ignimbrite

(a) Site ÞIG 1, taken from the lateral moraine of Gigjökull, looking approximately E up the Krossa towards Mýrdalsjökull.
(b) Sites ÞIG 3 & 7, taken from Valahnjúkur looking approximately E up the Krossa towards Mýrdalsjökull.
(c) Site ÞIG 5, taken from the top of site ÞIG 6, looking approximately NNE towards Tindfjalljökull in the distance.
(d) Close up of site ÞIG 5 with person in red jacket for scale.
(e) Site ÞIG 3 looking approximately W down the Krossa.
(f) Site ÞIG 7 taken from the Krossa sandur looking N at main sampling sites (k) and erratics near the top of the deposit.
(g) Site ÞIG 11 looking NNE with person at the bottom edge of the shadow for scale.
(h) Site ÞIG 12 taken from the top of the hill at site ÞIG 13 looking approximately N.
(i) Tindfjalljökull taken from Tindfjöll looking NW.
(j) Eyjafjalljökull taken from the Langidalur campsite looking SW.
(k) TL sampling at site ÞIG 7 in interbedded ash, pumice and lithic layers, similar to shown in (m), beneath an outcrop of welded ignimbrite.
(l) TL sampling at ÞIG 1b in ash rich co-ignimbrite ash and pumice layers.
(m) TL sampling of inter-bedded ash layers at ÞIG 3.
(n) Erratics near the top surface of site ÞIG 7
(o) Site ÞIG 12 taken from a vantage point on the south side of the Þronga, uncrossable at this point.
(p) Basalt pillow structures at river level opposite site ÞIG 12
(q) Flattened pumice clasts (fiamme), approximately 5 cm long, in a welded ash and lithic matrix at site ÞIG 5.
(r) Co-ignimbrite ash, black tuff and capping hyaloclastites at site ÞIG 1b.
(s) TL sampling of a large (*ca.* 25-30 cm in diameter) pumice clast in a welded ash and lithic matrix at site ÞIG 16.
(t) Poorly sorted, rounded boulders and pebbles in loose soil and fine-grained matrix (diamicton) contact with welded ignimbrite (hammer) at site ÞIG 11.

Sampling location map re-drawn and modified from Jørgensen (1980). For sites not visited, distribution and classification of ignimbrite deposits is as Jørgensen (1980; 1981).

Jørgensen (1980, 1981) who suggested that, on a macroscale, this palaeotopography was similar to today.

4.1.3 Holocene age control, highly silicic tephra deposits

Ash deposits from the Plinian phase of the Öræfi 1362 AD and Askja 1875 AD eruptions were sampled from locations indicated in Figure 4.4 and Table 4.1-a.

(a) Öræfi 1362 (Ö1362)

Layers of Ö1362 were sampled from locations indicated in Table 4.1-a. Sample ÖR 3 was sampled by SJR from the steep northern slope in Fossdalur. In total it is an 8 cm thick, fine white ash deposit with no pumice and bracketed by orange-brown aeolian soils and black tephra layers. Samples were taken from the 1-4 cm interval of this deposit.

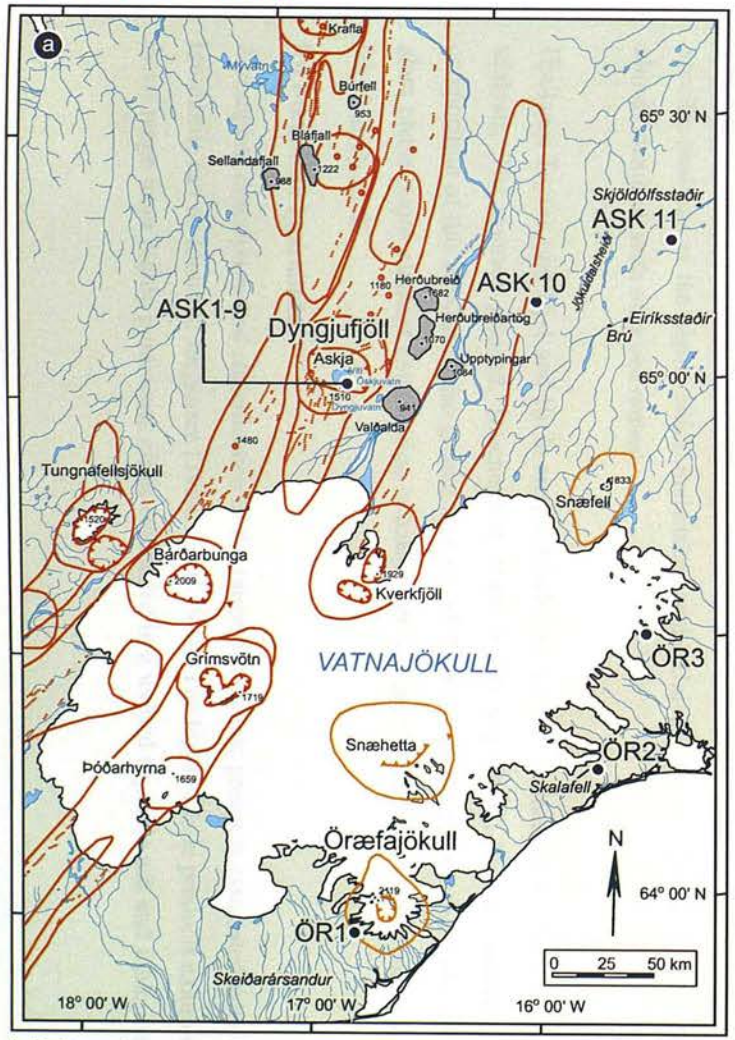
(b) Askja 1875 (A1875)

ASK 5 is located near to the crater floor. It is a 10-15 cm thick structureless white ash layer up to 1 m thick in places and bracketed by an uncertain basal deposit and layers of clast supported pumice that fines upwards into matrix supported pumice and ash. The structureless white ash layer was selected because it is almost completely devoid of visible phenocrysts. ASK 6 is located approximately 5 m above ASK 5, near the top of Layer 'D' of Sparks *et al.* (1981). The ASK 6 sample was taken from a layer of mixed white ash, pumice and black scoria immediately above a 30 cm thick layer of coarse pumice with clasts up to 20 cm in diameter. The deposit is capped by a 2-3 m thick unit of coarse volcanic breccia consisting predominantly of clast supported porphyritic basalt clasts typically 5-10 cm in diameter, but some up to 20-30 cm and larger.

ASK 10 and ASK 11 were sampled from roadside cuttings along the main 910-923-Route 1 from Askja to Egilsstadir in eastern Iceland. ASK 10 is a white ash and pumice deposit about 8 cm thick in total. The bottom 1-2 cm is airfall ash[29] and this grades up into a fine ash and pumice rich upper layer. The airfall ash was sampled with care to avoid sampling of the underlying grey-brown aeolian soil. ASK 11 is a white ash layer, 3 cm thick in total. The bottom 2 cm appear to be an airfall deposit with perhaps some secondary thickening due to slope wash. The deposit is bracketed by a orange-brown aeolian soil with interbedded, subhorizontal, black tephra deposits.

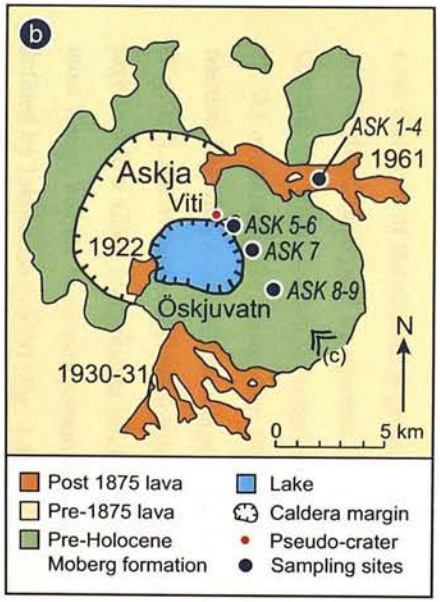
[29] An airfall ash layer in this context is structureless, evenly distributed in a laterally continuous manner so that it mantles the underlying topography with no visible signs of erosion. Reworked ash contains significant proportions (*e.g.* > 25%) of non-tephritic material with evidence for mixing and/or sedimentary structures. Reworked tephra or tephra that has experienced secondary thickening was not sampled to avoid contamination by non-tephra deposits.

1) Sample location map



(a) Solid red & orange lines are outlines of the the main volcanic systems; broken lines red and orange lines are fissure swarms; triangulated lines are caldera margin; red circles are craters and grey areas outlines of the main table mountains ('mobergs'). ÖR1 & 2 samples were identified by their stratigraphic position & collected in the same manner as ASK samples by Dr. Andrew Dugmore (AJD); ÖR3 was collected by SJR.

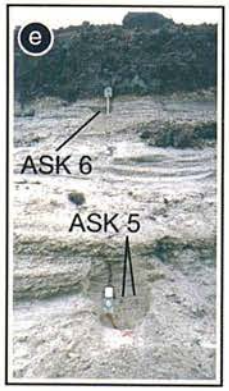
2) Askja 1875 summary geology, sample location map & TL sampling







(b) Summary geological map & ASK 1-9 sampling sites (adapted from Sparks *et al.*, 1981); **(c)** Askja caldera from SE rim & ASK 5-9 sampling sites; **(d)** A1875, Layer 'D' of Sparks *et al.* (1981) & capping lava flow. Sampling sites ASK 5-6 (e) are round the corner, beyond AJD.







(e) 'Zero age' TL sampling of Askja 1875 - ASK 5 (Layer 'C'); ASK 6 (Layer 'D'); **(f)** ASK 10 at Fiskidalur, 55 km NNE of Askja; **(g)** ASK 11 at Arnórsstaðamuli, 74 km NNE of Askja.

Figure 4.4 Askja 1875 and Öræfi 1362 sampling locations and Askja 1875 TL sampling.

4.2 Chemistry & Correlation Dating

A variety of methods were used to classify and discriminate between new and published chemical data. Firstly, new data was classified, and discrimination analysis of the datasets undertaken. Data classified as highly silicic was then selected for correlation dating analysis. The approach adopted, therefore, starts with simple bi- and tri-variate classification progressing to more complex multivariate hypothesis testing and validation methods to produce chemical correlation ages for the Óþoli Tephra and the Þörsmórk Ignimbrite.

4.2.1 Classification

(a) Óþoli and Hjallanes Tephra

The Óþoli Tephra is a glass-rich (>98 % bulk composition) pale yellow deposit (Figs. 4.5 & 4.6). The grain size of the bulk airfall component is uni-modal with a mean of 70 μm and median of 44 μm. Less than 1 % of the deposit is greater than sand grade (>500 μm) (Table C5.1). The mean grain size of 137 shards analysed by electron microprobe at the University of Edinburgh was *ca.* 110x80 μm. Overall, the Óþoli Tephra is compositionally bi-modal with the highly silicic component (SiO_2 = 72-73 %) accounting for more than 90% of the total glass shard population. The intermediate glass fraction has SiO_2 contents that range from 53-65 % and is classified as a basalt-andesite to andesite (Fig. 4.7). An evolutionary relationship exists within the intermediate-silicic glass compositions. Both high and low silica components belong to the medium-K calc-alkaline series. An Icelandic origin is most likely, but the basic component does not belong to the post-glacial basalt rock series of Iceland defined by Jakobsson (1979) (Fig. 4.8).

The highly silicic component is remarkably homogeneous. One hundred and ninety seven shard specific analyses of the highly silicic undertaken at the Universities of Edinburgh and Toronto were almost identical, with only one outlier.

Hjallanes Tephra unit Hj-1 and Hj-2a are glass-rich, but too fine grained for single-shard microprobe analysis. The coarser grained, structureless black tephra deposit Hj-2b was suitable. The bulk composition of this deposit is also greater than *ca.* 95 % brown platey glass shards (Fig. 4.5-1c;d). Its glass phase major element composition is basic-intermediate (50-53 SiO_2 wt %), but predominantly 50-52 SiO_2 wt %.

(b) Þörsmórk Ignimbrite

A complete description and classification of the range of volcanic products associated with Þörsmórk Ignimbrite can be found in Jørgensen (1980; 1981; 1987). The highly silicic products examined in this thesis range from highly pumiceous clasts embedded in a welded rhyolitic ash and lithic matrix (ÞIG

5, 11, 16) to pyroclastic surge related fallout ash, pumice (ÞIG 3, 7) and interbedded lithic-rich layers and co-ignimbrite ash and pumice surge or plume fallout deposits (ÞIG 1b).

The bulk ash deposits of ÞIG 1b and ÞIG 7 are dominated by highly silicic platey and bubble wall glass shards (ÞIG 1b >~80 %; ÞIG 7 > ~60 %) with some pumiceous shards (Fig. 4.5). The grain size distribution of ÞIG 1b is bi-modal and skewed towards coarser fractions, hence the mean grain size is *ca.* 290 μm, median 112 μm (Fig. 4.6-b). The grain size distribution for ÞIG 7 is uni-modal, but a significant proportion (~ 10 %; Table C5.1) is greater than sand grade. The mean grain size is ~315 μm and the median 105 μm. Unaltered highly silicic glass-phase deposits from all stages of the ignimbrite forming eruption are compositionally homogeneous. The early stage ashes and white pumice deposits are highly silicic. Post ignimbrite forming eruption stage deposits are dominated by black platey glass tuff deposits with a basic composition. These cap the highly silicic welded ignimbrite and the co-ignimbrite ash (ÞIG 1b). All deposits are part of the transitional alkaline, high-K calc-alkaline series (Fig. 4.7, 4.8-a). The basic fractions belong to the transitional alkali basalt series of Jakobsson (1972), all of which suggests an off-axial rift source (Fig. 4.8-b).

(c) Holocene age control deposits

(i) Öræfi 1362 AD (Ö1362)

The Öræfi 1362 AD tephra samples ÖR 1, 2, 3 are all glass-rich (>90% of bulk composition). OR 3 has a greater proportion of detrital contamination than OR 1 and 2. There is a morphological trend from pumiceous and bubble wall shard dominance in OR 1 to platey shard dominance in OR 3 (Fig. 4.5C-b) that mirrors the reduction in grain size and the transition from bi-modal to uni-modal grain size distribution (Fig. 4.6-a). The deposits are all highly silicic, compositionally homogeneous (transitional alkaline medium-high K calc-alkaline series) similar to ÞIG (silicic), but with reduced SiO_2, K_2O (respectively, 71.37±0.68 and 3.25±0.10 wt % compared to ÞIG silicic 72.34±0.76 and 4.10±0.26 wt %) and elevated CaO wt % (0.97±0.12 compared to ÞIG silicic 0.41±0.15) (Table 4.1; Fig. 4.7-a; 4.9; 4.10).

(ii) Askja 1875 AD (A1875)

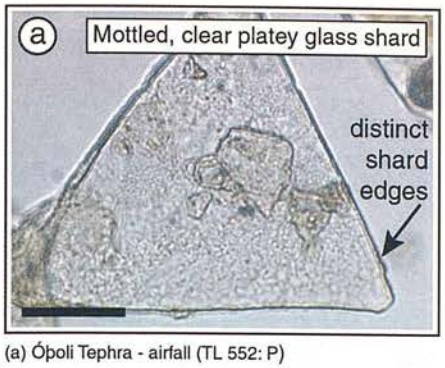
The Askja 1875 AD samples ASK 5, 10, 11 are glass-rich (at least 95% of bulk composition). All the samples are dominated by bubble wall shards (*e.g.* Fig. 4.5:3-a). Grain size distributions are uni-modal in the ash layers crater (ASK 5) and furthest from the crater (ASK 11) and bi-modal in the intermediate ash and pumice deposit (ASK 10). ASK 11 is well sorted and the mean and median grain size is approximately half that of ASK 5 and 10. All the samples are highly silicic, compositionally homogeneous (subalkaline, low-K tholeiites), but with elevated TiO_2, MgO and FeO_{tot} compared to the Óþoli Tephra (0.79±0.11, 0.64±0.09 and 3.34±0.37 compared to 0.16±0.04, 0.02±0.01, 2.36±0.09) (Table 4.1; Fig. 4.7-a; 4.9; 4.10).

(d) Discriminating between new analyses

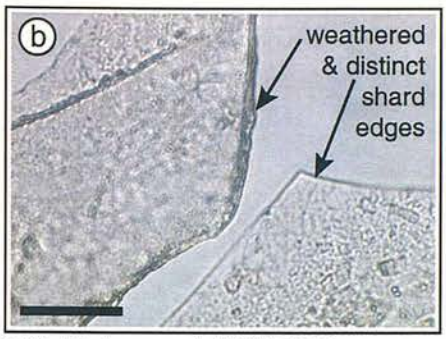
The nine major elements examined explain over 80 % of the variance between the datasets. New analyses from deposits examined in this study can be effectively separated using Fe-oxide bi-plots (Fig. 4.9) and PCA (Fig. 4.10). In addition, the Fe-oxide and PCA bi-plots show that manganese and aluminium are not important in discriminating between deposits, that silicic and basic deposits can be effectively separated using silica, sodium and potassium content alone, and that discrimination between highly silicic deposits is best achieved using ternary plots of combinations of calcium, total iron, magnesium and titanium oxides.

Morphological classification

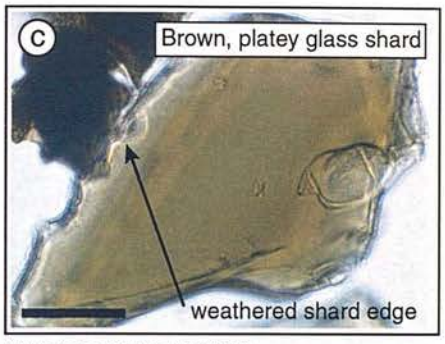
Other examples / features



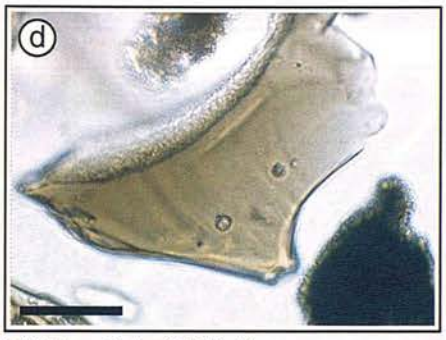
(a) Óþoli Tephra - airfall (TL 552: P)



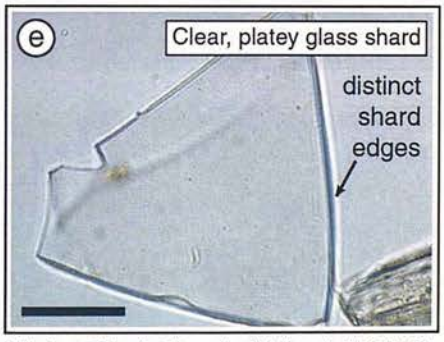
(b) Óþoli Tephra - reworked (SUTL 556: B)



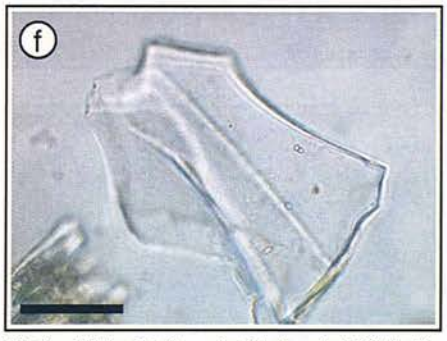
(c) Hjallanes Tephra (TL513: B)



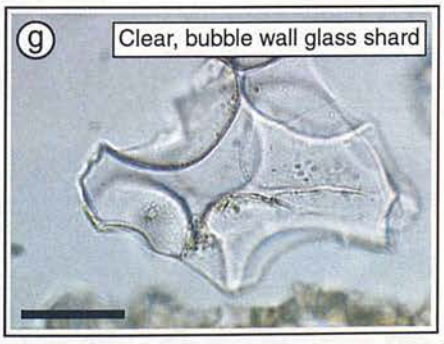
(d) Hjallanes Tephra (TL513: B)



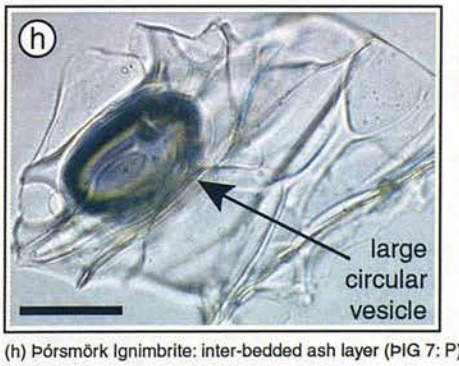
(e) Þórsmörk Ignimbrite: co-ignimbrite ash (ÞIG 1b: P)



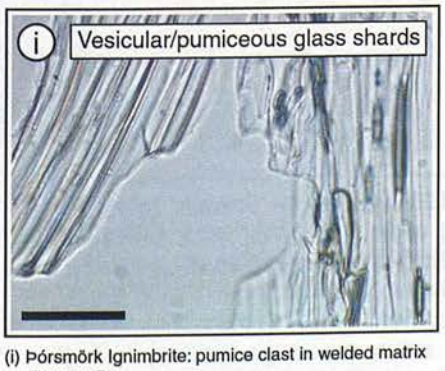
(f) Þórsmörk Ignimbrite: co-ignimbrite ash (ÞIG 1b: P)



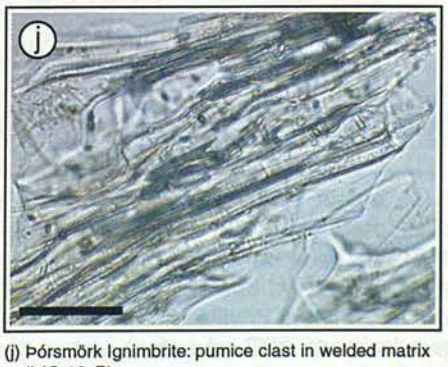
(g) Þórsmörk Ignimbrite: inter-bedded ash layer (ÞIG 7: B)



(h) Þórsmörk Ignimbrite: inter-bedded ash layer (ÞIG 7: P)



(i) Þórsmörk Ignimbrite: pumice clast in welded matrix (ÞIG 11: B)



(j) Þórsmörk Ignimbrite: pumice clast in welded matrix (ÞIG 16: P)

Figure 4.5-1: Variations in, and definitions of, typical glass shard morphology of selected Icelandic tephra deposits examined in this thesis. Scale bar = 25 μm; all photos x 400 magnification; P = purified fraction - 90-150 μm, 2.3-2.4 gcm^{-3} or <2.4 gcm^{-3}; B = bulk sample; samples mounted in Canada Balsam.

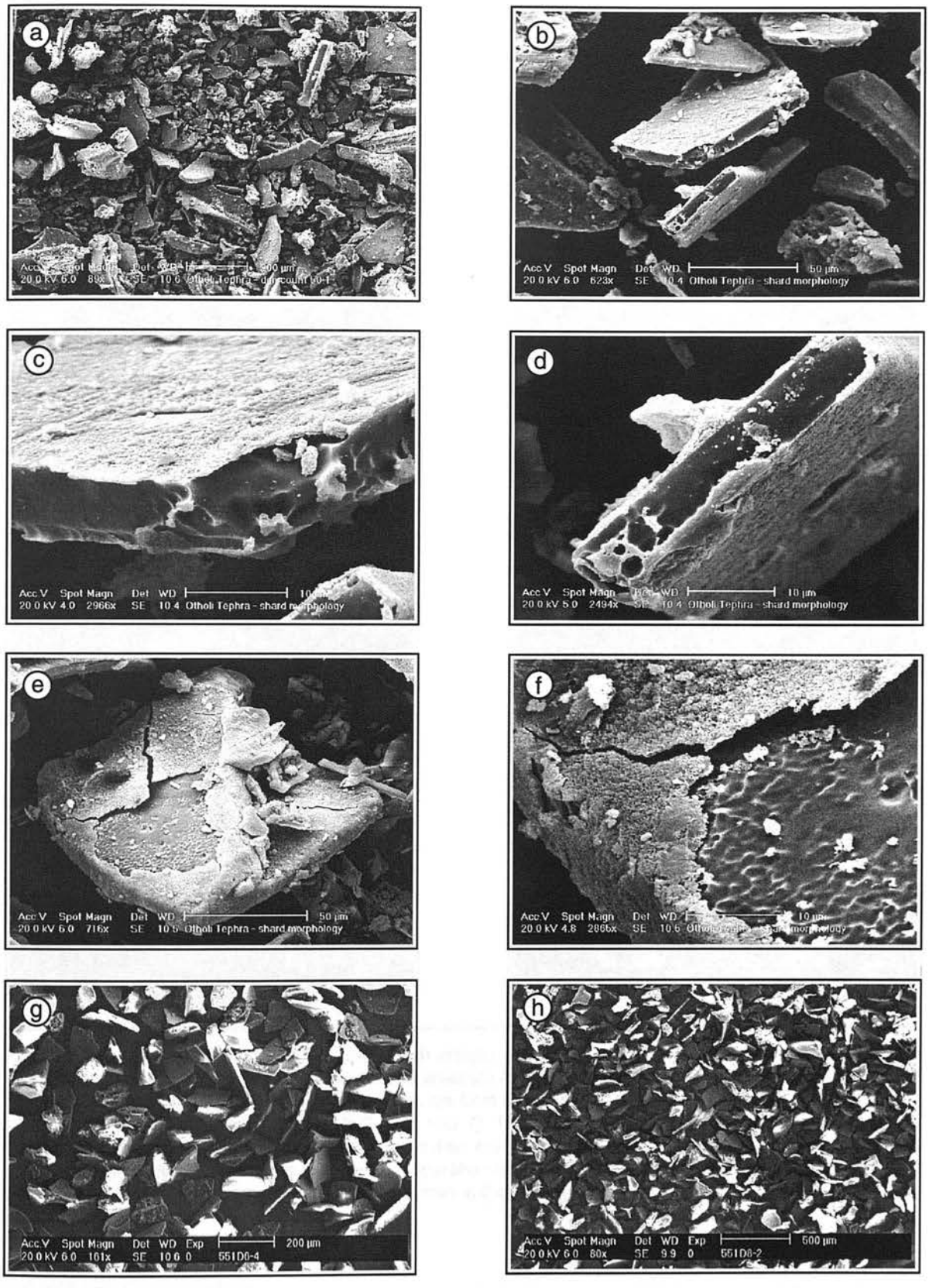


Figure 4.5-2 Scanning electron microscope (SEM) images of glass shards of the Óþoli Tephra. (a)-(f) are untreated bulk samples from SUTL 551, while (g)-(h) are images from SUTL 551 discs used in the TL regeneration experiment. These images are of purified fractions obtained by overnight acid wash with 10 % HCl, sieving to obtain the 90-150 µm fraction, ultra-sonic treatment for 45 minutes followed by 10 µm sieving and density separation at 2.3-2.4 gcm^{-3}. (a)-(f) were gold coated, hence the better quality of the images. Smectite weathering rinds < 1 µm thick are clearly visible. (g) & (h) were carbon coated for EDS chemical mapping, hence the charging of samples in these images. Although difficult to make out here, shards in (g) & (h) were significantly cleaner than shards in (a)-(f).

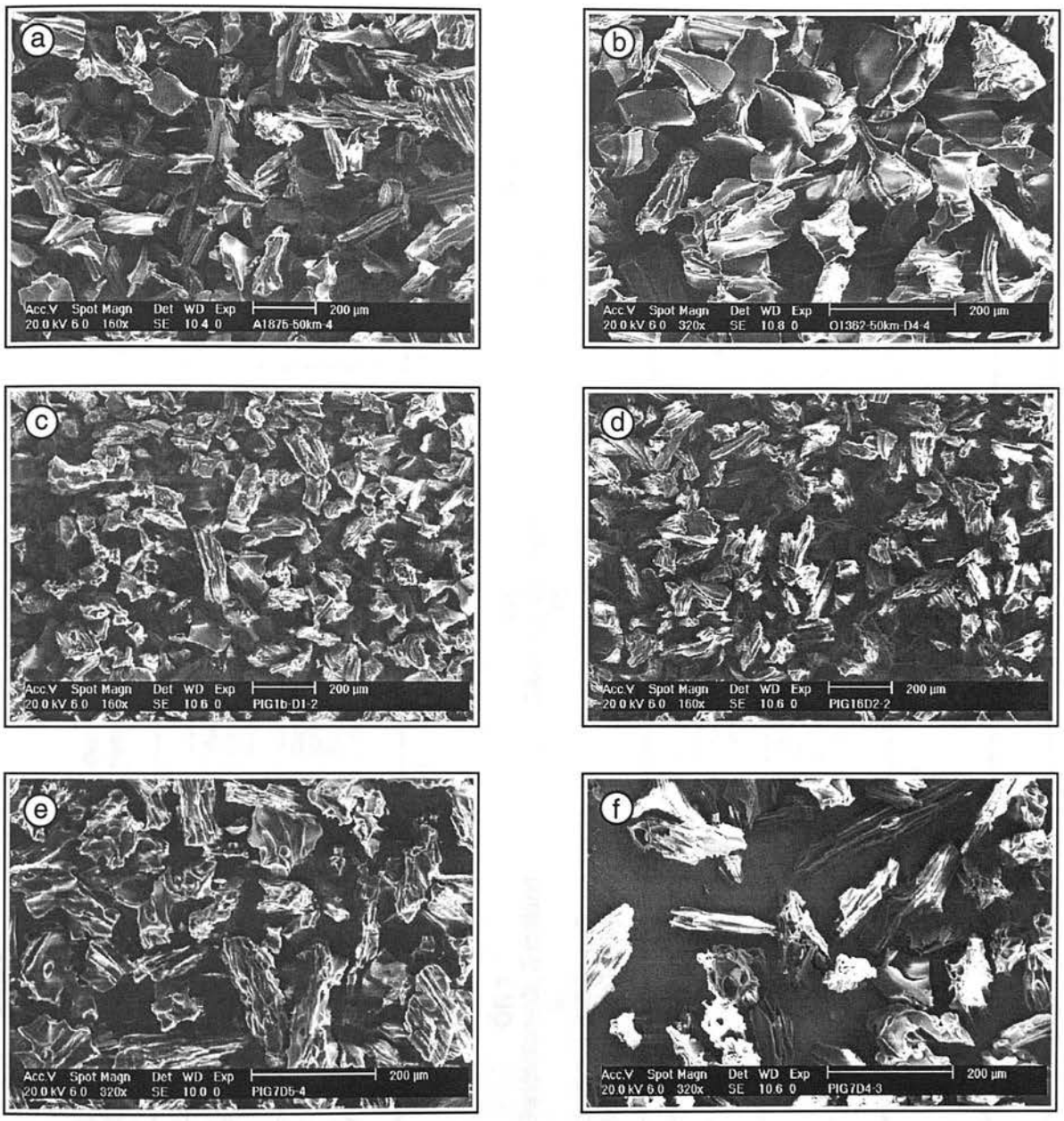


Figure 4.5-3 Scanning electron microscope (SEM) images of silcic glass shards of (a) SUTL-ASK 10 (Askja 1875 AD eruption) (b) SUTL-ÖR 2 (Öræfi 1362 AD eruption) (c) SUTL-ÞIG 1b (Þórsmörk Ignimbrite eruption) (d) SUTL-ÞIG 16 and (e) & (f) SUTL-ÞIG 7. All images are from discs used in the semi-quantitative (ASK 10; OR 2, ÞIG 16) and regeneration experiments (ÞIG 1b & ÞIG 7). These images are of purified fractions obtained by overnight acid wash with 10 % HCl, sieving to obtain the 90-150 µm fraction, ultra-sonic treatment for 45 minutes followed by 10 µm sieving and density separation at < 2.4 gcm^{-3}. All samples were carbon coated for EDS chemical mapping, hence the charging of samples in these images.

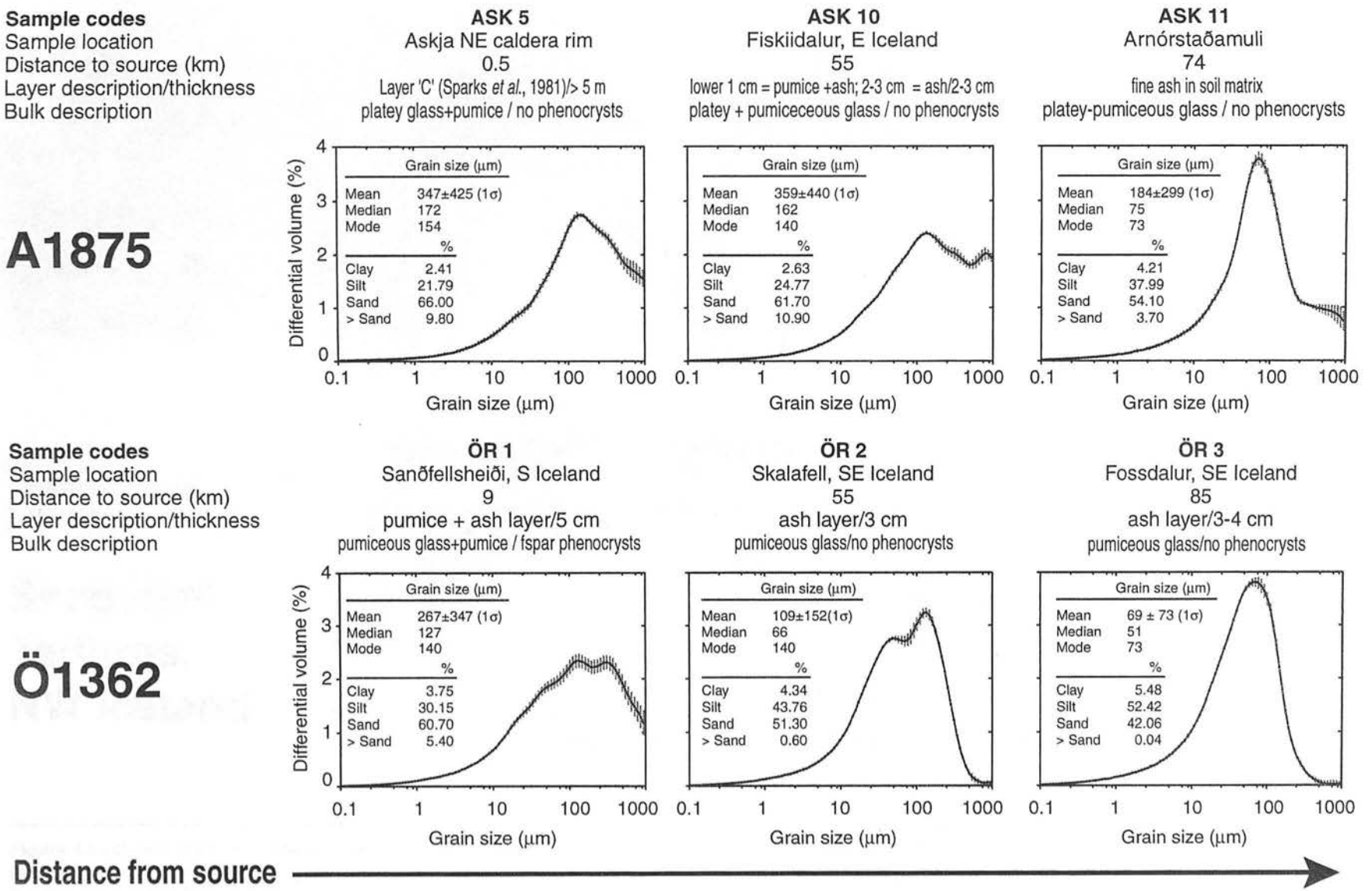


Figure 4.6 (a) Bulk grain size data and variation with distance from source for highly silicic tephra samples used as TL age and altitude signal inducement controls. See Table and Appendix C4.1 for details of method and full list of grain size statistics. Grey lines are 2σ error bars from 2 x 5 runs per sample.

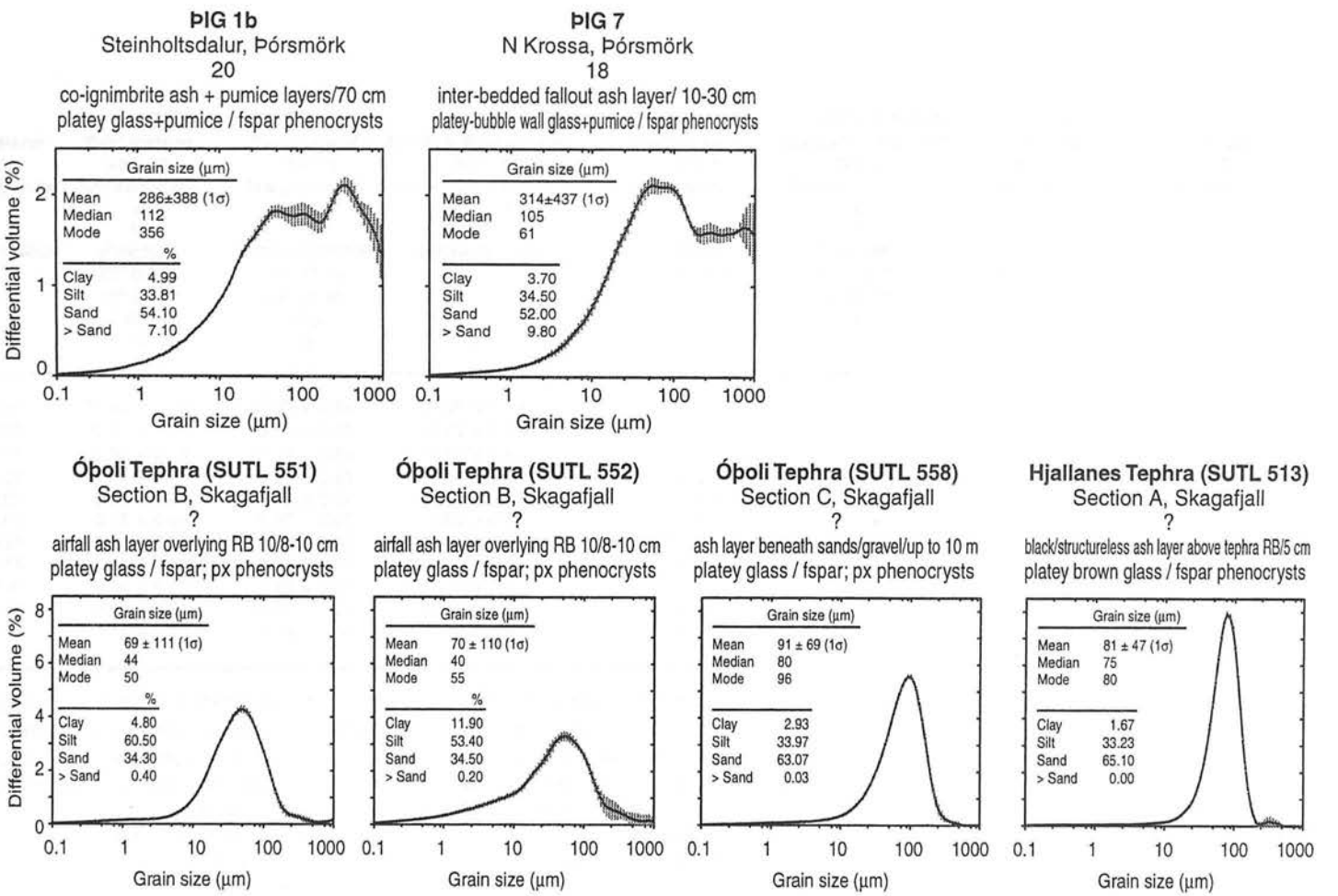


Figure 4.6 (b) Bulk grain size data and variation with distance from source for airfall or fallout components of highly silicic tephra samples (except Hjallanes Tephra) of pre-Holocene age used in dating analysis. See Table and Appendix C4.1 for details of method and full list of grain size statistics. Grey lines are 2σ error bars from a variable number of runs (see Table C4.1).

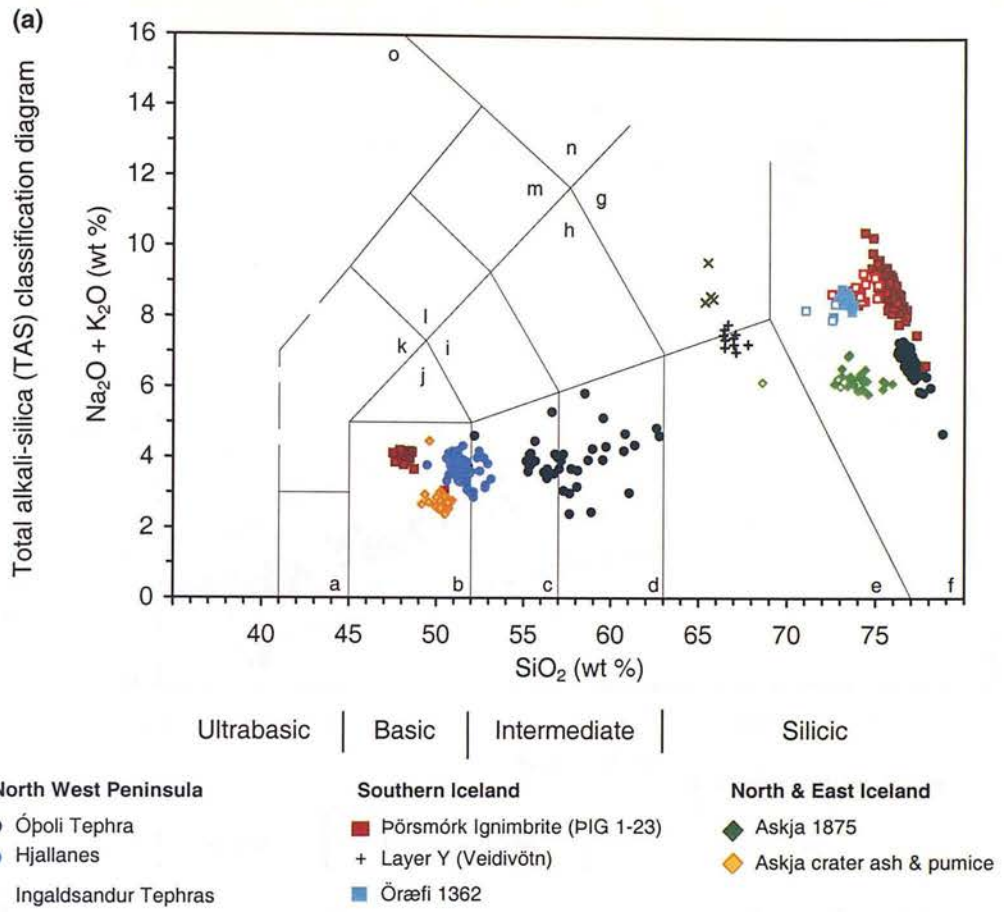
Eruption	ASKJA 1875 AD				ÖRÆFAJÖKULL 1362 AD			
Location of deposit	Askja, N Iceland	East Iceland	East Iceland	North & East Iceland	South Iceland	South-east Iceland	South-east Iceland	S & SE Iceland
Sample code	ASK 5	ASK 10	ASK 11	ASK 5/10/11	ÖR 1	ÖR 2	ÖR 3	ÖR 1/2/3
Classification	platey ash & pumice	fine platey ash	fine platey ash	platey/pumiceous ash	pumiceous ash	platey-pumiceous	platey-pumiceous	platey-pumiceous
Layer thickness (cm)	75	2	1.5	-	3	2	3	-
Sample-Source (km)	0.5	55	74	0.5-74	9	55	85	9-85
Location	NE crater shoreline	Fiskidalur	Arnórsstaðamuli	combined data	Sanðfellsheiði	Skalafell	Fossdalur	platey/pumiceous ash combined data
Latitude (°N)	65° 02.61'	65° 08.60'	65° 17.28	-	63° 57.3'	64° 14.02'	64° 29.13'	
Longitude (°W)	16° 43.45'	15° 40.47'	15° 10.75'	-	16° 51.6'	15° 40.50'	15° 19.88'	-
Altitude (m.a.s.l.)	1100	600	400	-	-	-	510	-
Shards analysed (n)	(10)	(8)	(9)	(27)	(10)	(8)	(10)	(27)
SiO_2	72.93 ± 0.64	71.93 ± 0.80	73.09 ± 0.84	72.69 ± 0.89	71.09 ± 0.74	71.79 ± 0.63	71.45 ± 0.55	71.40 ± 0.68
TiO_2	0.79 ± 0.09	0.81 ± 0.06	0.78 ± 0.15	0.79 ± 0.11	0.29 ± 0.21	0.20 ± 0.02	0.21 ± 0.04	0.24 ± 0.13
Al_2O_3	12.18 ± 0.19	12.22 ± 0.14	12.09 ± 0.21	12.16 ± 0.19	12.93 ± 0.16	13.01 ± 0.17	13.02 ± 0.20	12.99 ± 0.18
FeO_{tot}	3.25 ± 0.24	3.54 ± 0.27	3.26 ± 0.51	3.34 ± 0.37	3.31 ± 0.21	3.29 ± 0.16	3.31 ± 0.47	3.30 ± 0.31
MnO	0.07 ± 0.04	0.08 ± 0.01	0.10 ± 0.04	0.08 ± 0.03	0.15 ± 0.09	0.11 ± 0.27	0.13 ± 0.03	0.13 ± 0.06
MgO	0.65 ± 0.08	0.71 ± 0.06	0.57 ± 0.06	0.64 ± 0.09	0.05 ± 0.02	0.04 ± 0.01	0.05 ± 0.01	0.04 ± 0.02
CaO	2.33 ± 0.25	2.48 ± 0.18	2.12 ± 0.23	2.31 ± 0.26	0.92 ± 0.05	1.04 ± 0.20	0.96 ± 0.05	0.96 ± 0.12
Na_2O	3.53 ± 0.16	3.61 ± 0.11	3.48 ± 0.15	3.54 ± 0.15	4.96 ± 0.11	4.99 ± 0.11	5.06 ± 0.24	5.00 ± 0.17
K_2O	2.60 ± 0.27	2.54 ± 0.15	2.62 ± 0.28	2.59 ± 0.24	3.26 ± 0.12	3.29 ± 0.12	3.25 ± 0.08	3.26 ± 0.11
TOTAL	98.33 ± 0.78	97.92 ± 0.72	98.11 ± 1.20	98.14 ± 0.91	96.96 ± 0.88	97.76 ± 0.90	97.42 ± 0.65	97.34 ± 0.84
H_2O_d	1.67 ± 0.78	2.08 ± 0.72	2.15 ± 0.96*	1.94 ± 0.82*	3.04 ± 0.88	2.24 ± 0.90	2.58 ± 0.65	2.66 ± 0.84

Table 4.1 (a) Summary table of glass -phase major element chemistry of highly silicic Holocene age samples used luminescence dating experiments. FeO_{tot} = total iron oxide: $FeO_{tot} = 0.85FeO + 0.15Fe_2O_3$. Elements are expressed as wt %; analyses have not been re-cast on a volatile-free basis; data are mean ± 1σ from n shards; outliers were identified by multivariate analysis and removed before calculation of mean and 1σ; all samples were analysed on a Cambridge Microscan V wavelength dispersive (WDS) microprobe operating at 20 kV accelerating voltage, 5 μm beam diameter, 15 nA beam current, counting time of 10 seconds per element. To assess the degree of sodium mobilisation, this element was measured during the first and final counting period. Calibration to a mixture of pure metals and simple silicate minerals was performed at the start of each day and periodically checked against a synthetic oxide andradite standard. Spectrometer drift was checked if analytical totals were consistently poor and elements re-calibrated if this did not solve the problem. Counter dead time was corrected for and a ZAF correction applied to account for the effects of atomic number, absorption and fluorescence (Sweatman and Long, 1969); * = H_2O_d value affected by total(s) >100.

contd.

Tephra	ÞÓRSMÖRK IGNIMBRITE					ÓÞOLI TEPHRA			
Location of deposit	Þórsmörk, Southern Iceland					Skagafjall, North West Iceland			
Sample code (s)	ÞIG 1b (co-ig)		ÞIG 7 (ash)		ÞIG 1-23	OT(1-3 cm)	OT(1-8 cm)	OT(1-3 cm)	
	ÞIG 1b	TEX3	ÞIG 7	TEX4		TL551/2	UT1655-1659(FT)	TEX1	TEX2
Classification	co-ignimbrite ash		interbedded ash		unaltered ash & pumice		platey airfall ash		
Layer thickness (cm)	70		30		-		8 (airfall) *ca.* 200 (reworked)		
Latitude (°N)	63° 40.35'		63° 40.37'		combined data		65° 59.78'		
Longitude (°W)	19° 36.22'		19° 34.37'		-		23° 45.40'		
Altitude (m.a.s.l.)	*ca.* 250		*ca.* 220		200-500		580-582		
Shards analysed (n)	(24)	(XRF-bulk)	(20)	(XRF-bulk)	(218)	(137)	(60)	(XRF-pure*)	(XRF-bulk)
SiO_2	72.53 ± 0.79	65.90	72.61 ± 0.97	69.90	72.34 ± 0.75	72.89 ± 0.82	72.25 ± 0.65	69.10	66.30
TiO_2	0.18 ± 0.08	0.93	0.15 ± 0.04	0.48	0.16 ± 0.07	0.16 ± 0.04	0.17 ± 0.04	0.42	0.60
Al_2O_3	11.58 ± 0.19	13.00	11.48 ± 0.17	13.00	11.48 ± 0.17	11.60 ± 0.18	11.66 ± 0.13	12.20	12.50
FeO_{tot}	2.69 ± 0.41	5.79	2.51 ± 0.12	4.17	2.53 ± 0.21	2.36 ± 0.09	2.34 ± 0.09	4.97	6.29
MnO	0.10 ± 0.06	0.12	0.07 ± 0.04	0.11	0.07 ± 0.06	0.09 ± 0.03	0.08 ± 0.04	0.13	0.18
MgO	0.02 ± 0.01	1.04	0.02 ± 0.01	0.38	0.02 ± 0.01	0.02 ± 0.01	0.01 ± 0.01	0.39	0.77
CaO	0.43 ± 0.14	2.72	0.37 ± 0.03	1.34	0.40 ± 0.09	1.27 ± 0.07	1.44 ± 0.05	1.66	2.51
Na_2O	4.40 ± 0.16	4.78	4.14 ± 0.48	4.83	4.38 ± 0.30	3.68 ± 0.32	4.12 ± 0.10	4.06	3.03
K_2O	4.11 ± 0.61	3.28	4.06 ± 0.19	3.03	4.10 ± 0.26	2.75 ± 0.14	2.61 ± 0.07	2.49	2.16
Cl	-	-		-	-	-	0.06 - 0.02	-	-
P_2O_5	-	0.17	-	0.07	-	-	-	0.06	0.09
Cr_2O_3	-	-0.01	-	-0.01	-	-	-	-0.01	-0.01
LOI	-	2.35	-	2.55	-	-	-	4.40	5.43
TOTAL	96.04 ± 0.94	100.40	95.42 ± 0.93	100.20	95.48 ± 0.93	94.81 ± 0.93	94.75 ± 0.69	100.10	100.10
H_2O_d	3.96 ± 0.94	-	4.58 ± 0.93	-	4.52 ± 0.93	5.19 ± 0.93	5.25 ± 0.69	-	-
H_2O+	-	2.00	-	2.20	-	-	-	4.20	4.50
H_2O-	-	0.40	-	0.40	-	-	-	0.40	1.65

Table 4.1 (b) Summary table of glass-phase major element chemistry of highly silicic pre-Holocene age samples used in luminescence dating experiments. FeO_{tot} = total iron oxide: $FeO_{tot} = 0.85FeO + 0.15Fe_2O_3$. Elements are expressed as wt %; Operating conditions as in (a) except for samples with a UT- prefix which were analysed at University of Toronto by Shari Preece on a Cameca SX-50 WDS microprobe operating at 15 kV accelerating voltage, 10-15 μm beam diameter and 6 nA beam current; pure* = 90-150 μm; 2.3-2.4 gcm^{-3}.



Chemical classification and nomenclature of volcanic rocks (Le Maitre *et al*., 1989): a = Picrobasalt; b = Basalt; c = Basaltic andesite; d = Andesite; e = Dacite; f = Rhyolite; g = Trachyte (normative quartz <20%) or Trachydacite (normative quartz >20%); h = Trachyandesite; i = Basaltictrachyandesite; j = Trachybasalt; k = Tephrite (normative olivine <10%) or Basanite (normative olivine >10%); l = Phonotephrite; m = Tephriphonolite; n = Phonolite; o = Foidite. Unfilled datapoints represent outlier data, selected by cluster and principal components analysis of each dataset, were not included in mean and standard deviation calculations.

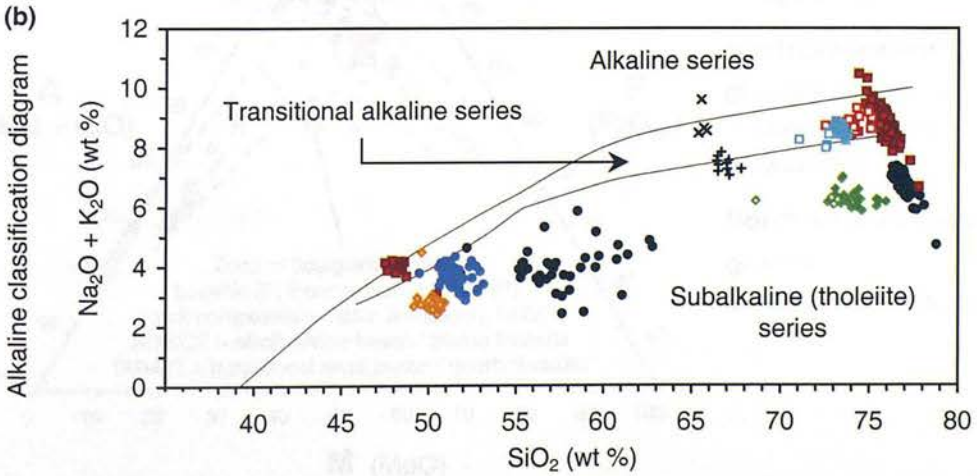


Figure 4.7 Classification bi-plots of glass-phase of Icelandic tephra deposits in this thesis. **(a)** Total alkali-silica (TAS) classification diagram and 624 new grain specific EPMA from glass shards of Icelandic tephra deposits presented in this thesis. **(b)** Subdivision of volcanic rocks into alkaline, transitional alkaline and subalkaline (tholeiitic) on a TAS diagram in relation to grain specific EPMA of glass shards from tephra deposits presented in this thesis. Upper line after Irvine and Baragar (1971), lower line after Kuno (1966). Key as (a). Data has been recalculated to 100% on a H_2O and CO_2 free basis. See text for further explanation.

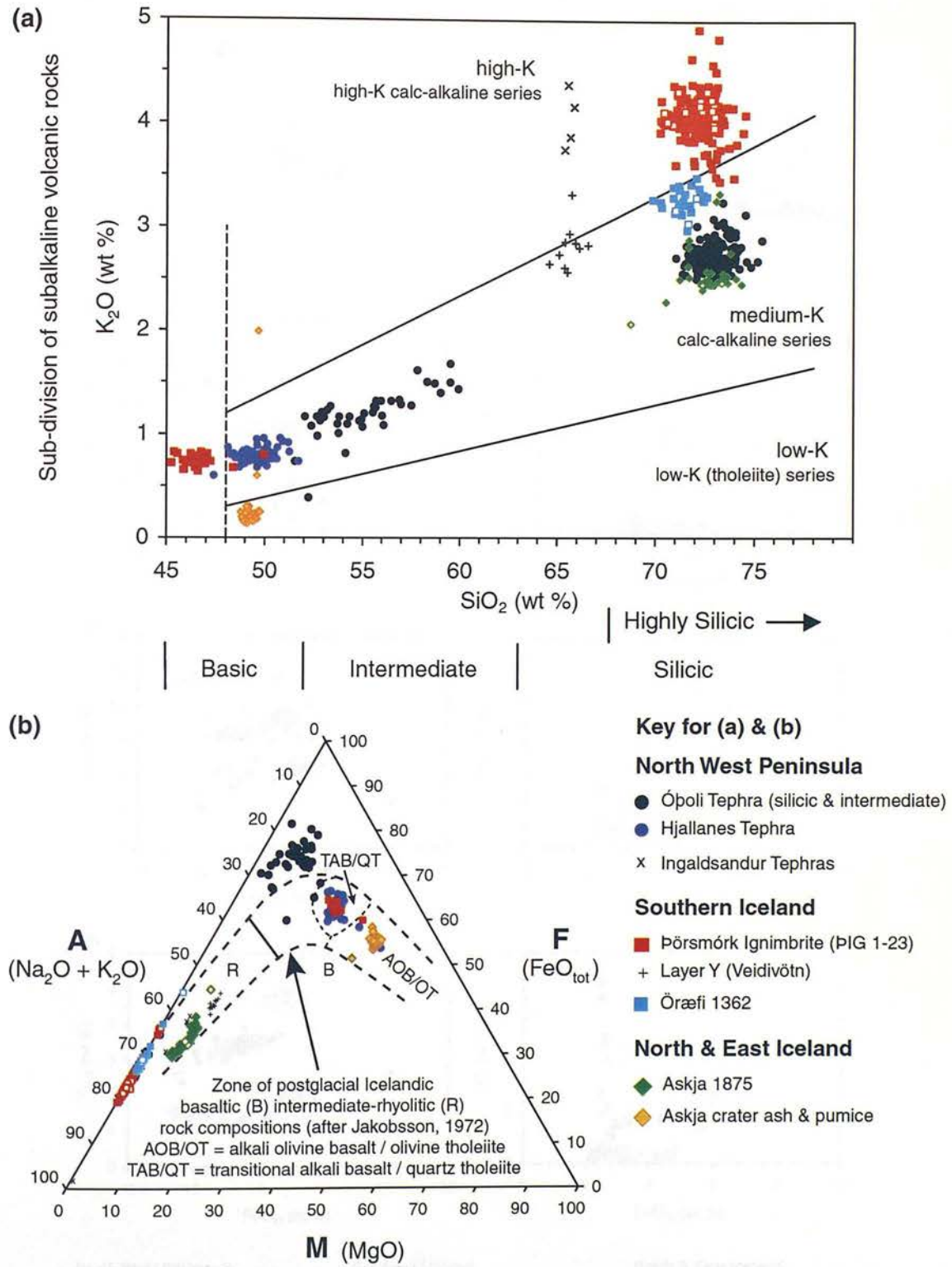


Figure 4.8 (a) Classification binary plot of K_2O vs SiO_2 of 624 new EPMA analyses from Icelandic volcanic glass shards presented in this thesis. This diagram is based on the sub-division of sub-alkalic rocks in Le Maitre *et al.* (1989) and Rickwood (1989). K_2O is a mobile element in volcanic glass and this sub-division was not originally intended for this purpose. Nevertheless, it provides a good starting point to sub-divide tephra analyses. A full list of data can be found in Appendix C1. **(b)** Total alkali (A), total iron (F), magnesium (M) diagram for new EPMA and comparison to classification scheme for postglacial Icelandic basalt rock compositions of Jakobsson (1972). The intermediate component of the Óþoli Tephra is the only deposit analysed that lies outside the zone for recent basaltic rocks from Iceland. Points for the silicic component of the Óþoli Tephra are beneath those of ÞIG 1-23 and Ö1362.

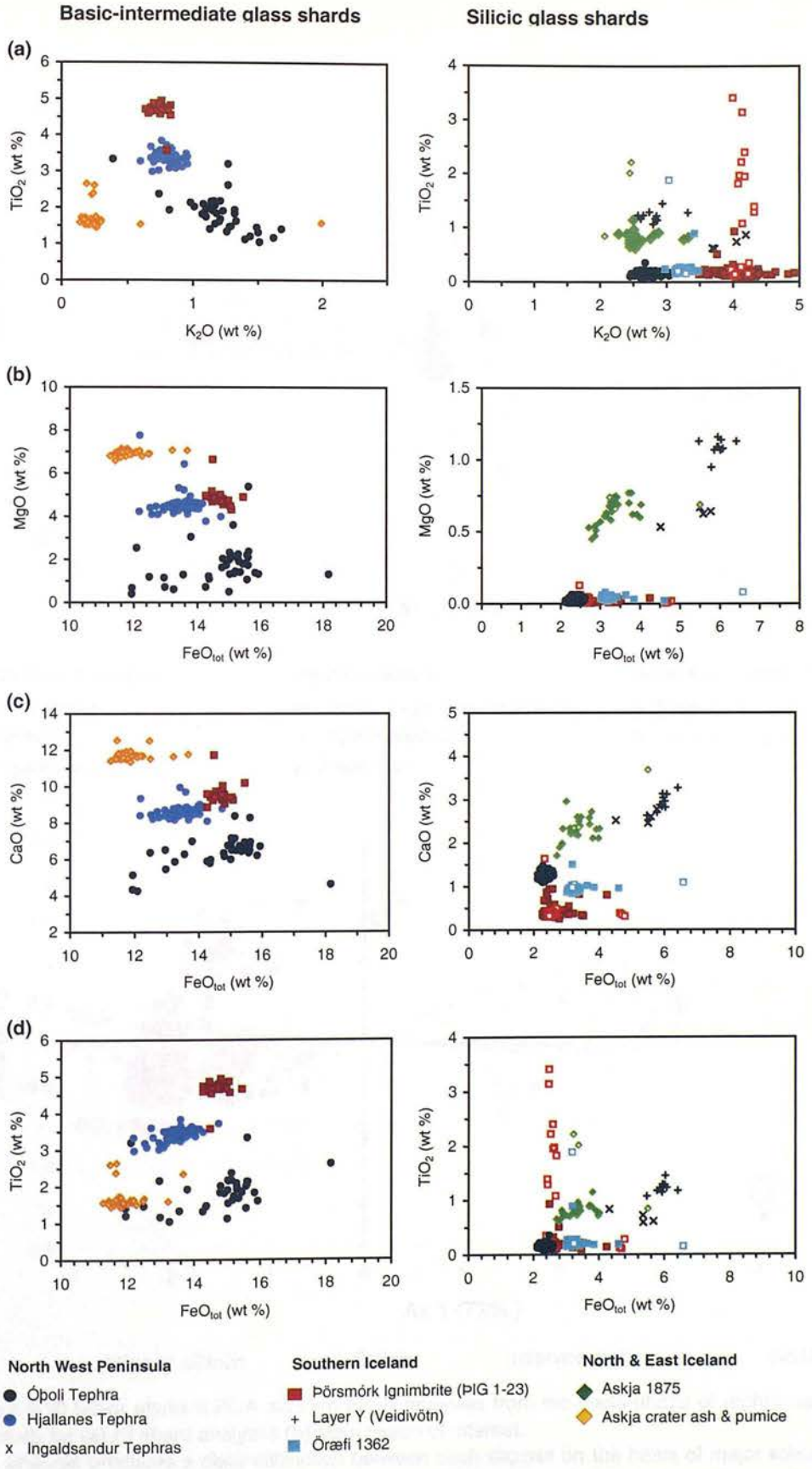


Figure 4.9 Discrimination binary plots for new EPMA glass shard analyses from tephra deposits in this thesis.
(a) TiO_2 vs K_2O. **(b)** FeO_{tot} (total FeO=FeO+Fe_2O_3) vs (b) MgO, (c) CaO and (d) TiO_2. All 'unburnt' shard data included (see text); in all cases data has not been recalculated to 100% on a H_2O and CO_2 free basis; unfilled datapoints represent outlier data not included in mean and standard deviation calculations.

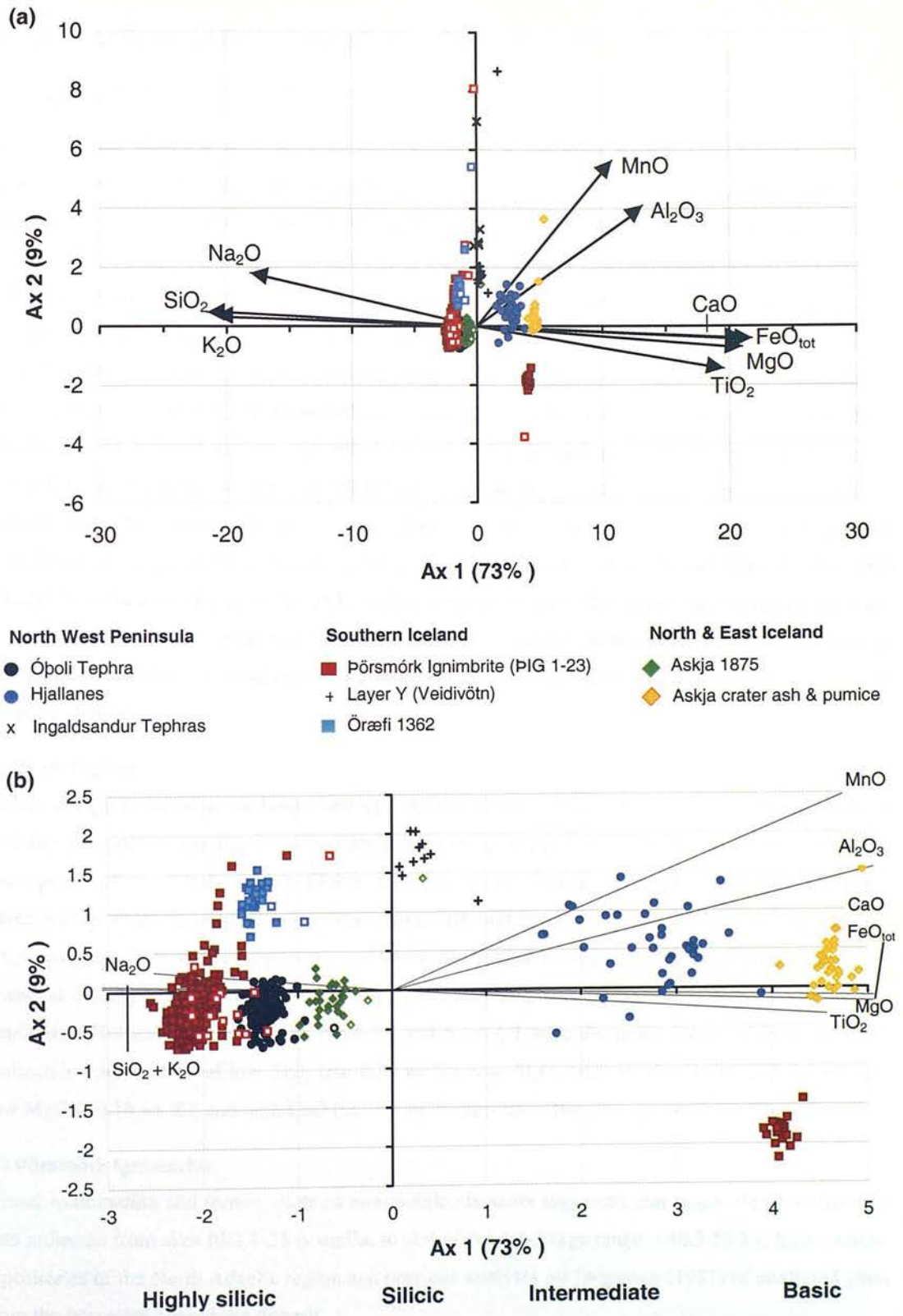


Figure 4.10 Major element PCA diagram for all analyses from the glass-phase of tephra deposits in this study for **(a)** All shard analyses **(b)** Main region of interest.
PCA analysis produces a clear distinction between each deposit on the basis of major element data alone. Variable coordinates have been modified to take account of the representation power of each axis and the scale of the plotted data. Square root transformation of the dataset produces similar results, but with a marginal increase in the the explanatory power of the first axis to 76 %, a reduction in the influence of SiO_2 and Al_2O_3 and a slight increase in the influence of Na_2O. (Analysed using XLSTAT, Kovach Computing Services, 2001)

4.2.2 Geochemical Correlation Dating Results

(a) Overview

Major element chemical correlation of the glass-phase is the most widely used correlation dating technique for Icelandic tephra deposits (Haflidason *et al.*, 2000). Correlation dating results presented are based solely on major element data. Incorporating trace element data in correlation dating analysis proved difficult. Apart from grain specific SIMS ion probe data of Clift and Fitton (1998) and Newton (1999), grain specific or purified trace element data for the other deposits is virtually non-existent. To produce correlation dating age estimates for the Óþoli Tephra and Þörsmórk Ignimbrite, multivariate statistical methods were applied to published major element data from most of the 65-0 Ma highly silicic tephra deposits from the terrestrial environment of Iceland and NW Europe, ocean cores of the northern North Atlantic and the Greenland ice cores. The locality numbers in Figure 4.11 refer to Table C2.1 in Appendix C where a full list of chemical data, ages, references and names of each deposit can be found. Some of the data in this table can be viewed in full at http://www.geo.ed.ac.uk/tephra/tbasehom.html. This is the most temporally and spatially extensive attempt at correlation dating of Icelandic tephra deposits to date. The multivariate methods used are statistically rigorous and empirically reproducible. The approach adopted aids identifying similarity within large datasets, is relatively straightforward and complements existing bi-plot and ternary diagram analysis.

(i) Óþoli Tephra

Before complex statistical analyses were undertaken, visual analysis identified 10 tephra deposits of mid-late Pleistocene age that have broadly similar major element compositions to the highly silicic glass-phase of the Óþoli Tephra (Table 4.2; Fig. 4.12). Ternary plots of non-mobile elements, identified by PCA as good discriminators, from 104 highly silicic tephra deposits of Tertiary and Quaternary age from various repositories of the North Atlantic region suggested the Óþoli tephra has a chemical affinity with deposits of early-mid Quaternary and Tertiary age (Fig. 4.13). Highly silicic deposits of Holocene age as well as NAAZ-1 and NAAZ-2 were dissimilar. None of these have the distinctive combination of low TiO_2 (*ca.* 0.20 wt %), low Al_2O_3 (<12 wt %), FeO_{tot} (2.3-2.5 wt %) , low MgO (<0.10 wt %), and high CaO (*ca.* 1.3 wt %) present in the glass-phase of the Óþoli Tephra.

(ii) Þörsmórk Ignimbrite

Visual examination and ternary plots of non-mobile elements suggested that major element chemical data collected from sites ÞIG 1-23 is similar to that of NAAZ-2 (age range = 48.5-58 ka) from various repositories of the North Atlantic region and previous analyses by Jørgensen (1981) of unaltered glass from the Þörsmórk Ignimbrite deposit.

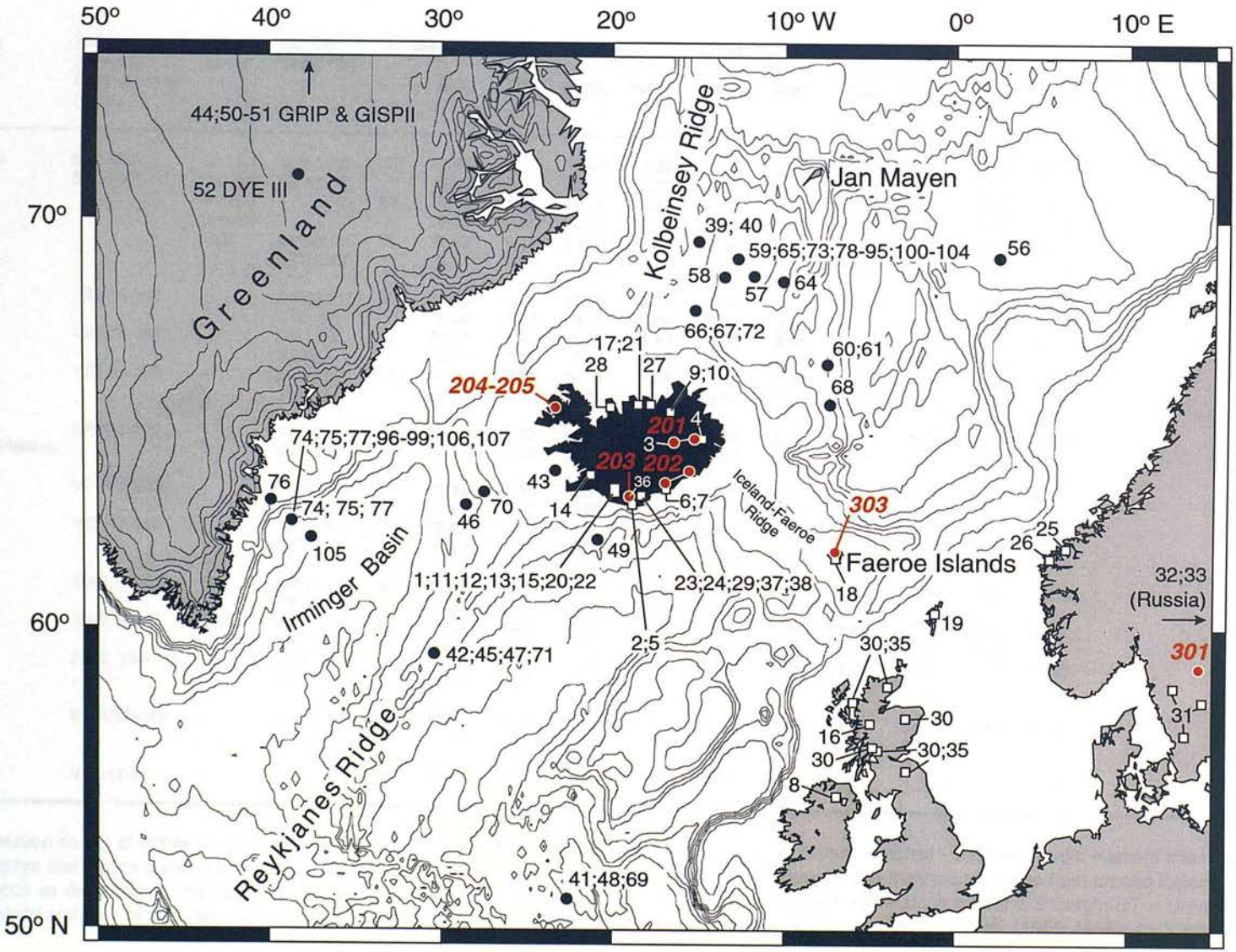


Figure 4.11 Map of the North Atlantic region showing the location of tephra deposits used in correlation dating analysis. Numbers are ID numbers on cluster and PCA diagrams. A full list of deposits, ID numbers & chemical data can be found in appendix C2.

ID no.	Site, Tephra	Height (m.a.s.l) Core-interval (cm)	Section Layer	Lat (N) Long (W)	n	Major element chemical composition (wt %) SiO_2	TiO_2	Al_2O_3	FeO_{tot}	MnO	MgO	CaO	Na_2O	K_2O	Total	Selected trace elements U	Th	Age PM	kyrs	$\delta^{18}O$	Refs.
204	Óþoli Tephra	580-582	B: 11.1	65°59.78'	137	**72.89**	**0.16**	**11.60**	**2.36**	**0.09**	**0.02**	**1.29**	**3.68**	**2.75**	**94.81**	2.3	8.5	-	-		sjr; UE;
	NW Iceland	580-590	0-3 cm	23°45.40'		0.82	0.04	0.18	0.09	0.03	0.01	0.33	0.32	0.14	0.93						11-12/98
205			B: 11.1		60	**72.25**	**0.17**	**11.66**	**2.34**	**0.08**	**0.01**	**1.44**	**4.12**	**2.61**	**94.75**			-	-		sp; UT;
			0-8 cm			0.65	0.04	0.13	0.09	0.04	0.01	0.05	0.10	0.07	0.69						5/00
-			C:11	65°58.11'	3	**71.42**	**0.17**	**11.26**	**2.66**	**0.36**	**0.01**	**1.32**	**4.40**	**2.51**	**94.11**						jrs; UI;
			-	23°43.43'		0.51	0.03	0.06	0.08	0.12	0.01	0.05	0.11	0.05	0.41						1983
56	DSDP 38:1	V23-73-393	-	68°32.8'	10	**71.85**	**0.16**	**11.78**	**2.74**	**0.10**	**0.06**	**1.13**	**4.60**	**2.73**	**95.15**	-	-	-	**115**		1, 2
	Iceland			2°43.0'		0.48	0.03	0.15	0.08	0.04	0.01	0.07	0.25	0.06							
64	Plateau	V23-74-688	-	68°11.0'	10	**71.85**	**0.18**	**11.80**	**2.84**	**0.10**	**0.05**	**1.18**	**4.35**	**2.69**	**95.04**	-	-	-	**190**		1, 2
				9°36.0'		0.68	0.14	0.10	0.03	0.07	0.15	0.13	0.03	0.03							
67		V23-58-375	-	65°46.0'	10	**72.05**	**0.17**	**11.74**	**2.84**	**0.11**	**0.06**	**1.22**	**4.31**	**2.71**	**95.21**	-	-	-	**225**		1, 2
				7°07.0'		0.63	0.20	0.14	0.01	0.04	0.22	0.09	0.03	0.08							
69	K708	K708-1-610	-	50°00.0'	16	**72.86**	**0.22**	**12.06**	**3.34**	**0.10**	**0.01**	**1.18**	**4.85**	**2.89**	**97.51**	-	-	-	***ca.* 320**		2
	SW Iceland Plateau			23°45.0'		0.57	0.03	0.11	0.18	0.08	-	0.05	0.32	0.13							
57	DSDP 38:2	V27-46-260	-	67°35.2'	10	**72.94**	**0.19**	**10.91**	**2.65**	**0.11**	**0.01**	**1.44**	**4.29**	**1.63**	**94.17**	-	-	-	**115**		1, 2
	Iceland			11°31.2'		0.67	0.03	0.25	0.15	0.03	0.01	0.05	0.10	0.06							
	Plateau	V27-47-180	-	13°32.50'	8	**72.86**	**0.17**	**10.98**	**2.71**	**0.09**	**0.00**	**1.45**	**4.52**	**1.62**	**94.40**	-	-	-	**120**		1, 2
				68°27.70'		0.61	0.03	0.13	0.09	0.03	-	0.03	0.23	0.12							
59	ODP 907A	1H-2, 50-51	B	69°14.9'	10	**73.79**	**0.23**	**11.04**	**2.78**	**0.06**	**0.03**	**1.50**	**4.83**	**1.84**	**96.10**	-	-	**97**	**122.3**		3
	Iceland			12°41.8'		1.66	0.11	0.39	0.98	0.06	0.03	0.49	0.32	0.11							
65	Plateau	1H-3, 53-55	C	69°14.9'	15	**71.28**	**0.24**	**11.94**	**3.35**	**0.11**	**0.08**	**1.81**	**4.83**	**2.37**	**96.01**	1.7	9.8	**170**	**204.6**		3
				12°41.8'		0.53	0.04	0.11	0.13	0.05	0.02	0.09	0.26	0.08		-	-				
73		2H-6, 139-141	G	69°14.9'	12	**72.80**	**0.22**	**11.29**	**2.69**	**0.10**	**0.04**	**1.32**	**4.40**	**2.69**	**95.55**	-	-	**789**	**774.1**		3
				12°41.8'		0.67	0.05	0.11	0.14	0.06	0.04	0.11	0.17	0.09							
70	ODP 902	SU9029-549	-	63°52.0'	14	**72.83**	**0.20**	**11.77**	**3.21**	**0.11**	**0.02**	**1.23**	**5.24**	**2.81**	**97.42**	-	-	-	***ca.* 320**		3
				28°56.0'		0.36	0.04	0.10	0.19	0.03	0.00	0.07	0.12	0.10							
70	ODP K708-7	III-RHY-I	-		18	**73.65**	**0.27**	**11.98**	**3.26**	**0.15**	**0.06**	**1.21**	**1.08**	**2.02**	**93.68**	-	-				4

Table 4.2 Correlation dating of highly silicic tephra deposits of Icelandic origin: Visual identification of Óþoli Tephra matches - summary major element chemical data (mean ± 1σ for the Óþoli Tephra and tephra layers with similar chemical composition found in deposits of mid-late Pleistocene age from marine cores from around Iceland. See Figure 4.11 for locations. Methods as described in chapter 3; sjr = Stephen Roberts, sp = Shari Preece, jrs = Jon Sigurvinsson; UE = University of Edinburgh; UT = University of Toronto; UI = University of Iceland and year of analysis. *References*: 1 = Sigurdsson and Loebner (1981); 2 = Sigurdsson (1982); 3 = Lacasse *et al*. (1995; 1996); 4 = Kvamme *et al*. (1989).

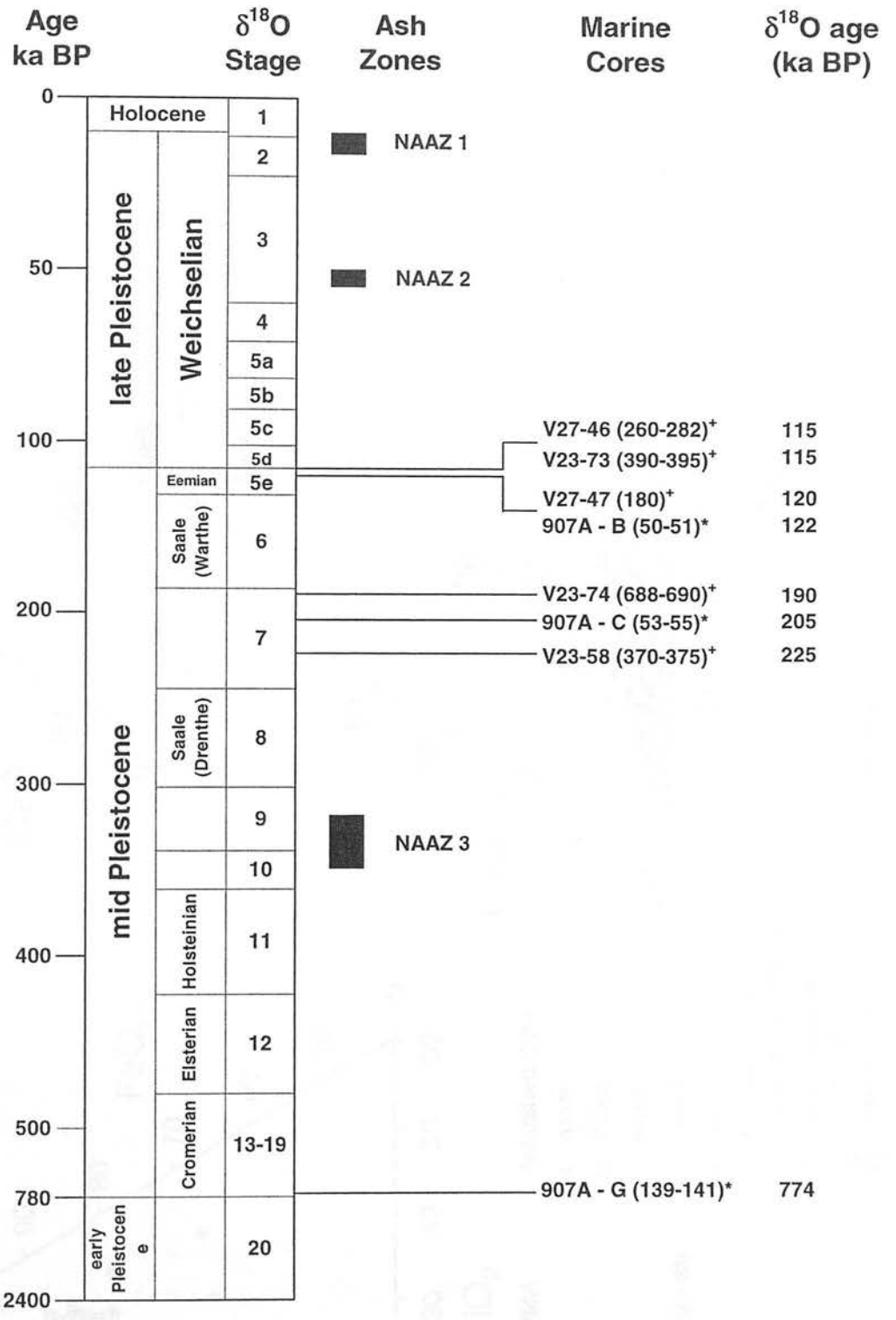


Figure 4.12 Visual major element correlation dating matches for the Óþoli Tephra in the Pleistocene era and their relationship to the classically defined North Atlantic Ash zones (NAAZ 1-3); references: + = Sigurdsson and Loebner (1981), * = Lacasse *et al*. (1996)

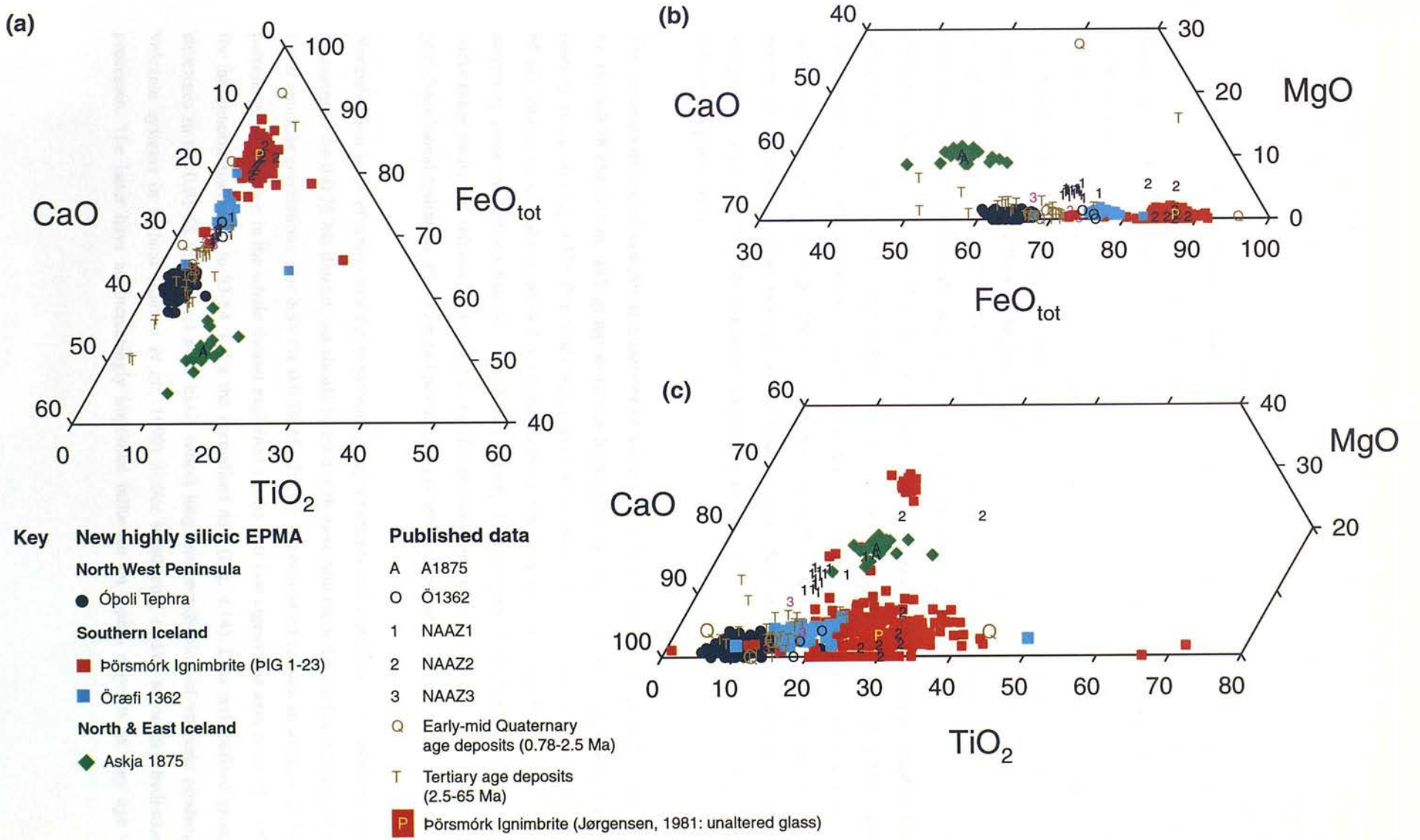


Figure 4.13 Non-mobile major element, ternary discrimination plots for the glass-phase of highly silicic EPMA data used for in numerical dating analysis compared to selected published data from 0-65 Ma tephra deposits of Icelandic origin. Published data are listed in full in Appendix C2: Table C2.

(b) Multivariate statistical analysis results

A variety of the clustering methods were applied to the original and normalised versions of data (Table C2.1). After several test runs, average linkage clustering analysis using Euclidean and Euclidean squared as a distance measure was selected as the best clustering method for the untransformed and normalised versions of this dataset. These methods produced the most accurate grouping of deposits of known or suggested geochemical similarity (*e.g.* A1875, Ö1362, Holocene Hekla tephras, NAAZ-1, NAAZ-2 and the Þörsmórk Ignimbrite). Ward's linkage imposed unrealistic group structures and produced some groups with negative percentage similarities that are clearly erroneous. Average linkage cluster analysis, using Euclidean distance as a similarity measure produces the largest percentage similarity differences between groups enabling clear distinctions to be made (Fig. 4.14). In addition, it highlighted potential differences between samples within these groups. For example, most of the Vedde-NAAZ-1 data is broadly similar, but there appears to be an inherent regional bias within the overall group. Data from Iceland and Greenland can be separated from data from NW Europe. This may be a result of different analytical procedures adopted. It is interesting to note, however, that Roberts (1997) and, more recently, Bond *et al.* (2001) have questioned whether all occurrences of Vedde-NAAZ-1 in the North Atlantic region are related to the same eruption event. Average linkage, Euclidean squared distance cluster analysis produces essentially the same grouping structure as Euclidean squared distance-average cluster analysis, dissimilarity at the high end of the similarity scale is less pronounced making it harder to visualise and delimit group structures.

The inclusion of control samples as a measure of acceptable levels of similarity appears to work well for the 0-0.78 Ma dataset, with group structures highlighted by cluster analysis confirmed by PCA primary axis plots (Fig. 4.14). Principal components analysis showed that groups formed in the 0.01-65 Ma dataset are less clearly defined compared to those formed in the 0-0.78 Ma dataset. This is not surprising since the 0.01-65 Ma. (*i.e.* pre-Holocene-early Tertiary) period incorporates data from a wider range variety of volcanic system types at different evolutionary stages. Furthermore, substantial post-depositional hydration, alteration and possible loss of mobile elements could have occurred.

Normalisation is an effective tool for improving group structures and confidence in correlation age estimates in the 0-0.78 Ma dataset, but should be used with more caution in the pre-Quaternary era to avoid spurious correlations. For both the 0-0.78 Ma dataset, normalisation creates an increase in the percentage of variance in the whole dataset explained by the first two eigenvalue axes from 72-73 % for the unnormalised data to 83-84 % for the normalised data (Fig. 4.14). Less well-defined group structures in the 0.01-65 Ma dataset most likely reflect long-term equifinality of volcanic products volcanic systems in Iceland (Larsen *et al.*, 1999) and/or weathering and/or secondary hydration processes. The latter have an increasingly important influence on tephra deposits as they age –

especially for deposits greater than 10 Ma (Steen-McIntyre, 1977). Tephras up to 5 Ma can retain their original chemical composition if they are deposited in low weathering/oxidising environments (Brown *et al.*, 1992).

Square root transformation of the data improved the clarity of group structures, but it was difficult to determine distinct groups from in all types of PCA based on the 0.01-65 Ma dataset, especially for the Óþoli Tephra. This highlights difficulties in using major element chemical correlation as a dating technique in the pre-mid Pleistocene era. Nevertheless, the use of multivariate statistical techniques provided an empirical method of defining similarity and has enabled several possible age estimates for the Óþoli Tephra and Þörsmórk Ignimbrite to be firmly eliminated.

(c) Evaluation of correlation dating hypotheses (Box 3.1)

(i) Óþoli Tephra

Major element chemical correlation dating was the least successful dating method for the Óþoli Tephra. In the 0-0.78 Ma age range, where published chemical data is most reliable, up to eight matches with an age range of 115-774.1 ka were obtained using a variety of multivariate statistical methods. Of these 115 ka, 225 ka, 774.1 ka were common in all cases. Average linkage, Euclidean distance cluster analysis of untransformed data proved to be the only reliable grouping method for the 0.01-65 Ma period, producing ten possible age matches of 115 ka, 190 ka, 225 ka, 320 ka (twice), 7.46-7.89 Ma and >10.83-12.94 Ma (three times).

Attempts to identify a single age match for the Óþoli Tephra were unsuccessful because of general trends towards long-term major element chemical equifinality of Icelandic volcanic systems (Larsen *et al.*, 1999) and, in particular, their highly silicic, explosive/Plinian style eruptives. Over shorter time scales, *i.e.* Holocene- to Lateglacial, discrimination to individual eruption level is possible for two main reasons. Firstly, a well-preserved, comparative terrestrial record exists and, secondly, there are relative few highly silicic eruptions. If the frequency of highly silicic producing eruptions in the Holocene period is extrapolated back 2.5 Ma there would be 3000 potential correlatives for the Óþoli Tephra. This is an overestimate because the temporal distribution of explosive eruptions from Iceland is uneven with more events occurring during interglacial periods (Sigurdsson and Loebner, 1981; Sigurdsson, 1982; Zielinski *et al.*, 1997; Clift and Fitton, 1998; Haflidason *et al.*. 2000). Nevertheless, this estimate highlights a significant barrier in extending the useful age range of major element correlation dating of Icelandic tephra deposits into the pre-^{14}C dating era.

(ii) Þörsmórk Ignimbrite

Major element chemical correlation dating of the 0-0.78 Ma dataset of highly silicic tephra deposits was the most successful method for dating the unaltered highly silicic glass-phase of the Þörsmórk Ignimbrite. All multivariate statistical methods and transformations of the original data in the 0-0.78 Ma age range unequivocally matched deposits of NAAZ-2 providing a correlation age estimate range

of 48.5-58 ka (Fig. 4.14; Table 4.3). Samples of unaltered glass from the Þörsmórk Ignimbrite analysed by Jørgensen (1980, 1981) and ocean core deposits of NAAZ-2 with ages of 48.5 ka were close matches to the new analyses in all statistical tests. Although sporadic matches with ages in the order of millions of years, the same age relationships were obtained from the 0.01-65 Ma dataset (Table 4.3b). In conclusion, the closest correlation age for the Þörsmórk Ignimbrite is 48.5 ka, but data from the whole NAAZ-2, 48.5-58 ka age range are broadly similar.

4.2.3 Palaeomagnetic reversal correlation dating of Skagafjall sediments

Preliminary palaeomagnetic reversal dating of the Skagafjall sediments provides an independent means to constrain the age of the Óþoli and Hjallanes Tephra. The polarity of the undisturbed sediments from Skagafjall sections A and B examined is predominantly reversed (Table 4.4), effectively ruling out a Mid-Pleistocene age. The notable exception are samples taken from the coarse-grained Hjallanes Tephra layer whose polarity is uncertain or possibly normal (Table 4.4). In addition, uncertain polarity measurements were obtained from two types of samples:

- Those from high energy depositional environments (*e.g.* I00PM1-4)
- Those collected in a torrential rainstorm (I0021-28)

Both of these effects could feasibly disturb any depositional detrital remnant magnetic polarity signal.

1) Cluster and Principal Components Analysis (PCA) of 0-0.78 Ma highly silicic tephra deposits of Icelandic origin

Data as analysed (not normalised)

a Average linkage, Euclidean distance cluster dendrogram

Average Euclidean distance % similarity dendrogram & similarity limit levels

A1875 | Similarity control sample limits | OUTLIERS

Óþoli

Groups		Tephra Deposit & ID number	Age (ka BP)	
A	1	65 907A-1H-3, 53-55-C (N. Iceland Plateau)	204.6	65
	2	70 SU9029-549 (III-RHY-I)	320	70
		69 K708-1-610 (III-RHY-I)	320	69
		204 Óþoli Tephra (Skagafjall, Vestfirðir; sjr)	*2260*	*204*
		73 907A-2H-6, 139-141-G (N. Iceland Plateau)	774.1	73
		205 Óþoli Tephra (Skagafjall, Vestfirðir; sp)	*2260*	*205*
		68 DSDP38:1-V23-58-375 (N. Iceland Plateau)	225	68
		64 DSDP38:1-V23-74-688 (N. Iceland Plateau)	190	64
		56 DSDP38:1-V23-73-393 (N. Iceland Plateau)	115	56
	3	303 Klaksvik, Faroe Islands (sw)	?	303
		63 MD-95-2009, 1830.5 (5e-Midt/RHY)	115-128	63
		60 HM79-31 (5e-Midt/RHY)	125	60
		59 907A-1H-2, 50-51-B (N. Iceland Plateau)	122.3	59
		58 V27-47-180 (N. Iceland Plateau)	120	58
		57 V27-46-260 (N. Iceland Plateau)	115	57
	4	16 Glen Garry, Scotland	2.1	16
		201 ASK 5/10/11 (N & E Iceland; sjr)	*0.126*	*201*
		301 4B-10/1-JB_UL (Sweden; sjr)	*0.126?*	*301*
		4 A1875 (E of Askja)	*0.126*	*4*
		3 A1875 (Askja)	*0.126*	*3*
	5	51 GRIP-2430.95-2430.97m (NAAZ2)	53.5	51
		52 DYE-3 (NAAZ2)	52	52
		48 K708-1-390 (NAAZ2)	48.5	48
		45 SO82-02,-5,-7,LO091-21,-23(NAAZ2)	58	45
	6	35 Borrobol Tephra (Scotland)	12.26	35
		34 Borrobol Tephra (Scotland)	12.26	34
	7	22 H5 (Hekla)	6.1	22
		21 H4 (N Iceland)	3.83	21
		20 H4 (Hekla)	3.83	20
		10 H1158 (H1-early) (N Iceland)	0.843	10
	8	62 ENAM33, 566 (5e-Top/RHY)	115-128	62
		53 ENAM33, 548 (5d-Low/RHY-I)	103-115	53
	9	55 ENAM33, 548 (5d-Low/RHY-III)	103-115	55
	10	49 SU9032-562 (NAAZ2)	48.5	49
		203 ÞIG 1-23 (Þórsmörk, S Iceland; sjr)	*(TL)*	*203*
		47 SO82-05/496 (II-RHY-I)	48.5	47
		36 Þórsmörk Ignim. (ÞIG) (S Iceland)	50/200	36
	11	1 H1970 (Hekla)	0.031	1
B	1	61 HM79-31 (5e-Midt/RHY)	125	61
	2	43 93030-006-LCF-278 (NAAZ1-Vedde?)	10.3	43
		44 GRIP-1639.54-1639.55m (NAAZ1-Vedde?)	11.98	44
		41 K708-1 (NAAZ1-Vedde?)	ca. 10	41
		29 Katla ob. Pumice (S Iceland)	10.3	29
		27 Skogar Tephra (N Iceland)	10.3	27
		8 Ö1362 (Ireland)	0.639	8
		202 ÖR 1-3 (S & SE Iceland; sjr)	*0.639*	*202*
		7 Ö1362 (Svinafell)	0.639	7
		6 Ö1362 (Öræfi)	0.639	6
	3	37 Solheimar Ignim. (SIG) (S Iceland)	65?	37
		38 6 km SW of SIG (S Iceland)	?	38
		33 Vedde Ash (≡) (Russia)	10.3	33
		32 Vedde Ash (≡) (Russia)	10.3	32
		31 Vedde Ash (≡) (Sweden)	10.3	31
		42 SO82-02,-5,-7,LO091-21,-23(NAAZ1?)	10.3	42
		30 Vedde Ash (≡) (Scotland)	10.3	30
		26 Vedde Ash (≡) (W Norway)	10.3	26
	4	5 E1821 (S Iceland)	0.18	5
		2 H1947 (S Iceland)	0.054	2
	5	15 Settlement (Afang)	1.131	15
		14 Settlement (Thing)	1.131	14
	6	19 H-S (Shetland Islands)	3.5	19
		18 H-S (Faroe Islands)	3.5	18
		13 H1104 (N of Hekla)	0.901	13
		17 H3 (N Iceland)	2.855	17
		12 H1104 (Hekla)	0.901	12
	7	9 H1300 (N Iceland)	0.701	9
D		66 HM57-7/410-412 (St. 7-RHY-I)	210	66
		71 K708-7 (III-RHY-I)	320	71
		46 V23-42, 246-245; V27-114, 396 (II-RHY-1)	ca. 50	46
		72 HM57-7/653-655 (St. 9-RHY-I)	330	72
		67 HM57-7/410-412 (St. 7-RHY-I)	210	67
		40 P57-7, 21-23 (NAAZ1?)	0-11.670	40
		39 P57-7, 16-18 (NAAZ1?)	0-11.670	39
		28 Vedde Ash (°) (N Iceland)	10.5	28
		25 Vedde Ash Stratotype (W Norway)	*10.6*	*25*
		54 ENAM33, 548 (5d-Low/RHY-II)	103-115	54
		24 SILK layer A12 (S Iceland)	ca. 7.2	24
		23 SILK layer A11 (S Iceland)	ca. 7.0	23
		11 H1158 (H1-late) (N of Hekla)	0.843	11
		50 GISP2-2464.25-2464.30m (NAAZ2)	52.682	50

100 90 80 70 60 50

Similarity (%)

A & B are the main groups (see text for explanation). These have been divided into subgroups by comparison with the similarity control samples of A1875 and Opoli Tephra (see text for explanation); C and D are outlier groups - group C members, where they occur, are outliers associated with the group A or B as indicated by the suffix - group D members are outliers to both A and B.

b PCA Principal Axes Bi-plots: *Axis 2* vs *Axis 1*

Numbers in (i) & (iii) are tephra deposit ID numbers from (a)

(i) 0-0.78 Ma: Untransformed data

Sample data point graph

Group structure unclear without aid of clustering analysis in diagram (ii)

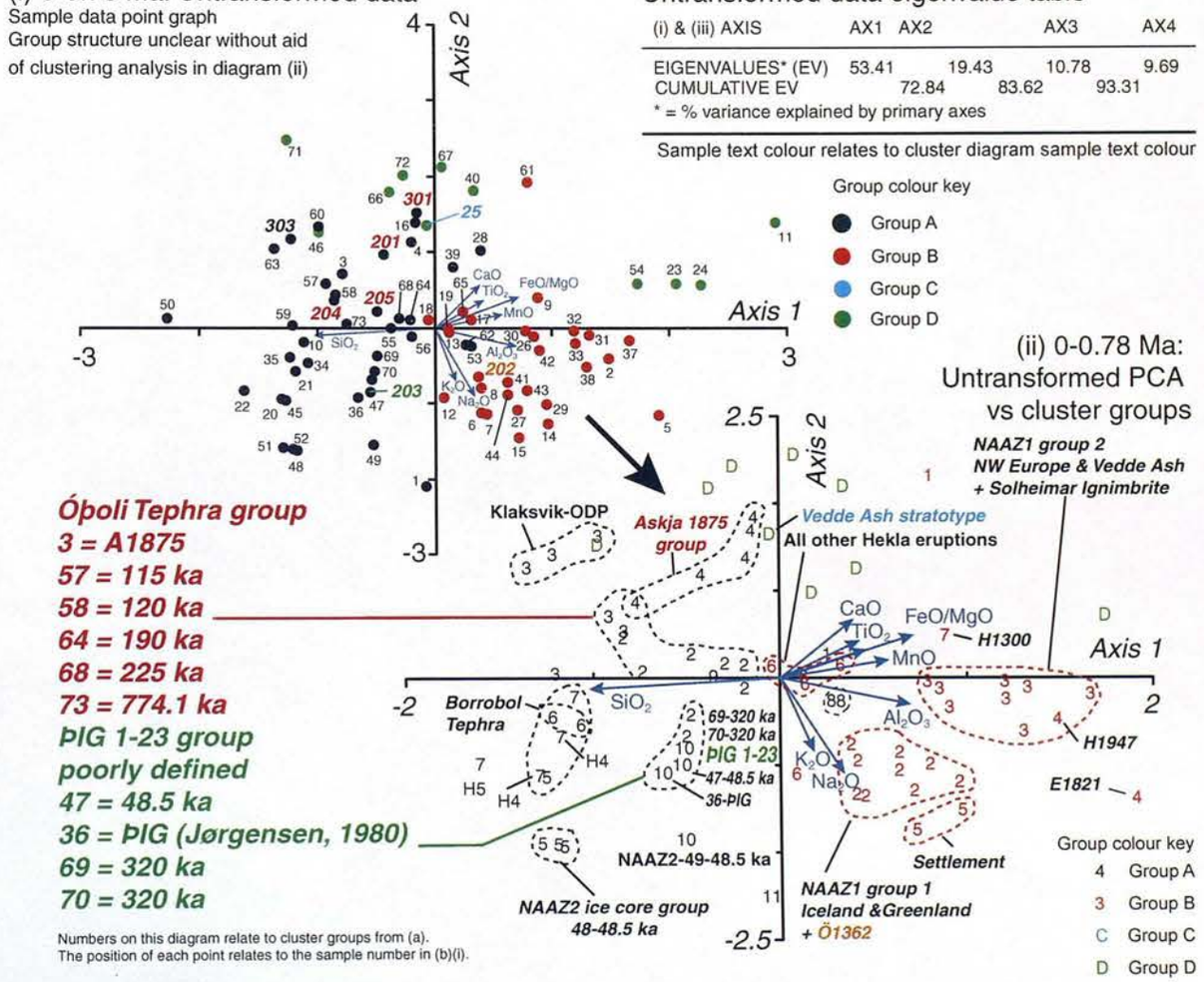
Untransformed data eigenvalue table

(i) & (iii) AXIS	AX1	AX2	AX3	AX4
EIGENVALUES* (EV)	53.41	19.43	10.78	9.69
CUMULATIVE EV	72.84	83.62	93.31	

* = % variance explained by primary axes

Sample text colour relates to cluster diagram sample text colour

Group colour key: Group A; Group B; Group C; Group D



Óþoli Tephra group
3 = A1875
57 = 115 ka
58 = 120 ka
64 = 190 ka
68 = 225 ka
73 = 774.1 ka
ÞIG 1-23 group
poorly defined
47 = 48.5 ka
36 = ÞIG (Jørgensen, 1980)
69 = 320 ka
70 = 320 ka

Numbers on this diagram relate to cluster groups from (a).
The position of each point relates to the sample number in (b)(i).

(ii) 0-0.78 Ma: Untransformed PCA vs cluster groups

NAAZ1 group 2
NW Europe & Vedde Ash
+ Solheimar Ignimbrite

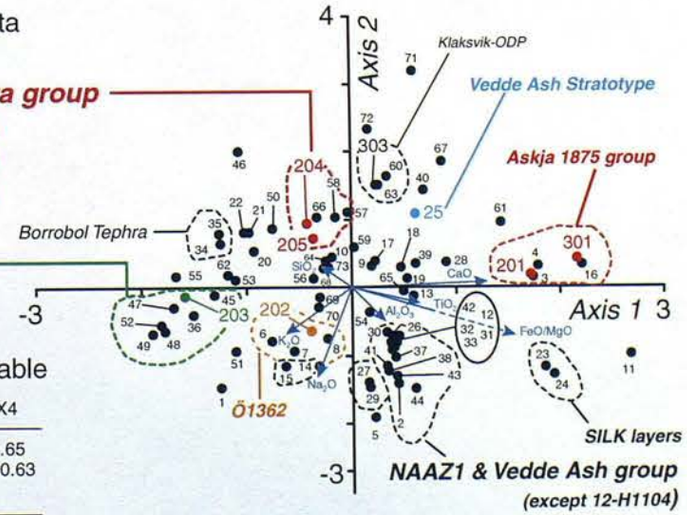
Group colour key: 4 Group A; 3 Group B; C Group C; D Group D

(iii) 0-0.78 Ma: Square root transformed data

Sample data point graph; group structure clearer than (i)

ÞIG 1-23 group
45 = 58 ka
47 = 48.5 ka
48 = 48.5 ka
49 = 48.5 ka
ODP-NAAZ2
52 = 52 ka (DYE 3 ice core)
36 = ÞIG (Jørgensen, 1980)

Óþoli Tephra group
66 = 210 ka
58 = 120 ka
57 = 115 ka



Square root transformed data eigenvalue table

(ii) AXIS	AX1	AX2	AX3	AX4
EIGENVALUES* (EV)	39.57	24.86	17.55	8.65
CUMULATIVE EV	64.43		81.98	90.63

* = % variance explained by primary axes

Figure 4.14-1 Example of correlation dating analysis for the Óþoli Tephra and Þórsmörk Ignimbrite using multivariate clustering and PCA analysis applied to most of the known highly silicic tephra deposits of Icelandic origin in the 0-0.78 Ma age range. Diagrams based on data that has not been recast to 100% on a volatile free basis (*i.e.* data presented is not normalised).

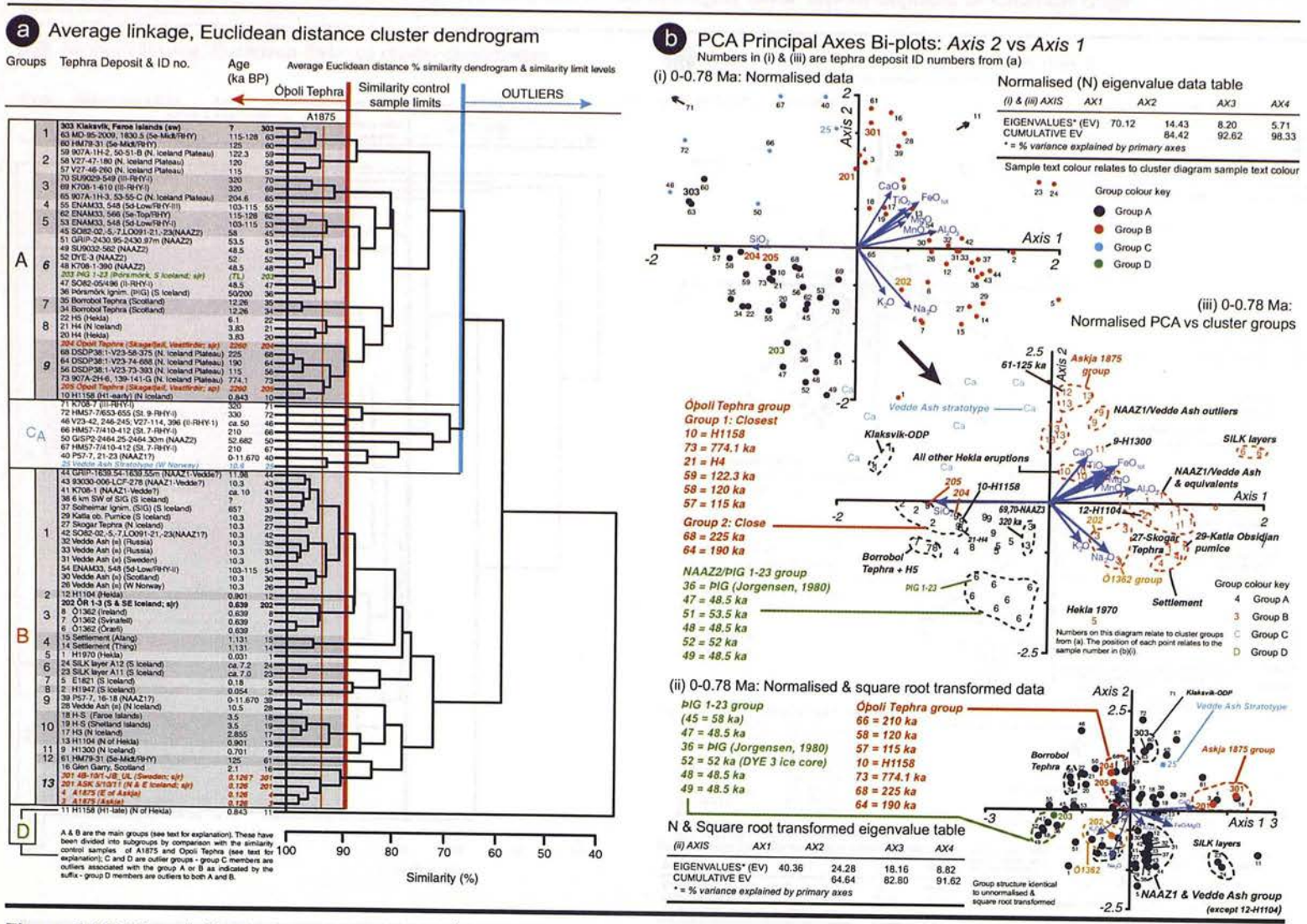


Figure 4.14-2 Correlation dating analysis for the Óþoli Tephra and Þórsmörk Ignimbrite using multivariate clustering and PCA analysis applied to most of the known highly silicic tephra deposits of Icelandic origin in the 0-0.78 Ma age range. Diagrams based on data that has been recast to 100% on a volatile free basis (*i.e.*data presented is normalised).

3) Cluster and Principal Components Analysis (PCA) of 0.01-65 Ma highly silicic tephra deposits of Icelandic origin

Data as analysed; published data only & ODP-P57 outliers removed

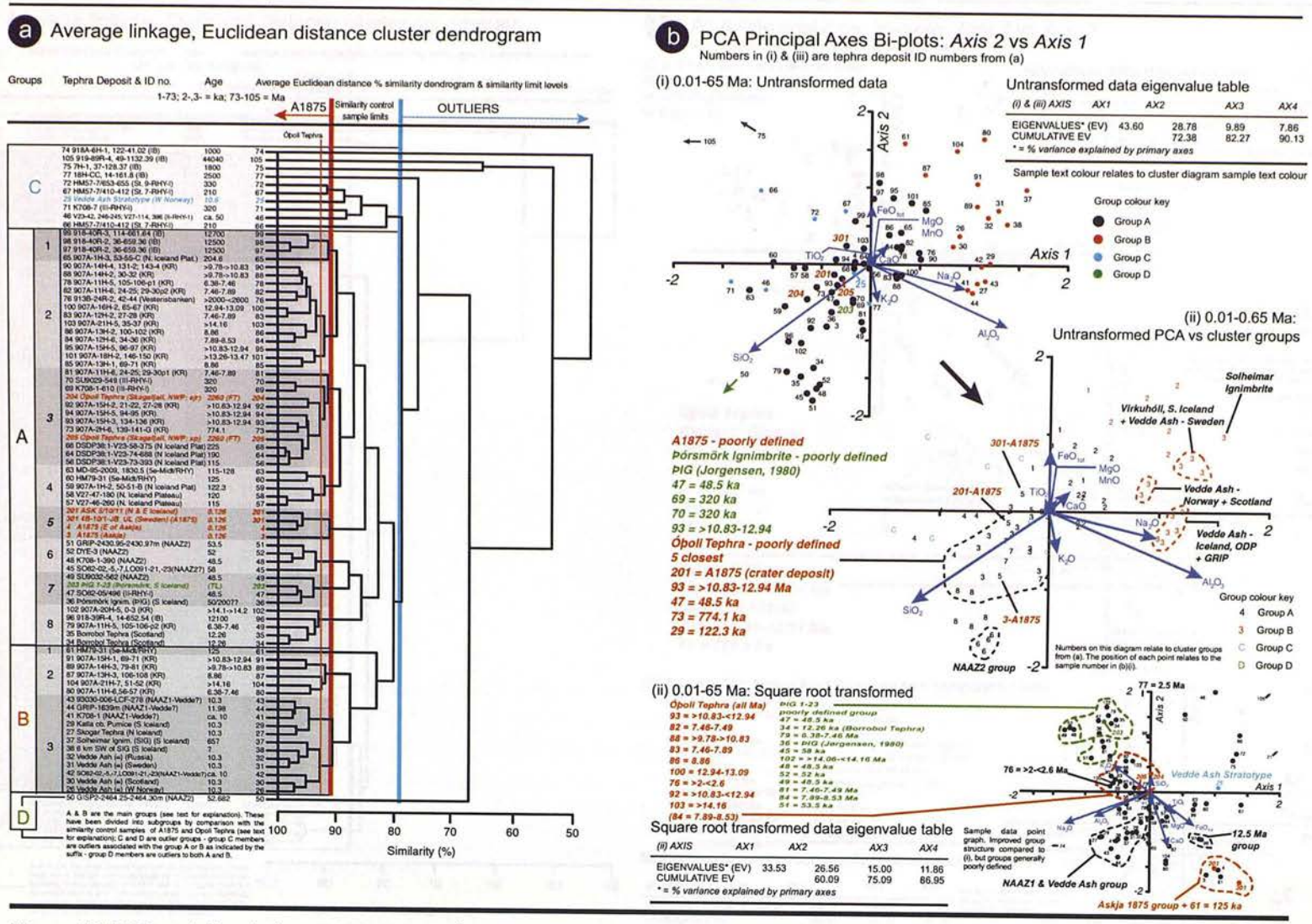


Figure 4.14-3 Correlation dating analysis for the Óþoli Tephra and Þórsmörk Ignimbrite using multivariate clustering and PCA analysis applied to most of the known highly silicic tephra deposits of Icelandic origin in the 0.01-65 Ma age range. Diagrams based on data that has not been recast to 100% on a volatile free basis (*i.e.*data presented is unnormalised).

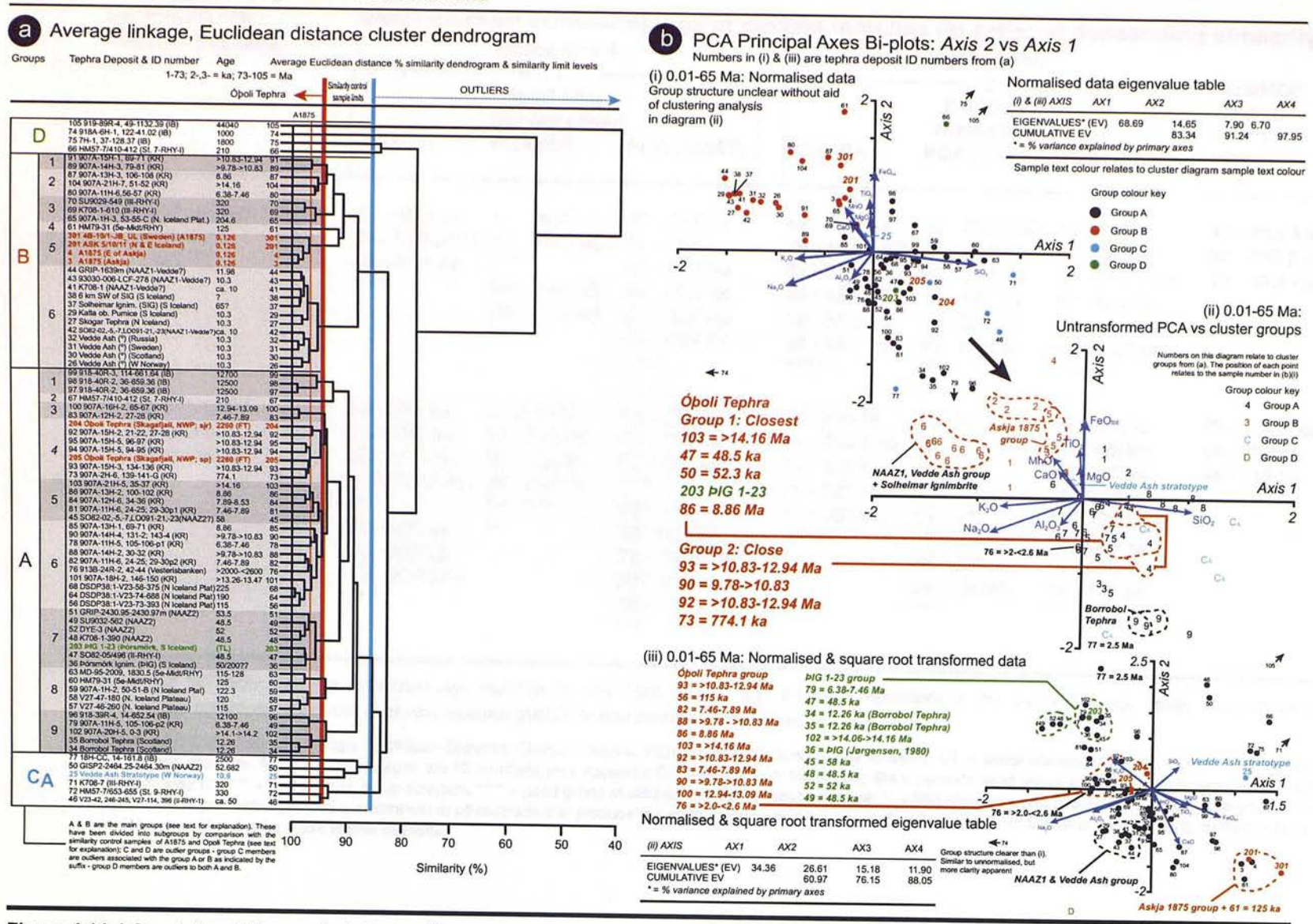


Figure 4.14-4 Correlation dating analysis for the Óþoli Tephra and Þórsmörk Ignimbrite using multivariate clustering and PCA analysis applied to most of the known highly silicic tephra deposits of Icelandic origin in the 0.01-65 Ma age range. Diagrams based on data that has been recast to 100% on a

(a) 0-0.78 Ma Tephra deposit	Major element correlation age of closest matches (in order of descending similarity)						
	Figure 4.14-1			Figure 4.14-2			
	1			2			
	0-0.78 Ma Unnormalised			0-0.78 Ma Normalised			COMMON TO ALL (> ***)
	AED-CA	PCA (UT)	PCA (SQRT)	AED-CA	PCA (UT)	PCA (SQRT)	
A Þörsmórk Ignimbrite Þörsmórk S Iceland	47 - 48.5 ka 36 - ÞIG (UD) 49 - 48.5 ka *****	47 - 48.5 ka 36 - ÞIG (UD) ***** [69 - 320 ka] [70 - 320 ka] **	45 - 58.0 ka 47 - 48.5 ka 48 - 48.5 ka 49 - 48.5 ka 52 - 52.0 ka 36 - ÞIG (UD) *****	47 - 48.5 ka 36 - ÞIG (UD) 51 - 53.5 ka 49 - 48.5 ka 52 - 52.0 ka 48 - 48.5 ka *****	36 - ÞIG (UD) 47 - 48.5 ka 51 - 53.5 ka 48 - 48.5 ka 52 - 52.0 ka 49 - 48.5 ka *****	45 - 58.0 ka 47 - 48.5 ka 36 - ÞIG (UD) 52 - 52.0 ka 48 - 48.5 ka 49 - 48.5 ka *****	**47 - 48.5 ka** **36 - ÞIG (UD)** **49 - 48.5 ka**
B Óþoli Tephra Skagafjall NW Iceland	68 - 225 ka 64 - 190 ka 56 - 115 ka 73 - 774.1 ka ***** 69 - 320 ka 70 - 320 ka 65 - 204.6 ka ****	3 - A1875 57 - 115 ka 58 - 120 ka 64 - 225 ka 73 - 774.1 **	66 - 210 ka 58 - 120 ka 57 - 115 ka **** 59 - 122.3 ka 10 - H1158 73 - 774.1 ka 68 - 225 ka 56 - 115 ka ***	10 - H1158 73 - 774.1 ka 56 - 115 ka 68 - 225 ka 64 - 190 ka *****	10 - H1158 73 - 774.1 ka 21 - H4 59 - 122.3 ka 58 - 120 ka 57 - 115 ka 68 - 225 ka 64 - 190 ka ***	66 - 210 ka 58 - 120 ka 57 - 115 ka 10 - H1158 73 - 774.1 ka 68 - 225 ka 64 - 190 ka 56 - 115 ka ***	**73 - 774.1 ka** **68 - 225 ka** **56 - 115 ka**

Table 4.3 (a) Major element correlation age matches for the Óþoli Tephra and Þörsmórk Ignimbrite in the 0-0.78 Ma age range obtained using multivariate statistical techniques of cluster analysis (AED-CA) and principal components analysis (PCA).

Notes: AED-CA = Average linkage, Euclidean Distance Cluster Analysis; PCA = Principal Components Analysis; UT = untransformed datasets; SQRT = square root transformed datasets. Numbers before ages are ID numbers (see Appendix C: Table 2C.1 for full details) Stars beneath each group are a subjective measure of group definition where: ***** = well-defined group structure, **** = good group structure; *** = some group structure; ** = little obvious group structure; * = no group structure. The final column represents ages that are common to all methods that produce group structures with *** or more. See Table C2.1 for full list of data & dating methods used to produce age estimates for these tephra deposits.

(b) 0.01-65 Ma Tephra deposit	Major element correlation age of closest matches (in order of descending similarity)						
	Figure 4.14-3 — 3 — 0.01-65 Ma Unnormalised			Figure 4.14-4 — 4 — 0.01-65 Ma Normalised			COMMON TO ALL (> **)
	AED-CA	PCA (UT)	PCA (SQRT)	AED-CA	PCA (UT)	PCA (SQRT)	
A Þörsmórk Ignimbrite Þörsmórk S Iceland	47 - 48.5 ka 36 - ÞIG (UD) 49 - 48.5 ka *****	47 - 48.5 ka 36 - ÞIG (UD) [69 - 320 ka] [70 - 320 ka] *	47 - 48.5 ka 34 - 12.26 ka 79 - 6.38-7.46 Ma 36 - ÞIG (UD) 45 - 58 ka 102 - >14.06-<14.16 48 - 48.5 ka 52 - 52.0 ka 49 - 48.5 ka 81 - 7.46-7.49 Ma 84 - 7.89-8.53 Ma 51 - 53.5 ka **	47 - 48.5 ka 36 - ÞIG (UD) 51 - 53.5 ka 49 - 48.5 ka 52 - 52.0 ka 48 - 48.5 ka *****	47 - 48.5 ka 103 - >14.16 Ma 86 - 8.86 Ma 205 - Óþoli Tephra 50 - 52.3 ka [36 - ÞIG (UD)] ***	79 - 6.38-7.46 Ma 47 - 48.5 ka 34 - 12.26 ka 35 - 12.26 ka 102 - >14.06->14.16 Ma 36 - ÞIG (UD) 45 - 58 ka 48 - 48.5 ka 52 - 52.0 ka 49 - 48.5 ka ***	**47 - 48.5 ka** **36 - ÞIG (UD)**
B Óþoli Tephra Skagafjall NW Iceland	68 - 225 ka 64 - 190 ka 56 - 115 ka 73 - 774.1 ka 93 - >10.83-12.94 Ma 94 - >10.83-12.94 Ma 92 - >10.83-12.94 Ma 69 - 320 ka 70 - 320 ka 81 - 7.46-7.89 Ma *****	201 - A1875 (ASK5) 93 - >10.83-12.94 Ma 47 - 48.5 ka 73 - 774.1 ka 29 - 122.3 ka *(5 closest to 204/205)* *	93 - >10.83-<12.94 Ma 82 - 7.46-7.89 Ma 88 - >9.78->10.83 Ma 83 - 7.46-7.89 Ma 86 - 8.86 Ma 100 - 12.94-13.09 Ma ***76 - >2-<2.6 Ma*** 92 - >10.83-<12.94 Ma 103 - >14.16 Ma ***	93 - >10.83-<12.94 Ma 73 - 774.1 ka 94 - >10.83-<12.94 Ma 95 - >10.83-<12.94 Ma 92 - >10.83-<12.94 Ma *****	103 - >14.16 Ma 47 - 48.5 ka 50 - 52.3 ka 203 - ÞIG 1-23 86 - 8.86 Ma 93 - >10.83-<12.94 Ma 90 - 9.78->10.83 Ma 92 - >10.83-<12.94 Ma 73 - 774.1 ka **	93 - >10.83-<12.94 Ma 56 - 115 ka 64 - 190 ka 68 - 225 ka 73 - 774.1 ka 82 - 7.46-7.89 Ma 88 - >9.78->10.83 Ma 86 - 8.86 Ma 103 - >14.16 Ma 92 - >10.83-<12.94 Ma 83 - 7.46-7.89 Ma 90 - 9.78->10.83 Ma 100 - 12.94-13.09 Ma ***76 - >2-<2.6 Ma*** ***	**Unnormalised** **93 - >10.83-<12.94 Ma** **Normalised** **93 - >10.83-<12.94 Ma** **73 - 774.1 ka** **92 - >10.83-<12.94 Ma** **All** **93 - >10.83-<12.94 Ma**

Table 4.3 (b) Major element correlation age matches for the Óþoli Tephra and Þörsmórk Ignimbrite in the 0.01-65 Ma age range obtained using multivariate statistical techniques of cluster analysis (AED-CA) and principal components analysis (PCA). Key as (a)

CODE	SECTION	UNIT	DESCRIPTION	SECTION BEARING (°)	UNIT DIP (N°W)	NRM MAGNETISM LAB DEC	LAB INC	CORRECTED DEC	CORRECTED INC	N or R
I00PM 1	B	11.27	Reworked Óþoli Tephra	120	18*	87.6	-60.3	117.6	-60.3	R?
I00PM 2	B	11.27		120	18*	86.2	-59.3	116.2	-59.3	R?
I00PM 3	B	11.27		120	18*	63.1	-54.9	93.1	-54.9	?
I00PM 4	B	11.27		120	18*	184.3	9.0	214.3	9.0	N?
I00PM 5	B	11.27		120	18*	188.2	-28.8	218.2	-28.8	R
I00PM 6	B	11.27		120	18*	195.5	-51.5	225.5	-51.5	R
I00PM 7	B	11.10	Airfall Óþoli Tephra	116	10-18	160.0	-49.9	186.0	-49.9	R
I00PM 8	B	11.10		118	10-18	119.8	-24.9	147.8	-24.9	R
I00PM 9	B	11.10		118	10-18	156.2	-59.0	184.2	-59.0	R
I00PM 10	B	10	RB 10 silt/clay (upper)	112	10-18	153.6	-17.2	175.6	-17.2	R
I00PM 11	B	10		112	10-18	185.4	-10.9	207.4	-10.9	R
I00PM 12	B	10		112	10-18	142.9	-24.9	164.9	-24.9	R
I00PM 13	B	10		112	10-18	136.1	-49.9	158.1	-49.9	R
I00PM 14	B	10	RB 10 silt/clay (lower)	90	10-18	161.8	-32.7	161.8	-32.7	R
I00PM 15	B	10		108	10-18	157.0	-46.1	175.0	-46.1	R
I00PM 16	B	10		78	10-18	153.4	-24.0	141.4	-24.0	R
I00PM 17	B	10		82	10-18	140.3	-29.6	132.3	-29.6	R
I00PM 18	A	8	RB 8 silt/clay	63	<10	207.4	-72.8	180.4	-72.8	R
I00PM 19	A	8		63	<10	231.7	-75.1	204.7	-75.1	R
I00PM 20	A	8		63	<10	220.5	-76.4	193.5	-76.4	R
I00PM 21	A	4.3	RB 4 clay varves above Hjallanes Tephra	61	<10	50.6	-78.7	21.6	-78.7	R?
I00PM 22	A	4.3		61	<10	37.7	-70.7	8.7	-70.7	R?
I00PM 23	A	4.3		61	<10	192.7	-88.3	163.7	-88.3	R
I00PM 24	A	4.2	Hjallanes Tephra (Hj-2b)	41	<10	142.8	-22.8	93.8	-22.8	?
I00PM 25	A	4.2		51	<10	314.8	35.0	275.8	35.0	N?
I00PM 26	A	4.2		49	<10	263.5	60.3	222.5	60.3	N?
I00PM 27	A	4.1	RB 4 varves below Hjallanes Tephra (Hj-1, Hj-2a)	63	<10	296.2	-75.4	269.2	-75.4	R?
I00PM 28	A	4.1	(samples collected in torrential rain)	63	<10	290.9	-87.9	263.9	-87.9	R?

Table 4.4 Preliminary palaeomagnetic polarity data for Skagafjall sediments. Acceptable declinations are between NW-NE (315-45°) and SE-SW (135-225°); * = measured unit dip; units correspond to stratigraphic diagrams; RB = rhythmite bed. Samples I0021-I0028 were collectd in a prolonged rainstorm.

4.3 Fission-track Dating

4.3.1 ITPFT & DCFT of the Óþoli Tephra

The weighted mean fission-track age of the Óþoli Tephra is 2.26±0.11 Ma (Table 4.5). The combined weighted mean age error estimate is less than 5%, as precise as the method allows (cf. ITPFT dating errors in Table 2.3). All ages are within single standard deviation error range of each other. The accuracy of the fission-track age obtained from the Óþoli Tephra is crucial. Above all, an early Pleistocene age for the Skagafjall sedimentary sequence has major implications for landscape development in the Vestfírðir Peninsula and the Icelandic glacial history. Secondly, it provides an opportunity to test the reliability of the correlation and the experimental thermoluminescence dating methods used in this study. The accuracy of the fission-track ages was evaluated in the following three ways:

(a) Methodological consistency & accuracy

There is a recognised element of subjectivity in fission-track dating. This effect was minimised by identifying and counting fission-tracks in the systematic, unbiased and consistent manner. Experience is the key factor in producing accurate fission-track ages, hence initial ages were undertaken by John Westgate and Amanjit Sandhu, who have twenty years of experience in this field. Large platey glass shards (>100 μm) of the Óþoli Tephra were ideal for counting fission-tracks and identifying fission-tracks on the glass-shard surfaces was straightforward. Figure 4.15 shows a typical field of view observed when counting fission-tracks on shards of the Óþoli Tephra at 500x magnification and illustrates the ease with which tracks can be identified and distinguished from vesicles and other features. Spontaneous tracks are formed by natural decay of ^{238}U and single spontaneous fission-tracks were observed on most large shards (Fig. 4.15a). Induced tracks were formed artificially in a nuclear reactor by an artificially high flux of ^{235}U decay; hence the high number of tracks per shard compared to the spontaneous portion.

The isothermal plateau is identified and the effects of track fading minimised when the ratio of spontaneous to induced track diameters is close to unity. ITPFT ages with D_s/D_i values close to unity are accurate assessments of the 'true' age of the glass. Figure 4.16 shows track-size distribution histograms. In all cases etching was successful producing a mean track size of 5-8 μm, as recommended by Westgate *et al.* (1997). Confidence in the ITPFT ages increases when track size distributions with a mean track size of 5-8 μm are obtained because this ensures that the tracks are of the optimum size for counting at 500x magnification. All ITPFT samples (UT1655, 1656, 1659) have D_s/D_i values close to unity indicating that the isothermal plateau dating method used has successfully corrected for the effects of partial track fading (Table 4.5). Figure 4.17 shows track count ratio data for UT1656 as an example of the counting procedure used. Post depositional thermal annealing can be ruled out because of the non-thermal nature, geologically stable and periglacial-glacial environment of

high plateau regions of the Vestfírðir Peninsula. In addition, the 1.97 ± 0.21 DCFT age obtained from the Huckleberry Ridge Tephra internal standard is similar to its established single-grain Ar-Ar age of 2.003 ± 0.014 Ma (Gansecki *et al.*, 1998) (Table 4.5). The major element composition of 197 silicic shards is homogeneous justifying the use of the population method (Fig. 4.18).

(b) Independent evaluation of fission-track age accuracy

The 2.26 ± 0.11 Ma age places the Óþoli Tephra firmly in the Matuyama reversed polarity epoch (2.48-0.73 Ma; McDougall, 1979). All of the samples that have a definite polarity signal are reversely magnetised (Table 4.4). While a floating single polarity signal does not provide enough information to fully test the fission-track age, the preliminary palaeomagentic results are encouraging because they reinforce confidence in the accuracy of the fission-track age.

4.3.2 Hjallanes Tephra

The bulk grain size of the Hjallanes Tephra was too small and its composition too basic for effective fission-track dating analysis.

4.3.3 Þörsmórk Ignimbrite

No spontaneous fission-tracks were observed on test slides of platey glass shards for samples of the Þörsmórk Ignimbrite (Westgate, *pers. comm.*). Tephra deposits as young as 75 ka with uranium contents of 5-6 ppm have sufficient spontaneous fission-tracks to be dated (*e.g.* Westgate *et al.*, 1998). Therefore, the absence of spontaneous fission-tracks in the Þörsmórk Ignimbrite samples (uranium content of 3-4 ppm) suggests an age of <100-150 ka would not be an unreasonable age estimate assuming no post-depositional partial or whole track annealing has occurred.

Sample number	Spontaneous track density	Corrected spontaneous track density	Induced track density	Track density on muscovite detector over dosimeter glass	Etching conditions HF: temp: time	D_s	D_i	D_s / D_i or	Age
(Analyst)	10^2 tcm^{-2}	10^2 tcm^{-2}	10^5 tcm^{-2}	10^5 tcm^{-2}	%: °C: s	μm	μm	D_i / D_s[#]	10^6 years
Óþoli Tephra, Skagafjall, North West Peninsula, Iceland									
UT1657 (AS)	22.75 ± 0.98 (540)		2.32 ± 0.02 (20826)	4.94 ± 0.04 (12744)	24: 21.5: 105	5.59 ± 0.08 (298)	7.87 ± 0.08 (597)	0.71 ± 0.01	1.54 ± 0.14
UT1657* (AS)		32.01 ± 1.38 (540)	2.31 ± 0.02 (20826)	4.94 ± 0.04 (12744)	24: 21.5: 105	5.59 ± 0.08 (298)	7.87 ± 0.08 (597)	1.41 ± 0.02[#]	2.18 ± 0.19
UT1659[$] (JAW)	15.36 ± 0.81 (360)		1.04 ± 0.01 (8590)	4.97 ± 0.04 (12744)	24: 21.3:140	5.91 ± 0.12 (133)	5.87 ± 0.08 (398)	1.01 ± 0.02	2.32 ± 0.22
UT1655[$] (JAW)	16.80 ± 0.72 (543)		1.14 ± 0.01 (6041)	5.11 ± 0.05 (12744)	24: 21.3: 140	5.91 ± 0.12 (133)	5.87 ± 0.08 (398)	1.01 ± 0.02	2.40 ± 0.28
UT1656[$] (SJR)	14.88 ± 0.77 (381)		1.21 ± 0.02 (6149)	5.63 ± 0.05 (43478)	24: 22.5: 145	6.60 ± 0.19 (100)	6.36 ± 0.10 (398)	0.96 ± 0.05	2.23 ± 0.24
							Weighted Mean Age		**2.26 ± 0.11**
Huckleberry Ridge Tephra: internal standard (UT1655/ UT1657/ UT1659)									
UT1094 (JAW)	43.23 ± 1.42		4.21 ± 0.03 (25152)	4.87 ± 0.04 (12744)	24: 21: 120	6.09 ± 0.07	7.54 ± 0.09	0.81 ± 0.01	1.59 ± 0.17
UT1094* (JAW)		53.57 ± 1.76 (931)	4.20 ± 0.03 (25152)	4.87 ± 0.04 (12744)	21: 21: 120	6.09 ± 0.07	7.54 ± 0.09	1.24 ± 0.02[#]	**1.97 ± 0.21**
Gansecki *et al*. (1998): Single-crystal (sanidine) laser fusion $^{40}Ar/^{39}Ar$ age (2σ)									**2.00 ± 0.01**

Table 4.5 (*contd.*) Glass phase fission-track age estimates for the Óþoli Tephra, Skagafjall, NW Iceland.

Methods and notes:
Thick platey glass shards were separated from the bulk component of the tephra to maximise the surface area of glass for dating. The bulk tephra is sieved to recover the +120 μm (0.125 mm) size fraction and cleaned with a Branson Scrufier Model 350. Platey bubble wall shards are separated from the pumiceous glass and mineral grains by magnetic methods, using a Franz Isodynamic separator. Population subtraction method was used, the reported induced track density being the measured track density minus the spontaneous track density. "AS" is Amanjit Sandhu; "JAW" is John Westgate; "SJR" is Stephen Roberts. Samples with asterisk (*) corrected for partial track fading by the track-size (DCFT) method (Sandhu and Westgate, 1995). Samples with dollar sign ($) corrected for partial track fading by the isothermal plateau (ITPFT) method (Westgate, 1989); uncorrected age is given for the other samples. Ages calculated using the zeta approach (Hurford and Green, 1983) and λ_D = 1.551 x 10 -10 yr $^{-1}$. Zeta value is 318 ± 3 based on 6 irradiations at the McMaster Nuclear Reactor, Hamilton, Ontario, using the NIST SRM 612 glass dosimeter and the Moldavite tektite glass (Lhenice locality) with an $^{40}Ar/^{39}Ar$ plateau age of 15.21±0.15 Ma (Staudacher *et al.*, 1982). UT1656 was irradiated separately and experienced a different neutron flux. Samples UT1655 and UT1659 were etched together and are assumed to have the same track size distribution. Samples were counted in reflected light on a Nikon 275437 microscope at 500x magnification. Area estimated using the point-counting technique (Sandhu *et al.*, 1993). D_s = mean spontaneous track diameter and D_i = mean induced track diameter. Number of tracks counted is given in brackets. Error (±1σ) is calculated according to Bigazzi and Galbraith (1999) by combining Poisson errors in the spontaneous induced tracks and on the number of tracks in the muscovite detector covering the glass dosimeter. The single-crystal (sanidine) laser-fusion $^{40}Ar/^{39}Ar$ age of Huckleberry Ridge tephra, the internal standard, is 2.003±0.014 Ma (2σ error) (Gansecki *et al.*, 1998). UT1655 = 6-7 cm above rhythmite bed (RB) no. 10, section B; reworked. UT1656 = 7-8 cm above RB10, section B. UT1657 = 2-3 cm above RB10, section B; airfall. UT1659 = 3-4 cm above RB10, section B; airfall.

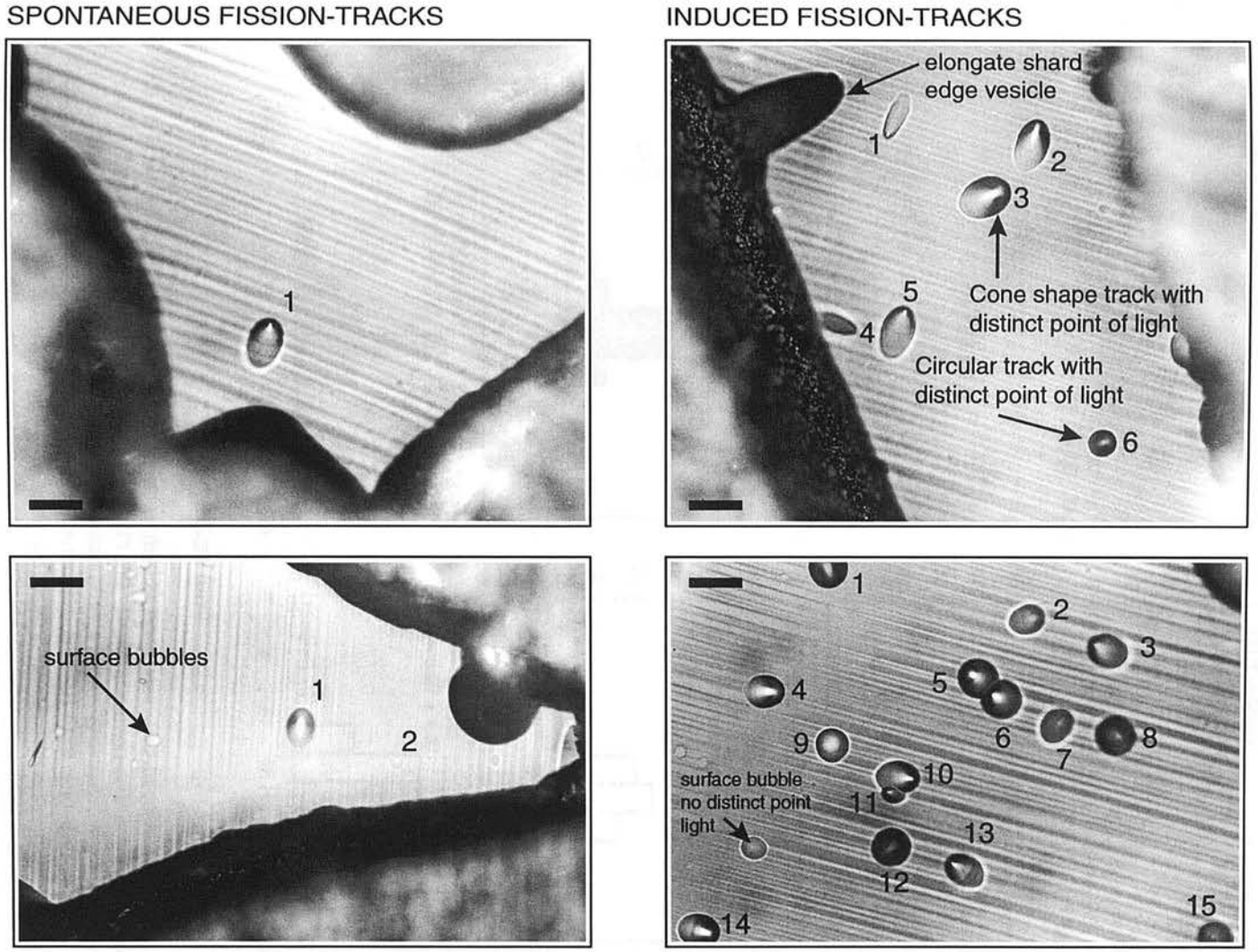


Figure 4.15 Micro-photographs of spontaneous and induced fission-tracks formed in glass shards of Ōpoli Tephra (sample UT1656). The difference between tracks and vesicles/surface bubbles is indicated; numbers are tracks per shard. Photos taken at x 500 magnification; scale bar is 10 μm; lines on the shard were created by uni-directional polishing using 1 μm diamond paste to allow identification of tracks on the shard surface.

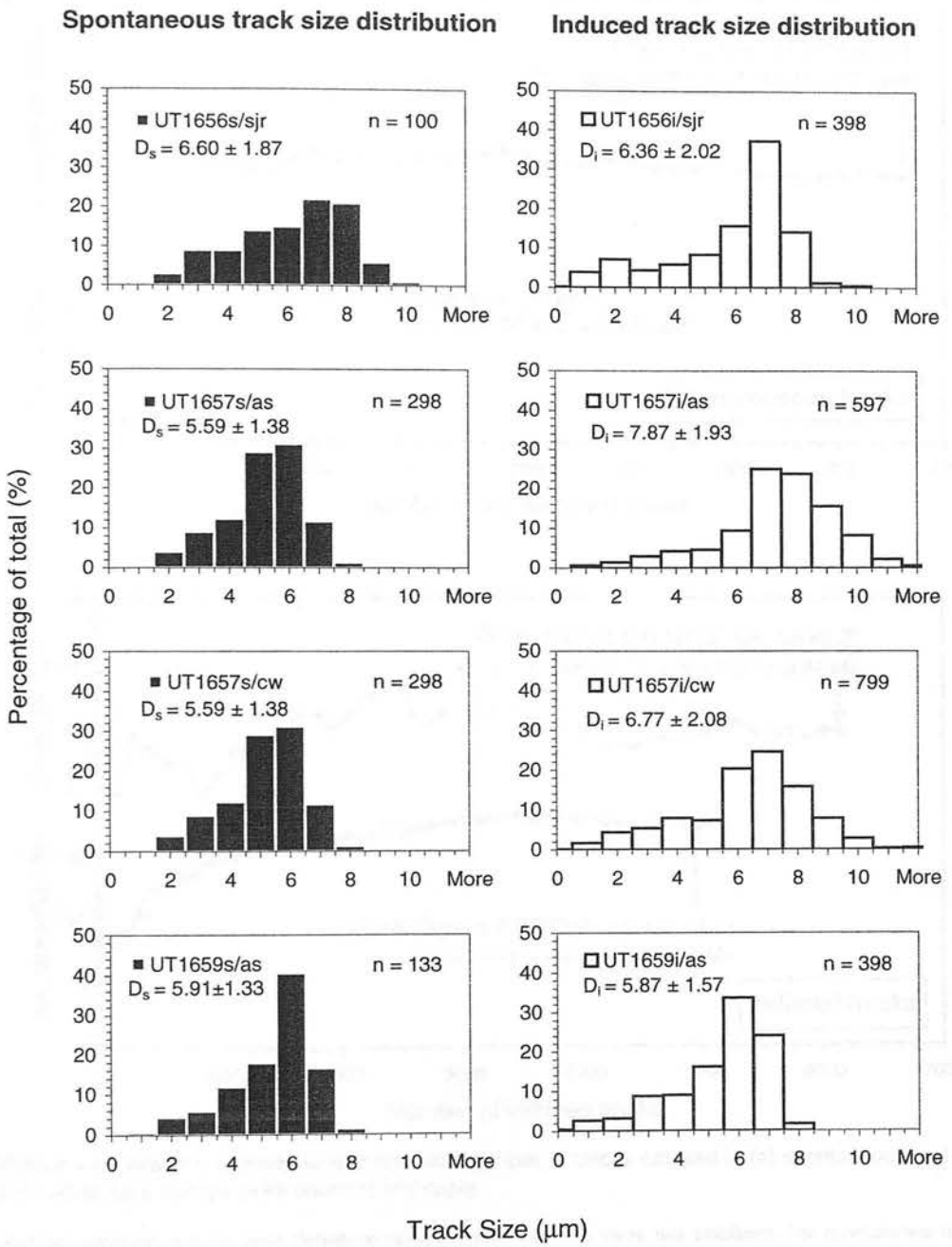


Figure 4.16 Induced (white) and spontaneous (black) track size distibution histograms for Óþoli Tephra samples UT1656, UT1657 and UT1659. The mean track size is 5-8 μm in all cases. sjr = Stephen Roberts; as = Amanjit Sandhu; cw = Corra Westgate; n = number of tracks measured. UT1655 was etched simultaneously with UT1659 and the track size distribution is assumed to be similar. Track sizes are mean ± 1σ.

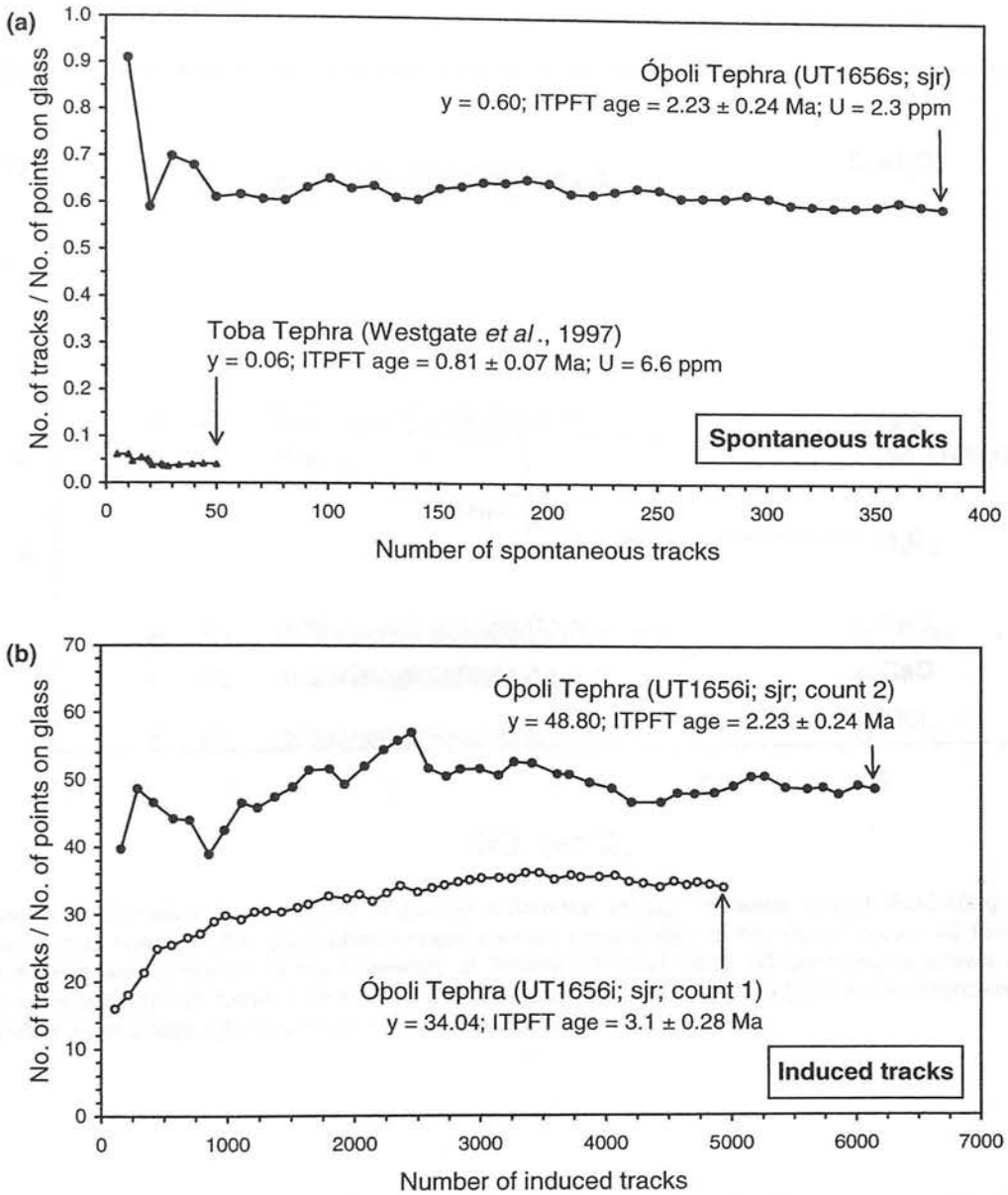


Figure 4.17 Variation of track density ratio with number of tracks counted in (a) spontaneous and (b) induced sample, using a point-counting technique.

A good estimation of areal track density is obtained when the ratio value has stabilised. For spontaneous track density ratios, results of the Toba Tephra counted on the same equipment have been included for comparison (Westgate *et al.*, 1997). Note the higher uranium content and significantly lower areal track density and age compared to the Óþoli Tephra. For the induced track density ratio two counts are included to emphasise the influence counting errors can have on age estimates. Count one was the SJR's first attempt at counting fission-tracks and was undertaken after an age estimate for the Óþoli Tephra had been produced by JAW and AS. SJR under-counted induced tracks on this first run by about a thrird, lead to a track density underestimate and age overestimate. After further practice the second count was undertaken. More tracks between 1-3 μm in diameter and some shard-edge tracks not counted in the first attempt were counted on the second attempt. Both sets of count data were included to illustrate the importance of experience in obtaining accurate glass-phase fission-track ages from tephra deposits of unknown age.

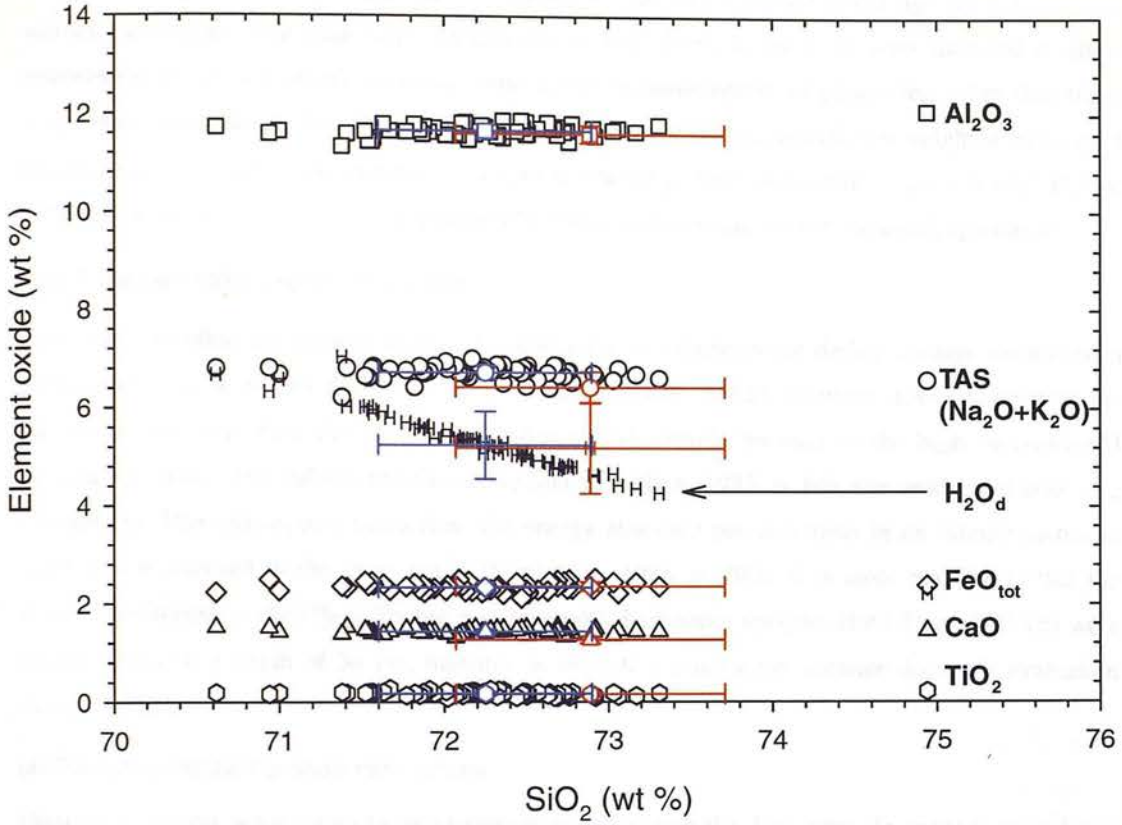


Figure 4.18 Selected element and water by difference (H_2O_d) vs silica bi-plot illustrating the homogeneous nature of the glass-phase major element composition of the Óþoli Tephra. All fission-track sample data analysed at the University of Toronto (UT1655-1659; 60 analyses) is shown with mean ± 1σ errors (blue). Mean ± 1σ of 137 other analyses of the Óþoli Tephra (red) were undertaken at the University of Edinburgh. See Table 4.1 for more analytical details.

4.4 Thermoluminescence (TL) Dating

The two main parameters that need to be evaluated to calculate a luminescence age are the dose rate and the palaeodose. The data tables in this section are complex, but have been included to allow examination of age variations associated with different combinations of parameters other than those considered 'most-likely'. In addition, they show that variations from the chosen weighted mean final palaeodose, and/or dose rate values do not alter the broad picture of an 'old' (> *ca.* 1.5 Ma) TL age estimate for the Óþoli Tephra and a 'young' (40-50 ka) age estimate for the Þörsmórk Ignimbrite.

4.4.1 Dose Rate Determination

Dose rates are often the biggest source of imprecision in luminescence dating because variations in palaeowater content are, by definition, best estimates (Aitken, 1985). Accurate dose rate calculations are particularly important for the Óþoli Tephra (SUTL 551/2) because of the high reconstructed palaeodose values. The infinite matrix assumption of Aitken (1985; p. 66) was used in all dose rate calculations. This assumption states that 'the energy absorbed per unit mass in an infinite matrix is equal to that released in the same mass' (Sanderson, 1988; p. 203). It is more than likely that the airfall components of the Óþoli Tephra and Þörsmórk Ignimbrite samples (ÞIG 7 and ÞIG 1b) were buried rapidly to a depth of 30 cm, meeting an important criteria for accurate dose rate evaluation (Aitken, 1998).

(a) Factors influencing dose rate values

Three main factors were found to be important in calculating the dose rates. In order if precedence they are:

1) The 'best estimate' of palaeowater content variability in the Icelandic environment since the eruption event being dated. Increased interstitial matrix water content leads to increased attenuation of environmental radiation. Three quantitative palaeowater content parameters exist:
   - Palaeowater content is equal to the 'as found' or sampled value during burial
   - Palaeowater content is equal to the saturation value of the tephra deposit
   - Palaeowater content is equal to the mid-point between the 'as found' and saturation value with errors set to encompass both values

   The first two are measurable. The last has been used as a good compromise for average palaeowater content in seasonally wet and/or cold environments (*e.g.* Balescu *et al.*, 1997) and has been adopted in final dose rate calculations in this study.

2) The choice of dose rate matrix model used to calculate the dose rate. Dating glass-rich tephra deposits presents an opportunity to develop homogeneous and heterogeneous matrix models for the glass-phase and examine their influence on dose rate values on a case by case basis. The contribution of alpha dose to the total dose rate is included because samples were not HF etched and it is undoubtedly more complex than the broad dose rate models outlined

- **Homogeneous matrix model** of dose rate calculation is the simpler of the two models. It assumes that the total environmental dose rate emanates from a chemically homogeneous medium that is broadly equivalent to the bulk composition of the tephra. On a macroscale, the internal and external contributions from the glass shards to the total dose rate are in equilibrium and no microscopic dose boundaries were assumed to exist between shards (Fig. 4.19). Comparisons of dose rates and age estimates obtained using 'as found' ($WF_{in\text{-}situ}$) and the mid-point between 'as found' and saturation water content ($WF_{in\text{-}situ\text{-}sat}$) as palaeowater content parameters and elemental versus spectrometry methods were evaluated using the homogeneous matrix model (Fig. 4.20; Table 4.6, 4.7).
- **Heterogeneous matrix model** is more complex. Assessment of the internal and external contribution of alpha and beta dose rate is necessary for feldspar-phase dating because the bulk chemical composition of the matrix and the internal composition of the grains is different. Heterogeneous matrix dose rate values were calculated by using grain specific or purified fraction chemical data to calculate internal shard dose rates and the bulk and/or spectrometry based measurements to calculate the external matrix shard dose rates (Table 4.8). $WF_{in\text{-}situ\text{-}sat}$ values were used to attenuate the external dose rates (Table 4.6).

3) The choice of elemental and spectrometry based dose rate values

- **Óþoli Tephra:** Dose rate values were calculated using elemental and spectrometry methods (Table 4.6). Elemental and spectrometry based dose rate values were not combined into a single weighted mean value to allow the full impact of dose rate variations on age estimates to be assessed (Table 4.7; see notes below table for further explanation). The airfall component of the Óþoli Tephra was chosen for all dating analysis because it is least likely to have been contaminated by reworked material. The airfall sampling positions (551/552) are located approximately 5 cm above rhythmite bed 10, that has an *in-situ* gamma dose rate an order of magnitude less than the overlying tephra bed. The gamma dose rate for RB 10, at 0.08±0.01 $mGya^{-1}$, is an order of magnitude less than the 0.30±0.03–0.52±0.05 $mGya^{-1}$ readings from the airfall and reworked components of the Óþoli Tephra (Fig. 4.2). The spectrometry based dose rate is significantly less than the dose rate calculated from bulk elemental compositions and conversion factors. Elemental dose rate calculations were not considered an accurate representation of total environmental dose rate because the elemental dose rate method does not account for the reduction in gamma dose rate associated with the position of the underlying rhythmite bed (Bell, 1979a; Nambi and Aitken, 1986; Adamiec and Aitken, 1996). To overcome this problem and avoid overestimating the gamma dose rate, the spectrometry dose rate method was chosen to calculate total environmental dose rate for the airfall Óþoli Tephra samples (551/552).

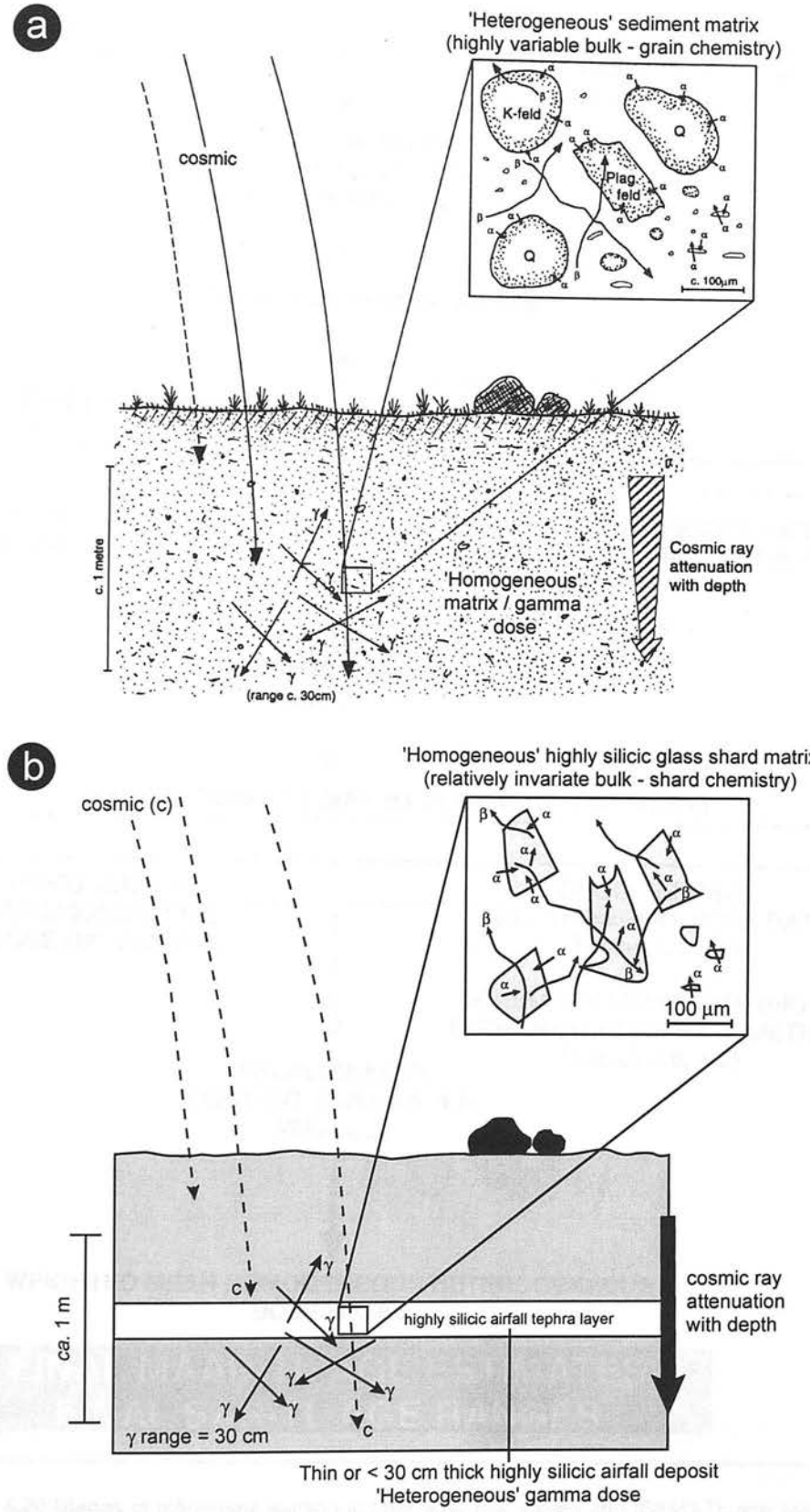


Figure 4.19 Schematic represenation of aspects of natural radioactivity for **(a)** regular sediment matrix and **(b)** samples from the centre of a thin (6-30 cm) highly silicic airfall tephra deposit. (a) is as described in Figure 3.10-b (adapted from Aitken, 1998). Radioactivity in an approximately homogeneous highly silicic glass-rich, phenocryst-poor matrix is fundamentally different to a 'normal' sediment because all glass shards are affected to approximately the same internal and external α and β radioactivity. Gamma dosimetry is complex because of the thin nature of airfall deposits. The *in-situ* spectrometry based γ-dose for the Óþoli Tephra was approximately half that obtained by the elemental concentration method because of the proximity of the underlying rhythmite bed no. 10 with a *in-situ* gamma dose an order of magnitude less.

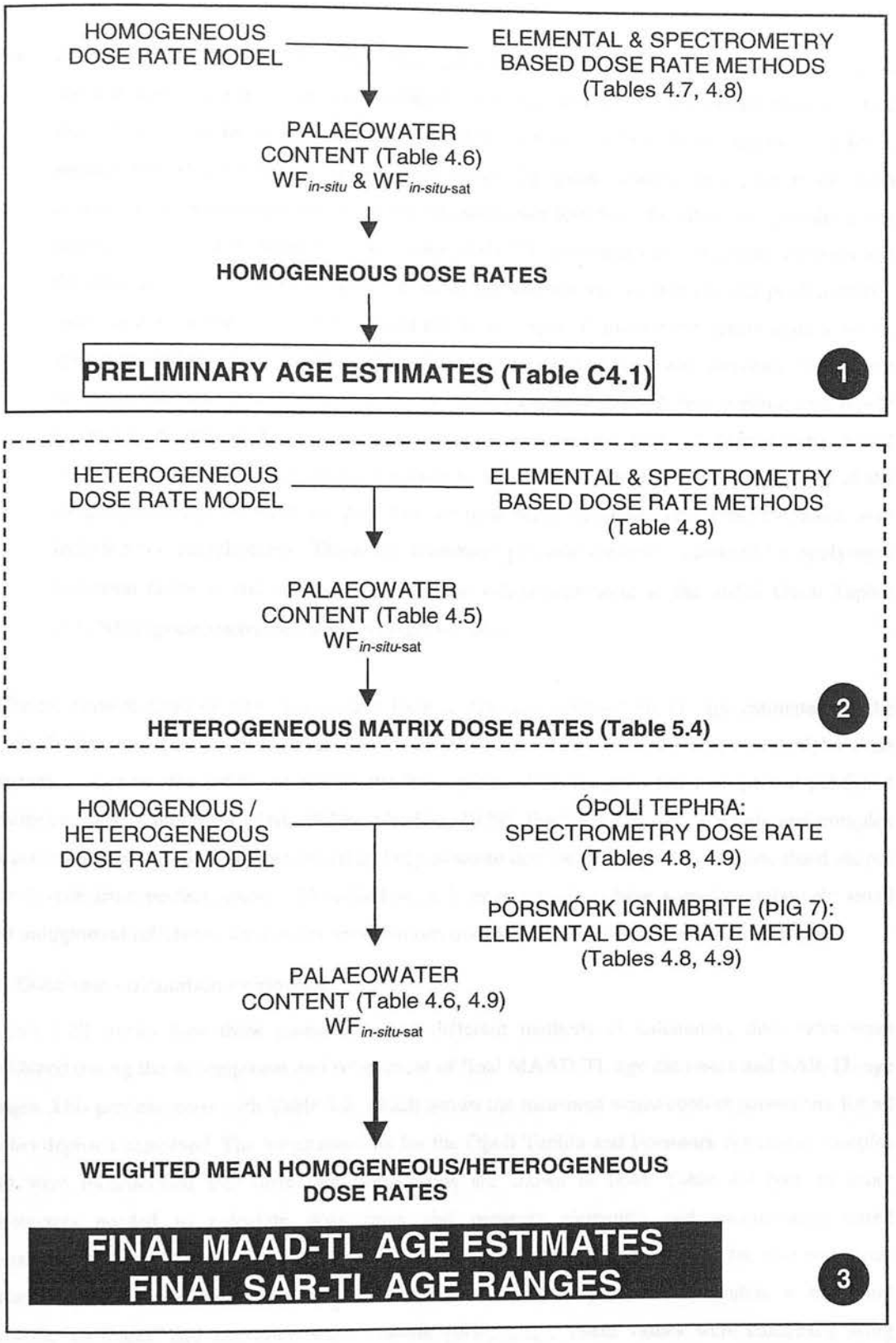


Figure 4.20 Stages of refinement leading to final dose rate values and MAAD-TL age estimates and SAR-TL age ranges. Further details of each stage can be found in the tables specified in brackets. Reasons for choosing the combinations of methods and parameters outlined in 3 for final TL age estimates and ranges are summarised in Table 4.9.

- **Þörsmórk Ignimbrite:** Elemental dose rates were used in all age calculations. ÞIG-TL samples were taken from the centre of thick ash or ash and pumice dominated exposures that were at least one metre thick. The co-ignimbrite ash at site ÞIG 1b is overlain by a black welded tuff deposit which is also dominated by glass shards. The glass-phase K_2O concentration is approximately an order of magnitude less than the silicic co-ignimbrite ash deposit. Samples were taken from the centre of the 50-60 cm thick co-ignimbrite ash layer and the gamma dose therefore emanates from decay process in the layered, but predominantly silicic deposit alone. White pumice and silicic ash layers dominant the matrix from a 30 cm sphere around the ÞIG 7 sample. The elemental-based dose rates are, therefore, considered accurate. Although *in-situ* spectrometry measurements from each of the sampling sites would be highly beneficial for comparison purposes, the current lack of spectrometry based measurements for the Þörsmórk Ignimbrite is of relatively minor importance because of the sampling strategy for these samples. For the time being, estimated spectrometry values were included for completeness. These are minimum possible estimates obtained by applying a reduction factor to the elemental γ-dose rate values equivalent to the airfall Óþoli Tephra (551/552) spectrometry:elemental γ-dose rate ratio.

Different combinations of these parameters have a significant impact on TL age estimates for the Óþoli Tephra and Þörsmórk Ignimbrite. In addition, the effect of shard shape and alpha dose attenuation is most effected by deviations the from spherical quartz grain shard shape that published dosimetric data is based on (Bell, 1979a; Mejdahl, 1979). Further laboratory analysis and complex numerical modelling would be beneficial to fully evaluate dosimetric properties of glass shard shapes that deviate from perfect spheres. Nevertheless, it is envisaged that these would be relatively small and unimportant relative to the current uncertainties involved in palaeowater content estimation.

(b) Dose rate calculation refinement

Figure 4.20 shows how these parameters and different methods of calculating dose rates were combined during the development and refinement of final MAAD-TL age estimates and SAR-TL age ranges. This process starts with Table 4.6, which shows the measured water content parameters for all tephra deposits examined. The water contents for the Óþoli Tephra and Þörsmórk Ignimbrite samples that were incorporated into dose rate calculations are shown in bold. Table 4.7 lists all other parameters needed to calculate dose rates and presents elemental and spectrometry based homogeneous matrix dose rates for the Óþoli Tephra and ÞIG 7 and ÞIG 1b for two scenarios: palaeowater content = 'as found' water content ($WF_{in\text{-}situ}$) and palaeowater content = mid-point between 'as found' and saturation water content ($WF_{in\text{-}situ\text{-}sat}$). These values were calculated using equations described in the caption and then incorporated into Table 4.8 to calculate MAAD-TL homogeneous matrix dose rate age estimates for the Óþoli Tephra and SAR-TL homogeneous matrix

dose rate age ranges for the Óþoli Tephra and Þörsmórk Ignimbrite. Table 4.8 illustrates the different dose rates obtained using elemental and spectrometry based and homogeneous and heterogeneous matrix dose rate models when palaeowater content = mid-point between 'as found' and saturation water content. The homogeneous matrix dose rates in this table are taken from the last column in Table 4.7. Heterogeneous matrix dose rate values were calculated using elemental or spectrometry parameters listed in Table 4.7 and equations and methods described in the caption of Table 4.8. Table 4.9 presents a summary of the final dose rate parameters used to calculate final TL age estimates and lists criteria for choosing certain parameters. These final dose rates are incorporated into Tables 4.10, 4.11, which show final MAAD-TL age estimates and final SAR-TL age ranges for the Óþoli Tephra and Þörsmórk Ignimbrite (ÞIG 7). Possible variations in palaeodose, examined in the next section, are summarised and evaluated in this table. Final weighted mean and mean MAAD-TL age estimates and SAR-TL ages are highlighted in black. Although complex, the presentation of all possible combinations allows the reader to examine and evaluate the effect different dose rate and palaeodose calculation methods and parameter inputs have on TL age estimates. The difference between TL ages based on homogeneous and heterogeneous matrix dose rate models is of most interest.

Overall, the calculated dose rates of 3-6 $Gyka^{-1}$ are typical of environments that are not dominated by quartz. All types of dose rates for the Þörsmórk Ignimbrite samples ÞIG 1b and ÞIG 7 are similar and consistently higher than the Óþoli Tephra (Tables 4.7, 4.8, 4.9) because of elevated potassium uranium and thorium concentrations in bulk and shard specific/purified fractions (Table 4.6). For example, the bulk K_2O, U and Th values for ÞIG 7 are 3.03±0.15 wt %, 3.80±0.19 ppm and 13.4±0.7 ppm respectively compared to 2.16±0.11 wt %, 2.26±0.11 ppm and 8.49±0.36 ppm respectively for the same fraction of the Óþoli Tephra. In all cases the higher concentrations of these elements are found in the purified fractions, the difference most likely due to the presence of minor basic glass component in the Óþoli Tephra and/or feldspars with lower concentrations of these elements in the ÞIG samples ÞIG 7 and ÞIG 1b.

Homogeneous and heterogeneous matrix model, spectrometry method dose rates for the airfall component of the Óþoli Tephra (SUTL 551/552) were similar at 2.70±0.62 and 2.92±0.54 $Gyka^{-1}$ respectively (Table 4.8). These two values were therefore combined into a weighted mean value for calculation of final age estimates and age ranges (Tables 4.10, 4.11). Furthermore, the homogeneous/heterogeneous weighted mean 'as-found' palaeowater dose rate of 3.28±0.31 $Gyka^{-1}$ is similar to the weighted mean '*in-situ*-saturation' palaeowater dose rate of 2.83±0.62 $Gyka^{-1}$ and the heterogeneous matrix, '*in-situ*-saturation' palaeowater dose rate value of 2.92±0.54 $Gyka^{-1}$. Confidence that the final dose rate value of 2.83±0.41 $Gyka^{-1}$ is an accurate reflection of average dose rate since burial is high because all combinations of spectrometry based dose rate values for the Óþoli Tephra are within single standard deviation analytical error ranges of each other.

Same matrix model, elemental dose rate values for ash deposits from sites ÞIG 7 and ÞIG 1b are broadly similar, *e.g.* homogeneous matrix model dose rates are 5.18±2.38 and 5.17±2.64 $Gyka^{-1}$ respectively and heterogeneous matrix dose rates are 6.97±1.96 and 6.71±2.14 $Gyka^{-1}$ respectively (Tables 4.7, 4.8). Homogeneous matrix model dose rates are approximately 75 % less than heterogeneous matrix model dose rates. The higher weighted mean homogeneous/heterogeneous dose rate of 6.25±1.51 $Gyka^{-1}$ is considered the most accurate estimate of the average dose rate since burial because it is the most representative average value that encompasses all dose rate heterogeneities associated with the bulk composition of ÞIG 7. The 6.10±1.66 $Gyka^{-1}$ homogeneous/heterogeneous matrix model dose rate for ÞIG 1b is similar to the ÞIG 7 value. Bulk fractions of both samples contain a fractionally larger proportion of non-glassy material compared to the Óþoli Tephra samples and have a bi-modal grain size distribution. Both of these factors are due to the relatively close proximity (<25 km) of the sampling sites to Tindfjalljökull, the Þörsmórk Ignimbrite source volcano (Thórarinsson, 1969).

The large errors on final ÞIG 7 6.25±1.51 $Gyka^{-1}$ dose rate create large standard analytical age errors of ± 7-10 ka (± 24 %). This dose rate means that the final mean ÞIG 7 SAR-TL age estimate of 39±9 ka[30] is significantly[31] younger than the oldest correlation age estimate of *ca.* 53 ka. The lowest fading and sensitivity corrected palaeodose and elemental homogenous dose rate combination (Table 4.9) produces a maximum mean SAR-TL age of 45±21 ka for ÞIG 7. This age is closer to the 48.5 ka correlation age than the 39±9 ka age.

The most important conclusion of this section is that the broad age patterns are similar for both dose rate models once the palaeowater content parameters and the type of method (*i.e.* elemental or spectrometry method) has been decided on.

[30] This age was obtained using the fading and sensitivity corrected palaeodose value 241±7 Gy and weighted mean homogeneous/heterogeneous matrix model dose rate of 6.25±1.51 Gya^{-1}.
[31] Significantly in this context means outside overlapping single standard deviation or standard analytical error ranges

Sample	Code	Matrix Description	$F_{in\text{-}situ}$	W_{sat} (≡W)	A $WF_{in\text{-}situ}$	$F_{in\text{-}situ\text{-}sat}$	B $WF_{in\text{-}situ\text{-}sat}$
Óþoli Tephra	SUTL551a	Platey ash	0.29 ± 0.01	0.83 ± 0.06	0.24 ± 0.04	0.56 ± 0.27	0.46 ± 0.33
	SUTL552a	Platey ash	0.35 ± 0.02	0.61 ± 0.05	0.21 ± 0.04	0.48 ± 0.13	0.29 ± 0.15
	SUTL552b	Platey ash	0.38 ± 0.02	0.59 ± 0.08	0.22 ± 0.07	0.49 ± 0.11	0.29 ± 0.14
	SUTL 551/2^{wm}	**Platey ash**	**0.33 ± 0.01**	**0.68 ± 0.03**	**0.23 ± 0.03**	**0.49 ± 0.08**	**0.30 ± 0.10**
	SUTL558	Platey ash	0.30 ± 0.02	0.76 ± 0.06	0.23 ± 0.04	0.53 ± 0.23	0.40 ± 0.28
Öræfi 1362	ÖR 1	Pumice+vesicular ash	0.43 ± 0.02	0.63 ± 0.17	0.27 ± 0.14	0.53 ± 0.10	0.33 ± 0.19
	ÖR 2	Vesicular ash	0.50 ± 0.03	0.97 ± 0.02	0.49 ± 0.04	0.74 ± 0.24	0.71 ± 0.28
	ÖR 3	Ash+soil	0.30 ± 0.02	0.93 ± 0.07	0.28 ± 0.05	0.62 ± 0.32	0.57 ± 0.40
Askja 1875	ASK 5	Platey ash (2)	0.39 ± 0.02	0.87 ± 0.13	0.34 ± 0.09	0.63 ± 0.24	0.55 ± 0.30
	ASK 10	Platey ash+pumice	0.23 ± 0.01	-	-	-	-
	ASK 11	Platey ash	0.30 ± 0.02	0.89 ± 0.06	0.27 ± 0.04	0.60 ± 0.30	0.53 ± 0.37
Þórsmórk Ignimbrite	ÞIG 1a	Ash+pumice	0.21 ± 0.01	-	-	-	-
ÞIG 1-23	**ÞIG 1b**	**Platey ash (2)**	**0.26 ± 0.01**	**0.70 ± 0.11**	**0.18 ± 0.07**	**0.48 ± 0.22**	**0.34 ± 0.28**
	ÞIG 1c	Slope ash+pumice	0.38 ± 0.02	-	-	-	-
	ÞIG 1d	Pumice+ash (2)	0.24 ± 0.01	0.50 ± 0.23	0.12 ± 0.16	0.37 ± 0.13	0.19 ± 0.25
	ÞIG 2	Slope ash+pumice	0.17 ± 0.01	0.46 ± 0.21	0.08 ± 0.13	0.32 ± 0.15	0.14 ± 0.25
	ÞIG 3	Platey-vesicular ash	0.31 ± 0.02	0.83 ± 0.03	0.26 ± 0.03	0.57 ± 0.26	0.47 ± 0.31
	ÞIG 5 (S4)	Pumice clast	0.05 ± 0.001	1.16 ± 0.15	0.06 ± 0.03	*	*
	ÞIG 7	**Inter-bedded platey ash (2)**	**0.27 ± 0.01**	**0.89 ± 0.09**	**0.24 ± 0.05**	**0.58 ± 0.31**	**0.52 ± 0.39**
	ÞIG 11$^{\$}$	Pumice clast	0.40 ± 0.02	1.05 ± 0.08	0.42 ± 0.06	*	*
	ÞIG 13	Slope ash+pumice	0.17 ± 0.01	-	-	-	-
	ÞIG 15	Slope ash+pumice	0.36 ± 0.02	-	-	-	-
	ÞIG 16	Pumice clast	0.11 ± 0.01	1.28 ± 0.13	0.14 ± 0.04	*	*

Table 4.6 Fractional water contents for Icelandic tephra deposits whose thermoluminescence characteristics were examined in this study. See notes overpage for description of terms.

contd.

Table 4.6 ***(contd.)*** Fractional water contents for Icelandic Tephra deposits

Notes: Full dose rate estimates were calculated for samples in bold in columns A and B (see Table 4.7). Samples were collected during June-August 1998-2000, i.e. warmest and driest part of the year. It is unlikely that the $WF_{in\text{-}situ}$ values above are even representative of a single year in the Icelandic environment, because, typically, the climate of both NW and S Iceland is significantly colder and wetter outside sampling months of June-August. $WF_{in\text{-}situ\text{-}sat}$ is, therefore, considered to be a good best estimate of the likely palaeowater content.

W = (saturation wet weight – dry weight) / (dry weight)
F = average fractional water content during burial history and was determined for two situations:

A) Average palaeo-water content = *in-situ* (as received) fractional water content for each sample. Therefore:
$F_{in\text{-}situ}$ = average fractional water content during burial history is equivalent to as received (measured) water content for each sample

B) Average palaeo-water content is at the mid-point between *in-situ* water content and water content at saturation

$F_{in\text{-}situ\text{-}sat} = Fi_{in\text{-}situ} + (F_{in\text{-}situ} + F_{in\text{-}situ\text{-}sat})/2$, *i.e.* the mid-point between measured and saturated water content for each sample with error limits that encompass the measured $F_{in\text{-}situ}$ and W_{sat} values

Where duplicate measurements produced the same result (indicated by the number of duplicate measurements in brackets after the sample name), or when duplicate measurements were not possible, due to insufficient material measurement, errors are estimated at ± 5%. Errors in $F_{in\text{-}situ}$ for TL551/2 are mean ± 1σ of three measurements for this sample; W_{sat} errors are measurement errors from six duplicate measurements.

^{wm} = weighted mean
* = judging the saturation point of pure pumice proved difficult and in some cases too much water was added leading to fractional water contents greater than unity
$ = sampling tube penetrated welded pumice/ash matrix

Terms used here are minor adaptations of those in Aitken (1985, 1998).

(a) ELEMENTAL METHOD Sample	Code	Latitude (°N)	Longitude (°W)	Sampling Depth (m)	Elemental concentrations[1] K (wt %)	 U (ppm)	 Th (ppm)	 Rb (ppm)	α-efficiency[2] k-value	D_{cosmic}[3]	$WF_{in\text{-}situ}$[4]	$WF_{in\text{-}situ\text{-}sat}$	D_T[5] WF_{insitu}	D_T $WF_{insitu\text{-}sat}$
(i) Elemental dose rates from bulk measurements														
Óþoli Tephra	**SUTL551/2**	65°59.78	23°45.40	5 ± 1	2.16 ± 0.11	2.26 ± 0.03	8.49 ± 0.36	55 ± 3	0.15 ± 0.01	0.11 ± 0.04	0.22 ± 0.03	0.30 ± 0.10	**4.21 ± 0.30**	**3.90 ± 0.66**
Þörsmórk Ignimbrite: Site 7	**ÞIG 7**	63°40.37	19°34.37	1 ± 0.5	3.03 ± 0.15	3.8 ± 0.19	13.4 ± 0.7	107 ± 5	0.16 ± 0.01	0.16 ± 0.06	0.24 ± 0.06	0.52 ± 0.39	**6.59 ± 0.91**	**5.18 ± 2.38**
Þörsmórk Ignimbrite: Site 1b	ÞIG 1b	63°40.35	19°36.22	20 ± 5	3.28 ± 0.16	3.13 ± 0.16	10.1 ± 0.5	73 ± 4	*0.16 ± 0.01*	0.04 ± 0.01	0.18 ± 0.07	0.34 ± 0.28	6.04 ± 1.36	5.17 ± 2.64
(ii) Elemental dose rates from grain specific and purified fraction measurements														
Óþoli Tephra	**SUTL551/2**	65°59.78	23°45.40	5 ± 1	2.75 ± 0.14 (137)	2.6 ± 0.1 (3)	10.8 ± 0.5 (3)	55 ± 3	0.15 ± 0.01	0.11 ± 0.04	0.22 ± 0.03	0.30 ± 0.10	5.14 ± 0.33	4.76 ± 0.73
Þörsmórk Ignimbrite: Site 7	**ÞIG 7**	63°40.37	19°34.37	1 ± 0.5	4.07 ± 0.19 (20)	4.37 ± 0.22	14.3 ± 0.7	107 ± 5	0.16 ± 0.01	0.16 ± 0.06	0.24 ± 0.06	0.52 ± 0.39	7.73 ± 0.99	6.08 ± 2.59
Þörsmórk Ignimbrite: Site 1b	ÞIG 1b	63°40.35	19°36.22	20 ± 5	4.11 ± 0.61 (24)	3.39 ± 0.17	11.6 ± 0.6	73 ± 4	*0.16 ± 0.01**	0.04 ± 0.01	0.18 ± 0.07	0.34 ± 0.28	7.03 ± 1.48	6.02 ± 2.86

(b) SPECTROMETRY METHOD Sample	Code	Latitude (°N)	Longitude (°W)	Sampling Depth (m)	Dry α-dose[6] (bulk elemental)	Dry TSBC[7] (mGya⁻¹)	*In-situ* γ (wet)[8] (mGya⁻¹)		α-efficiency k-value	D_{cosmic}	$WF_{in\text{-}situ}$[4]	$WF_{in\text{-}situ\text{-}sat}$	D_T[5] WF_{insitu}	D_T $WF_{insitu\text{-}sat}$
Óþoli Tephra	**SUTL551/2**	65°59.78	23°45.40	5 ± 1	1.41 ± 0.21	1.19 ± 0.31	0.30 ± 0.03		0.15 ± 0.01	-	0.22 ± 0.03	0.30 ± 0.10	2.91 ± 0.38	**2.70 ± 0.62**
Þörsmórk Ignimbrite: Site 7	**ÞIG 7**	63°40.37	19°34.37	1 ± 0.5	2.41 ± 0.61	2.69 ± 0.81	*0.48 ± 0.09*	*	0.16 ± 0.01	-	0.24 ± 0.06	0.52 ± 0.39	5.58 ± 1.02	***4.44 ± 2.11***
Þörsmórk Ignimbrite: Site 1b	ÞIG 1b	63°40.35	19°36.22	20 ± 5	2.04 ± 0.80	2.22 ± 0.89	*0.42 ± 0.08*	*	*0.16 ± 0.01*	-	0.18 ± 0.07	0.34 ± 0.28	4.68 ± 1.19	*4.05 ± 2.12*

Table 4.7 Summary data table for evaluation of the homogeneous matrix model annual total dose rate for samples of Óþoli Tephra and Þörsmórk Ignimbrite analysed in this study. See overpage for explanatory notes. Values in bold have been carried over to Table 4.8. ***contd.***

Table 4.7 *(contd.)* Dose rate data table and homogeneous matrix model dose rates for the Óþoli Tephra and Þórsmórk Ignimbrite analysed in this study. Figures in bold have been carried over to Table 4.8.

General notes for above table:
The three tables represent dose rates obtained from (a-i) XRF and ICP-MS elemental concentration of the bulk matrix (a-ii) Grain specific EPMA and ICP-MS elemental concentrations of purified (90-150 μm; <2.4 gcm^{-3} fraction) and (b) *In-situ* gamma-spectrometry, thick source beta counting (TSBC) of bulk dry matrix and elemental based alpha dose rate. In (b) α-dose contribution to the total dose rate is calculated from XRF elemental concentrations. For simplicity in dose rate calculations, samples are assumed to be homogenous with an overall composition that equates to either (a-i) bulk XRF values (which is considered the most likely) or (b) pure volcanic glass. (b) is unlikely and has not been carried over into age estimate calculations, but provides useful comparative dose rate data. All dose rate calculations are based on the infinite matrix assumption (see Aitken, 1985; p. 66) that assumes samples are homogeneous on a macroscale. A major assumption is that the chemical compositions are representative of the whole sample. Therefore, the sample is considered to be 100 % tephra with a composition that is equal to the bulk or purified fraction composition. This also assumes that there are no microscopic boundaries, at spatial scales of alpha and beta track lengths between concentrations of radioelements and the luminescence sensitivity so that uncertainties concerning glass shard shape can be ignored. This is an important assumption because dose rate equations and calculations presented in Aitken (1985, 1998) are based on dose rates that would be expected from a matrix of perfectly spherical grains. It is unlikely that this situation is totally applicable to a matrix of flat, rectangular platelets (*i.e.* volcanic glass shards), but it is a good first level approximation. See text for issues concerning dose rate calculations. More complex evaluations of dose rates and their influence on final TL age estimates are presented in Tables 4.8-4.11. Ages calculated with homogeneous matrix model dose rates in this table can be found in Table C4.1.

Specific notes for above table:
1 = K_2O was measured by EPMA and XRF, U and Th by ICP-MS and Rb_2O by XRF; EPMA errors are 1σ; the number of shards analysed or the number of replicate measurements is indicated by the number in brackets below the elemental concentrations; XRF and ICP-MS errors are estimated at 5 % as sufficient replicate measurements were not possible. Conversion factors from Nambi and Aitken (1986; Table 3.3) were used to convert elemental concentrations into 'dry' dose rate values. All 'dry' dose rates (elemental and spectrometry based) were then attenuated by appropriate factors before calculation of final 'wet' dose rates using equations in Aitken (1985, 1998), as follows: α-wet = α-dry / (1+1.5WF); β-wet = β-dry / (1+1.25WF); γ-wet = γ-dry / (1+1.14WF), where W and F are as defined in Table 4.6 and Aitken (1985). No thoron or radon loss is assumed in conversion calculations because samples are believed to be sufficiently compact. Equilibrium between U and Th decay is assumed. Similarities between elemental and TSBC β-dose rates suggest that disequilibrium between decay products is minimal. In any case, any potential errors in dose rate calculations associated with disequilibrium are significantly outweighed by variations in dose rate associated with palaeowater content estimation.
2 = Dry alpha-dose is reduced by an alpha efficiency factor which accounts for the reduced effectiveness of alpha-radiation compared to beta-radiaton. The k-value system for alpha efficiency measurements was used (see Zimmerman, 1971), where k = TL per unit dose of α-radiation / TL per unit dose of β-radiation (McKeever, 1985) and was measured in a separate experiment; alpha efficiency measurements for ÞIG 1b are assumed to be similar to ÞIG 7 because there was insufficient material to include this deposit in the alpha efficiency experiment.
3 = See Table 3.3 for explanation of cosmic dose rate values and their attenuation with depth. *In-situ* gamma spectrometry incorporates measurements for cosmic dose (Berger, 1995)
4 = See Table 4.6 for notes on water content evaluation. No measurement error was recorded in duplicate measurements of ÞIG 1b and ÞIG 7 WF_{insitu}, but an maximum error estimate of 15 %, approximately equivalent to the measurement error of SUTL 551/2 WF_{insitu}, has been included above to cover all eventualities.
5 = D_T = total dose rate; $D_T = kD_\alpha + D_\beta + D_\gamma + D_{cosmic}$ where k is the alpha efficiency value.
6 = The α-dose rate estimate is calculated from bulk concentration of elements because the SURRC laboratory does not have a set up for taking alpha spectrometry readings.
7 = TSBC is thick source beta counting. Measurements were obtained using equipment and methods described in Sanderson (1988). Background β-dose rate was measured in response to international dose rate standard minerals, in this case, Shap Granite. Background dose rate was obtained from three cycles of 100 seconds each. Sample dose rate was obtained from six cycles with a count time of 100 seconds per cycle.
8 = Gamma spectrometry measurements for the Óþoli Tephra were made using a portable Ortec Micro Nomad spectrometer with a 3x3 inch sodium-iodide spectrometer crystal and photo-multiplier assemblage. Spectra were collected over 512 channels using a preset live-time of 300 seconds. Accurate *in-situ* measurements of gamma dose are required for sites ÞIG 7 and 1b. * = data in italics have not been measured directly, and are minimum possible estimates. Gamma spectrometry measurements for ÞIG 7 and ÞIG 1b are based on a scaled reduction factor. This value was obtained from comparisons between elemental and *in-situ* gamma spectrometry measurements of the Óþoli Tephra and were calculated in the following manner: Óþoli Tephra *in-situ* gamma dose rate = 0.3 ± 0.03 $mGya^{-1}$, wet elemental gamma dose rate (based on $WF=WF_{in-situ}$ attenuation factor) = 0.82 ± 0.09 $mGya^{-1}$. Therefore, *in-situ* to wet elemental gamma dose rate scaling factor for the Óþoli Tephra = 0.36 ± 0.05 $mGya^{-1}$. Applied to ÞIG 7 the elemental gamma dose rate is reduced from ÞIG 7: elemental, $WF=WF_{insitu}$ γ-dose rate = 1.33 ± 0.18 $mGya^{-1}$ to ÞIG 7: *in-situ* scaled γ-dose rate = 0.48 ± 0.09 $mGya^{-1}$, the number in table above. Applied to ÞIG 1b the elemental gamma dose rate is reduced from ÞIG 1b: elemental, $W=WF_{insitu}$ γ-dose rate = 1.19 ± 0.17 $mGya^{-1}$ to ÞIG 1b: *in-situ* scaled γ-dose rate = 0.42 ± 0.08 $mGya^{-1}$, the number in table above.

Tephra Lab ID	WF (*in-situ*-sat)	GS (μm)		(1) Homogenous matrix dose rates $D\alpha_T$	$D\beta_T$	$D\gamma_T$	D_c	**Total**	(2) Heterogeneous matrix dose rates $D\alpha_T$	$D\beta_T$	$D\gamma_T$	D_c	Total	(3) W MEAN of (1) & (2)	(4) W MEAN ALL S & E
Óþoli Tephra															
SUTL 551/2	0.30±0.10	44.3	S	1.30	1.11	0.30	-	**2.70 ± 0.62**	1.51	1.11	0.30	-	**2.92 ± 0.54**	**2.83 ± 0.41**	3.32 ± 0.45
			%	48.0	40.9	11.1	-		51.7	37.9	10.3	-			
			E	1.30	1.65	0.85	0.11	3.90 ± 0.66	1.51	1.58	0.85	0.11	4.04 ± 0.67	3.97 ± 0.47	
			%	33.3	42.3	21.7	2.7		37.5	39.0	20.9	2.7			
Þörsmórk Ignimbrite															
ÞIG 7	0.52±0.39	105.2	#	1.84	2.12	0.48	0.16	4.44 ± 2.11	3.04	2.12	0.48	0.16	5.64 ± 2.07	5.05 ± 1.48	5.64 ± 1.38
			%	41.5	47.7	10.8	3.6		53.9	37.6	8.5	2.8			
			E	1.84	2.09	1.09	0.16	**5.18 ± 2.38**	3.04	3.32	1.09	0.16	**6.97 ± 1.96**	**6.25 ± 1.51**	
			%	35.5	40.3	21.1	3.0		43.7	47.6	15.7	2.3			
ÞIG 1b	0.34±0.28	111.6	#	1.72	1.91	0.42	0.04	4.09 ± 2.12	2.43	1.91	0.42	0.04	4.80 ± 2.03	4.46 ± 1.47	5.18 ± 1.47
			%	42.0	46.8	10.3	1.0		50.6	39.8	8.8	0.8			
			E	1.71	2.30	1.11	0.05	**5.17 ± 2.64**	2.43	3.122	1.113	0.05	6.71 ± 2.14	6.10 ± 1.66	
			%	33.1	44.5	21.5	1.0		36.2	46.5	16.6	0.7			

Table 4.8 Comparisons of dose rates obtained using the homogenous and heterogeneous matrix models for the Óþoli Tephra and ash samples from sites ÞIG 7 and ÞIG 1b of the Þörsmórk Ignimbrite.

Values in black boxes were used to calculate final TL ages summarised in Table 4.9. $D\alpha_T$, $D\beta_T$, $D\gamma_T$ are total dose rates and incorporate attenuation factors based on WF values shown. W is the saturation water content and F the average palaeowater content, both as defined in Table 4.5 (after Aitken,1985; 1998); GS = bulk median grain size - see Figure 4.6. The homogeneous model dose rate was calculated using equations in Table 4.7 notes 1 & 5 (after Zimmerman, 1971; Aitken, 1985; 1999; McKeever, 1985). These values are based on bulk compositions and/or spectrometry measurements were used to calculate ages in Table 4.10, 4.11 for reasons explained in text. The heterogeneous model partitions dose rate into internal glass shard, based on data from grain specific or purified fractions, and external matrix components, based on bulk data; $D\alpha_T = k[\phi_g D\alpha_g + (1-\phi_M)WFD\alpha_M]$ and $D\beta_T = \phi_g D_\beta + (1-\phi_M)WFD\beta_M]$, where: ϕ_g, ϕ_M are absorbed dose factors and $(1-\phi_M)$ attenuation factors from Bell (1980) and Mejdahl (1979) that correspond to the median grain size for glass shards and matrix respectively; S = spectrometry based measurements; E = elemental measurements; # = minimum estimate of dose rate based on elemental-*in-situ* gamma spectrometry reduction factor from Óþoli Tephra - see Table 4.7 note 8 for full explanation; % = percentage of total dose rate.

Tephra	Dose rate parameter	Parameter chosen	Reason	Value
Óþoli Tephra (SUTL 551/552)	Palaeowater content	Mid-point *In-situ*-sat	Most representative of burial period	0.30 ± 0.10
	Dose rate method	Spectrometry based	Proximity of RB-10 with reduced γ-dose to airfall ash sampling location	
	Dose rate model	Weighted mean of homogeneous & heterogeneous matrix models	Approximately equal values obtained Weighted mean chosen to reduce dose rate errors	2.83 ± 0.41 Gya^{-1}
Þörsmórk Ignimbrite (ÞIG 7)	Palaeowater content	Mid-point *In-situ*-sat	Most representative of burial period	0.52 ± 0.39
	Dose rate method	Elemental based	30 cm matrix of similar composition No *in-situ* measurements taken	
	Dose rate model	Weighted mean of homogeneous and heterogeneous matrix models	Bulk matrix contains greater proportion of non-glassy material than the Óþoli Tephra Best average estimate of dose rate as homogeneous & heterogeneous model dose rate values overlap. Weighted mean were chosen to reduce dose rate errors	6.25 ± 1.51 Gya^{-1}

Table 4.9 Summary of chosen dose rate parameters, reasons and most representative parameter and dose rate values for the Óþoli Tephra and Þörsmórk Ignimbrite.

4.4.2 TL Characterisation & Palaeodose Evaluation Experiments

Box 4.1 summarises the results of the TL characterisation experiments 1-3.

(a) TL Expt. 1: Natural vs 50 Gy response experiments (Figs. 4.21, 4.22)

The Natural vs 50 Gy laboratory dose response experiment demonstrated that uncontaminated, highly silicic volcanic glass shards retain an age and laboratory dose dependent TL signal that is reproducible. The largest signals were obtained from platey glass shards. A typical glass-phase response of highly silicic Icelandic tephra deposits to 50 Gy artificial radiation exists. For samples that have not been pre-heated, the glass-phase 50 Gy response is characterised by a broad band of near equal TL intensity between 100-400°C.

Askja 1875 and Öræfi 1362 produce near-zero ages. For both deposits, the natural TL signal is predominantly stored in the less stable, lower energy traps that are readily evicted at lower temperatures of 200-300°C. A small amount of storage occurs in the more stable >250°C temperature range. With technical modifications to the SUERC-TL readers it might be possible to produce direct ages from these and other highly silicic Holocene tephra deposits from Iceland. Multiple samples from the Þörsmórk Ignimbrite with different shard morphologies were included to illustrate the importance of shard morphology on the magnitude of the natural signal. This effect is related to area of the disc covered by glass, with platey shards providing glass coverage of a much greater proportion of the total disc area relative to pumiceous shards. Platey-glass shards are recommended for future work because they have the highest TL sensitivity, but other fractions produce usable signals. In fact, pumice clast samples from the Þörsmórk Ignimbrite (ÞIG 5, 11, 16, 22) were more easily purified than the fallout ash deposits (ÞIG 1b, 7) or weathered slope deposits (ÞIG 13, 21). For ignimbrite deposits stratigraphically well-constrained glass-rich fallout and co-ignimbrite ash layers and/or surge related ash deposits are the prime targets for dating. The natural and 50 Gy response plateau ratio of the Óþoli Tephra is an order of magnitude greater than that of ÞIG 7 and ÞIG 1b.

A serendipitous by-product of this experiment was the ability to identify non-glass phase contaminants with a higher TL sensitivity than the typical volcanic glass-phase 50 Gy response (Fig. 4.21). The anomalously high 50 Gy response of ÞIG 1b and ÞIG 13, with multiple peaks in the glow curve profile, and a well-defined and highly stable N/50 Gy plateau is thought to be indicative of contamination by a feldspathic phase with a higher TL sensitivity than the glass matrix. All other samples have a 50 Gy dose response $<10^2$ cps and highly fluctuating, but relatively stable, N/50 Gy plateau profile.

The rhythmite beds and the Hjallanes Tephra (Hj-2b) have a natural TL signal and 50 Gy dose response plateau ratio that is approximately an order of magnitude less than the Óþoli Tephra (Fig. 4.22). Contamination of the Óþoli Tephra by rhythmite bed deposits cannot therefore be recognised

using the 50 Gy dose response test, but this is not a serious concern given the low natural TL signal and fine-grain size (much less than the 90 μm) of these deposits. It is assumed that the TL signal in these deposits emanates from the volcanic feldspar phase, but it is uncertain what the signal represents; hence the initial decision to concentrate TL dating on the glass phase of the Óþoli Tephra with its well-defined thermal/formational event. Possible explanations for the origin and magnitude of the signal include: 1) TL from a phase with lower sensitivity than the glass phase of the Óþoli Tephra; 2) Geological TL that has experienced significant anomalous fading; 3) TL obtained since a well-bleached 'zeroing event' (and, perhaps, subsequent anomalous fading of that TL signal).

(b) Experiments 2 & 3: Optical bleaching & inducement TL signal in volcanic glass (Fig. 4.23)

It was not possible to remove the stored natural TL signal completely from the Óþoli Tephra and the Þörsmórk Ignimbrite or induce a signal equivalent to the natural signal of the Óþoli Tephra by optical stimulation. In addition, an optically-stimulated luminescence signal could not be obtained from the Óþoli Tephra. These results could suggest that there was little or no residual OSL in the tephra and/or the TL signal in volcanic glass is almost entirely due to long-term storage in heat sensitive traps. For these reasons, stored natural doses had to be thermally removed for the regeneration experiments. This undoubtedly caused sensitisation of the sample; hence the inclusion of minimum-maximum age ranges rather than specific age estimates for the SAR-TL experiment.

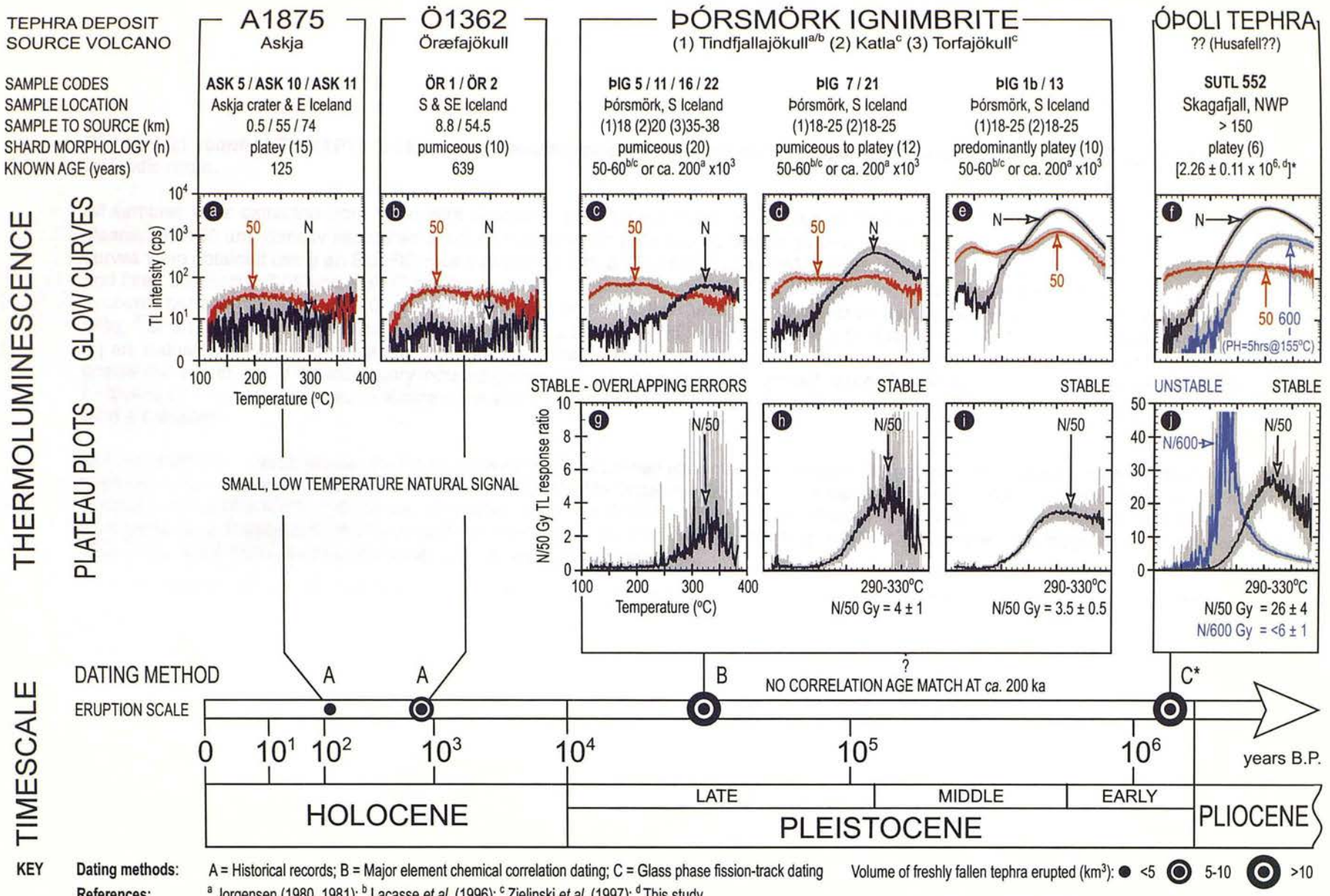


Figure 4.21 TL Expt. 1: Natural and 50 Gy thermoluminescence response glow curves for the glass phase of selected Icelandic tephra deposits.

contd. overpage

Figure 4.21 ***(contd.)*** **TL EXPT. 1:** Natural thermoluminescence (TL) and 50 Gy response 'glow curves' for selected highly silicic tephra deposits of Icelandic origin.

All samples were extracted from the centre of organic poor tephra deposits that are at least 3 cm thick. In all cases, the ultrasonically and 10% HCl cleaned 90-150 μm, density separated 2.3-2.4 or <2.4 gcm^{-3} (followed by 90 μm sieving to remove clay size particles) fraction was used. All TL glow curves were obtained using an SUERC research reader with an Electron Tubes 9883 QB Photo-multiplier Tube (PMT) continuously flushed with nitrogen and fitted and Schott 7/59 and KG1 filters; heating rate = 5° $Csec^{-1}$ from 0-400° C. In graphs a-f black lines represent the mean natural TL intensities (N) in counts per second (cps), at 1° C intervals. Red lines represent the mean TL intensity produced by applying a 50 Gy laboratory dose (50) using a 1.85 GBq, ^{90}Sr β-ray source with a silicate dose rate of 3.27 ± 0.015 $Gymin^{-1}$. Grey lines are ± 1σ deviations from (n) discs for each degree in all plots. Graphs g-j are natural and 50 Gy ratio plateau plots, *i.e.* the mean ratio and single standard deviation of the N/50 Gy TL response. No pre-heats were used to enable the true shape of the laboratory induced growth curve to be examined - the only exception being the 600 Gy response of the Óþoli Tephra (graph f - blue line). This was included to illustrate the effect of pre-heating. This sample was preheated to 155° C for 5 hours and the 600 Gy dose applied at 32.6 ± 0.6 $Gymin^{-1}$.

Sub-samples of all fractions used in this experiment were examined under the microscope. Non-glassy, minerogenic material (predominantly plagioclase feldspars) was observed in purified fractions of ÞIG 1b. No large microphenocrysts were observed in other purified fractions. Note the high 50 Gy response of the ÞIG 1b/13 and the smooth plateau ratio plot of ÞIG 1b/13 which are thought to be caused by microphenocrystic feldspar contamination. Comparisons of fractional Eu/Eu* rare earth element ratios for the Óþoli Tephra (Fig. 4.28) and SEM chemical maps of the Óþoli Tephra, ÞIG 1b and ÞIG 7 (Fig. 4.27) were used as additional 'ad-hoc' tests of sample purity.

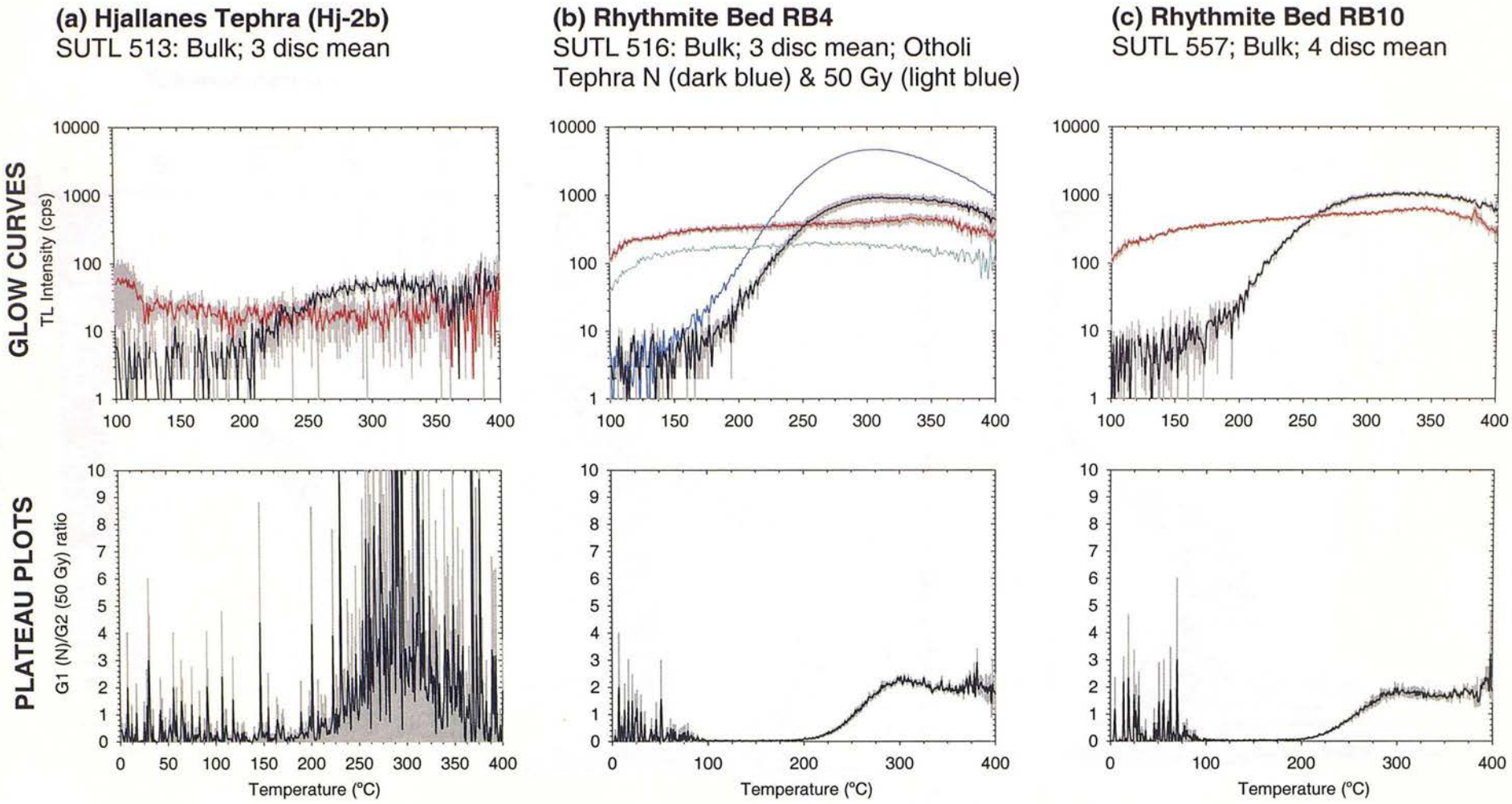
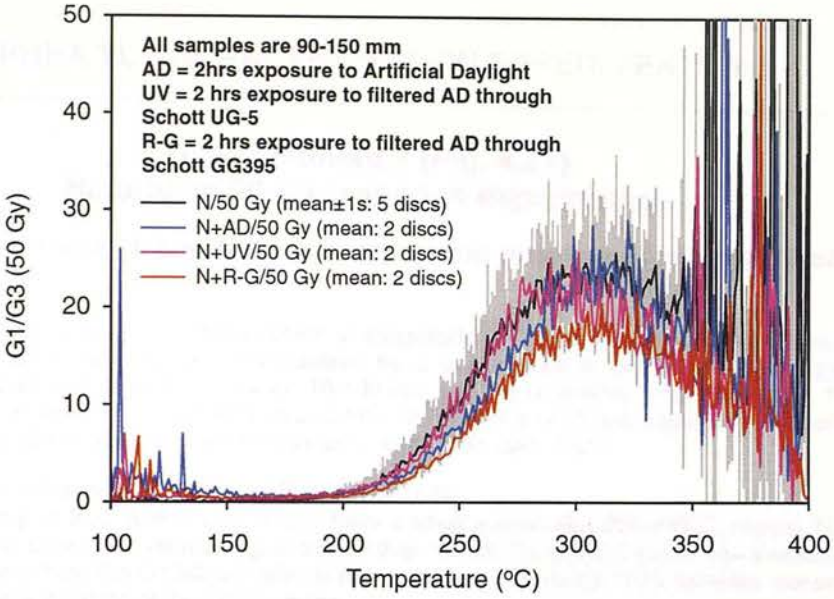
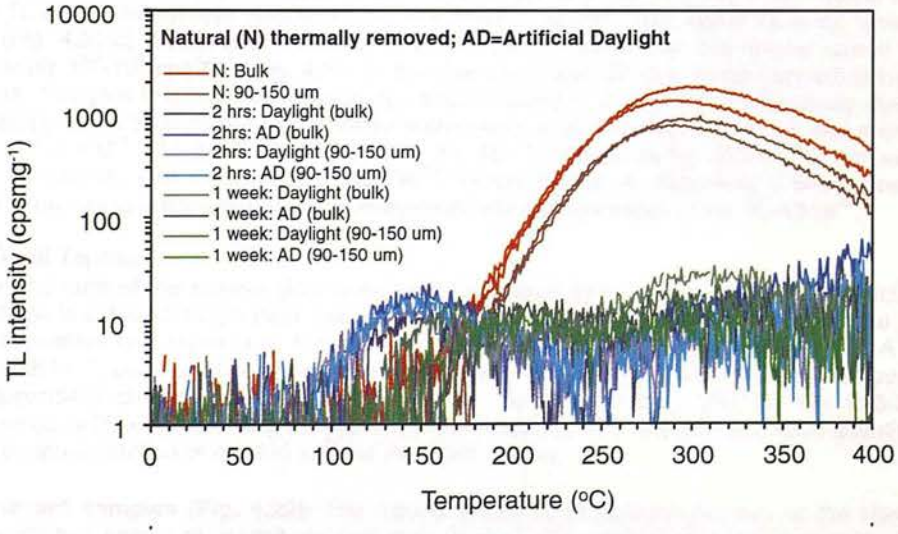


Figure 4.22 Natural and 50 Gy dose response glow curves and plateau plots for selected non-tephra deposits of the Skagafjall sedimentary sequence

(a) TL Expt. 2: Laboratory bleaching the Óþoli Tephra natural signal



(b) TL Expt. 3: Laboratory inducement of TL signal in the Óþoli Tephra



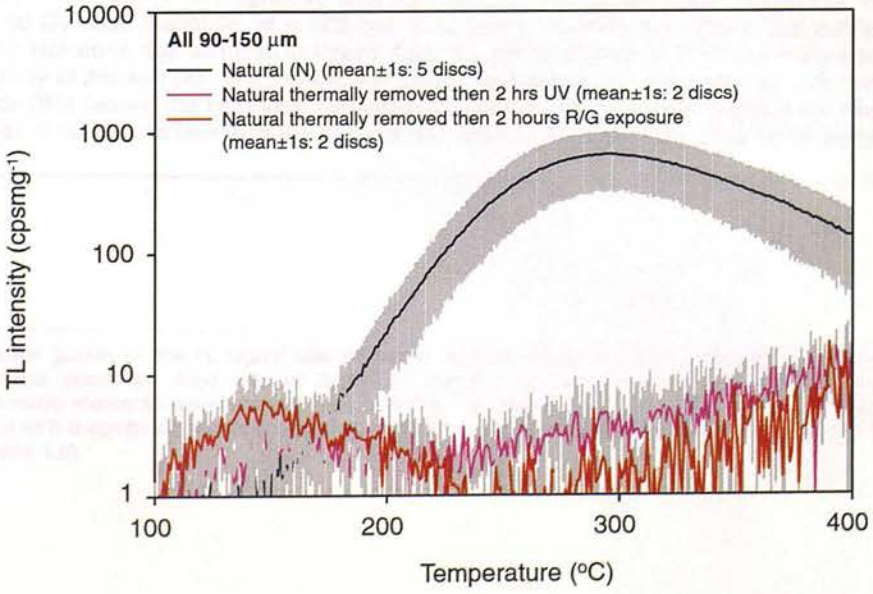


Figure 4.23 TL Expts. 2-3: Bleaching and inducement characterisation tests for the Óþoli Tephra

TEPHRA TL CHARACTERISATION EXPERIMENTS 1-3

TL Experiment 1 (Fig. 4.21)
Natural vs 50 Gy response experiments

(a) Natural glass-phase TL and 50 Gy laboratory dose response of Icelandic Tephra

General
Natural TL intensities ranged over three orders of magnitude. All pre-Holocene samples have similar and reproducible glow curve forms, characterised by a single peak in the 280-360°C temperature range. The 50 Gy dose response is between 10-100 cps and the laboratory –induced 110°C TL peak poorly-defined for all samples except ÞIG 1b and ÞIG 13. ÞIG 1b and 13 has a greater TL sensitivity of between 100-1000 cps and three well-defined peaks at *ca.* 130, 220, 300°C.

Holocene age control samples: Askja 1875 & Öræfi 1362
Near zero age samples from A1875 and Ö1362 have a small magnitude, 200-400°C, natural TL signal 10^1 cps°C^{-1}. In both cases, the natural signal is less than the 50 Gy artificial dose. The intensity of the intensity of the signal from the Ö1362 samples is not as great as the Askja 1875 samples, possibly due to the more pumiceous nature of the Ö1362 glass.

ÞIG samples: Þórsmórk Ignimbrite
There is an apparent relationship between shard morphology and the intensity if the stored natural glass-phase TL signal. Pumiceous deposits have the smallest stored peak signal intensity, typically < 10^2 cps°C^{-1} (Fig. 4.21-c). Samples dominated by platey glass shards have the largest stored signal intensity, typically 10^3-10^4 cps°C^{-1} (Fig. 4.21-d), but this could also be due to contamination by non-glassy material. Samples that have approximately equal proportions of pumiceous and platey shards or are dominated by pumiceous-platey hybrid shard morphologies lye between these two end members, typically 10^2-10^3 cps°C^{-1}. The peak area for ÞIG 7, 21, 1b, 13 occurs in the 290-330°C temperature range. N/50 Gy plateau plot ratios in the 290-330°C range are *ca.* 4. Assuming a linear dose-age response, this equates to a semi-quantitative, entry-level age approximation of *ca.* 30-40 ka[32].

SUTL 552: Óþoli Tephra
The intensity and form of the natural glow curve was consistent and reproducible. The characteristic glow curve shape is a 'broad' single peak between 10^3-10^4 cps°C^{-1} in the 280-360°C region. The 50 Gy response is consistent and reproduce, has an even profile and intensity of *ca.* 100 cps°C^{-1}. A slight temperature shift in TL peak position during pre-heating experiments, which could indicate temperature and dose dependent change in sensitivity. The N/50 Gy plateau plot ratio for the 290-330°C temperature range is 26 ± 4. Assuming a linear dose-age response, this equates to a semi-quantitative, entry-level age approximation of *ca.* 460 ka[33] for the Óþoli Tephra.

(b) Other relevant samples (Fig. 4.22): The natural signal of Hj-2b basic fraction of the Hjallanes Tephra is nearly two orders of magnitude less than that of the purified silicic fraction of the Óþoli Tephra. The 50 Gy dose response, at < 100 cps, is of similar magnitude to that of the purified silicic fractions of the Holocene age samples in Figure 4.21. No stable plateau exists most likely because of the low sensitivity of this sample. The natural and 50 Gy dose response of the silt-clay bulk fractions of rhythmite beds RB4 (above the Hjallanes Tephra) and RB10 (below the Óþoli Tephra) are similar and nearly an order of magnitude less than the signal in the purified silicic fraction of the Óþoli Tephra.

contd.

[32] Assuming linear growth of the TL signal with no supra- or sub- linear growth effects and a weighted mean homogenous-matrix elemental dose rate of 5.18±1.77 mGya^{-1} for the maximum age estimate and mean heterogeneous-matrix elemental dose rate of 6.18±1.12 mGya^{-1} for the minimum age estimate (see Table 4.8).
[33] As above, but with a combined homogeneous-heterogeneous matrix spectrometry based dose rate of 2.8 ± 0.4 mGya^{-1} (see Table 4.8).

TL Experiment 2 (Figs. 4.21, 4.22)
Optical bleaching of TL signals

(a) Field based experiments

ÞIG Samples: Þörsmórk Ignimbrite
For samples with similar glass-shard morphology, stored natural glass-phase TL signal intensity is approximately the same for slope ash and buried deposits (Fig. 4.21-d, e). Slope deposits (*i.e.* ÞIG 1d, ÞIG 13) have been exposed significant post depositional natural light exposure of unknown duration or intensity. It is assumed that buried ash deposits (*i.e.* ÞIG 1b) were buried rapidly and have not experienced post-depositional light exposure.

(b) Laboratory based
It was not possible to completely remove the natural TL signal from the Óþoli Tephra using artificial daylight lamps; hence the use of thermal resetting for regeneration experiments.

TL Experiment 3 (Fig. 4.21, 4.23)
Optical inducement of TL signal in the Óþoli Tephra

(a) Inducement of TL in the upper atmosphere during plume transport
There is no substantial stored dose in the 250-400°C temperature range of any of the Holocene age samples.

(b) Laboratory inducement of TL signal
It was not possible to induce a TL signal of equal to the magnitude or similar form to that of the Óþoli Tephra in these experiments. It is interesting to note the elevated bulk TL compared to TL from the 90-150 μm fraction. Possible explanations for this include: 1) The presence of coarse grained volcanic feldspars whose TL sensitivity is greater than the 90-150 μm fraction. The 90-150 μm fraction is overwhelmingly dominated by glass shards even before further purification; 2) The possibility that the TL per unit mass of coarser glass shards is greater than those in the 90-150 μm fraction.

Box 4.1 Thermoluminescence characterisation experiments of glass-phase of Icelandic tephra.

The Óþoli Tephra and Þörsmórk Ignimbrite sample ÞIG 7 were chosen for glass-phase quantitative dating analysis because of their higher TL sensitivity and the consistent/uncontaminated nature of the natural and 50 Gy dose response. ÞIG 7 was chosen for a further two reasons:

1) It is a stratigraphically well-constrained deposit, most probably related to fallout from a pyroclastic ground surge. The purified were are not contaminated by feldspathic material.
2) It was possible to retrieve a greater quantity of the 90-150 μm fraction from the sample without resorting to crushing.

4.4.3 Quantitative TL Dating Experiments 4 & 5

In each of the following sections there is a summary of data analysis applicable to each method and a summary of the main quantitative luminescence dating results. For reasons outlined in the previous section the final MAAD-TL age estimates and the SAR-TL minimum-maximum age ranges for the Óþoli Tephra and Þörsmórk Ignimbrite quoted in this section were calculated using the weighted mean dose rate values of the homogenous/heterogeneous matrix model with palaeowater content

estimated as the mid-point between 'as-found' and saturation values. Spectrometry based dose rate ages are highlighted for the Óþoli Tephra and elemental dose rates for the Þörsmórk Ignimbrite for reasons discussed in the previous section.

(a) MAAD-TL & SAR-TL experiments 4 & 5: Overview

For the Óþoli Tephra, quantitative dating results were mixed. Eight out of eleven dating attempts were successful and had an age range = 0.6-4.8 Ma. During the early stages of this study, results of the preliminary additive and regenerative dose (Fig. 3.7), the multiple aliquot additive dose (MAAD) (Fig. 4.24) and the single aliquot regeneration (SAR) (Fig. 4.25) TL experiments were seemingly incompatible. Regeneration experiments on the microphenocryst- and inclusion-free, rigorously purified 90-150 μm, 2.3-2.4 gcm^{-3} airfall glass-phase of the Óþoli Tephra indicated that the natural TL signal is greater than the first saturation growth phase. but in multiple aliquot experiments, the dose response grew in approximately linear manner, if at all. Furthermore, it was difficult to explain how the natural signal was greater than two additive test doses, natural + 600 Gy and natural + 1200 Gy in the preliminary experiments.

It was apparent from an early stage that both the preliminary regenerative and SAR-TL growth curves could be split into two components. Firstly, an exponential component which saturates at around 2000 Gy and secondly, an approximately linear component that does not saturate, but continues to grow in an approximately linear manner, similar to the high, glass-phase dose response described in Ward (1988). The natural signal of the Óþoli Tephra lies in the second phase of approximately linear signal growth beyond the first, main phase of saturation (Fig. 4.26). Ward (1988) and Wintle (1997) suggested that fitting a saturating exponential and linear growth function is the best way to deal with samples whose natural signal lies beyond the first phase of linear dose response growth and saturation. In addition, second phase, approximately linear dose response growth characteristics have been observed in, for example, glass dosimetry TL studies (Ward, 1988), TL dating studies of quartz extracted from low radiation, late Pleistocene dune sequences in South Australia and the Thar Desert of India (Chawla *et al.*, 1992; Huntley *et al.*, 1994; Huntley and Prescott, 2001).

Comparing all the regeneration and additive dose growth profiles it is clear that the additive-dose growth profiles most likely represent a second phase of approximately linear, post-saturation growth in the TL signal (Fig. 4.24). Linear regression curves were therefore fitted to the G1/G3 MAAD-TL data to obtain equivalent dose (ED) values. The negative supra/sublinearity correction dose value (I) obtained by fitting linear regression curves to the G2/G3 ratio was considered to be a good estimate the sub-linear or first phase growth to saturation dose. The sum of ED + I is then a good estimation of the palaeodose (P) (Fig. 4.24). Individual palaeodose plateau values were constructed in this manner. Individual palaeodose plateau values within runs because a large disc-disc variation in dose response was noted. Palaeodose plateau values were not combined across runs because different experimental

conditions were used. In this way individual, fading corrected MAAD-TL palaeodose dose values and age estimates were obtained and these can be found in Tables 4.7 and 5.6. Final weighted mean palaeodose values and age estimates were calculated for runs that shared similar pre-heat conditions (Table 4.11). MAAD-TL ages obtained in this manner should be viewed with a degree of caution because the form of the luminescence growth curve up to the completion of the first saturation phase has not been reconstructed. The 'Australian-slide' method (*e.g.* Prescott and Robertson, 1997) could be used in future MAAD-TL analysis to overcome this problem.

It should be noted that the final TL age estimates for the Óþoli Tephra presented in this section are significantly greater than the commonly accepted maximum age limit for luminescence dating of 0.5-0.8 Ma (Aitken, 1998; Forman *et al.*, 2000). Calculating ages beyond the commonly accepted upper limit of TL dating is justified because:

1) Independent age estimates were successfully established for both the Óþoli Tephra and Þörsmórk Ignimbrite
2) The position of the natural signal of the Óþoli Tephra in a secondary phase of approximately linear growth of the TL signal dose response growth profile meant meaningful palaeodose values and therefore TL age estimates could be produced.

The weighted mean age estimates from MAAD-TL experiment runs that use a 5 hour 155°C pre-heat is 2.06±0.27 Ma. This was calculated using a weighted mean dose rate value of 2.83±0.41 $Gyka^{-1}$ and a weighted mean palaeodose value of 5800±410 Gy (Table 4.11) and is broadly similar to the fission-track age for the Óþoli Tephra. The SAR-TL age range encompasses the fission-track age. Changes in sensitivity test were relatively minor during the course of the SAR-TL experiment indicating that an age slightly older than the 1.74±0.37 minimum SAR-TL age is more likely to be accurate than one closer to the 4.91±0.12 Ma maximum age. The minimum age was calculated using the same dose rate used in the MAAD-TL age estimate above and a mean palaeodose value of 4925±750 Gy. This palaeodose value was obtained by interpolation. The maximum age was calculated using the same dose rate used in the MAAD-TL age estimate above and a mean palaeodose value of 13265±855 Gy. This palaeodose value was obtained by extrapolation (Table 4.11)

Glass-phase SAR-TL ages for ÞIG 7 of the Þörsmórk Ignimbrite range from 29±7 to 48±22 ka. The natural TL signal lies within the first linear growth phase before the first phase of TL signal saturation. Palaeodose values were obtained by interpolation. The type of growth curve fitted through has little impact on the final ages produced (Table 4.10, 4.11), but the ages obtained from the Þörsmórk Ignimbrite vary significantly between 30-50 ka with minor variations in dose rate estimate (Table 4.8). The minimum age was calculated using the homogeneous/heterogeneous matrix model and elemental method dose rate value of 6.25±1.15 $Gyka^{-1}$ and maximum mean fading and sensitivity corrected palaeodose value of 244±7 Gy. The fading and sensitivity corrected SAR-TL palaeodose value is

considered a more accurate assessment of the 'true' palaeodose values for ÞIG 7 because changes in TL sensitivity were significant for this sample (Fig. 4.26).

(b) TL Expt. 4: MAAD-TL dating of the Óþoli Tephra (Fig. 4.24)

The multiple aliquot additive dose TL (MAAD-TL) experiment was used to reconstruct the glass-phase palaeodose by applying successively greater laboratory doses to each disc in a set of eight. This builds a dose response profile from which the palaeodose value can be obtained by extrapolation.

Each of five MAAD-TL experiment runs consisted of two sets of discs (A & B). Each set from each run (1-5) was analysed individually because of the different set up conditions and the wide variation in dose response. Distinct shifts in the peak position of individual glow curves from the single, broad peak centred on the 290-310°C temperature band (Fig. 4.24a) were observed during all runs. Simple linear regression curves were, therefore, fitted through the 250-400°C, G1/G3 and G2/G3 data. Equivalent dose (ED) values and a correction for sub-linearity in TL dose response growth curve (I) were combined to produce the palaeodose dose value (P) (Eq. 2.5, 2.6). This procedure was successful for 6 out of 10 runs (Fig. 4.24b; Table 4.10). Four of these runs, 2B, 3A, 4A, 5A, have regression correlation coefficient r^2 values greater than 0.5, while the best, 3A, has an r^2 value of 0.80 ± 0.17. No regression curve of any description could be fitted through data from 1A, 1B, 4B and 5B. 4A was set up in the same way and analysed under identical conditions to 4B. Saturating exponential curves could not be fitted through G1/G3 data from any of the ten runs. The temperature range of stable palaeodose values varies between runs (Table 4.10). The palaeodose values presented represent mean values across the stable temperature range indicated. Attempts at MAAD palaeodose evaluation were inconsistent and not always individually successful. Combining these inconsistent and not always successful datasets, collected under different laboratory conditions into a mean palaoedose value had great potential for producing erroneous palaeodose values. For this reason they have been presented as individual runs and experiments (Fig. 4.24). Final ages within error ranges were combined into weighted mean ages (Table 4.11).

Secondary growth phase linear extrapolation and sub-linear growth and fading corrected TL response curves, produced six MAAD-TL age estimates from nine attempts. The six final ages range from 0.64±0.15 Ma to 2.54 ± 0.50 Ma (Table 4.11). Three out of four final age estimates produced with a pre-heating regime of 5 hours at 155° C are similar to the weighted mean fission-track age. These age estimates are 2.54±0.50, 2.08±0.38 and 1.80±0.34 Ma. Longer 16 hour 135°C pre-heats produced age estimates more than 50 % younger with final age estimates of 1.09± 0.26, 0.81±0.20 and 0.64±0.15 Ma. No results were produced from the other three attempts. The long-term weighted mean fractional loss of signal (fading) of eight out of nine runs that exhibited some degree of fading was 0.95 ± 0.05 (Table 4.10)

(c) TL Expt. 5: SAR-TL dating of the Óþoli Tephra & Þórsmórk Ignimbrite (Figs. 4.24, 4.25)

The single aliquot regeneration TL (SAR-TL) experiment was used to calculate glass-phase palaeodose values by thermally removing the natural or stored TL signal and attempting to reconstruct a signal of equivalent magnitude by applying a series of laboratory radiation doses to each disc. Changes in sample sensitivity during the laboratory irradiation and pre-heat cycle were corrected for by normalising the regeneration dose against a small test dose applied after each regeneration dose.

(i) Óþoli Tephra

The minimum to maximum SAR-TL final age range for the Óþoli Tephra is 1.59±0.33-4.69±0.74 Ma (Table 4.11) The fading corrected, SAR-TL experiment produced ages with a range of 1.59±0.33-1.89±0.40 Ma for sample SUTL 551 of the Óþoli Tephra. These ages are based on palaeodose plateau values, obtained from the thermally stable 290-330°C, 260-340°C temperature band, respectively, by interpolation of the experimental data (Fig. 4.25-1) and spectrometry based homogeneous/heterogeneous dose rate values (Table 4.11). Regression coefficients (r^2) for fitted curves in this temperature range are greater than 0.98 (Fig. 4.23-1c; 2c). Fading and sensitivity (test-dose) corrected single aliquot experiments produced ages with a range 4.63±0.73-4.74±0.75 Ma. The highest of these is based on ED 290-330°C ED plateau values obtained by extrapolation of the saturating exponential-linear curve, fitted to the 10°C data, to more than 7000 Gy beyond the maximum laboratory dose of 6000 Gy. Sixty-seventy day fractional fading coefficients of 0.86±0.02 were obtained during the course of this experiment.

Changes in TL sensitivity for the Óþoli Tephra occurred during the course of the SAR-TL. There is substantial overlap, however, in the single standard deviation error bars for 100 Gy test-dose response relative to the TL intensity of the first test dose. Furthermore, no definite linear increase in test dose TL intensity was observed during the course of the experiment (Fig. 4.25-e, f). Therefore, the 1.74±0.37 Ma sensitivity and fading corrected interpolated SAR-TL age estimate is a minimum age estimate, but probably a more accurate reflection of the 'true' age than the extrapolated fading and sensitivity corrected age. Furthermore, the 4.69±0.74 Ma age estimate obtained from fading and sensitivity corrected dataset should be treated with caution because it is based on extrapolation of > 7000 Gy beyond the highest laboratory dose. It does, however, provide a working maximum age estimate. Data was not collected for irradiations beyond the 6000 Gy (*ca.* 2 Ma when dose rate is *ca.* 3 $mGya^{-1}$) mark for three reasons:

1) Laboratory time constraints on adding > 6000 Gy at 32 $Gymin^{-1}$ to 8 discs
2) Preliminary additive dose and early MAAD results (runs 1 & 2) were either unsuccessful or indicated ages in the region of 500-150 ka
3) Each disc had been irradiated and heated to 400°C 22 times up to and including the 100 Gy test dose following the 6000 Gy dose. It was decided at this point that a less potentially detrimental and time-consuming approach to high dose irradiation was needed.

(ii) Þörsmórk Ignimbrite (ÞIG 7)

In contrast to the Óþoli Tephra, the natural signal of the Þörsmórk Ignimbrite is located in the first phase of linear growth of the SAR-TL signal before first phase saturation. Linear and saturating exponential curves fitted to data collected produce broadly similar palaeodose values that are two orders of magnitude less than those obtained from the Óþoli Tephra (Figs. 4.26). The minimum to maximum SAR-TL final age range for ÞIG 7 of the Þörsmórk Ignimbrite is 29±7–40±10 ka (Tables 4.10, 4.11). All ages are based on interpolation of data points. The younger age estimate is based on minimum fading corrected palaeodose dose plateau values from the thermally stable 290-330°C temperature band and homogeneous/heterogeneous matrix model dose rates calculated from bulk elemental compositions (Tables 4.9, 4.10). The older age is based on maximum fading and sensitivity corrected palaeodose plateau values from the thermally stable 260-340°C temperature band (Fig. 4.24-1) homogeneous/heterogeneous matrix model dose rates calculated from bulk elemental compositions (Tables 5.5, 5.6). Fading and sensitivity corrected (25 Gy test-dose) single aliquot experiments produced age estimates between 39±9–40±10 ka. The younger and older age estimates are as outlined above. It is interesting to note that the weighted mean age of the average ages using a homogeneous matrix model, elemental and spectrometry based dose rate method is 48±16 ka (Table 4.7). Further dose rate data, particularly multiple-site, *in-situ* gamma dosimetry measurements from several depositional facies, is required before a firm conclusions can be drawn from the age data presented for the Þörsmórk Ignimbrite. Sixty-seventy day fractional fading coefficients of 0.92 ± 0.01 were obtained at the end of this experiment (Fig. 4.26-d).

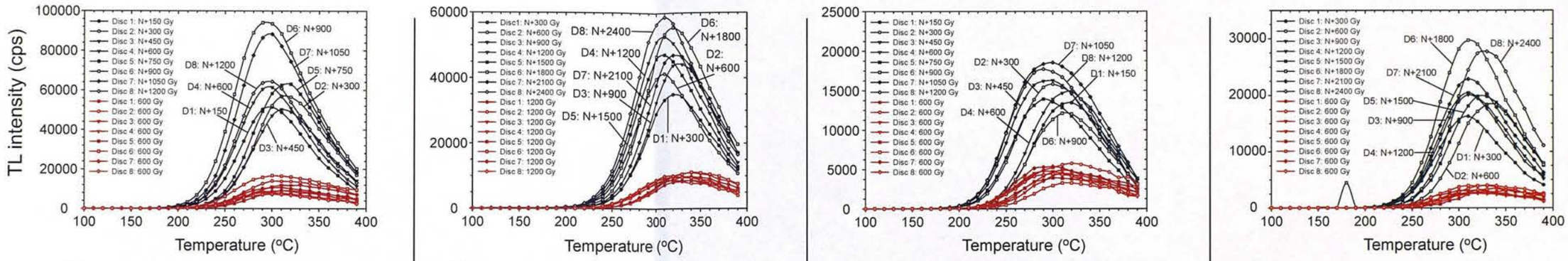
There is a linear increase in the 25 Gy test dose response indicating that the sensitivity of this sample changed significantly during the course of the ÞIG 7 SAR-TL experiment. Significant in this context is defined as the occurrence of single standard deviation error bars for the second and last test dose that do not overlap and a TL signal response to the 25 Gy test dose that increases in a linear manner (r^2>0.9) during the course of this experiment (Fig. 4.26-f). The weighted mean fading and sensitivity corrected age of 40±10 ka is therefore more likely to be accurate than the fading corrected age. The fractional fading coefficient is within the 0.9-1 range associated with experimental error (Forman *et al.*, 2000) indicating no anomalous fading occurred during long-storage. The large errors of *ca.* 46 % on individual age estimates are due to large uncertainties placed on estimates of palaeowater content estimates (Table 4.6). Nevertheless, the TL age of the Þörsmórk Ignimbrite sits firmly in the *ca.* 40-50 ka age bracket and is the best numerical age evidence obtained thus far from the type site of this deposit.

Óþoli Tephra: Equal Total Dose Multiple Aliquot Additive Dose (MAAD) Experiment

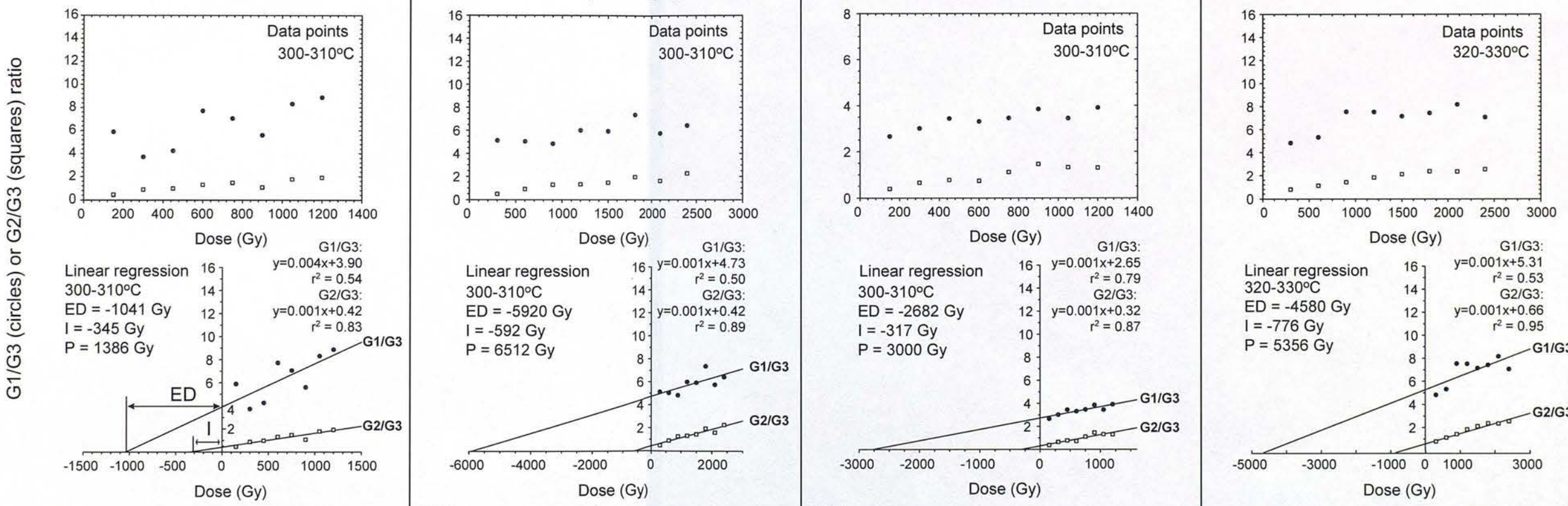
SUTL552: 0-8 cm airfall ash deposit; at least 150 km from source; 90-150 μm; 2.3-2.4 gcm^{-3}; sample distribution on disc - see below; regeneration β-dose rate = 32.00±0.0.6 Gymin^{-1} + 5.19 Gy transit dose.

Lab / run no.	1) SUTL552: 2B	2) SUTL552: 3A	3) SUTL552: 4A	4) SUTL552: 5A
Distribution on disc (radius, r, covered; mass)	whole disc covered (r=10 mm; 5-6 mg)	whole disc covered (r=10 mm; 5-6 mg)	inner area covered (r=5 mm; 2-3 mg)	inner area covered (r=5 mm; 2-3 mg)
Pre-heat	16 hrs @ 135° C	5 hrs @ 155° C	16 hrs @ 135° C	5 hrs @ 155° C
Additive dose range (Gy)	150-1200	300-2400	150-1200	300-2400
Dose interval (Gy)	150	300	150	300
Normalisation dose (Gy)	600	1200	600	600

a GLOW CURVES



b EXAMPLE G1/G3 &G2/G3 DATA PLOTS & REGRESSION



c PLATEAU PLOTS A & B

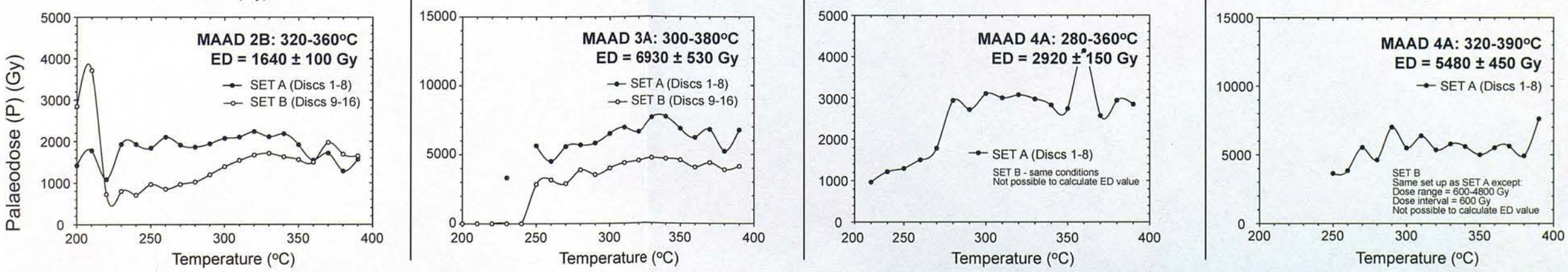


Figure 4.24 Glass phase, multiple aliquot additive dose (equal total dose) results for the 0-8 cm airfall component of the Óþoli Tephra, Skagafjall NW Iceland. See overpage for further explanation and Section 5.1 for discussion.

contd.

Figure 4.24 ***(contd.)*** **TL EXPT. 4:** Glass phase, equal total dose, multiple aliquot additive dose thermoluminescence (MAAD-TL) experiment for 0-8 cm airfall component of the Óþoli Tephra, Skagafjall, NW Iceland.

Set-up conditions vary-see set up information below title for details. All data was analysed on an individual run basis due to large variability in dose response between runs. All results presented are based on 10°C-integrals of original 1°C-data. Not all runs are included for clarity. It was not possible to fit regression curves of any type through results from MAAD1 and this run has not been included. Where a choice existed the sample with the highest G1/G3 r^2 regression value was chosen. Samples were analysed using equipment described in Figure 4.21, except dose rate = 32.00 ± 0.60 Gy min^{-1} + 5.19 $Gymin^{-1}$ transit dose.

(a) G1 and G3 glow curves for sets of eight discs.

(b) Example of G1/G3 and G2/G3 data-plots and regression analysis for a representative 10°C temperature band from the plateau region. Data from the 300-310°C temperature region was chosen when this temperature range was representative of the palaeodose (P) plateau. Otherwise, the first 10°C-temperature band from the thermally stable palaeodose range was chosen. P = ED + I as in Eq. 3.6 where P = Palaeodose, ED = Equivalent Dose and I = Dose correction for the effects of supra- or sublinear dose response.

(c) Individual run-based palaeodose (P) plateau plots for both sets in runs 2-5. Palaeodose plots were not combined because there was substantial run-run variation in dose response. Measurement of the natural signal was not included because preliminary tests showed that it was significantly and unexpectedly higher than the N+xGy additive dose response.

Óþoli Tephra: Dose Corrected - Single Aliquot Regeneration (SAR-TL) Experiment

SUTL 551: 0-8 cm airfall ash deposit; at least 150 km from source; 90-150 μm; 2.3-2.4 gcm^{-3}; sample centred on disc; regeneration β-dose rate = 5.19+32.00±0.6 Gymin^{-1} + 5.19 Gy transit dose; pre-heat = 2 minutes @ 220°C; test dose: TD = 100 Gy

1) Fading Corrected Results

2) Sensitivty Test Dose (TD) & Fading Corrected Results

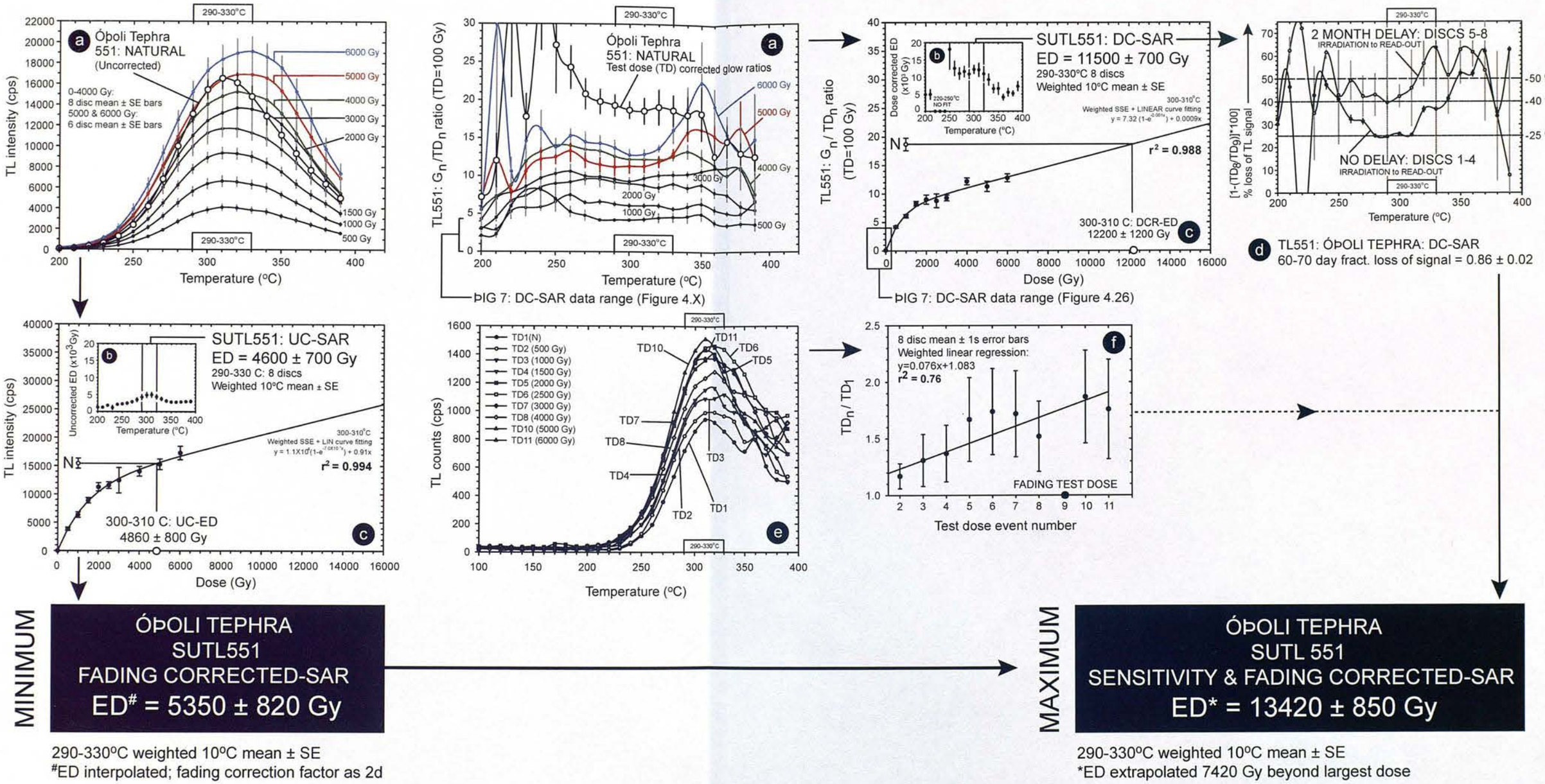


Figure 4.25 Glass phase, single aliquot TL regeneration experiment for air-fall component of the Óþoli Tephra, Skagafjall, NW Iceland.

All results presented above are based on 10°C integrals of original 1°C data. SE = standard error.

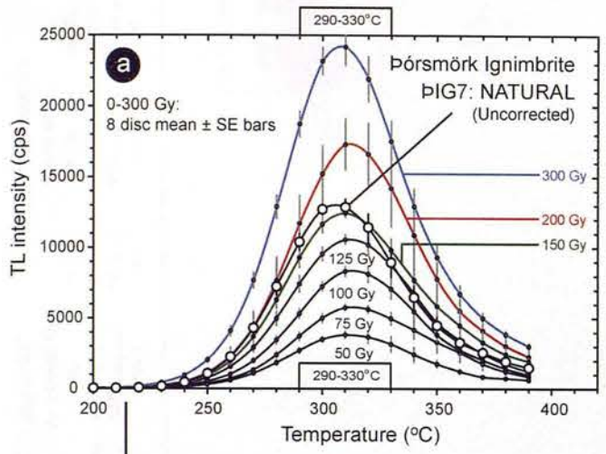
1) Fading corrected equivalent dose (ED) calculation process: (a) Regeneration dose (G_n) TL response glow curves; n = irradiation run number *e.g.* G1 = 500 Gy; G2 = 1000 Gy *etc.* (b) 200-400°C ED vs temperature (ED plateau) plot (c) Example of saturating exponential (SSE) + linear weighted regression curve fitting to the 300-310°C temperature integral. The 300-310°C is the central area of the 290-330°C thermally stable ED range and coincides with the peak intensity of the natural TL glow curve. The final 290-330°C ED value in the black box is corrected for the effects of thermal and anomalous fading using the correction factor calculated in 2d. Simple thermal fading, within the boundaries of experimental error, occurs when the fractional fading factor is between 0.9-1. Anomalous fading occurs when this factor is substantially below 0.9, *e.g.* 0.75 (see text for further details; Forman *et al.*, 2000).

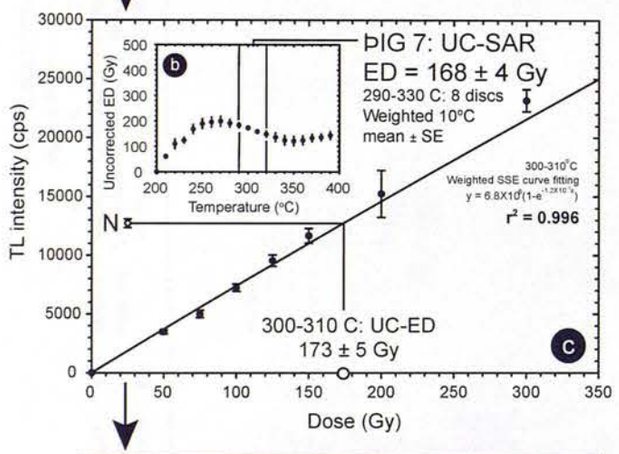
2) Sensitivity and fading corrected ED calculation process: (a) Normalised regeneration TL response glow curves calculated as follows: a 100 Gy test dose (TD_n) was added after each regeneration dose (G_n) to assess changes in TL sensitivity for each disc; n = 100 Gy test dose applied after the corresponding G_n dose *e.g.* TD1 = test dose applied after G1 (500 Gy). The 10°C glow curve profiles from 1a and 2e are then used to construct the normalised or test dose corrected glow curve ratio profiles (G_n/TD_n) (1a) and ED values (1b & c) (b) 200-400°C ED vs temperature (ED) test dose corrected plateau plot (c) Example of saturating exponential + linear weighted regression curve fitting to the 300-310°C temperature integral. The 300-310°C temperature band is the central area the 290-330°C thermally stable ED range. Therefore, the final 290-330°C ED value in the black box has been corrected for variations in the test dose TL response (2a & b) and for the effects of fading using the correction factor calculated in 2d (d) Comparative percentage loss of 100 Gy TL response signal for discs 1-4 that were read out immediately after irradiation and discs 5-8 that experienced a 60-70 day delay between irradiation and read out (e) 100 Gy test dose (TD_n) TL response glow curves used to calculate ratio based glow curve profiles and ED values and asses the magnitude and significance of changes in TL sensitivity for each disc (f) Variation in 100 Gy test dose TL response for TD2-11 compared to TD1. Significant change in sample sensitivity is considered to have occurred if the linear regression gradient is greater than 1 and the 8 disc 1σ errors bars for each run do not overlap.

Þórsmörk Ignimbrite: Dose Corrected - Single Aliquot Regeneration (SAR-TL) Experiment

SUTL ÞIG7: 5 cm unwelded co-ignimbrite airfall ash in inter-bedded layers of partially welded pumice, ash and lithic pyroclasts; *ca.* 25 km from source; 90-150 μm; <2.4 gcm^{-3}; sample covers whole disc; β-dose rate = 5.19 Gy transit dose + 32.00±0.19 Gymin^{-1}; applied dose; pre-heat = 2 minutes @ 220°C; test dose: TD = 25 Gy

1) Fading Corrected Results



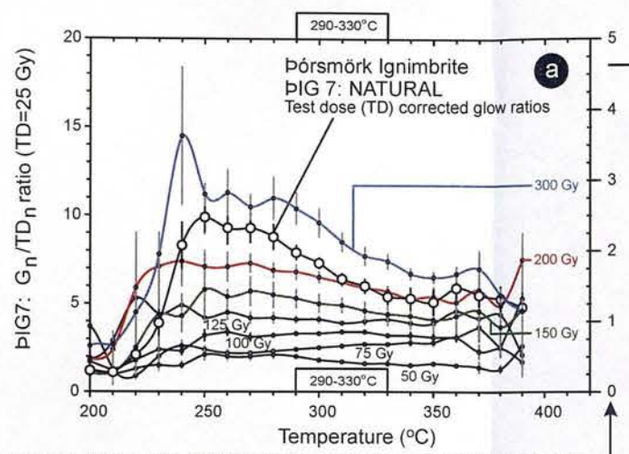


MINIMUM

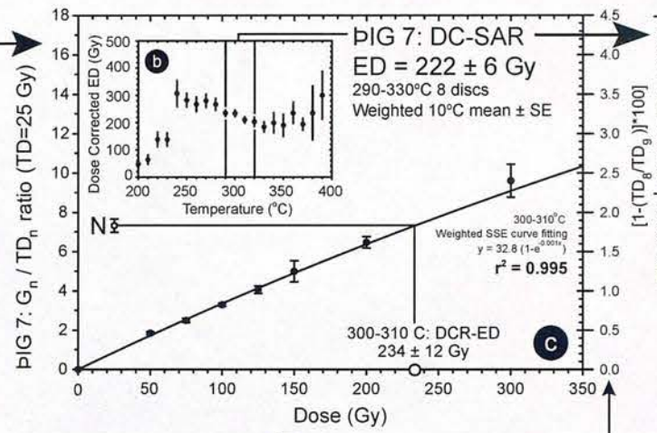
ÞÓRSMÖRK IGNIMBRITE
SUTL: ÞIG 7
FADING CORRECTED-SAR
ED# = 182 ± 5 Gy

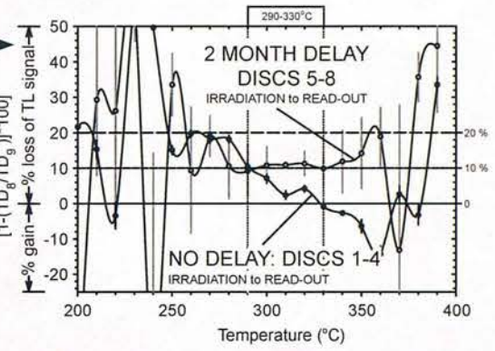
290-330°C weighted 10°C mean ± SE
#ED interpolated; fading correction factor as 2d

2) Sensitivty Test Dose (TD) & Fading Corrected Results

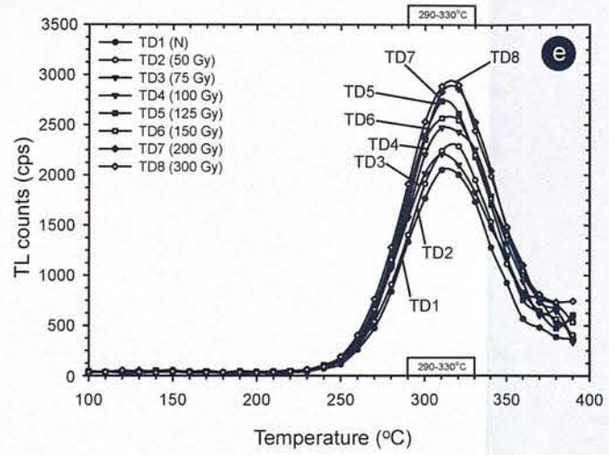


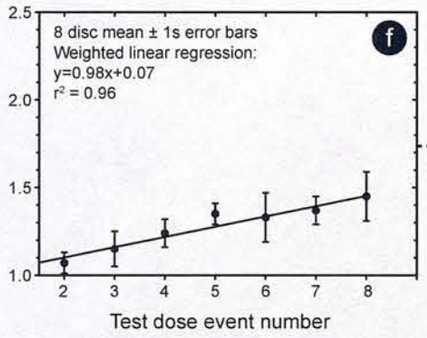
SUTL551: G_n / TD_n ratio (TD=25 Gy) : approximately equivalent scale





d ÞIG 7: ÞÓRSMÖRK IGNIMBRITE: DC-SAR
60-70 day fract. loss of signal = 0.92 ± 0.01





MAXIMUM

ÞÓRSMÖRK IGNIMBRITE
SUTL: ÞIG 7
SENSITIVITY & FADING CORRECTED-SAR
ED# = 241 ± 7 Gy

290-330°C weighted 10°C mean ± SE; #ED interpolated SSE
260-340°C = 247 ± 7 Gy; conditions as 290-330 C

Figure 4.26 Glass phase, single aliquot TL regeneration of the natural TL signal from unwelded ash layer at site ÞIG 7 of the Þórsmörk Ignimbrite, Þórsmörk, S Iceland.

All results presented above are based on 10°C integrals of original 1°C data. SE = standard error.

1) Fading corrected equivalent dose (ED) calculation process: (a) Regeneration dose (G_n) TL response glow curves; n = irradiation run number e.g. G1 = 50 Gy; G2 = 75 Gy etc. (b) 200-400°C ED vs temperature (ED plateau) plot (c) Example of saturating exponential (SSE) weighted regression curve fitted to the 300-310°C temperature integral data. The 300-310°C temperature band is the central area of the 290-330°C thermally stable ED range and coincides with peak intensity of the natural TL glow curve. The final 290-330°C ED value in the black box is corrected for the effects of thermal and anomalous fading using the correction factor calculated in 2d. Simple thermal fading, within the boundaries of experimental error, occurs when the fractional fading factor is between 0.9-1. Anomalous fading occurs when this factor is substantially below 0.9, *e.g.* 0.75 (see text for further details; Forman *et al.*, 2000).

2) Sensitivity and fading corrected ED calculation process: (a) Normalised regeneration TL response glow curves calculated as follows: a 25 Gy test dose (TD_n) was added after each regeneration dose (G_n) to assess changes in TL sensitivity for each disc; n = 100 Gy test dose applied after the corresponding G_n dose e.g. TD1 = test dose applied after G1 (500 Gy). The 10°C glow curve profiles from 1a and 2e are then used to construct the normalised or test dose corrected glow curve ratio profiles (G_n/TD_n) (1a) and ED values (1b & c) (b) 200-400°C ED vs temperature (ED) test dose corrected plateau plot (c) Example of saturating exponential (SSE) weighted regression curve fitted to the 300-310°C temperature integral data. The same procedure was repeated for for 10°C intergral data between 200-400°C to generate the ED plateau plot. The 300-310°C temperature band is the central area the 290-330°C thermally stable ED range. Therefore, the final 290-300°C ED value in the black box has been corrected for variations in the test dose TL response (2a & b) and for the effects of fading using the correction factor calculated in 2d (d) Comparative percentage gain/loss of 25 Gy TL response signal for discs 1-4 that were read out immediately after irradiation and discs 5-8 that experienced a 60-70 day delay between irradiation and read out (e) 25 Gy test dose (TD_n) TL response glow curves used to calculate ratio based glow curve profiles and ED values and asses the magnitude and significance of changes in TL sensitivity for each disc (f) Variation in 25 Gy test dose TL response for TD2-8 compared to TD1. Significant change in sample sensitivity is considered to have occurred if the linear regression gradient is greater than 1 and the 8 disc 1σ errors bars for each run do not overlap.

SAMPLE DATA		EQUIVALENT DOSE (ED) DATA									TOTAL BULK DOSE RATE (D_T) DATA[8] Highest D_T → Lowest D_T				TL AGE ESTIMATES Based on		
Sample name (Lab no.) Expt. Name Run no.	Set	Pre-heat[1] time @ temp. (hrs/min @ °C)	Dose range (Gy)	Dose interval (Gy)	ND or TD[2] (Gy)	Reg.[3] Type	Stable ED[4] Range (°C)	Regression r^2 G1/G3-MAAD G_T/TD_T-DC-SAR	ED[5] (Gy)	60-70 day[6] fading ratio	A Fading[7] Corrected ED (Gy)	B_1 ELEMENTAL D_T $WF_{in\text{-}situ}$ ($mGya^{-1}$)	B_2 ELEMENTAL D_T $WF_{in\text{-}situ\text{-}sat}$ ($mGya^{-1}$)	B_3 SPECT D_T (WM H-H) ($WF_{in\text{-}situ\text{-}sat}$) ($mGya^{-1}$)	A / B_1 ELEMENTAL D_T $WF_{in\text{-}situ}$ (ka)	A / B_2 ELEMENTAL D_T $WF_{in\text{-}situ\text{-}sat}$ (ka)	A / B_3 SPECT D_T ($WF_{in\text{-}situ\text{-}sat}$) (ka)	
(a) Óþoli Tephra (SUTL551/552)																		
(i) Multiple Aliquot Additive Dose(MAAD) Experiment (SUTL552)																		
MAAD1	A	16 hrs @ 135	150-1200	150	600	-	-	-	-	-	-	-	-	-	-	-	-	
	B	16 hrs @ 135	150-1200	150	600	-	-	-	-	0.87 ± 0.41	-	-	-	-	-	-	-	
MAAD2	A	16 hrs @ 135	150-1200	150	600	L	300-340	0.30 ± 0.02	2130 ± 90	0.93 ± 0.19	**2290 ± 440**	4.21 ± 0.30	3.97 ± 0.47	**2.83 ± 0.41**	544 ± 111	**577 ± 130**	**809 ± 195**	
	B	16 hrs @ 135	150-1200	150	600	L	320-360	0.56 ± 0.04	1640 ± 100	0.90 ± 0.17	**1810 ± 320**	4.21 ± 0.30	3.97 ± 0.47	**2.83 ± 0.41**	430 ± 82	**456 ± 97**	**640 ± 146**	
MAAD3	A	5 hrs @ 155	300-2400	300	1200	L	300-380	0.80 ± 0.17	6930 ± 530	0.96 ± 0.11	**7210 ± 940**	4.21 ± 0.30	3.97 ± 0.47	**2.83 ± 0.41**	1713 ± 254	**1816 ± 320**	**2548 ± 497**	
	B	5 hrs @ 155	300-2400	300	1200	L	320-360	0.44 ± 0.05	4640 ± 320	0.91 ± 0.11	**5090 ± 640**	4.21 ± 0.30	3.97 ± 0.47	**2.83 ± 0.41**	1209 ± 175	**1282 ± 221**	**1799 ± 345**	
MAAD4[9]	A	16 hrs @ 135	150-1200	150	600	L	280-360	0.57 ± 0.22	2920 ± 150	0.94 ± 0.18	**3090 ± 570**	4.21 ± 0.30	3.97 ± 0.47	**2.83 ± 0.41**	734 ± 145	**778 ± 171**	1092 ± 256	
	B	16 hrs @ 135	150-1200	150	600	-	-	-	-	1.21 ± 0.08	-	-	-	-	-	-	-	
MAAD5[9]	A	5 hrs @ 155	300-2400	300	600	L	320-390	0.64 ± 0.08	5480 ± 450	0.93 ± 0.08	**5880 ± 640**	4.21 ± 0.30	3.97 ± 0.47	**2.83 ± 0.41**	1397 ± 182	**1481 ± 238**	**2078 ± 377**	
	B	5 hrs @ 155	600-4800	600	600	-	-	-	-	0.99 ± 0.20	-	-	-	-	-	-	-	
											EXTRAPOLATED ED - NO COHERENT SINGLE AGE ESTIMATE - AGE RANGE:						**600 → 2700**	
(ii) Dose Corrected Single Aliquot Regeneration (DC-SAR) Experiment (SUTL551)																		
Uncorrected		2 min @ 220	0-6000	500/1000	-	SSE+L	290-330	0.996 ± 0.001	4600 ± 700	0.86 ± 0.02	**5350 ± 820**	4.21 ± 0.30	3.97 ± 0.47	**2.83 ± 0.41**	1271 ± 215	**1348 ± 261**	**1890 ± 399**	
		2 min @ 220	0-6000	500/1000	-	SSE+L	260-340	0.994 ± 0.002	3870 ± 580	0.86 ± 0.02	4500 ± 680	4.21 ± 0.30	3.97 ± 0.47	**2.83 ± 0.41**	1069 ± 179	1134 ± 218	1590 ± 333	MIN
											INTERPOLATED ED - UNCORRECTED MEAN AGE ESTIMATES 260-340 & 290-330°C:				1170 ± 197	1241 ± 239	1740 ± 366	
TD corrected (11)[10]		2 min @ 220	0-6000	500/1000	100	SSE+L	290-330	0.988 ± 0.003	11540 ± 730	0.86 ± 0.02	**13420 ± 850**	4.21 ± 0.30	3.97 ± 0.47	**2.83 ± 0.41**	3188 ± 304	**3380 ± 454**	**4742 ± 750**	
		2 min @ 220	0-6000	500/1000	100	SSE+L	260-340	0.985 ± 0.007	11280 ± 740	0.86 ± 0.02	13110 ± 860	4.21 ± 0.30	3.97 ± 0.47	**2.83 ± 0.41**	3114 ± 302	3302 ± 447	4633 ± 737	
											EXTRAPOLATED ED - DOSE CORRECTED MEAN AGE ESTIMATES 260-340 & 290-330°C:				3151 ± 303	3341 ± 450	4687 ± 743	MAX
(b) Þörsmórk Ignimbrite (ÞIG 7)																		
(i) Dose Corrected Single Aliquot Regeneration (DC-SAR) Experiment (ÞIG 7)																		
Uncorrected		2 min @ 220	0-300	50/100	-	L	290-330	0.991 ± 0.005	168 ± 4	0.92 ± 0.01	**182 ± 5**	6.59 ± 0.91	**6.25 ± 1.51**	*5.05 ± 1.48*	28 ± 4	**29 ± 7**	*36 ± 11*	MIN
						SSE		0.996 ± 0.003	168 ± 4	0.92 ± 0.01	**182 ± 5**	6.59 ± 0.91	**6.25 ± 1.51**	*5.05 ± 1.48*	28 ± 4	**29 ± 7**	*36 ± 11*	
		2 min @ 220	0-300	50/100	-	L	260-340	0.990 ± 0.008	169 ± 3	0.92 ± 0.01	**184 ± 4**	6.59 ± 0.91	**6.25 ± 1.51**	*5.05 ± 1.48*	28 ± 4	**29 ± 7**	*36 ± 11*	
						SSE		0.978 ± 0.015	169 ± 3	0.92 ± 0.01	**184 ± 4**	6.59 ± 0.91	**6.25 ± 1.51**	*5.05 ± 1.48*	28 ± 4	**29 ± 7**	*36 ± 11*	
											INTERPOLATED ED - UNCORRECTED MEAN AGE ESTIMATES:				28 ± 4	**29 ± 7**	***36 ± 11***	
TD corrected (9)[10]		2 min @ 220	0-300	50/100	25	L	290-330	0.986 ± 0.007	207 ± 5	0.92 ± 0.01	**225 ± 6**	6.59 ± 0.91	**6.25 ± 1.51**	*5.05 ± 1.48*	34 ± 5	**36 ± 9**	*45 ± 13*	
						SSE		0.996 ± 0.002	222 ± 6	0.92 ± 0.01	**241 ± 7**	6.59 ± 0.91	**6.25 ± 1.51**	*5.05 ± 1.48*	37 ± 5	**39 ± 9**	*48 ± 14*	
		2 min @ 220	0-300	50/100	25	L	260-340	0.942 ± 0.110	210 ± 5	0.92 ± 0.01	**228 ± 6**	6.59 ± 0.91	**6.25 ± 1.51**	*5.05 ± 1.48*	35 ± 5	**36 ± 9**	*45 ± 13*	
						SSE		0.991 ± 0.007	227 ± 6	0.92 ± 0.01	**247 ± 7**	6.59 ± 0.91	**6.25 ± 1.51**	*5.05 ± 1.48*	37 ± 5	**40 ± 10**	*49 ± 14*	
											INTERPOLATED ED - DOSE CORRECTED MEAN AGE ESTIMATES:				36 ± 5	**39 ± 9**	***47 ± 14***	MAX

Table 4.10 Equivalent dose and TL age estimate summary data table for multiple aliquot additive dose and single aliquot regeneration thermoluminescence dating experiments on volcanic glass fractions of the Óþoli Tephra and Þörsmórk Ignimbrite. Dose rate data is based on weighted mean homogenous/heterogeneous matrix model calculations summarised in Table 4.8 rather than homogeneous matrix model dose rate calculations in Table 4.7; reasons for choosing final dose rates are summarised in Table 4.9. Palaeodose values are from Figures 4.24-4.26

Table 4.10 ***(contd.)*** Equivalent dose data and age estimates for thermoluminescence dating experiments on volcanic glass fractions of the Óþoli Tephra and Þörsmórk Ignimbrite.

General notes for above table:
Full details of dose rate data can be found in Tables 4.8 and Table 4.9. Errors in MAAD are mean ± 1σ errors from individual set based ED reconstructions. Errors for regeneration data are mean ± standard errors from sets of 8 discs. All data is based on measured parameters except data in italics which is based on elementally scaled estimates of *in-situ* gamma spectrometry – see Table 4.7: specific note 7 for details.

Specific notes for above table:
1 = 135°C and 155°C pre-heats were undertaken in a muffle furnace; 220°C pre-heats were undertaken on the heater plate within the PMT assemblage.
2 = ND = normalisation dose (G3) in MAAD experiment; TD = test dose normalisation which was undertaken after each regeneration dose in the DC-SAR experiment.
3 = L = linear regression growth curve of the form y = ax + b fitted to data points; SSE = single saturating exponential regression growth curve of the form y = a(1-e-bx) fitted to data; SSE+L = weighted single saturating exponential + linear regression growth curve of the form $y = a(1-e^{-bx}) + cx$ fitted to mean +/- standard error values from 8 discs.
4 = Thermally stable region of equivalent dose vs temperature (plateau) plot.
5 = ED = P + Q where P = palaeodose and Q = correction for supra-, sub-linearity in dose response (Aitken, 1985). Where regression curves could be fitted all MAAD-G2/G3 Q values are negative indicating a sub-linear dose response associated with samples whose luminescence signal is fully saturated or experiencing further growth in luminescence beyond first phase of saturation.
6 = 60-70 day fractional fading ratio. Half the samples in each MAAD and DC-SAR run were irradiated with normalisation or test doses and pre-heats indicated in the respective columns and left in the dark for 60-70 days. The other half were left unirradiated in dark storage then irradiated at the end the 60-70 day period and TL signals read-out with no delay. Fading ratios greater than 0.9 are within experimental measurement errors (cf. Forman *et al.*, 2000). Samples that exhibit severe anomalous fading have fractional fading ratios of 0.75 or less.
7 = ED x 60-70 day fractional fading ratio.
8 = $WF_{in\text{-}situ\text{-}sat}$ dose rates are based on weighted mean homogeneous/heterogeneous infinite matrix model dose rate calculations presented in Tables 4.8 and 4.9. Summary reasons for their inclusion over other values in that table can also be found in Table 4.9. WFin-situ dose rates are based on homogenous matrix dose rates in Table 4.7.
9 = Sample concentrated in centre of disc in an attempt to reduce potential centre to edge of disc irradiation dose variations (cf. Spooner and Allsop, 2000).
10 = Number in brackets is the number of test doses added.

ÓÞOLI TEPHRA	Palaeodose (Gy)	Dose Rate ($mGya^{-1}$)	Age Estimate (Ma)		% age error
MAAD-TL					
5 hr @ 155°C					
3A (300-380°C)	7210 ± 940*	2.83 ± 0.41	2.54 ± 0.50		22.9
3B (320-360°C)	5090 ± 640*	(Spectrometry)	1.80 ± 0.34		19.5
5A (320-390°C)	5880 ± 640	(*In-situ*-sat)	2.08 ± 0.38		18.1
Weighted mean	**5800 ± 410**	(Homogeneous/	**2.06 ± 0.27**		**11.0**
16hr @ 135°C		Heterogeneous)			
2A (300-380°C)	2290 ± 440	2.83 ± 0.41	0.81 ± 0.20		24.1
2B (320-360°C)	1810 ± 320		0.64 ± 0.15		22.9
4A (280-360°C)	3090 ± 570		1.09 ± 0.26		23.5
Weighted mean	**2166 ± 236**		**1.03 ± 0.11**		**10.4**
SAR-TL					
2 mins @ 220°C					
FC (290-330°C)	5350 ± 820	2.83 ± 0.41	1.89 ± 0.40		21.1
FC (260-340°C)	4500 ± 680		1.59 ± 0.33		21.0
Mean age	**4925 ± 750**		**1.74 ± 0.37**	**MIN**	**21.0**
F+SC (290-330°C)	13420 ± 850		4.74 ± 0.75	↓	15.8
F+SC (260-340°C)	13110 ± 860		4.63 ± 0.73	↓	15.9
Mean age	**13265 ± 855**		**4.69 ± 0.74**	MAX	15.9
ÞÖRSMÓRK IGNIMBRITE (ÞIG 7)					
SAR-TL (SSE)					
2 mins @ 220°C					
FC (290-330°C)	182 ± 5	6.25 ± 1.51	29 ± 7		24.3
FC (260-340°C)	184 ± 4	(Elemental)	29 ± 7		24.3
Mean age	**183 ± 5**	(*In-situ*-sat)	**29 ± 7**	MIN	24.3
F+SC (290-330°C)	241 ± 7	(Homogeneous/ heterogeneous)	39 ± 9	↓	24.3
F+SC (260-340°C)	247 ± 7		40 ± 10	↓	24.3
Mean age	**244 ± 7**		**39 ± 9**	**MAX**	**24.3**

Table 4.11 Final age estimates for the Óþoli Tephra and Þörsmórk Ignimbrite

Notes: Palaeodose estimates are as in the appropriate columns of Table 4.7; dose rates from Table 5.5; summary of the conditions used is in brackets beneath dose rate value. Times and temperatures are pre-heating regimes used; SSE = saturating exponential regression based values; SSE+LIN = saturating exponential + linear regression based values; FC = fading corrected; F+SC = fading and sensitivity corrected; temperature range is range over which a stable palaeodose plateau exists; * = non-parallel G1/G2 and G2/G3 regression lines indicative of G1-G3 sensitivity change; all SAR-TL ages are affected by sensitivity change; the age considered to be closest to the 'true' age is in black – dose cycle sensitivity changes were not less significant for the Óþoli Tephra compared to the Þörsmórk Ignimbrite.

4.4.4 Testing phase-TL signal relationship

Determining the phase-origin of the TL signal is important because the TL methods used are not grain-specific. For the Óþoli Tephra, contamination by non-tephra material, *e.g.* the underlying rhythmite bed, RB-10, is not a significant problem. The dose stored in sediments of RB-10 is less than 10% of that stored in the Óþoli Tephra (Fig. 4.22), which is less than the standard analytical error for all the Óþoli Tephra TL age estimates. Contamination by co-genetic feldspar phenocrysts cannot be completely ruled out for ÞIG 1b, but for other samples the purification procedure used was highly effective. Each purification check has its drawbacks. Sub-samples taken for visual examination might not be representative of the whole sample. EDS chemical mapping of unpolished glass shards is not as an effective analytical tool as shard specific WDS analysis of polished grains. Detector alignment within the SEM set up creates 'shading' effects that could hide contaminant grains. The absence of any non-glassy material in all the discs examined is, however, a convincing argument against such effects. Europium anomalies are common for glass-rich, feldspar depleted volcanic products from Iceland and Eu/Eu* values only give a relative indication of the degree of feldspathic fractionation. Eu/Eu* values cannot be used in isolation as there is no established Eu/Eu* value that represents complete removal of feldspathic material from the melt. Nevertheless, the combined techniques are useful semi-quantitative indicators of glass purity.

In summary, no co-genetic or detrital feldspar contamination was detected by visual examination, trace and rare earth element (RRE) analysis and SEM-EDS chemical mapping of discs for samples used in quantitative TL dating analysis.

(a) Microscopic examination of sub-samples

During the course of fission-track dating, large feldspar grains were observed in the 60-200 μm fraction of the Óþoli Tephra after this sample had been mechanically cleaned. No other microphenocrysts or inclusions were observed. Sub-samples were taken from all purified glass samples used in TL dating analysis and examined under optical (polarising) and scanning electron microscope (Figs. 4.5-1; 4.5-2-g, h; 4.5-3). No definitive evidence for feldspathic contamination was found, but ÞIG 1b contained evidence for microphenocrystic and/or xenolithic contamination. This is the main reason why no further quantitative TL dating was undertaken on this sample.

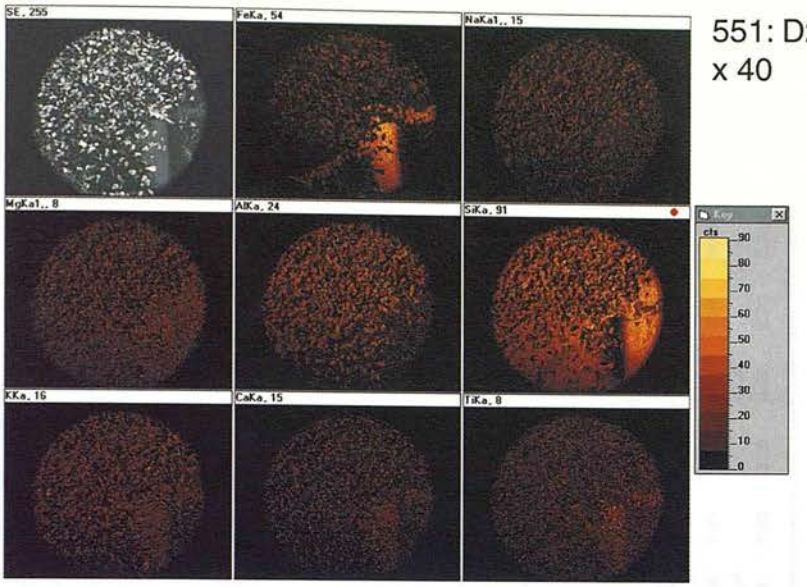
(b) EDS chemical mapping of discs used in SQ-TL and SAR-TL experiment

EDS chemical maps for all discs for samples of A1875, Ö1362, ÞIG 1b, ÞIG 7, SUTL 551 produced similar results. All contained elements associated with the glass-phase of tephra in the correct proportions (Fig. 4.27). No grains of exceptionally high potassium or sodium, indicative of possible feldspar contamination were found.

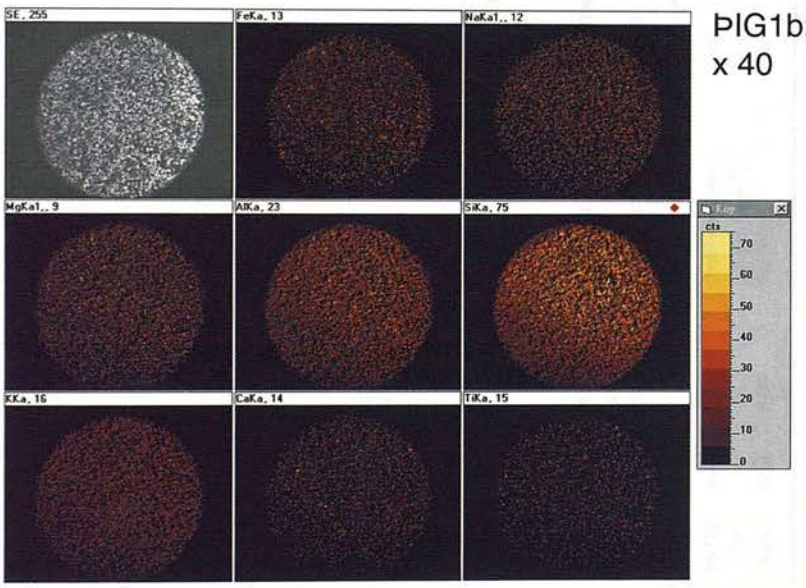
(c) Bulk vs purified Rare Earth Element (REE) composition

In the Óþoli Tephra chondrite normalised diagram (Fig. 4,25-a) the largest negative europium (Eu) anomalies occurred in the bulk sample and the 90-150 μm, 2.3-2.4 gcm-3 purified fraction used in TL dating experiments described above. There was no obvious negative anomaly in the bulk fraction of the Hjallanes Tephra. All fractions analysed have negative Eu/Eu* anomalies, except the <90 μm, >2.4 gcm^{-3} fraction. The largest Eu/Eu* negative anomaly of 0.59 occurs in the 90-150 μm, 2.3-2.4 gcm^{-3} fraction used in the TL dating studies described above. This is similar to the 0.62 value obtained for the bulk fraction of the Óþoli Tephra and the bulk fraction of ÞIG 7 (Fig. 4.25-b). The bulk fraction of ÞIG 1b has an Eu/Eu* value of 0.70. All fractions that used a <2.4 gcm^{-3} produced negative anomalies. The smallest negative anomalies of 0.81 and 0.88 were found in the 90-150 μm, >2.4gcm^{-3} of the Óþoli Tephra and the bulk fraction of the Hjallanes Tephra. The largest negative Ce values occurred in the 90-150 μm, <2.3 gcm^{-3} and <90 mm, <2.3 gcm^{-3}.

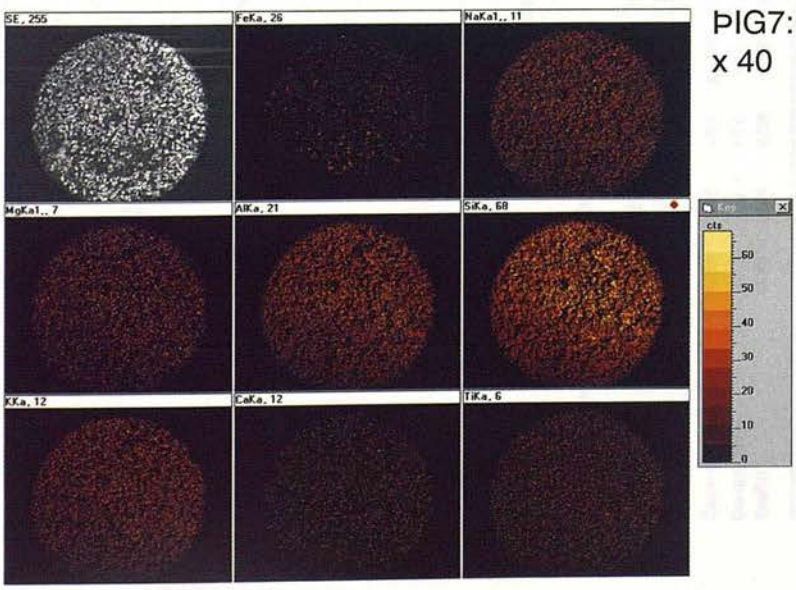
The REE experiment of different size and density fractions from the Óþoli Tephra proved a useful quantitative test of glass-phase purity. The Eu/Eu* value quantifies the extent of the Eu anomaly. Values less than unity are negative anomalies indicating fractionation of feldspar from the melt in geological studies, in this case, relative purity of the glass in fractions examined. The Óþoli Tephra Eu/Eu* anomaly results are consistent with results from the optical examination of sub-samples and EDS chemical mapping tests that indicate uncontaminated glass-phase purity. These combined results justify the selection and description of the 90-150 μm; 2.3-2.4 or <2.4 gcm^{-3} fraction as a pure fraction most suitable for glass-phase TL dating. The similarity in Eu/Eu* the bulk and 90-150 μm; 2.3-2.4 gcm^{-3} indicates that this phase is most representative of the bulk composition for the Óþoli Tephra. In addition, the large negative Eu/Eu* anomalies for the bulk ash fractions of ÞIG 1b and ÞIG 7 suggest that the feldspathic component of these deposits is depleted.



551: D2
x 40

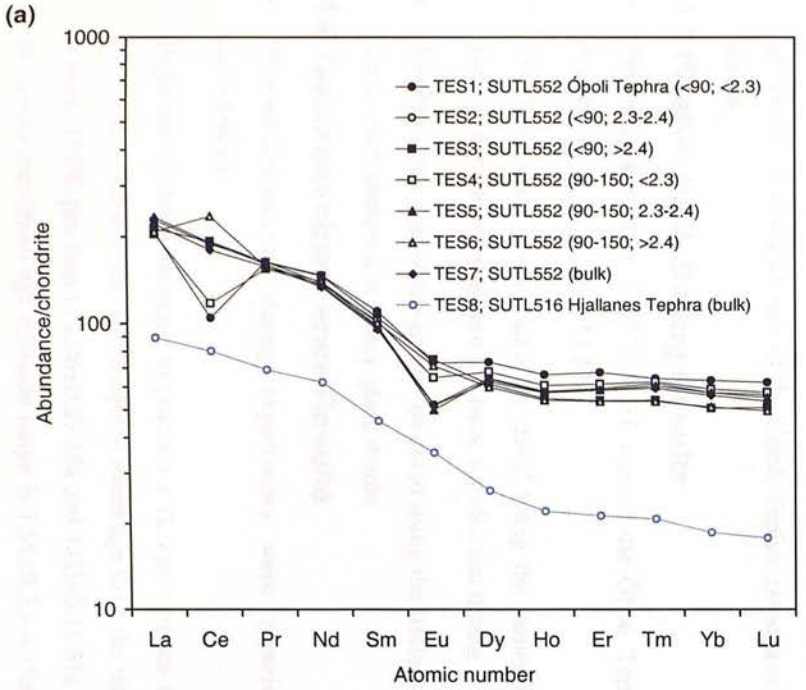


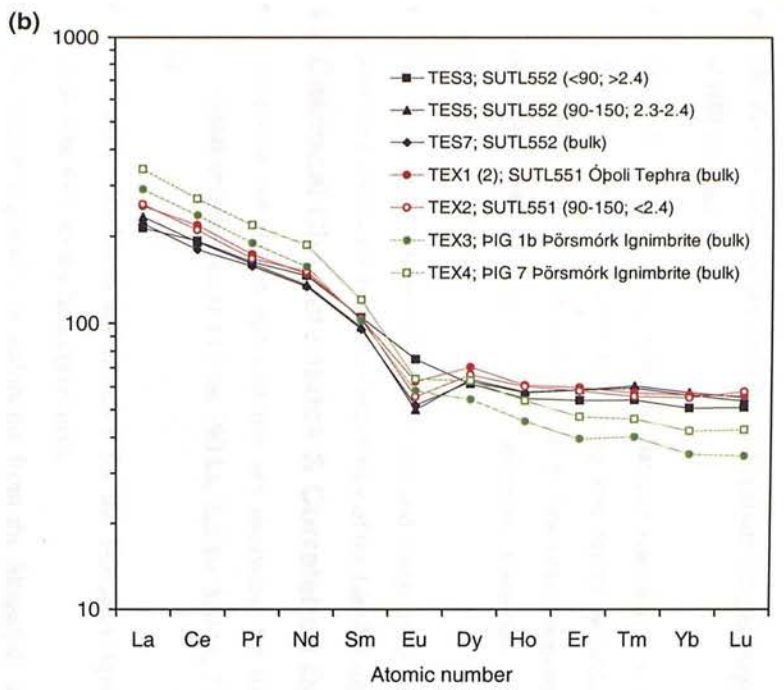
ÞIG1b: D1
x 40



ÞIG7: D4
x 40

Figure 4.27 Examples of SEM chemical maps from discs used in thermoluminescence dating of **(a)** the Óþoli Tephra (551) and Þórsmörk Ignimbrite samples **(b)** ÞIG1b and **(c)** ÞIG7. Other discs quoted in the text produced similar results. Silicon grease was use as a sample mountant for the TL discs and this explains the high SiO_2 counts in areas not covered by ash *e.g.* SUTL551.





(a) Eu/Eu* values	Óþoli Tephra							Hjallanes Tephra
Analysis code	TES1	TES2	TES3	TES4	TES5	TES6	TES7	TES8
SUTL no.	552	552	552	552	552	552	552	516
Grain size (mm)	<90	<90	<90	90-150	90-150	90-150	bulk	bulk
Density (gcm^{-3})	<2.3	2.3-2.4	>2.4	<2.3	2.3-2.4	>2.4	-	-
Eu/Eu*	**0.75**	**0.61**	**2.06**	**0.72**	**0.59**	**0.81**	**0.62**	**0.88**

(b) Eu/Eu* values	Óþoli Tephra					Þörsmórk Ignimbrite	
Analysis code	TES3	TES5	TES7	TEX1 (2)	TEX2	TEX3	TEX4
SUTL no.	552	552	552	551	551	ÞIG 1b	ÞIG 7
Grain size (mm)	<90	90-150	bulk	bulk	90-150	bulk	bulk
Density (gcm^{-3})	>2.4	2.3-2.4	-	-	<2.4	-	-
Eu/Eu*	**2.06**	**0.59**	**0.62**	**0.70**	**0.62**	**0.70**	**0.65**

Figure 4.26 Rare earth element (REE) abundances normalised to chondiritic meteorite values (Boynton, 1984) for bulk and purified glass fractions of the Óþoli Tephra and the Þörsmórk Ignimbrite samples used in TL dating. First number in brackets is the size fraction in μm, the second the denstiy fraction in gcm^{-3}. Eu* = interpolated geometric mean between Sm and Gd defined by Taylor and McLennan (1985) as $Eu^* = Eu_N / [(Sm_N) \times (Gd_N)]^{0.5}$ where subscript N is the chondrite normalised value of the indicated element.

Chapter 4 Summary

4.1 Identification of Tephra

- The diverse sedimentary record on Skagafjall is highly significant because it is unique in this part of NW Iceland
- The wide range of glassy volcanic material available in an accessible location made the Þörsmórk Ignimbrite an ideal deposit for testing new dating methods applied to the Óþoli Tephra. Detailed logs of the Þörsmórk Ignimbrite and its bracketing deposits have been used to link stratigraphic profiles in the Þörsmórk region allowing landscape evolution process to be examined in unprecedented detail.
- Holocene age eruptions of Öræfi 1362 and Askja 1875 were sampled to provide near zero and zero age controls for luminescence dating of the Óþoli Tephra and the Þörsmórk Ignimbrite

4.2 Chemical Characteristics & Correlation Dating Results

- Composite correlation age matches are equivocal for the Óþoli Tephra, with at least seven consistent correlatives at 115 ka, 190 ka, 225 ka, 320 ka, 774 ka, 7.46-7.89 Ma and >10.83-12.94 Ma
- Composite correlation age matches for the Þörsmórk Ignimbrite are all in the 48.5-58 ka age range with 48.5 ka the best correlative.
- The magnetic polarity of sediments from the Skagafjall section is predominantly reversed and given the fission-track age of the Óþoli Tephra associated with the Matuyama reversed polarity epoch.

4.3 Fission-track Dating Results

- The weighted mean ITPFT/DCFT age of the Óþoli Tephra, based on four independent age determinations, is 2.26±0.11 Ma
- The Hjallanes Tephra cannot be dated using the fission-track method because it is too fine-grained and the composition too basic for efficient dating.
- The Þörsmórk Ignimbrite cannot be dated using the fission-track method because no spontaneous tracks were observed in platey glass shards

4.4 Thermoluminescence Results

- Thermoluminescence dating experiments were experimental. Results were mixed, but encouraging.
- Eight out of eleven attempts to produce a TL age estimate for the Óþoli Tephra were successful, age range = 0.6-4.8 Ma. The weighted mean age from the three successful MAAD-TL runs with a 5 hour, 155°C pre-heat is 2.06±0.27 Ma and 1.03±0.11 Ma with a 16 hour, 135°C. The SAR-TL minimum-maximum age estimate range is 1.59±0.33–4.74±0.75 Ma. The fading corrected mean

SAR-TL of 1.74±0.37 Ma (pre-heat: 2 minutes, 220°C) is considered a minimum age estimate and the fading and sensitivity corrected mean age of 4.91±1.17 Ma is considered a maximum age estimate. Sensitivity changes occurred during the course of this experiment, but were not as significant as during the SAR-TL ÞIG 7 experiment and the minimum age estimate is thought to be more representative of the 'true' geological age.

- The ÞIG 7 SAR-TL minimum-maximum age estimate range is 29±7-40±10 ka. The mean fading corrected age estimate of 29±7 ka is considered a minimum age estimate. The fading and sensitivity corrected age estimate of 39±9 ka is considered a maximum age estimate. The latter age estimate is thought to be more representative of the 'true' geological age because significant changes in TL sensitivity were observed during the course of this experiment.

4.5 Testing FT & TL ages of the Óþoli Tephra

- The reversed magnetic polarity of most of the samples collected supports the fission-track age obtained for the Óþoli Tephra.

Chapter 5 Discussion
(A) Assessment of Tephra Ages
(B) Palaeoenvironmental Applications

The 2.26±0.11 Ma fission-track age of the Óþoli Tephra is highly significant. It allows the accuracy of new thermoluminescence dating methods to be fully assessed (Section 5.1). In addition, it provides the first numerical age constraint on pre-Holocene glacial activity on the Vestfírðir Peninsula, which allows glacially driven, macroscale landscape evolution processes on the Vestfírðir Peninsula and the dynamic relationship between Vestfírðir glaciation and mainland volcanic activity at the Plio-Pleistocene transition in Iceland to be examined and placed in a regional and/or global context. To achieve the latter, source volcanic systems of the Óþoli and Hjallanes Tephra are examined (Section 5.2) and formation models for the Skagafjall sedimentary sequence and its relationship to regional and global climatic changes are presented (Section 5.3). To explain the exceptional preservation of the Skagafjall sedimentary sequence, reference to existing models of Iceland-wide LGM-present day glacial activity is described and evaluated (Section 5.4). Particular reference is made to the four hypotheses introduced in Section 1.4.3 and recent ideas of preservation of relict landforms beneath major ice-sheets. Section 5.5 outlines new ideas relating to the formation and preservation of the Þörsmórk Ignimbrite and introduces new landscape evolution and eruption event models for the Þörsmórk region, the Þörsmórk Ignimbrite and NAAZ-2.

Chapter 5A: Final assessment of Tephra Ages

Fission-track dating of the Óþoli Tephra was highly successful. The weighted mean fading corrected (ITPFT & DCFT) age of 2.26 ± 0.11 Ma of the Óþoli Tephra reflects the high degree of experimental reproducibility obtained and is considered an accurate age against which the results of other dating techniques can be compared. No single correlation age could be obtained for the Óþoli Tephra highlighting the limitations of this technique in the pre-Holocene era. The fission track age of *ca.* 2.26 Ma for the Óþoli Tephra is two orders of magnitude older than Sigurvinsson's (1983) age estimate and an order of magnitude greater than anticipated at the outset of the luminescence experiments. Dating samples, such as the Óþoli Tephra, that lie beyond the generally quoted 0.5-0.8 Ma limit for TL dating (Aitken, 1998; Forman *et al.*, 2000) is not usually undertaken for three main reasons.

1) Most samples are specifically chosen because they are thought to lie within the 2-200 ka zone for which luminescence techniques are well-constrained and reasonably well-understood (Forman *et al.*, 2000).
2) For some quartz and feldspars the environmental dose rate is too low and/or the samples dose response to the laboratory dose is not sufficient to produce a second, post saturation linear dose response growth phase (Chawla *et al.*, 1998; Wintle, 1997).
3) High palaeodose values need higher levels of accuracy and precision in dose rate evaluation.

Furthermore, issues such as anomalous fading in volcanic deposits and phenocrystic or xenolithic contamination of glass were thought to be an insurmountable barriers to developing successful coarse-grain thermoluminescence methods for thermoluminescence dating of the glass-phase of tephra deposits.

5.1 Evaluation of TL age estimates & age ranges

The results of the TL dating experiments are groundbreaking. A new method of dating volcanic glass was developed and proved reasonably successful for the Óþoli Tephra and Þörsmörk Ignimbrite. The ability to produce contaminant-free, purified glass fractions from the already glass-rich, phenocryst- and micro-inclusion-poor nature of highly silicic tephra deposits from Iceland was the key factor for successful dating. This study has demonstrated, for the first time, that it is possible to obtain accurate TL ages from the glass phase of Icelandic tephra deposits of pre-^{14}C age. More significantly, it has been possible to use the special dose response properties of the Icelandic volcanic-glass to produce ages for the glass-rich tephra deposits older than the 0.8 Ma upper age limit of luminescence dating (Berger, 1994; Aitken, 1998; Forman *et al.* 2000), opening up new possibilities for TL dating of glass-rich highly silicic tephra beds across a broad age range.

In view of the potential importance of the work, it is important to critically assess the laboratory methods used. Table 5.1 compares procedures used in this study with recent recommendations for

luminescence dating. Table 5.2 provides a quantitative summary assessment of parameters that affect accuracy and precision of TL ages obtained from the Óþoli Tephra and Þörsmórk Ignimbrite. Potential percentage under/overestimates are presented for both deposits.

5.1.1 Evaluation of factors affecting dose rate values

(a) Palaeowater estimates

It is not always possible to constrain dose rates to a sufficient degree of accuracy needed for luminescence dating of the pre-0.5 Ma era for two reasons. Firstly, dating in this era is more susceptible to problems of disequilibrium between daughter products of U and Th (Aitken, 1985, 1998). Secondly, and more significantly, it is difficult to estimate palaeowater variations especially in areas, such as Iceland, with unstable climates. Palaeowater content estimation is also problematic for younger deposits such as ÞIG 7. If the palaeowater content of the ÞIG 7 remained at the 'as found' level during burial an 'absolute minimum' age estimate of 30±3 ka would be obtained. If the sample remained fully saturated during burial an 'absolute maximum age' estimate of 60±5 ka would be obtained. Both of these scenarios are equally unlikely because:

1) The 'as found' samples were collected on sunny days near the end of an unusual two week dry spell in late July/early August 1999 when temperatures reached *ca.* 25°C in parts of southern and southeastern Iceland. However, Þörsmórk and Skagafjall are located in some of the wettest parts of Iceland with average annual precipitation of up to 4000 mm (Fig. 5.1).
2) Extended periods at full saturation are unlikely given the porosity of the matrix.
3) It is likely that significant volumes of ice covered all the sampling sites for extended periods during burial. The effect this has on dose rates is difficult to assess quantitatively in anything but a broad manner; hence the use of a compromise solution of the mid-point between 'as found' and saturation water contents as a best estimate of palaeowater content.

(b) HF Etching

Inclusion and fine-grain luminescence dating methods described in Aitken (1985) relate principally to the dating of quartz. Compared to feldspar and glass, quartz is relatively resistant to HF etching and grains are approximately spherical. Quartz has no internal shard radioactivity. Extended etching is used in quartz-phase TL/OSL dating for two reasons:

1) To remove unwanted feldspars that have different dosimetric characteristics and might be susceptible to anomalous fading (see below).
2) Simplify dose rate calculations. The contribution of alpha decay from feldspars in the matrix to the total dose rate is complex, but can effectively be ignored if coarse-grained quartz separates are etched (Aitken, 1985). HF etching removes the outer rind effected by external alpha-radiation (Fig. 4.19-a).

Table 5.1 Recent recommendations & TL dating methods used in this study (notes at end)

FIELD CRITERIA (from Forman *et al.*, 2000)		Notes / problems encountered or potential problems with the approach used in this study / actual or possible solutions
1) Depositional environment of sediment must be known, particularly in reference to the completeness of solar resetting of the luminescence signal	☑	N/A – see (2)
2) The relation between the solar resetting event of the geological event must be understood	☑	The event being dated is the formation of the volcanic glass, *i.e.* the geological signal
3) Sediments must receive either negligible or little light exposure during sampling	☑	Section were cut back 30-50 cm; samples were extracted using copper tubes
4) Field sampling should concentrate on minimising dose rate heterogeneities	?	Óþoli Tephra – the airfall tephra was sampled. This is 5 cm above a unit with a gamma dose rate an order of magnitude less than the tephra. *In-situ* gamma spectrometry measurements were taken and spectrometry based dose rates rather than elemental dose rates used in age calculations ÞIG 7 – ash layers sampled surrounded by >30 cm of interbedded pumice/ash/lithic layers with approximately the bulk elemental composition as the sampled ash ÞIG 1b – ash layer sampled is in the middle of a *ca.* 1m thick co-ignimbrite ash deposit with pumice lenses, both of the same composition as the sample
LABORATORY CRITERIA		
1) Samples should be prepared in a low energy light environment	☑	
2) All samples should be pre-heated to isolate the most stable luminescence component	☑	MAAD-TL – 16 hrs 135°C & 5 hrs 155°C SAR-TL – 2 min. 220°C
3) Only calibrated radioactive sources should be used	☑	Irradiator 1 (~ 3 Gymin^{-1}) was calibrated to NPL in 1998 and recalibrated internally in Jan 2000; Irradiator 2 (~32 Gymin^{-1}) was calibrated against irradiator 1 by SJR in Dec. 1999 before quantitative dating analysis
4) Quadruplicate measurements should be used for luminescence age measurements	☑	MAAD-TL – 8 x 2 duplicates used per run; SAR-TL - 8 discs used
5) The sensitivity to solar resetting of the luminescence signal should be assessed for each sample to provide better definition of the residual level	☑	The glass-phase of the Óþoli Tephra is not sensitive to solar resetting, hence the use of thermal resetting in regeneration experiments. No residual in regeneration experiments, hence ED = palaeodose.
6) Growth curve functions should be constrained by at least 5 additive dose data sets and the projection used to determine the individual equivalent dose values should be < 20 % of the highest applied dose	☒	Óþoli Tephra – MAAD-TL - 5 datasets used in a heuristic manner due to disc-disc variations in response to irradiation. Projections were > highest applied dose due to unexpectedly old age of the Óþoli Tephra (see also 7)
8) Standard statistical procedures should be used to define mean and errors	☑	Errors in ages are overall errors propagated from various errors in palaeodose and dose rate measurements. Individual errors are standard analytical errors unless stated
9) Equivalent dose data should be plotted for each sample to provide maximum data for final ED determination and enable evaluation of the stability of the luminescence signal	☑	Figures 4.22-4.24
10) An alpha efficiency factor should be determined for each sample	☑	Table 4.6



11) Forman *et al.*(2000) advocate the use of total and partial bleach methods for TL analysis.	☒	SAR-TL was developed because significant disc to disc variation was encountered in MAAD-TL experiments. Further experiments on the Óþoli Tephra should concentrate on multiple aliquot and regeneration from HF etched samples. MAAD will probably be the most suitable technique for ÞIG samples and further attempts should concentrate on rigorous purification and TL dating of the co-ignimbrite ash layer ÞIG 1b because it is stratigraphically well-constrained
12) All samples should be tested for anomalous fading by storage of irradiated discs for at least 30 days with subsequent measurement and comparison with non-stored discs.	☑	60-70 day fading tests used on half the discs in each sets for MAAD-TL and SAR-TL experiments. NO significant anomalous fading was encountered.
13) At least duplicate luminescence age estimates should be obtained on each stratigraphic unit	?	The bracketing stratigraphic units at Skagafjall and Þörsmórk are unsuitable. The ages of the Óþoli Tephra and the Þörsmórk Ignimbrite were independently constrained using fission-track and/or correlation dating techniques
Prescott & Robertson (1997) (not in Forman *et al.*, 2000)		
1) Zero age samples should be included in the test program and should return zero ages	☑	There is a small detectable signal from the glass-phase of the A1875 and Ö1362 tephras. In both cases it is located in the unstable low temperature region of the glow curve, but there is also a small stable component. This is consistent with 'zero' and 'near–zero' ages, respectively, and possibly datable with adaptation of standard SURRC-TL reader equipment.

Notes: A tick indicates that the recommendations were completely satisfied; a question mark indicates that the recommendations were partially satisfied; a cross indicates that the recommendations were not fully satisfied and/or further work needs to be undertaken to meet the recommendations. Recommendations are from Prescott and Robertson (1997, p. 918) and Forman *et al.* (2000, p. 169-170).

Table 5.2 Common factors affecting the accuracy and precision of luminescence dating (from Forman *et al.*, 2000) and detailed assessment of their impact on TL age estimates for the Óþoli Tephra (OT: SUTL 551/552) and Þörsmórk Ignimbrite (ÞIG 7).

FACTOR	General & specific effect on TL age estimates[1]	Assessment of the effect on Óþoli Tephra (ÓT) & Þórsmörk Ignimbrite (ÞIG) age estimates
Inadequate compensation for partial solar resetting of the luminescence signal	**Overestimate in age by 10-200%** **OT – 0%** **ÞIG – 5-10%** **(overestimate)**	• Event being dated is the thermally well-defined formation of volcanic glass, *i.e.* the quench-phase of an explosive eruption. Effective optical bleaching of the natural TL signal in the Óþoli Tephra was not possible. Slope deposits of the Þörsmórk Ignimbrite have approximately the same level of stored signal as their buried equivalents. This suggests the natural TL signal in volcanic glass is overwhelmingly due to the release of electrons from heat sensitive traps and that volcanic glass is insensitive to optical resetting. • No thermal or optical partial resetting of the TL signal occurred during burial for the Óþoli Tephra. • Thermally-induced, partial resetting is possible, but unlikely, for the Þörsmórk Ignimbrite. ÞIG 1b and ÞIG 7 are located in a volcanically active region, but were capped by a thick black tuff deposit associated with the same eruption. There is no evidence for direct contact with lava flows, but this cannot be completely ruled out because of intense glacial erosion in the region.
Inadequate compensation for non-linearity in luminescence	**Overestimate in age by 10-100%** **OT – 10-20 %** **ÞIG – 0-5 %** **(overestimate)**	• Natural signal in the Óþoli Tephra is beyond first linear growth and saturation phase. For SAR-TL, fitting a single saturating + linear regression curve produces a second phase of linear growth. Goodness of fit is high. Sample sensitivity change during heating is not considered significant. Fading corrected SAR-TL ED values, obtained by interpolation, and spectrometry based dose rates are considered most accurate. ED values from MAAD-TL experiments with a 5 hour, 155°C pre-heat, obtained by linear regression of second phase growth and corrected for the effects of sub-linear growth produce ages similar to independent, fission-track age estimates. • Natural signal of ÞIG7 falls within the first linear growth phase. Sensitivity changes are significant, hence the ED value, obtained by interpolation, is likely to be accurate assuming sensitivity changes have been adequately accounted for (see below). Ages obtained are similar, but slightly younger than expected correlation ages of *ca.* 48.5 ka. Regeneration techniques commonly produce age underestimates (Rendell and Townsend, 1988). Given its age, an additive dose technique might be more suitable for the Þörsmórk Ignimbrite if a homogeneous dose response can be obtained.
Uncertainty in moisture content	***Decrease in precision by 10-40%*** ***OT – 5-10 % accuracy error; up to 30% precision error*** ***ÞIG – 5-10 % accuracy error; up to 50% precision error***	• This is the largest source of inaccuracy and imprecision for TL dating of both samples. Uncertainties in seasonal water content fluctuations make assessing average palaeowater content difficult. It is unlikely that the summer 'as found' water content are representative of a whole year in the Icelandic environment. Therefore, the mid-point between summer 'as found' and saturation water contents were chosen as best representing average palaeowater content for both the Óþoli Tephra and Þörsmórk Ignimbrite samples.

contd.

Disequilibrium in U and Th decay series	***Variable, over or underestimate by 5-50%*** ***OT- 0-5%*** ***ÞIG – 5-10%***	• Not measured directly; assumed to be minimal for the Óþoli Tephra because of similarity between elemental and spectrometry and homogeneous and heterogeneous dose rate estimates. • Possibly exists for the Þörsmórk Ignimbrite due to difference in homogenous and heterogeneous dose rates, but insignificant compared to uncertainty associated with palaeowater content estimates.
Anomalous fading	Underestimate in age by 5-50% OT – 0-5% ÞIG – 0%	• Two month fading test results indicate that there is a ~15 % loss in the overall TL signal from the Óþoli Tephra in the SAR-TL experiment and ~8 % total loss of signal for the Þörsmórk Ignimbrite (ÞIG7) sample. Anomalous fractional loss of signal (greater than 0.90 which is within experimental error; Forman *et al.*, 2000) for the Óþoli Tephra is 0.04 ± 0.01 for SAR-TL. Fractional loss from the Þörsmórk Ignimbrite, at 0.92 ± 0.01 is within experimental error. For the MAAD-TL experiment the weighted mean fractional loss for the Óþoli Tephra is 0.95 ± 0.05, *i.e.* within the bounds of experimental error. Additional notes: (1) Overall fading losses are 10-15 % less than losses encountered in volcanic feldspars of a much younger age (*e.g.* Wintle, 1973). (2) Short, high temperature pre-heats of 220°C for 2 minutes were used in this experiment to maximise the available laboratory time. This invites problems associated with anomalous fading and can lead to plateau artefacts (Berger, 1992). Longer, low temperature pre-heats may reduce fading losses and produce more precise ED estimates
Non-analogous response to laboratory irradiation, due to sensitivity change	Variable, but could result in underestimates by >25% OT – 10% ÞIG (FC^2) – 25 % ÞIG (FSC^3) – 0-5%	• This could be a factor in MAAD-TL dating of the Óþoli Tephra with possible ED underestimation of up to *ca.* 10%. Potentially a significant problem for fading corrected SAR-TL experiments, but the inclusion of a test dose after each applied dose allowed sensitivity changes to be monitored and corrected for. For SAR-TL dating of the Óþoli Tephra the TL intensity of the 100 Gy test dose not show a linear increase. Variations in 100 Gy TL intensity are within a single standard deviation throughout. This suggests changes in sensitivity exist, but are not significant, perhaps leading to age underestimates of 10%. • For the Þörsmórk Ignimbrite the TL intensity of the 25 Gy test dose increases in a linear manner and variations in 25 Gy test dose intensity increase in a similarly linear manner. This suggests changes in sensitivity are more significant and need to be corrected for. Without correction ED underestimates of up to 25 % occur (*e.g.* 241 Gy fading and sensitivity corrected vs 182 Gy fading only corrected *i.e.* ED underestimate of 25%). With correction ED underestimate possibly reduced to 0-5%.
TOTAL + or –	**OT: 0-5 % max age overestimate** **ÞIG 7 (FSC): 5-10% max age overestimate**	

Notes: [1]Factors that cause age overestimates are in bold type; factors that cause age underestimates are in normal type; factors that can cause under- or over-estimates are in italics. [2]FC=fading corrected; FSC=fading and sensitivity corrected.

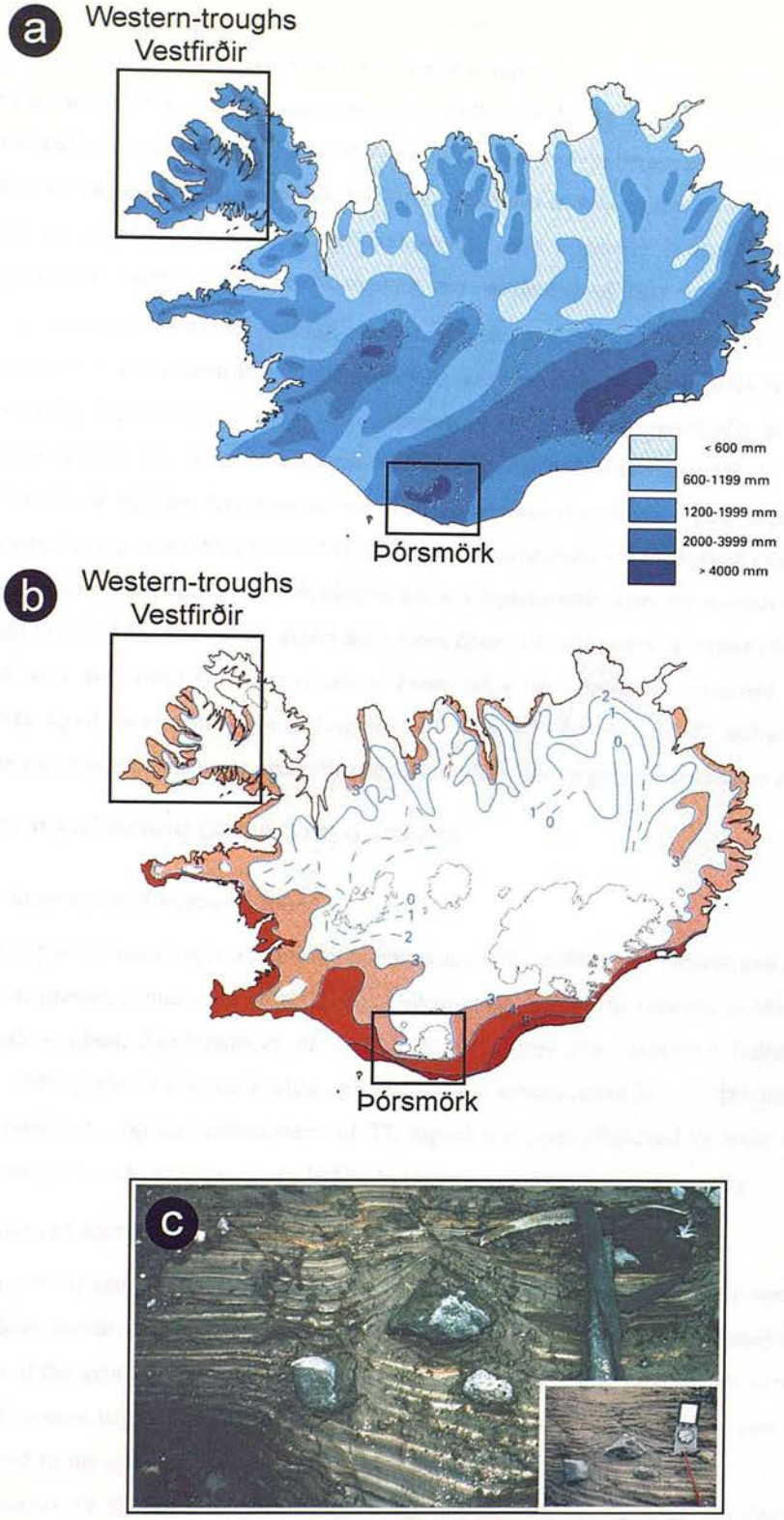


Figure 5.1 (a) Mean annual precipitation map of Iceland for the period 1931-1960 **(b)** Mean annual temperature map for Iceland (from 1:250,000 map series - all sheets, Icelandic Geodetic Survey). The Western Troughs of Vestfirðir and the Þórsmörk region are amongst the wettest and coldest parts of Iceland with annual mean temperatures less than 4°C and more than 2 m of rainfall on average each year **(c)** Dropstones in near-saturated rhythmite bed no. 8 near the end of July 1999 with, in inset, the same deposit from mid-July 1998. Section A from Unit 3 upwards was fully exposed in mid-July 1998. In July 1999 snow patch covered section A from this point downwards. (a)-(c) illustrate the influence of snow patch development on sample water content. In addition, this figure illustrates the variability and atypical nature of sampling conditions encountered in June-August 1998 and late June-early July 1999 when the Skagafjall secton B samples SUTL 500 and SUTL 551-558 were collected respectively.

In feldspar-phase TL/OSL dating, radioactive element composition varies significantly between grains because of the range of feldspar compositions in the bulk matrix (Fig. 4.19-a). Hence, the contribution from internal and external grain radioactivity is variable. Incomplete removal of the alpha-dosed outer layer is a known cause of inter-grain and disc-disc variations in luminescence dose response (Stokes 1994). Since no micro-inclusions or microphenocrysts were observed in the Óþoli Tephra shards during fission-track analysis, this could explain the variations of this type observed during the MAAD-TL experiment. Brief HF etching is used in feldspar dating to remove the outer 3-4 μm of density separated fractions contribution from internal and external grain radioactivity is variable. The bulk matrix of the deposits examined is overwhelmingly composed of chemically homogeneous silt-sand sized glass shards. The proportional compositions of radioactive elements (K, U, Th) for the bulk and grain specific or purified fractions of the deposits examined and the, Óþoli Tephra in particular are broadly similar, *e.g.* K_2O (bulk) = 2.16±0.11, K_2O (grain-specific) = 2.75±0.14 (Tables 4.1-b, 4.7). More complex treatment of dose rate calculation did not significantly alter the overall dose rate for the Óþoli Tephra (Table 4.8). Therefore, alpha dose from decay of radioactive elements from within each glass shard and the outer-rim contribution from adjacent shards is assumed to have been approximately equal on a macroscale during burial[35] (Fig. 4.19-b). Hence, HF etching may not be a pre-requisite for obtaining accurate age estimates from glass-rich highly silicic tephra deposits.

5.1.2 Factors affecting palaeodose values

(a) TL characteristics of volcanic glass

Resistance to optical bleaching is a common phenomena in TL studies of volcanic and certain types of archaeological glasses (Sanderson *et al.*, 1983; Göksu *et al.*, 1988). In relation to bleaching tests on modern window glass, Sanderson *et al.* (1983, p. 291) state that '[thermal fading] and optical bleaching ... take place as expected, although the highest temperatures [*i.e.* > 300-400°C] are barely affected.' Conversely, optical inducement of TL signal has been observed in most man-made and archaeological glasses (Sanderson *et al.*, 1983), but it was not observed in this study.

(b) Distribution of sample on disc

Zimmerman (1970) and Spooner and Allsop (2000) suggested that sample centre-periphery applied laboratory dose variations are significant. The critical area for luminescence dating applications is within 5 mm of the axial centre of the disc *i.e.* the radius of 10 mm aluminium discs used in this study. For a 15 mm source to sample gap the reduction in dose received by the sample can be as much as 15% compared to the axial centre. Overall, the peripheral 10 % of a 10 mm disc (*i.e.* the outer 0.26 mm rim) receives 12 % less dose than that received by the central 10 % of the disc (Spooner and Allsop, 2000). No age dependent pattern directly related to this effect emerged from the MAAD TL dating studies from the Óþoli Tephra. Only 50 % of runs with the sample centred on the disc were successful. Runs 3A&B (sample distributed evenly across disc) and run 5A (sample centred on disc)

[35] Assuming no microscopic dose boundaries exist

produced similar palaeodose values (Fig. 4.22; Table 4.10). This suggests when high, well-calibrated laboratory doses are applied, the centre-periphery dose variations are a relatively minor concern compared to other more important controls on dose response, *e.g.* pre-heating regime chosen.

(c) Pre-heating

The pre-heating regime chosen can cause significant palaeodose inaccuracies (Roberts *et al.*, 1993, 1994). The main purpose of pre-heating is, firstly, to empty unstable traps that give rise to the low temperature artificially induced 100-150°C peak and secondly, to reduce the effects of anomalous fading from unstable traps at higher temperatures. All pre-heating regimes used in this study achieved the former. The success of the latter is evaluated in this section.

The MAAD-TL ages of the Óþoli Tephra indicate a relationship between pre-heating regime and age accuracy, assuming the final weighted mean homogeneous/heterogeneous matrix model dose rates are an accurate representation of average palaeodose rate (Fig. 5.4; Table 5.3). Sixteen hour, 135°C pre-heats had an unexpectedly detrimental affect on the palaeodose, producing apparent age shortfalls of on average 50 %, while ages obtained using shorter, higher temperature pre-heats (*i.e.* 5 hour, 155°C or 2 minute, 220°C) are closer to the fission-track age. These findings contradict ideas and recommendations in glass-phase tephra TL dating and alkali feldspars IRSL studies where shorter pre-heats are generally discouraged because they invite problems of anomalous fading (Berger, 1991; Clarke and Rendell, 1997). However, the choice of pre-heating regime remains a contentious issue (Berger, 1992, 1995; Roberts *et al.*, 1993, 1994; Stokes 1996). For example, Roberts *et al.*, (1993, 1994) found that even long, low temperature pre-heats can lead to palaeodose underestimates. The 5 hour 155°C preheating regime appears particularly robust because it produce age estimates similar to the fission-track age even though different normalisation doses of 600 Gy (MAAD5) and 1200 Gy (MAAD3) were used. The findings of this study concur with those of Roberts *et al.* (1993, 1994). It is possible that deep trapping sites in the glass matrix are not as stable as those in feldspar matrices at above ambient temperatures. Electrons in glass-matrix deep traps are, therefore, more susceptible to eviction during long pre-heats. In conclusion, if the effects of anomalous fading can be contained and/or corrected for by shorter high temperature pre-heating regimes then longer low temperature preheats would appear to be both detrimental and unnecessarily time-consuming in volcanic glass-phase dating. Further investigation of this effect using volcanic glass would be beneficial.

(d) Anomalous fading

Despite the age of the Óþoli Tephra no serious fading beyond that associated with normal experimental error was measured during the course of the TL dating experiments. Aitken (1998: p. 218) warned that 'samples showing age shortfall do not always show loss during laboratory storage tests'. Nevertheless, the absence of serious anomalous fading in 60-70 day fading tests is encouraging. A simple explanation is that the pre-heating regimes chosen were adequate. A more complex one is

that anomalous fading is not an issue for the samples examined. If the latter is the case it requires further explanation for the following reasons:

1) Volcanic glass-phase fission-track ages became accepted as accurate over the last decade and a half as the mechanisms of glass-phase track fading were progressively understood. This led to the development of experimental methods such as the isothermal plateau and diameter correction procedures that compensate for the loss of signal and allow accurate ages to be produced (Westgate, 1988; Westgate *et al.*, 1997).

2) Anomalous fading is serious problem that compromises the accuracy of luminescence ages (Wintle, 1991). Fading can be either thermal or athermal (anomalous). Berger (1991, 1992) refers to anomalous fading in relation to pre-heat selection (see above), but published data for TL dating of highly silicic volcanic glass formed by explosive eruptions is sparse. In contrast, the anomalous fading literature for felspathic minerals of volcanic origin is extensive and detailed. Feldspars of volcanic origin are common, have a high TL sensitivity and linear dose response, but anomalous fading is problematic reducing confidence in ages obtained. Wintle (1973, 1977, 1978) first demonstrated that labrodorite minerals from volcanic lavas exhibited substantial anomalous fading. No simple relationship between chemistry and anomalous fading has been found, but a relationship between order and fading has been suggested (Spooner, 1994). The highly ordered end members of the alkali feldspar series do not exhibit anomalous fading (Spooner, 1994), unlike calcium rich, plagioclase feldspars (*e.g.* andesine, labradorite and bytownite) which exhibit the most dramatic fading (Visocekas, 1985; Prescott and Robertson, 1997).

Anomalous fading is considered an unassailable barrier to the successful dating of volcanic products (Prescott and Robertson, 1997). However, various studies have produced evidence to the contrary. Göksu *et al.* (1988) showed that dose dependent fading of obsidians only occurs at high doses close to the saturation level. Zink and Visocekas (1997) found that the near infrared TL emission from sanidine feldspars are stable. Smith and Sanderson (*submitted*) suggested that the TL signal from volcanic feldspars is composed of stable and unstable components and that a structured distribution of traps and centres leads to "periods of loss at distinct rates" rather than progressive decay. Accurate TL dating is, therefore, possible where evidence for signal stabilisation over laboratory time scales exists (Clark and Templer, 1988; Smith and Sanderson, *submitted*). Studies have shown that two months storage at room temperature is often long enough for stability to be achieved (Visocekas, 1985; Clark and Templer, 1988); hence its application in this study.

(i) Existing Models of Anomalous Fading

Models of possible mechanisms for anomalous fading are described in detail in Aitken (1985; p. 274-281; 1998: p. 219-225) and Smith and Sanderson (*submitted*), but the process is still not fully understood. Suggested mechanisms include recombination by quantum mechanical tunnelling, loss of signal due to localised transitions where luminescence acceptor centres in an excited state facilitate the escape of electrons from neighbouring traps (Templer, 1986) or by decay of luminescence centres during the burial period (Wintle, 1977). Templer (1986) and Smith and Sanderson (*submitted*) proposed that anomalous fading is temperature dependent with tunnelling dominant at low temperatures and localised transitions more prevalent at high temperatures. Quantum mechanical tunnelling is currently the favoured mechanism for anomalous fading (Aitken, 1998). In the tunnelling model trapped electrons can escape by wave-mechanical tunnelling in addition to conduction band escape. No additional energy in the form of temperature induced lattice vibrations is needed; hence the term athermal fading. Unlike conduction band escape, which is proportional to the energy input, athermal escape proceeds in decreasingly logarithmic manner until it becomes difficult for electrons to escape (Aitken, 1998). For anomalous fading to occur via the tunnelling mechanism activated acceptor centres are required. Acceptor centres are abundant in highly disordered structures that have a high density of lattice defects; hence the relationship between disorder and anomalous fading (Aitken, 1998). For this reason volcanic glass with little long term periodic order might be expected to exhibit serious anomalous fading effects.

(ii) New cooling rate model for model for anomalous fading

Two factors are suggested to explain the absence of anomalous fading in the highly silicic volcanic glass examined:

1) Experimental procedures

In this scenario the glass matrix is as susceptible to anomalous fading as certain other volcanic products and anomalous fading would have occurred if the chosen correction procedures had not been employed. Fractional fading coefficients outside the 0.9-1 range associated with experimental error (Forman *et al.*, 2000) only occurred in the SAR-TL experiment on the Ôpoli Tephra where a 220°C, 2 minute pre-heat was used and a coefficient of 0.86±0.02 was measured. A fractional fading coefficient of 0.92±0.01 for the Þórsmörk Ignimbrite was measured in the SAR-TL experiment. The SAR-TL fading coefficient for the Ôpoli Tephra is not significantly less than 0.90 or the SAR-TL fading coefficient of the Þórsmörk Ignimbrite. The lower fading coefficients approaching or exceeding the 0.90 experimental error limit both occurred in the SAR-TL experiment. The weighted mean fractional fading coefficient for the MAAD-TL dating experiment on the Ôpoli Tephra is 0.95±0.05. The loss due to athermal fading processes in the SAR-TL is not serious, but the lower fading coefficients recorded are possibly related to shorter, high temperature pre-heats that were only just adequate in dealing with the effects of anomalous fading.

2) The formation process and nature of the material

The event being dated in volcanic glass-phase dating is the formation of the glass matrix. Highly silicic volcanic glass has a uniquely rapid formation process: near instantaneous quenching (from the melt) followed by explosive ejection and exceptionally rapid liquid-solid phase cooling creates a tephra matrix overwhelming dominated by glass. It is proposed that this exceptionally rapid rate of cooling could be a significant factor controlling anomalous fading. Volcanic glass in the tephra deposits from highly explosive eruptions has little long-term periodic order and is best visualised as a rapidly frozen liquid. Exceptionally rapid cooling creates very few defect, acceptor centre pairs in close proximity or widely spaced, randomly distributed defect, acceptor centre pairs whose spacing in the disordered lattice is sufficient to prevent tunnelling processes. Both of these scenarios explain the relatively low TL sensitivity of highly silicic volcanic glass from explosive volcanic eruptions.

The wide range of glassy or minerogenic extrusive volcanic products, such as obsidian and certain feldspar minerals, that are created by relatively slow-medium rates of cooling are most effected by anomalous fading (Fig. 5.2). A greater degree of order is established in obsidian compared to rapidly-cooled volcanic glass, but the slower cooling rate provides an opportunity for the creation of a high density network or preferential clustering of lattice defect, acceptor centre pairs in close proximity (Smith and Sanderson, *submitted*). These are not randomly distributed and serious anomalous fading occurs.

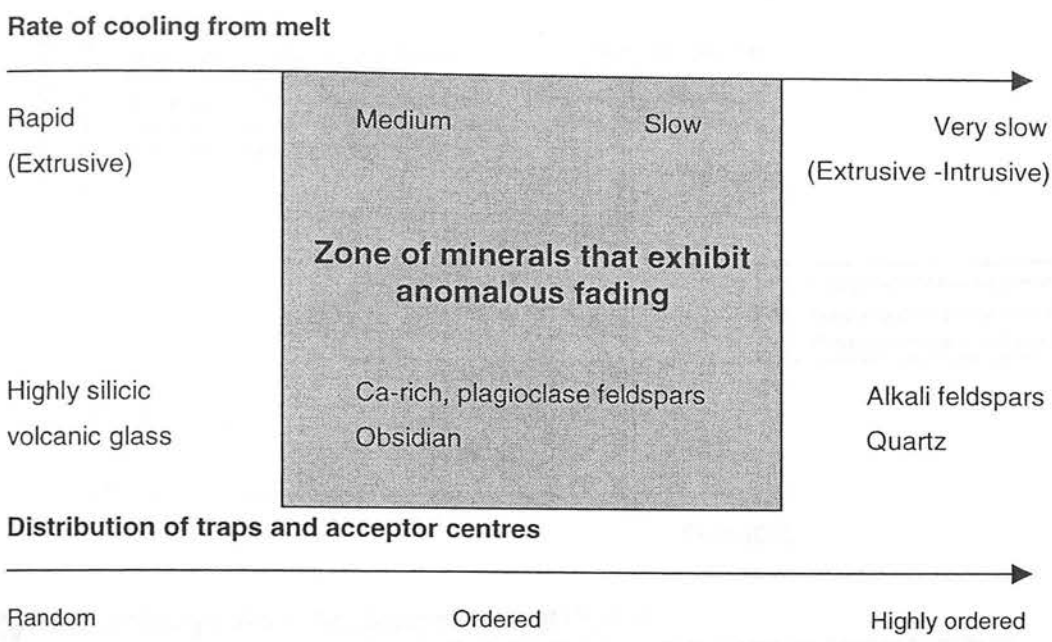


Figure 5.2 Proposed model illustrating the relationship between rate of cooling and anomalous fading for volcanic products

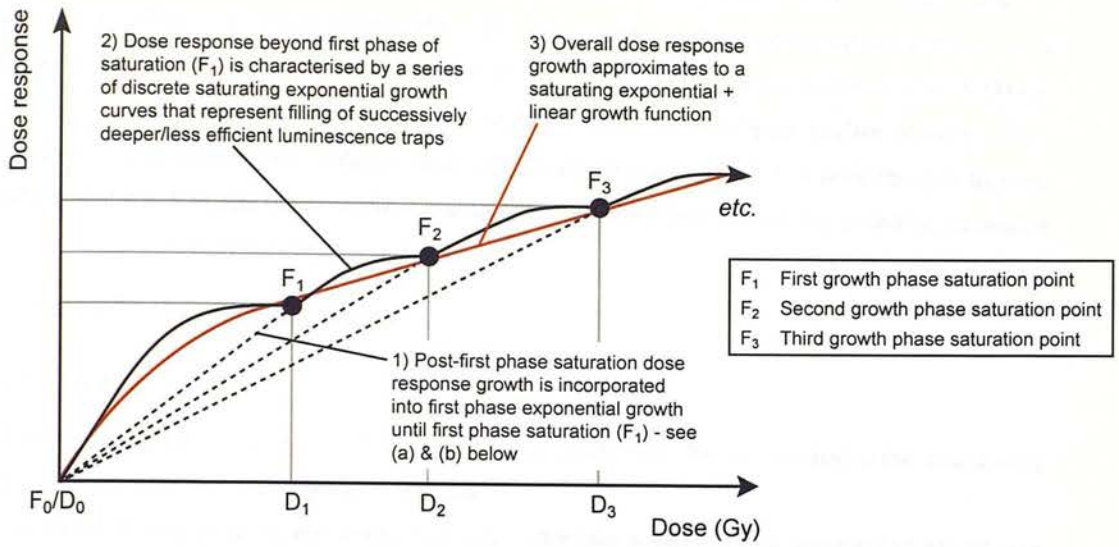
(e) Mechanisms of post-saturation dose response growth characteristics

Establishing a mechanism for the observed post-saturation growth of the glass-phase signal is important because of the enormous potential for direct TL dating glass-rich tephra deposits older than 0.5 Ma. Post saturation growth of the Óþoli Tephra SAR-TL signal after first phase saturation is only approximately linear. Additive dose and regeneration experiments suggest that this phase is constructed from a series of progressively stepped saturating exponential components of similar saturating exponential form to the first, or primary growth phase of the TL signal. In combination this creates a post saturation growth characteristic that is best and most easily described by fitting a linear regression function. The following explanation deals with the first and second growth phases only, but is applicable to all successive growth phases, *e.g.* second and third, third and fourth *etc.*

The proposed model is summarised in Figure 5.3. Trap combination and emptying processes are far less efficient for the second phase of TL signal growth compared to the primary growth phase of the TL signal. Trapped electrons for the second phase are from deeper traps that those released during first phase growth. During first phase growth, second phase traps are relatively inefficient at realising their luminescence potential. Linear growth occurs for the second phase TL growth throughout first phase growth. It does not contribute significantly to the first phase of linear growth and only becomes apparent when the first growth phase has fully saturated. This 'stacking' process continues with each successive growth curve representing eviction of electrons from traps at progressively deeper energy levels within the conduction band. The TL capability (efficiency) of each level of deeper trap is less

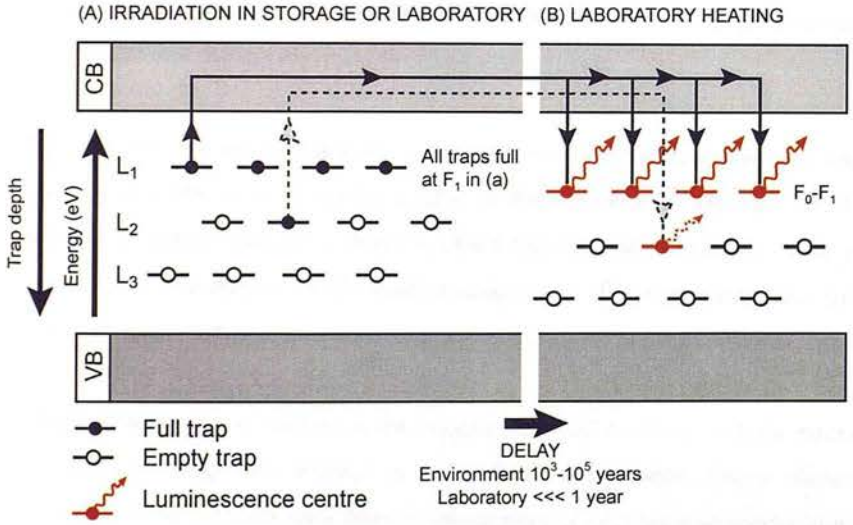
a Multi-phase TL dose response model for the volcanic glass-phase of Icelandic tephra

(based on MAAD-TL & SAR-TL dose response characteristics of the glass-phase of the Óþoli Tephra)



b First phase growth to first saturation point (F_0-F_1)

Storage time ≡ time represented by D_0-D_1 in (a); arrows relate to laboratory heating transitions

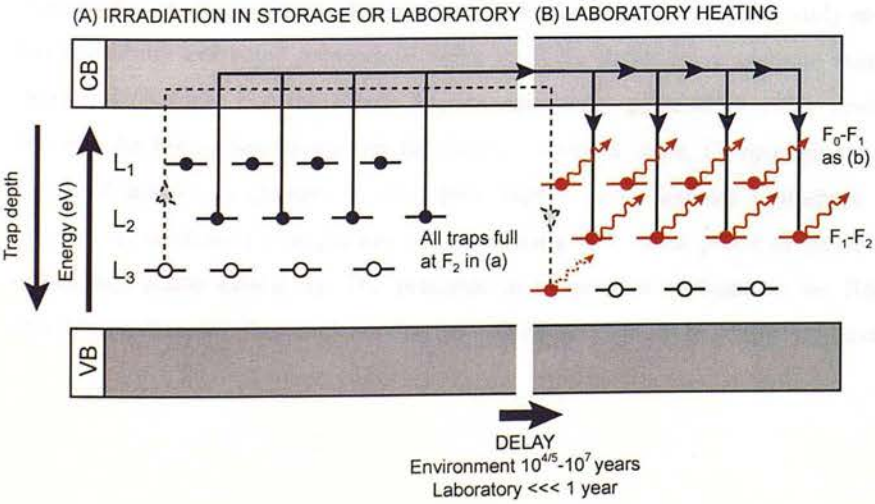


(A) Most samples used in luminescence dating represent trap filling storage times represented by the D_0-D_1 storage dose range. Relatively few L_2 traps are filled and

(B) Luminescence from L_1 recombination overwhelming contributes to first phase F_0-F_1 growth to full saturation at F_1. There is some contribution from electrons trapped at level L_2. There is a small contribution to F_0-F_1 growth from L_2 level recombination. Luminescence from L_2 is limited because because few traps were filled during storage and/or recombination is less efficient compared to L_1 level traps

c Multiple phase growth (F_0-F_3 *etc.*) (Illustrated using F_0-F_2 growth)

Storage time ≡ time represented by D_0-D_2 in (a); D_0-D_1 as (b)



(A) Extended storage time fills progressively deeper traps

(B) F_0-F_1 growth is as in (b) above. There is a small contribution to F_0-F_1 growth from L_2 level recombination. This greater than as described in (b), but still relatively insignificant because recombination processes are far less efficient for L_2 traps compared to L_1 traps during first phase (F_0-F_1) growth. Once first phase saturation is complete, *i.e.* at F_1 in (a), second phase growth dominates until it saturation point at F_2 with some contribution from partially filled L_3 level traps. Third phase growth dominates once second phase saturation is complete, i.e. at F_2, and so on.

Figure 5.3 Highly simplified multi-phase thermoluminescence dose response growth model for volcanic glass **(a)** Form of observed dose response **(b)** Simplified electron-hole trap depth/energy representation of luminescence production for (a). See also Figure 2.10.

than the immediately proceeding one. This explanation accounts for all the results obtained, including the preliminary additive dose test results (Fig. 3.7). In the preliminary experiments the natural signal in the Óþoli Tephra was greater than the N+600 Gy and N+1200 Gy. A palaeodose of *ca.* 1200 Gy was obtained, hence early, Mid-Pleistocene age underestimates for the Óþoli Tephra (Roberts *et al.*, 1999, 2000). These preliminary additive dose tests were misleading and it is now thought that the N+600 Gy and the N+1200 Gy were from the initially rapidly rising part of the post-first saturation phase TL growth curve profiles shown in Figure 5.3.

5.1.3 Final TL Age Assessment

(a) Óþoli Tephra

Two explanations were put forward before fission-track results were known to explain the quantitative TL dating results obtained from the Óþoli Tephra.

1) The Óþoli Tephra is an exceptionally 'old' (*i.e.* >0.5 Ma) tephra deposit and the MAAD-TL age estimates obtained using a 5 hour 155°C pre-heat and the SAR-TL age range are accurate assessments of the 'true' geological age.
2) The single aliquot regeneration approach adopted and/or the high laboratory dose rate of *ca.* 32 $Gymin^{-1}$ fundamentally altered the TL characteristics of the glass creating spurious regeneration results that did not replicate the natural dose cycle.

Initially, the second explanation was favoured, principally because a slight discolouring of disc material was observed during the course of the regeneration experiments. This was thought to be an artificial-radiation induced colouring effect that has been noted in other glass-phase luminescence studies (*e.g.* Sanderson, 1982). Further support for this explanation was provided by the apparently heterogeneous response to artificial radiation observed in the MAAD-TL experiment.

Changes in sample sensitivity is the biggest potential problem with the equivalent dose and dose rate reconstruction approach adopted in the SAR-TL experiments. Single aliquot procedures have so far been limited to optically stimulated luminescence (OSL) because thermoluminescence is a destructive technique that changes the samples TL sensitivity (Duller, 1995; Murray and Roberts, 1998; Forman *et al.*, 2000; Zander *et al.*, 2000). Test dose normalisation in the SAR-TL provided useful indicators of relative changes in sensitivity during the experimental process, but they only show whether the fading and sensitivity corrected palaeodose value is likely to be more accurate than the fading corrected palaeodose values. For the Óþoli Tephra, the 'true' palaeodose value probably lies somewhere between the fading-sensitivity and the fading corrected value. Comparisons between the degree and nature of sensitivity changes in the Óþoli Tephra and Þörsmörk Ignimbrite SAR-TL experiments suggest TL sensitivity changes are greatest during first linear phase of linear dose response growth before first phase saturation. The presence of palaeodose plateaux in the SAR-TL experiments is encouraging because they indicate that no non-linear changes in sensitivity have occurred. Moreover,

the SAR-TL method adopted has produced TL age estimates that are similar to independent and accurate fission-track age controls. Nevertheless, quoting minimum-maximum age ranges with suggestions as to which age is considered more accurate was considered the most appropriate way to quantifying sensitivity changes that occurred in the SAR-TL procedure adopted.

A second potential problem with the experimental procedure is that even the smallest laboratory dose rates are several orders of magnitude greater than those experienced in the natural environment. This creates two problems:

1) High laboratory doses tend to fill or saturate shallow, thermally unstable traps. This does not occur in natural irradiation processes and may lead to a differences in deep trap sensitivity (Wintle, 1997).
2) Chawla *et al.* (1998) showed that laboratory irradiation at 10^8-10^{11} (*ca.* 0.1-100 Gymin^{-1}) times greater than that experienced in the natural environment leads to defect creation, migration and, ultimately, defect complex creation that does not occur during natural irradiation. The higher than usual laboratory dose rates used in the quantitative experiments might exacerbate these effects.

The obvious solution is to reduce the applied dose rate. Dose rates for the preliminary regeneration tests were *ca.* 3 Gymin^{-1}. The higher dose rate was chosen for the quantitative experiments because applying kGy doses at this rate was time consuming and invited fading during the long exposure time. It is interesting to note, however, that the same general picture emerged for the preliminary regeneration experiment, *i.e.* the natural dose level at *ca.* 3600 Gy is far greater than expected.

(b) Þörsmórk Ignimbrite

A well-defined 48.5-58 ka correlation age was obtained for the unaltered glass-phase of the Þörsmórk Ignimbrite, but there were no spontaneous fission-tracks in the glass-shards of this deposit, suggesting an age approximation of <100-150 ka. The *ca.* 40 ka ÞIG 7-SAR-TL age estimate is less than the lowest correlation age and requires an explanation. In a similar study, the glass-phase TL age of 23.4±2.4 ka was obtained for deposits of the 75 ka Toba eruption (Horn *et al.*, 1993). This was substantially younger than expected. TL age underestimates were related to post eruption exposure to light during the last reworking event at the Bori site at Kukdi River, Pune, India or the difficulties in obtaining pure glass separates from silt-grade tephra. Local reworking had concentrated the tephra into a bed that was more than 1m thick and post-depositional light exposure was the preferred explanation. Exposure to light can be excluded as a reason for the slight age underestimate of the dated ÞIG 7 sample because:

- The undisturbed nature of the inter-bedded ash layers at site ÞIG 7,
- The depth from which the deposits were retrieved
- The resistance of volcanic glass to optical resetting (section 5.12-a)

If the correlation age is assumed to be correct, the SAR-TL age underestimate is most likely associated with various dose rate, equivalent dose parameter estimation problems already discussed and/or well-documented general problems with the regeneration technique that can lead to age underestimates (Rendell and Townsend, 1988; Duller, 1991). If the higher dose rates are correct, it is possible that equivalent values have been underestimated. Implementing a series of multiple aliquot additive dose experiments can check this. These should be successful given the *ca.* 40 ka age estimate obtained in this study. Reducing the age error ranges requires further *in-situ* dose rate measurements and a full assessment of seasonal fluctuations in water content. This task is more easily achievable for the Þörsmórk Ignimbrite than the Óþoli Tephra because of its accessible location.

A major concern for both fission-track and thermoluminescence dating of the Þörsmórk Ignimbrite is that the ÞIG samples have been affected by post-depositional thermal annealing. This would have the effect of partially resetting the formation age signal and lead to age underestimates. Although there are currently no thermal areas in the Þörsmórk region, post depositional thermal annealing cannot be completely ruled out because Þörsmórk is located in a active volcanic region. Nevertheless, the thick deposit of welded syn-depostional black tuff is assumed to have instantaneously capped the highly silicic ÞIG deposits providing a degree of insulation for the main ignimbrite unit. ÞIG 1b is better protected than exposed sections, *e.g.* ÞIG 7. It is likely that most of the sites had a similar protection to ÞIG 1b at some stage and that this has been removed by intense fluvio-glacial action along the Krossa and across the flat highland plateaux of the central Þörsmórk area.

5.1.4 Final Tephra Age Assessment

Many of the issues raised in the previous section, and summarised in Table 5.3, remain unresolved and need further investigation. Nevertheless, the range of dating evidence collected from the Óþoli Tephra and the Þörsmórk Ignimbrite suggest the TL age estimates and ranges for these deposits are reasonably accurate representations of the geological age. With issues discussed in the previous section in mind, Table 5.3 and Figure 5.4 presents a summary of the final ages for the Óþoli Tephra and Þörsmórk Ignimbrite. The ages considered most likely are shown in bold.

Type of Dating Method	**RADIOGENIC**			**CORRELATION**	
	Fission-track	Thermoluminescence		Geochemical	Palaeomagnetic
		MAAD-TL	SAR-TL		
Type of Dating Result	←	**NUMERICAL AGE**	→	← **CORRELATION AGE** →	
ÓÞOLI TEPHRA (Ma) [551/552] (airfall ash)	**2.26±0.11**	**2.06±0.27*** 1.03±0.11#	**Min: 1.74±0.37** Max: 4.69±0.74	-	**R: ~2.48-1.88**
ÞÖRSMÓRK IGNIMBRITE (ka) [ÞIG 7] (interbedded surge ash)	- (<<100-150)	-	Min: 29±7 **Max: 39±9**	**48.5**	-

Table 5.3 Final ages for the Óþoli Tephra and Þörsmórk Ignimbrite
This table is a summary of Figure 4.11 with ages considered most representative of the geological age highlighted in bold. See relevant tables in chapter four for explanation chosen methods used to calculate these ages; *Pre-heat = 5 hours @ 155°C; #Preheat=16 hours @ 135°C.

Óþoli Tephra

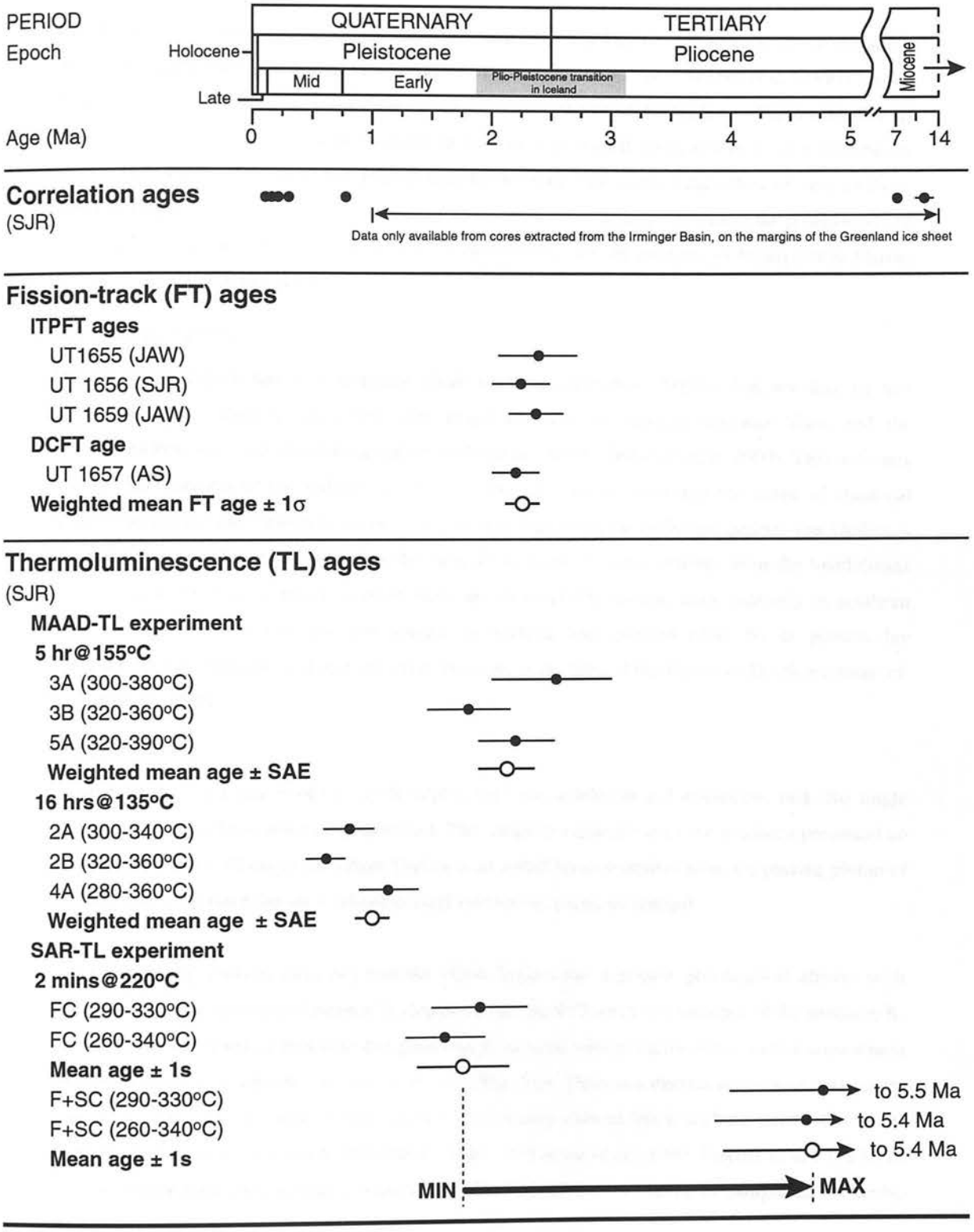


Figure 5.4 Summary of new ages from the Óþoli Tephra based on Tables 4.3-b (Correlation) , 4.5 (FT) & 4.11 (TL).For FT ages errors are as defined in Table 4.4. For TL ages, errors are standard age errors (SAE) propagated from standard analytical errors in each parameter measured. See Figure 5.16 for a summary of ages from the Þórsmörk Ignimbrite.

Chapter 5B: Palaeoenvironmental Implications

5.2 Source volcanoes

The sources volcanoes of the Þörsmórk Ignimbrite and other late Pleistocene deposits examined in this thesis are already well established (Thórarinsson, 1969; Jørgensen, 1981; Sparks *et al.*, 1981; Larsen *et al.*, 1999). The Óþoli Tephra and the massive basic component of the Hjallanes Tephra (Hj-2b) are from the two main types of volcanic system in Iceland (transitional alkali and tholeiitic) (Jakobsson, 1972; 1979). Figure 5.5 shows the relationship between the chemical composition of new analyses from this study and known evolution trends for the most active volcanic systems in the postglacial era. Figure 5.5-b is an attempt to identify source-sample distance for the products of highly silicic Plinian eruptions examined in this study.

(a) Hjallanes Tephra

The Hjallanes Tephra has a transitional alkali basalt composition. Tephra deposits that fit this classification are currently associated with eruptions from the Eastern Volcanic Zone and the Snæfellsnes Peninsula, off the main axial rift (Jakobsson, 1979; Gudmunðsson, 2000). This indicates that the configuration of the volcanic systems in the neovolcanic zone and the range of chemical products during the early Pleistocene is similar to eruptions from the Holocene period. The Hjallanes Hj-2b eruption may be related to either the early Pleistocene volcanic activity from the Snæfellsnes Volcanic Zone (SnVS) or to an eruption from an off-axial rift system, most probably in southern Iceland. This confirms that the rift system in Iceland had evolved close to its present-day configuration with distinct axial and off-axial rift zones at the time of the Hjallanes Hj-2b eruption (cf. Stecher *et al.*, 1999).

(b) Óþoli Tephra

Establishing the exact source of the Óþoli Tephra has been a difficult and incomplete task. No single volcanic system has been positively identified. The simplest explanation of the evidence presented so far is that the basal 8-10 cm of the Óþoli Tephra is an airfall layer deposited from the passing plume of a Plinian style eruption from an axial-rift central volcano in mainland Iceland.

Correlation dating analysis indicates that the Óþoli Tephra has a greater geochemical affinity with Tertiary and certain early-mid Quaternary deposits. The Óþoli Tephra is a member of the medium-K, calc-alkaline subdivision of tholeiitic compositions associated with a highly-silicic source somewhere along north and west axial-rift, *e.g.* Askja/Húsafell (Fig. 5.6). There is a distinct absence of data points in the SiO_2 = 60-70 wt % range. Compositional bi-modality such as this is a characteristic feature of certain Icelandic central volcanoes (McGarvie, 1984; McGarvie *et al.*, 1990; Stecher *et al.*, 1999). In addition, shards with intermediate compositions plot outside the envelopes of postglacial Icelandic

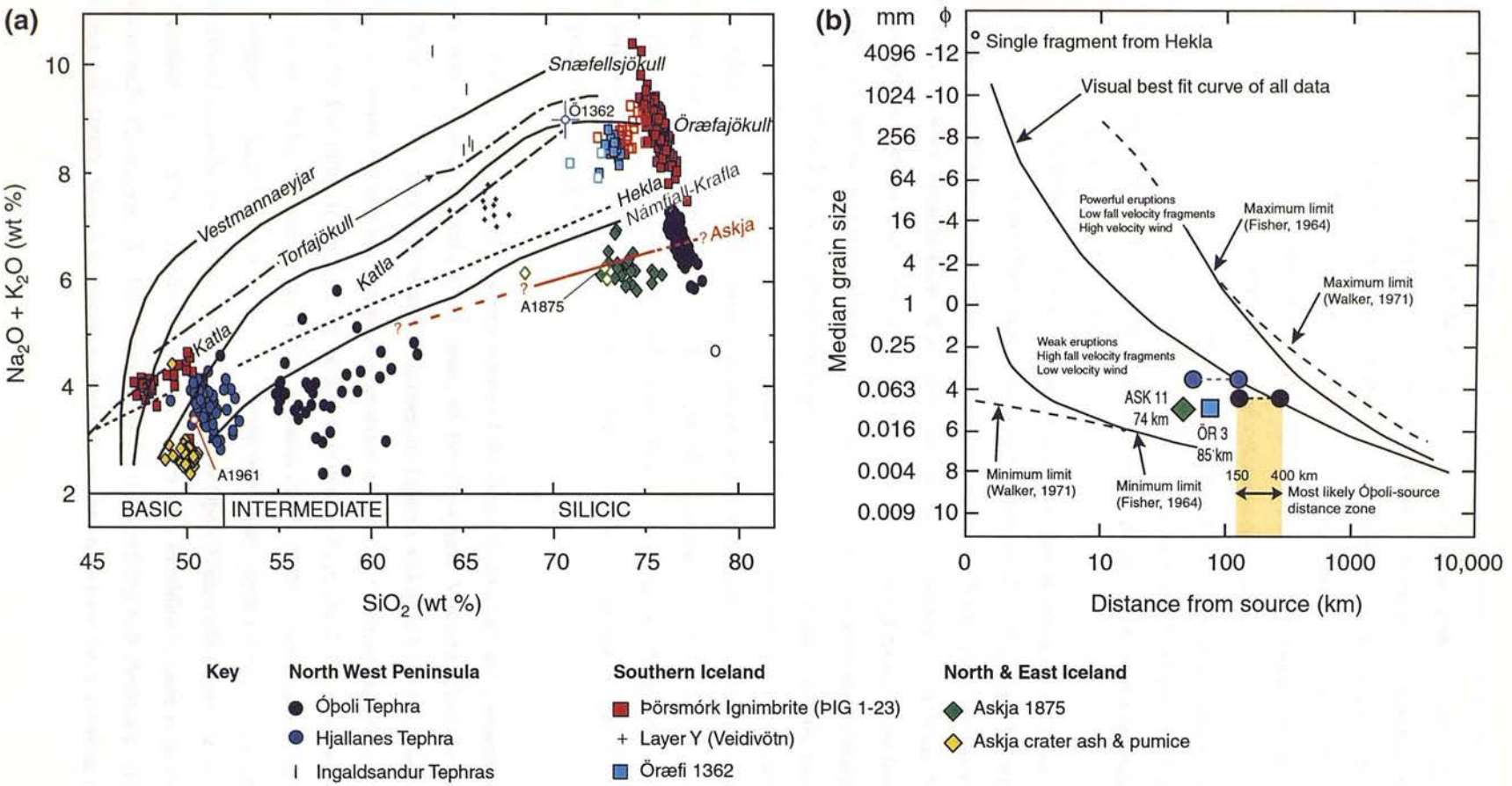


Figure 5.5 (a) Total alkali ($Na_2O + K_2O$) - silica (TAS) diagram showing the geochemical evolution trends of the most active Icelandic volcanic systems & zones of data with new glass analyses from 1998-2000. Evolution trends are based on hard rock analyses from Jakobsson (1979) & Óskarsson *et al.* (1985) except for the Askja evolution trend which is based on data analysed in this study with additional data from Sparks *et al.* (1981) & Larsen *et al.* (1999). Additional data for Ö1362 (blue circle with 1σ error bars) is from Sigurdsson (1982). New data has been recalculated to 100% on a volatile-free basis. **(b)** Median grain size vs distance from source for various tephra deposits (after Fisher & Schmincke, 1982). The yellow shaded area is a tentative distance from source range for the Óþoli tephra

eruptions suggesting, at the very least, a pre-Holocene-Lateglacial age for the Óþoli Tephra (Jakobsson, 1979). A simultaneous eruption from Jan Mayen cannot be entirely ruled out as an explanation for the intermediate composition. This scenario seems highly unlikely, however, given the direction of prevailing winds and Jan Mayen's remote location in the northern North Atlantic. It could be suggested that the Óþoli Tephra is a reworked deposit. Remnants of rhyolitic volcanism in Vestfírðir are restricted to the Drangajökull Peninsula, but there is evidence for at least five other extinct rhyolitic centres in the Vestfírðir Peninsula (Fig. 1.5) (Gudmunðsson *et al.*, 1996; Jóhannesson and Sæmundsson, 1998). It is unlikely that the Óþoli Tephra is a reworked deposit from glacial overriding and erosion of mid-late Pliocene central volcanoes because:

1) The basal 8-10 cm is structureless, very well-sorted and its thickness is laterally continuous as shown by its presence on the eroded upper surface of rhythmite bed 10 in sections B and C. These are characteristic features of extended upper-atmosphere plume transport and deposition (Cas and Wright, 1987; Sparks *et al.*, 1981; 1997).
2) The 2.26±0.11 Ma fission-track age is considered an accurate assessment of the 'true' age of the Óþoli Tephra. Although the Óþoli Tephra is similar to deposits from ODP site 917 with a >10.93-12.94 Ma palaeomagnetic age, there are numerous mid-late Pleistocene correlatives of similar composition; hence identification of a single correlation age estimate is difficult. Furthermore, palaeomagnetic ages are also correlation ages and it is likely that sediments in the Irminger Basin have had a complex depositional and burial history that might complicate palaeomagnetic age profiles. The Óþoli Tephra and Hjallanes Tephra have a chemical affinity with the two main types of volcanic system that exist in present day Iceland. This suggests that they were erupted at a time when tholeiitic rift-axis and transitional alkali-off-axis central volcanoes existed. Combinations of complex styles of volcanism, such as those described, appeared *ca.* 6 Ma (Stecher *et al.*, 1999) long after active volcanism had ceased on the Vestfírðir Peninsula. Mainland-Vestfírðir plume transport and airfall deposition is, therefore, responsible for at least one of, but most likely, both the Óþoli and Hjallanes Tephra.

The grain size characteristics and tholeiitic nature of the Óþoli Tephra indicate a source in the south-western or north-eastern, off-axis, flank zones of the Reykjanes Volcanic Zone or the Northern Volcanic Zone (Fig. 5.5, 5.6). The central volcanoes the Eastern Volcanic Zone have been eliminated on the basis of major element and correlation analysis as there is no chemical affinity to NAAZ1, NAAZ2 and the Þörsmórk Ignimbrite all of which originate from the EVZ (Thórarinsson, 1969; Mangerud *et al.*, 1984; Lacasse *et al.*, 1996; Zielinski *et al.*, 1997). Snæfellsjökull is the closest volcanic complex to Skagafjall. It is responsible for the only visible tephra layers in Holocene deposits in the Vestfírðir Peninsula, but the thoeliitic affinity of the Óþoli Tephra eliminates the alkalic centres of the Snæfellsnes Peninsula as a source (Figs. 4.7, 4.8, 5.5-b). In addition, there is no indication of late Pliocene–early Pleistocene (3.3-0.8 Ma) activity on the Snæfellsjökull Peninsula (Jóhannesson and Sæmundsson, 1998). Very few central volcanoes are known to have been active at the time of

Óþoli eruption *ca.* 2 ¼ Ma (Jóhannesson and Sæmundsson, 1998) (Fig. 5.2) and even fewer lie within the principal fallout source distance radius of 200-300 km suggested by the grain size of the airfall component of the Óþoli Tephra.

(i) Askja (Dyngjufjöll)

Sigurvinsson (1983) suggested Askja (Dyngjufjöll) was the most likely source of the Óþoli Tephra. Askja is located in the axial rift zone and produces rocks of tholeiitic composition. Some of the oldest rocks in the neovolcanic zone are found on the flanks of main caldera (Askja). These are presumed to be of mid-late Pleistocene age, but precise ages are unknown because the rocks are predominately basaltic in composition and are therefore difficult to produce numerical ages from (NVI, 2000). The Pleistocene formations have been subdivided into four distinct stratigraphic units. The units are all associated with sub-glacial or shallow sub-aqueous environments and consist of pillow lavas and hyaloclastites mixed with water-lain and mass flow sediments, air-fall ash and tuff deposits. No tillites have been found in the caldera[1]. Most of the deposits were formed in a predominantly shallow water environment created by ice dammed lakes. Each unit may represent a separate deglaciation period and it is possible that glacier unloading triggered a large but short-lived production pulse leading to their formation (Sigurdsson and Sparks, 1981; NVI, 2000).

During our visit in 1999 deposits were sampled from the eastern margins of the caldera (ASK 6-9). All were basaltic despite their yellow-white appearance in the field (Fig. 4.4, 4.7: Askja cater pumice and ash). The A1875 is currently the best available constraint on rhyolitic activity in the Askja-Dyngjufjöll volcanic system. Multivariate clustering and principal components analysis produced a clear distinction between the highly silicic A1875 eruption and the Óþoli Tephra (Fig. 4.10). This difference may reflect a shift in the major element composition at some time during the mid-late Pleistocene and/or a loss of mobile elements from the glass shards of the Óþoli Tephra during burial.

(ii) SW Iceland, Húsafell-Ok-Þorisdalur/jökull, Esja & Skálafell area

About half of the currently active volcanic systems are tholeiitic in composition (Jakobsson, 1979). However, the number known to be active at the time of the Óþoli eruption is much more limited. A potential source area for the Óþoli eruption is the former SW axial rift axis to north-east of Reykjavík, where evidence for at least four extinct central volcanoes has been found (Sæmundsson and Noll, 1974; Kristjánsson *et al.*, 1980). Of those, the interbedded ignimbrite, tillite and other volcanic products in the Húsafell area provide evidence for explosive volcanism from a central volcano that was active in the area between 3.1-1.5 Ma (Fig. 5.6) (Grönvold, 1972; Sæmundsson and Noll, 1974). The repetitious tillite interbeds indicate that volcanism during this period was intrinsically linked to the periodic build up and decay of local and, perhaps, regional ice-sheets (Sæmundsson and Noll, 1974; Geirsdóttir and Eiríksson, 1994). A '3rd acid phase' began *ca.* 2.4 Ma, but there is an erosional unconformity between. 2.4-1.8 Ma, which means that potential source deposits for the Óþoli eruption are not well represented in the Húsafell region. Chemical data is generally limited and not specifically

related to the glass phase (Grönvold, 1972), but its bulk tholeiitic nature (Fig. 5.6-a) and the optimum source-distance grain size zones (Fig. 5.6-b) and dispersal patterns (Fig. 5.7) for the Óþoli Tephra suggest that the Húsafell complex is the most likely source region of the Óþoli eruption.

(iii) Proposed source eruption site-Skagafjall dispersal of the Óþoli Tephra

The platey glass shard morphology and the thickness of the airfall deposit on Skagafjall suggests that Óþoli Tephra was the product of a massive Plinian style sub-aerial eruption. Compared to the rest of Iceland, visible tephra deposits are uncommon in Holocene deposits of the Vestfírðir Peninsula. Prevailing north/north-north-westerly winds at the time of the eruption transported ash *ca.* 200 km (Fig. 5.7-b) and deposition most probably occurred across much of the Vestfírðir Peninsula. The dispersal direction of the Óþoli Tephra was similar to that of the H-1104 eruption (Fig. 5.7-c) with Skagafjall located on the principal plume dispersal axis (Larsen and Thórarinsson, 1977). The Óþoli eruption was of a similar magnitude to (but possibly greater than) the H-3 eruption; hence an airfall component of 8-10 cm thick[36] (Fig. 5.7-c). Reworked deposits are up to 10 m thick in section C suggesting substantial amounts of tephra fell onto the glaciers that occupied Dýrafjörður and the other Western Troughs of the Vestfírðir Peninsula.

(c) Þörsmórk Ignimbrite

The new chemical evidence presented is similar to the unaltered glass compositions of Jørgensen (1980); hence, in the absence of any new field evidence to suggest the contrary, Thórarinsson (1969) and Jørgensen's (1980, 1981, 1987) identification of Tindfjalljökull as the source of the Þörsmórk Ignimbrite is supported.

[36] The known distribution of the Óþoli Tephra is currently restricted to the Skagafjall outcrop. Isopach data and minimum volume of tephra fall is therefore difficult to assess fully (cf. Pyle, 1995).

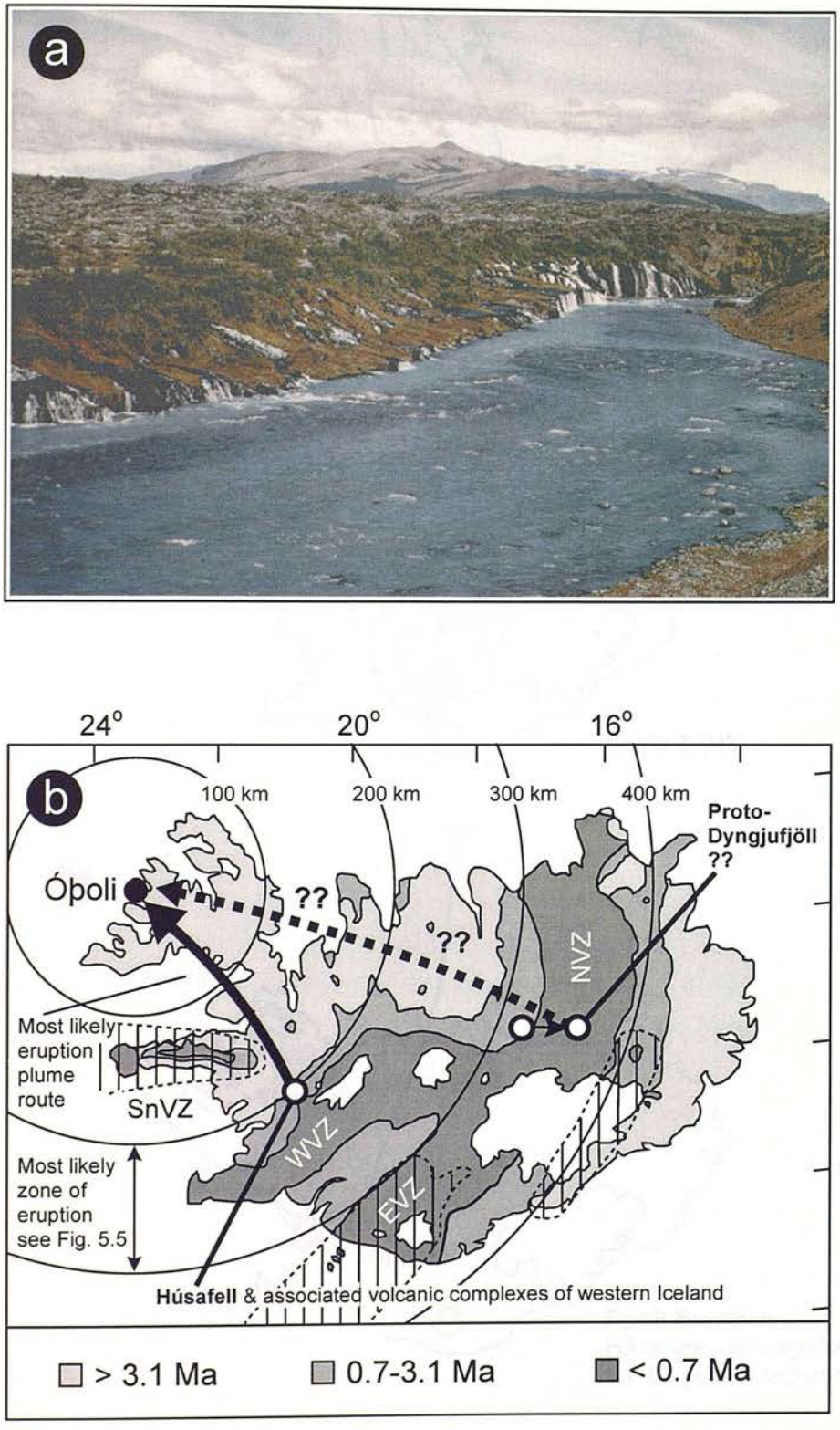


Figure 5.6 (a) Húsafell, western Iceland **(b)** Source range map for the Óþoli Tephra based in grain-size data curve fitting of Figure 5.5. Open circles are possible eruption source volcanoes; areas shaded with straight lines are alkali olivine basalt and transitional alkali basalt zones (after Jakobsson, 1979). Proto-Dyngjufjöll is an more unlikely source for the Óþoli Tephra based on present day wind directions and patterns of Holocene tephra plume dispersal (cf. Fig. 2.2).

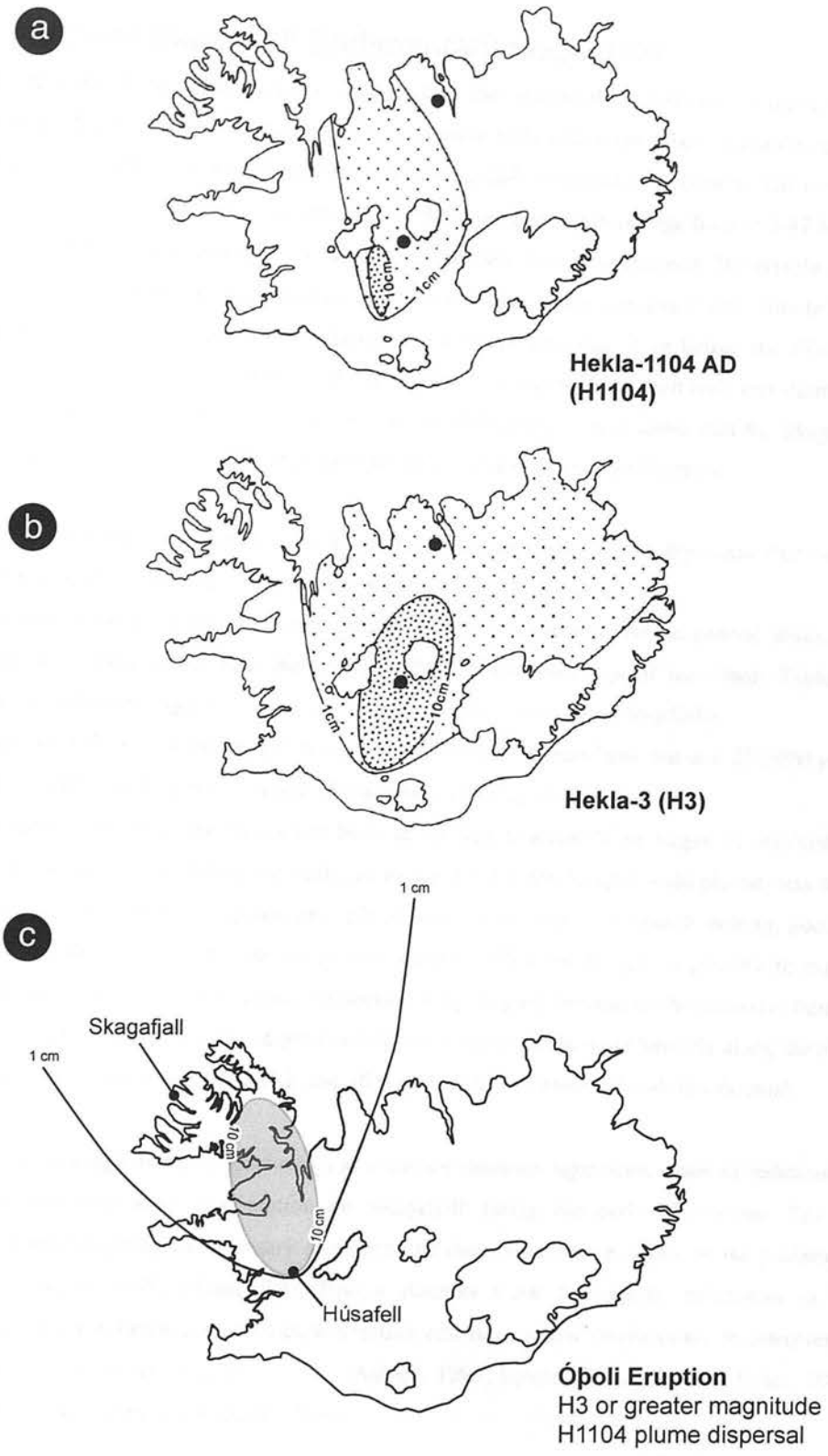


Figure 5.7 (a)-(c) Diagram to illustrate the feasibility of 10 cm of airfall ash being deposited on Skagafjall from an eruption and/or wind strength of slightly greater magnitude than the Hekla-3 (H3) eruption in the Husafell region. The plume dispersal pattern is analogous to the Hekla-1104 AD (H1104) eruption. The Óþoli eruption was at least the same order of magnitude or an order of magnitude greater than the H3 eruption. (a and b are from Kirkbride and Dugmore, 2001).

5.3 Formation of Skagafjall Sedimentary Sequence

New numerical ages of the Óþoli Tephra indicate that the Skagafjall sedimentary sequence was formed between 2.5-2.1 Ma. An older age for the rhythmite beds below the Óþoli Tephra cannot be ruled out as there are several erosional contacts in the Skagafjall sedimentary sequence. The reversed polarity of all the rhythmite beds above rhythmite bed three suggests an upper age limit of 2.47 Ma for units 3-11. It should be noted that the SW margin of the lake is not constrained. Nevertheless, the most likely explanation for the formation of an ice-dammed lake of this size and at this altitude is the existence of a fjord network of similar configuration to the present day at or before the Pliocene-Pleistocene transition. In addition, because of the presence of interbedded rhythmite and diamicton deposits in a sequence estimated to cover a duration of 3000 years, it is possible that the Skagafjall sedimentary sequence is a record of rapid global climate change in the early Quaternary.

It is only possible to make broad conclusions about the timing and processes of deposition that existed on Skagafjall around the time of the Óþoli eruption for the following reasons:

1) The fragmentary nature of the geomorphological record in Vestfírðir and the general absence of chronological control means that the *ca.* 2.26 Ma fission-track age of the Óþoli Tephra is currently the only direct age control on pre-Holocene glacial activity on Vestfírðir.
2) The precision of the fission-track ages from the Óþoli Tephra is excellent, but at ± 100,000 years, it is approximately the length of a single glacial-interglacial cycle.
3) Accurate interpretation of the diamicton beds is the key to identifying stages of regional ice advance versus stagnation during the build up to the 2.2-2.1 Ma Iceland-wide glacial maximum (Fig. 5.10) and the Skagafjall deposits are only exposed by seasonal snowpatch melting. Sections were restricted to approximately one metre wide during 1998-1999. It was not possible to expose parts of Section A and the lower regions of Section B by digging because of the extensive boulder cover on the slopes. Consequently, it proved difficult to trace all the units laterally along the cliff-edge. The evolutionary models (SSM-1 and SSM-2) should be examined with this in mind.

Nevertheless, the new age and geomorphological evidence contains significant clues to sedimentary formation processes that were in operation on Skagafjall during the early Pleistocene. The re-interpretation of the Skagafjall sedimentary sequence and their significance builds on the pioneering work of Sigurvinsson (1983) (Table 5.4). Recent theories show that subtle differences in the relationship between rhythmite and diamicton deposits can have major implications in interpreting glaciolacustrine environments (Appendix D1.1) (Ashley, 1995; Eyles, 1983; Eyles and Eyles, 1983; Hart and Boulton, 1991; Hart and Roberts, 1994).

Table 5.4 (next 5 pages) Summary descriptions, interpretations & sedimentary evolution model SSM-1 for the Skagafjall sedimentary sequence (notes at end).

Section, Unit & thickness (m)	DESCRIPTION OF SEDIMENTS General	Largest boulder or no./ thickest rhythmite	Upper contact	KNOWN AGE (Additional features – Sigurvinsson, 1983 + sjr+js 1998-2000)	NEW INTERPRETION (SJR) Existing interpretation (Sigurvinsson, 1983) Environment of Deposition (PE) & Landscape Development & Model Stage →	
Section A						
Tertiary basalt lava bedrock 500 m	**Layer 4 of Gudmundsson (1989) (?)**		Erosional	**BEDROCK AGE 15-13 Ma**	**Localised Pliocene glacial activity occurs in proto-Dýrafjörður (or Dýradalur) and other western troughs. Glacial flow follows the existing fluvial drainage pattern from central volcanic highlands across lava plains (that dipped towards the west at this time; Lárusson, 1983) to form proto-fjord versions of the western troughs.**	1
Unit 1 (DB-1) 3.5 m	Poorly sorted diamicton; subangular-subrounded boulders & pebbles in silt-sand matrix	-	Sharp Non-erosional	**Not exposed in 1998-1999**	**Localised glacial activity continues and preferentially erodes weak tuff and scoria inter-beds in the Tertiary lava pile. This leads to the formation of lateral erosion platforms. These provide stable depositional bases and basins for lateral ice-dammed lakes that formed in (at least) Skagafjall, Sauðanes. Intensification of glacial activity occurs during the Plio-Pleistocene transition. Localised ice caps merge to form a regional Vestfirðir ice sheet centred on the highlands that extended across present day Glama to Drangajökull. Deposition of the Unit 1 basal diamicton occurs. Later, ice stagnation leads to the formation of the Skagafjall ice-marginal lake and the deposition of glaciolacustrine diamicton follows. The latter is shown by the upper non-erosional contact of DB-1 and silt and sand within the diamictons indicative of syn-depositional water currents.**	2
Unit 2 (RB-2) 6 m	Laminated silt layers (mostly brown) Massive clay layers (orange) All rhythmite beds consist of brown silt – orange clay couplets with fine laminations in both throughout Fine to medium sand layers common at base of each silt layer Uppermost laminae convoluted with some overturned folds in WNW direction; fold planes dip ESE	? / 15 cm ? / 1cm	Sharp Erosional	**Not exposed in 1998-1999**	**Thinning and retreat of ice at the lateral margins of the fjord ice sheet creates a deep water lake and the deposition of glaciolacustrine lake floor facies. Convolutions and well developed folding are most likely due to advance of ice creating soft sediment glaciotectonic deformation push structures in the direction of ice flow. During glacial phases of glacial overriding WNW is the predominant plateaux top to centre of Dýrafjörður direction of ice flow. This is the same as the WNW direction of overturned folds.** The sedimentological characteristics of the rhythmite beds are most similar to deposits that are the result of deposition from underflow and overflow/interflow deposition in a glaciolacustrine environment (O' Cofaigh and Dowdeswell, 2001). Silt = summer layers; clay = winter layers; clay thickness < silt thickness, *i.e.* Group III type rhythmites of Ashley (1975) - formed relatively close to delta front; sand = occasional turbidity current formation	3
Unit 3 (DB-3) 3 m*	Sub-angular-sub-rounded boulders & pebbles in silt-sand matrix	-	Sharp-non erosional	**Not exposed in 1998-1999**	PE similar to unit DB-1	

Unit 4 (RB-4) **Hjallanes Tephra**	9.5 m	4.3 - 3m - silt & clay couplets each up to 35 cm thick in total; partially lithified fine clay laminations within brown silt 4.2 - 2 m - 40 couplets of silt & clay 4.1 - 1 m – thinly laminated yellow silt *(Hj-1)* & grey clay with sand partings; **Hj-1 = Hjallanes Tephra (silicic) 15-20 cm-25 couplets each fine upwards to a sharp upper contact; microfaulting structures in bottom 5-6 cm related to irregular upper surface of DB-3; Hj-1 is capped by Hj-2a (basic) -10-12 cm of fine black tephra (fbT) & brown clay/silt laminatons capped by 4 cm massive fbT (Hj-2b)**	4.1 - 5 cm 4.2 – 3.5 cm (clay) **4.1 - <1 cm silt & clay; Hj-1 up to 3 cm; Hj-2 up to 5 cm**	Locally gradational , but erosional	**Hjallanes Tephra (Hj-2b) magnetic polarity uncertain-possibly normal; other RB – uncertain-reversed polarity (>*ca.* 2.4 Ma ??)** 4.3 - top 1 m convoluted with overturned folds; sedimentary dyke through convoluted beds dip = 40° WNW 4.2 - silt layers commonly graded with sand layer in basal units 4.1-4.2 - general thinning upwards of rhythmites	**Establishing the relationship between the Hjallanes Tephra Hj-2b and the Óþoli Tephra is fundamental to the Skagafjall sedimentary evolution models. Two possible evolutionary models are suggested in this study - see Box 6.1 & 6.2 for more details. This table relates to the SSM-1 model.** **The massive nature of the Hj-2b and its relationship to the Óþoli Tephra in this model is explained by one of the following scenarios:** **(i) Hj-2b is not from the same eruption as Hj-1 and Hj2a and was deposited sub-aerially directly into the lake, hence its significantly coarser grain size.** **(ii) Hj-2b is from the same eruption as Hj-1 and Hj2b, but represents a prolonged and/or more effusive stage of the Hjallanes eruption during which the Skagafjall lake remained or became ice-free.** **(iii) Hj-2b is from the same eruption as Hj-1 and Hj-2a and represents a pulse of increased deposition after delayed glacier throughput (*e.g.* up to 1000-2000 years; Larsen, 2000).** **From the Hjallanes rhythmites upwards unit RB-4 is as RB-2.** Thin clay laminae within silts formed on cold summer days when little/no meltwater entered lake. The general upwards thinning of rhythmite beds is indicative of reduced sedimentation rate.
Unit 5 (DB-5)	2 m	Subangular-subrounded boulders & pebbles in silt-sand matrix	60 cm	Gradational -non erosional	-	**PE similar to unit DB-1.**
Unit 6 (RB-6)	19 m	6.2 Rhythmites - total thickness = 16 m; 300 couplets of thick laminated, fine graded silt + clay layers *(Figure 4.1-j)* 6.1 thick bedded sand + gravel capped by consolidated silt/sand layer	6.2 clay - 3.5 cm 6.1 - 2.7 m thick bedded sand	Sharp; erosional	6.2 Basal laminae convoluted; basal silt layers thin upwards Top 9 m of rhythmite beds are convoluted with overturned WNW folds and shear planes	**PE similar to unit RB-2.**
Unit 7 (DB-7)	10 m	**Poorly sorted, coarsening upwards sequence of well-rounded to sub-rounded clasts with no preferential orientation**	1 m	Sharp; non-erosional	**1998-1999 exposure limited to < 1m wide snowpatch meltwater channels**	**Unit 7 is the thickest diamicton unit in the Skagafjall sequence. It represents a period of increased and sustained glacial activity/overriding, hence the thickness of the diamicton deposits, the general increase in boulder size and intense glaciotectonism, *i.e.* shear planes + folds, in RB 6. Unit 7 possibly represents a glacial maximum (and/or climatic optimal phase of climatic deterioration) in the 2.5-2.2 Ma period of the early Pleistocene. This is followed by period of stagnation (and, perhaps, regional retreat) because there is no firm evidence for glacial overriding, *i.e.* convolution/folding of rhythmite beds or sharp erosional contacts, in units RB 8-12 of Sections A-C.**
Unit 8 (RB-8)	4 m	124 couplets; average thickness 2.8 cm; slight deformation of upper beds –	clay - 4 cm	Gradational & locally	**Numerous dropstones up to 10 cm diameter**	**PE similar to RB-2 except there is evidence for increased influence of ice rafting and turbidity current deposition in upper rhythmites. Evidence of a reduction in**

		no large scale fold structures or shear planes		erosional	(e.g. Figure 4.1-j); micro-ripples (0.1 mm long x 1.5 mm high) and cross lamination in thin section	glaciotectonic activity exists (see DB-9, below). This suggests a sustained period of ice stagnation, and possibly minor retreat of the down-fjord ice margin, occurred.	
Unit 9 (DB-9)	7 m	Coarsening upwards sequence of poorly sorted pebbles and boulders	1 m	Sharp-non-erosional	1998-1999 exposure limited to < 1m wide snowpatch meltwater channels; upper part of RB reversely magnetised	A sustained phase of ice-rafting and glaciolacustrine diamicton deposition is tentatively suggested, based the characteristics of RB-8 (*i.e.* non-erosional or locally erosional upper contacts, lack of deformation in the rhythmite beds), which are not indicative of glaciotectonism (*cf.* Eyles and Eyles, 1983).	
Unit 10 RB-10	8 m	Undisturbed silt and clay laminae	*ca.* 3cm - clay	Not visible	Bottom 4 m not exposed in 1983 & 1998-99	PE similar to RB-8	
Unit 11 (-)	NV	Obscured by slope boulders					?
Unit 12 (GB-12) & plateau surface	10-12 m	Coarse gravel and boulders; periglacial patterned ground and shattered bedrock are the dominant features of the plateau surface	5 cm – gravel 30-50 cm – boulders	Plateau surface	SKAG 1 well-rounded olivine and pyroxene phenocryst rich rock on plateau top sampled for ^{3}He CSED	Iceland-wide ice-sheet modelling (Hubbard *et al.*, manuscript) and extensive field-based evidence from across Vestfirðir (Lárusson, 1983) suggests that Skagafjall was covered by a thin ice sheet at the LGM. Olivine and pyroxene phenocryst-rich erratics are rare on Skagafjall (2 from >20 examined) and Sauðanes (6 from >50 examined) due to the stratigraphically restricted nature of their olivine-basalt source layer on Langafjall (Layer 5; Gudmunðsson, 1989). The Langafjall-Skagafjall axis coincides with weak LGM ice-flow pathways. Preliminary helium-3/4 cosmogenic surface exposure dating (CSED) of all suitable plateau erratics was inconclusive due to high levels of magmatic helium that masked any cosmogenic helium present. Further CSED of other erratics will be needed to fully resolve the issue of when Skagafjall/Sauðanes were last ice-covered. Current periglacial activity on the plateau surface suggests that the LGM ice sheet in this area would have been cold-based and non-erosive aiding the preservation of the Skagafjall sediments.	

Section B							
Unit 10 (RB-10)	8 m *2 m*	Same altitude as the top of RB-10 section A; microfaulting structures in upper 1-2 cm (~ WNW-NW orientation)	*1-2 cm - clay*	Gradational Mottled-slightly erosional	Unit B begins ca.65 m above bedrock, 2-5 m below plateau surface; reversed magnetic polarity	Mottled upper surface consists of small-scale hummocks and troughs. Troughs have a maximum height of 1-2 cm and are interpreted as well-rounded flame structures. Flame structures are indicative of water flowing over freshly accumulated and/or saturated sediments (Allen, 1985; Brodzikowski & Haluszczak, 1987) Two modes of formation are suggested: (1) The upper surface of RB-10 in section B represents the final stages of infilling	



						in the ice-dammed lake and the start of the transition from glaciolacustrine to glaciodeltaic sedimentation (2) The upper surface created by catastrophic drainage as the stagnating ice near the current fjord entrance thins to beyond the breach-point altitude. In both cases flows from sediment laden supraglacial deltas pass over the upper surface of rhythmite beds and mottled surface is a result of eddies and currents within these flows
Unit 11 (OT-11) Óþoli Tephra	2.3 m *2.6 m*	11.2 Three layers of silt-sand grade tephra with climbing ripple, **ripple drift** and cross-bedding structures (WNW flow direction) and two inter-fingered, inter-bedded layers of silt, clay and tephra; 20 cm thick gravel lens near the top of the unit **11.1 fine-medium, structureless, yellow tephra with minor, discontinuous layers of black pumice 1-2 mm diameter in upper 5 cm** **11.1-base-coarse yellow sand grade deposit (*i.e.* coarse airfall ash)**	30-50 cm – clay-silt layers **8-10 cm** **< 1cm**	Erosional (dip = 18° N)	**ITPFT age of the Óþoli Tephra is 2.26 ± 0.11 Ma; all sub-units of Unit 11 have a reversed polarity** **Óþoli Tephra thickens towards the SE;**	Above all, the new fission-track, luminescence ages and the palaeomagnetic polarity of the Óþoli Tephra show that the Skagafjall sedimentary sequence is one of the most remarkably well-preserved, high-resolution records of early Pleistocene glacial activity in Iceland. Unit 11.1 is the airfall component of Óþoli Tephra, deposited directly into a shallow lake or directly into the exposed upper surface of the existing lake sediments. Significant volumes of ash are deposited onto the adjacent glacier. Although residence times of tephra in Vatnajökull can be up to 1000 years (Larsen, 2000), large volumes of the Óþoli Tephra were re-deposited over the existing Skagafjall units during the next few years via supraglacial delta outlets. Unit 11.2 represents a 3-4 year period during the transition from a glaciolacustrine-glaciodeltaic environment as the Dýrafjörður ice-sheet continued to stagnate. A low-angle delta front was located up-fjord beyond section C, hence the fine-grained ripple drift sequences present. Increased summer in-wash into shallow lake environment from supraglacial deltas creates climbing ripple and cross bedding structures in reworked tephra. Directional flow remains WNW (i.e. from the lateral margin to the centre of Dýrafjörður). Reduced sedimentation and frozen lake conditions in winter lead to the deposition of finer clay material; well developed recumbent folds in these deposits are the result of shear stress created by strong, sediment-saturated currents (Sigurvinsson, 1983). High sedimentation rates are due to the volume of tephra deposited onto the surface of the ice.
Unit 12 (DB-12)	10 m *2 m*	Boulder gravel grading upwards into diamicton; sub-rounded to rounded boulders; few small (<0.5 m) erratics scattered on plateau surface	1 m	Plateau surface	-	Diamicton of Unit 12 is possibly related to the LGM overriding of Skagafjall plateau (see description under Unit 12-section B); bedrock channels identified by Sigurvinsson (1983) are possibly glacier flow-scour channels from the last LGM ice-sheet (cf. Ingólfsson & Norðdahl, 2001). Alternatively, the bedrock channels could be stagnation meltwater channels as suggested by Sigurvinsson (1983).

Section C							
Unit 10 (RB-10)	4 m	Bedrock lower contact is erosional and 2m below observed rhythmites	-	Gradational	Not observed in 1998-99 due to slope coverage	PE similar to Section B – Unit RB-10	?



Unit 11 (OT-11)	10 m*	Unit 11.2 Numerous inter-beds of sand/gravel/tephra; upper layers dominated by cross-laminated and bedded structures; localised gravel lenses Unit 11.1 Inter-bedded sand/gravel; no capping deposit Structureless (airfall) tephra at base (~10 cm thick)	**Numerous inter-beds of variable thickness**	Erosional / inter-bedded with sands and gravels	**Stretches of grass growth and fragments of rhythmite bed on the plateau surface between sections B and C and 5-10 m from the top of section C (Figure 4.1-o; Óþoli Tephra in sections B and C has the same major element chemistry)**	**The coarse-grained nature of these deposits indicates a higher energy depositional environment. Section C is closer to the supra-glacial delta outlet than section B; Section C is located on an elevated terrace. It is possible that an additional rhythmite bed existed capping Section B Units 11-12. The reoccurrence of the rhythmic deposition means:** **(1) the glacial lake was re-established after re-deposition of the Óþoli Tephra and it capping diamicton.** **(2) the Skagafjall lake sequence was thicker than the preserved deposits. The missing deposits have been removed by ice-sheet advance over the surface. Further ice advance most likely occurred in one or perhaps both of the following periods: (a) during a phase of early Pleistocene glacial activity when sediments were easily eroded and the glacial margins were nearby and fluctuating rapidly (b) during a mid-late Pleistocene glacial maximum (most likely the Weichselian or Saalian) when climate deterioration was severe enough to create coalescing mainland and Vestfírðir ice sheets. The thickness of these single ice-sheets was sufficient to cover the high altitude plateaux of the NW Peninsula.** **The lack of capping diamicton suggests: (i) section C remained above the ice surface at the LGM; (ii) the LGM ice sheets covered section C, but were debris-poor due to their cold-based, non erosive nature; (iii) post-glacial periglacial activity or mass flow has removed unconsolidated diamicton material over the cliff edge**	
Unit 12 (DB-12)	20	Boulder gravel with 2 m thick cross-bedded sands and gravels at base; large sub-rounded-rounded boulders up to	1 m	Plateau surface	**Boulders not suitable for ^{3}He CSED**	**Further ice stagnation prior to up-valley retreat characterised by prograding / fluctuating delta front facies. Boulders most likely deposited by overriding ice-sheets of the LGM**	

Additional notes: This table should be read in combination with Table 5.5 to provide an integrated landsystems model for the Skagafjall sedimentary deposits. The dotted line after Unit 7 represents the dividing line between evidence for alternating phases of glacial overriding and stagnation and deposits associated with stagnation only.
General key: Normal font – Jon Sigurvinsson (js) (see 1982, 1983 references); bold font – Steve Roberts (sjr) (this study) throughout table; NV = not visible; all thicknesses except those marked with an asterisk are at least values; * = up to values; PE = palaeoenvironment.
Key for the last column: white = ice advance/thickening; grey-dark grey = ice stagnation; spotted grey = ice stagnation related deposits with overlying diamictons.

5.3.1 New Skagafjall Sedimentary Evolution Models

A glaciomarine environment for the Skagafjall sedimentary deposits is considered unlikely (Appendix D1). The Skagafjall deposits are more than 500 m above sea level and there is no evidence for marine (or any other) biota or bioturbation throughout the sequence (cf. Ó Cofaigh and Dowdeswell, 2001). This altitude is beyond the reach of the most optimistic estimates of relative increase in Pliocene-Pleistocene sea level (*e.g.* Haq *et al.*, 1997) even after taking partial uplift of the Vestfírðir into account. Instead, sedimentological evidence points to a glaciolacustrine depositional environment. The sharp nature of the contacts between most of the rhythmites and the general lack of normal grading are characteristics. If it were to form today, a stable ice surface of at least 750 metres above present sea level would be required in Ingaldsandur and Dýrafjörður to maintain an ice dammed lake for approximately 2000 years (Sigurvinsson, 1983). The Skagafjall deposits formed either in a 'proto-Dýrafjörður' or at peripheral reaches of the fluvially incised Tertiary plateau. The ice thickness required to form a topographic ice-dammed lake would have been substantially less than 750 m in both cases.

Two sedimentary evolution models have been developed to explain the deposits examined. The Skagafjall Sedimentary Model-1 (SSM-1) is described in detail in Table 5.4. This model assumes the stratigraphic profiles are related in the manner described in Sigurvinsson (1983) and Figure 4.1-f. A second stratigraphic evolutionary model (SSM-2) has been developed to investigate the stratigraphic implications of the potential relationship between the Óþoli and Hj-2a component of the Hjallanes Tephra (Fig. 5.7-5.9, Boxes 5.1, 5.2). Section A was used as a reference log to construct the SSM models. The key differences between the SSM-1 and SSM-2 is that in SSM-2 the Óþoli Tephra and the Hj-1 component of the Hjallanes Tephra have been linked. This means that sections B and C occupied a relatively elevated pre-eruption position compared to section A.

Box 5.1: SKAGAFJALL SEDIMENTARY MODEL 1 (SSM-1)

Stratigraphic relationships between sections A, B and C are as in Sigurvinsson (1983) and Figures 4.1-f. The age relationships between the sections and the Óþoli and Hjallanes Tephras are shown in Figure 6.2-a. The Hjallanes and Óþoli eruptions occurred at significantly different times. Hj-1 and Hj-2a (Fig. 4.1-k) were deposited supraglacially during a phase of lateral glacial advance and/or thickening (represented by the underlying unit DB-3). The Skagafjall lake did not exist at this time because of this increased glacial activity or had a permanent (and, perhaps, thick) ice cover with superficial glaciofluvial reworking of sediments. In addition, transitional alkali basalt compositions are predominantly Re-deposition occurred during RB-4 stagnation phase when delayed glacier throughput and in-wash into the lake occurred. If the Hjallanes (Hj-1 & Hj2a) couplets are varves this occurred over a period of at least 25 years. Thin couplet laminae indicate sedimentation rates were low or the lake was ice covered for most of the year. Alternatively, the numerous laminations could be highly resolved, sub-annual laminations that occur within the normal rhythmite bed formation type (*e.g.* RB-2; Figure 4.1-i).

The uncertain-normal magnetic polarity of the structureless basic component of the Hjallanes Tephra can be explained as follows:

(a) primary remanence was inherited from magma and is dominant over secondary detrital remnant magnetisation (DRM)
(b) the normal polarity is due to self reversal effect of reversed polarity found in about 1 % of volcanic rocks (Thompson, 1991)
(c) Hj-2b is one of the 20 % of sedimentary deposits (Thompson, 1991) that are not amenable to palaeomagnetic polarity dating
(d) the deposit has experienced significant post depositional disturbance either *in-situ* or during sampling. Both of these process can realign or disturbed the inherited/depositional polarity signal. The only palaeomagnetic samples with uncertain signals were those collected from sediments deposited in a high energy environment, *i.e.* the top half of OT-11.27 (I00PM1-4), or samples that were collected in a heavy and prolonged rainstorm, *i.e.* rhythmite bed 4 (RB-4) and the Hjallanes Tephra samples (I00PM21-28)

If (a) is correct or can be more firmly established, the Hjallanes Tephra eruption occurred during the Gauss normal polarity epoch, which ended *ca.* 2.47-2.43 Ma. If the 2.26 Ma ITPFT age of the Óþoli Tephra is accurate. The Skagafjall sedimentary sequence then represents a longer term record of ice build up and decay in Dýrafjörður of possibly glacial-interglacial cycle duration.

Box 5.2: SKAGAFJALL SEDIMENTARY MODEL (SSM-2)

In this model the laminated sub-units of the Hjallanes Tephra, Hj-1 and Hj-2a, are part of the same eruption. Hj-2b was deposited subaerially from a near simultaneous eruption. Hj-1 is the same as the Óþoli Tephra. Hj-2a is the latter basic phase of the Óþoli eruption that has been eroded out of sections B and C. The relative altitudes of sections A, B and C have a fundamental impact the development of the sedimentary sequence. The relative positions of units in these sections are determined by the assumed relationship between the Óþoli Tephra and Hj-1 of the Hjallanes Tephra (Fig. 6.2-b). The Óþoli eruption occurred when the Skagafjall lake was ice-covered, the lake level reduced and airfall deposition occurred onto exposed rhythmite beds at B and C. Coarse material was removed and/or reworked by superficial meltwater streams, hence the fine-grained nature of the Hj-1 and Hj-2b material. Fig. 6.4 shows the proposed sequence of events for this model. The normal-uncertain polarity of the Hjallanes Tephra is due to explanations (b)-(d) Box 6.1.

The two new sedimentary evolution models (Box 5.1, 5.2; Figs. 5.7-5.9; Table D1.1) emphasise the following:

1) The fundamental role that well-dated tephra layers can play in constraining landscape development at different scales, from local depositional lacustrine environments to changes in the regional and even global environment.

The Hjallanes Tephra was divided into the following sub-units:

- Hj-1 is a yellow, laminated, early highly silicic phase of the Hjallanes eruption
- Hj-2a represents a more evolved laminated black tephra that is either the basic phase of Hj-1 or from a separate eruption.
- Hj-2b is a massive, structureless, but slightly coarser-grained black tephra deposit.

The basic components of the Óþoli Tephra and Hjallanes Tephra (Hj-2b) are from eruptions in the tholeiitic and transitional alkali volcanic systems within Iceland respectively (section 5.2). Glass-phase EPMA was undertaken on Hj-2b, but it was too fine grained for effective fission-track dating analysis. Further subdivision based on chemistry was not possible because Hj-1 and Hj-2a were too fine-grained (< 5-10 μm, *i.e.* approximately equivalent to the electron beam diameter) for EPMA. Linking the Óþoli Tephra and Hj-1 more securely requires further developments in grain specific and/or purified fraction chemical and dating analysis of very fine-grained tephra deposits. Nevertheless, the SSM models provide testable hypotheses that could form the basis of a future study.

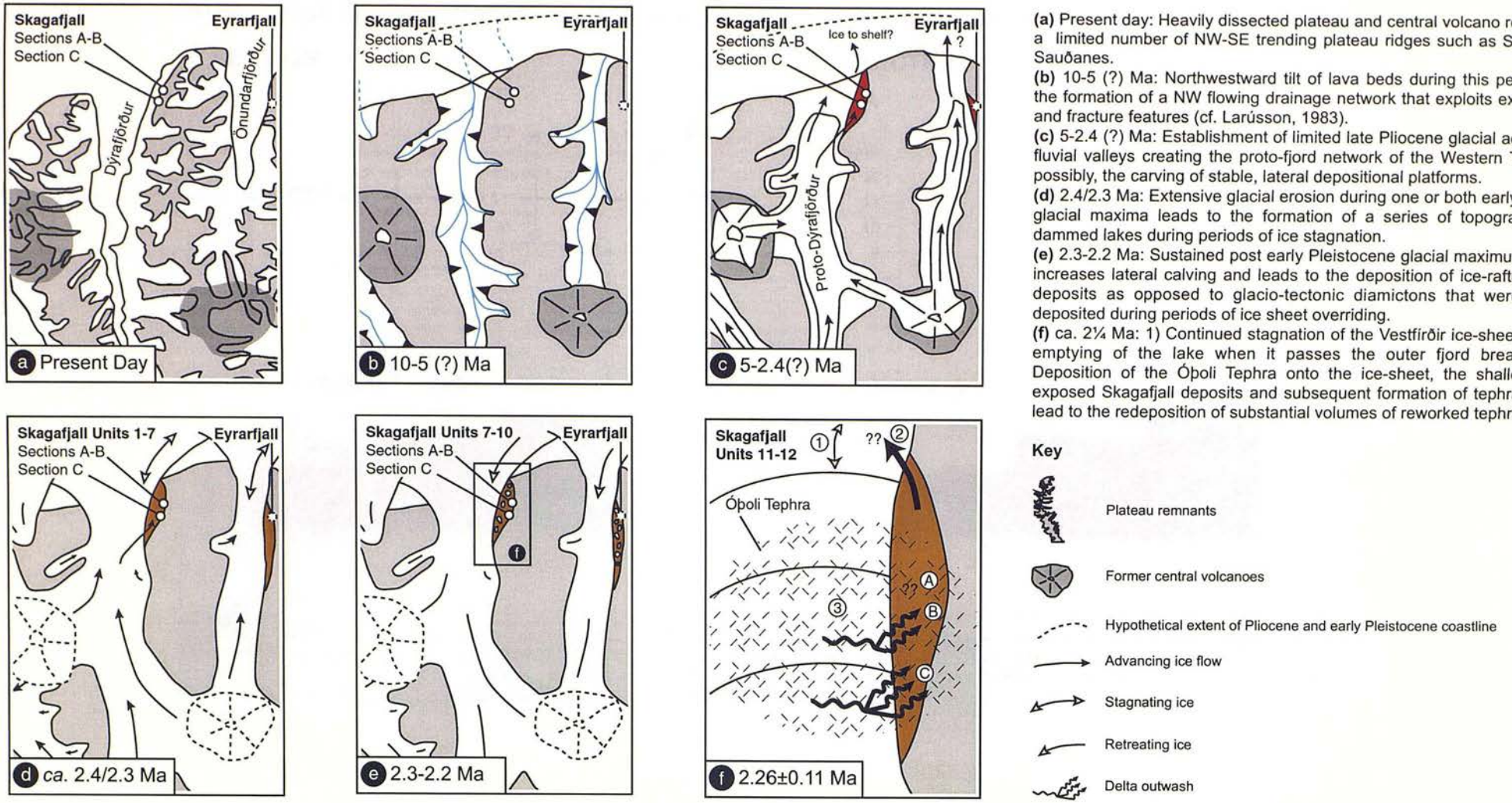
2) The dynamic interplay between Pliocene-early Pleistocene glacial activity in Dýrafjörður (and possibly the rest of the Vestfírðir Peninsula) and glacial and volcanic activity in mainland Iceland.

The Skagafjall sedimentary deposits have been split into two broad palaeoclimatic zones.

1) **Unit DB-1 to DB-7:** The palaeoenvironment of units 1-7 was persistently cold enough to maintain an ice-dammed lake for several hundreds of years at a time. The main evidence for this is the exceptionally thick summer rhythmite layers with sub-annual couplets that occur in most the observed rhythmite units up to and including RB-6. In addition, the erosional rhythmite to diamicton upper contacts and extensive deformation of the underlying rhythmite beds in the direction of assumed palaeo ice-flow (from the margins to the centre of proto-Dýrafjörður) only occur up to unit DB-7 (Table 5.4). This suggest that the rhythmite deposits were overridden intermittently, but at least four times, by thickening and/or advancing ice in proto-Dýrafjörður. Unit DB-7 represents a palaeoclimatic watershed and is a particularly extreme phase of glacial overriding associated with early Pleistocene glacial maximum event.
2) **Unit DB-7 to 12:** The evidence of unit 7 upwards is more indicative of a sustained period of stagnation and possibly ice retreat. The upper diamicton- rhythmite contacts are either gradational or locally erosional and there is an absence of large-scale deformation in units

RB-8 and RB-10 (cf. Eyles and Eyles, 1983). The presence of numerous dropstones suggests ice-rafting was increasingly influential during this period. It should be noted, however, that substantial parts of units 8, 9 and 10 were not as well exposed as some of the lower units in 1998 (Table 5.4).

A major difference between the two models of sedimentary evolution is the relative timing of the extreme cold phase (DB-7) and the Óþoli eruption. The Óþoli eruption occurs after the DB-7 extreme cold phase in SSM-1, but before it in SSM-2. In the former scenario, the Óþoli eruption occurred *ca.* 2.26 Ma during a period of sustained climatic amelioration after the DB-7 ice maximum. Model 2 assumes that the Óþoli Tephra and the Hj-1 silicic deposit are connected. In this scenario, the DB-7 ice maximum occurs after the *ca.* 2.26 Ma Óþoli Tephra eruption. The Óþoli eruption most probably occurred near the end of the DB-3 cold phase or at the start of the RB-4 ice stagnation phase (Figs. 5.8 & 5.9). Both sedimentary evolution models indicate that some degree of climatic upturn occurred before the eruption of the Óþoli Tephra. Broadly speaking, the timing of the Óþoli eruption is the same for both models. Table 5.5 and Figure 5.10 summarise major palaeoclimatic changes in Iceland and the circum-North Atlantic and their relationship to the evolution of the Skagafjall sedimentary sequence and potential influence on early Pleistocene landscape development processes on Vestfírðir.



(a) Present day: Heavily dissected plateau and central volcano remnants with a limited number of NW-SE trending plateau ridges such as Skagafjall and Sauðanes.
(b) 10-5 (?) Ma: Northwestward tilt of lava beds during this period leads to the formation of a NW flowing drainage network that exploits extensive dyke and fracture features (cf. Larússon, 1983).
(c) 5-2.4 (?) Ma: Establishment of limited late Pliocene glacial activity widens fluvial valleys creating the proto-fjord network of the Western Troughs and, possibly, the carving of stable, lateral depositional platforms.
(d) 2.4/2.3 Ma: Extensive glacial erosion during one or both early Pleistocene glacial maxima leads to the formation of a series of topographically ice-dammed lakes during periods of ice stagnation.
(e) 2.3-2.2 Ma: Sustained post early Pleistocene glacial maximum stagnation increases lateral calving and leads to the deposition of ice-rafted diamicton deposits as opposed to glacio-tectonic diamictons that were commonly deposited during periods of ice sheet overriding.
(f) ca. 2¼ Ma: 1) Continued stagnation of the Vestfirðir ice-sheet 2) Possibly emptying of the lake when it passes the outer fjord breach point 3) Deposition of the Óþoli Tephra onto the ice-sheet, the shallow water or exposed Skagafjall deposits and subsequent formation of tephra deltas that lead to the redeposition of substantial volumes of reworked tephra.

Figure 5.8 Schematic 10-2.2 Ma landscape evolution model for Dýrafjörður (and Önundarfjörður) and the Skagafjall (and Eyrarfjall) sedimentary sequence (see also Fig. 5.15)

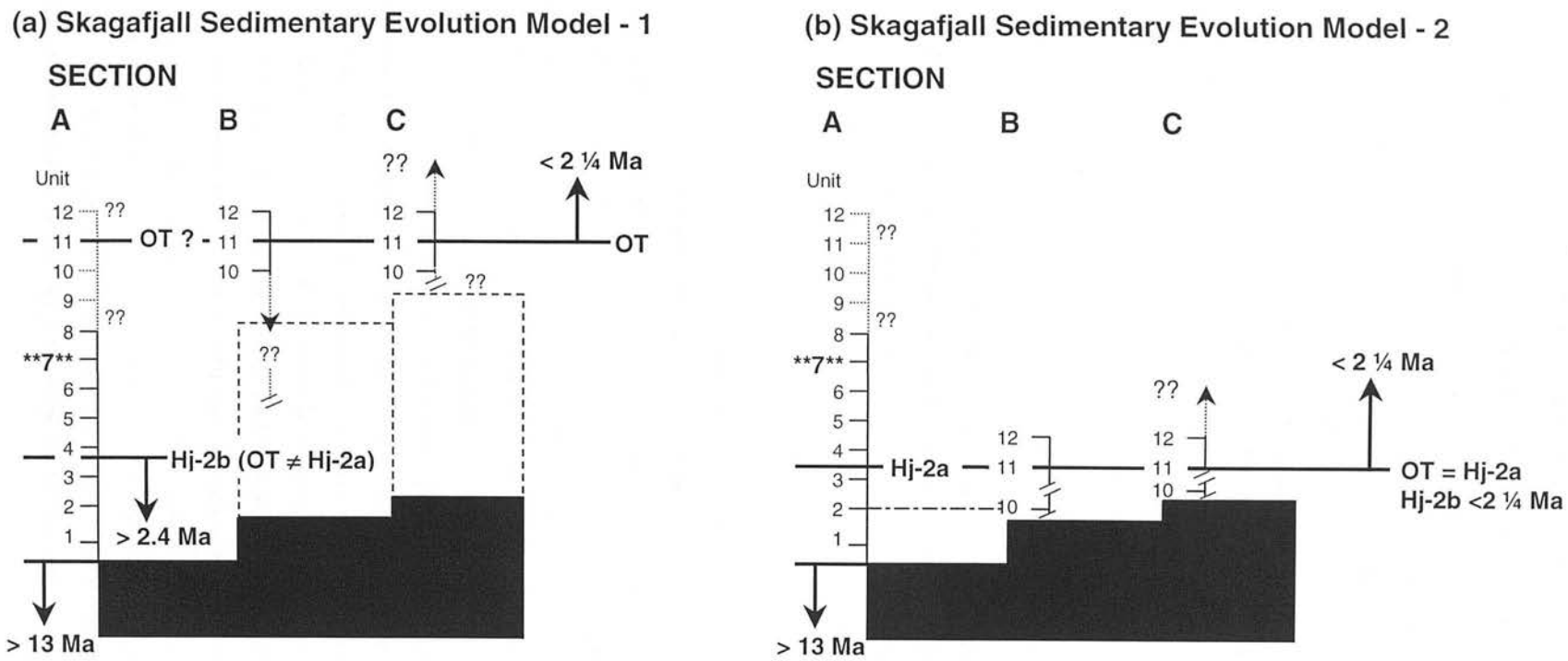


Figure 5.9 Comparison of Skagafjall sedimentary evolution models SSM-1 and SSM-2 illustrating how the tentative relationship between Hj-2b and Óþoli Tephra influences the interpretation of the Skagafjall sedimentary sequence **(a)** SSM-1 is as in Sigurvinsson (1983) with the Óþoli eruption occurring after the DB-7 extreme cold phase **(b)** SSM-2: new interpretation of stratigraphic relationship between sections A, B, and C with the Óþoli eruption occurring before the DB-7 extreme cold phase. The overall conclusion that the Skagafjall sedimentary sequence is a early Quaternary relict feature remains whichever evolutionary model is chosen. The black area is the Tertiary basalt bedrock.

5.3.2 The Plio-Pleistocene transition in Iceland:

Implications of the *ca.* 2.26 Ma age of the Óþoli Tephra

The start of the Plio-Pleistocene transition (*ca.* 2.5-2.4 Ma) is characterised by accelerated deterioration in global climate conditions (Kvasov and Blazhchishin, 1978; Shackleton *et al.*, 1984; De Jong, 1988; Bloemendal and deMenocal, 1989; Raymo *et al.*, 1989; Kukla 1989; Shackleton *et al.*, 1990; Krantz, 1991; Morley and Dworetzky, 1991; Ding *et al.*, 1993; Larsen *et al.*, 1994; Leroy and Dupont, 1994; Eyles, 1996; Kukla and Cilek, 1996). The 41,000 year obliquity cycle remained dominant in the late Pliocene and early Pleistocene (Dowsett and Poore, 1991). The full-scale 100,0000 year glacial/interglacial global ice volume cycle, which persists to the present day and plays an important role in the global deglaciation mechanism, developed during the 2.5-1.8 Ma interval, but only became dominant from *ca.* 0.8 Ma (Tiedemann *et al.*, 1989; Imbrie *et al.*, 1993; Williams *et al.*, 1997; Dalgleish *et al.*, 2000).

(a) Iceland

The unexpectedly old age of the Óþoli Tephra presents a new opportunity to develop chronologically constrained models of macroscale landscape evolution for Skagafjall and the Vestfírðir Peninsula. These models allow relationships between the different spatial and temporal scales of local-regional glaciation in Iceland to be tied to changes in global palaeoclimate during in the Pliocene-Pleistocene transition (*ca.* 2.6-2.0 Ma).

Forty years of research into the inter-bedded lava and diamicton sequences of mainland Iceland has identified two major pulses of amplified and widespread Plio-Pleistocene glacial activity at *ca.* 2.5-2.4 and 2.2-2.1 Ma (Wensink, 1964; McDougall and Wensink, 1966; Vilmundardóttir, 1972; Sæmundsson and Noll, 1974; Jóhannesson, 1975; Albertsson, 1976; McDougall *et al.*, 1976, 1977; Sæmundsson, 1979; Kristjánsson *et al.*, 1980; Albertsson, 1981; Eiríksson, 1981, 1985; Albertsson and Eiríksson, 1988; Geirsdottir, 1988, 1991; Eiríksson *et al.*, 1990; Eiríksson and Geirsdóttir, 1991; Geirsdóttir, 1991; Geirsdóttir and Eiríksson, 1994). Geirsdóttir and Eiríksson (1994) extended the 'Vaknajökull-centric' view of recent Icelandic glaciation to the progressive development of a Plio-Pleistocene transition ice sheet across most of mainland Iceland. They suggested that the onset of glaciation began as localised mountain ice caps in the SE during the Miocene. The 2.5-2.4 Ma event was the culmination of the first period of localised mountain ice cap coalescence and mainland ice sheet formation (Fig. 5.10) (Geirsdóttir and Eiríksson, 1994). Gradual enlargement of the main south-eastern ice sheets then occurred until they encompassed most of the central mainland 2.2-2.0 Ma. They suggested that at this time, and at other early Pleistocene glacial maxima, north and north-western ice sheets probably coalesced with the main ice sheet that advanced from the south and southeast. The unique imprint of early-mid Pleistocene glacial activity in the terrestrial record of Iceland and changes in the oxygen isotope record that indicate 100,000 cycles of global ice volume

build up are broadly synchronous (Sæmundsson, 1979; Shackleton *et al.*, 1984; 1990; Eiríksson and Geirsdóttir, 1991; Geirsdóttir and Eiríksson, 1994). The extent of early Quaternary ice sheets in Iceland is, therefore, of great significance because it suggests macroscale coeval linkage between terrestrial and oceanic climate systems.

This study shows that the first Icelandic ice sheets of the early Pleistocene covered a greater proportion of Iceland and/or were far more extensive than previously thought. The new fission-track age of the Óþoli Tephra suggests a substantial ice mass existed on the Vestfírðir Peninsula during or before 2.4-2.1 Ma and was large enough to reach from the central area to the outer Western Troughs. It is possible that a single ice-sheet encompassed the whole of the mainland and the NW Peninsula or an independent Vestfírðir ice cap developed centred on Glama.

In summary, the 2.26 Ma age for the Óþoli Tephra suggests that:

- The spatial extent and oceanographic impacts of early Pleistocene glaciations of Iceland have been significantly underestimated and/or
- The Vestfírðir Peninsula could have supported an independent ice cap from as far back as the early Pleistocene

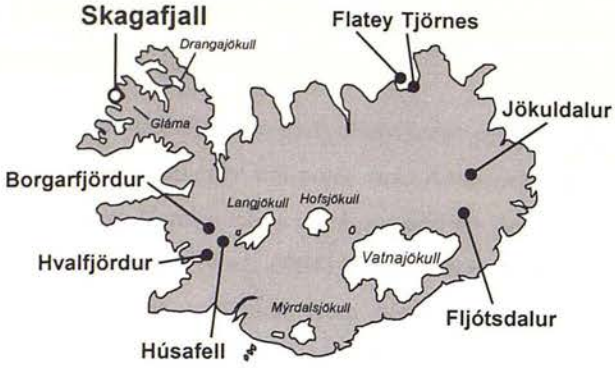
Evidence to support the former is provided by Stecher *et al.* (1999) who suggested the shape of Iceland was radically different during this period and the land area smaller because the neovolcanic zone along the current rift axes did not exist. Narrow land bridges and other topographic barriers that would currently impede the flow of early Pleistocene ice-sheets to the Vestfírðir Peninsula were possibly less well-developed features of the early Pleistocene Icelandic landscape. Support for the second hypothesis comes from the studies of the style of early Pleistocene glacial activity in Iceland (described above) and SE Greenland. Larsen *et al.* (1994) suggested that the early Pleistocene ice advances were predominantly localised and did not reach the coast until *ca.* 2 Ma.

(b) Skagafjall & Glaciation in the North Atlantic 7-2 Ma

The Skagafjall sequence is highly significant because it provides the first numerically dated, terrestrial, sedimentary record of glacial activity at the Plio-Pleistocene transition in the circum-North Atlantic. Other records are marine based (*e.g.* Larsen *et al.*, 1994; Ruddiman *et al.*, 1989) and/or based on either amino acid dating, strontium isotope ratio analysis (Sejrup *et al.*, 1995, 2000), correlation dating of oxygen isotope, magneto-, palyno- and other biostratigaphies (*e.g.* Raymo *et al.*, 1989; Suggate, 1991, Kleman and Stroeven, 1997) or inferred relationships between directly-dated lava flows that bracket diamicton deposits (*e.g.* Geirsdóttir and Eiríksson, 1994).

a Present Day

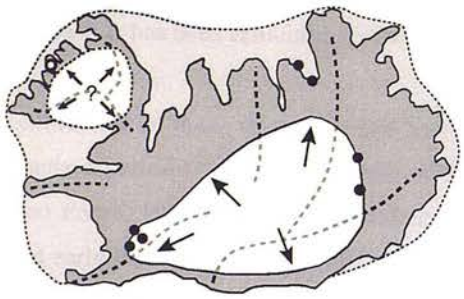
Location map of main sites where evidence for late Pliocene and early Pleistocene glacial activity has been found (see also Fig. 5.11)



- Site of new evidence for Pliocene & early Pleistocene glacial activity presented in this study
- Sites of known Pliocene & early Pleistocene glacial activity (after Sæmundsson & Noll, 1974; Geirsdóttir & Eiríksson, 1994)
- Present ice caps
- Outline of present day landmass

b 2.7-2.5 Ma

Expansion of the mainland ice sheets and possible development of an independent ice cap on central volcanoes of the Vestfírðir Peninsula.

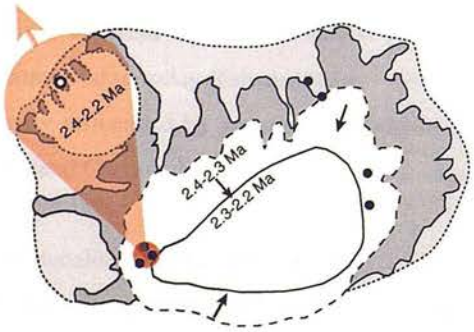


- Approximate outline of mainland ice sheet between 2.7-2.5 Ma
- Putative outline of Vestfírðir ice sheet between 2.7-2.5 Ma
- Main LGM ice divides (after Ingolfsson & Nordðahl, 2001; Hubbard *et al.*, manuscript)
- Putative outline of the late Pliocene landmass
- Main directions of ice expansion

Otherwise, key is as (a)

c 2.4-2.2 Ma

1) Expansion of mainland ice sheets at 2.4 Ma extreme cold phase to early Pleistocene maximum limits. Expansion of Vestfírðir ice sheet. Incision of the Western Trough fjords on the Vestfírðir Peninsula and the formation of ice-dammed lakes on the lateral margins of (at least) Skagafjall and Saudanes.
2) Rapid post 2.3 Ma glacial maximum deglaciation causes the Óþoli eruption in the Húsafell region and is one of the first massive pressure release induced eruptions of the early Pleistocene. The Vestfírðir ice cap stagnates, but remains relatively stable as it is fed by an independent precipitation supply (see Fig. 5.12).
3) The eruption plume drifts NNW and the Óþoli Tephra is deposited onto the Skagafjall sedimentary deposits.

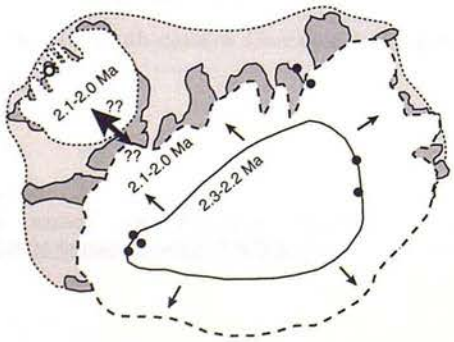


- Proposed Óþoli eruption site & plume dispersal

Otherwise, key is as (a)

d 2.2-2.0 Ma

Readvance of mainland ice sheet during the next extreme cold phase of the early Pleistocene. It is possible that the Vestfírðir and mainland ice sheets coalesced for the first time and that the fjord network of the Western Troughs was incised to almost its present depth in the 2.5-1.8 Ma interval (see Fig. 5.11 and text for further discussion).



Key as (b)

Figure 5.10 Development of late Pliocene and early Pleistocene ice sheets in Iceland and their relationship to the Óþoli eruption event (based on an original diagram in Geirsdóttir & Eiríksson, 1994).

Major interdisciplinary research programs, such as the multi-institutional PRISM[37] project, have been established to understand the patterns and causes of climate change 4-2 Ma. (*e.g.* Cronin, 1991; Dowsett *et al.*, 1994). Plio-Pleistocene transition climate change studies are important for two main reasons:

1) The mid-late Pliocene-early Pleistocene period spans the transition from relatively warm, ice-free and predominantly uni-polar (*i.e.* Antarctica) conditions to cooler global climates, increased Northern Hemisphere ice-volume and the development of the glacial-interglacial cycles (Krantz, 1991; Dowsett *et al.*, 1994). Furthermore, the Plio-Pleistocene transition is widely recognised as marking the transition from high frequency, low oscillations in global climate (that are characteristic of Pliocene climate regimes) to high frequency, high oscillations in climate that are common features of most of the Quaternary period (Krantz, 1991; Suggate, 1991).
2) Periods of exceptional warmth during the Pliocene (*e.g.* the 3 Ma 'event'; Edwards *et al.* 1991) are thought to be good analogues of future 'greenhouse' global climate (Cronin, 1991), although this approach is has been criticised (Crowley, 1993).

The main conclusion of many of studies that have contributed to this program is that the 4-2 Ma era was not simply a period of sustained warmth before the advent of Northern Hemisphere glaciation (Dowsett and Poore, 1991) with pronounced periods of global glacial activity occurring in the Late Miocene and early Pliocene (Krantz, 1991). In the circum-North Atlantic region there is evidence for ice-rafted detritus (IRD) in marine cores from the south-eastern coast of Greenland as early as 7 Ma (Larsen *et al.*, 1994) and the western coast of mid-Norway at *ca.* 5.5 Ma (Jansen and Sjøholm, 1991). It is likely that glacial activity also affected the Vestfirðir Peninsula at this time until relatively mild conditions returned in the mid-late Pliocene (4-3 Ma). The Icelandic and North Atlantic record for this period shows different oceanic circulation patterns with greater northward transfer of heat from the Tropics compared to today (Edwards *et al.*, 1991). Hence, between *ca.* 4-3 Ma coastal areas of Iceland were heavily influenced by warm oceanographic currents and, perhaps, a 'switching-off' of the cold East Greenland Current during summer (Fig. 5.12-a) (Cronin, 1991; Edwards *et al.*, 1991).

Cirque and localised plateau ice-caps were probably the dominant style of glaciation in mountainous North Atlantic peripheries until at least 2.75 Ma (Kleman and Storeven, 1997). In addition, pre-Pleistocene glaciations in Greenland were centred on the highlands of southern Greenland because of the high mountains and high levels of precipitation (Larsen *et al.*, 1994). The climate, mechanisms and style of Pre-Pleistocene glacial activity on the Vestfirðir Peninsula must have been remarkably similar to that of south-eastern Greenland, in particular, but also other terrestrial peripheries of the northern North Atlantic.

[37] PRISM stands for Pliocene Research, Interpretation and Synoptic Mapping project (see http://geochange.er.usgs.gov/pub/PRISM/.html for more details).

Jansen and Sjøholm (1991) showed that a significant expansion of the Scandinavian Ice Sheet occurred at 2.57 Ma. Mudie *et al.* (1990), Bringham-Grette and Carter (1992) and Bringham-Grette *et al.* (1994) suggested, however, that the Norwegian and Labrador Seas and the peripheral Arctic Ocean remained relatively warm and predominantly ice-free during summer until a rapid deterioration in climate 2.4-2.2 Ma. The first widespread occurrences of IRD across the northern North Atlantic are dated to *ca.* 2.4 Ma and this coincides with 'three closely-spaced significant ice build-up events' (Kleman and Stroeven, 1997, p. 40-41, Fig. 6.9-b; Raymo *et al.*, 1989). Evidence for two severe early Pleistocene glacial events, at *ca.* 2.4 and 2.3 Ma, has been found in the terrestrial glacial records of both hemispheres (Suggate, 1991; Kranz, 1991; Geirsdóttir and Eiríksson, 1994). Curry and Miller (1989) suggested that global ice volume during these 'events' was at least two thirds of late Pleistocene glacial maxima ice volumes. Ice-sheet glaciation in Greenland was not, however, severe enough to reach the coast until *ca.* 2.0 Ma (Larsen *et al.*, 1994). The 2.1-2.0 Ma broadly coincides with the intensified deterioration of global climate conditions (*e.g.* Tiedemann *et al.*, 1989).

Although glacial activity on the Vestfírðir Peninsula was probably initiated at least as far back as the late Miocene (cf. Larsen *et al.*, 1994), it is most likely that Dýrafjördur, and the western trough network was heavily incised by intensified glacial activity at the 2.4 Ma and 2.3 Ma climatic downturn 'events'. Incision most likely extended to the present depth of the main fjords; hence, in this scenario the major fjord network of Vestfírðir is a early Quaternary geomorphological relict. This supports old ideas that the first glaciation achieves the most erosion (Sugden, 1974; Sugden and John, 1976; Kleman, 1994)

(c) Evidence for, and implications of rapid climate change at the Plio-Pleistocene transition

Interglacial climate optima were 'noticeably cooler' between 2.1-1.8 Ma period compared to those in the 2.4-2.1 Ma era (Krantz, 1991). Hence, early Pleistocene deterioration to glacial-interglacial conditions was punctuated by a series of rapid climatic upturns in the 2.4-2.0 Ma era (Shackleton *et al.*, 1984) as the climate system attempted to shift to a new state of equilibrium. It is possible, therefore, that Geirsdóttir and Eiríksson's (1994) 'progressive' 2.7-2.2 Ma ice sheet growth across Iceland was, in fact, characterised by periods of regional ice sheet advance and decay to and from local, isolated ice caps between the gradual build up to early Pleistocene maxima at *ca.* 2.2 and 1.8 Ma (Fig. 5.11). The new 2.26 Ma minimum age of the Skagafjall sequence enables further refinement of established linkages between global and Icelandic stratigraphies and climate records at the Plio-Pleistocene transition (2.6-2.1 Ma). In comparison to glaciations in Greenland, which did not reach the coast until *ca.* 2.0 Ma (Larsen *et al.*, 1994), the 2.5-2.0 Ma glacial advances were not related to the development of an all encompassing ice-sheet in Iceland during the LGM (Ingólfsson and Norðdahl, 2001). Rather, an independent ice-centre developed on the Vestfírðir Peninsula during this period and only coalesced with the mainland ice-sheet when the 100,000 year glacial cycle intensified and became dominant *ca.* 0.8 Ma.

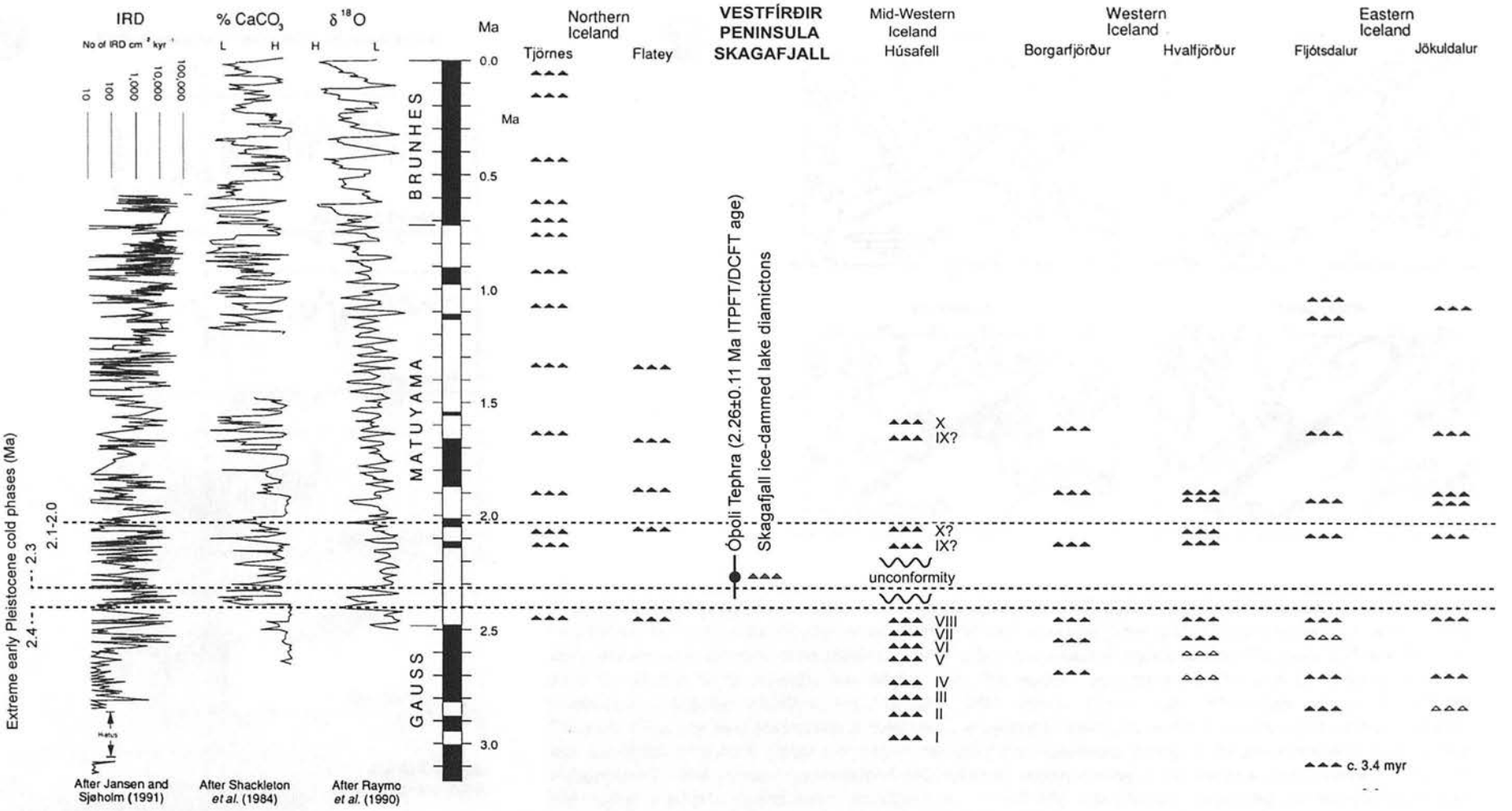
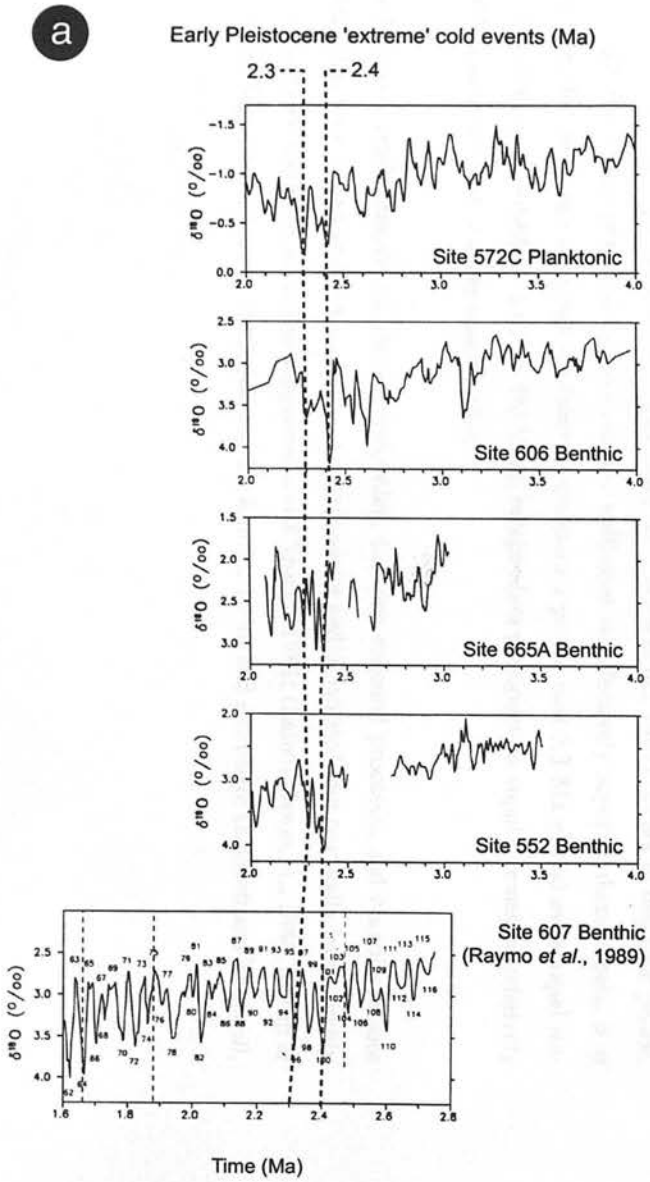


Figure 5.11 Integration of the Skagafjall sedimentary sequence into the glacial chronostratigraphy of Iceland and the oxygen-isotope ($\delta^{18}O$), carbonate ($CaCO_3$) and ice-rafted detritus (IRD) records from Shackleton *et al.* (1984), Raymo *et al.* (1989) and Jansen and Sjøholm (1991). Integration of the Skagafjall deposits is based on the 2.26±0.11 Ma fission-track age of the Óþoli Tephra. Black triangles are diamicton/diamictite horizons of glacial origin; unfilled triangles are diamicton/diamictite horizons of uncertain origin; red triangles are glaciotectonic/lacustrine diamicton units of the Skagafjall sedimentary sequence; L = low; H = high (diagram based on Fig. 8 of Geirsdóttir and Eiríksson, 1994 except for Husafell record, which is based on Sæmundsson and Noll, 1974).



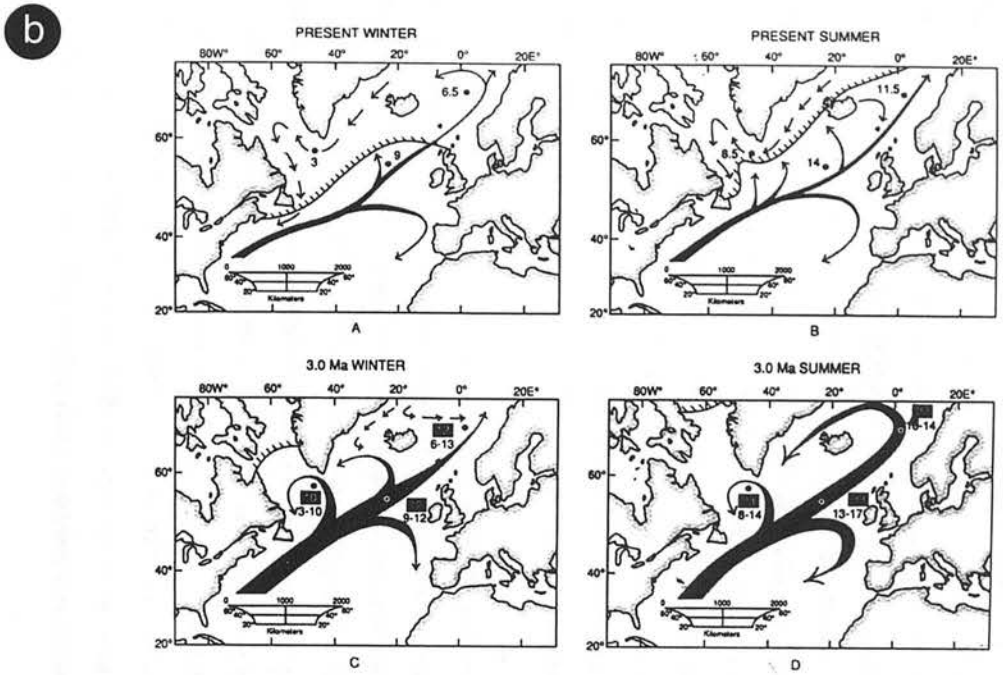


Figure 5.12 (a) Correlation of high resolution deep-ocean $\delta^{18}O$ DSDP and ODP records of planktonic and benthic forminifera to the Raymo *et al.* (1989) record illustrating the global nature of the 2.4 and 2.3 Ma early Pleistocene extreme cold phases. Site 572 is in the eastern equatorial Pacific; sites 606 and 607 are from the central North Atlantic; site 665 is from the eastern equatorial Atlantic and site 552 is from the northeastern Atlantic (modified from Krantz, 1991 where original data references can be found) **(b)** Possible Pliocene palaeocirculation illustrating a potential mechanism for a strong warm ocean currents and precipitation supply (large arrows) to the Vestfírðir Peninsula during 3 Ma summers and weaker, but independent cold surface currents and precipitation supply during 3 Ma winters (small arrows). The 3.0 Ma winter scenario could have persisted in 2.5-2.0 Ma interglacials providing an independent and continuously cold precipitation supply to the Vesfírðir Peninsula (small arrows). This helped to maintain an independent ice sheet that filled and continually incised the Western Troughs, perhaps to their present depth during the first part of the early Pleistocene. At the start of the post-2.3 Ma interglacial the precipitation starved mainland ice-sheet of Iceland collapsed rapidly from the west leading to the pressure release induced Óþoli eruption from Húsafell in mid-western Iceland ca. 2¼ Ma (Fig. 5.10) (from Edwards *et al.*, 1991).

The Skagafjall sediments reflect millennial (and perhaps even sub-millennial) climatically controlled fluctuations at the outer margins of the Vestfírðir regional ice-cap between 2.4-2.1 Ma. Evidence for less highly resolved, but high frequency Plio-Pleistocene climate oscillations, with timescales of tens of thousands of years, has been found in the foraminifera assemblages of the North Atlantic (Dowsett and Poore, 1991) and in sea-level highstands of the Middle Atlantic coastal Plain (Dowsett and Cronin, 1990; Krantz, 1991). It is reasonable, therefore, to assume that the early Pleistocene climate was as unstable and prone to rapid reorganisation in a similar manner to the last glacial cycle (cf. Dansgaard *et al.*, 1989; Hughen *et al.*, 1997). It is equally reasonable to assume that the early Pliocene ice-sheets were as responsive to these global climate variations and as equally prone to rapid advance and collapse as the LGM-Buði-present Holocene Inter-glacial ice-sheets in Iceland (Hansom and Briggs, 1991; Ingólfsson and Norðdahl, 2001; Hubbard *et al.*, *manuscript*).

It is possible that early Pleistocene ice-caps on Vestfírðir were either in anti-phase or at least partially out-of-phase with the decay of the mainland ice-sheet. Interestingly, the eruption age of 2.26 Ma dates the Skagafjall section to a time when inter-glacial lavas predominate in the central area of Iceland *ca.* 0.15 Ma years after evidence for widespread glaciation at 2.4 Ma, *ca.* 40,000 years after the 2.3 Ma glacial event and 0.05-0.1 Ma before the next extensive glacial phase 2.10-2.15 Ma. This observation undoubtedly reflects partial preservation of the geological history and the accuracy and precision of dating techniques used in this and/or previous studies. The 2.26 Ma fission-track age of the Óþoli Tephra might not reflect the 'true' eruption age for reasons discussed earlier. In addition, palaeomagetic correlations based on K-Ar ages of lavas with inter-bedded tillite deposits across mainland Iceland are described by Geirsdóttir and Eiríksson (1994) as 'tentative'.

Nevertheless, Ingólfsson and Norðdahl (2001) highlighted how susceptible the mainland section of the LGM ice-sheet in Iceland was to relative rises in sea level during the early stages of deglaciation, which created rapid calving-related collapse and retreat. As outlined earlier, the 2.4-2.1 Ma period is characterised by two severe glacial 'events' at *ca.* 2.4 and 2.3 Ma. In addition, a general rise in global sea levels from ca. –70 m.b.p.s.l. to 15-20 m.a.p.s.l.[38] (Haq *et al.*, 1987) occurs in this time period. Although the dating precision is not currently sufficient to effectively separate these events, it is possible, that while the mainland ice-sheet experienced a period post 2.3 Ma glacial event rapid ice-sheet collapse, the Vestfírðir ice cap, fed by an independent precipitation supply, remained relatively stable and/or decayed in a less rapid fashion.

Furthermore, rapid removal of glacial overburden, isostatic rebound processes and crustal pressure release has been linked to periods of increased volcanism and/or isolated, but unusually large, highly silicic volcanic eruptions in Iceland (Sigurdsson and Sparks, 1981; Gudmunðsson, A., 1986; Sejrup *et al.*, 1989; Sigvaldasson *et al.*, 1992; Jull and McKenzie, 1996) and elsewhere (Kennett and Thunnell,

1975; Nakada and Yokose, 1992). In addition, during the Pliocene and Pleistocene, and in the mid-late Pleistocene in particular, it has been noted that the most explosive Plinian-style eruptions occur in the initial phases of warm interglacial periods (Sigurdsson and Loebner, 1981; Clift and Fitton, 1998; Zielinski, 2000; Haflidason *et al.*, 2000).

It is possible that the first mainland coalescing ice sheets in the 2.7-2.3 Ma period covered the western edge of the axial rift around Húsafell, the favoured Óþoli eruption source volcano (section 5.2). Available evidence suggests that prior to the Óþoli eruption, glacial conditions existed in the western flank zone (Sæmundsson and Noll, 1974; Geirsdóttir and Eiríksson, 1994). The $\delta^{18}O$ record of global ice volume suggests 'rapid', but relatively sustained warming occurred shortly after 2.3 Ma (Shackleton *et al.*, 1984; Raymo *et al.* 1989). It is interesting to speculate that Húsafell became ice-free or substantially deglaciated by between 2.30-2.26 Ma. This could have triggered one of the first massive deglaciation-induced pressure-release, rhyolitic Plinian style eruptions of the Pleistocene in Iceland. The early phases of the eruption plume drifted north-north-westwards and deposited significant volumes of tephra across the Vestfírðir Peninsula, which remained largely ice-covered at the time of the eruption.

[38] Metres below present sea level

Stage Age (Ma)	I - Pre-Glacial-Early Glacial (a) 10-5 Ma →	(b) 5-3 Ma	II - Plio-Pleistocene Transition *ca.* 2.7-2.4 Ma	III – Early Quaternary (a) 2.4-2.2 Ma	(b) 2.2-1.6 Ma
Global climate change proxy Indicators (Haq *et al.*, 1987; Shackleton, *et al.*, 1990; Kukla & Cilek, 1996; Lowe & Walker, 1997; Williams *et al.*, 1998)	Gradual, but irregular climate cooling through middle-upper Miocene; rapid regressions and transgressions of *e.g.* 100 m in 1-2 Ma; marked decline in global sea level to -100 m.b.p.s.l. at *ca.* 10 Ma with gradual recovery to + 100 m.a.p.s.l. at *ca.* 5 Ma	Rapid fluctuations in global sea levels with marked decline to -100 m.b.p.s.l. at *ca.* 3-2.5 Ma. At *a.* 150 m.a.p.s.l. to *ca.* –100 m.b.p.s.l. at *ca.* 3-2.5 Ma	$\delta^{18}O$ record shows a marked increase in global ice volume at 2.7-2.5 Ma. The maximum at *ca.* 2.5 Ma is the most severe downturn in climate in the 3-1.2 Ma period; maximum dust input into Pacific *ca.* 2.5 Ma; max. deterioration in climate recorded at *ca.* 2.5 Ma in *e.g.* the Chinese loess record; marked fluctuations in sea-level from *ca.* –100 m.b.p.s.l. at 3-2.7 Ma to	$\delta^{18}O$ record shows marked decline in global ice volume between 2.4-2.3 Ma followed by marked increase at *ca.* 2.3 Ma; Early development of current *ca.* 100 ka (eccentricity) glacial-interglacial cyclicity with *ca.* 41 kyr (obiliquity) cycle established *ca.* 2.5-2.3 Ma and dominant between *ca.* 2.3-0.8 Ma	Further development of 100 ka glacial-interglacial cyclicity – 46 ka obliquity cycle remains dominant amplifying or modulating the effects of the underlying 100 ka eccentricity cycle; Underlying gradual climate warming with rapid oscillations in global ice volume
Icelandic mainland (mostly after Sæmundsson, 1979; Geirsdóttir & Eiríksson, 1994)	Continuing formation of Tertiary basalt plateau landscapes in NW, N and E Iceland; possible early localised glacial activity in N Iceland	Evidence for regional glacial activity across mainland Iceland *ca.* 6-2.7 Ma centred on main central volcanoes in the south-east; first appearance of hyaloclastite formations	First coalescing ice sheets on the mainland advance gradually from SE to N and NW; major glacial unconformity across Iceland reflecting maximum ice advance at *ca.* 2.45 Ma	Decay of thinning of *ca.* 2.4 or 2.3 Ma glacial 'event' maximum ice-sheets triggers explosive volcanism **(*e.g.* Óþoli eruption)** in western and/or northern parts of the axial-rift; regional and periodic advance and decay of ice between *ca.* 2.3-2.1 Ma	Development of full-scale glacial-interglacial cyclicity; further extensive ice sheet expansion 1.6 Ma
Vestfirðir Peninsula (mostly after Sæmundsson, 1979; Lárusson, 1983 & *new hypotheses / **this study***)	Tertiary basalt layer formation in S & E until *ca.* 7 Ma when rift axis shifts south-eastwards. Fluvial incision and valley formation similar to current fjord configuration. Flows guided from highlands and extinct central volcanoes (possibly with localised ice caps) by westwards tilt of bedrock strata	Further development of extensive fluvial network followed by cirque and proto-fjord development. Extinct central volcanoes that form topographic highs above the plateau basalt layers support regional ice caps as underlying climate progressively deteriorates towards Quaternary	*First independent ice cap forms across whole NW Peninsula, centred on Glama; possibly coalescing with mainland ice sheet that advances from the SE at ca. 2.5-2.45 Ma*	*Independent and periodic ice sheet development on the NW Peninsula possibly out of phase or even in anti-phase with expansion and contraction of mainland ice sheets (?); widespread deposition of tephra from **Óþoli eruption** as plume travels approximately northwards from eruption site at **Húsafell (?)***	*Currently no other evidence for early Pleistocene glaciation on Vestfirðir. It is speculated that glacial maxima widened and deepened early-formed glacial troughs removing large lateral sections of the Skagafjall lake sediments.*

Table 5.5 Summary of the main global palaeoclimatic changes in the 10-1.6 Ma and their influence on landscape development in Iceland and the Vestfirðir Peninsula. Speculative interpretations are in italics.

5.4 Preservation of the Skagafjall Sedimentary Sequence

This section examines how the Skagafjall sedimentary sequence survived for over two million years in a repeatedly glaciated environment. A new mid-late Tertiary and Quaternary landscape evolution model for the Vestfírðir Peninsula is presented and this assimilates information from previous research (*e.g.* Sigurvinsson, 1982; 1983; Lárusson, 1983; Geirsdóttir and Eiríksson, 1994), new geomorphological evidence from the elevated plateaux of the Western Troughs, new fission-track age data from the Óþoli Tephra and LGM-present day ice sheet field and modelling evidence (Ingólfsson and Norðdahl, 2001; Hubbard *et al.*, *manuscript*).

5.4.1 Modes of Pleistocene Glaciation

Kleman and Stroeven (1997) identified three modes of glaciation for the last 2.75 Ma in the Kebnekaise region of north-western Sweden (Table 5.6). These modes of glacial activity produced four important large-scale geomorphological units, three of which are visible in Vestfírðir today (Table 5.7).

Mode of Glaciation	$\delta^{18}O$* Values	Time in mode	% of 2.75-0 Ma	Dominant
1) Cirque Glaciation (CIG)	<3.7 ‰	1.2 Myrs	44 %	2.75-2.0 Ma IG-warm IS
2) Mountain Ice Sheets [≡ regional plateau ice caps]	3.7-4.5 ‰	1.3 Myrs	47 %	2.0-0.7 Ma
3) Fennoscandian Ice Sheets (FIS)	>4.5 ‰	0.25 Myrs	9 %	Late Pleistocene GM

Table 5.6 Modes of glaciation and length of time spent in those modes for Fennoscandian glaciations in the late Pliocene to Pleistocene (modified from information in Kleman and Stroeven, 1997).

While acknowledging the influence of local variations in ice-sheet growth and decay, the above modes and timings are assumed to be similar for the Icelandic-Vestfírðir system. Cirque Glaciation is equivalent to restricted 'Little Ice Age' style of and other Holocene glaciations in Vestfírðir; Mountain Ice sheets are equivalent to regional independent ice cap development on Glama in Vestfírðir, equivalent to 'Younger Dryas' style of glacial activity; Fennoscandian Ice Sheet mode is equivalent to LGM ice-sheet mode of the Icelandic ice-sheet and the development of multiple ice divides and flow regimes, *e.g.* Ingólfsson and Norðdahl (2001), Hubbard *et al.* (manuscript; see below). * modes were defined by Kleman and Stroeven (1997) using the $\delta^{18}O$ record of Deep Sea Drilling Project site 607 of Raymo *et al.* (1989), Ruddiman *et al.* (1989). IG = Interglacial; IS = Interstadial; GM = glacial maxima climate regime.

This section examines to what extent the Vestfírðir Peninsula was affected by the modes of glaciation outlined in Table 5.6 and the implications this has for preservation processes on the elevated plateaux interfluves of the Western Troughs. Sæmundsson (2000) suggested that most of Iceland might have been covered by glaciers for 80-90% of the last 0.5-1 million years.

Kleman & Storeven (1997) Northern Sweden, Norway	Lárusson (1983) equivalent Vestfírðir Peninsula
1) Intact preglacial surface remnants	1) Landscapes of selective linear erosion (interfluves)
2) Preglacial remnants with signs of glacial erosion or deposition	2) Relict landscapes of cirque glaciation
3) Glacially scoured troughs	3) Landscapes of selective linear erosion (troughs)
4) Deep fluvial valleys cut into preglacial surface	-

Table 5.7 Comparison between landscapes identified by Kleman and Storeven (1997) in northern Scandinavia and their Vestfírðir equivalents defined by Lárusson (1983). See also Figure 1.7(b).

The impact of cirque glaciation is evident across western Vestfírðir. Lárusson (1983) identified over 300 high altitude cirque features on the Western Trough plateau interfluves. Mountain ice caps are a feature of glacial activity of stadial rank (*e.g.* Tjaldanes Stage moraines in Dýrafjörður). Recent compilations of offshore and terrestrial evidence strongly suggests that Iceland was covered by a thick LGM ice sheet of similar mode and style to the Fennoscandian Ice Sheet that extended to approximately the 200 m.b.s.l. isobath (Ingólfsson and Norðdahl, 2001). In addition, new models of glaciation support this idea (Fig. 5.13) (Bingham, 1999; Bingham *et al.*, 2000; Bingham *et al.*, *submitted*; Hubbard *et al.*, *manuscript*). The Hubbard *et al.* LGM ice-sheet extends to the approximate position of the 'LGM' Látragunn morainal bank *ca.* 150 km west of mainland Iceland (Ólafsdóttir, 1975; Syvitski *et al.*, 1999). Other hypothesised LGM offshore limits of southern and northern Iceland have also been accurately reconstructed (Egloff and Johnson, 1979; Boulton *et al.*, 1988; Norðdahl, 1991) and the models' pattern of ice-divide formation is remarkably similar to that suggested by Ingólfsson and Norðdahl (2001) (Fig. 1.6-a). An assimilation of current field and modelling evidence suggests a single ice sheet existed across Iceland with mainland and ice-sheets inundating the regional ice-caps of the Vestfírðir Peninsula (Fig. 5.13). The main ice divide ran E-W through the centre of Iceland, but was most likely truncated by a secondary ice divide that ran approximately N-S from Glama along the western coastal fringes. A significant proportion LGM ice-flow is concentrated through the confined and deeply incised northern channel of Ísafjarðardjúp while less intense south-westerly flow occurs through the unconfined and presently shallower Breiðafjörður. This has the effect of reducing the ice thickness and flow-rates of ice across high altitude plateaux surfaces of the outer Western Trough interfluves (*e.g.* Skagafjall and Sauðanes) between these major fjords. Far less intense ice streaming occurs through the western troughs and 'strong' ice-flow that cross-cuts plateaux surfaces is restricted to exposed NE-SW outer Western Trough interfluves and NW-SE trending plateaux of the Hornstranðir Peninsula.

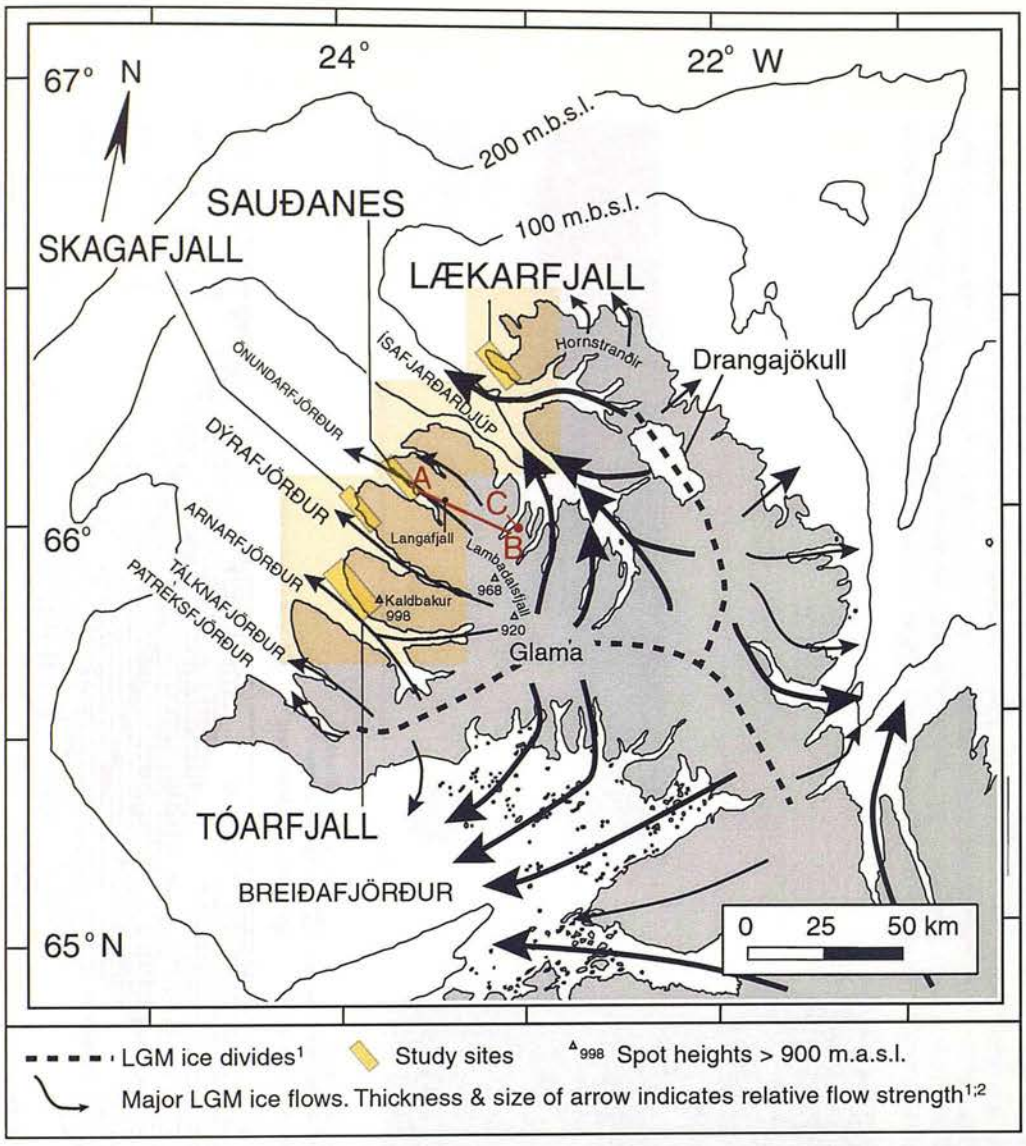


Figure 5.13 Summary of major LGM ice flow directions on the Vestfirðir Peninsula in relation to study sites (in capitals) (based in information and diagrams in principally [1]=Ingólfsson & Norðdahl, 2001, but also [2]=Hubbard *et al.*, (manuscript). Cross-section A-C is shown in Fig. 5.14.

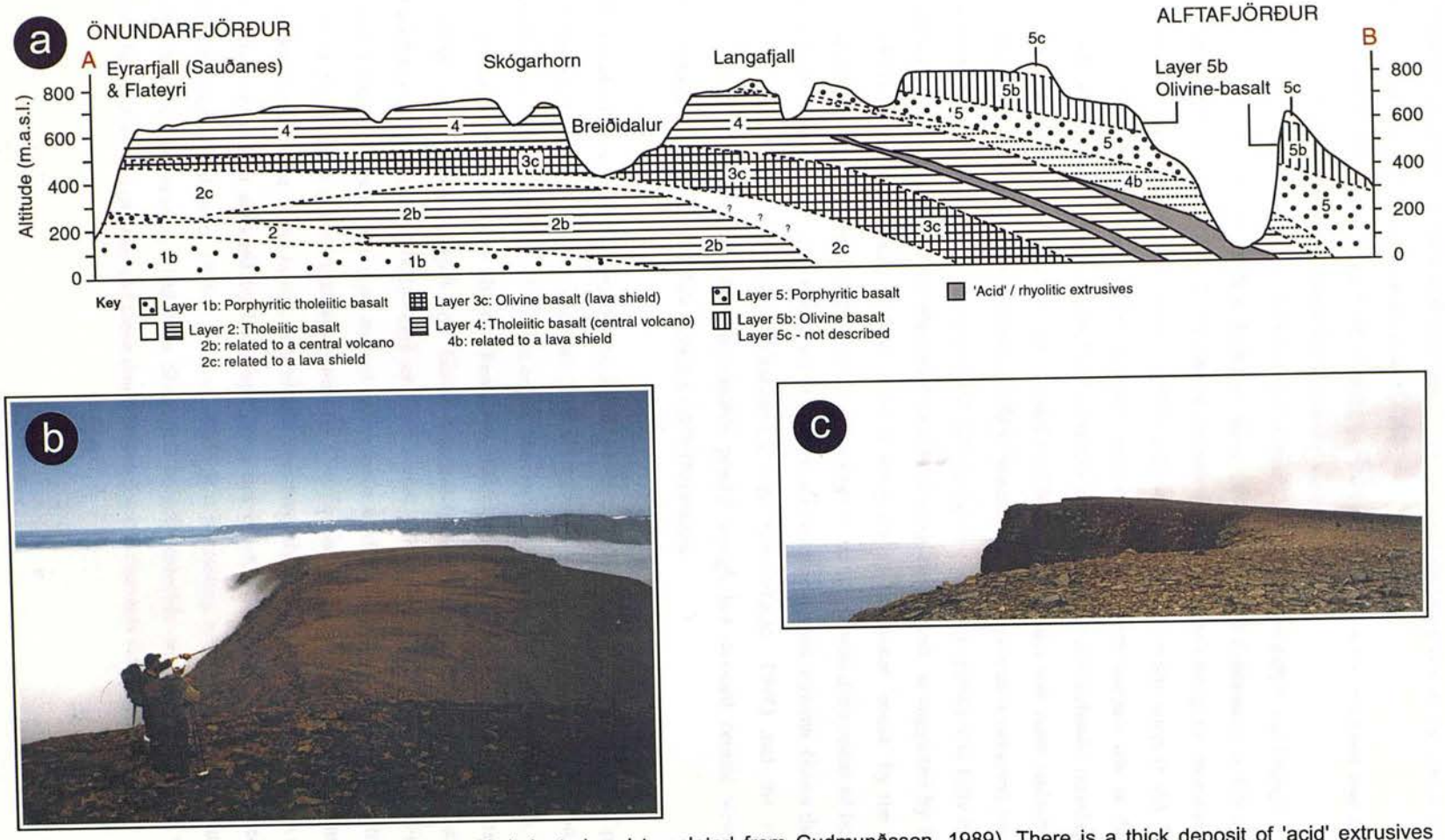


Figure 5.14 (a) Cross-section A-B from Fig. 5.13 (adapted and translated from Gudmundsson, 1989). There is a thick deposit of 'acid' extrusives between ca. 600-800 at C. A-B is the closest available cross section to Skagafjall. Olivine-basalt erratics on Skagafjall and Eyrarfjall (Sauðanes) are thought to be related to this layer, the main outcrop of which is on the Lambadalsfjall-Gláma plateau area, but its relatively restricted nature of this layer in the lava pile accounts for the scarcity of erratics of this composition. **(b)** & **(c)** Tertiary basalt bedrock is exposed at study sites with plateaux remnants that are orientated perpendicular to the LGM ice flow models shown in Fig. 5.13. (b) is Tóarfjall and (c) Lækarfjall. (b) was taken looking approximately NNE across Dýrafjörður. Skagafjall can be seen in the distance. The low cloud provides a good visual impression of what the Skagafjall would look like if Dýrafjörður was filled with ice today; (c) was taken looking approximately NW on the cliff-edge of Lækarfjall. The largest rocks in the foreground are *ca.* 50 cm in diameter.

The Ingólfsson and Norðdahl (2001) model of LGM ice build up suggest Lárusson (1983) was correct in identifying the main central area around Glama as the part of Vestfírðir where macroscale erosion has had most impact in reducing the lava pile. Lárusson (1983) suggested that Vestfírðir was completely covered by a thick and extensive LGM ice-sheet that extended to the 200 m.b.s.l. isobath. He suggested the following occurred at the LGM:

1) The large western troughs from Patreksfjörður to Jökulfirðir were widened and deepened by selective linear erosion beneath the advancing ice cap
2) Extensive areal scouring occurred on and around Gláma, Lambadalsfjall and Dranga
3) Ice thickness of up to 1170 m thick, *i.e.* about 200 m above the Kaldbakur, at 998 m.a.p.s.l., the highest point on the Vestfírðir Peninsula, extended to the offshore Látragunn moraine

Evidence in Ingólfsson and Norðdahl (2001) and new modelling results support the Thoroddsen-Lárusson hypothesis of thick LGM ice cover across Vestfírðir. They suggest that at the LGM the Vestfírðir Peninsula was overwhelmed by ice sheets advancing from the Icelandic mainland. A mode of pre-LGM coalescence with ice caps formed on Glama and Dranga was soon replaced by the all encompassing ice-sheet mode. Lárusson (1983) believed that this situation occurred several times, particularly during the late Pleistocene when full glacial-interglacial cyclicity was fully developed. It is possible that limited LGM ice-free areas existed in northern Iceland, as suggested by Rundgren *et al.*, (1997) because glaciation in these areas is not given an additional 'boost' by the presence of independent ice cap. In addition, the new models suggest that the present dimensions of Ísafjarðardjúp are a result of intense ice-stream incision at mid-late Pleistocene glacial maxima. Given the size of the adjacent extinct central volcano (Jóhannesson and Sæmundsson, 1998) and the existence of Drangajökull it is possible that this sizeable glacial trough has divided central Vestfírðir from Hornstranðir since at least the late Pliocene-early Pleistocene.

The LGM ice-flow model of Ingólfsson and Norðdahl (2001) highlights a mechanism of preservation for the Skagafjall sedimentary deposits (Fig. 5.14b).and provides an explanation for the frequency, distribution and composition of erratics on the plateau interfluves of the Western Troughs. Layer 5b is thought to be the source of olivine phenocryst-rich erratics on Skagafjall and Sauðanes because it outcrops on Glama-Skagafjall and Glama-Lambadalsfjall-Langafjall-Sauðanes flow axes of the Ingólfsson and Norðdahl (2001) LGM ice sheet model. Olivine and pyroxene phenocryst-rich coarse-grained basalt layers of this type are not as common as the fine-grained basalt layers that make up most of the lava pile in the Vestfírðir Peninsula. Consequently, most of the erratics encountered on the plateaux surfaces are of the latter composition. This possibly reflects high erosion rates in areas of the Vestfírðir Peninsula affected by landscape processes of areal scouring rather than selective linear erosion (Sugden and John, 1976; Lárusson, 1983). It is interesting to note that the meltwater channels identified by Sigurvinsson (1983) on Skagafjall broadly coincide with the position of weak LGM flow-lines across the plateau and these could be basal scour channels (cf. Rea *et al.* 1998).

A further assimilation of available field and modelling evidence suggests Vestfirðir supported an independent ice cap during the 'Younger Dryas', with two non-coalescing ice sheets centred on the central Glama area and the Hornstranðir Peninsula suggesting independent ice-cap formation on the Vestfirðir Peninsula has been restricted to periods of climatic deterioration of up to stadial rank. The greatest LGM-'Younger Dryas' reduction in ice volume appears to occur over the Vestfirðir Peninsula suggesting glacial activity in this area is the highly sensitive to rapid reorganisations of global and circum North Atlantic climate. Thin ice covered Glama and the north-western plateaux with ice stream fronts extending to the mid-points of the western troughs of Dýrafjörður, Önundarfjörður and Sugandarfjörður and Jökulfirðir and the eastern margins of Hornstranðir. Glacial activity extended westwards from the Glama into the north-western troughs of Dýrafjörður, Önundarfjörður, Sugandafjörður and Ísafjörður, but did not extend beyond the confines of the outer fjord. The maximum ice limit along Dýrafjörður broadly matched the positions of truncated lateral moraines assigned to the Tjaldanes stage by Lárusson (1983) (Fig. 1.7-a).

5.4.2 Preservation of the Skagafjall Sedimentary Sequence

The preservation of the Skagafjall sequence for 2.5 Ma is remarkable and provides major insights into several aspects of Pleistocene glacial activity in Iceland outlined in the previous section. A representative model of preservation for the Skagafjall sedimentary sequence probably lies somewhere between the following two end member scenarios[39]:

1) The Remnant Preservation Model

   In this model significant overburden of similar nature has been removed by glacial erosion at glacial maxima.

2) Whole Vertical Sequence Preservation Model

   This model suggests the sedimentary deposits are a relict feature preserved by uninterrupted frozen bed conditions during glacial overriding (cf. Nesje *et al.*, 1992; Nesje and Whillans, 1994).

A scenario close to the second preservation model, *i.e.* near whole vertical sequence preservation, with limited, but uniform, net erosion of the plateau surface, is considered most likely for the following reasons. Many of the <1-10 km scale plateau surface features on Skagafjall are similar to features preserved in a subglacial environment under frozen-bed conditions in northern Scandinavia and Arctic Canada. Large scale sorted rock polygons and blockfields cut by meltwater channels that represent two or more glaciations are common in areas that are known to have been glaciated at the LGM (Nesje *et al.*, 1988; Kleman, 1994; Kleman and Borgström, 1994). Both are delicate landforms that could not have survived basal sliding associated with warm-based glacier regimes. Hence, these landforms have been linked to cold-based, non-erosive areas within ice-caps or sheets where ice-sheet was continuously frozen to its bed (Kleman, 1994). Using this criteria over 60 km^2 of the Fulufjället plateau area in western Sweden was interpreted as a preglacial relict landscape (Kleman, 1994). Blockfields, large scale sorted polygons and cross-cutting meltwater channels are common features on Skagafjall (Fig. 1.9-a; Fig. 4.1-e). Applying the Kleman and Borgström (1994) and Kleman (1994) definition of a relict landscape[40] to Skagafjall, *ca.* 7.5 km^2, or 68%, of Skagafjall is a relict preglacial surface (*i.e.* blockfields, sorted polygons or sorted stripes). Large erratics (*e.g.* SKAG 1) on the surface of Skagafjall and Sauðanes were transported englacially and deposited from overriding cold-based glaciers from 'up-glacier summits' in a manner proposed by Rea *et al.* (1998: Figure 22, p. 46).

Two main stages of long term preservation are proposed. These correspond to broad periods during the Pleistocene associated with the development of full 100,000 glacial-interglacial cyclicity.

---

[39] It was not considered appropriate to calculate general erosion rates using criteria set out in Glasser and Hall (1997) because, firstly, there are wide local variations in styles and rates of erosion, secondly, there is a general lack of geomorphological evidence with which to calculate/reconstruct depth of weathering cover and, thirdly, estimating the volume of sediment of purely Icelandic origin in marine cores of Pleistocene age in the North Atlantic is a near impossible task because of the lithological similarity between all the Tertiary provinces of the North Atlantic.

[40] Relict in this context is defined as an unmodified ice covered surface that represents frozen bed areas (Kleman and Borgström, 1994)

1) Post 2 Ma Early-Mid Pleistocene Ice-Free Preservation Stage (Fig. 5.15-a, b)

The current general consensus is that fjords are the result of selective glacial erosion (Sugden and John, 1976; see Nesje and Whillans, 1994, p. 40 for an extensive list of appropriate references). Moreover, the fjords of Norway are thought to be of almost exclusively Quaternary age and early Pleistocene ice-sheets are thought to have had a greater landscape impact than more recent ones (Kleman and Stroeven, 1997; Glasser and Hall, 1997). Therefore, it is proposed that ice streams from early Pleistocene glacial activity incised deeply into the Tertiary basement of Dýrafjörður and the other Western Troughs of Vestfirðir (Fig. 5.15-a, b). At some stage during the early-mid Pleistocene the depth of the incised and overdeepened fjords of the Western Troughs was significantly greater than the thickness of ice that could be generated by glacial maxima-type deteriorations in climate. The glacial cycle was not sufficiently developed at this time to generate ice of sufficient thickness to encompass the whole of Iceland or even cover the highest Vestfirðir plateaux surfaces with ice. Extensive and highly erosive high altitude cirques were established and fed into the main ice sheet. This led to the development of a highly dissecting subsidiary N-S trending secondary trough network (*e.g.* Gerðhamradalur). Hence, the Skagafjall, Sauðanes plateaux and other Western Trough plateau interfluves were extensive ice-free areas that existed for a substantial part of the early-mid Pleistocene. It is possible that the distribution of ice-free areas on Vestfirðir at this time was similar to the putative LGM ice-free areas of Rundgren *et al.* (1997) (Fig. 1.8-a). High altitude ice-free plateaux and nunataks of the type suggested are common in parts of Antarctica, southern Greenland, South Iceland and Jan Mayen where high mountains are juxtaposed with a deep ocean basin and ice streaming and/or the plasticity of the ice lowers the overall altitude of the ice sheet (Miller, 1982; Forman and Miller, 1984; Dahl, 1992; Kleman and Stroeven, 1997).

2) Late Pleistocene Subglacial Preservation Stage (Fig. 5.15-c)

As the full 100,000 year glacial cycles developed and intensified during the mid-late Pleistocene, glacial maxima ice-free areas became increasingly uncommon. Although a near constant supply of IRD was maintained into the North Atlantic between 2.57-1.2 Ma, Nesje and Whillans (1994) and Sejrup *et al.*, (2000) identified two major pulses of increased in IRD into the North Atlantic at *ca.* 1.2-1.1 Ma ($\delta^{18}O$ stage 13) and 0.6 Ma. The latter occurs shortly after the establishment of full 100,000 glacial -interglacial cyclicity at *ca.* 0.8 Ma (Imbrie, *et al.* 1993) and represents the first time that the Scandinavian Ice Sheet reached the continental shelf edge (Nesje and Whillans, 1994). From 0.6 Ma-LGM(*ca.* 28-22 ka) Fennoscandian ice 'frequently' reached the continental shelf edge (Nesje and Whillans, 1994, p.40). The last three advances of the Fennoscandian Ice Sheet (Elsterian, Saalian and Weichselian) had a comparable outline and extent, indicating climatic forcing of similar magnitude and duration (Kleman and Stroeven, 1997).

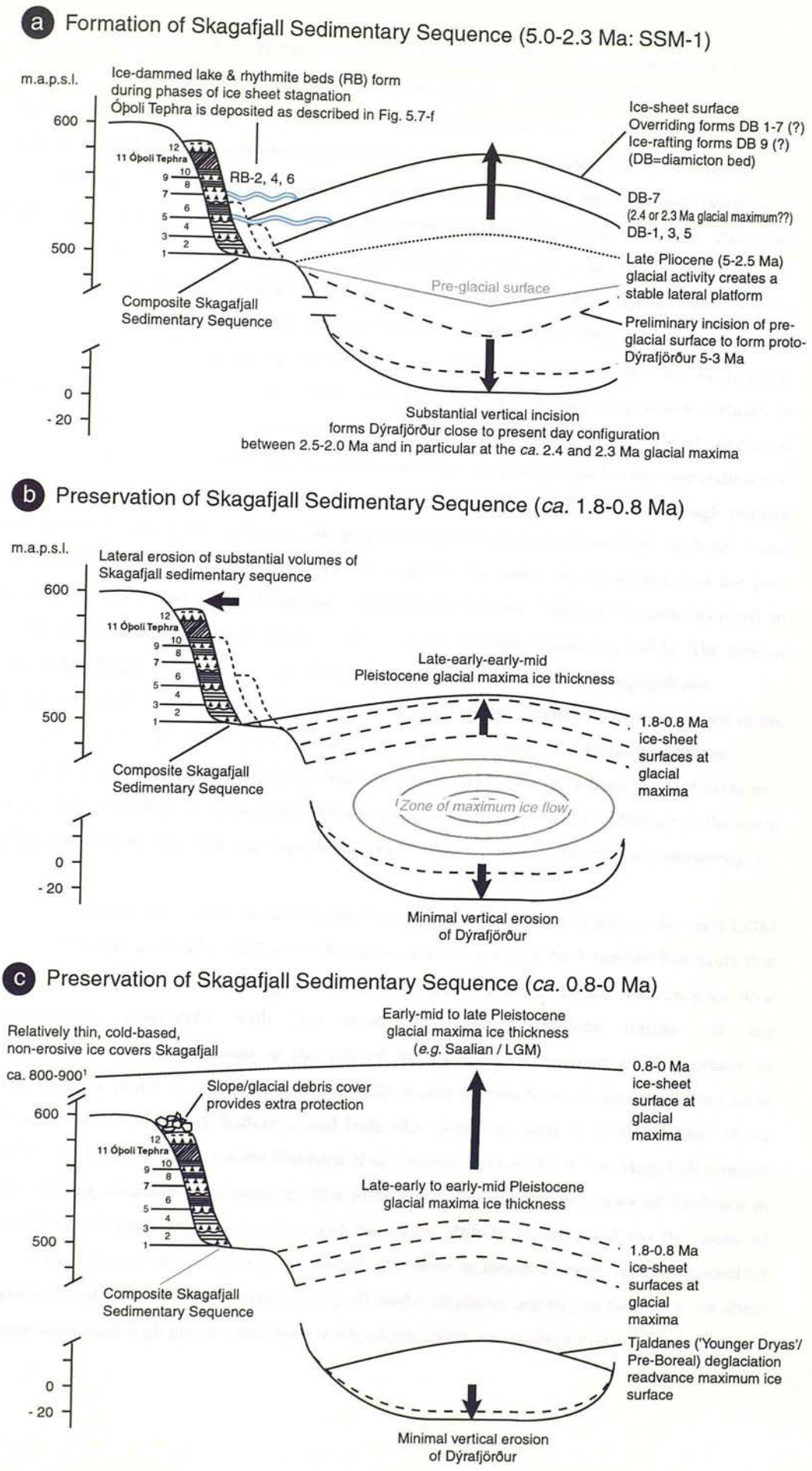


Figure 5.15 Formation and preservation of the Skagafjall sedimentary sequence as an example of macro scale landscape development of the Western Trough network of the Vestfirðir Peninsula

By analogy, it is likely that thick glacial maxima LGM-style ice sheets encompassed the whole of Iceland at least three times during the late Pleistocene when ice probably extended to Látragunn morainal bank and/or the 200 m.b.s.l. limit. The Vestfírðir Peninsula was covered by ice that was at least as thick as the LGM reconstructions presented in the previous section. Studies in high altitude plateaux regions of arctic Canada, the northern Scandinavian mountains and eastern Scotland have shown that cold-based Pleistocene ice-sheets, frozen to the bed, acted as a protective agent. This aided long-term preservation of geomorphological evidence of pre-LGM glacial activity and an extensive network of Cretaceous-Tertiary preglacial (paléic) surfaces (Gjessing, 1967; Sugden, 1968; Sugden and Watts, 1977; Hall and Sugden, 1987; Boulton and Clark, 1990; Doré, 1992; Kleman *et al.*, 1992; Kleman, 1994; Kleman and Borgström, 1994; Nesje and Whillans, 1994; Glasser and Hall, 1997; Kleman and Stroeven, 1997; Rea *et al.*, 1998). Preservation of pre-Quaternary plateaux surfaces in Vestfírðir during periods of glacial maxima ice coverage is associated with cold-based subglacial regimes within Pleistocene ice-sheets and selective linear erosion through fjords and other outlets (cf. Sugden and John, 1976). The high altitude NW-SE trending of the outer Western Trough plateau interfluves of the Vestfírðir Peninsula, *e.g.* Skagafjall and to a lesser extent Eyrarfjall-Sauðanes, were protected by cold-based non-erosive Pleistocene ice-sheets that aided the preservation of the pre-existing, Tertiary paléic and early Pleistocene sedimentary deposits. Selective erosion occurred in concentrated zones along the major fjords of the Western Troughs (Lárusson, 1983). The crucial factors that aided the preservation of early Pleistocene sedimentary deposits on Skagafjall are:

1) The elevation and location of the outer plateau interfluves of the Western Troughs marginal to the main ice divides of the LGM-style ice sheets and regional ice centres of Glama and Dranga.
2) The parallel orientation of Skagafjall and Sauðanes to the main flow directions of LGM-style ice-sheets and the diversion of main flows into the main outlet troughs of Ísafjarðardjúp to the north and Breiðafjörður to the south (*e.g.* Ingólfsson and Norðdahl, 2001; Hubbard *et al.*, *manuscript*).

No sedimentary deposits are found on plateau interfluves orientated at right angles to the main LGM flow axes, *i.e.* Tóarfjall and Lækjarfjall, or in the central plateau areas of the Vestfírðir Peninsula that experienced extensive areal scouring (Fig. 5.14-d, e). During the 'Younger Dryas' readvance ice flow along Dýrafjörður converges with ice from the outer peninsula interior of the Önundarfjörður/Dýrafjörður Peninsula at the site of the large lateral moraine at the entrance to Gerðhamradalur. Ice limits in the other fjords broadly match the positions of the lateral bars upon which the settlements of Flateyri, Suðureyri and Ísafjörður have been built. A notable feature of the 'Younger Dryas' re-advance stage in the Hubbard *et al.* (*manuscript*) model is that Skagafjall remains ice-free. In contrast, Sauðanes is covered by thin plateau ice. The relative proximity of Sauðanes to the Lambadalsfjall-Glama high-plateau area and the lower altitude of Eyrarfjall (to the south of Sauðanes, above Flateyri) are suggested as reasons. Ice flow is therefore more readily channelled across Eyrarfjall and glacial activity occurs during all modes of glacial activity on Sauðanes. Ice sheet development associated with glacial maximum mode of glaciation are required to cover Skagafjall.

In summary, the Western Trough plateaux interfluves of Skagafjall provided a remarkably stable and non-erosive environment that aided the unique preservation of an early Pleistocene record of rapid climate change. Elsewhere the three modes of glacial erosion were highly efficient at reducing and moulding the Tertiary lava pile. LGM-style ice sheets, regional and plateau style ice sheets and cirque glacial activity between Arnarfjörður and Ísafjarðardjúp led to:

1) Minor widening and deepening of the early Pleistocene fjord network during the build up to and at ice sheet maxima conditions.
2) Widespread modification of the interiors of the inner Western Trough interfluves by alpine style landscape erosion processes during periods of mountain ice cap and cirque glaciation (*i.e.* stadial stages of glacial advance).

5.5 Þörsmórk, S Iceland

The development of late Quaternary landscape in the Þörsmórk region of S Iceland provides a striking contrast to the Vestfírðir Peninsula. Detailed stratigraphic descriptions of the Þörsmórk Ignimbrite and its bracketing deposits presented in this study enable macroscale landscape evolution models to be constructed for the Þörsmórk area for the first time. It is possible to link these deposits the GRIP and GISP2 ice core records from Greenland, which provides a global palaeoclimatic framework for landscape development in this region.

5.5.1 Landscape evolution models

Volcanic aggradation, extensive and highly destructive glacial processes make evaluating the temporal evolution of landscapes in geologically active areas, such as Þörsmórk, a difficult task. There are four main reasons for this:

1) Volcanic products cannot always be dated because of their composition and/or are not representative of single eruption event because they have been reworked (*e.g.* hyaloclastite deposits).
2) Volcanism in active regions is often highly localised and making spatial correlation of stratigraphic units difficult (*e.g.* lava and hyaloclastite deposits).
3) Sedimentary deposits or volcanic deposits often have similar characteristics. Stratigraphic profiles, sometimes of markedly different age, can be represented by the similar configurations of deposits making distinctions between different periods of landscape development difficult. For example, Carswell (1983) had difficulties differentiating and correlating between hyaloclastite units around Sólheimajökull, the main southern outlet of Mýrdalsjökull (Fig. 1.10). Attempts to construct a regional chronological framework were compounded by the lack of exposed lavas and other potentially dateable material and the presence of only sporadic outcrops of the 'Ringing Ash' (Sólheimar Ignimbrite). Although a significant re-interpretation of the relative chronostratigraphy was possible, Carswell (1983; p. 70) was only able to determine that the 'volcanic rocks of the Sólheimajökull area were erupted in Pleistocene to Recent times'.
4) The preservation potential of volcaniclastic sediments is limited by their fragmentary and friable nature and repeated episodes of glacial advance.

Using the Þörsmórk Ignimbrite as a marker horizon, the following section illustrates how well-dated local stratigraphic profiles can be linked to regional and global records of palaeoenvironmental change to produce coherent models of landscape evolution for highly active volcanic areas. All currently available information has been assimilated to construct a working pre-, syn and post eruption model of macroscale landscape evolution for the Þörsmórk area (Figs 5.16 & 5.17; Table 5.8).

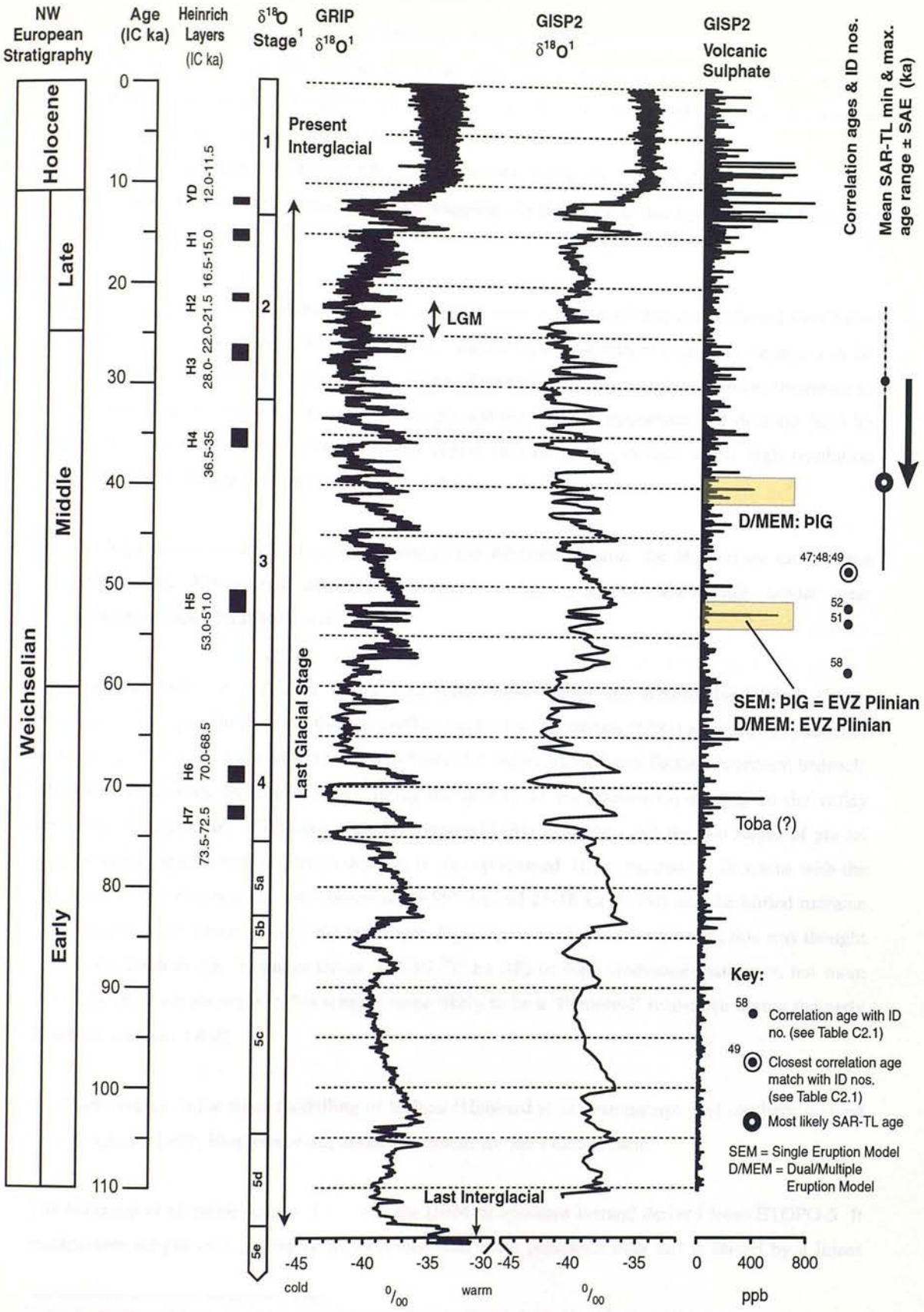


Figure 5.16 Comparison between the GISP2 Volcanic Sulphate record of palaeovolcansim, new ages for Þórsmörk Ignimbrite obtained using geochemical correlation and SAR-TL dating methods and the GRIP and GISP2 $\delta^{18}O$ proxy record of global ice volume variations for the last 110,000 years.

Notes: [1]The oxygen isotope record reflects variations in the total volume of fresh water separated from the ocean-atmosphere system (Kukla and Cliek, 1996) and is not uniformly distributed or only linked to climatic variations. The boundaries of the odd oxygen isotope stages do not correspond to the glacial/interglacial boundaries. The GRIP and GISP2 data was downloaded from The Greenland Summit Ice Cores CD-ROM (1997) obtained from NSIDC User services, University of Colorado and from the Internet at GISP2: www.gisp2.sr.unh.edu/GISP2; GRIP: www.esf.org/lp/lp_013a.htm. IC ka = ice core years before present.

The landscape model presented in Table 5.8 incorporates information from six sources:

1) The geochemically similar, unaltered, highly silicic glass-phase major element data from 23 outcrops of the Þörsmórk Ignimbrite has been used to link stratigraphic profiles across the Þörsmórk region in this study (Fig. 4.3).
2) ÞIG 1-23 correlation and ÞIG 7-SAR-TL age controls (Table 4.3; Table 4.10)
3) Jørgensen's (1981) comprehensive spatial mapping and petrological descriptions of the Þörsmórk Ignimbrite

Ignimbrite forming eruption events produce a large volume of material that is distributed over large areas. This key factor allows local stratigraphic sequences and terrestrial-marine correlations to be made (Chesner *et al.*, 1991; Westgate *et al.*, 1998). The similarity between major element chemistry of all the sites investigated, and the correlation age and provides an opportunity to develop 60-0 ka landscape evolution models for the Þörsmórk region and link these models to the high resolution record of climate change in the Greenland ice cores.

4) Geological and geophysical investigations of the Þörsmórk region, the Markarfljót sandur area (Haraldsson, 1981) and offshore boreholes 10 km south of Markarfljót sandur near Vestmannaeyjar (Pálmason *et al.*, 1965).

Þörsmórk has been inundated by ice at least three times during the Weichselian period. Cross-sectional seismic profiling across the Markarfljót sandur by Haraldsson (1981) revealed the existence of a glacially derived 15 km wide 150-200 m deep, N-S valley incised into Tertiary basement bedrock. Glaciofluvial deposits have buried this during the post-LGM era. Diamicton draping on the valley sides and an isolated arc of diamicton led Haraldsson (1981) to suggest that the two stages of glacial incision and a single phase of glacial deposition are represented. He associated the incisions with the two most severe Weichselian cold phases at 70-55[41] ka and 25-18 ka (LGM) and the buried moraine as the maximum advance limit of the last major deglaciation readvance. At the time this was thought to have occurred at the 'Younger Dryas' (11-10 ^{14}C ka BP) or Buði readvance maximum, but more recent studies have shown that this stage is more likely to be a 'Preboreal' readvance during the early Holocene (section 1.4.2).

5) High resolution ice sheet modelling of Iceland (Hubbard *et al.*, manuscript) and southern Iceland (Bingham, 1999; Bingham *et al.*, 2000, *submitted*) for the LGM-present.

The Bingham *et al.* model uses a 1 km x 1 km DEM of southern Iceland derived from ETOPO-5. It incorporates subglacial topography for Mýrdalsjökull from published data and is forced by a linear

[41] Ages are derived from ice core stratigraphic profiles in Figure 5.16. Haraldsson's (1981) ages are based on Weichselian glacial chronostratigraphy of the Northern Hemisphere of Flint (1970).

relationship between mass balance and altitude over Solheimajökull (Bingham *et al.*, 2000). Regional ice-sheet growth and LGM ice-sheet was reconstructed using a set of parameters that most accurately model present day ice cover (Bingham, 1999).

An assimilation of field and modelling evidence suggests the Þörsmórk area was inundated by ice up to and at the LGM. The strongest LGM flows were channelled along the Markarfljót. Ice flow from Torfajökull & Mýrdalsjökull merged into single ice centre with a regional N-S ice divide at the LGM and Younger Dryas. The western ice streams from Torfajökull-Mýrdalsjökull were channelled and intensified along the Markarfljót. This contributed to, but also deflected the primary flow from the interior, leaving the Krossa region relatively protected. Although inundated by ice, many deposits in the Þörsmórk region that were not aligned along the main ice flow axes were protected to some extent and large volumes of ignimbrite remain along the Krossa.

6) Ice core records of palaeovolcanism (*e.g.* Zielinski *et al.*, 1996; 1997) and the existence of Heinrich layers H4 (36.5-35 ka) and H3 (28.0-26.5 ka) (Fig. 5.16) suggest phases of glacial advance and retreat occurred in the Þörsmórk region rather than a gradual build up to LGM conditions. Build up characteristics and flow regimes in the area were probably of similar form, but of possibly lower magnitude to those of the LGM ice sheets. Palaeovolcanic ice core evidence for multiple eruptions in the 60-40 ka period is examined in more detail in the following section.

Table 5.8 (next 3 pages) The significance of the Þörsmórk Ignimbrite in constraining landscape development in the Þörsmórk region (notes at end).

Lithofacies Unit	ÞIG Site (approximate thickness) Sampling & Summary ages	General & site specific Description	NEW INTERPRETATION & MODEL STAGE
1) BASALT PILLOW LAVAS (observed at basal level on opposite river bank) [fg = fine grained; hc = hyaloclastite]	12 (10-30 m)	Elongate/cylindrical pillows with well-developed outer-rim radial and concentric cooling joints (20-30 cm thick) & intra-pillow cavities; up to 1-1.5 m long axis, but generally 0.5 m; up to 1 m short axis, but generally 0.3-0.5 m; long axis on average *ca.* 1-3 times the length of the short axis; composed of vesicular fg basalt (*ca.* 30-50 %); pillow-pillow contacts; volcanic breccia of vesicular fragments (hc?) up to 5 cm in diameter fills inter-pillow cavities (Figure 4.3-h, o, p); unable to trace unit vertically beyond eye level due to overhanging cliff face; basal contact not exposed	Proposed mode of formation is in meltwater ponds beneath the surface of an ice-sheet (cf. Jones, 1966, 1969, 1970), which was up to 150-200 m thick (see below). Proposed age of pillow formations is sometime during the *ca.* 70-60 ka glacial phase of the early Weichselian (Figure 6.8 & Bond *et al.*, 1992; Bond & Lotti, 1995). Pillow basalts are 'highly indicative' of direct magma-water contact (Moore, 1976; Cas & Wright, 1987). Emerging sea-mounts and early effusive phases of sub-glacial eruptions both produce pillows with shattered volcaniclastic inter-pillow breccia (Jones, 1970; Lonsdale & Batiza, 1980). In Iceland they are commonly associated with the initial phase of sub-glacial eruptions (Allen, 1980). The base of site 12 is *ca.* 250 m.a.s.l. Maximum relative change in sea-level in the Þörsmórk area during the Weichselian (*ca.* 80-10 ka) was probably no more than 100-120 m above or below present sea level. Minimum estimate is based on burial depths of moraines and marine abrasion limits and depths of glacial incision into the Markarfljót sandur (Pálmason *et al.*, 1965; Haraldasson, 1981. Maximum estimate is based on 110 m.a.s.l. postglacial marine limits on the lowlands NW of the Markarfljót (Kjártansson, 1970; Haraldsson, 1975) and marine limits and raised beaches in NE and E Iceland (summarised in Ingólfsson and Norðdahl, 1992). If unit 2 is a non-explosive emergent phase of sub-aerial lava flow, water depths were at least *ca.* 50 m; basalt vesicularity indicates water depth of up to ~100 m (Allen, 1980). The ice-sheet surface was, therefore, up to *ca.* 150-200 m above the current level of the Þrónga (200 m.a.s.l.) at the time of pillow eruption (assuming unit 1 does not extend significantly below the current level of the Þrónga).
2) LAVA FLOWS	ÞIG 12? (5-8 m) ÞIG 13?	Not accessible in field – mapped from opposite cliff-top (Figure 4.3-h), but grass covered, 0-5° ESE dipping near-horizontal strata *ca.* 8 m thick in total; up to 4 m for the thickest layer; most probably impermeable lava flows; fluvial channel basement rock at ÞIG 13, but no direct contact between lava and ÞIG observed	Sub-aerial deposition of lavas is either the emergent phase of subglacial volcanism during the latter stages of the 70-60 ka early Weichselian glacial event (see above; Figure 6.8) or represents the transition from sub-glacial pillow formation to sub-aerial lava flows. Proposed age for the latter is during one of the following mid-Weichselian warm interstadials (cf. Bond *et al.*, 1992 and Larsen *et al.*, 1987): (1) *ca.* 56-54 ka (2) 52-48 ka – given the correlation age of the Þörsmórk Ignimbrite eruption this is most likely (3) *ca.* 43-40 ka if the current ÞIG 7 SAR-TL ages of the Þörsmórk Ignimbrite are accurate and applicable to all occurrences of the Þörsmórk Ignimbrite

3) ÞÖRSMÓRK IGNIMBRITE (Further descriptions and petrology can be found in Jørgensen, 1980; 1981; 1987)	**ALL SITES (up to 200 m)** **Unaltered glass products sampled** **CORRELATION AGE 48-53 ka**	Þörsmórk Ignimbrite is the general name for three distinct phases of the eruption. The ignimbrite-forming stage is sandwiched between underlying white pumice and ash layered ground surge deposits and overlying black tuff, tuff breccia and co-ignimbrite breccia. Total thickness is highly variable, but up to *ca.* 150-200 m along Krossa valley.	**ÞÖRSMÓRK IGNIMBRITE:** All the currently exposed deposits in the Þörsmórk region most likely relate to a single eruption event. Main mode of emplacement was from a series of pyroclastic flows. Although Jørgensen (1981) identified up to ten different phases of activity. Five main stages of the eruption have been identified in this study: Stage 1: Pyroclastic flow surge deposition stage – Unit 3a – Sites 1, 2, 3, 5, 7, 15? Stage 2: Ignimbrite forming stage – Unit 3b – Sites – 1, 3, 5, 7, 11, 12?, 15?, 16 Stage 3: Co-ignimbrite (surge cloud) airfall ash stage – Unit 3c – 1 Stage 4: Co-ignimbrite airfall tuff stage – Unit 4a – 1 Stage 5: Tuff breccia flow and surge stage – Unit 4b – 5
3a) Inter-bedded ash/pumice/lithics	1 (10-20 m) 2 (8 m) 3 (8-10 m) 5 (15-20 m) 7 (10-20 m) ÞIG 1, 3, 7 sampled for TL **ÞIG 7 - SAR-TL *ca.* 40-45 ka** 15? (up to 100 m to Krossa)	Generally consists of well-defined layers of coarse pumice (clasts up to 10 cm diameter) – white pumice & coarse lithics (sands and gravels up to 3 cm) – ash – ash & fine lithics – thin layers of welded black pumice; variable layer thickness – each up to 20 cm thick, but generally < 10 cm thick; no evidence for overall grading, but pumice-ash fining upwards in some layers and reverse grading in others; faulting evident at ÞIG 3; post depositional dyke emplacement trending ~ NW-SE at ÞIG 1 & 7 and NE-SW (dip ~60° NE) and N (dip ~40°N) at ÞIG 2; basal contact not visible; upper contact with welded ignimbrite sharp, laterally continuous at sites 1, 5 and localised outcrops of welded ignimbrite at 7	**Stage 1: Unit 3a Pyroclastic ground surge stage** Early phreatomagmatic stage is followed by emission of pyroclastic flows with increasing explosivity (Jørgensen, 1981). Apparently random order of lithic, ash and pumice layers and lack of general grading suggests strong fluidisation deposition from a highly turbulent pyroclastic flow (cf. *e.g.* Wilson and Walker, 1981). Coarse pumice layers are due to explosive ejection of material jetted from the flow-head (*e.g.* Wilson, 1985). Jørgensen (1981, p. 349) suggested that ash-rich tephra layers are airfall deposits associated with minor periods of 'relative quiescence'. Ground surge and of pyroclastic flow deposits before full eruption column collapse that led to welded ignimbrite capping deposit. Over areas of reasonably flat topography such as ÞIG 5 and ÞIG 1b a near vertical layered sequence has developed. Sub-horizontal and/or angled layered sequences developed where surge deposits draped pre-existing, undulating topography, *e.g.* ÞIG 3. Down valley units and those off the main flow axis of the Markarfljót, *e.g.* ÞIG 1, 5, 8, 11, are relatively well-preserved, primarily because flat pre-existing topography or incised channels existed and welded ignimbrite and hyaloclastite capping units provided protection.
3b) Welded Ignimbrite	1 (up to 2 m) 3- (eroded) 5 (8-10 m) 7- (eroded) 11b (8-10 m) 13 (eroded) 16 (6-10 m) All sampled for TL **SQ-TL = 30-40 ka**	Total thickness is variable, but possibly up to *ca.* 100 m at site 15/16; elsewhere 5-10 m; white pumice clasts up to 30 cm diameter in a welded ash-fine xenolith dominated matrix (75 wt % xenoliths – Jørgensen, 1981); sporadic lenses of black pumice; at ÞIG 5 well-developed layer of flattened pumice (fiamme) up to 8x2 cm & E-W lineations in basal 0.5 m (Figure 4.3-q). Probable outcrops at ÞIG 12 and 15 buried by debris	**Stage 2 (Unit 3b): Ignimbrite stage** Welded ignimbrite formation is related to the culmination of the phreatomagmatic eruption stage during which collapse of the eruption column occurred (Jørgensen, 1981). Limited preservation of welded deposits occurs in areas that have had direct contact with major ice routes of LGM. Units are relatively well-preserved where pre-eruption topography was flat, *e.g.* ÞIG 1, 5, 11, and/or away from main flow axes (see ice flow models of Bingham, 1999; Bingham *et al.*, 2000; Hubbard *et al.*, manuscript). Along the main palaeo-ice-flow axes of the Markarfljót and the Mýrdalsjökull end of the Krossa, welded units have been completely eroded.
3c) Co-ignimbrite ash	1 (up to ~1 m) **Sampled for TL** **SQ-TL = 30-40 ka**	Eastern end of ÞIG 1b ~ 5 m long, 1 m thick unit of ash with six well-defined, continuous pumice layers with clasts up to 3 cm in diameter; numerous discontinuous lenses; no lower contact visible due to debris; upper contact is sharp, sub-horizontal and pinches out to the west of the sample location	**Stage 3 (Unit 3c): Co-ignimbrite ash stage** Co-ignimbrite ash deposited subaerially from later, lithic depleted and/or or distal portion of surge related or low altitude ash clouds, hence the lack of lithic material and well-defined pumice banding. Preservation of Unit 3c ÞIG 1 is due to basic airfall tuff cap deposit (Unit 4a). Sharp contact between the airfall tuff and the co-ignimbrite ash is due to sudden injection of basic magma into the chamber during the course of the eruption (Jørgensen, 1981; 1987).

4) BASIC TUFF & TUFF BRECCIA **4a) Basic airfall tuff**	1 (0.5-1 m)	At ÞIG 1, ~1 m thick layer of fine-medium partially welded-welded black tuff overlying unit 3c; pinches out down valley; sharp horizontal upper and lower contacts; overlain directly by hyaloclastite at the eastern end of ÞIG 1section, but a 5-10 m of unit 4b of coarse black tuff with large lithics similar to ÞIG 5 (i) & (iii) in Unit 4b, below, occurs at western end.	**Stage 4 (Unit 4a): Co-ignimbrite airfall tuff stage** These are possibly related to late eruption, highly explosive, basic 'lava fountaining' (Jørgensen, 1981; p.350) or could be the initial 'flow-head' airfall deposit of the basic pyroclastic surge phase. The former has been eroded from more proximal sites, *e.g.* ÞIG 5, by the latter.
4b) Basic tuff breccia	1 (up to 5 m) 5 (10-15 m) 15 (8-10 m) 3? 8?- 14?-	At ÞIG 5 ~ 12 m of chaotic, but generally coarsening upwards matrix supported partially welded-welded black tuff breccia (agglomerate); can be split into 3 sections (i) tuff and matrix supported gravel and lithics up to 5-10 cm diameter sharp and irregular contact with welded ignimbrite (ii) channelising and flow patterns in upper layers with well defined lenses of sorted coarse angular boulders and gravel and fine cross-bedding in tuff matrix; (iii) large randomly orientated and scattered lithic blocks in upper layers – mostly fg pillow lava (intact and fragments) and angular slabs of fg basalt lava up to 1 m in diameter and 2 m long respectively; predominantly matrix supported with some clast-clast contact; irregular and sharp upper and lower contacts	**Stage 5 (Unit 4b): Tuff breccia ground surge stage** Two possible modes of formation. The first is related to continuing explosive and pyroclastic activity from Tindfjalljökull. The second is related to post-ÞIG subglacial activity (1) Violent emplacement from a locally turbulent surge cloud is indicated by the size and lithological range of lithic clasts. Localised flows in the main surge axis from Tindfjalljökull to site ÞIG 5 create channelised deposits. (2) The tuff breccias are not related to the ÞIG eruption and represent sub-glacial flow-foot breccia (cf. Jones, 1970; Cas and Wright, 1987), hence the large pillows clasts, angular lava fragments in close proximity to well-development of subglacial channels. This aspect requires further investigation.
5) HYALOCLASTITE	1 (<1->12 m) 3- (~2 m) 5- (1-2 m) 8 (up to 2 m) 15 (10-20 m) 16 (up to 2 m) 12? 14?	Capping unit locally up to 20 m thick at ÞIG 1 and 15. Massive unit of welded volcanic breccia; consists of irregularly shaped vesicular, fg and glassy basalt fragments up to 20-30 cm, but typically 5-8 cm diameter; clast supported with little matrix; varying degrees of alteration of glass from black vitreous basalt to yellow-brown hydrated 'palagonite' breccia; At ÞIG 15 evidence for coarsening upwards of breccia with larger lobes of basalt; sharp lower contacts; no upper contact at ÞIG 1 and 15; upper parts of ÞIG 15 not accessible; angular to rounded hyaloclastite boulders up to 1 m diamter litter slopes up to ÞIG 1 & 6	These are interpreted as hyaloclastite capping deposits and are indicative of a period of renewed subglacial volcanism in the 40-20 ka build up to the LGM. The regional distribution and form suggests that subglacial volcanism was highly localised, but this could simply reflect intense post-ÞIG fluvioglacial processes in the region (Haraldsson, 1991; Bingham, 1999). There are two main sources in the area: (1) Subglacial activity along the Válahnukúr-Tindfjöll (E-W) axis creates hyaloclastite caps on the northern Krossa sites. It is possible that the bulk of Válahnukúr emerged in post-ÞIG times. Large dissected pillow structures (up to *ca.* 50 m in diameter) can be seen on the Krossa-facing side. Significant glacial erosion of the hyaloclastite deposits occurred during the LGM and deglaciation readvances. Due to its fragmentary nature hyaloclastite is easily eroded, hence its complete removal at some sites, *e.g.* ÞIG 7, by glacial activity and fluvial outlets form the retreating LGM and deglaciation ice sheets. (2) The main bulk of the Eyjafjalljökull complex did not exist at the time of the Þórsmórk eruption (Jørgensen, 1981). Intense subglacial activity during its emergence in post-ÞIG times created extensive hyaloclastite deposition over the ÞIG 1 ignimbrite deposits, at least. The current height



			of the Eyjafjalljökull complex is due to a combination of post-ÞIG subglacial accretion, regional upwarping and rapid tilting of the Eyjafjalljökull complex. A continuous vertical accretion rate of *ca.* 5 cm per year for 20,000 years would be required to build an edifice 1000 m in height. Again, significant volumes have been removed by fluvio-glacial activity, especially along the Steinholtsdalur, where periodic jökulhlaups occur.
6) DIAMICTON / DIAMICTITE	1# (localised) 6x (numerous layers – up to 2 m) 11 (2-4 m) 13 (~2 m)	Clast supported diamictons and diamictites in the Steinholtsjökull/Steinholtsdalur area (ÞIG 6, ÞIG 1); numerous layers of diamictite outcrop at ÞIG 6. Best exposure of 'fresh' matrix supported diamicton are at ÞIG 11 & 13. Poorly sorted, angular to subrounded matrix supported clasts up to 20-30 cm in diameter in grey-brown matrix (Figure 4.3-t); no striated boulders found at ÞIG 11; direct and sharp contact with underlying welded ignimbrite at ÞIG 11 and with weathered slope ignimbrite at ÞIG 13	Most likely related to retreat phases of last glaciers that covered the area either during the Buði readvance. The distribution of diamicton deposits is limited to areas that were in direct contact with Holocene glaciers (ÞIG 1, ÞIG 6), central upland areas (ÞIG 13) or channel depressions in the central upland areas (ÞIG 11).
7) INTER-BEDDED AEOLIAN SOILS & BLACK TEPHRA	3 5 8 11 12? 13 14-	Numerous orange soil and coarse-fine black ash layers well-eroded and unconformable with units 1-6	Holocene deposits related to subaerial tephra deposition and aeolian activity

Notes: This table concentrates on broad stratigraphical relationships and sedimentological characteristics of the Þörsmórk Ignimbrite and its surrounding units. Detailed petrological descriptions of the Þörsmórk Ignimbrite units can be found in Jørgensen (1980; 1981; 1987). Sites ÞIG 9 and 10 were viewed from a distance and not visited and are not included here; site ÞIG 4 is located between 3 and 5 on the side of Válahnúkur and is only a sample of weathered black tuff with no stratigraphy attached; samples were collected for TL and EMPA analysis from sites 21-23, but these sites were not visited by SJR. # = localised outcrop not directly overlying main section; - = thin or inaccessible outcrops viewed from a distance; x = not included due to major uncertainties over relationship between ignimbrite and other layers; ? inferred by position and weathering characteristics, not visible in field. Pillow lavas are defined by Jones (1970; p. 128) as a 'body of lava incorporating little or no fragmental material which, in vertical section, is seen to consist of abundant structural units, many of which display circular or elliptical outlines.'; Breccia is defined as 'fragmental rocks consisting of substantially (>25 %) of angular clasts larger than 1 cm.'; tuff and ash as defined in chapter 2; tuff is further defined here as 'fragmental volcanic rock 'with clasts predominantly (>75 %) less than 1 cm consisting largely or wholly of fragments of glass ... clasts are characteristically, although variably, vesicular, but rarely pumiceous (Jones, 1970, p. 129); all interpretations are by SJR unless stated.

5.5.2 Eruption Models for the 60-40 ka

The single and dual/multiple Þörsmórk Ignimbrite (ÞIG)/Eastern Volcanic Zone (EVZ) eruption models for the 60-40 ka presented below, and summarised in Table 5.9 are speculative. The distinction between them is based primarily on the discrepancy between the correlation and SAR-TL ages of the Þörsmórk Ignimbrite and the existence of two large sulphate peaks at *ca.* 53 and 40 ka in the GISP2 ice core record of palaoevolcanism (Zielinski *et al.*, 1996).

(a) ÞIG- Single Eruption Model (ÞIG-SEM) for the 60-40 ka period

This model assumes that the GRIP ice correlation age of *ca.* 53 ka is an accurate representation of the 'true' age of the Þörsmórk Ignimbrite. All the occurrences of the highly silicic tephra are from a single eruption. This scenario necessitates that the SAR-TL and correlation ages of *ca.* 40 and 48.5 ka, respectively, and most of the $\delta^{18}O$ chronologies of the North Atlantic are inaccurate. The following main reasons can all lead to significant SAR-TL age underestimates:

1) Fundamental problems associated with the regeneration method outlined in section 2.4.3 and in Duller (1991) and Forman *et al.* (2000).
2) Unaccounted for changes in sample sensitivity during reconstruction of the SAR-TL palaeodose value (see section 5.1.3).
3) Overestimation of the environmental dose rates that are sometimes encountered using the elemental method (see section 4.4.1). It is interesting to note that the 5.05±1.48 $Gyka^{-1}$ weighted mean homogeneous/heterogeneous model dose rate based on the difference in elemental to spectrometry method dose rates for the Óþoli Tephra produces a maximum SAR-TL age estimate of *ca.* 48 ka.

In the ÞIG-SEM, a pre-ignimbrite, Plinian phase of activity led to the deposition of glass shards with the same major element chemistry as unaltered glass products of the ÞIG in the Greenland ice cores. The Plinian phase of activity is not represented in the Þörsmórk region because it was either incorporated into the surge deposit by turbulent flow processes and/or was buried at the currently inaccessible base of the surge-related deposit.

(b) ÞIG Dual/Multiple Eruption Model (ÞIG-D/MEM) for the 60-40 ka period

This model assumes that the SAR-TL ages and the correlation ages are both accurate and the result of at least two eruptions from the EVZ in the 60-40 ka period. Although the error range of the ÞIG 7-SAR-TL age encompasses all possible correlation dating age estimates, the 29-45 ka[42] SAR-TL age range is significantly younger than the ice core correlation age estimates. As discussed in section 5.5.3 partial resetting is not considered a likely cause of this apparent age underestimate.

[42] The *ca.* 29 ka age is the minimum age estimate obtained using the heterogeneous matrix dose rate model while the *ca.* 45 ka is the maximum age estimate obtained using the homogeneous matrix dose rate model. The *ca.* 40 ka age is the age estimate obtained using weighted mean homogeneous/heterogeneous matrix dose rate model. All ages are based on dose rates calculated using the elemental method.

SINGLE ERUPTION MODEL (SEM)

Unit	General Field Description	GENERAL ENVIRONMENT OF DEPOSITION	Evidence	Chronology
1	Pillow lavas	SUBGLACIAL	ÞIG 12; marine cores of North Atlantic & GRIP/GISP2 (Bond *et al.*, 1992 & various others); Markarfljót incision channels (Haraldsson, 1981)	> 60 ka glacial activity
2	Lava	SUBGLACIAL - SUBAERIAL	ÞIG 12	*ca.* 70-55 ka
-	**EVZ PLINIAN ERUPTION**	**SUBAERIAL**	**GRIP/GISP2/DYE-3 (see Table C2.1); marine cores of N. Atlantic**	**53 / 48 ka**
3 & 4	**ÞÖRSMÓRK IGNIMBRITE**		**ÞIG 1-23 - WIDELY DISPERSED ERUPTION PRODUCT DISPERSAL**	
5	Hyaloclastite	SUBGLACIAL- SUBAERIAL (FLUCTUATING)	ÞIG 1; 3; 5; 8; 15; GRIP/GISP2; IRD & Heinrich Events in marine cores	40-18 ka
6	Diamicton	SUBGLACIAL - SUBAERIAL	ÞIG 11, 13; GRIP/GISP; Hubbard *et al.*, (manuscript); Bingham *et al.*, (submitted); Haraldsson, (1981); Pálmason (1965)	LGM and/or Last deglaciation re-advance
7	Inter-bedded aeolian soils and tephra	SUBAERIAL	ÞIG 3; 5; 8; 12; 13	Holocene

DUAL ERUPTION MODEL (DEM)

1	Pillow lavas	SUBGLACIAL	As SEM	> 60 ka glacial activity
2	Lava	SUBGLACIAL - SUBAERIAL	As SEM	*ca.* 70-55 ka
-	**EVZ PLINIAN ERUPTION (S)**	**SUBAERIAL**	**GRIP/GISP2/DYE-3 & various marine cores (Table C2.1)**	**53 / 48 ka**
-	-	SUBGLACIAL??	-	*ca.* 45-43
3 & 4	**ÞÖRSMÓRK IGNIMBRITE**	**SUBAERIAL**	**ÞIG 1-23 LOCALISED ERUPTION PRODUCT DISPERSAL**	***ca.* 40 ka**
5	Hyaloclastite	SUBGLACIAL - SUBAERIAL (FLUCTUATING)	Deposition and erosion of ÞIG capping deposits; erosion of Plinian deposits from southern Iceland	40-18 ka glacial activity (as SEM)
6	Diamicton	SUBGLACIAL - SUBAERIAL	As SEM	LGM and/or Last deglaciation re-advance
7	Inter-bedded aeolian soils and tephra	SUBAERIAL	As SEM	Holocene

Table 5.9 Summary of evidence for single and dual/multiple eruption models from the EVZ in the 60-40 ka period.

Black = eruption event; grey = deposition predominantly in a subaerial environment; white = deposition in a predominantly subglacial environment.

Sub-division, beyond the broad 58-48.5 ka NAAZ-2 correlation age match group identified by multivariate analysis is not possible with confidence. Nevertheless, subtle differences between the major element geochemistry exist and these may reflect different eruption events and/or differences in the analytical methods used. Particularly noteworthy is the consistent dissimilarity between the unaltered glass-phase composition of the Þörsmórk Ignimbrite and that of the *ca.* 58 ka $\delta^{18}O$ NAAZ-2 deposit of Lackschewitz *et al.* (1997). Both deposits were analysed in a similar manner and yet the 10 ka age difference between the Lackschewitz *et al.*, age and 48.5 ka $\delta^{18}O$ ages from various other marine cores in the North Atlantic is intriguing. The 58 ka age may relate to a combination of factors that include uncertainties in the $\delta^{18}O$ 'wiggle-matched' chronologies and delays in deposition by ice-rafting and/or mixing in cores with younger ashes (*e.g.* Andrews *et al.*, 2000; Bond *et al.*, 2001). There are numerous examples of the latter, but the most famous (and relevant) example is that of Ruddiman and Glover (1972) who originally suggested that NAAZ-2 was the result of a single eruption *ca.* 64±3.5 ka and that several 'secondary' volcanic ash peaks in the NAAZ-2 layer were due to ice-rafting events. It is interesting to note, however, that Ram *et al.* (1996) report a 57.3 ka age for the earliest of two silicic ash layer in the GISP2 ice core separated by a distinct break in the ice core stratigraphy. This age is similar to the Lackschewitz *et al.* (1997) age. Ram and Gayley (1991, p. 403) stated that 'the simplest mechanism that can explain the spreading out of our ash [across stratigraphic discontinuities in ice core stratigraphies] is multiple volcanic eruptions'. Multiple, highly-silicic explosive eruption events from Iceland between 60-40 ka are therefore a distinct possibility.

In this model, the SAR-TL age estimate is assumed to be correct. The ice and marine core deposits of NAAZ 2 are due to a highly silicic Plinian-style eruption (or eruptions) from the EVZ in the 48-58 ka period. As suggested by Zielinski *et al.*, (1997) this could be from any one of the central volcanoes in the area, but Tindfjalljökull, Torfajökull or Katla are considered most likely. If Tindfjalljökull was responsible for both eruptions the first eruption would have partially emptied or fundamentally altered the physiological characteristics of the magma chamber (cf. Larsen *et al.*, 2001). The repose time between the EVZ Plinian eruption and the ÞIG eruption was too small to generate sufficient pressure/magma and second Plinian-style eruption could not be sustained. When the ÞIG eruption at *ca.* 40 ka, 5000-10,000 years after the EVZ Plinian eruption. The ÞIG eruption, like the EVZ eruption before it, was triggered by rapid deglaciation across the EVZ shortly after the start of an interstadial period. Rapid eruption column collapse led to relatively localised deposition of the Þörsmórk Ignimbrite and provides an alternative explanation for the lack of Plinian phase eruption products in the Þörsmórk region. Tephra from the ÞIG eruption was not widely dispersed across the North Atlantic region, hence the absence of widespread and/or thick tephra deposits in marine cores. In addition, there are no reports of glass shards in the GRIP or GISP 2 records in the 45-38 ka period. It is interesting to note, however, that there is a larger than average volcanic sulphate peak in the GISP2 record at *ca.* 40 ka (Fig. 5.16). This provides additional support for the dual/multiple ÞIG eruption model. The *ca.* 40 ka event could be related to an exceptionally large and/or sulphur rich eruption

from outside Iceland (see above), but the simplest explanation is that this is the aerosol signature of the ÞIG eruption.

Chapter 6
Conclusions

Adding to the quote from Scourse (2000) on page one, this thesis has demonstrated, above all, and for the first time, that well-dated tephras from Iceland can provide otherwise unobtainable and, therefore, critical constraints on long-term landscape evolution processes in Iceland.

6.1 Tephra Ages

6.1.1 Óþoli Tephra

1) Numerical ages have been obtained from the Óþoli Tephra for the first time.

2) The 2.26±0.11Ma fission-track age of the Óþoli Tephra is significantly older than the previous estimate of 20-17 ka.

3) Preliminary palaeomagnetic results are consistent with the fission-track age. The 2.26 Ma Óþoli eruption occurred during the Matuyama magnetic reversal epoch, 0.21 Ma after the end of the Gauss normal epoch, *ca.* 2.47 Ma. The magnetic polarity of all Skagafjall sedimentary units, above unit 3 and apart from the Hjallanes Tephra, is reversed.

4) No single correlation age for the Óþoli Tephra could be determined by comparison to a geochemical dataset of published analyses of over 100 published geochemical datasets for 65-0 Ma highly silicic tephra deposits from various repositories of the North Atlantic region. Several deposits, particularly those in the mid-late Pleistocene and >10.83-<12.94 Ma age range, were close correlatives.

5) The absence of close chemical matches of comparable age to the fission-track age could be related to the location of the ocean cores and/or post depositional changes in shard chemistry. Tephra deposits in the 1.0-12.7 Ma age range were taken from cores extracted from the deep Irminger Basin, on the margins of the East Greenland ice-sheet, where parts of the Quaternary-Tertiary record might not be fully represented.

6) Thermoluminescence age estimates for the Óþoli Tephra are older than the commonly quoted upper age limit of luminescence dating of 0.5-0.8 Ma. The TL age estimates and age ranges for the should be viewed with a degree of caution. Nevertheless, TL ages comparable to the fission-track age have been obtained from the glass-phase of Icelandic tephra using simple adaptations of established luminescence techniques. TL dating was qualified success for the following reasons:

   - Spectrometry based calculations of dose rate are more accurate for the airfall component of the Óþoli Tephra because samples were extracted from *ca.* 5 cm above a rhythmite bed whose *in-situ* gamma dose rate is an order of magnitude less than the airfall and reworked components of the Óþoli Tephra.

- The near-homogeneous glassy matrix of the Óþoli Tephra produces identical dose rate estimates independent of the complexity of the dose-rate modelling method chosen.

- Eight out of eleven individual thermoluminescence dating attempts produced a final age, *i.e.* they were successful.

- Three out of four individual multiple aliquot additive dose thermoluminescence (MAAD-TL) dating experiments that used a 5 hour 155°C preheat were successful. They produced a weighted mean MAAD-TL age estimate of 2.06 ± 0.27 Ma, which is in statistical agreement with the fission-track age.

- Three out of six individual MAAD-TL experiments that used a 16 hour 135°C preheat were successful. These produced a weighted mean MAAD-TL age of 1.03 ± 0.11 Ma suggesting that the preheating regime chosen is a critical factor in producing 'accurate' ages and can result in age reductions of at least 50%.

- Significant changes in sample sensitivity were noted for the Óþoli Tephra during the course of the single aliquot regeneration thermoluminescence (SAR-TL) dating experiments. For this reason single age estimates have not been quoted, but the 1.74±0.37–4.69±0.74 Ma age range encompasses the fission-track age. The lower end of this age range (*i.e.* the 1.74±0.37 Ma fading corrected age) is considered to be closer to the 'true' age because test dose recycling plots did not grow in a strongly linear manner (*i.e.* $r^2 < 0.75$) and single standard deviation error bars for all test dose recycling points overlapped.

6.1.2 Þörsmórk Ignimbrite

(1) NAAZ-2 deposits in marine cores with a 48.5 ka $\delta^{18}O$ age are the closest geochemical match to the Þörsmórk Ignimbrite.

(2) The absence of spontaneous fission-tracks suggests the Þörsmórk Ignimbrite is less than *ca.* 100-150 ka.

(3) Semi-quantitative thermoluminescence dating analysis suggests that the age of all unaltered glass fractions from 23 sites in the Þörsmórk region from is broadly similar and in the 45-30 ka range.

(4) The SAR-TL age range estimate for the inter-bedded fallout ash component at site ÞIG 7 is 29±7–40±10 ka. The upper end of this age range (*i.e.* the 40±10 ka fading and sensitivity corrected age) is considered to be closer to the 'true' age because test dose recycling plots grew in a strongly

linear manner (*i.e.* r^2=0.96) and single standard deviation error bars for all test dose recycling points did not overlap.

(5) The different dose rates obtained from separate dose rate models for the Þörsmórk Ignimbrite emphasises the need for cross-checking measurements when determining dose rate characteristics in thermoluminescence dating.

6.2 Tephra Dating Methods

6.2.1 Correlation Dating

1) Correlation dating in the pre-^{14}C Quaternary era is possible if highly silicic ($SiO_2 \geq 68$ wt %) Icelandic tephra deposits with distinctive major element geochemistry are chosen *e.g.* Þörsmórk Ignimbrite. It is not always successful for highly silicic deposits with less distinctive geochemistry *e.g.* Óþoli Tephra. If possible a multi-site approach in the terrestrial and marine environment is preferable.

2) Multivariate statistical analysis, in particular, clustering analysis with similarity control samples, is a rapid and useful 'elimination tool' for the pre-^{14}C era correlation dating, which could be applied more widely.

3) New grain specific major element, glass-shard datasets from the Óþoli Tephra and Þörsmórk Ignimbrite presented in this thesis represent an exceptionally high quality comparative dataset for future studies that utilise pre^{14}C, Quaternary age, tephra deposits from Iceland.

4) The highly silicic glass-phase of the Óþoli Tephra is homogeneous and is ideal informal tephra glass shard 'standard' material for future EPMA. It is currently being used for this purpose in the Tephrochronological Unit at Edinburgh.

6.2.2 Fission-track Dating

1) This is the first application of glass-phase fission-track dating in Icelandic tephrochronological studies.

2) Routine preparation of slides to look for spontaneous fission-tracks would be beneficial for new deposits or deposits of uncertain, but probable pre-^{14}C age.

3) Glass-phase fission track dating analysis opens up new research opportunities for dating pre-^{14}C ash grade tephra deposits of Quaternary and Tertiary age in Iceland and could be more widely applied in a variety of situations.

6.2.3 Luminescence Dating

1) This is the first application of glass-phase thermoluminescence dating in Icelandic tephrochronological studies.

2) Although further refinement of the methods used is needed, quantitative volcanic glass-phase, coarse-grained TL dating was moderately successful. This was due to the following combination of factors:
   - The magma quenching-glass formation event being dated is thermally and chronologically unambiguous.
   - The luminescence signal in volcanic glass is overwhelmingly due to recombination from heat sensitive traps. Bleaching and inducement experiments demonstrated that no post-depositional light exposure occurred and/or traps in the glass matrix are not highly susceptible to emptying/resetting by light exposure.
   - The glass-phase TL signal dose response growth can be broken down into two main stages:
     (i) A first phase of linear dose response followed by first and main phase of signal saturation
     (ii) A second, approximately linear dose response, post-first phase saturation growth

     If the linear dose response second stage growth characteristics can be adequately constrained, and/or near accurate palaeodose values can be obtained by minor modification of established multiple aliquot additive dose and single aliquot regeneration methods, age estimates of great value and older than the generally assumed upper age limit of 800 ka for luminescence dating can be obtained.
   - In theory, consistent and highly accurate dose rates can be obtained from highly silicic Icelandic tephra deposits. Environmental radioactivity is broadly homogeneous in distal deposits because of the predominantly chemically homogeneous glassy nature of the highly silicic tephra matrix (*e.g.* Óþoli Tephra). In practice, dose rate accuracy (and precision) is currently compromised by:
     (i) Limited information on seasonal and annual fluctuations in sediment water content in the Icelandic environment.
     (ii) The airfall component of highly silicic distal deposits should be sampled because it is the least contaminated component of a single tephra unit. Distal airfall components sampled in this study were all less than 10 cm thick and adjacent to units whose environmental dose rate is known or presumed to be an order of magnitude less than the highly silicic deposit.

     These problems were overcome in this study by:
     (i) Assuming that the mid-point between measured summer water content and water saturation values is a reasonable approximation of average palaeowater content.

(ii) Sampling greater than 3 cm from the lower contact and only using *in-situ* gamma dosimetry measurements to calculate dose rates

- Anomalous fading of the stored luminescence signal is not a serious problem for highly silicic glass. A new, preliminary cooling-rate based model was presented. The underlying principal of this model is that the rapid liquid-solid phase cooling transition creates a random arrangement of defect-acceptor pairs, restricting signal loss by quantum mechanical tunnelling. An alternative explanation is that the pre-heating regimes used were adequate.
- Most of the above are unique to the highly silicic volcanic glass phase of explosively erupted tephra deposits.

3) TL age estimates of samples that used either a 5 hour, 155°C or 2 minute, 220°C preheat for palaeodose dose evaluation are more similar to the fission-track age of the Óþoli Tephra. Substantially younger ages were obtained from experiments that used a 16 hour, 135°C pre-heat. This suggests that shorter, high temperature are preferable for glass-phase TL dating and that the glass matrix is susceptible to additional signal loss, possibly from deeper trapping sites, at very high storage temperature.

4) Accuracy is the key when dating isolated events, such as volcanic eruptions. The precision of the fission-track and thermoluminescence ages of Óþoli Tephra is more than adequate for its intended purpose, *i.e.* constraining long-term landscape development of the Vestfírðir Peninsula. Reducing the level of uncertainty is desirable for the Þörsmórk Ignimbrite, however, because glass phase TL dating might prove to be the only method capable of determining whether all occurrences of the Þörsmórk Ignimbrite and/or NAAZ-2 are the result of single or multiple eruptions.

5) Significant changes in sample sensitivity were noted during the course of the single SAR-TL dating experiments. It was considered more appropriate, therefore, to quote SAR-TL age estimates as minimum-maximum age ranges than single age estimates. This proved useful for the Óþoli Tephra, but uncertainties remain over the 'true' age of the Þörsmórk Ignimbrite.

6) The age errors are for the both the Óþoli Tephra and the Þörsmórk Ignimbrite are large *ca.* 20-30% and 40-45% respectively. This is primarily due to the large errors ranges associated with palaeowater content estimation because current knowledge of the seasonal water content of the sediments examined is limited. Above all, the thermoluminescence dating experiments described highlight the need to refine, and define, luminescence dating procedures on sample-by sample basis rather than applying a single general dating strategy.

6.3 Palaeoenvironmental Applications

6.3.1 Skagafjall & the Vestfírðir Peninsula

(1) The Skagafjall sedimentary sequence is the first directly dated high resolution terrestrial record of early Pleistocene glacial activity and rapid climate change in the circum North Atlantic region.

(2) The new tephra based dating evidence from Skagafjall suggests that a macroscale fjord network of similar configuration to the present day existed across western Vestfírðir since the early Pleistocene.

(3) The establishment of the fjord system in the Vestfírðir Peninsula by at least 2 ¼ Ma had a significant impact on the extent and form of subsequent glaciations and aided the preservation of the Skagafjall deposits. Early formation of the fjord network provided outlet channels for regional ice streams, leading to the development of landscapes of selective linear erosion in and around the western troughs (Sugden and John, 1976; Lárusson, 1983). At times of maximum glacial activity during the mid-late Pleistocene the Vestfírðir Peninsula was covered by ice-sheets several hundreds of metres thick. Highly erosive ice streams were channelled through the pre-existing Western Trough network troughs. Outer plateau Western Trough interfluves were covered with cold-based, non-erosive ice which protected the 'pre-glacial' Tertiary topography and early Pleistocene glaciation features *e.g.* Skagafjall sedimentary sequence. Deposition of blockfields and basal deposits onto the plateau surface from the overriding ice sheets provided additional protection.

(4) The high altitude, sedimentary sequence of ice-dammed lake deposits on Skagafjall appears to be unique in NW Iceland. An ice dammed lake of similar size and configuration possibly existed on Sauðanes at the same time as the Skagafjall lake, but sedimentary evidence on Sauðanes is now limited to scattered fragments of similar nature to Skagafjall rhythmite beds, sizeable erratics (this study) and boulder gravels (Sigurvinsson, 1982; 1983). Sauðanes was more susceptible to mid-late Pleistocene glacial maxima erosion because it lies on the principal axis of outflow from the Gláma-Lambadalsfjall accumulation zone. It is possible that Lækjarfjall and other NW-SE trending plateaux supported ice-dammed lakes during the early Pleistocene. The Hubbard *et al.* LGM ice-model suggests that strong northwards flowing ice streams overran Lækjarfjall exposing the basalt strata.

6.3.2 Þörsmórk & Southern Iceland

1) In contrast to early Pleistocene plateau remnants of the Vestfírðir Peninsula, the Þörsmórk area has experienced rapid subglacial landscape accretion and highly erosive wet-based glacier erosion

processes in the last 60,000 years. A not unreasonsable vertical accretion/regional uplift rate of *ca.* 5 cma^{-1} for a 20,000 year period is needed to create the Eyjafjalljökull central volcano.

2) There is at least an 8,000 year age discrepancy between the SAR-TL and correlation age estimates of the Þörsmórk Ignimbrite presented.

3) The maximum SAR-TL age coincides with an major sulphate peak in the 110,000 year GISP2 record of palaeovolcanic activity. This study suggests, for the first time, that the Þörsmórk Ignimbrite could be the latter of at least two chemically similar eruptions from the Eastern Volcanic Zone in the 60-30 ka period.

6.4 Future Work

Further field- and experimental work is encouraged because of the significant nature of the preliminary results obtained.

6.4.1 Dating techniques

1) Full scale grain specific SIMS or laser ablation ICP-MS trace element analysis of glass separates would be beneficial. Investigations of this type for the NAAZ-2 deposits are in progress (Lacasse, *pers. comm.*). This data and further refinement to the TL dating methods used could help determine if the ignimbrite deposits in the Þörsmórk region are the result of single, dual, or multiple eruption events. Preliminary ICP-MS results from purified glass fractions of ÞIG 1b, ÞIG 7, ÞIG 13, ÞIG 16 suggest that subtle differences in trace element composition exist.

2) The Hj-2b fraction of the Hjallanes Tephra, found at a lower altitude in the Skagafjall sequence was too basic and fine grained for fission-track dating analysis. It is unlikely that TL or OSL methods would be successful given the age of the Óþoli Tephra, the low dose rate recorded the rhythmite beds and major uncertainties associated with the completeness of optical resetting in glaciolacustrine deposits (Berger, 1995; Prescott and Robertson, 1997). The absence of a clearly defined chemical correlation age and the general lack of suitable phenocyrstic material make further isotopic dating of the Óþoli Tephra difficult, but the unexpected antiquity of the Óþoli Tephra, means isotopic tephra dating techniques might be suitable for phenocryst (or even glass phases) of the Óþoli and Hjallanes Tephras.

3) The thermoluminescence dating results presented are highly encouraging, but further work needs to be undertaken to test the suitability of volcanic glass from Iceland as an accurate TL chronometer. Particular attention is needed to reproduce and establish the accuracy of the techniques developed for dating deposits in the > 0.5 Ma age range. TL signals were obtained from the Öræfi 1362 and Askja 1875 samples suggesting that TL dating of highly silicic ash layers of Lateglacial and Holocene age is possible with modifications to the equipment.

4) An awareness of the potential problems that exist in the TL dose rate calculations has been demonstrated in this study. The experimental procedures and the accuracy and precision of the TL ages needs to be improved for glass-phase TL dating of tephra deposits to be considered as reliable as the fission-track method. Differences in ED values have been noted between etched and non-etched samples of fine-grained volcanic glass (Berger and Huntley, 1985) and this aspect needs further investigation. Further HF etching experiments may reduce grain-grain variability, improve precision and perhaps accuracy of glass-phase tephra TL ages obtained so far.

5) Further refinement of the methods used is needed to improve the accuracy and precision of ages obtained. Monthly measurements of the ash layer water contents at sampled sites and its effect on total dose rate evaluation would be particularly beneficial, as would the further application of MAAD-TL methods to ash deposits of the Þörsmórk Ignimbrite.

6) Extensive experimental tests and, perhaps, numerical modelling are required to test the cooling rate hypothesis of anomalous fading further.

7) An unsuccessful attempt was made to obtain ^{3}He cosmogenic surface exposure ages from the only six olivine and pyroxene phenocryst-rich boulders found on the surface of Skagafjall and Sauðanes. Further attempts at ^{10}Be, ^{26}Al cosmogenic surface exposure dating of larger and more abundant plateaux surface erratics could provide an additional constraint on the last time the Vestfirðir Peninsula was inundated by ice.

6.4.2 Palaeoenvironmental applications

1) The direct ages from the Óþoli Tephra presented in this thesis are highly significant and open up new possibilities for connecting early Pleistocene terrestrial and marine records of palaeoenvironmental change. Future studies should concentrate on establishing the presence of the Óþoli Tephra in:
   - Marine cores from outside the Irminger Basin
   - Inter-bedded lava, till and sedimentary sequences in Iceland, *e.g.* Tjörnes, that span this period.
   - Glacial sedimentary sequences in south-east Greenland that are thought to date from between 2.0-1.8 Ma (Larsen *et al.*, 1994).

2) The age of the Óþoli Tephra provides an excellent 'circumstantial' constraint on early Pleistocene climate change. Further palaeoenvironmental and biological investigations of the Skagafjall sequence might be beneficial.

3) Further age estimates from other deposits would enable further refinement of the models presented. For example, high stratigraphic resolution (1 or 10 cm) palaeomagnetic analysis of the whole sequence, Hjallanes Tephra and other overlying erratics, would be beneficial if possible.

4) Further analysis of the Skagafjall deposits in uncharacteristically warm Vestfírðir summers would be beneficial. This could include detailed fabric analysis of the diamictons, because more extensive/different parts of the sequence would be exposed by melting snow patches. Detailed fabric analysis of the diamictons was unsuccessful because it was difficult to distinguish between slope debris and boulders/pebbles that had been deposited *in-situ*. In addition, most of the boulders were either subangular-subrounded with either no long axis or obvious orientation. In addition, micromorphological analysis of the deposits might reveal further insights into the genesis of the Skagafjall deposits.

5) Multiple aliquot additive dose (MAAD-TL) dating of samples used in SAR-TL dating of the Þörsmórk Ignimbrite would be beneficial for establishing the reliability of the technique and producing equivalent dose values of comparable or better accuracy and precision.

6.4.3 Other

1) Further identification and (fission-track) dating of the ash deposits in and around the Dyngjufjöll volcanic complex would be beneficial for establishing the source of Óþoli Tephra and a more accurate developmental history of Askja.

2) Further, glass-phase EPMA and fission-track analysis of tephra deposits from various ignimbrite formations in and around the Húsafell complex, and in particular those of the 3rd acid phase, as well as other volcanic complexes of SW axial rift area would help establish the source volcano of the Óþoli Tephra.

Appendix **A**: **Terminology, Definitions & Isotopic Dating of Tephras**

This appendix provides a list of commonly used abbreviations for reference (Table A1.1) extended definitions of terms introduced in the main body of text (Section A1), brief outlines of general issues applicable to all Quaternary dating techniques (Section A2) and, for completeness, a brief evaluation of the potassium argon and argon-argon method and it application to dating of tephra deposits (Section A3).

Chemical methods:		
EPMA		electron probe microanalysis
ICP		inductively coupled plasma emission spectrometry
ICP-MS		inductively coupled mass spectrometry
NAA		neutron activation analysis
SEM		scanning electron microscope
SIMS		secondary ion mass spectrometer
XRF		X-ray fluorescence
ME		major elements
TE		trace elements
REE		Rare Earth Elements
Dating methods:		
TL		thermoluminescence
PTTL		phototransferred TL
OSL		optically stimulated luminescence
PSL		photo stimulated luminescence
IRSL		infrared stimulated luminescence
MAAD		multiple aliquot additive dose
SAR		single aliquot regeneration
ESR		electron-spin resonance
ED		equivalent dose
FT		fission-track
ITPFT		isothermal plateau fission-track
DCFT		diameter corrected fission-track
K-Ar	(^{40}K-^{39}Ar)	potassium-argon dating
Ar-Ar	(^{40}Ar-^{39}Ar)	argon-argon dating
U-series		uranium series
PM		palaeomagnetic polarity
Age abbreviations:		
a		calendar years before present
ka		10^3 calendar years before present
Ma		10^6 calendar years before present
Ga		10^9 calendar years before present
^{14}C ka BP		10^3 uncalibrated radiocarbon years before 1950 AD
calibrated ^{14}C ka BP		10^3 calibrated ^{14}C years (after Stuvier and Reimer, 1993)
Radioactivity units		
Radiation dose		Gray: 1 Gy = 1 Jkg-1 = 100 rad
Dose rate		milli-Grays per year: mGya^{-1} = Gyka^{-1} Grays per thousand years
Radioactivity		Becquerel: 1 Bq = 1 radioactive decay per second
		Curie: 1 Ci = 37x10^9 Bq
Biologically effective dose		Sievert: 1 Sv = 1 Gy for radiation having a biological effectiveness of unity
Prefixes, other symbols, abbreviations & units:		
m	milli	(x 10^{-3})
μ	micro	(x 10^{-6})
n	nano	(x 10^{-9})
λ	wavelength	
ppm	parts per million	
ppb	parts per billion	
min	minute	
hr	hour	

Table A1.1 Principal terminology, abbreviations, symbols and units used in this thesis. Otherwise, SI units are used throughout. Other units and abbreviations are explained in text.

A1: Definitions & Classification of Volcanic Terms

An exhaustive description of volcanic processes and terminology can be found in Carmicheal *et al.* (1974), Gary *et al.* (1976), Fisher and Schmincke (1982), and Hall (1987). What follows is a summary of the main terms used in this thesis.

A1.1 Pyroclastic deposits

Pyroclastic fragments (**pyroclasts, pyroclastic material**) are unconsolidated volcanic products that are ejected through the vent during a volcanic eruption. They are produced directly from volcanic processes. Pyroclasts are the main constituents of volcaniclastic rocks. **Volcaniclastic** is a general term best defined as 'clastic volcanic materials formed by any process of fragmentation, dispersed by any transporting agent, deposited in any environment or mixed in any significant portion with non-volcanic fragments' (Fisher and Schmincke, 1982; p. 89).

Wright *et al.* (1980; 1981) proposed two different classification systems for pyroclastic deposits reflecting the complexity of their formation processes and their representation in the geological record (Table A1.2).

FIELD BASED		LABORATORY BASED
GENETIC	LITHOLOGICAL	CHEMICAL
Pyroclastic fall Pyroclastic flow Pyroclastic surge	Grain size distribution Dominant components	SiO_2 content Alkali - silica bi-plot

Table A1.2 Classification schemes for pyroclastic rocks. Terms in this table and used in this thesis are from Fisher (1961), Schmid (1981) and Wright *et al.* (1980; 1981b). Full details and definitions of terms used can be found in Wright *et al.* (1980; 1981b).

Genetic classification groups pyroclasts according to their eruptive mechanism and is related to the volcanoes history, location and behaviour pattern (Fig. 2.1). **Lithological classification** is purely descriptive, no mode of origin is implied. It is based on the grain size distribution of the constituent fragments and their degree consolidation or welding (Fisher and Schmincke, 1982).

PYROCLAST	GRAIN SIZE (mm)	PYROCLASTIC DEPOSITS UNCONSOLIDATED Tephra	CONSOLIDATED Pyroclastic rock
Block, Bomb	>256	Coarse agglomerate Coarse bomb/block tephra	Coarse agglomerate Coarse pyroclastic breccia
	64-256	Fine agglomerate Fine bomb/block tephra	Fine agglomerate Fine pyroclastic breccia
Lapilli	2 - 64	Layer Lapilli tephra	Lapillistone
Ash	1/16 - 2 <1/16	Coarse ash Fine ash	Coarse tuff Fine tuff

Table A1.3 Granulometric classification of the end member terms for pyroclastic fragments (adapted from Schmid, 1981; Wright *et al.*, 1981b). These definitions are used in this study.

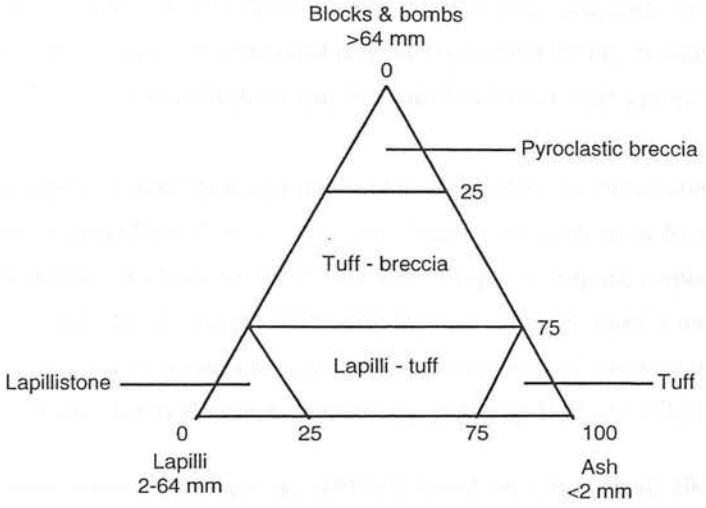


Figure A1.1 Lithological classification scheme for mixture terms of end-member pyroclastic fragments defined in Table A1.3. Numbers adjacent to the ternary diagram represent the percentage of ash in each mixture (adapted from Fisher and Schmincke, 1982). These definitions are used in this study.

Tephra is a non-genetic, collective term for unconsolidated accumulations of airborne pyroclasts of any size. It is synonymous with the term 'pyroclastic material' and includes all deposits listed in Table A1.3 and Figure A1.1 (Thórarinsson, 1944; Whitten and Brooks, 1972; Schmid, 1981; Fisher and Schmincke, 1982). The dominant constituent of tephra is volcanic glass. This is particularly true of highly silicic Icelandic tephra deposits (*e.g.* Mørk, 1984). Other components are crystal and lithic fragments. **Breccia** is defined as 'fragmental rocks consisting of substantially (>25 %) of angular clasts larger than 1 cm.' (Jones, 1970; p. 128). It should be noted that there minor variations in the definitions for some terms shown in Table A1.1 and Figure A1.1. For example, Gary *et al.* (1976; p. 759) define **tuff** as a 'compacted pyroclastic deposit of volcanic ash and dust that may or may not contain up to 50% sediments such as sand or clay' and **ash** (p. 41) as 'fine pyroclastic material (under 4.0 mm in diameter; under 0.25 mm in diameter for fine ash' whose use is usually restricted to

description of unconsolidated material. Jones (1970; p. 129) defines tuff more specifically as a 'fragmental volcanic rock 'with clasts predominantly (>75 %) less than 1 cm consisting largely or wholly of fragments of glass ... clasts are characteristically, although variably, vesicular, but rarely pumiceous.'

Combinations of these terms are used throughout this study. For example, Gary *et al.* (1976; p. 42) define **ash flow tuff** as a 'tuff deposited by an ash flow or gaseous cloud; a type of ignimbrite. It is consolidated, but not necessarily welded'. An **ash flow** (p. 42) is defined as ' a turbulent blend of unsorted, mostly fine-grained pyroclastics and high-temperature gas ejected explosively from fissures or craters.' And **ash fall** (p. 42) (synonymous with the term **air-fall ash** used in this study) as 'the descent of volcanic ash from an eruption cloud by *air-fall deposition*.'

A variety of **chemical classification** schemes exist volcaniclastic deposits. Terms used are applicable to both pyroclastic and non-pyroclastic material. Distinctions are made according to the different differentiation and evolution processes that magma experiences during its ascent to the Earth's surface (Le Maitre, 1976). In essence, magmas can be divided in to two main groups (Fisher and Schmincke, 1982):

1) Parental magmas formed by the partial melting of the upper mantle or crust.
2) Derivative magmas formed by differentiation from parent magmas or by mixing of magmas

Primary mafic basaltic magmas are the most primitive types of magma, erupting through fissures with no chemical change during transit. Such magmas are rare and most experience some degree of cooling, fractionation and mixing en-route. Explosive eruptions of silica-saturated and undersaturated magmas are probably due to abundant volatiles (*e.g.* primarily H_2O and CO_2) in the melt.

The classification scheme of Cox *et al.* (1979) is based on variations in alkali (Na_2O+K_2O) - silica (SiO_2) composition. This forms the basis of Figure 4.7-a. The classification scheme of Irvine and Baragar (1971; p. 524-525) groups rocks according to similarities in their chemistry, reflecting the degree mixing or differentiation from the parent magma. This classification scheme forms the basis of Figure 4.7-b. Both schemes provide a 'chemical definition of conventional [volcanic] rock names' that were originally defined on a mineralogical basis. Both schemes are simple, but useful, starting points for classifying the chemical composition of the glass component of Icelandic tephra deposits, although this was not their original purpose. Nevertheless, volcanic glass reflects the composition of the magma form which it formed and these chemical classification schemes are should be applicable to the volcanic glass component of tephra deposits provided no loss or migration of mobile elements has occurred. Further details can be found in Irvine and Baragar (1971), Carmichael *et al.* (1974), Cox *et al.* (1979), Fisher and Schmincke (1982) and Hall (1987).

A1.2 Common Icelandic Rock Types

Iceland is best classified as an oceanic-rhyolite-basalt system because many mixed eruptions of basaltic and rhyolitic material occur (Fisher and Schmincke, 1982). This activity reflects Iceland's position straddling the Mid-Atlantic Ridge spreading axis and directly above an eastward migrating 'deep-mantle hot-spot', currently located in the East Volcanic Zone beneath Vatnajökull (Fig. 1.3).

Basalts are the most abundant type of volcanic rock in Iceland occurring as **'ocean-island tholeiites'**, or as **'alkali basalts'**. Ocean-island tholeiites are richer than **ocean-floor tholeiites** (*e.g.* Mid-Ocean Ridge Basalts), in volatiles, alkalis and incompatible elements (*e.g.* K, P, Rb, Zr, Nb, U) indicating a greater degree of magma mixing or differentiation during their formation. In Iceland non-pyroclastic deposits of this type form voluminous shield forming lavas while pyroclastic rocks are mainly hyaloclastites (Fisher and Schmincke, 1982). Alkali basalts are more silica-undersaturated than tholeiites, but are enriched in incompatible elements and volatiles.

Pillow lavas are defined by Jones (1970; p. 128) as a 'body of lava incorporating little or no fragmental material which, in vertical section, is seen to consist of abundant structural units, many of which display circular or elliptical outlines.' **Hyaloclastite** is a fragmental pyroclastic rock formed from the comminuted glassy shells of pillow lava produced during submarine, sub-lacustrine or sub-glacial basalt eruptions by the intense chilling and brecciation of lava against water or ice (Gary *et al.*, 1976). Layered pillow-hyaloclastite-breccia complexes are common in Iceland, forming principally in sub-glacially or in shallow marine environments (Jones, 1970). Sigurdsson and Sparks (1981) suggested that rhyolitic rocks in Iceland formed by fractional crystallisation from basaltic melts. Several different melting models have also been proposed for their formation (*e.g.* Grönvold, 1972; Sigurdsson, 1977; Mørk, 1984; McGarvie, 1984; McGarvie *et al*, 1990). **Comendite** is a white or light coloured (leucrocratic) extrusive volcanic rock/deposit with 0-35% dark minerals. Comendite is a sub-class of pantellerite. **Pantellerite** is 'characterised by acmite-augite or diopside, anorthoclase and cossyrite phenocyrsts in a pumiceous, partly glassy, fine-grained microlite dominated groundmass of acmite and feldspar. Plagioclase is typically absent and quartz rare' (Gary *et al.*, 1976; p. 514). Pantellerites are **peralkaline** rocks, defined as $Na_2O+K_2O/Al_2O_3 > 1$ (agpaitic index, AI; molecular proportions) and comendites as $Al_2O_3 > (1.33*FeO) + 4.4$ (Civetta *et al.*, 1998).

A1.3 Type of eruptions mentioned in text

A **Plinian eruption** can be simply defined as a type of volcanic eruption characterised by periodic explosive events (Gary *et al.*, 1976). A quantitative definition is given in the caption of Fig. 2.1 (a). Ignimbrite forming eruptions are relatively uncommon in Iceland. The term **ignimbrite** and has been used in a variety of ways (Wright *et al.*, 1981b), but the broad definition of Gary *et al.* (1976; p. 353) as 'the rock formed by the deposition and consolidation of ash flows and nuée ardentes' is preferred in this thesis. A degree of welding is not defined; hence ignimbrites can consist of a variety of welded

and non-welded ash, tuff and volcanic breccia (Wright *et al.*, 1981b). Nuée ardentes are defined as 'swiftly flowing and turbulent gaseous cloud[s], sometimes incandescent, erupted from a volcano and containing ash and other pyroclasts in its lower part' (Gary *et al.*, 1976; p. 486).

A2: Quaternary Dating Techniques

The classification scheme proposed by Colman *et al.* (1987) for Quaternary dating techniques has been widely adopted elsewhere and is used throughout this thesis (Fig. 2.7). Smart (1991b) recommends this scheme because of its simplicity; other schemes exist (*e.g* Lowe and Walker, 1997). In the Colman *et al.* scheme, methods are grouped according to similarities in their fundamental mechanisms, assumptions and applications and the type of results produced form a second, distinct classification that are allowed to, and often do, overlap.

Smart (1991b) and Prescott and Robertson (1997) suggested that there are three critical criteria that to be satisfied when selecting a dating method:

1) Applicability	Is there dateable material in a deposit and if so which method is most appropriate?
2) Time Range	Does the time range of the method match the probable age of the deposit?
3) Accuracy & Precision	Does the method produce consistently accurate ages that are similar to those produce by other methods? Is the method precise enough to resolve the age difference in the events of interest? Would/do zero-age/lower limit controls return a zero age?

A2.1 Upper & Lower Age Limits

The upper and lower age limits of dating techniques are fixed by the techniques' underlying physical processes, the sensitivity of the measurement technique. Lower dating limits depend on the technique selected and the concentration of critical elements in a sample (*e.g.* the presence of carbon for ^{14}C dating, uranium for fission-track dating, principally potassium, uranium and thorium for luminescence dating). Upper limits depend on the technique selected and the stability of the sample (Smart, 1991b). Table A2.1 shows the generally applicable age limits for selected dating techniques.

Upper age limits for some techniques are universal. For example, methods based on the radioactive decay of parent isotopes are limited to approximately 10 half-life reductions because, in many cases, instrumentation is not sensitive enough to measure minute quantities of decay products present. Future improvements in instrumentation might extend the upper datable limits. However, this has not been the case for radiocarbon dating (Scott and Harkness, 2000). The introduction of AMS analysis reduced the amount of organic material required to obtain an age. However, it did not increase the upper age limit significantly because of the underlying half-life decay principle upon which it is based.

METHOD	AGE RANGE min.	max.	PRECISION (% unless stated)
Historical records	0	4000	minimal error
Dendrochronology	0	12 ka	± 0.5 years
Varve chronology	1000	30 ka	± 0.5 years
Ice core records	100	200 (700?)	±
Radiocarbon (^{14}C)			
Wood, resin	0	6 ka	± 60 years
Charcoal, peat	6 ka	30 ka	1 %
Shell, coral	> 30 ka	45 ka	1 %
Potassium & argon - argon (^{40}K-^{40}Ar & ^{39}Ar-^{40}Ar)			
K-rich/plagioclase feldspar	30	<20 Ma	0.5 %
Sanidine & feldspar			
Uranium Series (U-series)	0	500 ka	<0.5 %
Helium-uranium (He-U)	100	> 2 Ma (?)	(?)
Cosmogenic exposure dating (CED)[2]	1000	5-10 Ma	10-20 %
Fission-track (FT)[3]			
Zircon; apatite; muscovite	50 ka	10 Ma	5-10 %
Volcanic glass	50-100 ka	5 Ma	5- 10 %
Thermoluminescence (TL)[1]			
Pottery	100	100 ka	10 %
Tephras	1000	> 800 ka (?)	10-15%
Optically stimulated luminescence (OSL)[1]			
Quartz-rich sediments	100	100 ka	7-10 %
Feldspar rich sediments	1000	800	7-10 %
Electron Spin Resonance (ESR)			
Coral, teeth, calcite, gypsum	0	1 Ma	10-20 %
Tephrochronology	0	unlimited	errors in dating methods used in correlations
Palaeomagnetism	20-30	unlimited	

Table A2.1 General effective range of application of dating techniques classified in Figure 2.7. Abbreviations used in the text are shown in brackets after the method name. Ages are in years unless stated; (?) = uncertain (adapted from Smart, 1991a; Williams *et al.*, 1998; additional information from [1]Aitken, 1985, 1998; [2]Brook, 1993; Berger, 1994; [3]Lowe and Walker, 1997).

Upper age limits for certain techniques are variable. For example, in luminescence dating the palaeodose equivalent to the natural luminescence intensity that has accumulated in the sample since the last resetting event is reconstructed. If the dose rate, acquired from irradiation by radioactive minerals potassium, uranium and thorium in the sample, is established, and the rate of loss of the luminescence signal during burial is negligible, an age can be determined (McKeever, 1985). Concentrations of potassium, uranium and thorium are much smaller in quartz than feldspar. The dose rate in quartz is therefore smaller than feldspar and the first linear growth phase of the reconstructed palaeodose curve in quartz extends over a larger dose range than feldspar. Consequently, the upper age limit for luminescence ages obtained from quartz is generally higher than that of feldspars.

A2.2 Accuracy, precision & errors

Of the techniques applicable to tephra deposits (Fig. 2.6) only volcanic eruptions chronicled in historical archives and some incrementally dated pre-historic records produce an actual eruption 'date'. All the other applicable dating techniques produce 'ages' or 'age estimates' with inherent uncertainties. These terms imply that there might be differences between an experimentally obtained age and the true age (Smart, 1991b). The accuracy and reliability of age estimates if less than ages.

The overall accuracy of the experimental age obtained depends on three main factors (adapted from Smart, 1991b, Lowe and Walker, 1997):

1) The physical and chemical characteristics of the tephra deposit (because, above all, this determines which dating technique(s) can be used)
2) The legitimacy of the underlying principles and assumptions of the technique chosen
3) Establishment and/or adherence to the principles and assumptions of the technique employed during the experimental process

Overall uncertainties are usually expressed as ± 1 standard deviation (± 1σ) with a 68% probability that the 'true' age obtained lies within these limits. Certain isotopic methods are capable of producing high precision ages quotable to 2σ (*e.g.* Gansecki *et al.*, 1998). Most radiogenic ages are quoted with 1σ or standard analytical errors. Although less precise, they are not necessarily less accurate than isotopic methods and in circumstances where high precision is not crucial (*e.g.* widely spaced eruption events) radiogenic methods have proved very useful (Naeser and Naeser, 1988). Standard analytical errors (SAE) are often quoted (*e.g.* Summerfield *et al.* 1999; TL dating in this study) and these reflect the typical age errors that can be expected after propagation of individual errors associated with each dating parameter.

A3: Brief Review of K-Ar & Ar-Ar Dating of Tephra Deposits

Isotopic methods have been used in a variety of ways to date tephra deposits. Potassium-argon (^{40}K-^{40}Ar) and argon-argon (^{40}Ar/^{39}Ar) dating methods are the most commonly applied tephra dating techniques (Richards and Smart, 1991). Potassium or argon-argon dating of volcanic products utilises samples that are old enough (*i.e.* > 250 ka) or contain abundant potassium-rich feldspar phenocryst phases (K=10-20 wt %) that yield sufficient quantities of radiogenic argon (Pringle *et al.*, 1992; McDougall, 1995). These methods have been used to date basaltic lava flows, obsidians and phenocrysts from near-source tephra deposits in Iceland (Albertsson, 1981; McGarvie, 2000). Pre-^{14}C tephra deposits in the volcanic regions, particularly in the Eastern Volcanic Zone (EVZ) around the Torfajökull complex, have been dated using potassium argon techniques (McGarvie *et al.*, 1998).

Potassium-argon ages can be very precise and reliable and well-dated and reliable deposits provide age standards for other techniques (Pringle *et al.*, 1992; Westgate *et al.* 1997; Gansecki *et al.*, 1998). Step heating and single crystal laser fusion (SCLF) ^{40}Ar-^{39}Ar dating and isochron age assessment techniques have been developed to identify and minimise contamination problems that were common in ^{40}K-^{40}Ar dating (York *et al.*, 1981; Hurford and Hammerschmidt, 1985; LoBello *et al.* 1987; van den Bogaard *et al.*, 1989; Chesner *et al.*, 1991; Pringle *et al.*, 1991; 1992; Gansecki *et al.*, 1998; Renne, 2000). Nevertheless, discrepant ages have often been reported, however, between bulk and single grain analyses or between single-grain analysis of K-rich phases (*e.g.* Fitch *et al.*, 1976; Horn *et al.*, 1993; Mishra *et al.*, 1995; Pillans *et al.*, 1996).

Where no other methods can be applied, independent stratigraphic control and age measurement reproducibility are the only ways to test the reliability of ^{40}K-^{40}Ar ages (Lo Bello, *et al.*, 1987). Accurate, precise and even Holocene SCLF ^{40}Ar-^{39}Ar ages have been obtained from millimetre scale K-feldspar, hornblende, plagioclase and sanidine phenocrysts present in many tephra deposits (*e.g.* Table 2.7). van den Bogaard *et al.* (1989) used SCLF to produce ^{40}Ar-^{39}Ar ages of 215±4 ka for the Huttenberg Tephra and a *ca.* 13 ka age for the Laacher See Tephra, in the East Eifel volcanic province. They were able to recognise older detrital contamination in the latter by using single grain (K-feldspar) isochron methods (van den Bogaard, 1995). The ^{40}Ar-^{39}Ar age of the Huttenberg Tephra is almost half the conventional ^{40}K-^{40}Ar age of *ca.* 445 ka, while the ^{14}C and ^{40}Ar-^{39}Ar ages of the Laacher See tephra are broadly concordant.

Contamination by inherited atmospheric argon of a younger age and primordial or radiogenic argon in the melt is problematic in all forms of potassium based dating. Van den Bogaard *et al.*, (1989) found that xenocrystic feldspar was enriched in radiogenic argon. It was indistinguishable from feldspar phenocrysts and consequently bulk ages were in error by more than 100%. Hu *et al.* (1996) dated 63 sanidine crystals from the five sites of the Mono Craters complex in California. The weighted mean age of 12.56 ± 0.47 ka was similar to the upper ^{40}K-^{40}Ar age estimate of 6.4-10.2 ka (Dalrymple,

1967). Hu *et al.* (1996) concluded that the sanidine ^{40}Ar-^{39}Ar age could be too old because all the analyses were undertaken on a single chemically homogenous phase that may contain excess radiogenic argon.

Isotopic dating of phenocryst depleted distal deposits that are dominated by volcanic glass has proved to be more challenging. Precise measurement of the daughter products of radioactive decay is crucial. The relatively low potassium content of silicic glass of *ca.* 2-5% is often the initial obstacle. Potassium-argon age estimates from glass are considered unreliable because glass does not meet the assumptions of the method (McDougall and Harrison, 1988; Pillans *et al.*, 1996; Westgate *et al.*, 1998). More significantly, the key assumption of all isotopic dating methods is that a closed system has existed since the formation event being dated. This is not always true for glass because potassium is a mobile element and can be easily lost from the glass matrix during post depositional hydration and volatile substitution processes (Kaneoka, 1972; Naeser *et al.*, 1980). Volatiles can constitute as much as 8% of the glass composition. Icelandic tephra deposits are generally dry and even silicic glasses are not water saturated on eruption (Clift and Fitton, 1998). Even so, major element totals less than 100% are commonplace. Post-depositional or secondary hydration, alkali mobilisation, dissolution and other depletion processes can all alter the original volatile composition of the glass (Hodder *et al.*, 1991; Froggatt, 1992). Glass shards in ignimbrite deposits may also have experienced slow cooling, welding, rapid devitrification and vapour phase alteration processes (Hildreth and Mahood, 1985; McDougall and Harrison, 1988; Froggatt, 1992; Hunt and Hill, 1993; Dugmore *et al.*, 1995; Black *et al.*, 1996), all of which make isotopic glass-phase dating methods potentially unsuitable.

Appendix B
Experimental Theory Preliminary Methods

B1: Experimental Theory for Elemental Analysis

Major element chemical data from tephra deposits is most commonly obtained by electron probe microanalysis (EPMA) (Smith and Westgate, 1969; Larsen, 1981). X-ray fluorescence (XRF) can be used to obtain bulk major and trace composition chemical data. Detection limits for XRF are an order of 50 to 100 times lower than EPMA. However, separating sufficient masses (*ca.* 6-10 g) of pure glass or phenocrysts from tephra deposits for XRF analysis is difficult and time-consuming. Trace and rare earth elements can be analysed using ICP-MS techniques. Detection limits are comparable or better than XRF, but only ca. 0.1g of sample is required and purification of samples more efficient.

B1.1 Electron-probe microanalysis (EPMA)

EPMA has the ability to determine the composition of individual glass grains. The procedures that govern the technique were fully established by the work of Sweatman and Long (1969). Further details of experimental equipment and general analytical procedures here can be found in Potts (1987; chapter 10). EPMA involves the excitation of selected areas of sample that fall directly under the path of an electron beam, usually 5-10 μm in diameter and with a voltage of 15 or 30 kV (Potts, 1987). Unconsolidated samples for EPMA need to be set in resin and polished to ensure collection of good quality major element chemical data (Smith and Westgate, 1969; Sweatman and Long, 1969). Interactions between the primary electron beam and the sample cause a number of phenomena that include the generation of X-rays, backscattered electrons (BSE) and secondary electrons (SE) that are characteristic of the atoms in the excited sample. In theory, all elements between boron and uranium can be analysed, but machine and sample sensitivity needs to be taken into consideration. The intensity of the X-rays is measured by wavelength or energy dispersive spectrometers (WDS or EDS). EDS collect characteristic X-rays and sort them based on energy. The resulting spectrum plots the number of X-rays versus energy. Each set of spectra provides information on the different elements in the sample and their relative concentrations, but is not a quantitative measure of elemental composition.

B1.2 Scanning Electron Microscopy (SEM)

Scanning electron microscopy (SEM) works in a similar manner to EDS-EPMA except that instead of collecting X-ray emissions BSE and SE are collected in the electron column. BSE highlight contrasts in atomic mass. This difference is related to chemical composition and can be used to distinguish subtle variations in chemical composition not always visible using light microscopy. At high

magnifications (*e.g.* >200x) SEM can also be used to identify contaminant particles and chemical variations within individual tephra grains. Quantitative analysis of elemental compositions can only be obtained using WDS. Sample compositions are calculated by comparison to standards of known composition and after matrix corrections for the influence of atomic mass have been included (*e.g.* ZAF).

B1.3 X-Ray Fluorescence (XRF)

XRF is a technique used to analyse bulk samples. Samples can be prepared as compressed pellets or fused glass disc. These are excited with X-ray radiation and interactions between this and the atoms in the sample causes ionisation of discrete orbital electrons. When these return to their unexcited or ground state, fluorescence X-rays of energy that are characteristic of individual elements are emitted. These can be measured with an X-ray spectrometer and, after comparison to a standard sample, elemental composition can be calculated. XRF can be used to analyse all nine major elements commonly analysed in EPMA as well as phosphorus and trace elements Rb, Sr, Y, Nb, Zr, Cr, Ni, Cu, Zn, Ga, Ba, Pb, Th, and U. The main constraints on XRF precision is sample heterogeneity and the reliability and homogeneity of standards used for calibration (Potts, 1987). Samples are contaminated to a small degree by the agate mortar used to crush the sample.

B1.4 Inductively Coupled Plasma – Mass Spectrometry (ICP-MS)

Inductively coupled plasma mass spectrometry (ICP-MS) is powerful technique for the analysis of trace elements in geological materials (Jarvis *et al.*, 1992). Strong acids are used to place crushed samples into solution. This solution is passed as an aerosol from a neubuliser into argon plasma (Rollinson, 1993). The inductively coupled argon plasma is generated by heating inductive heating of a radio-frequency coil and ignited by a high frequency Tesla spark. This creates a source of ions that are extracted through a pinhole sized orifice into a pumped vacuum system. The ions are focussed into a quadruple mass spectrometer where they are measured (Potts, 1987; Rollinson, 1993). Accurate running conditions are monitored by the inclusion of a standard solution of known composition. When running a series of samples and standards drift in machine operating conditions can occur. This can be overcome by adding a solution of known concentration to samples and standards and normalising the analysed mass counts with respect to the appropriate standard counts (Potts, 1987).

The main advantage of the ICP-MS is that ICP-MS spectra are simple and matrix interferences commonly encountered in ICP emission spectra are eliminated because they occur in a predictable manner. The resulting signal to background ratios are higher. Consequently a wider range of 'heavier' trace elements, such as the Rare Earth Elements (REE) and, potentially, individual isotope ratios can be determined rapidly and precisely from a single solution that does not need to be pre-concentrated (Potts, 1987). All elements within a given mass range can be detected using a single analytical technique and set of instrumental conditions. Background mass interference contamination occurs from the argon plasma gas, the dissolution solvents and reagents, trapped gases and material eroded

from the machine assembly, but these are usually inconsequential. The amount of sample required is approximately 0.1g and detection limits are significantly lower than XRF. Further details of instrumentation and applications can be found in Potts (1987).

B2: Preliminary Experiments

B2.1 Density Separation Profiling of Selected Tephra Deposits

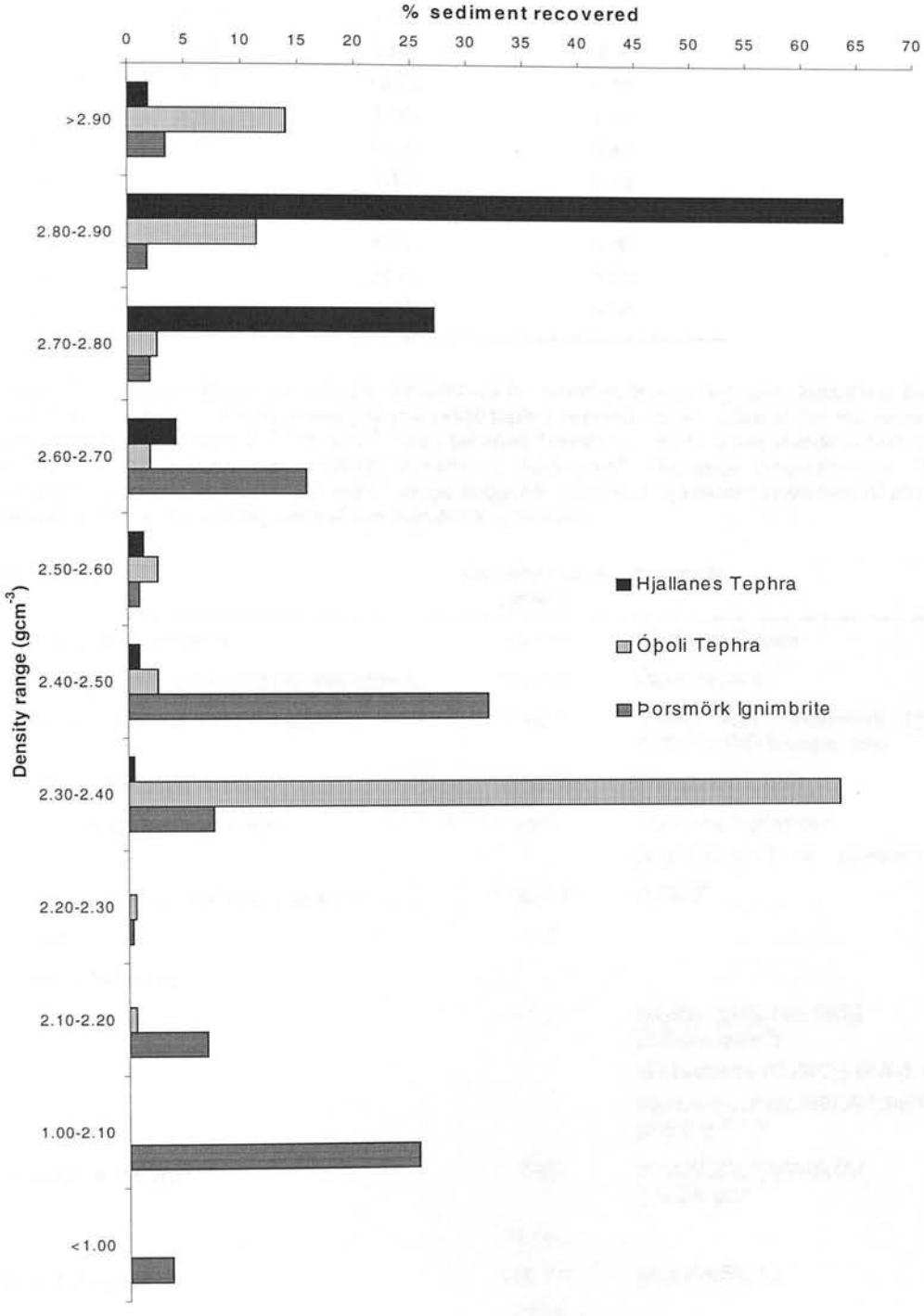


Figure B2.1 Density profiles for selected Icelandic Tephra deposits. The Óþoli Tephra sample is SUTL 551 airfall ash deposit; the Þörsmórk Ignimbrite sample is slope ash from ÞIG 5; the Hjallanes Tephra sample is Hj-2b.

(a) Density (gcm^{-3})	Óþoli Tephra (SUTL 552) (% recovered)	Þórsmörk Ignimbrite ÞIG 5 (slope-ash) (wt % recovered)	Hjallanes Tephra Hj-2b (SUTL 513) (wt % recovered)
>2.90	14.00	3.42	1.90
2.80-2.90	11.33	1.71	63.81
2.70-2.80	2.67	2.05	27.14
2.60-2.70	2.00	15.75	4.29
2.50-2.60	2.67	1.03	1.43
2.40-2.50	2.67	31.85	0.95
2.30-2.40	63.33	7.53	0.48
2.20-2.30	0.67	0.34	0.00
2.10-2.20	0.67	6.85	0.00
1.00-2.10	0.00	25.68	0.00
<1.00	0.00	3.77	0.00

Table B2.1 Density separation profiling experiment for selected tephra deposits, illustrating the use of 2.3-2.4 and <2.4 gcm^{-3} for separating highly silicic tephra deposits. Basic glass of the Hjallanes Tephra has a density of between 2.7-2.9 gcm^{-3}. The Hjallanes Tephra is > 95 % glass shards in bulk and over 90 wt % of this deposit has a density between 2.7-2.9 gcm^{-3}. The large proportion (*ca.* 15 %) of sediment recovered in the 2.6-2.7 gcm^{-3} range suggests there is a significant proportion of plagioclase feldspar in the slope ash deposits of the Þórsmörk Ignimbrite.

(b) Tephra	Density range (gcm^{-3})	Example
'Old' basic platey shards	2.8-2.9	Hjallanes Tephra
'Old' platey highly silicic (HS) tephra shards	2.3-2.4	Óþoli Tephra
'Younger' platey HS tephra shards	2.4-2.5	Vedde Ash*; Þörsmörk Ignimbrite (ÞIG 1b; ÞIG 5-slope ash)
Vesicular HS tephra shards	2.3-2.4	Borrobol Tephra*
Pumiceous HS tephra shards	<2.3	Þörsmörk Ignimbrite (*e.g.* ÞIG 5, 11, 16 – pumice clasts)
Recent/pumiceous HS tephra shards	1.18-2.45	Ö1362#
Pumice	<1.0	
Selected Minerals		
Heavy minerals	>2.7	Olivine [$(Mg, Fe)_2SiO_3$] (3.3-3.4 gcm^{-3})
		Wollastonite ($CaSiO_3$) (2.8-3.1 gcm^{-3})
		Muscavite [Kal2(AlSi3O10)(OH,F)] (2.8-2.9 $^{gcm-3}$)#
Plagioclase feldspar	2.65	[$NaAlSi_3O_8$-$CaAl_2Si_2O_8$] 2.6-2.8 gcm^{-3} #
Quartz	2.65	
Alkali Feldspars	2.5-2.6	[*e.g.* $KAlSi_3O_8$]
Clay minerals (<4 μm)	<2.53	

Table B2.2 Summary density characteristics of selected tephra deposits and minerals (# from Boygle, 1994; * from Roberts, 1997; no mark – this study).

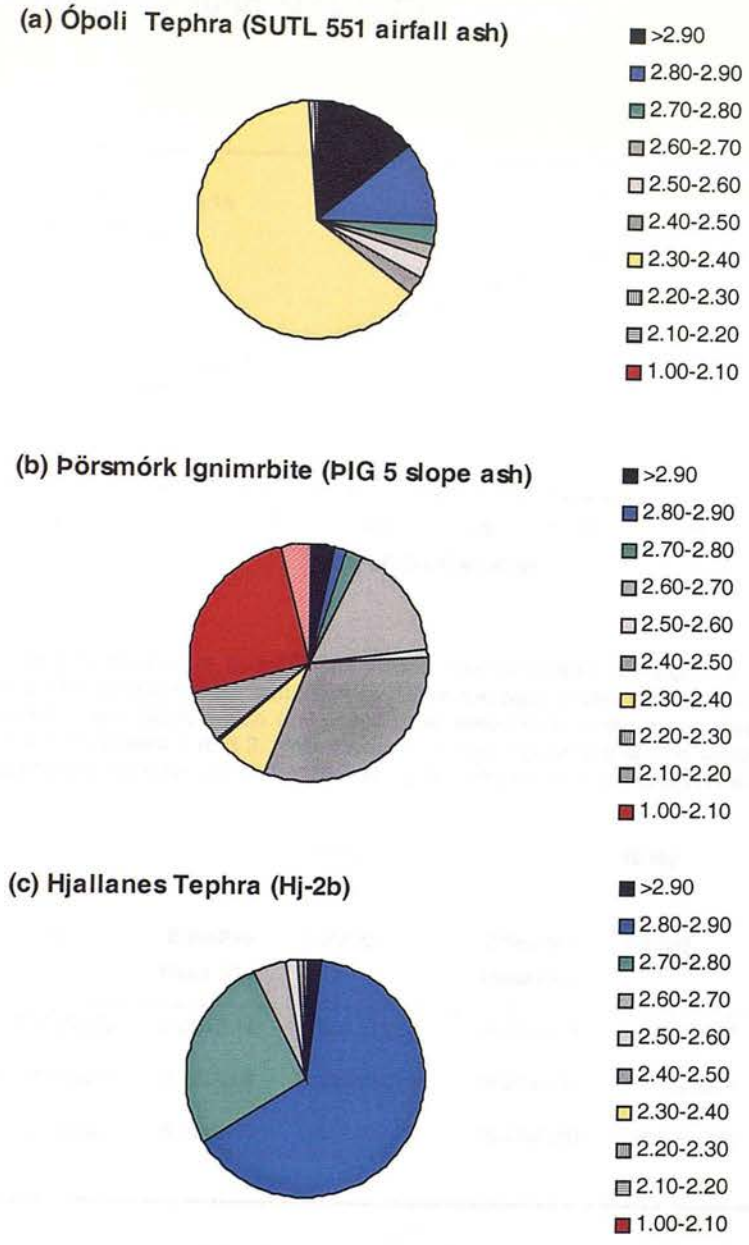


Figure B2.2 Density profile pie charts of data in Table B2.1 showing the transition from tephra deposits dominated by highly silicic glass shards to one dominated by basic glass shards **(a)** the Óþoli Tephra, a compositionally bi-model tephra deposit dominated by highly silicic, platey glass shards (> 60 wt %), but with a significant proportion (> 11 wt %) of shards with an intermediate composition and little feldspathic material (< 5 wt %) **(b)** slope ash from sample location ÞIG 5 of the Þörsmórk Ignimbrite with a mixture of highly silicic platey (> 30 wt %), vesicular glass shards (25-30 wt %), pumice (*ca.* 4 wt %), and a greater concentration of phenocrystic material compared to the Óþoli Tephra, in this case *ca.* 15 % plagioclase feldspar **(c)** the Hjallanes Tephra a deposit dominated by brown basic-glass shards (*ca.* 80-90 wt %).

B2.2 Working Calibration of SUERC Irradiator 2

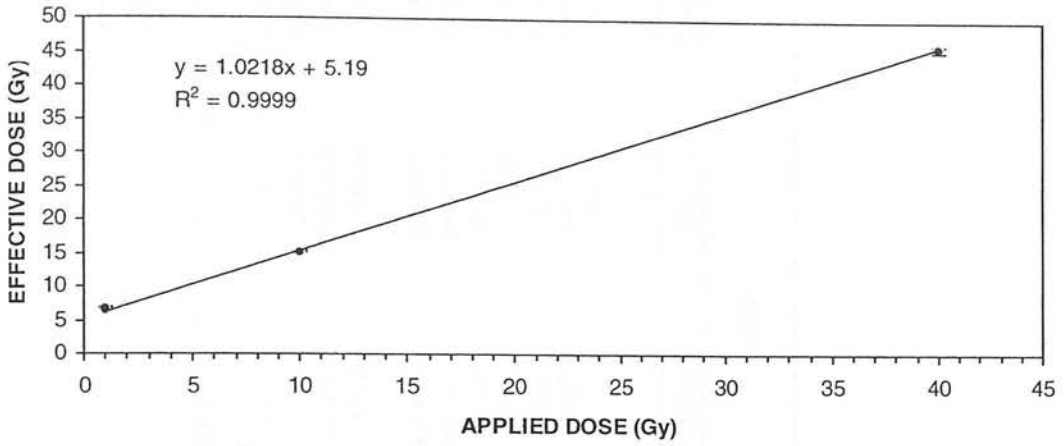


Figure B2.3 Working calibration of SUERC Irradiator 2 against SUERC Irradiator 1. IEA-F1 standard feldspar was used. The effective dose values were calculated from mean TL and IRSL dose response values in Tables B2.3 and B2.4, which compares dose responses of the same dose using existing dose rate values for Irradiators 1 and 2. The transit dose was calculated as the x-axis intersect point. The working calibrated dose rate was calculated using the gradient as a reduction coefficient.

Applied Dose	**1 Gy**		**10 Gy**		**40 Gy**	
Method	Set A/B	**Effective Dose (Gy)**	Set A/B	**Effective Dose (Gy)**	Set A/B	**Effective Dose (Gy)**
IRSL	0.124±0.029	8.06±0.14	0.649±0.040	15.41±0.21	0.882±0.007	45.35±0.50
TL	0.188±0.036	5.32±0.09	0.696±0.089	14.37±0.32	0.852±0.008	46.95±0.52
IRSL/TL (WM)	0.149±0.022	**6.71±0.10**	0.657±0.036	**15.22±0.20**	0.869±0.005	**46.02±0.51**

Table B2.3 Summary of calibration effective dose data for IRSL and TL analysis of IEA-F1 (listed in the order that doses were applied and readouts undertaken, *i.e.* IRSL followed by TL). Full datasets are listed in Table B2.4. See end of tables for full explanation and summary of methods. WM=weighted mean.

Working calibration dose for Irradiator 2:

$y = 1.0218x + 5.19$

Transit Dose = x-axis intersect = **5.19 Gy**

Calibrated dose rate = 2/9/97 dose rate/1.0218 = 32.6±0.6/1.0218 = **32.0±0.6 Gymin^{-1}**

Table B2.4 (a)-(f) (next 3 pages) Calibration data. Set A was used to calibrate Irradiator 2 against Irradiator 1. Set B was used to check changes in sample sensitivity over a double exposure/read-out irradiation cycle. No pre-heats were used.

(a) IRSL (10 Gy) Filenames: CAL 1-2

DOSE	10 Gy						IEA-F1
	0						
IRSL	CYCLE TIME (s): 1 CYCLE - 20 SECS						
SET	DISC NO.	CAL1	+/-	CAL2	+/-	CAL1/CAL2	1σ %
		IRRAD 1		IRRAD 2			
		1/1/99: 3.35±0.02 Gymin^{-1}		2/9/97: 32.6±0.6 Gymin^{-1}			
SET A	1	502055	709	514347	717	0.976	
	2	517304	719	512172	716	1.010	
	3	688707	830	692957	833	0.994	
	4	547583	740	541104	736	1.012	
	MEAN	563912.25	750	565145.00	751	**0.998**	
	1 STD	85321.01	40	86217.66	41	**0.017**	1.7
		IRRAD 1		IRRAD 1			
SET B	1	677092	823	494870	704	1.368	
	2	799549	894	503245	710	1.589	
	3	1024928	1013	623887	790	1.643	
	4	785689	887	505611	711	1.554	
	MEAN	821814.50		531903.25		**1.538**	
	1 STD	146059.92		61495.39		**0.119**	7.7
IRSL	A/B = 0.649		0.040				

(b) TL (10 Gy) Filenames: CAL 1-2

DOSE	10 Gy						IEA-F1
TL	300-380^{0}C - 5°Cs^{-1}						
SET	DISC NO.	CAL1	+/-	CAL2	+/-	CAL1/CAL2	1σ %
		IRRAD 1		IRRAD 2			
		1/1/99: 3.35±0.02 Gymin^{-1}		2/9/97: 32.6±0.6 Gymin^{-1}			
SET A	1	1182588		1208986		0.978	
	2	1044951		1107103		0.944	
	3	2047718		1622698		1.262	
	4	1160687		1236568		0.939	
	MEAN	1358986.00		1293838.75		**1.031**	
	1 STD	463108.52		226199.45		**0.155**	15.1
		IRRAD 1		IRRAD 1			
SET B	1	1477108		1118144		1.321	
	2	1829370		1181682		1.548	
	3	2305604		1463125		1.576	
	4	-		1176079		-	
	MEAN (1-3)	1870694.00		1234757.50		**1.482**	
	1 STD (1-3)	415791.01		154930.74		**0.140**	9.4
TL	A/B = 0.696		0.089				

Table B2.4 (a)-(b) Calibration of IRRAD 2 to IRRAD 1: Applied Dose = 10 Gy

(c) IRSL (40 Gy) Filenames: CAL 3-4

DOSE	40 Gy						IEA-F1
IRSL SET	CYCLE TIME (s): 1 CYCLE - 20 SECS DISC NO.	CAL 3	+/-	CAL 4	+/-	CAL3/CAL4	1σ %
		IRRAD 1 1/1/99: 3.35±0.02 Gymin^{-1}		IRRAD 2 2/9/97: 32.6±0.6 Gymin^{-1}			
SET A	1	1899725	1378	1931455	1390	0.984	
	2	2064878	1437	2124062	1458	0.972	
	3	2292796	1514	2350940	1533	0.975	
	4	2197095	1482	2234826	1495	0.983	
	MEAN	2113623.50		2160320.75		0.979	
	1 STD	170488.48		178494.59		0.006	0.6
SET B	1	2190144	1480	1977278	1406	1.108	
	2	2378099	1542	2114537	1454	1.125	
	3	2163375	1471	1976780	1403	1.094	
	4	143997	-	2449154	1565	0.059	
	MEAN (1-3)	2243872.67		2022865.00		1.109	
	1 STD (1-3)	117011.44		79390.67		0.015	1.4
IRSL	A/B =	0.882	0.007				

(d) TL (40 Gy) Filenames: CAL 3-4

DOSE	40 Gy						IEA-F1
TL SET	300-380°C - 5°Cs^{-1} DISC NO.	CAL3	+/-	CAL 4	+/-	CAL2/CAL3	1σ %
		IRRAD 1 1/1/99: 3.35±0.02 Gymin^{-1}		IRRAD 2 2/9/97: 32.6±0.6 Gymin^{-1}			
SET A	1	5213522		6014665		0.867	
	2	4992731		5779405		0.864	
	3	5846776		6782820		0.862	
	4	5791214		6750788		0.858	
	MEAN	5332489.00		6181619.33		0.863	
	1 STD	423629.40		511430.92		0.005	0.5
SET B	1	5994606		5902301		1.016	
	2	6378919		6214789		1.026	
	3	5739895		5758852		0.997	
	4	265320		6438334		0.041	
	MEAN (1-3)	6037806.67		5958647.33		1.013	
	1 STD (1-3)	321694.95		233132.62		0.015	1.5
TL	A/B =	0.852	0.008				

Table B2.4 (c)-(d) Calibration of IRRAD 2 to IRRAD 1: Applied Dose = 40 Gy

(e) IRSL (1 Gy) Filenames: CAL 5-6

DOSE	1 Gy						IEA-F1
IRSL SET	CYCLE TIME (s): 1 CYCLE - 20 SECS DISC NO.	CAL 5	+/-	CAL 6	+/-	CAL5/CAL6	1σ %
		IRRAD 1 1/1/99: 3.35±0.02 Gymin^{-1}		IRRAD 2 2/9/97: 32.6±0.6 Gymin^{-1}			
SET A	1	48193	220	48235	220	0.999	
	2	51826	228	53818	233	0.963	
	3	54387	234	59700	245	0.911	
	4	52078	229	54442	234	0.957	
	MEAN	51621.00		54048.75		**0.957**	
	1 STD	2559.48		4688.43		**0.036**	3.8
SET B	1	264551	515	49513	223	5.343	
	2	413284	643	51202	227	8.072	
	3	371432	610	47886	219	7.757	
	4	458624	677	62063	250	7.390	
	MEAN	376972.75		52666.00		**7.739**	
	1 STD	82975.46		6409.28		**0.341**	4.4
IRSL	A/B =	0.124	0.029				

(f) TL (1 Gy) Filenames: CAL 5-6

DOSE	1 Gy						IEA-F1
TL SET	300-380°C - 5°Cs^{-1} DISC NO.	CAL 5	+/-	CAL 6	+/-	CAL5/CAL5	1σ %
		IRRAD 1 1/1/99: 3.35±0.02 Gymin^{-1}		IRRAD 2 2/9/97: 32.6±0.6 Gymin^{-1}			
SET A	1	210138		156889		1.339	
	2	190552		155796		1.223	
	3	238998		178272		1.341	
	4	230470		177109		1.301	
	MEAN	223271.00		170574.50		**1.308**	
	1 STD	19190.29		11041.73		**0.046**	3.5
SET B	1	760234		156973		4.843	
	2	1157365		174427		6.635	
	3	1087236		149682		7.264	
	4	1183805		172529		6.861	
	MEAN (1-3)	1142802.00		165546.00		**6.949**	
	1 STD (1-3)	49904.45		13771.36		**0.444**	6.4
TL	A/B =	0.188	0.036				

Table B2.4 (e)-(f) Calibration of IRRAD 2 to IRRAD 1: Applied Dose = 1 Gy

EXPERIMENTAL CONDITIONS		SAMPLES & APPLIED DOSES (Gy)		
		HOLOCENE		
Sample code		A1875	Ö1362	LAYER Y
Tephra sample		ASKJA 1875	ÖRÆFI 1362	KATLA 1700 BP
Local location		0, 50 & 70 km from crater	0, 50 & 70 km from crater	GIGAJÖKULL
Regional location		N & E ICELAND	S ICELAND	S ICELAND
Glass fraction		ASH	ASH	ASH
No. of discs		5	5	5
Pre-heat conditions		-	-	-
Dose cycles		2	2	2
Natural TL	G1	N	N	N
Applied dose (Gy): Irradiator no.	G2	50:1	50:1	50:1

		PRE-HOLOCENE				
Sample code(s)		ÞIG 1b/1c/3/5/7 ÞIG 11/13/16/21	SUTL 552	SUTL 551	SUTL 551	SUTL 551
Tephra sample		ÞÓRSMÖRK IGNIMBRITE	ÓÞOLI TEPHRA	ÓÞOLI TEPHRA	ÓÞOLI TEPHRA	ÓÞOLI TEPHRA
Local location		ÞÓRSMÖRK	SKAGAFJALL	SKAGAFJALL	SKAGAFJALL	SKAGAFJALL
Regional location		S ICELAND	NW ICELAND	NW ICELAND	NW ICELAND	NW ICELAND
Glass fraction		ASH & PUMICE	ASH	ASH	ASH	ASH
No. of discs		5 each	8	8	8	8
Pre-heat conditions		-	-	2 mins @ 220°C	5 hrs @ 155°C	16 hrs @ 135°C
Dose cycles		2	2	4	4	4
Natural TL		N	N	N	N	N
Applied dose (Gy): Irradiator no.	G1	50:1	50:1	50:1	50:1	50:1
	G2			50:2	50:2	50:2
Fading test*	G3			50:1	50:1	50:1

* Discs 1-4: Dose & pre-heat applied. Stored in dark & TL read-out delayed for 2 months.
Discs 5-8: Dose & pre-heat applied. No delay to TL read-out

Table B2.5 Experiment 1: Natural TL and 50 Gy dose response: Experimental conditions and samples

RUN NUMBER	MAAD1	MAAD2	MAAD3	MAAD4	MAAD5
Sample code	SUTL 552	SUTL 552	SUTL 552	SUTL 552	SUTL 552
Tephra sample	Óþoli Tephra	Óþoli Tephra	Óþoli Tephra	Óþoli Tephra	Óþoli Tephra
Glass fraction	ASH	ASH	ASH	ASH	ASH
No. of discs	16	16	16	16	16
Sample distribution on disc	non-centred	non-centred	non-centred	centred	centred
Irradiator number	2	2	2	2	2
Pre-heat conditions	16 hrs@135°C	16 hrs@135°C	5 hrs@155°C	16 hrs@135°C	5 hrs@155°C
G1 CYCLE: ADDED DOSE	1 150 9 150	1 150 9 150	1 300 9 300	1 150 9 150	1 300 9 600
Discs Dose (Gy)	2 300 10 300	2 300 10 300	2 600 10 600	2 300 10 300	2 600 10 1200
	3 450 11 450	3 450 11 450	3 900 11 900	3 450 11 450	3 900 11 1800
	4 600 12 600	4 600 12 600	4 1200 12 1200	4 600 12 600	4 1200 12 2400
	5 750 13 750	5 750 13 750	5 1500 13 1500	5 750 13 750	5 1500 13 3000
	6 900 14 900	6 900 14 900	6 1800 14 1800	6 900 14 900	6 1800 14 3600
	7 1050 15 1050	7 1050 15 1050	7 2100 15 2100	7 1050 15 1050	7 2100 15 4200
	8 1200 16 1200	8 1200 16 1200	8 2400 16 2400	8 1200 16 1200	8 2400 16 4800
G2 CYCLE: REVERSE DOSE	1 1200 9 1200	1 1200 9 1200	1 2400 9 2400	1 1200 9 1200	1 2400 9 4800
Discs Dose (Gy)	2 1050 10 1050	2 1050 10 1050	2 2100 10 2100	2 1050 10 1050	2 2100 10 4200
	3 900 11 900	3 900 11 900	3 1800 11 1800	3 900 11 900	3 1800 11 3600
	4 750 12 750	4 750 12 750	4 1500 12 1500	4 750 12 750	4 1500 12 3000
	5 600 13 600	5 600 13 600	5 1200 13 1200	5 600 13 600	5 1200 13 2400
	6 450 14 450	6 450 14 450	6 900 14 900	6 450 14 450	6 900 14 1800
	7 300 15 300	7 300 15 300	7 600 15 600	7 300 15 300	7 600 15 1200
	8 150 16 150	8 150 16 150	8 300 16 300	8 150 16 150	8 300 16 600
G3 CYCLE: NORMALISATION Discs Dose (Gy)	1-16 600	1-16 600	1-16 1200	1-16 600	1-16 600
G4 CYCLE: FADING TEST	1-8 600 *2 months*	1-8 600 *2 months*	1-8 1200 *2 months*	1-8 600 *2 months*	1-8 600 *2 months*
Discs Dose (Gy) *Delay*	9-16 600 *no delay*	9-16 600 *no delay*	9-16 1200 *no delay*	9-16 600 *no delay*	9-16 600 *no delay*

Table B2.6 Experiment 2: Multiple aliquot additive dose runs 1-5. Experimental conditions and doses applied to discs in runs 1-5.

EXPERIMENTAL CONDITIONS		REGENERATION & NORMALISATION DOSES (Gy)					
Tephra deposit	**ÓÞOLI TEPHRA**	**G1**	N	**G9**	100	**G17**	100
Sample code	**SUTL 551**	**G2**	50	**G10**	2000	**G18**	100*
Glass fraction	ASH	**G3**	100	**G11**	100	**G19**	5000
No. of discs	8	**G4**	500	**G12**	2500	**G20**	100
Sample distribution on disc	centred	**G5**	100	**G13**	100	**G21**	6000
Disc mass (mg)	2-3	**G6**	1000	**G14**	3000	**G22**	100
Irradiator number	2	**G7**	100	**G15**	100		
Pre-heat conditions	2 mins @ 220°C	**G8**	1500	**G16**	4000		
Tephra deposit	**ÞÓRSMÖRK IGNIMBRITE**	**G1**	N	**G9**	125	**G17**	25*
Sample code	**ÞIG 7**	**G2**	25	**G10**	25		
Glass fraction	ASH	**G3**	50	**G11**	150		
No. of discs	8	**G4**	25	**G12**	25		
Sample distribution on disc	centred	**G5**	75	**G13**	200		
Disc mass (mg)	4-5	**G6**	25	**G14**	25		
Irradiator number	2	**G7**	100	**G15**	300		
Pre-heat conditions	2 mins @ 220°C	**G8**	25	**G16**	25		

Table B2.7 Experiment 3: Dose corrected regeneration thermoluminescence (DCRTL). Experimental conditions and doses applied to discs in regeneration cycles. Fading tests were carried out at the point marked with an asterisk (*).

Appendix C
Experimental Data

Experimental data can be found in this Appendix. Further lists of chemical data, fission-track count data, dose rate calculations, full 1°C and 10°C palaeodose reconstruction datasets for the TL Experiments 1-5, and a full list of regression analysis results can be found the enclosed CD-R in the appropriate Appendices folder. These datasets are in Word 97, Excel 97 and PDF format. They were not amenable to printing or were too big to include as part of the main thesis. They are included on the CD-R for completeness and to enable the reader to see how final answers in Chapter 4 were calculated. The copyright of these datasets rests with the author. Permission to use them should be sought from the author.

Appendix C and the folders in the CD-R Appendix C are structured in a similar manner to Chapter 4. Section C1 presents a list of major and trace element data while C2 has a list of all data used in correlation dating analysis. Section C3 is fission-track count and size data produced by SJR. Other fission-track data was received as presented in Section 4.3. Section C4 contains dose rate and palaeodose data used to characterise the Óþoli Tephra, Þörsmórk Ignimbrite, Ö1362 and A1875 samples as well as full data tables of palaeodose data. C5 contains any other data such as grain size analyses. From this point on all descriptions can be found in figure and table captions.

Table C1.1 (overpages) New grain specific glass-phase EPMA data presented in this thesis

Summary of methods: Samples were analysed by Stephen Roberts at Department of Geology, University of Edinburgh using a wavelength dispersive spectrometry (WDS), Cambridge Instruments Microscan V microprobe operating at 20 kV accelerating voltage, 5 μm beam diameter, and a 15 nA beam current. Slides were scanned systematically. Two second energy dispersive spectrometry (EDS) profiles were obtained for every well-polished grain of suitable size (*i.e.* usually >10 μm). Those with characteristic tephra chemical profiles were analysed using WDS. Before each analyses the beam was centred by 'burning' a hole in the araldite resin and the beam current was determined by the insertion of a Faraday cup into the path of the beam. Nine major elements were measured; counting time = 10 seconds each. Background counts (2 x 10 seconds) were established on a single grain for each sample. These results are not included in the data listed. Throughout, the beam was covered during spectrometer repositioning to minimise mobilisation of alkali elements. To assess the degree of sodium mobilisation, this element was measured during the first and final counting period. Counter dead time was corrected for and a ZAF correction applied for the effects of atomic number, absorption and fluorescence (Sweatman and Long, 1969).

Notes on results: All elements are expressed as weight percent. Data is presented in order of descending SiO_2 content. Data from shards with obvious 'burn' or superficial probe related marks are not included in this list, but can be found on the enclosed CD-R. Burnt data should be viewed/used with caution as low totals often reflect analytical complications not associated with shard characteristics (Froggatt *et al.*, 1992; Hunt and Hill, 1993; 1996).

RH = silicic glass phase data; INT = shard with intermediate composition; BS = shards with basic composition; 1s or 1σ = single standard deviation for sample and whole population respectively; mean and standard deviations are only presented when the data is normally distributed and exhibits no obvious evolution trend; n = number of analysis; FeO* = total iron oxide ($FeO^* = 0.85FeO + 0.15Fe_2O_3$); outliers are defined as shards with distinctly variant non-mobile element composition (*i.e.* variation in TiO2, FeO*, CaO and/or MgO); outliers were identified visually at first and by principal components analysis (PCA) and average linkage, Euclidean distance cluster analysis.

Standards: Calibration to standards of a mixture of pure metals, simple silicate minerals was performed at the start of each session (see Table C1.2). Smooth running conditions were periodically checked against a synthetic oxide andradite standard after every 15 analyses, at a change of sample, a relevant break in analysis or if problems developed. * = andradite standard analysis undertaken after shard analysis; ** = andradite standard analysis undertaken before shard analysis. Problems with low standard totals were corrected by, in the following order, checking that the beam is centred, verifying the position of the spectrometers and, as a last resort, re-reading standard compositions.

Please e-mail sjr@geo.ed.ac.uk for permission to use this chemical data.

Table C1.1 (1 of 12) New EPMA data presented in this thesis

Óþoli Tephra - Section B, Skagafjall, NW Peninsula, Iceland; silicic glass shard data; (n=137)

No.	SiO_2	TiO_2	Al_2O_3	FeO_{tot}	MnO	MgO	CaO	Na_2O	K_2O	TOTAL	H_2O_d	Sample / Analysis codes Sample	Date	RH no.
1	75.36	0.17	11.84	2.43	0.11	0.01	1.33	3.32	2.88	97.45	2.55	OT R6	11-12/98	237
2	75.15	0.18	11.92	2.52	0.14	0.03	1.32	3.06	2.68	97.00	3.00	OT A0-1	11/25/98	24
3	74.82	0.16	11.80	2.38	0.12	0.05	1.18	1.84	2.63	94.98	5.02	OT A0-1	11/25/98	28
4	74.58	0.35	11.89	2.48	0.11	0.02	1.27	3.76	2.68	97.14	2.86	OT A0-1	11/25/98	34
5	74.54	0.24	11.78	2.35	0.09	0.04	1.18	3.40	3.13	96.75	3.25	OT R6	11-12/98	238
6	74.32	0.14	11.42	2.17	0.12	0.02	1.24	3.23	2.82	95.48	4.52	OT A0-1	11/25/98	23
7	74.23	0.22	11.57	2.32	0.10	0.04	1.18	4.31	2.61	96.58	3.42	OT A 2-3	3/12/98	126
8	74.16	0.20	11.52	2.21	0.09	0.04	1.41	3.79	2.79	96.21	3.79	OT A 2-3	3/12/98	113
9	74.08	0.17	11.45	2.38	0.12	0.04	1.23	3.69	2.77	95.93	4.07	OT A0-1	11/25/98	21
10	74.04	0.10	11.51	2.39	0.14	0.01	1.35	3.45	2.71	95.70	4.30	OT A0-1	11/25/98	33
11	74.04	0.18	11.82	2.61	0.12	0.04	1.24	3.18	2.92	96.15	3.85	OT A0-1	11/25/98	35*
12	74.03	0.13	11.45	2.31	0.09	0.02	1.34	4.08	2.79	96.24	3.76	OT A 2-3	3/12/98	121
13	74.02	0.14	11.38	2.27	0.09	0.01	1.18	2.75	2.96	94.80	5.20	OT A0-1	11/25/98	26
14	74.00	0.14	11.68	2.40	0.05	0.02	1.25	3.81	2.68	96.03	3.97	OT R6	11-12/98	239*
15	73.99	0.13	11.65	2.45	0.08	0.04	1.22	3.63	2.66	95.85	4.15	OT R6	11-12/98	224
16	73.97	0.19	11.43	2.25	0.07	0.04	1.30	4.10	2.83	96.18	3.82	OT A 2-3	3/12/98	111
17	73.93	0.16	11.52	2.26	0.08	0.04	1.30	3.73	2.94	95.96	4.04	OT A 2-3	3/12/98	129
18	73.83	0.12	11.68	2.39	0.08	0.01	1.31	3.70	2.71	95.83	4.17	OT A0-1	11/25/98	13
19	73.82	0.11	11.60	2.40	0.11	0.04	1.25	3.68	2.81	95.82	4.18	OT A0-1	11/25/98	30
20	73.80	0.19	11.65	2.30	0.04	0.03	1.25	3.56	2.55	95.37	4.63	OT A0-1	11/25/98	15
21	73.75	0.17	11.62	2.48	0.09	0.02	1.24	3.92	2.99	96.28	3.72	OT A0-1	11/26/98	57*
22	73.74	0.17	12.07	2.39	0.07	0.02	1.26	3.82	2.91	96.45	3.55	OT R4	10/12/98	205$
23	73.70	0.16	11.70	2.33	0.15	0.02	1.29	3.66	2.65	95.66	4.34	OT A0-1	11/25/98	10
24	73.70	0.20	11.67	2.38	0.12	0.01	1.28	3.87	2.92	96.15	3.85	OT A0-1	11/25/98	18
25	73.69	0.16	11.44	2.12	0.10	0.02	1.27	3.43	2.68	94.91	5.09	OT A0-1	11/25/98	32
26	73.65	0.15	11.53	2.31	0.08	0.02	1.16	3.61	2.61	95.12	4.88	OT R6	11/12/98	236
27	73.61	0.15	11.53	2.30	0.06	0.00	1.35	3.64	2.70	95.34	4.66	OT A0-1	11/25/98	20
28	73.59	0.18	11.86	2.30	0.05	0.01	1.31	3.81	2.94	96.05	3.95	OT A 2-3	10/12/98	202
29	73.51	0.20	11.47	2.48	0.10	0.01	1.28	3.60	2.71	95.36	4.64	OT A0-1	11/25/98	27
30	73.51	0.14	11.52	2.31	0.04	0.06	1.38	3.81	3.01	95.78	4.22	OT A 2-3	3/12/98	110
31	73.46	0.13	12.00	2.40	0.10	0.03	1.32	3.50	2.72	95.66	4.34	OT A 2-3	10/12/98	203
32	73.43	0.13	11.71	2.31	0.08	0.02	1.17	3.83	2.83	95.51	4.49	OT A0-1	11/25/98	25
33	73.43	0.13	11.61	2.28	0.11	0.00	1.35	3.99	3.06	95.96	4.04	OT A0-1	11/26/98	63
34	73.40	0.17	11.54	2.42	0.14	0.06	1.23	2.31	3.25	94.52	5.48	OT A 2-3	3/12/98	118
35	73.40	0.20	11.81	2.36	0.12	0.02	1.23	3.79	2.63	95.56	4.44	OT R4	11-12/98	207
36	73.34	0.16	11.82	2.53	0.14	0.04	1.27	3.56	2.71	95.57	4.43	OT A0-1	11/25/98	11
37	73.34	0.12	11.62	2.25	0.10	0.03	1.31	3.43	2.86	95.06	4.94	OT R4	11-12/98	206**
38	73.33	0.12	11.75	2.12	0.03	0.01	1.17	3.67	2.71	94.91	5.09	OT R4	11-12/98	216
39	73.29	0.19	11.77	2.36	0.07	0.01	1.22	3.83	2.69	95.43	4.57	OT R4	11-12/98	211
40	73.28	0.11	11.35	2.38	0.10	0.04	1.39	3.93	3.04	95.62	4.38	OT A 2-3	3/12/98	120
41	73.27	0.19	11.54	2.56	0.13	0.02	1.26	3.83	2.69	95.49	4.51	OT A0-1	11/26/98	52
42	73.23	0.15	11.32	2.44	0.10	0.02	1.31	3.72	2.69	94.98	5.02	OT A 2-3	3/12/98	125
43	73.22	0.16	11.57	2.46	0.09	0.01	1.41	3.58	2.82	95.32	4.68	OT R6	11-12/98	230
44	73.19	0.17	11.67	2.34	0.11	0.02	1.26	3.69	2.56	95.01	4.99	OT R6	11-12/98	233
45	73.16	0.18	11.88	2.28	0.10	0.06	1.47	4.01	2.78	95.92	4.08	OT A 2-3	3/12/98	130
46	73.15	0.14	11.61	2.28	0.08	0.03	1.19	3.46	2.68	94.62	5.38	OT A0-1	11/25/98	14
47	73.13	0.11	11.72	2.34	0.10	0.01	1.32	3.71	2.80	95.24	4.76	OT A0-1	11/26/98	73
48	73.13	0.16	11.75	2.60	0.11	0.02	1.31	3.85	2.89	95.82	4.18	OT A0-1	11/26/98	80
49	73.13	0.14	11.38	2.31	0.17	0.05	1.40	3.86	2.78	95.22	4.78	OT A0-1	11/26/98	85
50	73.12	0.13	11.65	2.48	0.07	0.00	1.36	2.70	2.88	94.39	5.61	OT A0-1	11/25/98	12
51	73.12	0.18	11.44	2.46	0.07	0.02	1.32	3.81	2.84	95.26	4.74	OT A 2-3	3/12/98	124*
52	73.11	0.11	11.65	2.46	0.10	0.02	1.35	3.24	2.70	94.74	5.26	OT A0-1	11/25/98	36
53	73.11	0.17	11.30	2.32	0.11	0.02	1.18	3.66	2.63	94.50	5.50	OT A 2-3	3/12/98	115
54	73.11	0.20	11.93	2.22	0.09	0.04	1.19	3.48	2.85	95.11	4.89	OT A 2-3	10/12/98	197
55	73.10	0.17	11.73	2.38	0.03	0.01	1.19	3.16	3.03	94.80	5.20	OT A 2-3	10/12/98	198
56	73.08	0.08	11.83	2.31	0.12	0.02	1.35	3.74	2.67	95.20	4.80	OT A0-1	11/25/98	9*
57	73.07	0.14	11.51	2.37	0.13	0.03	1.24	3.92	2.76	95.17	4.83	OT A0-1	11/26/98	79
58	73.05	0.18	11.62	2.48	0.03	0.03	1.22	3.80	2.74	95.15	4.85	OT A0-1	11/25/98	47*
59	73.03	0.13	11.88	2.29	0.06	0.01	1.22	3.72	2.67	95.01	4.99	OT A 2-3	10/12/98	201
60	73.01	0.16	11.53	2.34	0.07	0.01	1.22	3.76	2.78	94.88	5.12	OT R6	11-12/98	227
61	73.00	0.13	11.82	2.42	0.08	0.02	1.27	3.47	2.65	94.86	5.14	OT A0-1	11/25/98	7
62	72.98	0.12	11.41	2.23	0.10	0.02	1.23	3.82	2.94	94.85	5.15	OT A0-1	11/26/98	74
63	72.97	0.15	11.59	2.37	0.05	0.02	1.19	3.91	2.69	94.94	5.06	OT A0-1	11/26/98	54
64	72.96	0.21	11.81	2.23	0.11	0.04	1.25	4.16	2.83	95.60	4.40	OT R6	11-12/98	225
65	72.95	0.18	11.86	2.54	0.06	0.01	1.25	3.56	2.63	95.04	4.96	OT R4	11-12/98	210
66	72.93	0.15	11.96	2.39	0.08	0.03	1.21	3.32	3.09	95.16	4.84	OT R4	11-12/98	214
67	72.88	0.12	11.50	2.30	0.06	0.00	1.25	3.46	2.73	94.30	5.70	OT A0-1	11/25/98	19
68	72.88	0.11	11.58	2.32	0.09	0.03	1.32	3.59	2.72	94.64	5.36	OT A0-1	11/25/98	38
69	72.88	0.18	11.47	2.29	0.08	0.02	1.31	3.77	2.84	94.84	5.16	OT A0-1	11/26/98	58
70	72.87	0.11	11.48	2.26	0.08	0.02	1.29	3.94	2.52	94.57	5.43	OT A0-1	11/26/98	64
71	72.87	0.15	12.23	2.35	0.07	0.03	1.11	3.73	2.59	95.13	4.87	OT A 2-3	10/12/98	196
72	72.86	0.09	11.48	2.45	0.10	0.03	1.28	3.57	2.60	94.46	5.54	OT A0-1	11/25/98	8
73	72.86	0.10	11.41	2.30	0.11	0.02	1.35	3.80	2.45	94.40	5.60	OT A0-1	11/26/98	51**

(contd.)

Table C1.1 (2 of 12) New EPMA data presented in this thesis

74	72.84	0.18	11.68	2.41	0.08	0.02	1.29	3.65	2.81	94.96	5.04 OT R6	11-12/98	226
75	72.83	0.14	11.61	2.36	0.08	0.01	1.21	3.74	2.72	94.70	5.30 OT R6	11-12/98	228
76	72.81	0.19	11.48	2.33	0.08	0.03	1.36	3.85	2.82	94.95	5.05 OT A 2-3	3/12/98	117
77	72.80	0.18	11.71	2.36	0.09	0.03	1.28	3.75	2.81	95.01	4.99 OT R4	11-12/98	217
78	72.74	0.12	11.66	2.46	0.14	0.03	1.31	3.73	2.71	94.90	5.10 OT A0-1	11/25/98	44
79	72.74	0.15	11.56	2.21	0.11	0.03	1.21	4.07	2.62	94.70	5.30 OT A 2-3	3/12/98	123
80	72.72	0.15	11.81	2.45	0.10	0.04	1.22	3.63	2.76	94.88	5.12 OT A0-1	11/25/98	48
81	72.72	0.12	11.56	2.44	0.15	0.02	1.22	3.65	2.87	94.75	5.25 OT A0-1	11/26/98	56
82	72.72	0.16	11.69	2.43	0.08	0.01	1.23	3.58	2.57	94.47	5.53 OT R6 *(b)*	11-12/98	223
83	72.69	0.21	11.45	2.37	0.10	0.02	1.21	4.11	2.76	94.92	5.08 OT A0-1	11/26/98	53
84	72.69	0.20	11.85	2.32	0.09	0.00	1.25	3.49	2.70	94.59	5.41 OT R6	11/12/98	234
85	72.66	0.16	11.47	2.43	0.09	0.03	1.28	3.80	2.71	94.63	5.37 OT A0-1	11/26/98	55
86	72.64	0.18	11.52	2.35	0.04	0.02	1.35	4.10	2.85	95.05	4.95 OT A 2-3	3/12/98	116
87	72.63	0.15	11.44	2.27	0.12	0.04	1.23	3.53	2.47	93.88	6.12 OT A0-1	11/25/98	16
88	72.59	0.10	11.59	2.26	0.12	0.02	1.19	3.69	2.92	94.48	5.52 OT A0-1	11/26/98	84
89	72.58	0.20	11.46	2.37	0.07	0.04	1.39	4.00	2.73	94.84	5.16 OT A 2-3	3/12/98	119
90	72.54	0.11	11.58	2.40	0.13	0.02	1.37	3.90	2.84	94.89	5.11 OT A0-1	11/26/98	76
91	72.52	0.20	11.79	2.27	0.07	0.04	1.09	3.73	2.77	94.48	5.52 OT R4 *(b)*	10/12/98	204
92	72.50	0.07	11.54	2.35	0.09	0.01	1.27	4.02	2.80	94.65	5.35 OT A0-1	11/26/98	61
93	72.45	0.18	11.69	2.39	0.07	0.02	1.27	3.61	2.81	94.49	5.51 OT A0-1	11/25/98	40
94	72.45	0.14	11.52	2.39	0.07	0.03	1.23	3.91	2.70	94.44	5.56 OT A0-1	11/26/98	66
95	72.45	0.14	11.74	2.24	0.09	0.04	1.34	3.85	2.72	94.61	5.39 OT R4	11-12/98	208
96	72.43	0.20	11.62	2.39	0.09	0.02	1.16	3.73	2.65	94.29	5.71 OT R4	11-12/98	213
97	72.40	0.20	11.52	2.49	0.08	0.02	1.26	3.96	2.63	94.56	5.44 OT A 2-3	3/12/98	132
98	72.40	0.20	11.75	2.38	0.09	0.00	1.26	3.51	2.57	94.16	5.84 OT A 2-3	10/12/98	200
99	72.39	0.16	11.68	2.39	0.04	0.00	1.25	3.69	2.57	94.17	5.83 OT A0-1	11/26/98	78
100	72.34	0.14	11.42	2.20	0.11	0.02	1.28	3.91	2.72	94.14	5.86 OT A0-1	11/25/98	41
101	72.34	0.16	11.57	2.45	0.12	0.03	1.24	3.74	2.71	94.36	5.64 OT A0-1	11/25/98	49
102	72.34	0.15	11.54	2.39	0.09	0.03	1.26	3.93	2.67	94.40	5.60 OT A 2-3	3/12/98	131
103	72.29	0.12	11.48	2.51	0.05	0.03	1.24	3.67	2.47	93.86	6.14 OT R6	11-12/98	235
104	72.26	0.08	11.41	2.31	0.12	0.01	1.22	3.85	2.65	93.91	6.09 OT A0-1	11/26/98	62
105	72.24	0.10	11.61	2.40	0.06	0.02	1.33	4.02	2.73	94.51	5.49 OT A0-1	11/26/98	83
106	72.23	0.15	11.69	2.16	0.11	0.01	1.16	3.45	2.90	93.86	6.14 OT R6	11-12/98	232
107	72.22	0.17	11.49	2.32	0.03	0.01	1.28	3.53	2.71	93.76	6.24 OT R4	11-12/98	215
108	72.20	0.18	11.26	2.33	0.11	0.02	1.15	3.72	2.71	93.68	6.32 OT A0-1	11/25/98	39
109	72.14	0.15	11.48	2.30	0.14	0.01	1.14	3.88	2.63	93.87	6.13 OT A0-1	11/26/98	59
110	72.14	0.14	11.34	2.21	0.13	0.00	1.35	3.98	2.81	94.10	5.90 OT A 2-3	10/12/98	199
111	72.12	0.14	11.56	2.41	0.11	0.02	1.25	4.03	2.56	94.20	5.80 OT A0-1	11/26/98	72*
112	72.12	0.15	11.44	2.36	0.06	0.00	1.34	3.64	2.60	93.71	6.29 OT R4	11-12/98	219
113	72.11	0.17	11.55	2.36	0.15	0.03	1.26	3.45	2.75	93.83	6.17 OT A0-1	11/25/98	37
114	72.10	0.15	11.46	2.43	0.11	0.01	1.17	3.82	2.76	94.01	5.99 OT A0-1	11/25/98	43
115	72.08	0.15	11.70	2.37	0.11	0.02	1.29	3.45	3.02	94.19	5.81 OT A0-1	11/25/98	46
116	72.08	0.17	11.24	2.26	0.07	0.02	1.26	3.74	2.72	93.56	6.44 OT A 2-3	3/12/98	128
117	72.05	0.14	11.53	2.28	0.08	0.00	1.23	3.85	2.51	93.67	6.33 OT A 2-3	10/12/98	195
118	72.05	0.14	11.60	2.32	0.09	0.03	1.37	3.65	2.60	93.85	6.15 OT R4	11-12/98	209
119	72.04	0.21	11.60	2.19	0.14	0.03	1.38	3.90	2.69	94.18	5.82 OT A 2-3	3/12/98	133*
120	72.02	0.16	11.52	2.33	0.07	0.04	1.23	3.79	2.71	93.87	6.13 OT A 2-3	3/12/98	112
121	71.97	0.19	11.62	2.31	0.09	0.01	1.37	3.86	2.65	94.07	5.93 OT A0-1	11/26/98	77
122	71.92	0.15	11.38	2.20	0.05	0.02	1.14	3.60	2.72	93.18	6.82 OT R4	11-12/98	222*
123	71.85	0.10	11.60	2.57	0.15	0.01	1.36	3.78	2.82	94.24	5.76 OT A0-1	11/26/98	65
124	71.82	0.11	11.44	2.47	0.12	0.06	1.31	3.77	2.72	93.82	6.18 OT A0-1	11/26/98	86
125	71.80	0.14	11.57	2.47	0.09	0.01	1.30	3.51	2.76	93.65	6.35 OT A0-1	11/25/98	45
126	71.78	0.10	11.53	2.39	0.09	0.04	1.26	3.79	2.81	93.79	6.21 OT A0-1	11/25/98	50
127	71.68	0.15	11.51	2.34	0.08	0.02	1.19	3.70	2.71	93.38	6.62 OT A0-1	11/26/98	75
128	71.68	0.19	11.65	2.54	0.06	0.02	1.25	3.76	2.72	93.87	6.13 OT R4	11-12/98	221
129	71.67	0.17	11.40	2.43	0.13	0.02	1.31	3.85	2.69	93.67	6.33 OT A0-1	11/26/98	70
130	71.67	0.19	11.51	2.41	0.07	0.03	1.32	3.73	2.74	93.67	6.33 OT R6	11/12/98	231
131	71.64	0.20	11.58	2.30	0.04	0.02	1.22	3.55	2.75	93.30	6.70 OT R6	11-12/98	229
132	71.54	0.20	11.10	2.40	0.07	0.02	1.21	3.74	2.83	93.11	6.89 OT A 2-3	3/12/98	127
133	71.50	0.18	11.49	2.35	0.11	0.04	1.21	4.06	2.66	93.60	6.40 OT R4	11-12/98	218
134	71.49	0.21	11.22	2.49	0.11	0.02	1.17	3.71	2.55	92.97	7.03 OT A0-1	11/26/98	69*
135	71.45	0.10	11.79	2.30	0.11	0.00	1.37	3.88	2.64	93.64	6.36 OT A0-1	11/26/98	82
136	71.36	0.12	11.31	2.40	0.08	0.03	1.24	3.30	2.56	92.40	7.60 OT A0-1	11/26/98	71
137	71.03	0.11	11.54	2.35	0.07	0.03	1.26	3.25	2.71	92.35	7.65 OT R4	11-12/98	212

n=137	SiO_2	TiO_2	Al_2O_3	FeO_{tot}	MnO	MgO	CaO	Na_2O	K_2O	TOTAL	H_2O_d
Mean	**72.89**	**0.16**	**11.60**	**2.36**	**0.09**	**0.02**	**1.27**	**3.68**	**2.75**	**94.81**	**5.19**
1σ	**0.82**	**0.04**	**0.18**	**0.09**	**0.03**	**0.01**	**0.07**	**0.32**	**0.14**	**0.93**	**0.93**

Óþoli Tephra_UT1655-1659_samples_silicic glass shard data; (n=60)_Analysed by Dr. Shari Preece

No.	SiO_2	TiO_2	Al_2O_3	FeO_{tot}	MnO	MgO	CaO	Na_2O	K_2O	Cl	TOTAL	H_2O_d	UT no.
1	72.13	0.08	11.44	2.49	0.07	0.01	1.48	4.09	2.50	0.07	94.35	5.64	UT1655
2	72.64	0.21	11.67	2.29	0.09	0.03	1.41	4.25	2.76	0.06	95.40	4.60	UT1655
3	72.16	0.17	11.75	2.33	0.11	0.01	1.44	4.29	2.59	0.07	94.92	5.08	UT1655

(contd.)

Table C1.1 (3 of 12) New EPMA data presented in this thesis

4	72.34	0.18	11.81	2.25	0.12	0.03	1.41	4.07	2.68	0.05	94.95	5.04 UT1655
5	72.16	0.25	11.62	2.29	0.05	0.01	1.47	4.05	2.68	0.07	94.63	5.38 UT1655
6	71.95	0.17	11.57	2.30	0.03	0.00	1.41	3.99	2.49	0.06	93.97	6.03 UT1655
7	71.97	0.12	11.46	2.39	0.10	0.02	1.42	4.05	2.52	0.02	94.08	5.92 UT1655
8	72.88	0.18	11.66	2.45	0.06	0.02	1.34	4.12	2.55	0.09	95.34	4.65 UT1655
9	72.52	0.10	11.40	2.48	0.11	0.02	1.46	4.09	2.65	0.08	94.91	5.09 UT1655
10	71.55	0.18	11.75	2.41	0.11	0.01	1.52	3.87	2.54	0.06	93.99	6.02 UT1655
11	72.56	0.15	11.67	2.39	0.12	0.00	1.33	4.23	2.69	0.08	95.22	4.78 UT1655
12	72.51	0.20	11.54	2.47	0.14	0.02	1.48	4.10	2.57	0.09	95.12	4.88 UT1655
13	72.41	0.16	11.62	2.21	0.09	0.00	1.36	4.22	2.64	0.13	94.84	5.16 UT1655
14	72.20	0.09	11.61	2.42	0.05	0.00	1.46	4.18	2.58	0.05	94.65	5.35 UT1655
15	71.50	0.19	11.54	2.25	0.13	0.01	1.50	4.04	2.45	0.07	93.68	6.33 UT1655
Mean	**72.23**	**0.16**	**11.61**	**2.36**	**0.09**	**0.01**	**1.43**	**4.11**	**2.59**	**0.07**	**94.67**	**5.33 UT1655**
1σ	**0.38**	**0.04**	**0.12**	**0.09**	**0.04**	**0.01**	**0.06**	**0.11**	**0.09**	**0.02**	**0.54**	**0.54**
1	72.02	0.12	11.76	2.40	0.14	0.00	1.50	3.98	2.43	0.06	94.42	5.58 UT1657
2	72.43	0.19	11.64	2.42	0.13	0.02	1.44	4.30	2.64	0.06	95.26	4.75 UT1657
3	72.27	0.17	11.84	2.11	0.05	0.02	1.49	4.11	2.59	0.05	94.69	5.30 UT1657
4	71.91	0.25	11.63	2.31	0.08	0.00	1.44	4.15	2.61	0.06	94.42	5.58 UT1657
5	72.18	0.19	11.64	2.40	0.13	0.00	1.42	4.14	2.63	0.05	94.78	5.21 UT1657
6	72.59	0.18	11.83	2.24	0.01	0.02	1.44	4.18	2.64	0.07	95.19	4.82 UT1657
7	72.38	0.19	11.87	2.31	0.09	0.02	1.46	4.19	2.63	0.10	95.24	4.76 UT1657
8	72.18	0.08	11.70	2.39	0.06	0.01	1.39	4.27	2.55	0.05	94.66	5.35 UT1657
9	72.86	0.14	11.83	2.34	0.11	0.01	1.44	4.29	2.66	0.07	95.75	4.26 UT1657
10	72.61	0.18	11.70	2.21	0.01	0.02	1.49	4.22	2.70	0.03	95.16	4.84 UT1657
11	71.59	0.20	11.56	2.27	0.07	0.01	1.38	3.77	2.52	0.06	93.43	6.58 UT1657
12	71.20	0.22	11.68	2.23	0.10	0.00	1.46	3.86	2.54	0.01	93.31	6.68 UT1657
13	72.45	0.14	11.78	2.29	0.07	0.02	1.38	4.22	2.61	0.03	94.98	5.03 UT1657
14	71.95	0.19	11.50	2.26	0.10	0.00	1.50	4.08	2.66	0.05	94.30	5.70 UT1657
15	71.86	0.19	11.66	2.27	0.08	0.03	1.38	3.95	2.50	0.08	94.00	6.01 UT1657
Mean	**72.17**	**0.18**	**11.71**	**2.30**	**0.08**	**0.01**	**1.44**	**4.11**	**2.59**	**0.05**	**94.64**	**5.36 UT1657**
1σ	**0.43**	**0.04**	**0.11**	**0.08**	**0.04**	**0.01**	**0.04**	**0.16**	**0.07**	**0.02**	**0.68**	**0.68**
1	71.69	0.18	11.66	2.47	0.02	0.04	1.47	4.14	2.52	0.05	94.23	5.79 UT1658
2	72.50	0.09	11.55	2.35	0.00	0.01	1.54	4.16	2.69	0.09	94.97	5.03 UT1658
3	72.67	0.24	11.64	2.38	0.07	0.00	1.44	4.13	2.74	0.06	95.36	4.63 UT1658
4	72.78	0.20	11.64	2.50	0.11	0.00	1.43	4.32	2.60	0.09	95.67	4.35 UT1658
5	72.02	0.11	11.51	2.31	0.05	0.02	1.48	4.10	2.77	0.04	94.40	5.62 UT1658
6	72.47	0.13	11.75	2.37	0.07	0.01	1.50	4.26	2.58	0.07	95.21	4.78 UT1658
7	72.31	0.28	11.76	2.30	0.06	0.02	1.45	4.20	2.65	0.04	95.07	4.95 UT1658
8	72.46	0.19	11.88	2.26	0.04	0.01	1.42	4.09	2.64	0.08	95.07	4.92 UT1658
9	72.20	0.13	11.61	2.28	0.08	0.00	1.42	4.02	2.63	0.08	94.43	5.56 UT1658
10	71.89	0.16	11.74	2.53	0.09	0.01	1.54	4.12	2.79	0.06	94.94	5.07 UT1658
11	71.38	0.20	11.33	2.36	0.02	0.01	1.39	3.72	2.50	0.04	92.95	7.04 UT1658
12	72.20	0.13	11.84	2.37	0.04	0.01	1.41	4.19	2.54	0.05	94.78	5.22 UT1658
13	72.26	0.14	11.77	2.25	0.03	0.02	1.43	4.04	2.65	0.03	94.62	5.38 UT1658
14	72.54	0.18	11.60	2.42	0.00	0.00	1.35	4.04	2.49	0.06	94.69	5.29 UT1658
15	72.22	0.09	11.62	2.39	0.09	0.01	1.36	4.25	2.58	0.04	94.66	5.35 UT1658
Mean	**72.24**	**0.16**	**11.66**	**2.37**	**0.05**	**0.01**	**1.44**	**4.12**	**2.62**	**0.06**	**94.74**	**5.27 UT1658**
1σ	**0.37**	**0.05**	**0.14**	**0.08**	**0.04**	**0.01**	**0.06**	**0.14**	**0.09**	**0.02**	**0.63**	**0.62**
1	72.42	0.20	11.71	2.23	0.03	0.00	1.37	4.13	2.69	0.04	94.82	5.17 UT1659
2	72.51	0.14	11.60	2.25	0.09	0.02	1.45	4.18	2.62	0.08	94.95	5.05 UT1659
3	71.62	0.19	11.89	2.27	0.13	0.00	1.55	4.15	2.75	0.08	94.63	5.37 UT1659
4	72.35	0.21	11.52	2.24	0.11	0.00	1.44	4.16	2.62	0.05	94.70	5.30 UT1659
5	71.66	0.20	11.79	2.40	0.12	0.00	1.38	4.02	2.46	0.08	94.11	5.88 UT1659
6	72.77	0.11	11.67	2.20	0.10	0.02	1.46	4.09	2.72	0.06	95.20	4.80 UT1659
7	72.40	0.24	11.61	2.51	0.07	0.01	1.38	4.14	2.66	0.01	95.02	4.98 UT1659
8	72.43	0.18	11.62	2.29	0.10	0.00	1.34	4.16	2.59	0.06	94.77	5.23 UT1659
9	71.97	0.15	11.67	2.31	0.04	0.00	1.39	4.29	2.67	0.08	94.57	5.42 UT1659
10	72.53	0.19	11.71	2.27	0.15	0.00	1.38	4.07	2.73	0.07	95.10	4.90 UT1659
11	72.17	0.22	11.67	2.46	0.11	0.02	1.44	3.87	2.56	0.06	94.58	5.42 UT1659
12	71.82	0.15	11.58	2.43	0.05	0.00	1.39	4.11	2.49	0.03	94.04	5.96 UT1659
13	71.95	0.18	11.56	2.32	0.06	0.03	1.51	4.03	2.68	0.04	94.35	5.66 UT1659
14	72.06	0.21	11.52	2.39	0.12	0.01	1.46	4.22	2.62	0.04	94.65	5.34 UT1659
15	72.62	0.19	11.79	2.37	0.08	0.01	1.56	4.25	2.68	0.05	95.59	4.42 UT1659
Mean	**72.22**	**0.18**	**11.66**	**2.33**	**0.09**	**0.01**	**1.43**	**4.13**	**2.64**	**0.05**	**94.74**	**5.26 UT1659**
1σ	**0.36**	**0.03**	**0.11**	**0.09**	**0.04**	**0.01**	**0.07**	**0.10**	**0.08**	**0.02**	**0.41**	**0.40**
ALL	**72.25**	**0.17**	**11.66**	**2.34**	**0.08**	**0.01**	**1.44**	**4.12**	**2.61**	**0.06**	**94.75**	**5.30 UT1655-59**
MEAN	**0.65**	**0.04**	**0.12**	**0.09**	**0.04**	**0.01**	**0.06**	**0.13**	**0.08**	**0.02**	**5.25**	**0.56**

Óþoli Tephra, Section B, Skagafjall, NW Peninsula, Iceland; basic-intermediate glass shard data; (n=40)

											Sample / Analysis codes		
No.	**SiO_2**	**TiO_2**	**Al_2O_3**	**FeO_{tot}**	**MnO**	**MgO**	**CaO**	**Na_2O**	**K_2O**	**TOTAL**	**H_2O_d**	**Sample**	**Date**	**RH no.**

(contd.)

Table C1.1 (4 of 12) New EPMA data presented in this thesis

1	59.92	1.20	11.82	11.94	0.35	0.66	5.13	2.99	1.44	95.45	4.55	OP A0-1	26/11/98	69
2	59.50	1.31	11.81	14.26	0.35	0.71	5.88	2.62	1.50	97.94	2.06	OP A0-1	25/11/98	39
3	59.50	1.40	12.59	11.93	0.27	0.38	4.34	2.94	1.68	95.03	4.97	OP A0-1	26/11/98	47
4	59.00	1.12	11.72	15.00	0.41	0.49	5.99	1.51	1.40	96.64	3.36	OP A0-1	26/11/98	73
5	58.70	1.44	12.20	14.35	0.38	1.20	5.77	2.76	1.49	98.29	1.71	OP A0-1	26/11/98	72
6	58.30	1.04	11.89	13.25	0.41	0.60	5.86	2.99	1.51	95.85	4.15	OP A0-1	26/11/98	66
7	57.80	1.16	11.54	12.97	0.44	0.70	5.46	2.50	1.62	94.19	5.81	OP A0-1	26/11/98	54
8	57.50	1.46	12.25	12.48	0.35	1.18	6.37	3.69	1.28	96.56	3.44	OP A0-1	26/11/98	58
9	56.97	1.47	11.72	14.37	0.34	1.07	5.97	2.49	1.29	95.69	4.31	OP A0-1	26/11/98	70
10	56.89	1.62	12.33	15.16	0.40	1.35	6.49	1.04	1.33	96.61	3.39	OP A0-1	26/11/98	79
11	56.46	1.82	12.13	15.83	0.40	1.37	6.19	2.29	1.32	97.81	2.19	OP A0-1	26/11/98	81
12	56.06	1.86	12.11	15.43	0.39	1.81	6.70	1.82	1.09	97.27	2.73	OP A0-1	26/11/98	75
13	55.99	1.83	12.43	15.44	0.42	1.78	6.92	1.15	1.18	97.14	2.86	OP A0-1	26/11/98	85
14	55.92	1.83	11.86	14.78	0.42	1.61	6.34	2.19	1.32	96.27	3.73	OP A0-1	26/11/98	74
15	55.69	1.93	12.35	15.31	0.35	1.90	6.71	1.66	1.32	97.22	2.78	OP A0-1	26/11/98	44
16	55.64	1.33	11.86	13.55	0.42	1.28	6.27	2.76	1.26	94.37	5.63	OP A0-1	25/11/98	43*
17	55.56	3.20	11.66	12.09	0.15	2.52	4.26	4.28	1.27	94.99	5.01	OP A0-1	26/11/98	53
18	55.52	1.67	11.94	15.35	0.30	1.40	6.42	1.83	1.21	95.64	4.36	OP A0-1	26/11/98	78
19	55.08	1.60	11.95	15.93	0.45	1.31	6.69	2.78	1.20	96.99	3.01	OP A0-1	26/11/98	59
20	54.99	1.81	11.95	14.91	0.36	1.71	6.74	2.70	1.07	96.24	3.76	OP A0-1	25/11/98	40
21	54.93	2.16	13.95	12.95	0.24	1.14	6.51	4.01	1.14	97.03	2.97	OP A0-1	26/11/98	62
22	54.83	1.40	10.08	15.57	0.44	1.05	6.35	2.55	1.13	93.40	6.60	OP A0-1	26/11/98	77
23	54.31	1.54	11.81	15.03	0.44	1.30	6.50	2.72	1.17	94.82	5.18	OP A0-1	26/11/98	63
24	54.20	1.73	11.93	15.20	0.38	1.44	6.48	2.73	1.10	95.19	4.81	OP A0-1	26/11/98	82
25	54.11	1.92	11.72	13.79	0.41	3.03	6.99	2.57	0.82	95.36	4.64	OP A0-1	26/11/98	52
26	53.79	2.05	11.90	15.60	0.42	1.71	6.73	2.10	1.17	95.47	4.53	OP A0-1	25/11/98	41
27	53.77	2.01	11.69	14.80	0.35	2.02	6.15	2.47	1.01	94.27	5.73	OP A0-1	26/11/98	49
28	53.71	1.99	11.94	15.29	0.39	2.23	6.67	2.33	1.10	95.65	4.35	OP A0-1	26/11/98	84
29	53.35	2.61	11.27	18.16	0.28	1.29	4.61	3.02	1.27	95.86	4.14	OP A0-1	26/11/98	60
30	53.18	1.90	11.85	15.01	0.32	1.97	6.67	2.24	1.23	94.37	5.63	OP A0-1	26/11/98	50
31	53.01	2.17	12.05	15.02	0.37	2.30	7.15	2.47	1.16	95.70	4.30	OP A0-1	26/11/98	67
32	52.88	2.17	12.20	15.13	0.35	2.13	7.13	2.38	1.21	95.58	4.42	OP A0-1	26/11/98	61
33	52.82	1.91	12.11	15.29	0.45	1.98	6.63	2.56	1.15	94.90	5.10	OP A0-1	26/11/98	57*
34	52.80	2.00	11.94	15.57	0.35	2.19	6.68	2.77	1.13	95.43	4.57	OP A0-1	26/11/98	46
35	52.67	2.13	11.80	15.62	0.35	2.35	6.94	2.46	0.98	95.30	4.70	OP A0-1	26/11/98	64
36	52.65	2.13	11.81	15.60	0.36	2.08	6.47	2.75	1.17	95.02	4.98	OP A0-1	26/11/98	80
37	52.37	2.09	11.87	15.28	0.30	2.15	6.73	2.70	1.08	94.57	5.43	OP A0-1	25/11/98	42
38	52.21	3.33	11.89	15.61	0.31	5.38	8.27	3.39	0.39	100.78	-	OP A0-1	25/11/98	2
39	52.04	2.15	11.97	15.04	0.38	2.16	6.95	2.51	1.17	94.37	5.63	OP A0-1	26/11/98	65
40	51.52	2.36	12.83	15.13	0.40	3.58	8.36	3.82	0.74	98.74	1.26	OP A0-1	26/11/98	83

Hjallanes Tephra, Section A, Skagafjall, NW Peninsula, Iceland; basic glass shard data; (n=78)

											Sample / Analysis codes		
No.	SiO_2	TiO_2	Al_2O_3	FeO_{tot}	MnO	MgO	CaO	Na_2O	K_2O	TOTAL	H_2O_d	Sample	Date	RH no.
1	51.72	3.01	15.35	12.94	0.23	4.29	8.73	3.12	0.74	100.13	-	Hj 0-1	11/24/98	23
2	51.24	3.36	13.48	14.04	0.19	4.62	9.02	2.21	0.83	98.99	1.01	Hj 0-1	11/24/98	8
3	51.19	3.11	12.64	13.10	0.23	4.43	8.31	2.77	0.92	96.70	3.30	Hj 0-1	11/24/98	17
4	50.90	3.34	13.09	12.76	0.22	4.08	8.31	2.92	0.93	96.55	3.45	Hj 3-4	12/3/98	120
5	50.76	3.39	12.78	13.69	0.24	4.10	8.16	2.06	0.96	96.14	3.86	Hj 0-1	11/24/98	4
6	50.63	3.07	13.10	13.08	0.25	4.53	8.23	2.98	0.87	96.74	3.26	Hj 0-1	11/24/98	5
7	50.61	3.83	13.58	13.58	0.20	5.23	8.85	3.00	0.76	99.64	0.36	Hj 0-1	11/24/98	12
8	50.46	3.54	13.36	13.32	0.20	4.49	8.52	2.10	0.82	96.81	3.19	Hj 0-1	11/24/98	10
9	50.35	3.41	13.06	13.99	0.22	4.57	8.96	2.62	0.76	97.94	2.06	Hj 0-1	11/25/98	36
10	50.31	3.30	12.82	13.25	0.22	4.14	8.16	2.26	0.80	95.26	4.74	Hj 0-1	11/24/98	25
11	50.28	3.38	12.90	13.65	0.28	4.39	8.39	2.66	0.82	96.75	3.25	Hj 0-1	11/24/98	3
12	50.17	3.07	12.91	12.57	0.18	4.09	8.21	2.38	0.82	94.40	5.60	Hj 0-1	11/24/98	31
13	50.15	3.35	13.04	13.76	0.49	4.38	8.62	2.28	0.84	96.91	3.09	Hj 0-1	11/24/98	18*
14	50.12	3.33	13.08	12.17	0.22	4.23	8.41	3.09	0.90	95.55	4.45	Hj 3-4	12/3/98	117
15	50.10	2.97	10.73	12.19	0.26	7.76	9.35	2.06	0.69	96.11	3.89	Hj 0-1	11/25/98	37
16	50.09	3.58	12.66	14.04	0.32	4.34	8.47	2.63	0.81	96.94	3.06	Hj 3-4	12/3/98	136*
17	50.05	3.52	12.93	13.82	0.26	4.44	8.75	3.13	0.76	97.66	2.34	Hj 3-4	12/3/98	118
18	49.97	3.37	13.06	13.59	0.24	4.59	8.76	2.47	0.85	96.90	3.10	Hj 0-1	11/24/98	11
19	49.97	3.71	13.55	14.74	0.28	3.98	8.77	2.65	0.80	98.45	1.55	Hj 2-3	12/3/98	108
20	49.94	3.18	13.00	12.51	0.23	4.40	8.46	2.47	0.96	95.15	4.85	Hj 2-3	12/3/98	110
21	49.82	3.50	13.14	13.61	0.18	4.60	8.65	2.76	0.72	96.98	3.02	Hj 0-1	11/24/98	14
22	49.81	3.37	12.99	13.76	0.23	4.36	8.52	2.07	0.81	95.92	4.08	Hj 2-3	12/3/98	100
23	49.70	3.37	12.75	13.28	0.24	4.58	8.62	2.76	0.75	96.05	3.95	Hj 2-3	12/3/98	112
24	49.69	3.32	12.96	13.17	0.20	4.42	8.53	2.95	0.77	96.01	3.99	Hj 0-1	11/25/98	34*
25	49.67	3.45	12.98	13.96	0.27	4.65	8.67	2.49	0.74	96.88	3.12	Hj 3-4	12/3/98	134
26	49.63	3.23	11.96	13.59	0.28	6.43	9.70	2.56	0.70	98.08	1.92	Hj 3-4	12/3/98	133
27	49.60	3.49	12.94	13.68	0.24	4.66	8.79	2.40	0.78	96.58	3.42	Hj 2-3	12/3/98	103
28	49.59	3.35	12.88	13.67	0.27	4.72	8.74	2.69	0.68	96.59	3.41	Hj 0-1	11/25/98	35**
29	49.59	3.28	12.90	13.34	0.23	4.49	8.80	2.66	0.89	96.18	3.82	Hj 2-3	12/3/98	102
30	49.58	3.48	12.92	14.27	0.24	3.77	8.09	2.57	0.95	95.87	4.13	Hj 2-3	12/3/98	109
31	49.55	3.54	13.07	13.80	0.26	4.59	8.71	3.09	0.80	97.41	2.59	Hj 2-3	12/3/98	98

(contd.)

32	49.51	3.47	12.99	13.63	0.26	4.44	8.47	2.89	0.78	96.44	3.56	Hj 2-3	12/3/98	101
33	49.38	3.40	12.99	13.40	0.21	4.27	8.62	2.39	0.79	95.45	4.55	Hj 0-1	11/24/98	21
34	49.38	3.27	12.78	13.55	0.20	4.55	8.61	3.25	0.78	96.37	3.63	Hj 3-4	12/3/98	130
35	49.36	3.57	13.06	14.16	0.28	4.59	8.90	2.65	0.75	97.32	2.68	Hj 0-1	11/24/98	6
36	49.34	3.18	12.69	13.17	0.28	4.49	8.49	3.31	0.83	95.78	4.22	Hj 3-4	12/3/98	132
37	49.31	3.51	12.96	13.70	0.24	4.60	8.56	2.64	0.77	96.29	3.71	Hj 0-1	11/24/98	22
38	49.31	3.47	13.03	13.23	0.21	4.45	8.46	2.65	0.83	95.64	4.36	Hj 0-1	11/24/98	24
39	49.30	3.64	13.04	13.92	0.26	4.35	8.49	2.50	0.83	96.33	3.67	Hj 2-3	12/3/98	105
40	49.29	3.54	13.20	13.72	0.20	4.55	8.66	2.66	0.79	96.61	3.39	Hj 0-1	11/24/98	16
41	49.26	3.45	12.39	13.65	0.26	4.57	8.59	3.08	0.77	96.02	3.98	Hj 2-3	12/3/98	107
42	49.26	3.40	12.95	13.57	0.24	4.60	8.61	3.26	0.76	96.65	3.35	Hj 2-3	12/3/98	114
43	49.25	3.61	13.11	13.89	0.26	4.39	8.75	2.78	0.83	96.87	3.13	Hj 0-1	11/24/98	7
44	49.25	3.42	12.97	13.52	0.23	4.54	8.62	2.60	0.81	95.96	4.04	Hj 0-1	11/25/98	33
45	49.23	3.33	12.79	13.59	0.24	4.54	8.70	2.68	0.77	95.87	4.13	Hj 3-4	12/3/98	135
46	49.22	3.51	12.84	13.37	0.20	4.42	8.39	2.74	0.74	95.43	4.57	Hj 0-1	11/24/98	32
47	49.19	3.57	12.95	13.46	0.23	4.37	8.75	3.13	0.79	96.44	3.56	Hj 2-3	12/3/98	99
48	49.18	3.60	12.87	12.70	0.26	4.47	8.63	2.92	0.84	95.47	4.53	Hj 2-3	12/3/98	96
49	49.08	3.56	12.84	13.36	0.24	4.47	8.87	3.00	0.75	96.17	3.83	Hj 2-3	12/3/98	106
50	49.07	3.46	12.87	13.32	0.19	4.65	8.76	3.05	0.78	96.15	3.85	Hj 0-1	11/24/98	13
51	49.07	3.42	12.69	13.53	0.23	4.59	8.50	3.27	0.73	96.03	3.97	Hj 3-4	12/3/98	121
52	49.06	3.50	12.98	13.08	0.23	4.44	8.56	3.17	0.78	95.80	4.20	Hj 0-1	11/24/98	30
53	49.06	3.31	12.91	13.66	0.22	4.47	8.65	3.13	0.85	96.26	3.74	Hj 3-4	12/3/98	116
54	49.05	3.52	12.94	13.39	0.19	4.67	8.38	3.04	0.76	95.94	4.06	Hj 0-1	11/24/98	19
55	49.05	3.46	13.01	13.23	0.27	4.53	8.81	2.80	0.78	95.94	4.06	Hj 0-1	11/24/98	26
56	49.03	3.34	12.82	13.41	0.28	4.58	8.56	3.03	0.79	95.84	4.16	Hj 2-3	12/3/98	113
57	49.03	3.32	12.98	13.61	0.24	4.69	8.53	2.57	0.74	95.71	4.29	Hj 3-4	12/3/98	127
58	49.02	3.48	12.74	13.62	0.22	4.35	8.87	3.01	0.81	96.12	3.88	Hj 3-4	12/3/98	124
59	48.99	3.45	12.73	13.48	0.21	4.46	8.64	3.20	0.74	95.90	4.10	Hj 3-4	12/3/98	115*
60	48.96	3.50	12.79	13.85	0.23	4.65	8.74	2.94	0.72	96.38	3.62	Hj 3-4	12/3/98	123
61	48.96	3.43	12.64	13.78	0.22	4.94	8.70	2.95	0.71	96.33	3.67	Hj 3-4	12/3/98	126
62	48.94	3.54	12.96	13.70	0.23	4.62	8.66	2.73	0.78	96.16	3.84	Hj 3-4	12/3/98	131
63	48.91	3.38	12.41	13.79	0.24	4.63	8.41	2.91	0.81	95.49	4.51	Hj 0-1	11/24/98	20
64	48.90	3.20	12.73	12.94	0.24	4.46	8.39	2.49	0.84	94.19	5.81	Hj 2-3	12/3/98	94
65	48.82	3.35	12.57	13.63	0.27	4.45	8.88	2.82	0.82	95.61	4.39	Hj 2-3	12/3/98	95
66	48.80	3.55	13.01	13.38	0.19	4.65	8.59	2.96	0.78	95.91	4.09	Hj 0-1	11/24/98	29
67	48.80	3.57	12.82	13.35	0.24	4.55	8.56	3.03	0.77	95.69	4.31	Hj 2-3	12/3/98	97
68	48.80	3.46	12.82	14.02	0.27	4.62	8.69	3.07	0.76	96.51	3.49	Hj 3-4	12/3/98	122
69	48.79	3.51	13.01	13.71	0.24	4.57	8.48	3.00	0.75	96.06	3.94	Hj 0-1	11/24/98	28
70	48.78	3.52	12.71	13.38	0.26	4.53	8.63	3.00	0.80	95.61	4.39	Hj 3-4	12/3/98	125
71	48.71	3.66	12.85	13.59	0.18	4.62	8.66	2.89	0.68	95.84	4.16	Hj 0-1	11/24/98	27
72	48.49	3.43	12.60	13.32	0.28	4.56	8.53	3.21	0.77	95.19	4.81	Hj 2-3	12/3/98	111
73	48.39	3.52	12.84	13.21	0.23	4.61	8.81	2.94	0.81	95.36	4.64	Hj 3-4	12/3/98	128
74	48.25	3.39	12.58	13.45	0.20	4.53	8.49	2.78	0.80	94.47	5.53	Hj 3-4	12/3/98	119
75	48.11	3.43	12.49	13.37	0.20	4.62	8.77	3.03	0.87	94.89	5.11	Hj 2-3	12/3/98	93
76	47.39	3.26	12.60	13.41	0.24	5.33	9.95	3.01	0.60	95.79	4.21	Hj 2-3	12/3/98	104

Skagafjall basal tephras, Nupur-Fjallskagi, NW Peninsula,; silicic glass shard data; (n=9)

												Sample / Analysis codes		
No.	SiO_2	TiO_2	Al_2O_3	FeO_{tot}	MnO	MgO	CaO	Na_2O	K_2O	TOTAL	H_2O_d	Sample	Date	RH no.
1	74.55	0.11	11.62	2.44	0.05	0.02	1.24	4.38	1.99	96.40	3.60	SKBT2 (9(	2/16/01	45**
2	74.39	0.09	11.77	2.39	0.10	0.00	1.25	4.10	2.12	96.21	3.79	SKBT2	2/16/01	46
3	73.94	0.11	11.86	2.59	0.06	0.03	1.23	4.54	2.08	96.44	3.56	SKBT2	2/16/01	47
4	73.78	0.16	11.84	2.47	0.05	0.02	1.16	4.32	1.83	95.63	4.37	SKBT2	2/16/01	48
5	73.87	0.07	11.75	2.51	0.09	0.03	1.15	4.19	2.06	95.72	4.28	SKBT2	2/16/01	49*
6	74.37	0.14	11.60	2.42	0.09	0.04	1.34	4.21	1.98	96.19	3.81	SKBT2	2/16/01	78**
7	74.41	0.15	11.53	2.55	0.11	0.00	1.32	4.25	1.92	96.24	3.76	SKBT2	2/16/01	79
8	74.96	0.13	11.77	2.40	0.07	0.01	1.29	4.30	2.14	97.07	2.93	SKBT2	2/16/01	80
9	74.88	0.15	11.63	2.42	0.07	0.00	1.33	4.28	1.91	96.67	3.33	SKBT2	2/16/01	81
n=9	74.16	0.13	11.47	2.28	0.05	0.01	1.29	4.16	2.02	95.57	4.43	SKBT2	2/16/01	82*
Mean	**74.33**	**0.12**	**11.68**	**2.45**	**0.07**	**0.02**	**1.26**	**4.27**	**2.01**	**96.21**	**3.79**			
1σ	**0.40**	**0.03**	**0.13**	**0.09**	**0.02**	**0.01**	**0.07**	**0.12**	**0.10**	**0.47**	**0.47**			

Ingaldsandur Tephras, Ingaldsandur, NW Peninsula, Iceland; silicic glass shard data; (n=4)

												Sample / Analysis codes		
No.	SiO_2	TiO_2	Al_2O_3	FeO_{tot}	MnO	MgO	CaO	Na_2O	K_2O	TOTAL	H_2O_d	Sample	Date	RH no.
1	64.01	0.72	15.63	5.35	0.19	0.65	2.39	4.25	4.05	97.24	2.76	NWPT2	1/22/99	GS3
2	62.72	0.83	15.61	4.32	0.15	0.51	2.41	4.99	4.19	95.73	4.27	NWPT2	1/22/99	GS4
3	63.03	0.59	15.44	5.36	0.21	0.60	2.50	4.56	3.72	96.01	3.99	NWPT2	1/22/99	GS5
4	64.22	0.61	15.86	5.67	0.24	0.63	2.73	4.62	3.69	98.27	1.73	NWPT2	1/22/99	GS6
5	63.34	0.03	22.04	0.21	0.00	0.04	3.52	8.81	1.43	99.42	0.58	NWPT2	1/22/99	GS7
n=5														
Mean	**63.50**	**0.69**	**15.64**	**5.18**	**0.20**	**0.60**	**2.51**	**4.61**	**3.91**	**96.81**	**3.19**			
1σ	**0.73**	**0.11**	**0.17**	**0.59**	**0.04**	**0.06**	**0.16**	**0.30**	**0.25**	**1.17**	**1.17**			

(contd.)

ÞIG 1-23: Þórsmörk Ignimbrite, S Iceland; silicic glass shard data

No.	SiO_2	TiO_2	Al_2O_3	FeO_{tot}	MnO	MgO	CaO	Na_2O	K_2O	TOTAL	H_2O_d	Sample / Analysis codes Sample	Date	RH no.
1) ÞIG 1b														RH
1	73.94	0.19	11.57	2.81	0.29	0.02	0.33	4.91	3.48	97.54	2.46	ÞIG 1b	8-10/02/00	87*
2	73.24	0.51	11.49	2.78	0.15	0.00	0.26	4.40	3.76	96.59	3.41	ÞIG 1b	8-10/02/00	79
3	73.23	0.12	11.58	2.43	0.06	0.01	0.30	4.32	5.76	97.81	2.19	ÞIG 1b	8-10/02/00	75
4	73.20	0.15	11.45	2.53	0.07	0.00	0.35	4.59	3.93	96.27	3.73	ÞIG 1b	8-10/02/00	82
5	73.18	0.14	11.78	2.52	0.05	0.00	0.52	4.35	4.83	97.37	2.63	ÞIG 1b	8-10/02/00	80
6	73.16	0.18	11.56	2.67	0.19	0.00	0.44	4.36	4.02	96.58	3.42	ÞIG 1b	8-10/02/00	73
7	73.08	0.20	11.61	2.52	0.06	0.03	0.44	4.34	3.73	96.01	3.99	ÞIG 1b	8-10/02/00	93
8	73.04	0.14	11.64	2.64	0.08	0.01	0.54	4.54	3.49	96.12	3.88	ÞIG 1b	8-10/02/00	88
9	72.86	0.13	11.53	3.21	0.05	0.01	0.38	4.53	4.58	97.28	2.72	ÞIG 1b	8-10/02/00	91
10	72.82	0.16	11.50	2.55	0.06	0.01	0.43	4.34	3.83	95.70	4.30	ÞIG 1b	8-10/02/00	77
11	72.74	0.12	11.28	2.51	0.10	0.01	0.32	4.35	4.18	95.61	4.39	ÞIG 1b	8-10/02/00	76
12	72.64	0.15	11.51	2.52	0.06	0.04	0.37	4.35	4.00	95.64	4.36	ÞIG 1b	8-10/02/00	83
13	72.55	0.18	11.54	2.53	0.06	0.05	0.42	4.28	5.91	97.52	2.48	ÞIG 1b	8-10/02/00	84
14	72.55	0.12	11.54	2.51	0.08	0.00	0.47	4.46	3.92	95.65	4.35	ÞIG 1b	8-10/02/00	86
15	72.44	0.22	11.62	2.49	0.09	0.04	0.36	4.49	3.71	95.46	4.54	ÞIG 1b	8-10/02/00	95
16	72.42	0.15	11.55	2.64	0.09	0.01	0.46	4.35	4.02	95.69	4.31	ÞIG 1b	8-10/02/00	96
17	72.41	0.23	11.71	2.58	0.08	0.03	0.42	4.14	4.01	95.61	4.39	ÞIG 1b	8-10/02/00	99*
18	72.35	0.17	11.54	2.59	0.09	0.03	0.41	4.54	4.22	95.94	4.06	ÞIG 1b	8-10/02/00	97
19	72.23	0.13	11.50	2.45	0.25	0.01	0.36	4.43	4.10	95.46	4.54	ÞIG 1b	8-10/02/00	98
20	71.90	0.13	11.34	2.41	0.06	0.02	0.37	4.19	3.84	94.26	5.74	ÞIG 1b	8-10/02/00	90
21	71.73	0.22	11.74	2.50	0.09	0.02	0.39	4.53	3.84	95.06	4.94	ÞIG 1b	8-10/02/00	89
22	71.61	0.20	11.46	2.54	0.12	0.02	0.35	4.30	3.85	94.45	5.55	ÞIG 1b	8-10/02/00	81
23	70.99	0.14	11.47	4.25	0.19	0.04	0.81	4.44	3.61	95.94	4.06	ÞIG 1b	8-10/02/00	78
24	70.34	0.22	12.31	3.40	0.07	0.01	0.83	4.17	4.02	95.37	4.63	ÞIG 1b	8-10/02/00	74
Mean	**72.53**	**0.18**	**11.58**	**2.69**	**0.10**	**0.02**	**0.43**	**4.40**	**4.11**	**96.04**	**3.96**	*24*		
1s	**0.79**	**0.08**	**0.19**	**0.41**	**0.06**	**0.01**	**0.14**	**0.16**	**0.61**	**0.94**	**0.94**			
2) ÞIG 1c														RH
1	73.88	0.22	11.77	3.05	0.07	0.02	0.42	4.83	4.16	98.42	1.58	ÞIG 1c	8-10/02/00	103
2	73.16	0.18	11.56	2.63	0.10	0.01	0.39	4.40	3.99	96.42	3.58	ÞIG 1c	8-10/02/00	109*
3	73.14	0.32	11.72	2.61	0.11	0.02	0.41	4.67	4.00	97.00	3.00	ÞIG 1c	8-10/02/00	104
4	73.01	0.21	11.54	3.52	0.11	0.03	0.33	4.43	3.94	97.12	2.88	ÞIG 1c	8-10/02/00	107
5	72.85	0.16	11.51	2.54	0.17	0.00	0.41	4.35	4.13	96.12	3.88	ÞIG 1c	8-10/02/00	106
6	72.42	0.22	11.34	2.56	0.14	0.02	0.42	4.44	3.92	95.48	4.52	ÞIG 1c	8-10/02/00	101
7	71.89	0.22	11.57	2.58	0.10	0.03	0.48	4.46	4.20	95.53	4.47	ÞIG 1c	8-10/02/00	105
Mean	**72.91**	**0.22**	**11.57**	**2.78**	**0.11**	**0.02**	**0.41**	**4.51**	**4.05**	**96.58**	**3.42**	*7*		
1s	**0.63**	**0.05**	**0.14**	**0.37**	**0.03**	**0.01**	**0.04**	**0.17**	**0.11**	**1.03**	**1.03**			
3) ÞIG 1d														RH
1	73.62	0.14	11.67	2.60	0.03	0.03	0.39	4.30	4.16	96.94	3.06	ÞIG 1d	1/28/99	8
2	73.44	0.16	11.59	2.39	0.10	0.04	0.37	4.53	4.01	96.63	3.37	ÞIG 1d	1/28/99	3
3	73.05	0.19	11.57	2.44	0.10	0.03	0.35	4.27	3.67	95.67	4.33	ÞIG 1d	1/28/99	4
4	72.98	0.14	11.50	2.38	0.06	0.05	0.42	4.35	4.30	96.18	3.82	ÞIG 1d	1/28/99	10
5	72.97	0.17	11.61	2.54	0.04	0.01	0.36	4.27	4.02	95.99	4.01	ÞIG 1d	1/28/99	12
6	72.86	0.19	11.39	2.49	0.08	0.02	0.40	4.50	4.09	96.02	3.98	ÞIG 1d	1/28/99	14
7	72.73	0.16	11.50	2.45	0.05	0.04	0.39	4.27	4.02	95.61	4.39	ÞIG 1d	1/28/99	11
8	72.67	0.17	11.54	2.61	0.06	0.03	0.36	4.57	4.00	96.01	3.99	ÞIG 1d	1/28/99	16*
9	72.41	0.11	11.49	2.53	0.07	0.03	0.41	4.19	4.20	95.44	4.56	ÞIG 1d	1/28/99	15
10	72.40	0.11	11.19	2.55	0.16	0.03	0.36	4.08	3.88	94.76	5.24	ÞIG 1d	1/28/99	13
11	72.26	0.14	11.72	2.42	0.07	0.00	0.38	4.01	4.17	95.17	4.83	ÞIG 1d	1/28/99	7
12	71.72	0.13	11.41	2.48	0.10	0.04	0.42	4.26	4.16	94.72	5.28	ÞIG 1d	1/28/99	9
13	71.70	0.14	11.39	2.43	0.09	0.03	0.38	3.99	3.97	94.12	5.88	ÞIG 1d	1/28/99	2
14	71.51	0.19	11.54	2.40	0.10	0.01	0.37	4.24	4.27	94.63	5.37	ÞIG 1d	1/28/99	6
Mean	**72.59**	**0.15**	**11.51**	**2.48**	**0.08**	**0.03**	**0.38**	**4.27**	**4.07**	**95.56**	**4.44**	*14*		
1s	**0.64**	**0.03**	**0.13**	**0.08**	**0.03**	**0.01**	**0.02**	**0.18**	**0.17**	**0.81**	**0.81**			
4) ÞIG 2														RH
1	73.58	0.22	11.67	2.60	0.08	0.03	0.32	4.27	4.17	96.94	3.06	ÞIG 2	1/28/99	27*
2	73.12	0.15	11.30	2.50	0.08	0.06	0.37	4.28	4.37	96.23	3.77	ÞIG 2	1/28/99	24
3	72.98	0.17	11.53	2.65	0.11	0.05	0.34	4.54	4.08	96.45	3.55	ÞIG 2	1/28/99	19
4	72.79	0.21	11.47	2.54	0.10	0.02	0.38	4.32	4.05	95.88	4.12	ÞIG 2	1/28/99	18
5	72.67	0.16	11.52	2.58	0.06	0.02	0.36	4.29	4.10	95.76	4.24	ÞIG 2	1/28/99	21
6	72.59	0.21	11.39	2.62	0.08	0.01	0.36	4.61	4.19	96.06	3.94	ÞIG 2	1/28/99	25
7	72.58	0.16	11.48	2.39	0.10	0.05	0.34	4.25	4.00	95.35	4.65	ÞIG 2	1/28/99	23
8	72.56	0.24	11.47	2.57	0.09	0.02	0.34	4.31	4.21	95.81	4.19	ÞIG 2	1/28/99	26
9	72.47	0.17	11.67	2.55	0.08	0.03	0.34	4.34	4.19	95.84	4.16	ÞIG 2	1/28/99	22
10	72.16	0.22	11.38	2.51	0.07	0.02	0.38	4.44	4.26	95.44	4.56	ÞIG 2	1/28/99	20
Mean	**72.75**	**0.19**	**11.49**	**2.55**	**0.09**	**0.03**	**0.35**	**4.37**	**4.16**	**95.98**	**4.02**	*10*		
1s	**0.39**	**0.03**	**0.12**	**0.07**	**0.02**	**0.02**	**0.02**	**0.12**	**0.11**	**0.47**	**0.47**			
5) ÞIG 3														RH
1	73.26	0.14	11.67	2.53	0.00	0.01	0.41	4.43	4.16	96.61	3.39	ÞIG 3	1/28/99	12
2	73.25	0.15	11.30	2.51	0.02	0.00	0.42	4.41	4.14	96.20	3.80	ÞIG 3	1/28/99	5
3	73.13	0.17	11.63	2.48	0.00	0.01	0.43	4.30	4.15	96.30	3.70	ÞIG 3	1/28/99	13

(contd.)

Table C1.1 (7 of 12) New EPMA data presented in this thesis

4	73.00	0.13	11.43	2.50	0.05	0.00	0.39	4.36	4.04	95.90	4.10	ÞIG 3	1/28/99	3
5	72.99	0.17	11.33	2.41	0.00	0.00	0.36	4.18	4.10	95.54	4.46	ÞIG 3	1/28/99	14
6	72.82	0.18	11.51	2.45	0.00	0.01	0.34	4.29	4.06	95.66	4.34	ÞIG 3	1/28/99	15
7	72.24	0.11	11.55	2.53	0.00	0.03	0.38	4.33	4.19	95.36	4.64	ÞIG 3	1/28/99	11
8	72.09	0.16	11.22	2.53	0.04	0.01	0.41	4.31	4.22	94.99	5.01	ÞIG 3	1/28/99	16
9	71.71	0.18	11.35	2.51	0.06	0.00	0.37	4.15	4.07	94.40	5.60	ÞIG 3	1/28/99	7
10	70.39	0.17	11.36	2.47	0.01	0.02	0.38	4.17	4.04	93.01	6.99	ÞIG 3	1/28/99	10
Mean	**72.49**	**0.16**	**11.44**	**2.49**	**0.02**	**0.01**	**0.39**	**4.29**	**4.12**	**95.40**	**4.60**	*10*		
1s	**0.91**	**0.02**	**0.15**	**0.04**	**0.02**	**0.01**	**0.03**	**0.10**	**0.06**	**1.06**	**1.06**			
6) ÞIG 5														
1	73.70	0.14	11.89	2.68	0.08	0.05	0.40	4.39	3.78	97.11	2.89	ÞIG 5	1/28/99	9
2	73.00	0.13	11.66	2.46	0.06	0.03	0.37	4.30	4.10	96.11	3.89	ÞIG 5	1/28/99	11
3	72.95	0.13	11.54	2.46	0.06	0.05	0.35	4.34	4.24	96.12	3.88	ÞIG 5	1/28/99	12
4	72.71	0.15	11.65	2.52	0.05	0.01	0.35	4.28	4.25	95.97	4.03	ÞIG 5	1/28/99	6
5	72.44	0.12	11.25	2.44	0.04	0.00	0.43	4.00	3.91	94.63	5.37	ÞIG 5	1/28/99	16
6	72.40	0.13	11.56	2.41	0.06	0.01	0.33	4.55	4.22	95.67	4.33	ÞIG 5	1/28/99	3
7	72.37	0.11	11.43	2.46	0.02	0.01	0.35	4.26	4.28	95.29	4.71	ÞIG 5	1/28/99	13
8	72.33	0.16	11.38	2.40	0.08	0.04	0.34	4.06	4.07	94.86	5.14	ÞIG 5	1/28/99	17*
9	72.06	0.13	11.44	2.44	0.01	0.02	0.41	4.10	4.07	94.68	5.32	ÞIG 5	1/28/99	4
10	71.98	0.17	11.24	2.38	0.09	0.01	0.36	3.68	3.89	93.80	6.20	ÞIG 5	1/28/99	5
11	71.94	0.14	11.52	2.49	0.04	0.03	0.36	4.29	3.87	94.68	5.32	ÞIG 5	1/28/99	14
12	71.83	0.14	11.41	2.53	0.03	0.01	0.42	4.08	3.99	94.44	5.56	ÞIG 5	1/28/99	7
13	71.15	0.19	11.26	2.58	0.07	0.02	0.37	4.15	3.97	93.76	6.24	ÞIG 5	1/28/99	8
14	71.08	0.19	11.29	2.67	0.05	0.01	0.34	4.01	4.29	93.93	6.07	ÞIG 5	1/28/99	15
Mean	**72.28**	**0.15**	**11.47**	**2.49**	**0.05**	**0.02**	**0.37**	**4.18**	**4.07**	**95.08**	**4.93**	*14*		
1s	**0.70**	**0.02**	**0.19**	**0.09**	**0.02**	**0.02**	**0.03**	**0.21**	**0.17**	**1.01**	**1.01**			
7) ÞIG 6														**BS**
1	73.27	0.23	11.20	2.58	0.04	0.05	0.40	4.35	4.07	96.19	3.81	ÞIG 6	1/28/99	24
2	72.83	0.16	11.50	2.50	0.08	0.00	0.42	4.42	3.97	95.88	4.12	ÞIG 6	1/28/99	23
3	72.69	0.13	11.33	2.61	0.06	0.04	0.38	4.49	4.11	95.84	4.16	ÞIG 6	1/28/99	28
4	72.63	0.18	11.42	2.58	0.05	0.01	0.36	3.66	3.86	94.75	5.25	ÞIG 6	1/28/99	19
5	72.62	0.15	11.57	2.44	0.06	0.02	0.40	4.15	3.91	95.32	4.68	ÞIG 6	1/28/99	27
6	72.31	0.13	11.56	2.54	0.13	0.03	0.35	3.88	4.17	95.10	4.90	ÞIG 6	1/28/99	20
7	72.20	0.18	11.17	2.51	0.06	0.02	0.40	4.28	4.27	95.09	4.91	ÞIG 6	1/28/99	29
8	72.18	0.21	11.46	2.49	0.11	0.03	0.39	4.50	3.95	95.32	4.68	ÞIG 6	1/28/99	26
9	72.15	0.20	11.58	2.88	0.08	0.02	0.47	5.21	3.90	96.49	3.51	ÞIG 6	1/28/99	22
10	72.08	0.12	11.49	2.58	0.08	0.03	0.39	4.37	4.25	95.39	4.61	ÞIG 6	1/28/99	21
11	71.92	0.20	11.41	2.48	0.09	0.03	0.32	4.48	4.20	95.13	4.87	ÞIG 6	1/28/99	25
Mean	**72.44**	**0.17**	**11.43**	**2.56**	**0.08**	**0.03**	**0.39**	**4.34**	**4.06**	**95.50**	**4.50**	*11*		
1s	**0.40**	**0.04**	**0.14**	**0.12**	**0.03**	**0.01**	**0.04**	**0.39**	**0.15**	**0.53**	**0.53**			
8) ÞIG 7														**RH**
1	74.54	0.10	11.77	2.56	0.08	0.01	0.39	2.29	4.09	95.83	4.17	ÞIG 7	2/16/01	84*
2	74.43	0.18	11.64	2.28	0.06	0.03	0.36	4.08	3.92	96.98	3.02	ÞIG 7	1/28/99	3
3	73.39	0.21	11.54	2.33	0.06	0.03	0.40	4.26	4.05	96.27	3.73	ÞIG 7	1/28/99	4
4	73.09	0.15	11.75	2.63	0.06	0.01	0.30	4.17	4.12	96.28	3.72	ÞIG 7	2/16/01	56**
5	72.94	0.11	11.30	2.45	0.08	0.02	0.35	3.98	4.35	95.58	4.42	ÞIG 7	2/16/01	83
6	72.86	0.13	11.57	2.65	0.07	0.04	0.38	4.37	4.07	96.14	3.86	ÞIG 7	2/16/01	10
7	72.85	0.09	11.49	2.64	0.12	0.01	0.36	4.03	4.06	95.65	4.35	ÞIG 7	2/16/01	37
8	72.82	0.23	11.66	2.67	0.09	0.01	0.29	4.58	3.58	95.93	4.07	ÞIG 7	1/28/99	6*
9	72.72	0.15	11.38	2.50	0.03	0.00	0.37	3.64	4.01	94.80	5.20	ÞIG 7	2/16/01	4
10	72.68	0.13	11.47	2.49	0.08	0.02	0.36	4.33	4.04	95.60	4.40	ÞIG 7	2/16/01	3
11	72.68	0.17	11.50	2.45	0.07	0.01	0.40	4.40	4.06	95.74	4.26	ÞIG 7	2/16/01	34
12	72.59	0.17	11.57	2.71	0.09	0.04	0.43	4.47	3.72	95.79	4.21	ÞIG 7	1/28/99	5
13	72.54	0.11	11.49	2.45	0.03	0.00	0.38	4.14	4.11	95.25	4.75	ÞIG 7	2/16/01	33**
14	72.48	0.11	11.27	2.46	0.03	0.02	0.36	4.31	4.35	95.39	4.61	ÞIG 7	2/16/01	35
15	72.45	0.17	11.54	2.33	0.05	0.02	0.39	4.15	4.25	95.35	4.65	ÞIG 7	2/16/01	RH2
16	72.41	0.15	11.64	2.57	0.06	0.01	0.36	4.47	4.35	96.02	3.98	ÞIG 7	2/16/01	36
17	71.76	0.16	11.12	2.53	0.02	0.01	0.35	4.24	4.20	94.39	5.61	ÞIG 7	2/16/01	9
18	71.54	0.13	11.37	2.58	0.20	0.02	0.38	4.43	4.02	94.67	5.33	ÞIG 7	2/16/01	7
19	71.23	0.15	11.27	2.48	0.05	0.03	0.36	4.34	3.98	93.89	6.11	ÞIG 7	2/16/01	6
20	70.20	0.26	11.27	2.51	0.12	0.01	0.37	4.20	3.92	92.86	7.14	ÞIG 7	1/28/99	GL2
Mean	**72.61**	**0.15**	**11.48**	**2.51**	**0.07**	**0.02**	**0.37**	**4.14**	**4.06**	**95.42**	**4.58**	*20*		
1s	**0.97**	**0.04**	**0.17**	**0.12**	**0.04**	**0.01**	**0.03**	**0.48**	**0.19**	**0.93**	**0.93**			
9) ÞIG 8														**RH**
1	74.10	0.14	11.83	2.49	0.10	0.04	0.44	4.12	3.81	97.07	2.93	ÞIG 8	1/28/99	14
2	73.24	0.20	11.77	2.56	0.08	0.01	0.44	4.41	4.05	96.76	3.24	ÞIG 8	1/28/99	19*
3	73.19	0.16	11.80	2.36	0.12	0.01	0.38	4.13	4.08	96.23	3.77	ÞIG 8	1/28/99	8
4	73.08	0.20	11.69	2.45	0.09	0.03	0.39	4.66	4.06	96.65	3.35	ÞIG 8	1/28/99	16
5	72.96	0.18	11.52	2.63	0.11	0.00	0.48	4.49	4.10	96.47	3.53	ÞIG 8	1/28/99	13
6	72.89	0.15	11.49	2.49	0.11	0.01	0.41	4.46	3.96	95.97	4.03	ÞIG 8	1/28/99	15
7	72.74	0.13	11.55	2.49	0.08	0.02	0.36	4.12	3.64	95.13	4.87	ÞIG 8	1/28/99	12
8	72.52	0.21	12.29	2.33	0.14	0.00	0.43	3.99	3.92	95.83	4.17	ÞIG 8	1/28/99	10
9	72.15	0.17	11.49	2.35	0.06	0.03	0.44	4.60	4.23	95.52	4.48	ÞIG 8	1/28/99	11
10	72.07	0.12	11.26	2.62	0.09	0.02	0.40	4.50	3.91	94.99	5.01	ÞIG 8	1/28/99	17
11	72.04	0.16	11.45	2.40	0.08	0.00	0.41	3.87	4.11	94.52	5.48	ÞIG 8	1/28/99	9
Mean	**72.82**	**0.17**	**11.65**	**2.47**	**0.10**	**0.02**	**0.42**	**4.30**	**3.99**	**95.92**	**4.08**	*11*		

(contd.)

Table C1.1 (8 of 12) New EPMA data presented in this thesis

1s	**0.61**	**0.03**	**0.27**	**0.10**	**0.02**	**0.01**	**0.03**	**0.27**	**0.16**	**0.81**	**0.81**			
10) ÞIG 11														**RH**
1	72.95	0.14	11.42	2.53	0.30	0.02	0.35	4.36	4.26	96.33	3.67	ÞIG 11	8-10/02/00	17**
2	72.41	0.19	11.48	3.08	0.07	0.03	0.55	4.10	4.17	96.08	3.92	ÞIG 11	8-10/02/00	19
3	72.40	0.19	11.39	2.38	0.10	0.00	0.42	4.27	4.00	95.15	4.85	ÞIG 11	8-10/02/00	24
4	72.29	0.12	11.33	2.39	0.12	0.04	0.36	4.53	4.09	95.27	4.73	ÞIG 11	8-10/02/00	25
5	72.26	0.19	11.55	2.91	0.10	0.01	0.44	4.46	3.30	95.22	4.78	ÞIG 11	8-10/02/00	20
6	72.24	0.18	11.47	2.44	0.38	0.02	0.43	4.45	4.20	95.81	4.19	ÞIG 11	8-10/02/00	18
7	72.16	0.16	11.41	2.43	0.14	0.00	0.38	4.37	4.92	95.97	4.03	ÞIG 11	8-10/02/00	30*
8	71.94	0.18	11.42	2.48	0.10	0.01	0.94	4.37	4.22	95.66	4.34	ÞIG 11	8-10/02/00	22
9	70.26	0.12	11.06	2.58	0.15	0.02	0.95	4.19	4.23	93.56	6.44	ÞIG 11	8-10/02/00	23
10	70.25	0.12	11.10	2.32	0.08	0.02	0.43	4.34	4.04	92.70	7.30	ÞIG 11	8-10/02/00	29
Mean	**71.92**	**0.16**	**11.36**	**2.55**	**0.15**	**0.02**	**0.53**	**4.34**	**4.14**	**95.18**	**4.83**	***10***		
1s	**0.91**	**0.03**	**0.16**	**0.25**	**0.10**	**0.01**	**0.23**	**0.13**	**0.39**	**1.16**	**1.16**			
11) ÞIG 13														**RH**
1	73.19	0.20	11.51	2.52	0.08	0.02	0.39	4.28	3.93	96.12	3.88	ÞIG 13	8-10/02/00	6
2	73.03	0.13	11.50	2.54	0.12	0.03	0.38	4.38	4.32	96.43	3.57	ÞIG 13	8-10/02/00	8
3	72.91	0.22	11.69	2.57	0.06	0.01	0.42	4.37	4.15	96.40	3.60	ÞIG 13	8-10/02/00	10
4	72.73	0.19	11.50	2.64	0.10	0.02	0.37	4.17	4.09	95.81	4.19	ÞIG 13	8-10/02/00	9
5	72.57	0.10	11.48	2.54	0.14	0.02	0.37	4.12	4.05	95.39	4.61	ÞIG 13	8-10/02/00	13
6	72.26	0.93	11.61	2.50	0.16	0.02	0.35	4.24	4.02	96.09	3.91	ÞIG 13	8-10/02/00	5
7	72.21	0.15	11.47	2.61	0.07	0.01	0.37	4.23	4.15	95.27	4.73	ÞIG 13	8-10/02/00	7
8	72.13	0.17	11.27	2.43	0.06	0.01	0.38	4.37	4.17	94.99	5.01	ÞIG 13	8-10/02/00	11
9	71.12	0.21	11.65	2.38	0.07	0.00	0.40	4.37	4.31	94.51	5.49	ÞIG 13	8-10/02/00	4
Mean	**72.46**	**0.26**	**11.52**	**2.53**	**0.10**	**0.02**	**0.38**	**4.28**	**4.13**	**95.67**	**4.33**	***9***		
1s	**0.63**	**0.26**	**0.12**	**0.08**	**0.04**	**0.01**	**0.02**	**0.10**	**0.13**	**0.67**	**0.67**			
12) ÞIG 15														**RH**
1	73.23	0.19	11.46	2.53	0.03	0.02	0.38	4.38	3.45	95.67	4.33	ÞIG 15	8-10/02/00	112
2	72.57	0.21	11.57	2.43	0.01	0.03	0.72	4.34	3.99	95.87	4.13	ÞIG 15	8-10/02/00	117
3	72.54	0.23	11.61	2.64	0.05	0.00	0.59	4.54	3.93	96.13	3.87	ÞIG 15	8-10/02/00	116
4	72.50	0.17	11.65	2.58	0.02	0.02	0.39	4.67	3.91	95.91	4.09	ÞIG 15	8-10/02/00	111
5	72.49	0.15	11.70	2.54	0.03	0.03	0.44	4.41	4.07	95.86	4.14	ÞIG 15	8-10/02/00	118
6	72.33	0.12	11.67	2.53	0.09	0.01	0.40	4.84	4.18	96.17	3.83	ÞIG 15	8-10/02/00	120
7	72.07	0.14	11.37	2.27	0.03	0.01	0.36	4.86	3.94	95.05	4.95	ÞIG 15	8-10/02/00	125
8	72.04	0.13	11.80	2.50	0.03	0.02	0.37	4.90	4.17	95.96	4.04	ÞIG 15	8-10/02/00	119
9	71.94	0.19	11.55	2.56	0.07	0.02	0.48	4.26	3.61	94.68	5.32	ÞIG 15	8-10/02/00	114
10	71.91	0.20	11.45	2.45	0.05	0.04	0.45	4.67	3.65	94.87	5.13	ÞIG 15	8-10/02/00	123
11	71.80	0.18	11.76	2.28	0.06	0.03	0.38	4.82	4.64	95.95	4.05	ÞIG 15	8-10/02/00	121
12	71.47	0.14	11.59	2.40	0.06	0.03	0.36	4.93	3.93	94.91	5.09	ÞIG 15	8-10/02/00	127*
13	71.30	0.17	11.57	2.43	0.06	0.02	0.38	4.60	4.35	94.88	5.12	ÞIG 15	8-10/02/00	115
14	71.22	0.16	11.16	2.46	0.02	0.04	0.35	4.61	3.86	93.88	6.12	ÞIG 15	8-10/02/00	126
15	70.92	0.14	11.35	2.56	0.01	0.03	0.37	4.66	4.38	94.42	5.58	ÞIG 15	8-10/02/00	124
16	70.41	0.20	11.62	2.46	0.07	0.03	0.34	4.67	4.06	93.86	6.14	ÞIG 15	8-10/02/00	122
Mean	**71.92**	**0.17**	**11.56**	**2.48**	**0.04**	**0.02**	**0.42**	**4.64**	**4.01**	**95.25**	**4.75**	***16***		
1s	**0.72**	**0.03**	**0.16**	**0.10**	**0.02**	**0.01**	**0.10**	**0.21**	**0.30**	**0.78**	**0.78**			
13) ÞIG 16														**RH**
1	73.14	0.11	11.32	2.49	0.08	0.00	0.37	2.93	4.19	94.63	5.37	ÞIG 16A	8-10/02/00	43
2	73.03	0.13	11.42	2.57	0.03	0.02	0.39	4.62	4.51	96.72	3.28	ÞIG 16B	8-10/02/00	62
3	72.92	0.15	11.53	2.37	0.06	0.02	0.67	4.49	4.09	96.30	3.70	ÞIG 16B	8-10/02/00	58
4	72.74	0.13	11.34	2.55	0.05	0.01	0.31	4.82	4.24	96.19	3.81	ÞIG 16A	8-10/02/00	42
5	72.68	0.13	11.20	2.46	0.10	0.04	0.34	4.54	4.23	95.72	4.28	ÞIG 16A	8-10/02/00	40
6	72.68	0.10	11.49	2.50	0.06	0.03	0.33	4.71	4.19	96.09	3.91	ÞIG 16B	8-10/02/00	50
7	72.65	0.24	11.35	2.42	0.13	0.02	0.36	4.23	4.38	95.78	4.22	ÞIG 16A	8-10/02/00	34
8	72.65	0.11	11.38	2.50	0.03	0.00	0.40	4.38	4.05	95.50	4.50	ÞIG 16A	8-10/02/00	41
9	72.56	0.11	11.33	2.42	0.06	0.02	0.37	4.51	4.19	95.57	4.43	ÞIG 16A	8-10/02/00	44
10	72.56	0.12	11.30	2.36	0.06	0.03	0.33	4.20	4.32	95.28	4.72	ÞIG 16B	8-10/02/00	48**
11	72.55	0.15	11.30	3.07	0.04	0.02	0.36	4.51	4.25	96.25	3.75	ÞIG 16B	8-10/02/00	67
12	72.48	0.10	11.40	3.47	0.08	0.02	0.35	4.36	4.24	96.50	3.50	ÞIG 16B	8-10/02/00	56
13	72.47	0.10	11.60	2.51	0.03	0.02	0.31	4.72	4.34	96.10	3.90	ÞIG 16B	8-10/02/00	49
14	72.47	0.15	11.37	2.54	0.04	0.01	0.35	4.53	4.13	95.59	4.41	ÞIG 16B	8-10/02/00	57
15	72.44	0.16	11.36	2.46	0.05	0.01	0.34	4.42	4.20	95.44	4.56	ÞIG 16A	8-10/02/00	47*
16	72.42	0.13	11.47	2.54	0.03	0.02	0.34	4.42	4.27	95.64	4.36	ÞIG 16B	8-10/02/00	65
17	72.35	0.16	11.44	2.58	0.17	0.02	0.41	4.73	4.21	96.07	3.93	ÞIG 16A	8-10/02/00	37
18	72.33	0.14	11.41	2.38	0.09	0.01	0.37	4.37	4.15	95.25	4.75	ÞIG 16A	8-10/02/00	33
19	72.32	0.15	11.38	2.70	0.04	0.01	0.37	4.68	4.23	95.88	4.12	ÞIG 16B	8-10/02/00	70
20	72.25	0.19	11.43	2.51	0.09	0.00	0.40	4.17	4.33	95.37	4.63	ÞIG 16A	8-10/02/00	31**
21	72.23	0.08	11.35	2.35	0.04	0.04	0.31	4.62	4.12	95.14	4.86	ÞIG 16B	8-10/02/00	69
22	72.20	0.13	11.37	2.67	0.08	0.01	0.33	4.39	4.15	95.33	4.67	ÞIG 16B	8-10/02/00	52
23	72.20	0.18	11.45	2.57	0.07	0.03	0.36	4.50	4.37	95.73	4.27	ÞIG 16B	8-10/02/00	71*
24	71.97	0.13	11.31	2.38	0.06	0.02	0.34	4.60	4.06	94.87	5.13	ÞIG 16B	8-10/02/00	51
25	71.97	0.15	11.35	2.49	0.05	0.01	0.42	4.55	4.19	95.18	4.82	ÞIG 16B	8-10/02/00	63
26	71.85	0.16	11.32	2.56	0.48	0.01	0.42	3.24	4.14	94.18	5.82	ÞIG 16A	8-10/02/00	36
27	71.77	0.14	11.27	2.41	0.05	0.03	0.36	4.44	4.21	94.68	5.32	ÞIG 16B	8-10/02/00	59
28	71.72	0.13	11.36	2.32	0.04	0.01	0.68	4.60	4.21	95.07	4.93	ÞIG 16A	8-10/02/00	45
29	71.66	0.15	11.27	2.41	0.03	0.03	0.37	4.68	4.23	94.83	5.17	ÞIG 16B	8-10/02/00	61
30	71.60	0.15	11.33	2.39	0.02	0.03	0.36	4.45	4.02	94.35	5.65	ÞIG 16B	8-10/02/00	55

(contd.)

31	71.56	0.15	11.47	2.54	0.05	0.03	0.34	4.61	4.14	94.89	5.11	ÞIG 16B	8-10/02/00	66
32	70.89	0.16	11.35	2.39	0.03	0.01	0.40	4.29	4.03	93.55	6.45	ÞIG 16B	8-10/02/00	68
33	70.80	0.07	11.06	2.41	0.03	0.03	0.30	4.25	4.09	93.04	6.96	ÞIG 16B	8-10/02/00	64
Mean	**72.25**	**0.14**	**11.37**	**2.52**	**0.07**	**0.02**	**0.38**	**4.41**	**4.20**	**95.35**	**4.65**	***33***		
1s	**0.54**	**0.03**	**0.10**	**0.22**	**0.08**	**0.01**	**0.08**	**0.38**	**0.11**	**0.81**	**0.81**			
14) ÞIG 21														**RH**
1	72.26	0.12	11.31	2.40	0.00	0.02	0.87	4.57	4.10	95.65	4.35	ÞIG 21	8-10/02/00	142
2	71.87	0.16	11.58	2.50	0.03	0.02	0.33	4.80	4.02	95.31	4.69	ÞIG 21	8-10/02/00	136
3	71.83	0.17	11.52	2.29	0.04	0.02	0.38	4.46	4.39	95.10	4.90	ÞIG 21	8-10/02/00	137
4	71.74	0.12	11.39	2.51	0.07	0.03	0.35	4.60	4.06	94.87	5.13	ÞIG 21	8-10/02/00	143
5	71.48	0.12	11.23	2.58	0.01	0.03	0.35	4.43	4.00	94.23	5.77	ÞIG 21	8-10/02/00	138
6	71.46	0.12	11.32	2.34	0.03	0.00	0.38	4.31	4.05	94.01	5.99	ÞIG 21	8-10/02/00	128**
7	71.14	0.17	11.36	2.80	0.04	0.02	0.35	4.24	4.08	94.20	5.80	ÞIG 21	8-10/02/00	144*
8	71.13	0.16	11.08	2.35	0.01	0.04	0.41	4.52	4.03	93.73	6.27	ÞIG 21	8-10/02/00	139
9	71.04	0.21	11.46	2.34	0.04	0.03	0.32	4.49	4.15	94.08	5.92	ÞIG 21	8-10/02/00	131
10	70.56	0.19	11.26	2.43	0.01	0.02	0.36	4.34	4.11	93.28	6.72	ÞIG 21	8-10/02/00	134*
11	70.45	0.14	11.56	2.47	0.01	0.00	0.42	4.68	4.00	93.73	6.27	ÞIG 21	8-10/02/00	129
Mean	**71.36**	**0.15**	**11.37**	**2.46**	**0.03**	**0.02**	**0.41**	**4.49**	**4.09**	**94.38**	**5.62**	***11***		
1s	**0.56**	**0.03**	**0.15**	**0.14**	**0.02**	**0.01**	**0.16**	**0.17**	**0.11**	**0.75**	**0.75**			
15) ÞIG 22														**RH**
1	71.21	0.13	11.45	2.57	0.02	0.00	0.32	4.32	4.22	94.24	5.76	ÞIG 22	8-10/02/00	145**
2	72.67	0.09	11.46	2.50	0.00	0.02	0.31	4.68	4.22	95.95	4.05	ÞIG 22	8-10/02/00	148
3	72.62	0.20	11.40	2.38	0.00	0.04	0.31	4.83	4.25	96.03	3.97	ÞIG 22	8-10/02/00	146
4	72.59	0.17	11.50	2.45	0.05	0.03	0.32	4.85	4.08	96.04	3.96	ÞIG 22	8-10/02/00	147
5	72.58	0.11	11.49	2.29	0.01	0.02	0.33	4.80	4.01	95.64	4.36	ÞIG 22	8-10/02/00	161*
6	72.41	0.10	11.33	2.46	0.02	0.03	0.41	4.69	4.09	95.54	4.46	ÞIG 22	8-10/02/00	153
7	72.14	0.15	11.62	2.33	0.00	0.02	0.37	4.08	3.95	94.66	5.34	ÞIG 22	8-10/02/00	152
8	72.02	0.11	11.22	2.39	0.00	0.00	0.39	4.62	4.12	94.87	5.13	ÞIG 22	8-10/02/00	154
9	71.91	0.15	11.31	2.51	0.01	0.02	0.37	4.94	3.99	95.21	4.79	ÞIG 22	8-10/02/00	149
10	71.86	0.08	11.49	2.36	0.06	0.02	0.36	4.72	4.23	95.18	4.82	ÞIG 22	8-10/02/00	150
11	71.86	0.13	11.47	2.46	0.03	0.00	0.42	4.62	4.12	95.11	4.89	ÞIG 22	8-10/02/00	156
12	71.82	0.16	11.33	2.48	0.02	0.04	0.39	4.57	4.23	95.04	4.96	ÞIG 22	8-10/02/00	157
13	71.68	0.19	11.41	2.35	0.07	0.02	0.31	4.56	4.13	94.72	5.28	ÞIG 22	8-10/02/00	155
14	71.57	0.14	11.55	2.43	0.05	0.03	0.44	4.55	4.04	94.80	5.20	ÞIG 22	8-10/02/00	158
15	70.85	0.14	11.22	2.36	0.02	0.02	0.30	4.40	3.99	93.30	6.70	ÞIG 22	8-10/02/00	159
Mean	**71.99**	**0.14**	**11.42**	**2.42**	**0.02**	**0.02**	**0.36**	**4.62**	**4.11**	**95.09**	**4.91**	***15***		
1s	**0.54**	**0.03**	**0.12**	**0.08**	**0.02**	**0.01**	**0.05**	**0.22**	**0.10**	**0.73**	**0.73**			
16) ÞIG 23														**RH**
1	72.97	0.21	11.69	2.44	0.09	0.03	0.33	4.72	4.03	96.51	3.49	ÞIG 23	8-10/02/00	229
2	72.34	0.11	11.74	2.72	0.09	0.04	0.40	4.79	4.06	96.29	3.71	ÞIG 23	8-10/02/00	226**
3	72.32	0.12	11.54	2.57	0.19	0.01	0.34	4.58	4.09	95.76	4.24	ÞIG 23	8-10/02/00	227
Mean	**72.54**	**0.15**	**11.66**	**2.58**	**0.12**	**0.03**	**0.36**	**4.70**	**4.06**	**96.19**	**3.81**	***3***		
1s	**0.37**	**0.06**	**0.10**	**0.14**	**0.06**	**0.02**	**0.04**	**0.11**	**0.03**	**0.39**	**0.39**			

ÞIG 1-23											
n=218	**SiO_2**	**TiO_2**	**Al_2O_3**	**FeO_{tot}**	**MnO**	**MgO**	**CaO**	**Na_2O**	**K_2O**	**TOTAL**	**H_2O_d**
Mean	**72.34**	**0.16**	**11.48**	**2.53**	**0.07**	**0.02**	**0.40**	**4.38**	**4.10**	**95.48**	**4.52**
1s	**0.75**	**0.07**	**0.17**	**0.21**	**0.06**	**0.01**	**0.09**	**0.30**	**0.26**	**0.93**	**0.93**

ÞIG 1-23: Þórsmórk Ignimbrite, S Iceland; silicic glass shard outlier data (PCA, cluster analysis)

												Analysis code	
No.	**SiO_2**	**TiO_2**	**Al_2O_3**	**FeO_{tot}**	**MnO**	**MgO**	**CaO**	**NaO**	**K_2O**	**TOTAL**	**H_2O_d**	**Sample**	**Date**	**RH no.**
1	73.02	1.97	11.68	2.64	0.07	0.01	0.48	4.50	4.10	98.47	1.53	ÞIG 1b	8-10/02/00	94
2	73.07	0.13	11.63	4.64	0.04	0.00	0.39	4.31	4.04	98.25	1.75	ÞIG 13	8-10/02/00	14
3	73.01	0.11	11.25	2.34	0.10	0.02	1.65	4.71	4.01	97.20	2.80	ÞIG 1b	8-10/02/00	85
4	72.98	1.82	11.65	2.71	0.60	0.02	0.50	4.53	4.08	98.89	1.11	ÞIG 1c	8-10/02/00	108
5	72.91	2.40	11.55	2.60	0.05	0.04	0.43	4.53	4.18	98.69	1.31	ÞIG 1c	8-10/02/00	102
6	72.91	0.11	11.73	4.70	0.07	0.01	0.36	4.35	4.00	98.24	1.76	ÞIG 16B	8-10/02/00	54
7	72.83	1.08	11.58	2.68	0.06	0.05	0.39	4.20	4.14	97.01	2.99	ÞIG 13	8-10/02/00	12
8	72.57	1.29	11.22	2.44	0.05	0.01	0.39	4.56	4.32	96.85	3.15	ÞIG 16B	8-10/02/00	60
9	72.32	3.14	11.57	2.47	0.08	0.00	0.42	4.36	4.14	98.50	1.50	ÞIG 13	8-10/02/00	16*
10	72.25	0.15	11.45	2.65	1.51	0.00	0.36	4.51	4.23	97.11	2.89	ÞIG 11	8-10/02/00	26
11	72.21	1.95	11.79	2.61	0.12	0.00	0.35	4.24	4.18	97.45	2.55	ÞIG 1c	8-10/02/00	100**
12	71.46	2.22	11.84	2.53	0.02	0.02	0.33	4.42	4.13	96.97	3.03	ÞIG 21	8-10/02/00	130
13	71.13	1.39	11.39	2.43	0.13	0.01	0.38	4.58	4.32	95.76	4.24	ÞIG 21	8-10/02/00	140
14	70.85	3.41	11.50	2.48	0.48	0.13	0.33	4.50	4.00	97.68	2.32	ÞIG 21	8-10/02/00	132
15	70.40	0.28	10.97	4.79	0.07	0.02	0.32	4.37	4.12	95.34	4.66	ÞIG 11	8-10/02/00	21
16	72.95	0.23	11.60	2.59	0.12	0.05	1.20	4.99	3.97	97.70	2.30	ÞIG 23	8-10/02/00	230*
17	72.81	0.35	11.55	2.40	0.04	0.03	1.04	4.54	4.24	97.00	3.00	ÞIG 22	8-10/02/00	160
18	70.58	0.14	11.24	2.47	0.12	0.03	1.78	4.38	4.03	94.77	5.23	ÞIG 11	8-10/02/00	27

ÞIG 1b & 4: Þórsmórk Ignimbrite, S Iceland; basic glass shard data

												Sample / Analysis codes		
No.	**SiO_2**	**TiO_2**	**Al_2O_3**	**FeO_{tot}**	**MnO**	**MgO**	**CaO**	**Na_2O**	**K_2O**	**TOTAL**	**H_2O_d**	**Sample**	**Date**	**Bs no.**

(contd.)

Table C1.1 (10 of 12) New EPMA data presented in this thesis

ÞIG 1b (Bs)														
1	46.34	4.76	12.38	14.47	0.00	4.69	9.49	3.03	0.72	95.88	4.12	ÞIG 1b	2/16/01	2
2	45.24	4.77	12.19	14.55	0.00	4.85	9.68	3.20	0.72	95.20	4.80	ÞIG 1b	2/16/01	3
3	45.57	4.74	12.50	14.27	0.00	4.96	8.87	3.08	0.81	94.80	5.20	ÞIG 1b	2/16/01	4
4	45.40	4.81	11.87	14.76	0.00	4.80	9.97	3.11	0.83	95.55	4.45	ÞIG 1b	2/16/01	5
5	45.86	4.61	12.44	14.45	0.00	4.84	9.24	3.29	0.66	95.39	4.61	ÞIG 1b	2/16/01	6
6	45.84	4.65	12.45	14.37	0.00	4.93	9.43	3.27	0.75	95.69	4.31	ÞIG 1b	2/16/01	7**
7	46.64	4.74	12.22	14.82	0.00	4.56	9.06	3.21	0.79	96.04	3.96	ÞIG 1b	2/16/01	8
8	46.36	4.74	12.46	14.74	0.00	4.87	9.27	3.11	0.75	96.30	3.70	ÞIG 1b	2/16/01	9
9	46.53	4.94	12.32	14.81	0.00	4.82	9.58	3.14	0.76	96.90	3.10	ÞIG 1b	2/16/01	10
10	46.24	4.75	12.36	14.72	0.00	4.78	9.36	3.14	0.81	96.16	3.84	ÞIG 1b	2/16/01	11
11	46.59	4.70	12.40	14.54	0.00	4.75	9.73	3.17	0.64	96.52	3.48	ÞIG 1b	2/16/01	12
12	46.57	4.75	12.10	14.56	0.00	4.74	9.53	3.13	0.68	96.06	3.94	ÞIG 1b	2/16/01	13
13	45.88	4.59	12.34	14.27	0.00	4.97	9.59	3.25	0.66	95.55	4.45	ÞIG 1b	2/16/01	14
14	46.81	4.57	12.29	15.08	0.00	4.31	9.26	3.24	0.75	96.31	3.69	ÞIG 1b	2/16/01	15
15	46.67	4.66	12.35	14.54	0.00	4.92	9.74	3.26	0.71	96.85	3.15	ÞIG 1b	2/16/01	16*
16	47.24	4.87	12.46	15.05	0.00	4.48	9.41	3.17	0.74	97.42	2.58	ÞIG 1b	2/16/01	17
17	46.00	4.66	12.28	14.70	0.00	4.78	9.51	3.20	0.74	95.87	4.13	ÞIG 1b	2/16/01	18
18	46.46	4.66	12.09	15.45	0.00	4.90	10.20	3.09	0.68	97.53	2.47	ÞIG 1b	2/16/01	19
19	49.93	3.58	9.53	14.48	0.00	6.64	11.73	2.22	0.80	98.91	1.09	ÞIG 1b	2/16/01	20
20	46.46	4.87	12.36	14.46	0.00	5.17	9.57	2.96	0.70	96.55	3.45	ÞIG 1b	2/16/01	21
21	46.77	4.54	12.46	14.52	0.00	4.86	9.44	3.21	0.83	96.63	3.37	ÞIG 1b	2/16/01	22
22	46.95	4.67	12.29	14.72	0.00	4.86	9.76	3.24	0.71	97.20	2.80	ÞIG 1b	2/16/01	23
23	48.37	4.65	13.11	14.76	0.00	4.70	10.05	2.96	0.68	99.28	0.72	ÞIG 1b	2/16/01	24
24	47.07	4.67	12.39	14.98	0.00	4.75	9.40	3.14	0.81	97.21	2.79	ÞIG 1b	2/16/01	25
25	46.67	4.69	12.62	14.72	0.00	5.02	9.56	3.21	0.76	97.25	2.75	ÞIG 1b	2/16/01	26*
ÞIG 4 (Bs)														
1	48.07	3.97	12.15	14.13	0.18	4.12	8.58	3.19	1.07	95.46	4.54	ÞIG 4	1/28/99	18
2	48.32	4.16	12.51	14.37	0.13	4.70	9.10	3.05	0.89	97.23	2.77	ÞIG 4	1/28/99	19
3	48.30	4.01	12.10	13.84	0.17	4.34	8.51	3.33	1.12	95.72	4.28	ÞIG 4	1/28/99	20
4	49.03	3.98	12.32	14.07	0.21	4.33	8.63	3.08	1.09	96.74	3.26	ÞIG 4	1/28/99	21
5	48.31	4.03	12.20	14.35	0.20	4.16	8.54	3.14	1.02	95.95	4.05	ÞIG 4	1/28/99	22
6	47.77	4.04	12.32	14.14	0.16	4.64	8.97	3.18	0.91	96.13	3.87	ÞIG 4	1/28/99	23
7	48.32	3.80	12.06	14.01	0.24	4.24	8.54	3.27	1.11	95.59	4.41	ÞIG 4	1/28/99	24
8	48.13	4.22	11.86	13.80	0.17	4.16	8.66	3.42	1.05	95.47	4.53	ÞIG 4	1/28/99	25
9	47.62	4.12	12.05	14.28	0.17	4.26	8.66	3.19	1.05	95.40	4.60	ÞIG 4	1/28/99	26
10	47.68	4.16	11.87	15.04	0.21	4.74	8.92	3.04	1.07	96.73	3.27	ÞIG 4	1/28/99	27*

A1875 (ASK 5, 10, 11): N & E Iceland; silicic glass shard data; (n=27)

											Sample / Analysis codes		
No.	**SiO_2**	**TiO_2**	**Al_2O_3**	**FeO_{tot}**	**MnO**	**MgO**	**CaO**	**Na_2O**	**K_2O**	**TOTAL**	**H_2O_d**	**Sample**	**Date**	**RH no.**
1) ASK5														**RH**
1	74.05	0.72	11.99	3.00	0.11	0.57	2.96	3.73	2.51	99.64	0.36	ASK 5	8-10/02/00	168
2	73.38	0.67	11.74	2.87	0.05	0.47	1.99	3.43	2.56	97.16	2.84	ASK 5	8-10/02/00	172
3	73.35	0.96	12.38	3.36	0.05	0.71	2.18	3.40	2.51	98.90	1.10	ASK 5	8-10/02/00	167
4	73.11	0.71	12.20	3.14	0.04	0.63	2.21	3.61	2.48	98.13	1.87	ASK 5	8-10/02/00	173*
5	73.06	0.78	12.31	3.34	0.06	0.70	2.37	3.61	3.26	99.49	0.51	ASK 5	8-10/02/00	169
6	72.87	0.77	12.16	3.26	0.14	0.71	2.26	3.36	2.45	97.98	2.02	ASK 5	8-10/02/00	164
7	72.76	0.78	12.21	3.22	0.05	0.68	2.29	3.77	2.46	98.22	1.78	ASK 5	8-10/02/00	171
8	72.70	0.72	12.28	3.14	0.10	0.61	2.26	3.62	2.45	97.88	2.12	ASK 5	8-10/02/00	163
9	72.35	0.88	12.19	3.42	0.02	0.74	2.39	3.39	2.40	97.78	2.22	ASK 5	8-10/02/00	166
10	71.69	0.90	12.31	3.72	0.11	0.70	2.43	3.36	2.88	98.10	1.90	ASK 5	8-10/02/00	170
2) ASK10														**RH**
1	72.80	0.80	12.25	3.45	0.08	0.69	2.60	3.59	2.57	98.83	1.17	ASK 10	8-10/02/00	177
2	72.68	0.76	12.00	4.02	0.08	0.69	2.33	3.59	2.56	98.71	1.29	ASK 10	8-10/02/00	182
3	72.59	0.79	12.14	3.27	0.08	0.58	2.21	3.70	2.58	97.94	2.06	ASK 10	8-10/02/00	179
4	72.28	0.72	12.29	3.34	0.10	0.71	2.60	3.77	2.47	98.28	1.72	ASK 10	8-10/02/00	183*
5	71.68	0.88	12.02	3.71	0.08	0.77	2.58	3.41	2.52	97.65	2.35	ASK 10	8-10/02/00	174**
6	71.66	0.87	12.36	3.39	0.10	0.75	2.50	3.62	2.82	98.07	1.93	ASK 10	8-10/02/00	175
7	71.22	0.79	12.31	3.33	0.06	0.74	2.32	3.56	2.50	96.83	3.17	ASK 10	8-10/02/00	178
8	70.53	0.88	12.35	3.78	0.09	0.77	2.72	3.67	2.28	97.07	2.93	ASK 10	8-10/02/00	176
3) ASK11														**RH**
1	74.34	0.65	11.90	2.71	0.05	0.53	1.71	3.56	2.45	97.90	2.10	ASK 11	8-10/02/00	189
2	73.79	0.80	12.49	3.92	0.04	0.62	2.32	3.49	2.76	100.23	-	ASK 11	8-10/02/00	185
3	73.64	0.81	11.95	2.87	0.06	0.54	1.97	3.37	2.47	97.68	2.32	ASK 11	8-10/02/00	192
4	73.60	0.62	12.05	2.79	0.14	0.45	1.90	3.54	2.53	97.62	2.38	ASK 11	8-10/02/00	194*
5	73.21	0.82	12.26	3.29	0.14	0.64	2.31	3.61	3.33	99.61	0.39	ASK 11	8-10/02/00	190
6	72.67	1.14	12.04	3.81	0.12	0.62	2.11	3.53	2.50	98.54	1.46	ASK 11	8-10/02/00	193
7	72.48	0.71	12.17	3.99	0.09	0.60	2.11	3.35	2.45	97.95	2.05	ASK 11	8-10/02/00	184**
8	72.47	0.70	12.16	3.11	0.11	0.61	2.34	3.18	2.49	97.17	2.83	ASK 11	8-10/02/00	191
9	71.64	0.76	11.76	2.89	0.12	0.51	2.33	3.67	2.63	96.31	3.69	ASK 11	8-10/02/00	186
ASK 5/10/11														
n=27	**SiO_2**	**TiO_2**	**Al_2O_3**	**FeO_{tot}**	**MnO**	**MgO**	**CaO**	**Na_2O**	**K_2O**	**TOTAL**	**H_2O_d**			
Mean	**72.69**	**0.79**	**12.16**	**3.34**	**0.08**	**0.64**	**2.31**	**3.54**	**2.59**	**98.14**	**1.94**			

(contd.)

1σ	0.89	0.11	0.19	0.37	0.03	0.09	0.26	0.15	0.24	0.91	0.82

A1875: ASK 5, 10, 11: N & E Iceland; silicic glass shard outlier data; (n=3)

No.	SiO_2	TiO_2	Al_2O_3	FeO_{tot}	MnO	MgO	CaO	Na_2O	K_2O	TOTAL	H_2O_d	Sample	Analysis code Date	RH no.
1	73.33	2.21	12.43	3.23	0.09	0.74	2.35	3.61	2.47	100.46	-	ASK 11	8-10/02/00	188
2	72.36	2.01	12.27	3.38	0.04	0.66	2.36	3.78	2.45	99.31	0.69	ASK 10	8-10/02/00	181
3	68.73	0.84	14.47	5.50	0.10	0.69	3.69	4.11	2.07	100.20	-	ASK 10	8-10/02/00	180

Askja, western caldera rim samples (ASK6,7), N Iceland; basic glass shards; (n=36)

No.	SiO_2	TiO_2	Al_2O_3	FeO_{tot}	MnO	MgO	CaO	Na_2O	K_2O	TOTAL	H_2O_d	Sample	Sample / Analysis codes Date	RH no.
1	49.78	2.60	13.57	11.47	0.21	6.98	11.57	2.63	0.25	99.06	0.94	ASK6T	8-10/02/00	3
2	49.72	1.74	13.62	11.74	0.22	6.79	11.56	2.46	0.26	98.11	1.89	ASK6T	8-10/02/00	18
3	49.70	1.58	13.55	11.58	0.23	7.02	11.67	2.53	0.25	98.11	1.89	ASK6T	8-10/02/00	17
4	49.66	1.57	13.41	12.13	0.22	7.01	11.67	2.48	1.99	100.14	-	ASK6T	8-10/02/00	16*
5	49.63	1.58	13.59	11.77	0.17	7.07	11.86	2.36	0.18	98.21	1.79	ASK6T	8-10/02/00	23
6	49.60	1.53	13.75	11.61	0.24	7.16	11.87	2.39	0.60	98.75	1.25	ASK6T	8-10/02/00	13
7	49.52	1.51	13.41	12.26	0.23	6.80	11.68	2.50	0.24	98.15	1.85	ASK6T	8-10/02/00	24
8	49.52	1.51	13.54	11.74	0.27	7.09	11.94	2.52	0.18	98.31	1.69	ASK6T	8-10/02/00	26*
9	49.44	2.34	13.41	13.67	0.20	7.07	11.77	2.45	0.23	100.58	-	ASK6T	8-10/02/00	4
10	49.44	1.67	13.49	12.49	0.22	6.91	11.53	2.44	0.22	98.41	1.59	ASK6T	8-10/02/00	7
11	49.44	1.57	13.67	11.26	0.22	6.81	11.42	2.49	0.21	97.09	2.91	ASK6P	8-10/02/00	30
12	49.43	1.62	13.48	12.46	0.80	6.91	12.52	2.79	0.16	100.17	-	ASK7	8-10/02/00	35
13	49.39	1.63	13.60	11.43	0.23	6.98	11.66	2.30	0.17	97.39	2.61	ASK7	8-10/02/00	38
14	49.38	1.60	13.48	11.66	0.21	7.05	11.69	2.42	0.16	97.65	2.35	ASK6T	8-10/02/00	20
15	49.33	2.64	13.78	11.66	0.21	6.98	11.60	2.38	0.19	98.77	1.23	ASK6T	8-10/02/00	11
16	49.32	1.56	13.22	11.91	0.18	6.87	11.73	2.35	0.20	97.34	2.66	ASK6P	8-10/02/00	31
17	49.31	1.57	13.58	11.72	0.16	7.01	11.51	2.59	0.23	97.68	2.32	ASK6T	8-10/02/00	22
18	49.25	1.58	13.36	12.06	0.46	7.00	11.72	2.35	0.20	97.98	2.02	ASK6T	8-10/02/00	21
19	49.23	1.53	13.63	12.00	0.24	6.94	11.71	2.46	0.21	97.95	2.05	ASK6T	8-10/02/00	8
20	49.23	1.56	13.47	11.45	0.21	6.96	12.55	2.49	0.18	98.10	1.90	ASK6P	8-10/02/00	29
21	49.22	1.64	13.47	12.08	0.25	6.96	11.62	2.60	0.30	98.14	1.86	ASK6T	8-10/02/00	2
22	49.22	1.45	13.63	11.50	0.25	7.02	11.84	2.57	0.26	97.74	2.26	ASK6T	8-10/02/00	19
23	49.20	1.50	13.34	11.59	0.23	6.75	11.53	2.42	0.21	96.77	3.23	ASK6P	8-10/02/00	32
24	49.13	1.44	13.38	11.79	0.16	7.15	11.82	2.48	0.27	97.62	2.38	ASK6T	8-10/02/00	6
25	49.10	2.38	13.43	11.64	0.23	7.06	11.80	2.31	0.24	98.19	1.81	ASK6T	8-10/02/00	10
26	49.10	1.50	13.56	11.87	0.14	7.04	11.36	2.53	0.27	97.37	2.63	ASK6T	8-10/02/00	14
27	49.09	1.58	13.69	11.90	0.21	6.96	11.66	2.52	0.14	97.75	2.25	ASK6T	8-10/02/00	25
28	49.08	1.59	13.22	11.55	0.22	7.02	11.50	2.35	0.23	96.76	3.24	ASK6P	8-10/02/00	27**
29	49.07	1.59	13.50	13.21	0.20	7.08	11.65	2.40	0.30	99.00	1.00	ASK6T	8-10/02/00	12
30	49.02	1.56	13.69	11.65	0.28	7.10	11.56	2.52	0.24	97.62	2.38	ASK7	8-10/02/00	34
31	48.96	1.64	13.48	12.18	0.18	7.06	11.70	2.31	0.16	97.67	2.33	ASK6T	8-10/02/00	5
32	48.95	1.72	13.36	11.75	0.28	7.01	11.77	2.57	0.15	97.56	2.44	ASK6T	8-10/02/00	15
33	48.93	1.72	13.69	11.79	0.20	7.00	11.57	2.32	0.18	97.40	2.60	ASK6T	8-10/02/00	9
34	48.88	1.66	13.53	11.64	0.19	6.99	11.61	2.14	0.17	96.81	3.19	ASK7	8-10/02/00	37
35	48.83	1.57	13.47	11.87	0.30	6.88	11.95	2.60	0.20	97.67	2.33	ASK6P	8-10/02/00	33
36	48.76	1.53	13.59	11.42	0.21	6.60	11.51	2.37	0.25	96.24	3.76	ASK7	8-10/02/00	36

ASK 6/7

n=36	SiO_2	TiO_2	Al_3O_2	FeO_{tot}	MnO	MgO	CaO	NaO	K_2O	TOTAL	H_2O_d
Mean	49.27	1.68	13.52	11.88	0.24	6.97	11.71	2.46	0.27	98.01	2.20
1σ	0.27	0.30	0.13	0.48	0.11	0.12	0.24	0.12	0.30	0.94	0.65

Öræfajökull 1362: ÖR 1, 2, 3, SE Iceland; silicic glass shard data; (n=27)

No.	SiO_2	TiO_2	Al_2O_3	FeO_{tot}	MnO	MgO	CaO	Na_2O	K_2O	TOTAL	H_2O_d	Sample	Sample / Analysis codes Date	RH no.
OR1														
1	72.20	0.21	13.04	3.18	0.15	0.04	0.93	4.84	3.38	97.97	2.03	OR1	8-10/2/00	199
2	71.77	0.89	12.97	3.20	0.40	0.05	0.87	4.89	3.42	98.46	1.54	OR1	8-10/2/00	197
3	71.59	0.24	12.97	3.27	0.13	0.06	0.97	4.98	2.98	97.19	2.81	OR1	8-10/2/00	205*
4	71.37	0.25	12.89	3.17	0.09	0.02	0.84	4.87	3.26	96.76	3.24	OR1	8-10/2/00	196
5	71.27	0.20	13.02	3.27	0.10	0.06	0.93	5.15	3.24	97.24	2.76	OR1	8-10/2/00	202
6	71.18	0.28	12.80	3.13	0.11	0.08	0.92	5.12	3.37	96.99	3.01	OR1	8-10/2/00	200
7	71.14	0.19	13.22	3.42	0.12	0.05	0.90	4.97	3.19	97.20	2.80	OR1	8-10/2/00	203
8	70.30	0.28	12.98	3.33	0.16	0.04	1.00	4.96	3.20	96.25	3.75	OR1	8-10/2/00	201
9	70.23	0.21	12.85	3.28	0.19	0.03	0.86	4.83	3.25	95.73	4.27	OR1	8-10/2/00	204
10	69.84	0.18	12.60	3.85	0.09	0.03	0.98	4.94	3.27	95.78	4.22	OR1	8-10/2/00	198
OR2														
1	72.59	0.20	13.24	3.64	0.11	0.06	1.02	5.08	3.30	99.24	0.76	OR2	8-10/2/00	209
2	72.40	0.20	13.20	3.18	0.07	0.02	0.97	5.11	3.32	98.47	1.53	OR2	8-10/2/00	211
3	72.04	0.21	13.13	3.16	0.11	0.04	1.03	4.77	3.48	97.97	2.03	OR2	8-10/2/00	210

(contd.)

Table C1.1 (12 of 12) New EPMA data presented in this thesis

4	71.76	0.21	12.92	3.36	0.12	0.05	0.90	4.95	3.16	97.43	2.57	OR2	8-10/2/00	207
5	71.53	0.16	12.78	3.19	0.16	0.03	1.51	5.03	3.22	97.61	2.39	OR2	8-10/2/00	208
6	71.30	0.23	13.00	3.20	0.11	0.05	0.95	5.08	3.13	97.05	2.95	OR2	8-10/2/00	215*
7	70.88	0.22	12.79	3.33	0.10	0.03	0.90	4.91	3.39	96.55	3.45	OR2	8-10/2/00	213
OR3														
1	72.41	0.27	13.33	3.04	0.13	0.06	0.93	4.92	3.26	98.35	1.65	OR3	8-10/2/00	223
2	72.37	0.25	13.11	3.15	0.13	0.06	0.89	5.20	3.28	98.44	1.56	OR3	8-10/2/00	224
3	71.71	0.17	12.71	3.42	0.17	0.05	0.97	5.13	3.22	97.55	2.45	OR3	8-10/2/00	219
4	71.47	0.22	13.09	3.19	0.11	0.04	1.01	5.00	3.33	97.46	2.54	OR3	8-10/2/00	225*
5	71.19	0.26	12.69	3.21	0.15	0.06	0.99	5.04	3.19	96.78	3.22	OR3	8-10/2/00	220
6	71.17	0.19	13.11	4.61	0.09	0.02	0.96	4.47	3.41	98.03	1.97	OR3	8-10/2/00	216**
7	71.17	0.16	13.13	3.02	0.17	0.04	0.87	5.10	3.24	96.90	3.10	OR3	8-10/2/00	218
8	71.10	0.15	13.04	3.13	0.11	0.05	0.92	5.16	3.14	96.80	3.20	OR3	8-10/2/00	221
9	70.97	0.19	12.90	3.20	0.16	0.05	1.03	5.29	3.14	96.93	3.07	OR3	8-10/2/00	222
10	70.89	0.23	13.10	3.09	0.09	0.03	0.98	5.29	3.29	96.99	3.01	OR3	8-10/2/00	217

OR 1/2/3											
n=27	SiO_2	TiO_2	Al_2O_3	FeO_{tot}	MnO	MgO	CaO	Na_2O	K_2O	TOTAL	H_2O_d
Mean	71.40	0.24	12.99	3.30	0.13	0.04	0.96	5.00	3.26	97.34	2.66
1σ	0.68	0.13	0.18	0.31	0.06	0.02	0.12	0.17	0.11	0.84	0.84

Ö1362: ÖR 1, 2, 3, SE Iceland; silicic glass shard outlier data; (n=3)

												Analysis code	
No.	SiO_2	TiO_2	Al_2O_3	FeO_{tot}	MnO	MgO	CaO	Na_2O	K_2O	TOTAL	H_2O_d	Sample	Date	RH no.
1	72.05	0.15	13.02	6.58	0.11	0.08	1.09	5.05	3.29	101.42	-	OR2	8-10/2/00	206**
2	70.99	0.20	13.04	3.25	0.86	0.04	1.05	5.04	3.17	97.64	2.36	OR2	8-10/2/00	212
3	71.63	1.88	13.06	3.19	0.12	0.03	0.98	4.81	3.04	98.74	1.26	OR2	8-10/2/00	214

Layer Y, Gigajokull, S Iceland; silicic glass shard data; (n=11)

												Sample	Analysis code	
No.	SiO_2	TiO_2	Al_2O_3	FeO_{tot}	MnO	MgO	CaO	Na_2O	K_2O	TOTAL	H_2O_d	Code	Date	RH no.
LY *(90-150)*														
1	65.36	1.17	13.73	6.41	0.22	1.13	3.27	4.44	2.61	98.34	1.66	LY	8-10/2/00	2
2	65.61	1.45	13.85	6.03	0.26	1.14	2.82	4.65	2.94	98.75	1.25	LY	8-10/2/00	3
3	66.57	1.17	13.75	5.78	0.18	0.95	2.70	4.30	2.83	98.23	1.77	LY	8-10/2/00	4
4	65.71	1.28	13.64	6.01	0.21	1.07	2.96	4.39	3.32	98.59	1.41	LY	8-10/2/00	5
5	65.40	1.14	13.98	5.93	0.22	1.09	2.84	4.00	2.86	97.46	2.54	LY	8-10/2/00	6
6	64.59	1.23	13.62	6.07	0.26	1.08	3.12	4.53	2.65	97.15	2.85	LY	8-10/2/00	7
7	65.09	1.29	13.87	5.95	0.19	1.16	3.13	4.63	2.74	98.05	1.95	LY	8-10/2/00	8
8	66.11	1.07	13.54	5.47	1.45	1.13	2.63	4.55	2.80	98.75	1.25	LY	8-10/2/00	9
9	65.31	4.23	13.87	6.01	0.18	1.12	2.97	4.48	2.94	101.11	-	LY	8-10/2/00	10
10	65.93	1.22	13.65	5.86	0.28	1.07	2.88	4.57	2.85	98.31	1.69	LY	8-10/2/00	11
11	65.50	1.23	13.64	5.96	0.25	1.09	3.04	4.52	2.57	97.80	2.20	LY	8-10/2/00	12*
Mean	65.59	1.23	13.73	5.95	0.35	1.09	2.94	4.46	2.82	98.14	1.86	n=10		
1σ	0.55	0.10	0.14	0.24	0.39	0.06	0.20	0.19	0.21	0.54	0.54			

(contd.)

Table C1.2 (1 of 5) Andradite standard data for EPMA analyses presented in this thesis

(1) Andardite Standard: 11-12/98

11-12/98:AD	UNEDITED DATA		EDITED DATA*		Hill (pers. comm.)	
n	87		56		200	OK range
SiO_2	35.55	0.44	35.60	0.30	35.5	35-36
Al_2O_3	1.73	0.04	1.73	0.04	1.74	1.6-1.9
Fe_2O_3	30.28	0.27	30.32	0.20	30.2	30-30.5
MnO	0.40	0.02	0.41	0.02	0.42	0.40-0.45
MgO	0.10	0.01	0.10	0.01	-	-
CaO	32.36	0.26	32.40	0.22	32.4	32-32.8
TOTAL	100.42	0.71	100.55	0.45	100.26	100-101
					Camebax	

AD STD_General notes:
(a) * Edited data removes unrepresentative duplicate analyses (x), undertaken during calibration, recalibration & verification process, from the mean and 1σ calculation.
(b) Additional AD analyses were undertaken while analysing other samples not included in this thesis. This data is included here for completeness.

UNEDITED DATA_11-12/98:AD1-87

AD no.	SiO_2	Al_2O_3	FeO_{tot}	MnO	MgO	CaO	TOTAL	Notes
1	35.62	1.73	30.14	0.40	0.07	32.38	100.34	
2	35.41	1.70	30.57	0.34	0.09	32.75	100.86	
3	35.18	1.73	29.67	0.37	0.07	32.42	99.44	
4	35.18	1.68	29.66	0.40	0.10	32.40	99.42	
5	35.06	1.76	29.66	0.41	0.10	32.10	99.09	x
6	35.05	1.73	29.26	0.37	0.09	31.73	98.23	x
7	35.72	1.75	30.42	0.43	0.09	32.41	100.82	x
8	35.70	1.82	30.53	0.44	0.13	32.74	101.36	x
9	35.96	1.70	30.17	0.43	0.11	32.56	100.93	
10	36.12	1.78	30.12	0.45	0.08	32.86	101.41	
11	36.07	1.77	30.44	0.42	0.08	32.61	101.39	
12	35.97	1.72	30.07	0.41	0.09	32.68	100.94	x
13	35.22	1.74	30.41	0.42	0.10	32.54	100.43	x
14	35.68	1.70	30.58	0.40	0.12	32.52	101.00	
15	35.32	1.76	30.18	0.43	0.11	32.68	100.48	
16	34.77	1.75	29.74	0.38	0.11	32.02	98.77	
17	35.84	1.69	30.34	0.43	0.10	32.14	100.54	
18	35.63	1.74	30.06	0.40	0.10	32.04	99.97	x
19	34.92	1.69	30.45	0.37	0.10	32.00	99.53	
20	35.14	1.68	30.37	0.40	0.09	32.16	99.84	x
21	35.28	1.74	30.47	0.38	0.13	32.20	100.20	x
22	35.48	1.76	30.00	0.41	0.09	32.36	100.10	x
23	35.14	1.74	30.11	0.41	0.10	32.18	99.68	
24	35.41	1.66	30.38	0.41	0.10	32.32	100.28	
25	34.93	1.75	30.78	0.41	0.10	31.98	99.95	
26	35.05	1.76	30.18	0.37	0.10	32.35	99.81	
27	35.27	1.72	30.50	0.40	0.09	32.23	100.21	x
28	34.92	1.73	30.25	0.39	0.09	32.12	99.50	
29	34.78	1.70	30.34	0.44	0.10	32.63	99.99	
30	34.91	1.70	30.36	0.42	0.12	32.47	99.98	x
31	35.46	1.73	30.49	0.39	0.08	32.60	100.75	x
32	35.25	1.73	30.10	0.42	0.09	32.52	100.11	x
33	35.33	1.73	30.38	0.40	0.09	32.35	100.28	
34	35.63	1.75	30.63	0.41	0.08	32.74	101.24	
35	36.01	1.72	30.85	0.41	0.09	32.70	101.78	
36	35.82	1.72	30.36	0.42	0.10	32.53	100.95	
37	35.89	1.67	30.24	0.42	0.09	32.29	100.60	x
38	36.06	1.73	30.08	0.44	0.11	32.21	100.63	
39	36.02	1.71	30.40	0.38	0.09	32.10	100.70	
40	35.48	1.72	30.10	0.41	0.10	32.07	99.88	
41	35.16	1.67	30.18	0.42	0.11	32.26	99.80	
42	34.91	1.74	30.67	0.42	0.09	31.88	99.71	
43	35.78	1.73	30.30	0.37	0.07	31.90	100.15	x
44	35.09	1.73	30.18	0.38	0.08	31.76	99.22	x
45	34.96	1.69	30.44	0.38	0.08	31.89	99.44	
46	35.51	1.64	30.27	0.43	0.11	32.21	100.17	x
47	36.27	1.73	30.36	0.42	0.10	32.32	101.20	x
48	35.39	1.72	30.27	0.40	0.13	32.48	100.39	
49	35.40	1.72	29.81	0.40	0.09	32.11	99.53	x
50	35.16	1.73	30.38	0.41	0.10	32.40	100.18	
51	35.54	1.66	30.15	0.38	0.09	32.15	99.97	

(contd.)

Table C1.2 (2 of 5) Andradite standard data for EPMA analyses presented in this thesis

52	35.34	1.72	30.37	0.39	0.09	32.15	100.06
53	35.60	1.73	30.20	0.40	0.09	32.07	100.09 x
54	35.46	1.75	30.44	0.41	0.12	32.73	100.91
55	35.45	1.70	30.27	0.44	0.10	32.61	100.57
56	35.69	1.72	30.21	0.42	0.11	32.80	100.95
57	35.64	1.67	30.25	0.41	0.09	32.78	100.84
58	35.63	1.75	30.82	0.39	0.09	32.37	101.05
59	35.44	1.75	30.40	0.42	0.10	32.49	100.60
60	35.64	1.73	30.67	0.37	0.09	32.60	101.10
61	35.89	1.74	30.72	0.39	0.10	32.39	101.23
62	35.82	1.74	30.29	0.37	0.07	32.19	100.48
63	35.97	1.79	30.16	0.42	0.08	32.22	100.64
64	36.41	1.80	30.19	0.39	0.10	32.44	101.33 x
65	36.86	1.80	30.65	0.40	0.08	32.66	102.45
66	36.41	1.73	30.09	0.38	0.10	32.80	101.51 x
67	36.29	1.79	30.09	0.43	0.10	32.32	101.02 x
68	35.50	1.75	29.86	0.39	0.11	32.47	100.08 x
69	35.51	1.71	30.12	0.39	0.08	32.29	100.10 x
70	36.20	1.71	30.08	0.40	0.10	31.94	100.43 x
71	36.02	1.76	30.06	0.45	0.09	32.58	100.96
72	36.05	1.73	30.10	0.39	0.09	32.41	100.77
73	35.59	1.75	30.24	0.41	0.09	32.34	100.42
74	35.54	1.76	30.11	0.41	0.10	32.22	100.14
75	35.67	1.74	30.23	0.42	0.09	32.43	100.58
76	35.81	1.81	30.41	0.43	0.10	32.40	100.96
77	35.88	1.75	30.70	0.41	0.08	32.64	101.46
78	35.78	1.85	30.48	0.39	0.09	32.35	100.94
79	35.95	1.78	30.53	0.41	0.11	32.60	101.38
80	35.98	1.83	30.19	0.41	0.10	32.60	101.11
81	35.87	1.76	30.41	0.41	0.09	32.52	101.06
82	35.57	1.70	30.41	0.41	0.10	32.14	100.33 x
83	34.56	1.76	30.30	0.41	0.10	31.85	98.98 x
84	35.02	1.73	30.13	0.38	0.10	32.62	99.98
85	34.63	1.74	30.38	0.39	0.10	32.47	99.71 x
86	35.59	1.73	30.28	0.41	0.10	32.26	100.37 x
87	35.77	1.71	30.34	0.40	0.09	32.39	100.70
	SiO_2	Al_3O_2	FeO_{tot}	MnO	MgO	CaO	TOTAL
Mean	35.55	1.73	30.28	0.40	0.10	32.36	100.42
1σ	0.44	0.04	0.27	0.02	0.01	0.26	0.71

(2) Andardite Standard: 22/1/99

21/1/99:AD	UNEDITED DATA		EDITED DATA*		Hill (pers. comm.)	
n	19		17		200	OK range
SiO_2	35.57	0.18	35.57	0.19	35.5	35-36
Al_2O_3	1.74	0.04	1.74	0.04	1.74	1.6-1.9
FeO_{tot}	30.34	0.24	30.31	0.23	30.2	30-30.5
MnO	0.45	0.04	0.45	0.04	0.42	0.40-0.45
MgO	0.09	0.01	0.09	0.01	-	-
CaO	32.12	0.17	32.14	0.16	32.4	32-32.8
TOTAL	100.30	0.32	100.30	0.33	100.26	100-101
					Camebax	

UNEDITED DATA_22/1/99:AD

AD no.	SiO_2	Al_2O_3	FeO_{tot}	MnO	MgO	CaO	TOTAL	Notes
1	35.42	1.70	29.83	0.53	0.10	32.03	99.61	
2	35.60	1.75	30.05	0.43	0.07	32.16	100.06	
3	35.71	1.74	30.19	0.43	0.10	32.07	100.24	
4	35.44	1.78	30.39	0.49	0.09	31.90	100.09	
5	35.44	1.82	30.00	0.45	0.10	32.23	100.04	
6	35.43	1.76	30.31	0.42	0.10	32.05	100.07	
7	35.81	1.72	30.53	0.47	0.10	32.20	100.83	
8	35.69	1.76	30.35	0.39	0.10	31.93	100.22	
9	35.44	1.74	30.54	0.43	0.11	31.99	100.25	

(contd.)

Table C1.2 (3 of 5) Andradite standard data for EPMA analyses presented in this thesis

10	35.77	1.78	30.21	0.42	0.10	32.09	100.37
11	35.37	1.69	30.33	0.51	0.08	32.05	100.03
12	35.60	1.71	30.26	0.47	0.07	32.28	100.39
13	35.29	1.70	30.61	0.42	0.09	32.14	100.25
14	35.34	1.81	30.56	0.49	0.09	32.04	100.33
15	35.45	1.70	30.55	0.47	0.08	31.98	100.23 X
16	35.65	1.73	30.75	0.42	0.09	31.87	100.51 X
17	35.72	1.74	30.65	0.46	0.09	32.31	100.97
18	35.92	1.71	30.10	0.43	0.09	32.47	100.72
19	35.67	1.75	30.28	0.38	0.09	32.40	100.57
	SiO_2	Al_3O_2	FeO_{tot}	MnO	MgO	CaO	TOTAL
Mean	35.57	1.74	30.34	0.45	0.09	32.12	100.30
1σ	0.18	0.04	0.24	0.04	0.01	0.17	0.32

(3) Andradite Standard: 28/1/99

28/1/99:AD	UNEDITED DATA		EDITED DATA*	Hill (pers. comm.)	
n	10		n/a	200	OK range
SiO_2	35.77	0.15		35.5	35-36
Al_2O_3	1.73	0.04		1.74	1.6-1.9
FeO_{tot}	30.25	0.12		30.2	30-30.5
MnO	0.44	0.03		0.42	0.40-0.45
MgO	0.10	0.01		-	-
CaO	32.32	0.13		32.4	32-32.8
TOTAL	100.60	0.25		100.26	100-101
				Camebax	

UNEDITED DATA_28/1/99:AD

AD no.	SiO_2	Al_3O_2	FeO_{tot}	MnO	MgO	CaO	TOTAL	Notes
1	35.78	1.74	30.02	0.48	0.09	32.24	100.35	
2	35.53	1.73	30.29	0.49	0.10	32.36	100.50	
3	35.96	1.75	30.44	0.47	0.10	32.15	100.87	
4	35.72	1.69	30.27	0.41	0.10	32.17	100.36	
5	35.91	1.72	30.36	0.45	0.12	32.42	100.98	
6	35.52	1.71	30.24	0.42	0.08	32.28	100.25	
7	35.72	1.67	30.32	0.42	0.11	32.51	100.75	
8	35.85	1.76	30.17	0.44	0.09	32.49	100.80	
9	35.87	1.80	30.18	0.42	0.08	32.28	100.63	
10	35.86	1.71	30.19	0.39	0.11	32.25	100.51	
	SiO_2	Al_3O_2	FeO_{tot}	MnO	MgO	CaO	TOTAL	
Mean	35.77	1.73	30.25	0.44	0.10	32.32	100.60	
1σ	0.15	0.04	0.12	0.03	0.01	0.13	0.25	

(4) Andradite Standard: 8-10/2/00

8-10/2/00:AD	UNEDITED DATA		EDITED DATA*		Hill (pers. comm.)	
n	46		39		200	OK range
SiO_2	35.55	0.21	35.59	0.18	35.5	35-36
Al_2O_3	1.72	0.02	1.72	0.02	1.74	1.6-1.9
FeO_{tot}	30.42	0.30	30.41	0.31	30.2	30-30.5
MnO	0.43	0.12	0.44	0.13	0.42	0.40-0.45
MgO	0.09	0.01	0.09	0.01	-	-
CaO	32.26	0.30	32.26	0.31	32.4	32-32.8
TOTAL	100.46	0.56	100.49	0.49	100.26	100-101
					Camebax	

UNEDITED DATA_AD1-46:8-10/2/00

AD no.	SiO_2	Al_2O_3	FeO_{tot}	MnO	MgO	CaO	TOTAL	Notes
1	35.86	1.72	30.31	0.37	0.08	32.11	100.45	
2	35.57	1.71	30.32	0.38	0.08	31.91	99.97	

(contd.)

Table C1.2 (4 of 5) Andradite standard data for EPMA analyses presented in this thesis

3	35.67	1.70	30.44	0.42	0.09	31.92	100.24
4	35.48	1.69	30.26	0.37	0.09	32.08	99.97 X
5	35.50	1.74	30.58	0.40	0.10	32.58	100.90
6	35.35	1.73	30.35	1.03	0.11	31.97	100.54
7	35.37	1.70	30.52	0.35	0.09	32.21	100.24
8	35.37	1.69	30.28	0.33	0.07	32.47	100.21
9	35.43	1.75	30.41	0.37	0.09	32.21	100.26
10	35.69	1.68	30.14	0.38	0.08	32.05	100.02
11	35.84	1.73	31.88	0.39	0.09	32.24	102.17
12	35.77	1.71	30.18	0.65	0.13	32.31	100.75
13	35.45	1.70	30.88	0.45	0.08	32.26	100.82
14	35.66	1.70	30.51	0.40	0.10	31.92	100.29
15	35.65	1.71	30.13	0.46	0.10	32.26	100.31
16	35.62	1.70	30.60	0.59	0.08	32.06	100.65
17	35.85	1.77	30.37	0.37	0.09	32.14	100.59
18	35.62	1.77	30.45	0.39	0.08	32.34	100.65
19	35.73	1.70	30.24	0.38	0.10	32.23	100.38
20	35.66	1.73	30.37	0.37	0.08	32.30	100.51
21	35.69	1.73	30.27	0.38	0.08	32.67	100.82
22	35.52	1.72	30.09	0.42	0.10	33.15	101.00
23	35.63	1.72	30.10	0.39	0.07	32.19	100.10
24	35.62	1.69	30.04	0.39	0.11	32.18	100.03
25	35.64	1.72	30.34	0.63	0.09	32.68	101.10
26	35.84	1.71	30.36	0.40	0.09	32.39	100.79
27	35.79	1.73	30.25	0.42	0.09	33.00	101.28
28	36.01	1.71	31.09	0.49	0.11	32.88	102.29 X
29	35.43	1.71	30.29	0.44	0.08	32.02	99.97 X
30	35.05	1.75	30.52	0.45	0.10	32.12	99.99 X
31	35.24	1.74	30.67	0.40	0.11	32.32	100.48
32	35.26	1.76	30.56	0.35	0.09	32.66	100.68
33	35.18	1.71	30.38	0.33	0.11	32.26	99.97 X
34	35.16	1.73	30.40	0.41	0.09	32.18	99.97 X
35	35.55	1.66	30.46	0.52	0.10	31.70	99.99
36	35.58	1.72	30.77	0.37	0.08	32.02	100.54
37	35.64	1.69	30.13	0.33	0.09	31.82	99.70
38	35.33	1.69	30.30	0.34	0.09	32.17	99.92 X
39	35.51	1.69	30.26	0.39	0.11	31.86	99.82
40	35.54	1.73	30.13	0.43	0.08	32.15	100.06
41	35.73	1.72	30.34	0.39	0.09	32.21	100.48
42	35.76	1.73	30.42	0.40	0.10	32.67	101.08
43	35.38	1.72	30.40	0.43	0.09	32.13	100.15
44	35.23	1.70	30.32	0.41	0.07	32.09	99.82
45	35.30	1.71	30.47	0.41	0.08	32.13	100.10
46	35.72	1.68	30.58	0.65	0.11	32.51	101.25
	SiO_2	Al_3O_2	FeO_{tot}	MnO	MgO	CaO	TOTAL
Mean	35.55	1.72	30.42	0.43	0.09	32.26	100.46
1σ	0.21	0.02	0.30	0.12	0.01	0.30	0.56

(5) Andardite Standard: 16/2/01

16/2/01:AD1-	UNEDITED DATA		EDITED DATA*		Hill (pers. comm.)	
n	17		13		200	OK range
SiO_2	35.71	0.29	35.71	0.25	35.5	35-36
Al_2O_3	1.70	0.03	1.70	0.03	1.74	1.6-1.9
FeO_{tot}	30.59	0.24	30.57	0.21	30.2	30-30.5
MnO	0.42	0.03	0.43	0.03	0.42	0.40-0.45
MgO	0.09	0.01	0.09	0.01	-	-
CaO	32.47	0.21	32.46	0.18	32.4	32-32.8
TOTAL	100.99	0.68	100.96	0.53	100.26	100-101
					Camebax	

UNEDITED DATA_16/2/01:AD1-17

AD no.	SiO_2	Al_2O_3	FeO_{tot}	MnO	MgO	CaO	TOTAL	Notes
1	35.13	1.65	30.16	0.38	0.08	32.16	99.56 X	

(contd.)

Table C1.2 (5 of 5) Andradite standard data for EPMA analyses presented in this thesis

2	35.41	1.67	30.23	0.42	0.10	32.29	100.12
3	35.32	1.69	30.35	0.40	0.10	32.53	100.39
4	35.70	1.65	30.31	0.40	0.12	32.47	100.65
5	35.62	1.72	30.34	0.41	0.08	32.06	100.23
6	35.69	1.69	30.53	0.47	0.10	32.32	100.80
7	35.72	1.72	30.78	0.40	0.09	32.45	101.16
8	35.90	1.73	30.86	0.41	0.10	32.52	101.52 X
9	35.61	1.75	30.64	0.40	0.07	32.45	100.92 X
10	35.76	1.68	30.67	0.42	0.09	32.64	101.26
11	35.85	1.73	30.89	0.39	0.08	32.52	101.46
12	36.11	1.75	30.97	0.45	0.10	32.95	102.33 X; V
13	35.55	1.71	30.55	0.43	0.08	32.57	100.89
14	36.28	1.69	30.62	0.43	0.10	32.70	101.82
15	35.51	1.67	30.72	0.45	0.08	32.54	100.97
16	36.04	1.69	30.74	0.46	0.08	32.65	101.66
17	35.79	1.76	30.72	0.45	0.08	32.25	101.05
	SiO_2	Al_3O_2	FeO_{tot}	MnO	MgO	CaO	TOTAL
Mean	35.71	1.70	30.59	0.42	0.09	32.47	100.99
1σ	0.29	0.03	0.24	0.03	0.01	0.21	0.68

(contd.)

Site no.	Site name	Lat (N)* Long (W)	Bulk matrix	Fraction analysed	n	SiO_2	TiO_2	Al_2O_3	FeO_{tot}	MnO	MgO	CaO	Na_2O	K_2O	TOTAL
ÞIG 1b	STEINHOLTSDALUR (W)	63° 40.35'	co-ignimbrite ash	bulk	24	**72.53**	**0.18**	**11.58**	**2.69**	**0.10**	**0.02**	**0.43**	**4.40**	**4.11**	**96.04**
	[Krossa S]	19° 36.22'				0.79	0.08	0.19	0.41	0.06	0.01	0.14	0.16	0.61	0.94
ÞIG 1c			co-ignimbrite pumice	bulk	7	**72.91**	**0.22**	**11.57**	**2.78**	**0.11**	**0.02**	**0.41**	**4.51**	**4.05**	**96.58**
						0.63	0.05	0.14	0.37	0.03	0.01	0.04	0.17	0.11	1.03
ÞIG 1d			slope ash + pumice	bulk	14	**72.59**	**0.15**	**11.51**	**2.48**	**0.08**	**0.03**	**0.38**	**4.27**	**4.07**	**95.56**
						0.64	0.03	0.13	0.08	0.03	0.01	0.02	0.18	0.17	0.81
ÞIG 2	HAFTFELL (ALFAKIRKA)	63° 40.75'	ash + pumice	bulk	10	**72.75**	**0.19**	**11.49**	**2.55**	**0.09**	**0.03**	**0.35**	**4.37**	**4.16**	**95.98**
	[Krossa S]	19° 30.32'				0.39	0.03	0.12	0.07	0.02	0.02	0.02	0.12	0.11	0.47
ÞIG 3	LANGIDALUR (E)	63° 41.12'	pumice	bulk	10	**72.49**	**0.16**	**11.44**	**2.49**	**0.02**	**0.01**	**0.39**	**4.29**	**4.12**	**95.40**
	[Krossa N]	19° 30.44'				0.91	0.02	0.15	0.04	0.02	0.01	0.03	0.10	0.06	1.06
ÞIG 5	HESTAGIL	63° 40.91'	welded pumice clasts	bulk	14	**72.28**	**0.15**	**11.47**	**2.49**	**0.05**	**0.02**	**0.37**	**4.18**	**4.07**	**95.08**
	[Krossa N]	19° 32.70'				0.70	0.02	0.19	0.09	0.02	0.02	0.03	0.21	0.17	1.01
ÞIG 6	RJUPNAFELL	63° 40.37'	slope ash+pumice	bulk	11	**72.44**	**0.17**	**11.43**	**2.56**	**0.08**	**0.03**	**0.39**	**4.34**	**4.06**	**95.50**
	[Steinholtsjokull snout]	19° 34.37'				0.40	0.04	0.14	0.12	0.03	0.01	0.04	0.39	0.15	0.53
ÞIG 7	STORAENDAHRYGGUR	63° 40.37'	interbedded ash	bulk	20	**72.54**	**0.15**	**11.46**	**2.50**	**0.07**	**0.02**	**0.37**	**4.15**	**4.07**	**95.33**
	[Krossa N]	19° 34.37'				1.00	0.04	0.19	0.12	0.04	0.01	0.03	0.47	0.19	0.99
ÞIG 8	ENGIDALUR	63° 40.94'	slope ash + pumice	bulk	11	**72.82**	**0.17**	**11.65**	**2.47**	**0.10**	**0.02**	**0.42**	**4.30**	**3.99**	**95.92**
	[Krossa N]	19° 32.97'				0.61	0.03	0.27	0.10	0.02	0.01	0.03	0.27	0.16	0.81
ÞIG 11	HAMRASKÓGAR	63° 41.94'	welded pumice	90-150 µm	10	**71.79**	**0.16**	**11.35**	**2.55**	**0.15**	**0.02**	**0.64**	**4.35**	**4.13**	**95.14**
	[Central E]	19° 28.96'				0.95	0.03	0.16	0.24	0.10	0.01	0.44	0.12	0.37	1.11
ÞIG 13	HAMRASKÓGAR	63° 41.94'	slope ash + pumice	90-150 µm	9	**72.46**	**0.26**	**11.52**	**2.53**	**0.10**	**0.02**	**0.38**	**4.28**	**4.13**	**95.67**
	[Central E]	19° 28.96'				0.63	0.26	0.12	0.08	0.04	0.01	0.02	0.10	0.13	0.67
ÞIG 15	STÖNG (W)	63° 40.98'	slope ash + pumice	90-150 µm	16	**71.92**	**0.17**	**11.56**	**2.48**	**0.04**	**0.02**	**0.42**	**4.64**	**4.01**	**95.25**
	[Krossa N]	19° 27.93'				0.72	0.03	0.16	0.10	0.02	0.01	0.10	0.21	0.30	0.78
ÞIG 16	STÖNG (E)	63° 40.89'	1 welded pumice clast	90-150 µm	33	**72.25**	**0.14**	**11.37**	**2.52**	**0.07**	**0.02**	**0.38**	**4.41**	**4.20**	**95.35**
	[Krossa N]	19° 28.41'				0.54	0.03	0.10	0.22	0.08	0.01	0.08	0.38	0.11	0.81
ÞIG 21	KLAPPIR	63° 42.1'	welded pumice	90-150 µm	11	**71.36**	**0.15**	**11.37**	**2.46**	**0.03**	**0.02**	**0.41**	**4.49**	**4.09**	**94.38**
	[Central W]	19° 30.5'				0.56	0.03	0.15	0.14	0.02	0.01	0.16	0.17	0.11	0.75
ÞIG 22	TINDFJALLAGIL	63° 41.7'	welded pumice	90-150 µm	15	**71.99**	**0.14**	**11.42**	**2.42**	**0.02**	**0.02**	**0.36**	**4.62**	**4.11**	**95.09**
	[Central SE]	19° 28.6'				0.54	0.03	0.12	0.08	0.02	0.01	0.05	0.22	0.10	0.73
ÞIG 23	TINDFJALLAGIL	63° 41.7'	welded pumice	90-150 µm	3	**72.54**	**0.15**	**11.66**	**2.58**	**0.12**	**0.03**	**0.36**	**4.70**	**4.06**	**96.19**
	[Central SE]	19° 28.5'				0.37	0.06	0.10	0.14	0.06	0.02	0.04	0.11	0.03	0.39
ÞIG 1-22	Þörsmörk Region	-	-	-	218	**72.34**	**0.16**	**11.48**	**2.53**	**0.07**	**0.02**	**0.40**	**4.38**	**4.10**	**95.48**
						0.75	0.07	0.17	0.21	0.06	0.01	0.09	0.30	0.26	0.93

Table C1.3 Summary EPMA major element data from silicic glass shards from sites ÞIG 1-23 in the Þörsmörk region. * ÞIG 1-16 are handheld GPS coordinates

(a) ALL DATA (including outliers)

	SiO2	TiO2	Al2O3	FeOtot	MnO	MgO	CaO	Na2O
TiO2	-0.904							
Al2O3	-0.547	0.44						
FeOtot	-0.969	0.886	0.471					
MnO	-0.413	0.288	0.31	0.474				
MgO	-0.933	0.809	0.561	0.853	0.334			
CaO	-0.969	0.843	0.578	0.929	0.406	0.972		
Na2O	0.717	-0.608	-0.204	-0.756	-0.389	-0.708	-0.777	
K2O	0.886	-0.784	-0.55	-0.875	-0.414	-0.865	-0.934	0.809

(b) ALL DATA (excluding outliers)

	SiO2	TiO2	Al2O3	FeOtot	MnO	MgO	CaO	Na2O
TiO2	-0.924							
Al2O3	-0.553	0.452						
FeOtot	-0.97	0.906	0.473					
MnO	-0.495	0.345	0.367	0.568				
MgO	-0.932	0.824	0.567	0.852	0.404			
CaO	-0.97	0.862	0.582	0.929	0.492	0.972		
Na2O	0.726	-0.634	-0.206	-0.766	-0.494	-0.713	-0.785	
K2O	0.89	-0.81	-0.548	-0.878	-0.51	-0.868	-0.936	0.818

(c) OT Si vs OT Bs

	SiO2	TiO2	Al2O3	FeOtot	MnO	MgO	CaO	Na2O
TiO2	-0.966							
Al2O3	-0.447	0.477						
FeOtot	-0.988	0.955	0.448					
MnO	-0.93	0.86	0.399	0.949				
MgO	-0.897	0.943	0.431	0.868	0.794			
CaO	-0.985	0.95	0.492	0.986	0.949	0.904		
Na2O	0.704	-0.643	-0.323	-0.756	-0.762	-0.575	-0.735	
K2O	0.978	-0.955	-0.451	-0.971	-0.917	-0.904	-0.976	0.684

(d) OT Si vs Hj Bs

	SiO2	TiO2	Al2O3	FeOtot	MnO	MgO	CaO	Na2O
TiO2	-0.996							
Al2O3	-0.888	0.902						
FeOtot	-0.997	0.998	0.902					
MnO	-0.895	0.897	0.792	0.903				
MgO	-0.989	0.988	0.863	0.989	0.895			
CaO	-0.997	0.997	0.895	0.998	0.901	0.994		
Na2O	0.791	-0.8	-0.728	-0.806	-0.746	-0.805	-0.804	
K2O	0.992	-0.991	-0.889	-0.992	-0.891	-0.986	-0.992	0.787

(e) PIG 1-23 vs PIG 1b

	SiO2	TiO2	Al2O3	FeOtot	MnO	MgO	CaO	Na2O
TiO2	-0.994							
Al2O3	-0.677	0.712						
FeOtot	-0.993	0.996	0.688					
MnO	0.381	-0.365	-0.217	-0.364				
MgO	-0.99	0.99	0.641	0.994	-0.373			
CaO	-0.992	0.992	0.658	0.997	-0.371	0.998		
Na2O	0.819	-0.821	-0.48	-0.826	0.215	-0.835	-0.834	
K2O	0.967	-0.97	-0.674	-0.971	0.343	-0.968	-0.97	0.804

(f) PIG 1-23 vs PIG 4

	SiO2	TiO2	Al2O3	FeOtot	MnO	MgO	CaO	Na2O
TiO2	-0.985							
Al2O3	-0.573	0.628						
FeOtot	-0.985	0.993	0.627					
MnO	-0.348	0.378	0.281	0.382				
MgO	-0.988	0.995	0.62	0.995	0.365			
CaO	-0.989	0.995	0.624	0.996	0.369	0.998		
Na2O	0.674	-0.684	-0.38	-0.681	-0.379	-0.684	-0.686	
K2O	0.915	-0.926	-0.594	-0.926	-0.37	-0.924	-0.925	0.634

(g) ASK 1875 vs ASK Bs crater pumice

	SiO2	TiO2	Al2O3	FeOtot	MnO	MgO	CaO	Na2O
TiO2	-0.882							
Al2O3	-0.975	0.876						
FeOtot	-0.995	0.887	0.971					
MnO	-0.676	0.576	0.645	0.682				
MgO	-0.999	0.885	0.976	0.995	0.673			
CaO	-0.998	0.881	0.974	0.995	0.692	0.999		
Na2O	0.97	-0.864	-0.944	-0.966	-0.602	-0.971	-0.966	
K2O	0.973	-0.864	-0.944	-0.966	-0.662	-0.971	-0.971	0.948

(h) 65-0 Ma_HIGHLY SILICIC CORRELATION DATASET

	SiO2	TiO2	Al2O3	FeOtot	MnO	MgO	CaO	Na2O
TiO2	-0.254							
Al2O3	-0.282	0.059						
FeOtot	-0.465	0.541	-0.09					
MnO	-0.394	0.253	0.174	0.521				
MgO	-0.294	0.739	0.133	0.35	0.06			
CaO	-0.255	0.568	0.233	0.327	0.266	0.314		
Na2O	-0.256	-0.108	0.475	-0.084	0.029	-0.075	-0.059	
K2O	0.032	-0.151	0.248	-0.147	0.027	-0.103	-0.566	0.171

Table C1.4 Pearson product moment correlation coefficients (PPMCC) for combinations of major element data presented in this thesis. Explanation of correlation coefficient values: 0 = no linear relationship between elements; 1 = perfect linear relationship between elements; -1 = no relationship between variables. PPMCC values have no petrological significance (Rollinson, 1993). They were used to decide which element bi-plot would be the most powerful discrimination tools (see Figure 4.9). The most reliable and best discriminator elements are the non-mobile elements TiO_2, FeO_{tot}, MgO, & CaO. For new data collected in the course of this study, *i.e.* (a)-(g), all combinations of these elements have correlation coefficients > 0.8. Correlation coefficients in the 65-0 Ma highly silicic dataset are generally closer to 0 than those for new data. This is due to two factors: (1) Different operating conditions used to collect this dataset, & (2) post-depositional alteration of glass composition deposits of pre-Holocene age.

SUTL no.	Fraction	Density	Lab code		La	Ce	Pr	Nd	Sm	Eu	Gd	Tb	Dy	Ho	Er	Tm	Yb	Lu	
552	<90	<2.3	TES1; SUTL552 Óþoli Tephra (<90; <2.3)	-	64.40	84.45	20.00	88.22	21.51	5.37	22.35	3.71	23.60	4.76	14.19	2.08	13.22	2.01	
552	<90	2.3-2.4	TES2; SUTL552 (<90; 2.3-2.4)	-	70.95	152.28	19.99	83.01	19.11	3.83	19.49	3.27	20.75	4.17	12.44	2.00	11.98	1.82	
552	<90	>2.4	TES3; SUTL552 (<90; >2.4)	-	66.21	156.12	19.90	87.84	20.42	5.51	3.26	20.75	19.78	3.93	11.31	1.75	10.58	1.64	
552	90-150	<2.3	TES4; SUTL552 (90-150; <2.3)	-	63.34	94.97	18.91	82.21	19.88	4.76	20.39	3.42	21.87	4.37	12.90	2.03	12.32	1.85	
552	90-150	2.3-2.4	TES5; SUTL552 (90-150; 2.3-2.4)	-	72.45	154.19	19.56	81.37	18.88	3.67	19.28	3.26	20.53	4.14	12.32	1.96	11.97	1.78	
552	90-150	>2.4	TES6; SUTL552 (90-150; >2.4)	-	64.58	190.50	19.20	83.72	19.62	5.24	19.99	3.18	19.32	3.87	11.23	1.73	10.69	1.60	
552	bulk	-	TES7; SUTL552 (bulk)	-	68.75	145.47	19.24	80.42	18.59	3.81	19.16	3.20	20.16	4.12	12.27	1.93	11.74	1.73	
516	bulk	-	TES8; SUTL516 Hjallanes Tephra (bulk)	-	27.62	64.77	8.42	37.32	8.89	2.60	9.23	1.40	8.39	1.59	4.47	0.67	3.89	0.57	
				Y	La	Ce	Pr	Nd	Sm	Eu	Gd	Tb	Dy	Ho	Er	Tm	Yb	Lu	
OT(0-3 cm)	bulk	-	TEX1	124.00	78.90	180.00	21.50	90.20	20.00	4.62	20.00	3.50	22.90	4.47	12.40	1.90	11.90	1.75	
OT(0-3 cm)	bulk	-	DTEX1	119.00	78.90	173.00	20.70	87.80	20.50	4.59	20.50	3.40	22.40	4.27	12.70	1.80	11.60	1.84	
OT(0-3 cm)	bulk	-	TEX1 (2)	121.50	78.90	176.50	21.10	89.00	20.25	4.61	20.25	3.45	22.65	4.37	12.55	1.85	11.75	1.80	
OT(0-3 cm)	90-150 mm	2.3-2.4	TEX2	117.00	80.00	170.00	20.40	90.80	20.30	4.07	19.90	3.50	21.30	4.32	12.20	1.80	11.50	1.86	
ÞIG 1b	bulk	-	TEX3	88.00	90.20	191.00	23.10	94.20	19.90	4.27	17.50	2.90	17.50	3.27	8.30	1.30	7.30	1.11	
ÞIG 7	bulk	-	TEX4	102.00	106.00	218.00	26.70	112.00	23.50	4.70	20.80	3.40	20.30	3.86	9.90	1.50	8.80	1.37	
Chondrite Norm	**Boynton (1984)**			**2.10**	**0.31**	**0.81**	**0.12**	**0.60**	**0.20**	**0.07**	**0.26**	**0.05**	**0.32**	**0.07**	**0.21**	**0.03**	**0.21**	**0.03**	
	***=Taylor & McLennan (1985)**			**Y***	**La**	**Ce**	**Pr**	**Nd**	**Sm**	**Eu**	**Gd**	**Tb**	**Dy**	**Ho**	**Er**	**Tm**	**Yb**	**Lu**	**Eu/Eu***
552	<90	<2.3	TES1; SUTL552 Óþoli Tephra (<90; <2.3)	-	207.73	104.52	163.92	147.03	110.29	73.03	86.28	78.19	73.31	66.34	67.55	64.24	63.27	62.31	**0.75**
552	<90	2.3-2.4	TES2; SUTL552 (<90; 2.3-2.4)	-	228.86	188.46	163.88	138.36	97.99	52.10	75.25	69.00	64.43	58.02	59.21	61.83	57.32	56.50	**0.61**
552	<90	>2.4	TES3; SUTL552 (<90; >2.4)	-	213.58	193.22	163.14	146.39	104.73	74.92	12.59	437.73	61.42	54.71	53.84	54.02	50.61	50.91	**2.06**
552	90-150	<2.3	TES4; SUTL552 (90-150; <2.3)	-	204.31	117.54	155.03	137.02	101.95	64.82	78.74	72.07	67.91	60.86	61.43	62.55	58.96	57.51	**0.72**
552	90-150	2.3-2.4	TES5; SUTL552 (90-150; 2.3-2.4)	-	233.69	190.83	160.35	135.62	96.82	49.90	74.45	68.84	63.75	57.63	58.67	60.52	57.27	55.13	**0.59**
552	90-150	>2.4	TES6; SUTL552 (90-150; >2.4)	-	208.33	235.77	157.41	139.53	100.62	71.32	77.18	67.11	60.01	53.96	53.47	53.45	51.13	49.58	**0.81**
552	bulk	-	TES7; SUTL552 (bulk)	-	221.77	180.04	157.73	134.03	95.35	51.80	73.97	67.60	62.62	57.36	58.45	59.42	56.18	53.65	**0.62**
516	bulk	-	TES8; SUTL516 Hjallanes Tephra (bulk)	-	89.11	80.16	69.00	62.21	45.60	35.37	35.62	29.52	26.06	22.09	21.27	20.73	18.60	17.80	**0.88**
OT(0-3 cm)	bulk	-	TEX1	59.05	254.52	222.77	176.23	150.33	102.56	62.86	77.22	73.84	71.12	62.26	59.05	58.64	56.94	54.35	**0.71**
OT(0-3 cm)	bulk	-	DTEX1	56.67	254.52	214.11	169.67	146.33	105.13	62.45	79.15	71.73	69.57	59.47	60.48	55.56	55.50	57.14	**0.68**
OT(0-3 cm)	bulk	-	TEX1 (2); SUTL551 Óþoli Tephra (bulk)	57.86	254.52	218.44	172.95	148.33	103.85	62.65	78.19	72.78	70.34	60.86	59.76	57.10	56.22	55.75	**0.70**
OT(0-3 cm)	90-150 µm	2.3-2.4	TEX2; SUTL551 (90-150; <2.4)	55.71	258.06	210.40	167.21	151.33	104.10	55.37	76.83	73.84	66.15	60.17	58.10	55.56	55.02	57.76	**0.62**
ÞIG 1b	bulk	-	TEX3; ÞIG 1b Þórsmórk Ignimbrite (bulk)	41.90	290.97	236.39	189.34	157.00	102.05	58.10	67.57	61.18	54.35	45.54	39.52	40.12	34.93	34.47	**0.70**
ÞIG 7	bulk	-	TEX4; ÞIG 7 Þórsmórk Ignimbrite (bulk)	48.57	341.94	269.80	218.85	186.67	120.51	63.95	80.31	71.73	63.04	53.76	47.14	46.30	42.11	42.55	**0.65**

References
Boynton, W. V. (1984). Geochemistry of rare earth elements: meteorite studies. In: Henderson, P. (Ed.), Rare Earth Element Geochemistry. Elsevier, pp. 63-114.
Taylor, S. R., & McLennan, S. M. (1981). The composition and evolution of the continental crust: rare earth element evidence from sedimentary rocks. Philosophical Transactions of the Royal Society, A301, 381-399.

Table C1.5 Summary of ICP-MS trace element data

MAJOR ELEMENTS Sample	OT(0-3 cm)	OT(0-3 cm)	OT(0-2 cm)	ÞIG 1b	ÞIG 7	STANDARDS SXRAL04	DETECTION LIMITS
Fraction	bulk	bulk	90-150 μm	bulk	bulk	bulk	
Density (gcm^{-3})	-	-	2.3-2.4	-	-	-	
XRAL lab code	TEX1	DTEX1	TEX2	TEX3	TEX4	certified ok	
XRAL run no.	(5001)	(05001)	(05002)	(05003)	(05004)	-	
SiO_2	66.3	66.3	69.1	65.9	69.9	48.2	0.01
TiO_2	0.604	0.604	0.424	0.93	0.483	0.376	0.001
Al_2O_3	12.5	12.5	12.2	13	13	14.7	0.01
FeO_{tot}	6.27	6.31	4.97	5.79	4.17	9.32	0.01
MnO	0.18	0.18	0.13	0.12	0.11	0.16	0.01
MgO	0.76	0.77	0.39	1.04	0.38	11.6	0.01
CaO	2.51	2.51	1.66	2.72	1.34	11.0	0.01
NaO	3.03	3.03	4.06	4.78	4.83	1.33	0.01
K_2O	2.16	2.16	2.49	3.28	3.03	0.39	0.01
P_2O_5	0.09	0.09	0.06	0.17	0.07	0.04	0.01
Cr_2O_3	-0.01	-0.01	-0.01	-0.01	-0.01	0.06	0.01
LOI	5.46	5.40	4.40	2.35	2.55	2.45	0.01
TOTAL	100.1	100.1	100.1	100.4	100.2	99.7	0.01
H_2O+	4.5	-	4.2	2.0	2.2	1 (SSY)	0.1
H_2O-	1.90	1.40	0.40	0.40	0.40	1 (SXRAL06)	0.1
TRACE ELEMENTS							
Rb	55	55	55	73	107	11	2
Sr	136	135	111	152	83	104	2
Y	140	140	120	103	147	10	2
Zr	548	547	441	807	1140	27	2
Nb	81	80	76	107	147	-2	2
Ba	529	528	545	640	627	81	20

Table C1.6 Summary of XRF data for samples used in dating analysis
All samples analysed using scheme XRF103 at SGS-XRAL Laboratories, Don Mills, Toronto, Canada. Major element data are expressed as wt % and trace element data as ppm.

Table C2.1 Summary grain specific EPMA major element chemical data for most of the highly silicic tephra layers (SiO_2>68%; MgO & TiO_2 < 1%) of known Icelandic origin for the last 50-60 Ma. Data are mean values from the number of shards indicated in the n column (see notes at end of list) - 1σ data in original reference.

ID no.	Site location; core number[1]	Tephra name; loc.[2]	Volcano	Reference (s)	Age[3] (ka BP) & method	n	SiO_2	TiO_2	Al_2O_3	FeO_{tot}	MnO	MgO	CaO	Na_2O	K_2O	Total
Terrestrial deposits																
1	Hekla volcano	H1970	Hekla	Sigvaldson (1974)	0.031 HR	1	72.22	0.30	13.23	2.08	0.09	0.35	0.33	5.92	3.89	98.41
2	‡ Gígjujökull, S Iceland	H1947	Hekla	Larsen *et al*. (1999)	0.054 HR	2	69.77	0.37	13.47	4.72	0.11	0.15	1.15	5.32	3.41	98.46
3	† Askja volcano	A1875	Askja	Sparks *et al* (1981)	0.126 HR	27	73.72	0.80	12.81	3.34	0.08	0.60	2.31	3.65	2.40	99.71
4	‡ Snidanes, 50 km E of Askja	A1875	Askja	Larsen *et al.* (1999)	0.126 HR	18	72.21	0.79	12.42	3.28	0.11	0.64	2.30	3.38	2.43	97.56
5	‡ Gígjujökull, S Iceland	E1821	Eyjafjalljökull	Larsen *et al.* (1999)	0.18 HR	11	69.13	0.36	14.10	4.29	0.15	0.13	1.10	6.14	3.50	98.90
6	† Öræfajökull volcano	Ö1362	Öræfajökull	Sigurdsson (1982)	0.639 HR	14	71.46	0.22	13.13	3.16	0.05	0.00	0.99	5.45	3.53	97.99
7	‡ Svinafell, 10 km W of Öræfi	Ö1362	Öræfajökull	Larsen *et al.* (1999)	0.639 HR	15	71.36	0.22	13.14	3.12	0.10	0.03	0.98	5.55	3.38	97.89
8	$† Ireland	Ö1362	Öræfajökull	Pilcher *et al*. (1995)	0.639 HR	23	71.60	0.30	13.54	3.33	0.00	0.06	1.13	5.06	3.35	98.37
9	Myvatn, N Iceland	H1300	Hekla	Einarsson *et al*. (1988)	0.701 HR	1	70.58	0.23	14.69	3.07	0.11	0.12	1.09	3.46	2.68	96.03
10	Myvatn, N Iceland	H1158 (H1-early)	Hekla	Einarsson *et al.* (1988)	0.843 HR	4	73.72	0.17	12.07	2.18	0.12	0.13	1.45	4.15	2.85	96.84
11	‡ Áfangagil, 7 km N of Hekla	H1158 (H1-late)	Hekla	Larsen *et al.* (1999)	0.843 HR	12	67.42	0.48	14.39	5.71	0.20	0.45	3.11	4.56	2.24	98.55
12	† Hekla volcano (Burfell)	H1104	Hekla	Sigurdsson (1982)	0.901 HR	10	72.56	0.21	14.05	3.04	0.15	0.10	1.96	5.39	2.80	100.26
13	‡ Áfangagil, 7 km N of Hekla	H1104	Hekla	Larsen *et al.* (1999)	0.901 HR	14	72.24	0.19	13.95	3.23	0.12	0.14	1.85	4.30	2.74	98.78
14	Thingvallavatn, SW Iceland	Settlement	Torfajökull	Haflidason *et al*. (1982)	1.131 HR	9	70.41	0.30	14.34	2.29	0.24	0.23	1.20	4.69	4.73	98.43
15	‡ Áfangagil, 7 km N of Hekla	Settlement	Torfajökull	Larsen *et al.* (1999)	1.131 HR	22	70.97	0.25	14.46	2.32	0.09	0.24	0.89	4.78	4.64	98.64
16	‡ Glen Garry, N Scotland	Glen Garry	?	Dugmore *et al*. (1995)	2.1 ^{14}C	9	72.60	0.63	12.73	4.19	0.13	0.56	2.61	3.51	1.95	98.91
17	Eyjafjordur, N Iceland	H3	Hekla	Haflidason (1983)	2.855 ^{14}C	26	71.60	0.09	13.95	2.76	0.09	0.04	1.85	4.10	2.51	96.99
18	‡ Skaelingsvatn, Faroe Islands	H-S	Hekla	Dugmore & Newton (1998)	3.5 ^{14}C	2	72.30	0.20	13.75	2.72	0.09	0.13	1.83	4.03	2.52	97.57
19	‡ Kebister, Shetland Islands	H-S	Hekla	Dugmore *et al.* (1995)	3.5 ^{14}C	5	72.03	0.18	13.83	2.78	0.11	0.14	1.87	4.29	2.42	97.65
20	† Hekla volcano (Burfell)	H4	Hekla	Sigurdsson (1982)	3.83 ^{14}C	10	74.37	0.12	12.97	1.60	0.14	0.00	1.28	4.73	2.59	97.80
21	Eyjafjordur, N Iceland	H4	Hekla	Haflidason (1983)	3.83 ^{14}C	27	74.08	0.07	13.02	1.73	0.07	0.00	1.22	4.22	2.67	97.08
22	† Hekla volcano	H5	Hekla	Sigurdsson (1982)	6.1 ^{14}C	16	74.80	0.12	12.62	1.37	0.12	0.00	1.29	4.54	2.53	97.39
23	† A-Site, SE of Mydralsjökull	SILK layer A11	Katla	Newton (1999)	*ca.* 7.0 ^{14}C	10	68.37	0.90	13.74	4.14	0.15	0.73	2.02	4.35	3.17	97.56
24	† A-Site, SE of Mydralsjökull	SILK layer A12	Katla	Newton (1999)	*ca.* 7.2 ^{14}C	10	68.00	0.87	13.75	4.21	0.15	0.74	2.15	4.53	3.12	97.51
25	Ξ Ålesund, Western Norway	Vedde Ash	Katla (K)	Mangerud *et al*. (1984)	10.6 ^{14}C	26	72.02	0.28	13.16	3.67	0.15	0.21	1.33	2.10	3.49	96.41
26	† Krakanes, Western Norway	Vedde Ash (≡)	Katla / Öræfi	Birks *et al*. (1996)	10.3 ^{14}C	11	70.46	0.29	12.95	3.63	0.17	0.20	1.38	4.64	3.34	97.06
27	Fnjoskadalur, N Iceland	Skogar Tephra	Öræfajökull	Norddahl & Haflidason (1992)	10.3 ^{14}C	10	71.08	0.27	13.32	3.51	0.14	0.22	1.30	5.64	3.57	99.05
28	L. Torfadalsvatn, N Iceland	Vedde Ash (≡)	Öræfajökull	Bjorck *et al*. (1992)	10.5 ^{14}C	7	71.53	0.31	13.81	4.01	0.21	0.28	1.47	2.72	3.37	97.71
29	Katla volcanic system	Katla ob. Pumice	Katla	Lacasse *et al*. (1995; 1996)	10.3 ^{14}C	16	70.60	0.29	13.28	3.69	0.11	0.21	1.29	5.58	3.76	98.81
30	‡ 6 LGIT sites, Scotland	Vedde Ash (≡)	Katla / Öræfi	Lowe/Turney (1997)+Roberts (1997)	10.3 ^{14}C	203	70.66	0.28	13.16	3.71	0.14	0.23	1.24	4.35	3.50	97.25
31	‡ 4 LGIT sites S Sweden	Vedde Ash (≡)	Katla / Öræfi	Wastegård *et al*. (2000a)	10.3 ^{14}C	57	69.57	0.28	13.21	3.71	0.14	0.24	1.31	4.68	3.42	96.56
32	‡ L. Medvedevskoe, W Russia	Vedde Ash (≡)	Katla / Öræfi	Wastegård *et al*. (2000b)	10.3 ^{14}C	11	69.84	0.29	13.23	3.73	0.18	0.25	1.25	4.61	3.28	96.65

contd. overpage

ID no.		Site location or core number	Extra ID	Volcano	Reference	Age[3] (ka BP) & method	n	SiO_2	TiO_2	Al_2O_3	FeO_{tot}	MnO	MgO	CaO	Na_2O	K_2O	Total
33	‡	L. Pastorskoye, W Russia	Vedde Ash (≡)	Katla / Öræfi	Wastegård *et al.* (2000b)	10.3 ^{14}C	7	69.92	0.25	13.42	3.73	0.15	0.25	1.27	4.77	3.31	97.07
34	‡	Borrobol, Scotland	Borrobol Tephra	Hekla (?)	Turney *et al.* (1997)	12.26 ^{14}C	18	73.36	0.11	12.29	1.47	0.06	0.12	0.76	3.58	3.76	95.51
35	‡	6 LGIT sites, Scotland	Borrobol Tephra	?	Turney *et al.* (1997)+Roberts (1997)	12.26 ^{14}C	71	73.65	0.12	12.30	1.45	0.04	0.11	0.75	3.44	3.69	95.55
36	Ξ	Þórsmörk, S Iceland	Þórsmörk Ignim. (ÞIG)	Tindfjalljökull	Jørgensen (1980; 1981); unaltered	50/200 UD	25	72.74	0.17	11.42	2.81	0.07	0.02	0.41	4.80	4.03	96.47
37	‡	Solheimajökull, S Iceland	Solheimar Ignim. (SIG)	Katla (?)	Newton (1999)	65? UD	25	68.92	0.29	13.25	3.74	0.14	0.21	1.39	4.89	3.47	96.28
38	‡	Víkurhóll, S Iceland	6 km SW of SI	SIG (≡?)	Newton (1999)	? UD	31	69.76	0.31	13.27	3.74	0.15	0.23	1.30	5.21	3.47	97.44
Quaternary age ocean & ice core deposits																	
39		P57-7, 16-18	NAAZ1	Vedde Ash (º)	Sjøholm *et al.* (1991)	0-11.670 ^{14}C	11	72.07	0.28	13.888	3.97	0.15	0.21	1.32	2.74	3.61	98.24
40		P57-7, 21-23	NAAZ1	(?)	Sjøholm *et al.* (1991)	0-11.670 ^{14}C	16	71.16	0.31	13.326	3.84	0.15	0.21	1.10	1.84	2.90	94.84
41	†	K708-1	NAAZ1	Katla	Sigurdsson (1982)	*ca.* 10 δ^{18}O	20	71.44	0.29	13.70	3.93	0.14	0.18	1.29	5.19	3.37	99.53
42	†	SO82-02,-5,-7,LO091-21,-23	NAAZ1	Katla	Lackschewitz *et al.* (1997)	*ca.* 10 δ^{18}O	12	70.72	0.26	13.84	3.71	0.15	0.19	1.35	4.57	3.45	98.24
43	†	93030-006-LCF-278	NAAZ1	Vedde Ash (≡)	Jennings *et al.* (2000)	10.3 ^{14}C	25	71.10	0.27	13.70	3.80	0.13	0.25	1.38	5.44	3.30	99.37
44	*	GRIP-1639.54-1639.55m	NAAZ1	Katla	Grönvold *et al.* (1995)	11.98 ICY	2	71.55	0.41	13.70	4.03	0.23	0.32	1.29	5.52	3.27	100.31
45	$†	SO82-02,-5,-7,LO091-21,-23	NAAZ2	Tindfjalljökull (?)	Lackschewitz *et al.* (1997)	58 δ^{18}O	5	74.42	0.19	12.51	2.76	0.07	0.01	0.51	4.40	3.78	98.65
46	$	V23-42, 246-245; V27-114, 396	II-RHY-1	Tindfjalljökull (?)	Kvamme et al. (1989)	*ca.* 50 δ^{18}O	77	72.84	0.17	11.70	2.51	0.10	0.04	0.36	1.88	3.21	92.83
47	†	SO82-05/496	II-RHY-1	Tindfjalljökull (?)	Haflidason *et al.* (2000)	48.5 δ^{18}O	7	72.26	0.17	11.05	2.53	0.07	0.02	0.36	4.72	4.11	95.29
48	†	K708-1-390	NAAZ2	Tindfjalljökull (?)	Sigurdsson (1982)	48.5 δ^{18}O	20	74.22	0.16	12.02	2.64	0.06	0.01	0.33	5.25	4.04	98.73
49	†	SU9032-562	NAAZ2	Tindfjalljökull (?)	Lacasse *et al.* (1995; 1996)	48.5 δ^{18}O	10	72.62	0.16	11.69	2.47	0.07	0.00	0.37	5.52	4.04	96.94
50	*	GISP2-2464.25-2464.30m	NAAZ2	Torfajökull;K(?)	Zielinski *et al.* (1997)	52.682 ICY	12	76.50	0.30	12.80	3.30	0.00	0.20	0.40	2.30	4.30	100.10
51	*	GRIP-2430.95-2430.97m	NAAZ2	Tindfjalljökull (?)	Grönvold *et al.* (1995)	53.5 ICY	5	74.60	0.20	12.20	2.90	0.00	0.20	0.50	5.30	4.00	99.90
52		DYE-3	NAAZ2	-	Grönvold *et al.* (1995)	52 ICY	-	74.00	0.16	11.90	2.33	0.07	0.01	0.38	5.26	4.04	98.15
53	†	ENAM33, 548	5d-Low/RHY-I	?	Wastegård & Rasmussen (sub.)	103-115 δ^{18}O	10	70.78	0.07	12.49	2.37	0.05	0.08	0.66	3.96	3.75	94.19
54	†	ENAM33, 548	5d-Low/RHY-II	?	Wastegård & Rasmussen (sub.)	103-115 δ^{18}O	3	68.32	0.21	12.42	3.97	0.18	0.06	1.28	4.18	3.46	94.07
55	†	ENAM33, 548	5d-Low/RHY-III	?	Wastegård & Rasmussen (sub.)	103-115 δ^{18}O	2	71.80	0.08	10.73	3.26	0.07	0.01	0.28	3.84	4.23	94.29
56	†	DSDP38:1-V23-73-393	N. Iceland Plateau	?	Sigurdsson & Loebner (1981)	115 δ^{18}O	10	71.85	0.16	11.78	2.74	0.10	0.06	1.13	4.60	2.73	95.15
57	†	V27-46-260	N. Iceland Plateau	?	Sigurdsson & Loebner (1981)	115 δ^{18}O	10	72.94	0.19	10.91	2.65	0.11	0.01	1.44	4.29	1.63	94.17
58	†	V27-47-180	N. Iceland Plateau	?	Sigurdsson & Loebner (1981)	120 δ^{18}O	8	72.86	0.17	10.98	2.71	0.09	0.00	1.45	4.52	1.62	94.40
59	†	907A-1H-2, 50-51-B	N. Iceland Plateau	?	Lacasse *et al.* (1995; 1996)	122.3 δ^{18}O	10	73.79	0.23	11.04	2.78	0.06	0.03	1.50	4.83	1.84	96.10
60		HM79-31	5e-Midt/RHY	?	Fronval *et al.* (1998)	125 δ^{18}O	12	73.09	0.22	11.18	3.00	0.05	0.03	1.55	3.21	1.71	94.04
61		HM79-31	5e-Midt/RHY	?	Fronval *et al.* (1998)	125 δ^{18}O	1	70.34	0.33	11.95	4.73	0.01	0.01	2.46	3.69	1.53	95.05
62	†	ENAM33, 566	5e-Top/RHY		Wastegård & Rasmussen (sub.)	115-128 δ^{18}O	7	70.76	0.09	12.41	2.13	0.08	0.09	0.62	3.85	3.82	93.85
63	†	MD-95-2009, 1830.5	5e-Midt/RHY		Wastegård & Rasmussen (sub.)	115-128 δ^{18}O	7	73.81	0.15	10.96	2.77	0.14	0.05	1.57	3.51	1.68	94.64
64	†	DSDP38:1-V23-74-688	N. Iceland Plateau	?	Sigurdsson & Loebner (1981)	190 δ^{18}O	10	71.85	0.18	11.80	2.84	0.10	0.05	1.18	4.35	2.69	95.04
65	†	907A-1H-3, 53-55-C	N. Iceland Plateau	?	Lacasse *et al.* (1995; 1996)	204.6 δ^{18}O	15	71.28	0.24	11.94	3.35	0.11	0.08	1.81	4.83	2.37	96.01

contd. overpage

ID no.		Site location or core number	Extra ID	Volcano	Reference	Age[3] (Ma BP) & method	n	SiO_2	TiO_2	Al_2O_3	FeO_{tot}	MnO	MgO	CaO	Na_2O	K_2O	Total
66		HM57-7/410-412	St. 7-RHY-I	?	Sjøholm *et al*. (1991)	210 $\delta^{18}O$	7	72.12	0.31	10.67	5.17	0.20	0.05	0.37	2.22	3.68	94.79
67		HM57-7/410-412	St. 7-RHY-I	?	Sjøholm *et al*. (1991)	210 $\delta^{18}O$	15	71.34	0.22	12.34	3.63	0.10	0.08	1.74	2.07	2.33	93.85
68	†	DSDP38:1-V23-58-375	N. Iceland Plateau	?	Sigurdsson & Loebner (1981)	225 $\delta^{18}O$	10	72.05	0.17	11.74	2.84	0.11	0.06	1.22	4.31	2.71	95.21
69	†	K708-1-610	III-RHY-I	?	Sigurdsson (1982)	320 $\delta^{18}O$	16	72.86	0.22	12.06	3.34	0.10	0.01	1.18	4.85	2.89	97.51
70	†	SU9029-549	III-RHY-I	?	Lacasse *et al*. (1995; 1996)	320 $\delta^{18}O$	14	72.83	0.20	11.77	3.21	0.11	0.02	1.23	5.24	2.81	97.42
71		K708-7	III-RHY-I	?	Kvamme *et al*. (1989)	320 $\delta^{18}O$	18	73.65	0.27	11.98	3.26	0.15	0.06	1.21	1.08	2.02	93.68
72		HM57-7/653-655	St. 9-RHY-I	?	Sjøholm *et al*. (1991)	330 $\delta^{18}O$	6	71.29	0.20	11.72	2.49	0.08	0.13	1.16	1.77	2.40	91.24
73	†	907A-2H-6, 139-141-G	N. Iceland Plateau	?	Lacasse *et al*. (1995; 1996)	774.1 $\delta^{18}O$	12	72.80	0.22	11.29	2.69	0.10	0.04	1.32	4.40	2.69	95.55
74	†	918A-6H-1, 122-41.02	Irminger basin	?	Clift & Fitton (1998)	1000 $\delta^{18}O$	-	67.72	0.04	18.64	1.90	0.02	0.87	0.38	8.24	2.09	99.91
75	†	7H-1, 37-128.37	Irminger basin	?	Clift & Fitton (1998)	1800 $\delta^{18}O$	-	70.89	0.23	7.83	6.39	0.28	0.02	0.28	4.03	2.81	92.75
76		913B-24R-2, 42-44	Vesterisbanken	?	Werner et al. (1996)	>2000- <2600 PM	58	70.92	0.15	12.25	2.33	0.09	0.00	1.07	4.78	2.32	93.91
77		18H-CC, 14-161.8	Irminger basin	?	Clift & Fitton (1998)	2500 PM	-	71.09	0.03	12.58	1.49	0.09	0.03	0.65	2.34	5.41	93.70
Pre-Quaternary age ocean core deposits																	
78		907A-11H-5, 105-106-p1	Kolbeinsey Ridge	?	Werner *et al.* (1998)	6.38-7.46 PM	5/10	71.06	0.30	12.33	2.54	0.08	0.09	1.49	4.00	2.68	94.57
79		907A-11H-5, 105-106-p2	Kolbeinsey Ridge	?	Werner *et al.* (1998)	6.38-7.46 PM	5/10	73.72	0.07	11.92	1.03	0.02	0.03	0.95	3.52	3.18	94.44
80		907A-11H-6,56-57	Kolbeinsey Ridge	?	Werner *et al.* (1998)	6.38-7.46 PM	7/13	69.00	0.29	12.38	4.13	0.15	0.02	1.97	4.57	2.15	94.66
81		907A-11H-6, 24-25; 29-30p1	Kolbeinsey Ridge	?	Werner *et al.* (1998)	7.46-7.89 PM	7/17	72.35	0.15	12.24	1.81	0.05	0.05	0.75	4.31	3.11	94.82
82		907A-11H-6, 24-25; 29-30p2	Kolbeinsey Ridge	?	Werner *et al.* (1998)	7.46-7.89 PM	14/35	70.98	0.19	11.98	2.50	0.10	0.04	1.05	4.51	2.68	94.03
83		907A-12H-2, 27-28	Kolbeinsey Ridge	?	Werner *et al.* (1998)	7.46-7.89 PM	8/13	71.28	0.11	12.15	1.68	0.04	0.13	1.21	4.43	2.50	93.53
84		907A-12H-6, 34-36	Kolbeinsey Ridge	?	Werner *et al.* (1998)	7.89-8.53 PM	9/37	70.77	0.14	11.71	2.14	0.10	0.02	0.85	4.43	3.22	93.38
85		907A-13H-1, 69-71	Kolbeinsey Ridge	?	Werner *et al.* (1998)	8.86 PM	5/10	70.31	0.28	12.25	3.18	0.14	0.04	1.28	4.18	2.73	94.39
86		907A-13H-2, 100-102	Kolbeinsey Ridge	?	Werner *et al.* (1998)	8.86 PM	6/17	70.77	0.20	11.59	2.20	0.08	0.01	1.08	4.30	2.82	93.05
87		907A-13H-3, 106-108	Kolbeinsey Ridge	?	Werner *et al.* (1998)	8.86 PM	12/30	70.24	0.33	11.95	4.13	0.16	0.02	1.63	4.47	2.27	95.20
88		907A-14H-2, 30-32	Kolbeinsey Ridge	?	Werner *et al.* (1998)	>9.78->10.83 PM	8/16	71.47	0.15	12.42	2.34	0.08	0.02	1.17	4.28	2.87	94.80
89		907A-14H-3, 79-81	Kolbeinsey Ridge	?	Werner *et al.* (1998)	>9.78->10.83 PM	7/16	69.69	0.31	12.65	3.17	0.15	0.08	0.98	4.90	2.68	94.61
90		907A-14H-4, 131-2; 143-4	Kolbeinsey Ridge	?	Werner *et al.* (1998)	>9.78->10.83 PM	21/54	70.89	0.15	12.48	2.53	0.10	0.00	1.08	4.39	3.07	94.69
91		907A-15H-1, 69-71	Kolbeinsey Ridge	?	Werner *et al.* (1998)	>10.83-12.94 PM	10/21	69.47	0.22	12.72	3.48	0.12	0.08	1.49	4.46	2.44	94.48
92		907A-15H-2, 21-22, 27-28	Kolbeinsey Ridge	?	Werner *et al.* (1998)	>10.83-12.94 PM	21/56	73.29	0.17	11.73	2.1	0.07	0.03	0.86	4.25	2.56	95.06
93		907A-15H-3, 134-136	Kolbeinsey Ridge	?	Werner *et al.* (1998)	>10.83-12.94 PM	12/32	72.59	0.20	11.65	2.75	0.10	0.00	1.11	4.49	2.35	95.24
94		907A-15H-5, 94-95	Kolbeinsey Ridge	?	Werner *et al.* (1998)	>10.83-12.94 PM	6/15	72.21	0.32	11.45	2.65	0.10	0.10	1.48	4.21	2.00	94.52
95		907A-15H-5, 96-97	Kolbeinsey Ridge	?	Werner *et al.* (1998)	>10.83-12.94 PM	9/24	70.50	0.30	11.39	2.64	0.09	0.12	1.50	4.37	2.03	92.94
96	†	918-39R-4, 14-652.54	Irminger basin	?	Clift & Fitton (1998)	12.1 PM	-	73.28	0.07	11.97	1.25	0.10	0.17	1.15	2.92	2.90	93.81
97	†	918-40R-2, 36-659.36	Irminger basin	?	Clift & Fitton (1998)	12.5 PM	-	71.01	0.30	11.79	3.40	0.15	0.07	1.85	3.60	1.83	94.00
98	†	918-40R-2, 36-659.36	Irminger basin	?	Clift & Fitton (1998)	12.5 PM	-	70.74	0.19	11.71	3.56	0.07	0.09	1.91	3.60	1.79	93.66

contd. overpage

ID no.		Site location or core number	Extra ID	Volcano	Reference	Age[3] (Ma BP) & method	n	SiO_2	TiO_2	Al_2O_3	FeO_{tot}	MnO	MgO	CaO	Na_2O	K_2O	Total
99	†	918-40R-3, 114-661.64	Irminger basin	?	Clift & Fitton (1998)	12700 PM	4	71.29	0.24	11.77	2.97	0.10	0.12	1.55	3.29	2.21	93.54
100		907A-16H-2, 65-67	Kolbeinsey Ridge	?	Werner *et al.* (1998)	12.94-13.09 PM	12/25	71.31	0.11	12.31	1.80	0.07	0.03	1.26	4.46	2.33	93.68
101		907A-18H-2, 146-150	Kolbeinsey Ridge	?	Werner *et al.* (1998)	>13.26-13.47 PM	12/15	70.27	0.19	11.66	2.90	0.09	0.04	1.21	4.42	2.74	93.52
102		907A-20H-5, 0-3	Kolbeinsey Ridge	?	Werner *et al.* (1998)	>14.06->14.16 PM	28/74	73.01	0.18	11.53	1.38	0.04	0.06	0.61	3.74	3.97	94.52
103		907A-21H-5, 35-37	Kolbeinsey Ridge	?	Werner *et al.* (1998)	>14.16 PM	7/12	71.19	0.18	11.46	2.34	0.10	0.02	1.08	3.94	3.44	93.75
104	$	907A-21H-7, 51-52	Kolbeinsey Ridge	?	Werner *et al.* (1998)	>14.16 PM	8/10	69.31	0.37	11.81	3.74	0.12	0.17	2.05	4.67	2.70	94.94
105	†	919-89R-4, 49-1132.39	Irminger basin	?	Clift & Fitton (1998)	44040 PM	-	70.84	0.47	3.51	5.28	0.01	1.05	0.30	0.29	1.52	83.25
106		918D-40R-3	Irminger basin	?	Werner *et al.* (1998)	60000 PM	<30	72.42	0.31	11.45	2.94	0.10	#	1.68	2.90	1.98	93.78
107		918D-42R-1	Irminger basin	?	Werner *et al.* (1998)	60000 PM	<30	73.88	0.10	12.18	1.22	0.04	#	1.21	2.99	2.94	94.56
New correlation dating data in this thesis						Age[3] (ka BP) & method											
201	‡$	N & E Iceland[3]	ASK 5/10/11	Askja	sjr; this study	0.126 HR	27	72.69	0.79	12.16	3.34	0.08	0.64	2.31	3.54	2.59	98.14
202	‡	S & SE Iceland[3]	ÖR 1-3	Öræfajökull	sjr; this study	0.639 HR	27	71.40	0.24	12.99	3.30	0.13	0.04	0.96	5.00	3.26	97.34
203	‡	Þórsmörk, S Iceland	ÞIG 1-23	Tindfjalljökull (?)	sjr; this study	(TL) TL	218	72.34	0.16	11.48	2.53	0.07	0.02	0.40	4.38	4.10	95.48
204	‡	Skagafjall, Vestfirðir	Óþoli Tephra	Husafell (??)	sjr; this study	2260 FT	137	72.89	0.16	11.60	2.36	0.09	0.02	1.29	3.68	2.75	94.84
205	‡	Skagafjall, Vestfirðir	Óþoli Tephra	Husafell (??)	sp; this study (FT-dating analyses)	2260 FT	60	72.25	0.17	11.66	2.34	0.08	0.01	1.44	4.12	2.61	94.745
Other new data included in cluster analysis																	
301	‡	Sweden	4B-10/1-JB_UL	A1875 (?)	sjr; Swedish tephra project	0.126 HR	15	72.19	0.80	12.33	3.65	0.09	0.76	2.61	3.11	2.41	97.94
302	‡	Sweden	93 10/1-JB_UL	?	sjr; Swedish tephra project	? -	4	72.88	0.09	12.68	1.92	0.08	0.03	1.31	4.00	3.04	96.04
303	‡$	Klaksvik, Faroe Islands	Eemian lake sediments	?	sw; unpublished	? -	11	73.46	0.15	10.80	2.88	0.09	0.06	1.51	3.39	1.80	94.14

Table C2.1 Notes: [1]last number is core depth in cm unless stated; [2]loc. = additional locational information. Elemental compositions are wt % mean values from the number of shards indicated in the n column; *e.g.* 5/10 in the n column represents 10 analyses from 5 shards. Dating methods: post-settlement tephra ages are taken from historical records (HR) and incrementally counted ice core ages (ICY) are calendar ka BP; ages of pre-settlement terrestrial deposits (^{14}C) are ^{14}C ka BP; ages for ocean cores deposits ($\delta^{18}O$) are astronomically tuned $\delta^{18}O$ ka BP; PM ages are based on palaeomagnetic reversal correlation dating ages; some ages taken from Werner *et al*. (1998) are estimated Ma BP, based on comparison to single-grain Ar-Ar ages from core 917; TL = thermoluminescene ages; FT = fission-track ages. [4] Based on long Quaternary time scale of 0-2.5 Ma. ID nos. relate to cluster dendrograms and location map. Ξ indicates stratotype location. All data are grain specific obtained by EPMA; most analyses are WDS; where known, EDS analyses are marked with a *. For accurate comparison volatiles (*e.g.* P_2O_5,SO_2) and other elements (*e.g.* F, Cl) measured in some of the above analyses have been omitted and totals presented in this table adjusted accordingly. Data obtained using EDS has been included in correlation and multivariate analysis, but matches between EDS and WDS data should be treated with more caution than those made between WDS data. Matches between WDS data should be treated with a degree of caution because data listed represents analyses obtained from several microprobes using different running conditions over the last 30 years. Analyses marked with a ‡ were undertaken on the Mk V Cambridge Instruments microprobe in Edinburgh using the same operating conditions as specified in the methods section. Analyses marked with a † are known to include a correction for sodium mobilisation; data from Sjøholm *et al.* (1991) not in the table above has been omitted from correlation because of low Na_2O wt % that contribute to low overall totals. 1σ standard deviation errors are not included for clarity, but these are generally 10% or less when known; known SiO_2: 1σ >10 % are marked with a $; # = data not published or error in published data - blacked out nu mbers are not included in statistical analysis. Table based in part on Table A1 of Haflidason *et al*. (2000; p. 19-22) with additional data from pre-mid Pleistocene deposits, Scottish Lateglacial tephra data obtained by SJR and studies undertaken since publication of this paper. Original data was selected when considered reliable; a comprehensive list of analyses from some Holocene silicic deposits can be found on Tephrabase - http://www.geo.ed.ac.uk/tephra/tbasehom.html (Newton, 1996). SW is Dr. Stefan Wastegard, JB is Jonas Bergman, both University of Stockholm, who kindly allowed their submitted and unpublished data to be included; SP is Dr. Shari Preece, University of Toronto, who undertook analyses as part of the fission-track dating program to establish the chemical homogeneity of dated samples. Samples with blacked out ID nos. were not included in cluster analysis.

contd. overpage

Table C2.1 (*contd.*): Alphabetical reference list for correlation dating data. Numbers in italics at the end of each reference are deposit ID numbers.

1) **Birks, H.H., Gulliksen, S., Halfidason, H., Mangerud, J., and Possnert, G. (1996).** New radiocarbon dates for the Vedde Ash and the Saksunarvatn Ash from Norway. *Quaternary Research*, **45**, 119-127; *(26)*

2) **Björck, S., Ingolfsson, O., Haflidason, H., Hallsdottir, M., and Anderson, N. J. (1992).** Lake Torfadalsvatn: a high resolution record of the North Atlantic Ash Zone I and the last glacial-interglacial environmental changes in Iceland. *Boreas*, **21**, 15-22; *(28)*

3) **Clift, P. D. & Fitton, J. G. (1998).** Trace and rare earth element chemistry of volcanic ashes from sites 918 and 919: Implications for Icelandic volcanism. *Proceedings of the Ocean Drilling Program, Scientific Results*, **152**, 67-83; *(74, 75, 77, 96-99, 105)*

4) **Dugmore, A. J., & Newton, A. J. (1998).** Holocene tephra layers in the Faroe Islands. *Fróðskaparrit*, **46**, 191-204; *(18)*

5) **Dugmore, A. J., Larsen, G, & Newton, A. J. (1995).** Seven tephra isochrones in Scotland. *The Holocene*, **5/3**, 257-266; *(16, 19)*

6) **Einarsson, A. Haflidason, H., Oskarsson, H. (1988).** Lake Myvatn: palaeoliminology and tephrochronology of the Sydrifloi Basin. *Naturuvernarrad Report*, **17**, pp. 96. (In Icelandic with English summary; cited in Haflidason *et al.*, 2000); *(9, 10)*

7) **Fronval, T., Jansen, E., Haflidason, H., & Serjup, H. P. (1998).** Variability in surface and deep water conditions in the Nordic Seas during the last interglacial period. *Quaternary Science Reviews*, **17**, 963-985; *(60, 61)*

8) **Grönvold K., Oskarsson N., Johnsen S.J., Clausen H.B., Hammer C.U., Bond G., & Bard E. (1995).** Ash layers from Iceland in the Greenland GRIP ice core correlated with oceanic and land sediments. *Earth and Planetary Science Letters*, **135**, 149-155; *(44, 50, 51)*

9) **Haflidason, H. (1983).** *The Marine Geology of Eyjafjordur, North Iceland: Sedimentological, Petrological and Stratigraphical Studies.* Mphil Thesis, University of Edinburgh, Edinburgh. pp. 281; *(17, 21)*

10) **Haflidason, H., Eiríksson, J., & Van Kreveld, S. (2000).** The tephrochronology of Iceland and the North Atlantic region during the Middle and Late Quaternary: a review. *Journal of Quaternary Science*, **15**(1), 3-22; *(47)*

11) **Haflidason, H., Larsen, G., & Olafsson, G. (1992).** The recent sedimentation history of Thingvallavatn, Iceland. *Oikos*, **64**, 80-95; *(14)*

12) **Jennings, A. E., Syvitski, J. P. M., Gerson, L., Grönvold, K., Geirsdottir, A., Hardardottir, J., Andrews, J. T., & Hagen, S. (2000).** Chronology and palaeoenvironments during the late Weichselian deglaciation. *Boreas*, **29**, 167-183; *(43)*

13) **Jørgensen, K. A. (1980).** The Þórsmörk Ignimbrite: An unusual comenditic pyroclastic flow from southern Iceland. *Journal of Volcanology and Geothermal Research*, **8**, 7-22; *(36)*

14) **Jørgensen, K. A. (1981).** The eruption of Þórsmörk Ignimbrite, south Iceland. *Nordic Volcanological Institute, Reykjavik*, Report no. 8103;

15) **Kvamme T., Mangerud J., Furnes H., & Ruddiman W.F. (1989).** Geochemistry of Pleistocene ash zones in cores from the North Atlantic. *Norsk Geologisk Tidsskrift* **69**, 251-272; *(46, 71)*

16) **Lacasse, C., Sigurdsson, H., Carey, S., Paterne, M., & Guichard, F. (1996).** North-Atlantic deep-sea sedimentation of late Quaternary tephra from the Iceland hotspot. *Marine Geology*, **129(3-4)**, 207-235; *(29, 49, 59, 65, 70, 73)*

17) **Lacasse, C., Sigurdsson, H., Johannesson, H., Paterne, M., & Carey, S. (1995).** Source of Ash Zone 1 in the North Atlantic. *Bulletin of Volcanology* **57**, 18-32; *(29, 49, 59, 65, 70, 73)*

18) **Lackschewitz, K. S., & Wallrabe-Adams, H-J. (1997).** Composition and origin of volcanic ash zones in Late Quaternary sediments from the Reykjanes Ridge: evidence for ash fallout and ice-rafting. *Marine Geology*, **136**, 209-224; *(42, 45)*

19) **Larsen, G., Dugmore, A., & Newton, A. (1999).** Geochemistry of historical-age silicic tephras in Iceland. *The Holocene*, **9**(4), 463-471; *(2, 4, 5, 7, 11, 13, 15)*

20) **Lowe J. J., & Turney C. S. M., (1997).** Vedde Ash discovered in a small lake basin on the Scottish mainland. *Journal of the Geological Society* **154**, 605-612; *(30, 35)*

21) **Mangerud, J., Lie, S. E., Furnes, H., Kristiansen, I. L., & Lomo, L. (1984).** A Younger Dryas ash bed in western Norway and its possible correlations with tephra in cores from the Norwegian Sea and the North Atlantic. *Quaternary Research*, **21**, 85-104; *(25)*

22) **Newton, A. J. (1999).** *Ocean Transported Pumice in the North Atlantic.* Unpublished PhD Thesis, University of Edinburgh. p. 394.; ***(23, 24, 37, 38)***

23) **Norðdahl, H., & Haflidason, H. (1992).** The Skógar Tephra, a Younger Dryas marker in north Iceland. *Boreas.* **21(1)**, 23-41; *(27)*

24) **Pilcher, J. R., Hall, V. A., & McCormac, F. G. (1995).** Dates of Holocene Icelandic volcanic eruptions from tephra layers in Irish peats. *The Holocene* **5(1)**, 103-110; *(8)*

25) **Roberts, S. J. (1997).** *The spatial distribution and geochemical characteristics of Lateglacial tephras in Scotland.* Unpublished MSc. Thesis. University of London; *(30, 35)*

26) **Roberts, S. J., Turney, C. S. M. & Lowe, J. J. (1998).** Icelandic tephra in Late-glacial sediments of Scotland (14 - 9,000 ^{14}C BP). *Fróðskaparrit*, **46**, 335-339; *(30, 35)*

27) **Sigurdsson, H. (1982).** Útbreidsla íslenskra gjóskulaga à botni Atlantshafs. (Atlantic ocean circulation and Icelandic eruptions). In *Eldur er í nordri*, Thorarainsdóttir, H., Oskarsson, O. H., Steinthorsson, S., & Einarsson. Th. (Eds.) Sögufélag, Reykjavík. p. 119-127; *(6, 12, 20, 22, 41, 48, 69)*

28) **Sigurdsson, H., & Loebner, B. (1981).** Deep sea record of Cenozoic explosive volcanism in the North Atlantic. In: S. Shelf & R. S. J. Sparks (Eds.). *Tephra Studies.* Reidel, Dordrecht. pp. 289-316; *(56, 57, 58, 64, 68)*

29) **Sigvaldson, G. (1974).** The petrology of Hekla and origin of silicic rocks in Iceland. In: *The Eruption of Hekla, 1947-1948, Vol. 1*, Einarsson, T., Kjartansson, G., Thórarinsson, S. (Eds.). Societas Scientiarum Islandica, Reykjavík. pp. 1-44; *(1)*

30) **Sjøholm, J., Sejrup, H. P., & Furnes, H. (1991).** Quaternary volcanic ash zones on the Iceland Plateau, southern Norwegian Sea. *Journal of Quaternary Science* **6(2)**, 159-173; *(39, 40, 66, 67, 72)*

31) **Sparks, R. S. J., Wilson, L., & Sigurdsson, H. (1981).** The pyroclastic deposits of the 1875 eruption of Askja, Iceland. *Philosophical Transactions of the Royal Society of London*, **299**, 241-273; *(3)*

32) **Turney, C. S. M., Harkness, D. D. & Lowe, J. J. (1997).** The use of micro-tephra horizons to correlate lake sediment successions in Scotland. *Journal of Quaternary Science*, **12** (6), 525-531; *(34, 35)*

33) **Wastegård, S., & Rasmussen (submitted);** *(53, 54, 55, 62, 63)*

34) **Wastegård, S., Turney, C. S. M., Lowe, J. J. & Roberts, S. J. (2000a).** New discoveries of the Vedde Ash in southern Sweden and Scotland. *Boreas*, **29**, 72-78; *(31)*

35) **Wastegård, S., Wohlfarth, B., Subetto, D. A., & Sapelko, T. V. (2000b).** Extending the known distribution of Younger Dryas Vedde Ash into north-western Russia. *Journal of Quaternary Science*, **15**(6), 581-586; *(32, 33)*

36) **Werner, R., Wallrabe-Adams, H-J., Lacasse, C., Schmincke, H-U., & Theide, J. (1996).** Distribution, chemical composition, and sources of Oligocene to Miocene volcanic ashes from sites 907, 908, and 913. In: Theide, J., Myhre, A. M., Firth, J. V., Johnson, G. L., & Ruddiman, W. F. (Eds.). *Proceedings of the Ocean Drilling Program, Scientific Results*, **151**, 333-350; *(76, 78-95, 100-104, 106-107)*

37) **Zielinski, G. A., Mayewski, P. A., Meeker, D., Grönvold, K., Germain, M. S., Whitlow, S., Twickler, M. S., & Taylor, K. (1997).** Volcanic aerosol records and tephrochronology of the Summit, Greenland, ice cores. *Journal of Geophysical Research*, **102**, 26,625-26,640; *(50)*

(a) Induced slides track size data - UT1656i/sjr mean 6.360 stdev 2.016

	1-25	26-50	51-75	76-100	101-125	126-150	151-175	176-200	201-225	226-250	251-275	276-300	301-325	326-350	351-375	375-400
1	7.061	7.380	8.446	7.122	8.628	7.496	7.548	8.306	7.054	3.258	2.249	7.597	6.007	7.355	2.650	8.135
2	10.106	7.713	3.822	6.573	7.982	4.594	5.939	6.667	2.127	7.122	7.774	8.135	6.890	7.285	3.891	7.420
3	6.942	8.058	7.423	4.313	8.311	2.650	4.170	5.151	7.999	7.984	3.258	4.704	7.919	1.249	5.244	8.236
4	7.244	7.244	7.512	7.087	6.537	7.263	7.506	8.399	6.247	8.058	7.548	3.485	8.127	8.221	8.058	4.950
5	5.124	7.901	7.423	9.409	8.939	3.970	7.069	7.122	1.424	4.273	4.624	5.099	9.095	7.378	7.397	4.594
6	7.036	8.306	8.106	4.594	3.642	2.697	7.244	7.628	2.480	8.628	5.488	7.250	6.537	7.744	6.632	7.218
7	4.079	8.482	2.263	1.380	7.496	6.762	4.861	7.054	2.135	7.782	6.480	8.729	2.263	6.872	1.943	6.007
8	4.255	6.728	2.627	2.674	5.634	7.397	5.160	9.724	8.356	2.297	6.861	7.423	5.217	1.060	2.068	2.832
9	6.615	6.632	7.244	7.679	7.102	7.211	6.400	8.399	7.067	4.255	6.244	6.017	8.587	1.060	7.244	7.244
10	5.939	7.901	7.448	7.599	7.679	6.622	5.768	8.326	7.762	2.511	7.500	3.534	8.834	7.321	7.758	7.285
11	7.517	8.340	5.373	6.184	7.800	7.218	4.922	8.394	6.900	1.380	7.665	6.893	8.499	3.009	8.058	7.901
12	5.698	8.221	6.266	7.616	6.954	8.066	7.872	6.102	7.597	8.356	7.383	7.001	6.714	6.911	5.503	6.072
13	2.014	7.750	4.988	7.599	7.671	6.575	6.989	8.261	7.679	7.911	5.939	4.947	7.968	2.656	7.246	4.331
14	6.911	4.420	6.989	6.651	9.391	6.723	7.034	8.317	5.172	7.431	7.597	7.067	8.058	3.398	6.893	6.716
15	8.379	7.599	3.793	1.951	7.717	7.800	7.420	7.506	3.430	7.034	8.185	1.600	10.001	7.810	4.033	5.520
16	6.714	8.242	7.616	2.697	2.703	6.996	7.218	1.380	3.714	6.085	8.219	7.911	8.429	6.751	7.111	4.214
17	6.539	7.285	7.278	7.671	7.278	6.728	7.792	8.198	7.597	7.246	8.304	5.124	7.776	2.461	7.776	2.794
18	5.000	5.408	7.597	7.822	8.490	7.548	7.599	7.263	7.887	0.999	7.554	5.196	8.011	7.523	6.601	6.688
19	7.061	7.244	5.722	3.573	6.728	6.048	7.423	7.806	4.431	6.496	8.249	7.067	8.371	2.304	7.454	7.937
20	7.069	1.667	8.046	1.819	7.822	6.660	7.194	7.644	5.253	2.849	2.297	6.597	3.727	7.597	7.951	6.751
21	7.982	7.646	6.247	8.221	7.999	7.423	7.533	5.679	7.548	4.851	5.300	7.982	1.346	7.822	8.152	3.998
22	7.423	5.271	2.304	7.599	1.185	6.881	6.007	4.170	8.772	5.722	5.884	9.167	7.067	3.642	6.714	7.887
23	7.014	7.768	2.297	5.656	6.942	5.579	3.781	6.942	2.650	6.972	7.304	8.554	2.120	8.272	8.334	5.420
24	6.881	7.774	1.767	6.125	7.072	8.013	6.622	1.131	8.304	7.329	8.446	5.812	7.774	7.889	8.129	
25	7.209	7.423	8.196	2.941	6.714	7.429	7.548	7.500	7.842	7.846	7.776	5.160	5.897	7.423	5.612	

(b) Spontaneous slides track size data - UT1656i/sjr mean 6.597 stdev 1.866

	1-8	9-16	17-24	25-32	33-40	41-48	49-56	57-64	65-72	73-80	81-88	89-96	97-100
1	8.129	4.515	2.876	7.597	8.106	4.140	8.878	7.846	7.774	8.158	7.548	5.612	3.286
2	5.830	7.548	7.380	5.747	7.246	6.274	6.861	9.066	6.573	8.058	4.037	7.244	6.667
3	5.124	9.174	5.488	2.760	9.187	3.710	9.054	6.431	7.244	8.772	7.244	8.005	8.236
4	7.244	8.091	7.397	3.534	8.722	6.872	5.303	7.941	7.776	5.199	7.744	3.480	8.455
5	7.454	9.654	6.875	8.144	4.607	6.516	3.887	5.253	3.430	9.169	7.285	5.454	
6	3.357	8.830	6.827	6.186	4.678	6.421	8.060	3.398	8.481	8.127	4.270	5.830	
7	8.356	7.244	10.637	2.060	7.420	5.477	7.014	8.326	8.490	6.010	7.448	6.989	
8	3.538	8.304	4.374	4.200	6.370	5.300	4.214	5.315	7.824	5.689	6.723	8.995	

Table C3.1 Track size diameter data for sample UT1656 as an example of the the precise measurement of track diameters. Other track size data is summarised in Table C3.2. Full datasets can be found on the CD-R; filename: C3.1UTFT_OT_track-EPMA_sjr_data.xls.

(a) UT1656-1659 SUMMARY	UT1656i/sjr	UT1656s/sjr	UT1657i/as	UT1657s/as	UT1657i/cw	UT1657s/cw	UT1659i/as	UT1659s/as
Mean	6.36	6.60	7.87	5.59	6.77	5.59	5.87	5.91
Standard Error	0.10	0.19	0.08	0.08	0.07	0.08	0.08	0.12
Median	7.07	7.00	8.09	5.83	7.09	5.83	6.35	6.33
Mode	7.42	7.24	8.31	5.94	7.67	5.94	7.12	6.37
Standard Deviation	2.02	1.87	1.93	1.38	2.08	1.38	1.57	1.33
Sample Variance	4.06	3.48	3.74	1.89	4.32	1.89	2.47	1.77
Kurtosis	0.16	-0.65	0.75	0.50	0.14	0.50	0.48	0.36
Skewness	-1.06	-0.44	-0.68	-0.74	-0.48	-0.74	-1.05	-0.92
Range	9.11	8.58	11.28	8.27	13.41	8.27	7.90	6.61
Minimum	1.00	2.06	1.58	0.71	0.18	0.71	0.95	1.95
Maximum	10.11	10.64	12.86	8.98	13.59	8.98	8.85	8.56
Sum	2531.15	659.69	4698.36	1666.91	5411.11	1666.91	2335.68	785.64
Count	398	100	597	298	799	298	398	133
Confidence Level (95.0%)	0.20	0.37	0.16	0.16	0.14	0.16	0.15	0.23
D_s/D_i		1.04		0.71		0.83		1.01
Standard Error		0.05		0.01		0.01		0.02
D_i/D_s		0.96		1.41		1.21		0.99
Standard Error		0.05		0.01		0.01		0.02

(b) Track size (μm)	Percentage frequency							
	UT1656i/sjr	UT1656s/sjr	UT1657i/as	UT1657s/as	UT1657i/cw	UT1657s/cw	UT1659i/as	UT1659s/as
0	0.25	0.00	0.00	0.34	0.25	0.34	0.50	0.00
1	4.02	0.00	0.67	0.67	1.75	0.67	2.76	0.75
2	7.29	3.00	1.51	4.03	4.51	4.03	3.27	4.51
3	4.52	9.00	3.02	9.06	5.51	9.06	8.79	6.02
4	6.03	9.00	4.36	12.42	8.01	12.42	9.05	12.03
5	8.54	14.00	4.69	29.19	7.38	29.19	16.08	18.05
6	15.83	15.00	9.55	31.21	20.40	31.21	33.67	40.60
7	37.44	22.00	25.13	11.74	24.66	11.74	24.12	16.54
8	14.32	21.00	23.95	1.34	15.89	1.34	1.76	1.50
9	1.26	6.00	15.75	0.00	7.88	0.00	0.00	0.00
10	0.50	1.00	8.38	0.00	2.88	0.00	0.00	0.00
11	0.00	0.00	2.35	0.00	0.38	0.00	0.00	0.00
More	0.00	0.00	0.67	0.00	0.50	0.00	0.00	0.00
Total	100	100	100	100	100	100	100	100

Table 3.2 (a) Track size summary statistics and Ds/Di ratios **(b)** Track size distributions used to construct Figure 4.16

Notes: UT1655 was irradiated and etched under same conditions and at the same time as UT1659. Track size distribution is assumed to be approximately similar. UT1657 age corrected using the diameter correction technique that is based on the ratio of Di/Ds. UT16555/56/59 age corrected using the isothermal plateau heating 30 days @ 130C. When Ds/Di >= 1 plateau reached & indicates suitable for dating. Track size distributions shaded in grey are from preliminary etching experiments; sjr is Steve Roberts; as ia Amanjit Sandhu; cw is Corra Westgate.

Óþoli Tephra_IT1656_sjr

Spontaneous			Induced					
1st count			1st count			Recount		
Notes		ok		Undercounted				ok
1	2	3	1	2	3	1	2	3
10	11	0.91	112	7	16.00	159	4	39.75
20	34	0.59	217	12	18.08	292	6	48.67
30	43	0.70	342	16	21.38	420	9	46.67
40	59	0.68	448	18	24.89	575	13	44.23
50	82	0.61	560	22	25.45	704	16	44.00
61	99	0.62	690	26	26.54	856	22	38.91
71	117	0.61	787	29	27.14	978	23	42.52
81	134	0.60	897	31	28.94	1117	24	46.54
91	144	0.63	985	33	29.85	1238	27	45.85
101	155	0.65	1111	38	29.24	1376	29	47.45
111	176	0.63	1215	40	30.38	1516	31	48.90
121	190	0.64	1310	43	30.47	1645	32	51.41
131	214	0.61	1427	47	30.36	1805	35	51.57
141	232	0.61	1552	50	31.04	1924	39	49.33
151	239	0.63	1638	52	31.50	2081	40	52.03
161	253	0.64	1799	55	32.71	2234	41	54.49
171	265	0.65	1941	60	32.35	2344	42	55.81
181	281	0.64	2042	62	32.94	2454	43	57.07
191	293	0.65	2142	67	31.97	2587	50	51.74
201	312	0.64	2258	68	33.21	2731	54	50.57
211	339	0.62	2364	69	34.26	2841	55	51.65
221	356	0.62	2501	75	33.35	2999	58	51.71
231	368	0.63	2615	77	33.96	3146	62	50.74
241	379	0.64	2714	79	34.35	3270	62	52.74
251	397	0.63	2823	81	34.85	3416	65	52.55
261	424	0.62	2915	83	35.12	3616	71	50.93
271	440	0.62	3011	85	35.42	3712	73	50.85
281	456	0.62	3153	89	35.43	3873	78	49.65
291	467	0.62	3252	92	35.35	4051	83	48.81
301	488	0.62	3366	93	36.19	4207	90	46.74
311	516	0.60	3473	96	36.18	4440	95	46.74
321	535	0.60	3591	102	35.21	4570	95	48.11
331	554	0.60	3725	104	35.82	4707	98	48.03
341	571	0.60	3803	107	35.54	4866	101	48.18
351	585	0.60	3950	111	35.59	5015	102	49.17
361	593	0.61	4077	114	35.76	5156	102	50.55
371	618	0.60	4187	120	34.89	5263	104	50.61
381	640	0.60	4297	124	34.65	5433	111	48.95
			4433	130	34.10	5608	115	48.77
1 = No. of spontaneous or induced tracks			4543	130	34.95	5733	117	49.00
2 = No. of points on glass			4643	135	34.39	5859	122	48.02
3 = No. of tracks / No. of points on glass			4728	136	34.76	6014	122	49.30
			4827	140	34.48	6149	126	48.80
			4936	145	34.04			

Table C3.3 Track count data for sample UT1656 analysed by sjr as an example of track counting process. The recount of induced tracks includes all edge & small (1-3 mm) tracks not counted in the first count; hence the greater number of tracks counted.

SAMPLE DATA		EQUIVALENT DOSE (ED) DATA									TOTAL BULK DOSE RATE (D_T) DATA[8] Highest D_T ⟶ Lowest D_T				TL AGE ESTIMATES Based on		
Sample name (Lab no.) . Expt. Name Run no.	Set	Pre-heat[1] time @ temp. (hrs/min @ °C)	Dose range (Gy)	Dose interval (Gy)	ND or TD[2] (Gy)	Reg.[3] Type	Stable ED[4] Range (°C)	Regression r^2 G1/G3-MAAD G_n/TD_n-DC-SAR	ED[5] (Gy)	60-70 day[6] fading ratio	A Fading[7] Corrected ED (Gy)	B_1 ELEMENTAL D_T $WF_{in\text{-}situ}$ ($mGya^{-1}$)	B_2 ELEMENTAL D_T $WF_{in\text{-}situ\text{-}sat}$ ($mGya^{-1}$)	B_3 SPECT $D_{T\ (WM\ H\text{-}H)}$ ($WF_{in\text{-}situ\text{-}sat}$) ($mGya^{-1}$)	A/B_1 ELEMENTAL D_T $WF_{in\text{-}situ}$ (ka)	A/B_2 ELEMENTAL D_T $WF_{in\text{-}situ\text{-}sat}$ (ka)	A/B_3 SPECT D_T ($WF_{in\text{-}situ\text{-}sat}$) (ka)
(a) Óþoli Tephra (SUTL551/552)																	
(i) Multiple Aliquot Additive Dose(MAAD) Experiment (SUTL552)																	
MAAD1	A	16 hrs @ 135	150-1200	150	600	-	-	-	-	-	-	-	-	-	-	-	-
	B	16 hrs @ 135	150-1200	150	600	-	-	-	-	0.87 ± 0.41	-	-	-	-	-	-	-
MAAD2	A	16 hrs @ 135	150-1200	150	600	L	300-340	0.30 ± 0.02	2130 ± 90	0.93 ± 0.19	**2290 ± 440**	4.21 ± 0.30	**3.90 ± 0.66**	2.83 ± 0.41	544 ± 111	**587 ± 150**	**809 ± 195**
	B	16 hrs @ 135	150-1200	150	600	L	320-360	0.56 ± 0.04	1640 ± 100	0.90 ± 0.17	**1810 ± 320**	4.21 ± 0.30	**3.90 ± 0.66**	2.83 ± 0.41	430 ± 82	**464 ± 114**	**640 ± 146**
MAAD3	A	5 hrs @ 155	300-2400	300	1200	L	300-380	0.80 ± 0.17	6930 ± 530	0.96 ± 0.11	**7210 ± 940**	4.21 ± 0.30	**3.90 ± 0.66**	2.83 ± 0.41	1713 ± 254	**1849 ± 395**	**2548 ± 497**
	B	5 hrs @ 155	300-2400	300	1200	L	320-360	0.44 ± 0.05	4640 ± 320	0.91 ± 0.11	**5090 ± 640**	4.21 ± 0.30	**3.90 ± 0.66**	2.83 ± 0.41	1209 ± 175	**1305 ± 275**	**1799 ± 345**
MAAD4[9]	A	16 hrs @ 135	150-1200	150	600	L	280-360	0.57 ± 0.22	2920 ± 150	0.94 ± 0.18	**3090 ± 570**	4.21 ± 0.30	**3.90 ± 0.66**	2.83 ± 0.41	734 ± 145	**792 ± 198**	**1092 ± 256**
	B	16 hrs @ 135	150-1200	150	600	-	-	-	-	1.21 ± 0.08	-	-	-	-	-	-	-
MAAD5[9]	A	5 hrs @ 155	300-2400	300	600	L	320-390	0.64 ± 0.08	5480 ± 450	0.93 ± 0.08	**5880 ± 640**	4.21 ± 0.30	**3.90 ± 0.66**	2.83 ± 0.41	1397 ± 182	**1508 ± 303**	**2078 ± 377**
	B	5 hrs @ 155	600-4800	600	600	-	-	-	-	0.99 ± 0.20	-	-	-	-	-	-	-
											EXTRAPOLATED ED - NO COHERENT SINGLE AGE ESTIMATE - AGE RANGE:						**600→2700**
(ii) Dose Corrected Single Aliquot Regeneration (DC-SAR) Experiment (SUTL551)																	
Uncorrected		2 min @ 220	0-6000	500/1000	-	SSE+L	290-330	0.996 ± 0.001	4600 ± 700	0.86 ± 0.02	**5350 ± 820**	4.21 ± 0.30	**3.90 ± 0.66**	2.83 ± 0.41	1271 ± 215	**1372 ± 313**	**1890 ± 399**
		2 min @ 220	0-6000	500/1000	-	SSE+L	260-340	0.994 ± 0.002	3870 ± 580	0.86 ± 0.02	4500 ± 680	4.21 ± 0.30	3.90 ± 0.66	2.83 ± 0.41	1069 ± 179	1154 ± 262	1590 ± 333
											INTERPOLATED ED - UNCORRECTED MEAN AGE ESTIMATES 260-340 & 290-330°C:				1170 ± 197	1263 ± 287	1740 ± 366
TD corrected (11)[10]		2 min @ 220	0-6000	500/1000	100	SSE+L	290-330	0.988 ± 0.003	11540 ± 730	0.86 ± 0.02	**13420 ± 850**	4.21 ± 0.30	**3.90 ± 0.66**	2.83 ± 0.41	3188 ± 304	**3441 ± 622**	**4742 ± 750**
		2 min @ 220	0-6000	500/1000	100	SSE+L	260-340	0.985 ± 0.007	11280 ± 740	0.86 ± 0.02	13110 ± 860	4.21 ± 0.30	3.90 ± 0.66	2.83 ± 0.41	3114 ± 302	3362 ± 610	4633 ± 737
											EXTRAPOLATED ED - DOSE CORRECTED MEAN AGE ESTIMATES 260-340 & 290-330°C:				3151 ± 303	3401 ± 616	4687 ± 743
(b) Þórsmórk Ignimbrite (ÞIG 7)																	
(i) Dose Corrected Single Aliquot Regeneration (DC-SAR) Experiment (ÞIG 7)																	
Uncorrected		2 min @ 220	0-300	50/100	-	L	290-330	0.991 ± 0.005	168 ± 4	0.92 ± 0.01	**182 ± 5**	6.59 ± 0.91	**6.25 ± 1.51**	*4.44 ± 2.11*	28 ± 4	**29 ± 7**	*41 ± 20*
						SSE		0.996 ± 0.003	168 ± 4	0.92 ± 0.01	**182 ± 5**	6.59 ± 0.91	**6.25 ± 1.51**	*4.44 ± 2.11*	28 ± 4	**29 ± 7**	*41 ± 20*
		2 min @ 220	0-300	50/100	-	L	260-340	0.990 ± 0.008	169 ± 3	0.92 ± 0.01	**184 ± 4**	6.59 ± 0.91	**6.25 ± 1.51**	*4.44 ± 2.11*	28 ± 4	**29 ± 7**	*41 ± 20*
						SSE		0.978 ± 0.015	169 ± 3	0.92 ± 0.01	**184 ± 4**	6.59 ± 0.91	**6.25 ± 1.51**	*4.44 ± 2.11*	28 ± 4	**29 ± 7**	*41 ± 20*
											INTERPOLATED ED - UNCORRECTED MEAN AGE ESTIMATES:				28 ± 4	**29 ± 7**	*41 ± 20*
TD corrected (9)[10]		2 min @ 220	0-300	50/100	25	L	290-330	0.986 ± 0.007	207 ± 5	0.92 ± 0.01	**225 ± 6**	6.59 ± 0.91	**6.25 ± 1.51**	*4.44 ± 2.11*	34 ± 5	**36 ± 9**	*51 ± 24*
						SSE		0.996 ± 0.002	222 ± 6	0.92 ± 0.01	**241 ± 7**	6.59 ± 0.91	**6.25 ± 1.51**	*4.44 ± 2.11*	37 ± 5	**39 ± 9**	*54 ± 26*
		2 min @ 220	0-300	50/100	25	L	260-340	0.942 ± 0.110	210 ± 5	0.92 ± 0.01	**228 ± 6**	6.59 ± 0.91	**6.25 ± 1.51**	*4.44 ± 2.11*	35 ± 5	**36 ± 9**	*51 ± 24*
						SSE		0.991 ± 0.007	227 ± 6	0.92 ± 0.01	**247 ± 7**	6.59 ± 0.91	**6.25 ± 1.51**	*4.44 ± 2.11*	37 ± 5	**40 ± 10**	*56 ± 26*
											INTERPOLATED ED - DOSE CORRECTED MEAN AGE ESTIMATES:				36 ± 5	**39 ± 9**	*53 ± 25*

Table C4.1 Equivalent dose and TL age estimate summary data table for multiple aliquot additive dose and single aliquot regeneration thermoluminescence dating experiments on volcanic glass fractions of the Óþoli Tephra and Þórsmórk Ignimbrite. Dose rate data is based on weighted mean homogenous/heterogeneous matrix model caculations summarised in Table 5.4 rather than homogeneous matrix model dose rate calculations in Table 4.6; reasons for choosing final dose rates are summarised in Table 5.5. Otherwise explanatory notes are as for Table 4.7.

Sample	Disc	TL dose response (300-350°C)			Alpha irradiation unit			Alpha efficiency values	
		Natural	TL_b 15 mins	TL_a 30 mins	Position	S-factor (S)	a-dose ($Gymin^{-1}$)	a^1	k^2
Óþoli Tephra (SUTL 551/2)	1	152390	13228	6142	1	0.308	4.004	0.190	0.157
	2	123993	11762	5486	2	0.349	4.537	0.168	0.139
							Mean ± 1s	**0.18 ± 0.02**	**0.15 ± 0.01**
Þörsmórk Ignimbrite (ÞIG 7)	2	29962	14253	6707	3	0.313	4.069	0.189	0.157
	3	28669	13768	6996	4	0.315	4.095	0.203	0.168
							Mean ± 1s	**0.20 ± 0.01**	**0.16 ± 0.01**

Table C4.2 Alpha efficiency measurements for the samples of the Óþoli Tephra and Þörsmórk Ignimbrite used in quantitative TL dating analysis. Irradiator 1 was used (β-dose rate = 3.27 ± 0.015 $Gymin^{-1}$) to re-calibrate the six seater Littlemore Scientific alpha irradiation unit and work out alpha efficiency values. [1] = a-value system defined by Aitken and Bowman (1975) where S = α track length exposure per unit volume and $a = \{\beta\text{-dose}/[13S^{*}\alpha\text{-dose rate}]\} \times [TL_\alpha/TL_\beta]$; [2] = k-value system defined by Zimmerman (1971) where k = 0.83a.

Sample	Run Cycle	[No. of counts, count time (s)]	Mean counts	Mean count rate (cps)
Óþoli Tephra (SUTL 551/2)	Standard	[6,100]	661.17	6.612 ± 0.087
	Background	[6,300]	302.83	1.009 ± 0.088
	SUTL 551/2	[6,300]	506.50	1.688 ± 0.093
	Background	[6,300]	308.50	1.028 ± 0.060
	Standard	[6,100]	656.17	6.550 ± 0.120
	Average standard count rate	Std_{ave}	659	6.591 ± 0.014
	Average background count rate	$Bkgrd_{ave}$	306	1.022 ± 0.004
	Sensitivity	S	-	2.270 ± 0.015
	Sample count rate average	G	507	1.688 ± 0.093
	Net count rate (cps)	N	-	0.666 ± 0.093
SUTL 551/2	**Dry beta-dose rate ($mGya^{-1}$)**	**(see caption)**		**1.513 ± 0.211**
	Wet beta dose rate			
Þörsmörk Ignimbrite (ÞIG 7 & ÞIG 1b)	Standard	[6,100]	700.17	7.002 ± 0.325*
	Background	[6,300]	347.67	1.159 ± 0.237
	ÞIG 7	[6,300]	798.83	2.663 ± 0.243
	ÞIG 1b	[6,300]	694.83	2.316 ± 0.247
	Background	[6,300]	305.50	1.019 ± 0.266
	Standard	[6,300]	1970.67	6.569 ± 0.284
	Average standard count rate	Std_{ave}	1335	6.756 ± 0.080
	Average background count rate	$Bkgrd_{ave}$	327	1.097 ± 0.070
	Sensitivity	S	-	2.233 ± 0.107
ÞIG 7	Sample count rate average	G	799	2.663 ± 0.243
	Net count rate (cps)	N	-	1.566 ± 0.253
	Dry beta-dose rate ($mGya^{-1}$)	**(see caption)**		**3.498 ± 0.589**
ÞIG 1b	Sample count rate average	G	695	2.316 ± 0.061
	Net count rate (cps)	N	-	1.219 ± 0.093
	Dry beta-dose rate ($mGya^{-1}$)	**(see caption)**		**2.723 ± 0.245**

Table C4.3 Summary of thick source beta-counting (TSBC) results for tephra TL dating samples from the Óþoli Tephra and the Þörsmörk Ignimbrite. *ca.* 15 g of each sample and standard was used; dry β dose = $(G_{ave}\text{-}Bkgrd_{ave}) \times [12.64/(Std_{ave}\text{-}Bkgrd_{ave})]$, *i.e.* N*S; where 12.64 = the known count rate for 15 g of Shap Granite standard with a count rate of 6.25 $mGya^{-1}$. See Sanderson (1988) for more details of TSBC equipment and theory; * = elevated standard count rate due to minor pulse in attached oscilloscope

File	Location (time in brackets)	°N	°W	^{40}K cts	Channel 1(>450 keV) Counts	Channel 1(>450 keV) mGya^{-1}	Channel 2 (>1350 KeV) Counts	Channel 2 (>1350 KeV) mGya^{-1}	Combined dose rates mGya^{-1}	Notes; meaurement dimensions ~ 4p unless stated
Skag 1	Hotel room 1 (09:30)	-	-	244 [1]	7201	0.144 ± 0.002	1401	0.130 ± 0.003	0.130 ± 0.01	
Skag 2	Hotel room 2	-	-	245 [1]	8079	0.160 ± 0.002	1520	0.140 ± 0.003	0.150 ± 0.01	
Skag 3	Isafjordur tunnel	-	-	236 [2]	5317	0.106 ± 0.001	1045	0.097 ± 0.003	0.100 ± 0.01	environmentally shielded
Skag 4	Nupur section	-	-	237 [2]	2449	0.050 ± 0.001	467	0.043 ± 0.003	0.050 ± 0.005	
Skag 5	Nesdalur 'car park' (11:01)	66 01.03	23 43.82	238 [2]	5952	0.119 ± 0.001	781	0.073 ± 0.003	0.040 ± 0.005	^{137}Cs (Chernobyl?)
Skag 6	Skag boulder 1	66 00.27	23 45.60	240 [2]	4733	0.094 ± 0.001	712	0.066 ± 0.003	0.080 ± 0.005	fg bs+<1 mm p fsp pheno
Skag 7	Skag boulder 3	66 00.08	23 45.55	238 [2]	4427	0.088 ± 0.001	731	0.068 ± 0.003	0.080 ± 0.005	fg bs+<1 mm p fsp pheno
Skag 8	500 m W of section A (13:20)	65 59.78	23 44.67	230 [3]	11559	0.231 ± 0.001	2237	0.210 ± 0.003	0.220 ± 0.01	2p-general background reading
Skag 9	Section B: samples 1/2 (TL555/6)	65 59.78	23 45.40	234 [3]	26545	0.531 ± 0.001	5452	0.510 ± 0.003	0.520 ± 0.01	3.5-3.8p
Skag 10	Section B: samples 5/6 (TL551/2)	65 59.78	23 45.40	237 [2]	15170	0.303 ± 0.001	3188	0.296 ± 0.003	0.300 ± 0.01	3.5-4p
Skag 11	Section B: samples 3/4 (TL553/4)	65 59.78	23 45.40	240	23369	0.467 ± 0.001	4643	0.430 ± 0.003	0.450 ± 0.01	3.5-4p
Skag 12	Section B: sample 7 (TL557)	65 59.78	23 45.40	233	4250	0.085 ± 0.001	835	0.777 ± 0.003	0.080 ± 0.01	
Skag 13	Plateau grass 1 (16:35)	-	-	239	3848	0.077 ± 0.001	591	0.055 ± 0.003	0.070 ± 0.01	^{137}Cs (Chernobyl?)
Skag 14	Plateau grass 2	-	-	233	3254	0.065 ± 0.001	614	0.057 ± 0.003	0.064 ± 0.01	
Skag 15	Rhythmite bed 12(?)	65 59.13	23 43.83	232	3553	0.071 ± 0.001	675	0.063 ± 0.003	0.070 ± 0.01	
Skag 16	Section C: sample 8 (TL558)	65 58.11	23 43.43	240	22873	0.450 ± 0.001	4628	0.430 ± 0.003	0.440 ± 0.01	~3p
Skag 17	Section C: gravel/tephra (18:30)	65 58.18	23 43.43	241	20608	0.412 ± 0.001	4299	0.399 ± 0.003	0.410 ± 0.01	~3p
Skag 18	Hotel room 3 (11:53)	-	-	231	3781	0.136 ± 0.001	1296	0.120 ± 0.003	0.130 ± 0.01	
CES-SKAG1 (a & b)		66 00 .08	23 45.40							

[1] ch. 1	75-500	ch. 2	225-500	Conversion factors
[2] ch. 1	73-500	ch. 2	219-500	Channel 1 0.0060 ± 0.0004
[3] ch. 1	-	ch. 2	262-500	Channel 2 0.0280 ± 0.003

Table C4.4 *In-situ* gamma spectrometry readings taken on 1/7/99 in the course of measuring the gamma dose rates for the Óþoli Tephra at section B, Skagafjall, NW Peninsula, Iceland. Samples collected for ^{3}He cosmogenic surface dating from boulder 4 (SKAG 1) (*ca*. 1 m diameter erratic - ol/px phenocrysts > 1-5 mm). Only boulder found of significant size of this composition on Skagafjall on 1/7/99; fg = fine-grained; cg = coarse-grained; bs = basalt; ol = olivine; p = plagioclase; pheno = phenocrysts. Total gamma dose was measured in-situ for all samples of Óþoli Tephra and underlying rhythmite bed (unit 10) from sections B and C at sampling sites TL551-558 (Fig. 4.2). A portable Ortec Micro Nomad spectrometer with a 3x3 inch sodium-iodide spectrometer crystal and photo-multiplier assemblage was used. This was initially connected to a Toshiba laptop running Ortec Micro (MCB) program that integrates spectra and calculates the dose rates. Several test runs were undertaken before disconnection from the laptop to ensure correct operation. The spectrometer was then operated in field mode that collects spectra without viewing or computation. Spectra were collected over 512 channels using a preset live-time of 300 seconds.

(a) Icelandic Tephra: Palaeowater content estimates

WATER CONTENT: W & F values

SAMPLE	CODE	WATER CONTENTS			SATURATION LEVEL VARIATION: EFFECT ON F VALUE (% time @ saturation : % time @ measured)					
		DRY	SATURATED	1σ	1	2	3	4	5	6
			W		F_1[3]	F_2	F_3	F_4	F_5	F_6
		H_2O/dry[1]	wt H_2O_{SAT}/dry[2]	±[5]	mean H_2O/H_2O_{SAT} 0:100[4]	mean H_2O/H_2O_{SAT} 20:80	mean H_2O/H_2O_{SAT} 67:33	mean H_2O/H_2O_{SAT} 75:25	mean H_2O/H_2O_{SAT} 80:20	mean H_2O/H_2O_{SAT} 100:0
ÖÞOLI TEPHRA	TL551a	0.29	0.83	0.06	0.35	0.48	0.78	0.84	0.87	1.00
	TL551b*	0.30	0.80	0.08	0.38	0.50	0.79	0.84	0.88	1.00
	TL552a	0.35	0.61	0.05	0.57	0.66	0.86	0.89	0.91	1.00
	TL552b	0.38	0.59	0.08	0.64	0.71	0.88	0.91	0.93	1.00
	TL558*	0.30	0.78	0.05	0.38	0.51	0.80	0.85	0.88	1.00
		0.30	0.73	0.03	0.41	0.53	0.81	0.85	0.88	1.00
ÖRÆFI 1362	ÖR1	0.43	0.63	0.17	0.67	0.74	0.89	0.92	0.93	1.00
	ÖR2	0.50	0.97	0.02	0.52	0.62	0.84	0.88	0.90	1.00
	ÖR3	0.30	0.93	0.07	0.32	0.45	0.77	0.83	0.86	1.00
ASKJA 1875	ASK5	0.39	0.91	0.10	0.43	0.54	0.81	0.86	0.89	1.00
		0.39	0.83	0.09	0.48	0.58	0.83	0.87	0.90	1.00
	ASK10	0.23	0.94	0.04	0.25	0.40	0.75	0.81	0.85	1.00
	ASK11	0.30	0.89	0.06	0.34	0.47	0.78	0.83	0.87	1.00
ÞÓRSMÖRK	ÞIG1a	0.21	-	-	-	-	-	-	-	-
IGNIMBRITE	ÞIG1b	0.26	0.76	0.10	0.34	0.47	0.78	0.83	0.87	1.00
		0.26	0.64	0.05	0.40	0.52	0.80	0.85	0.88	1.00
	ÞIG1c	0.38	-	-	-	-	-	-	-	-
	ÞIG1d	0.24	0.50	0.06	0.48	0.58	0.83	0.87	0.90	1.00
		0.24	0.50	0.22	0.48	0.58	0.83	0.87	0.90	1.00
	ÞIG2	0.17	0.46	0.21	0.38	0.51	0.80	0.85	0.88	1.00
	ÞIG3	0.31	0.83	0.03	0.37	0.50	0.79	0.84	0.87	1.00
	[6] ÞIG5:S4	0.05	1.16	0.15	0.04	0.23	0.68	0.76	0.81	1.00
	ÞIG7	0.27	0.87	0.02	0.31	0.45	0.77	0.83	0.86	1.00
		0.27	0.91	0.09	0.30	0.44	0.77	0.83	0.86	1.00
	ÞIG11	0.40	1.05	0.08	0.38	0.51	0.80	0.85	0.88	1.00
	ÞIG13	0.17	-	-	-	-	-	-	-	-
	[6] ÞIG16A	0.11	1.28	0.13	0.09	0.27	0.70	0.77	0.82	1.00

[1] (wt sample - dry wt) / (dry wt)
[2] (wt sat sample - dry wt) / (dry wt)
[3] assuming the average water content during burial = measured water content
[4] %of time spent @ saturation value : % of time spent at measured water content value
[5] error value carries throughout F_1-F_7
[6] highly pumiceous samples
W=W_7 (i.e. dose rate in the surrounding sediment = dose rate in the tephra)
* = estimated H_2O dry value

Table C4.5 (a) Fractional water content (W) and the influence of proportional variations in average fractional water content (F1-F7) scenarios outlined in **(b)** overpage. Terms are as defined in **(b)** overpage.

(b) Icelandic Tephra: Palaeowater content scenarios

F1: Average, 'as-found' model (minimum saturation model)
Average water content = measured water content for the whole time since burial

F2: Glacial cycle saturation model (with no seasonal variations/no snow patch formation in winter)
Milankovitch timescales: 20,000 years at full saturation per 100,000 year glacial cycle; 80,000 years as measured
Sub-Milankovitch Timescale: 5000 years at full saturation in full interglacial

Tephra	Age	% & time at full saturation
Óþoli	2.3 Ma	20%: 0.5 Ma
ÞIG samples	50 ka	20%: 10 ka
Ö1362	640 years	8%: 50 years
A1875	125 years	0%: 0 years

F3: Glacial cycle saturation model with snow patches
As F2, but with 8 month seasonal full saturation

Tephra	Age	% & time at full saturation
Óþoli	2.3 Ma	67%: 1.5 Ma
ÞIG samples	50 ka	67%: 33.5 ka
Ö1362	640 years	67%: 430 years
A1875	125 years	67%: 84 years

F4: Glacial cycle saturation model with 75% non-glacial saturation

Tephra	Age	% & time at full saturation
Óþoli	2.3 Ma	75%: 1.7 Ma
ÞIG samples	50 ka	75%: 38 ka
Ö1362	640 years	66%: 420 years
A1875	125 years	67%: 84 years

F5: Glacial cycle saturation model with 80% non-glacial saturation

Tephra	Age	% & time at full saturation
Óþoli	2.3 Ma	80%: 1.8 Ma
ÞIG samples	50 ka	80%: 40 ka
Ö1362	640 years	92%: 590 years
A1875	125 years	80%: 100 years

F6: 100% saturation model

(a) MAAD 1

G1/G3	TEMPERATURE (°C)	G3=600 Gy				PH=16 hrs@135 C																G2/G3	TEMPERATURE (°C)	G3=600 Gy				PH=16 hrs@135 C															
SET A	DOSE (Gy)	200	210	220	230	240	250	260	270	280	290	300	310	320	330	340	350	360	370	380	390	SET A	DOSE (Gy)	200	210	220	230	240	250	260	270	280	290	300	310	320	330	340	350	360	370	380	390
1	150	5.08	4.35	4.70	4.38	4.67	4.67	4.80	4.80	4.90	4.80	4.60	4.37	4.00	3.77	3.31	3.04	2.84	2.81	2.87	2.69	1	1200	2.47	1.99	2.10	1.96	1.97	1.88	1.82	1.72	1.67	1.63	1.55	1.54	1.51	1.55	1.47	1.50	1.41	1.51	1.76	1.49
2	300	2.04	1.55	1.75	1.74	1.77	1.83	2.02	2.23	2.30	2.42	2.33	2.24	2.13	1.88	1.63	1.40	1.17	1.03	0.89	0.93	2	1050	1.13	1.10	1.10	1.13	1.06	1.08	1.12	1.20	1.22	1.31	1.28	1.36	1.41	1.36	1.35	1.32	1.30	1.26	1.25	1.37
3	450	9.17	10.55	4.93	6.88	6.36	6.92	7.28	7.65	8.42	8.32	8.15	7.84	7.40	6.41	5.80	5.41	5.08	5.48	7.32	7.96	3	900	2.74	4.34	1.98	2.57	2.11	2.05	1.89	1.71	1.71	1.58	1.53	1.51	1.52	1.41	1.51	1.48	1.45	1.48	2.06	2.33
4	600	7.30	3.47	5.00	4.84	5.35	5.90	6.40	7.44	8.21	8.84	9.19	8.94	8.47	7.05	6.02	5.45	5.07	4.92	3.09	2.84	4	750	2.04	0.79	1.20	1.26	1.38	1.38	1.32	1.36	1.32	1.32	1.38	1.38	1.38	1.28	1.24	1.30	1.20	1.29	0.86	0.60
5	750	2.02	2.44	2.36	2.35	2.53	2.83	3.30	3.72	4.25	4.51	4.68	4.76	4.47	4.22	3.85	3.42	2.82	2.48	2.32	2.15	5	600	0.85	0.93	0.85	0.85	0.85	0.89	0.94	0.97	1.02	1.02	1.02	1.04	1.03	1.04	1.03	0.99	0.94	0.91	0.94	0.85
6	900	9.71	5.45	5.29	5.60	6.17	6.12	6.93	7.40	8.40	9.14	9.59	9.68	9.36	8.14	7.30	6.16	5.89	4.93	4.54	3.82	6	450	7.44	4.29	3.60	3.63	3.94	4.01	4.44	4.76	5.27	5.80	6.46	6.94	7.60	7.48	7.58	7.36	7.77	7.37	7.98	6.86
7	1050	1.17	1.21	1.13	1.03	1.10	1.15	1.16	1.16	1.16	1.12	1.03	0.93	0.81	0.70	0.59	0.50	0.42	0.36	0.29	0.24	7	300	-0.22	0.03	0.09	0.10	0.11	0.11	0.10	0.11	0.10	0.10	0.09	0.08	0.07	0.07	0.06	0.07	0.05	0.06	0.04	0.04
8	1200	2.75	3.76	3.54	3.56	3.83	3.82	4.13	4.18	4.41	4.32	4.29	4.22	3.78	3.61	3.21	2.98	2.92	2.69	2.50	1.96	8	150	-0.35	-0.04	0.24	0.30	0.33	0.34	0.39	0.38	0.42	0.40	0.41	0.42	0.39	0.39	0.39	0.37	0.42	0.40	0.50	0.35
SET B																						SET B																					
1	150	2.75	2.75	2.70	2.72	2.75	3.10	3.57	3.88	4.36	4.75	5.00	4.98	4.83	4.21	3.73	3.37	3.06	2.97	2.63	2.37	1	1200	1.29	1.48	1.35	1.38	1.28	1.25	1.31	1.27	1.31	1.33	1.37	1.38	1.39	1.34	1.29	1.25	1.28	1.46	1.35	1.58
2	300	2.15	2.82	2.49	2.95	3.25	3.60	3.93	4.45	4.79	5.13	5.15	5.08	4.80	4.40	4.01	3.68	3.10	3.17	2.52	1.88	2	1050	0.92	1.49	1.41	1.52	1.51	1.55	1.47	1.44	1.37	1.30	1.20	1.07	1.05	1.05	1.03	1.07	1.00	1.07	1.07	0.95
3	450	3.89	109.50	4.38	4.03	3.90	4.26	4.94	5.07	5.45	5.86	6.44	6.50	6.67	6.13	5.45	5.12	4.87	4.37	4.39	3.47	3	900	3.07	59.43	2.15	1.81	1.69	1.67	1.67	1.51	1.46	1.43	1.49	1.47	1.56	1.54	1.49	1.51	1.56	1.48	1.56	1.36
4	600	0.00	15.19	4.53	4.60	4.26	4.55	4.94	5.25	5.38	5.52	5.44	5.48	5.32	4.94	4.68	4.12	3.64	3.05	2.71	2.41	4	750	-5.81	6.16	1.81	1.67	1.57	1.54	1.57	1.51	1.46	1.46	1.38	1.37	1.37	1.36	1.40	1.42	1.38	1.21	1.15	1.19
5	750	13.94	7.59	5.88	6.13	6.23	6.55	6.19	5.80	5.34	4.88	4.56	4.11	3.79	3.62	3.30	3.10	2.86	2.56	2.42	2.33	5	600	4.76	2.61	1.98	2.07	1.94	1.83	1.66	1.38	1.16	1.00	0.88	0.80	0.73	0.75	0.69	0.71	0.70	0.69	0.66	0.78
6	900	1.49	1.98	1.83	2.20	2.32	2.39	2.43	2.46	2.50	2.44	2.36	2.18	2.00	1.69	1.51	1.30	1.12	1.00	0.92	0.77	6	450	0.69	0.71	0.71	0.82	0.85	0.80	0.78	0.77	0.79	0.77	0.79	0.77	0.79	0.75	0.77	0.77	0.75	0.73	0.78	0.75
7	1050	0.41	0.41	0.38	0.40	0.42	0.48	0.52	0.58	0.62	0.63	0.62	0.57	0.51	0.45	0.40	0.35	0.32	0.28	0.27	0.26	7	300	0.25	0.24	0.20	0.21	0.20	0.20	0.20	0.21	0.21	0.21	0.21	0.21	0.21	0.20	0.20	0.20	0.20	0.19	0.18	0.20
8	1200	9.08	12.47	13.09	11.77	9.46	8.16	7.55	7.25	7.36	7.09	6.91	6.52	6.17	5.54	4.74	4.52	4.04	3.61	3.01	2.54	8	150	0.24	0.43	0.31	0.35	0.29	0.26	0.27	0.26	0.28	0.27	0.28	0.29	0.31	0.31	0.29	0.29	0.28	0.29	0.41	0.43

(b) MAAD 2

G1/G3	TEMPERATURE (°C)	G3=600 Gy				PH=16 hrs@135 C																G2/G3	TEMPERATURE (°C)	G3=600 Gy				PH=16 hrs@135 C															
SET A	DOSE (Gy)	200	210	220	230	240	250	260	270	280	290	300	310	320	330	340	350	360	370	380	390	SET A	DOSE (Gy)	200	210	220	230	240	250	260	270	280	290	300	310	320	330	340	350	360	370	380	390
1	150	-0.83	0.87	1.84	3.25	3.38	3.74	3.76	4.18	4.50	4.80	5.06	5.09	5.05	4.91	4.51	4.06	3.66	3.41	2.73	2.56	1	1200	0.27	0.53	1.35	1.53	1.57	1.70	1.63	1.78	1.79	1.87	1.84	1.84	1.84	1.81	1.78	1.74	1.72	1.75	1.67	1.51
2	300	5.05	1.43	2.00	1.71	2.10	2.11	2.37	2.59	2.84	3.08	3.40	3.52	3.52	3.42	3.14	2.82	2.40	1.95	1.59	1.38	2	1050	4.41	2.73	2.18	2.04	2.11	2.06	2.00	1.92	1.96	1.99	2.07	2.05	2.10	2.12	2.16	2.20	2.13	2.00	1.94	1.85
3	450	6.66	5.02	5.39	5.63	5.40	5.73	5.58	5.78	5.94	5.71	5.70	5.21	4.88	4.27	3.97	3.60	3.10	2.77	2.44	2.09	3	900	1.35	1.00	1.11	1.26	1.28	1.33	1.27	1.30	1.29	1.22	1.19	1.11	1.09	1.02	1.03	1.04	0.98	1.03	0.97	0.97
4	600	2.86	4.11	3.36	3.85	3.83	4.29	4.95	5.28	5.73	6.28	6.53	6.73	6.84	6.11	5.71	4.88	4.54	3.86	3.37	3.19	4	750	1.41	1.53	1.10	1.09	1.17	1.24	1.31	1.36	1.37	1.44	1.50	1.51	1.60	1.66	1.64	1.62	1.65	1.59	1.50	1.87
5	750	1.92	1.83	2.10	2.08	2.09	2.21	2.30	2.58	2.85	3.16	3.44	3.56	3.48	3.24	2.96	2.64	2.35	2.12	1.80	1.71	5	600	0.49	1.21	1.44	1.42	1.39	1.46	1.43	1.44	1.48	1.51	1.51	1.53	1.51	1.53	1.53	1.52	1.51	1.54	1.45	1.47
6	900	4.14	5.25	4.98	5.24	5.17	5.53	5.53	5.83	6.32	6.44	6.91	6.87	6.54	6.24	5.71	5.53	4.95	4.52	4.37	3.47	6	450	0.21	1.35	1.10	1.23	1.12	1.07	1.05	1.00	1.03	1.01	1.04	1.03	1.03	1.03	1.04	0.99	0.96	0.99	1.04	0.69
7	1050	1.77	3.57	4.58	5.29	5.75	6.29	6.27	7.05	7.42	7.57	7.63	7.49	7.04	6.76	5.90	5.32	5.01	4.20	3.94	3.35	7	300	0.54	1.08	0.55	0.82	0.85	0.79	0.71	0.72	0.69	0.72	0.68	0.67	0.68	0.73	0.68	0.69	0.70	0.69	0.73	0.71
8	1200	5.29	6.50	8.00	4.59	4.58	4.80	4.72	5.16	5.62	5.89	6.05	6.01	5.99	5.82	5.48	5.10	5.04	4.26	4.16	3.31	8	1200	-0.71	0.58	0.98	0.55	0.58	0.52	0.53	0.47	0.46	0.48	0.48	0.46	0.43	0.48	0.47	0.48	0.52	0.46	0.58	0.52
SET B																						SET B																					
1	150	3.88	5.78	4.26	5.39	4.98	5.17	5.44	5.57	5.69	5.87	5.89	5.39	5.03	4.83	4.03	3.52	3.19	3.19	2.48	1.82	1	1050	3.45	3.76	2.65	2.80	2.56	2.41	2.35	2.18	2.03	2.02	1.92	1.77	1.72	1.74	1.61	1.53	1.57	1.67	1.57	1.16
2	300	1.46	1.22	1.70	1.97	1.90	2.06	2.21	2.55	2.94	3.36	3.72	4.11	4.11	4.00	3.74	3.50	3.01	2.74	2.59	2.38	2	900	2.23	1.01	2.30	2.25	2.06	1.90	1.85	1.84	1.85	1.80	1.78	1.80	1.80	1.73	1.72	1.76	1.62	1.64	1.74	1.82
3	450	16.05	5.47	3.39	3.45	3.76	3.55	4.03	3.85	3.89	4.11	4.25	4.24	4.20	3.81	3.59	3.28	2.83	2.54	2.35	2.01	3	750	7.05	1.35	1.09	1.35	1.13	1.27	1.29	1.10	1.06	1.10	1.07	1.06	1.09	1.00	1.00	0.99	0.96	0.92	0.90	1.00
4	600	5.93	5.51	4.94	5.70	5.81	6.06	6.33	6.85	7.14	7.52	7.72	7.32	6.87	6.41	5.74	5.27	4.76	4.23	3.76	3.65	4	600	1.34	0.80	0.83	0.96	1.03	1.03	1.17	1.22	1.33	1.39	1.47	1.47	1.45	1.49	1.47	1.46	1.47	1.53	1.41	1.59
5	750	28.75	-77.71	6.91	5.13	6.70	5.99	6.42	6.76	6.87	6.96	7.06	6.86	6.94	6.65	6.34	5.43	4.91	4.64	4.43	4.13	5	450	17.17	-25.71	3.04	1.71	1.88	1.77	1.61	1.61	1.46	1.42	1.31	1.25	1.23	1.21	1.25	1.18	1.22	1.26	1.28	1.40
6	900	7.71	6.79	6.13	6.56	6.65	6.39	6.26	6.27	6.05	5.96	5.60	5.37	4.91	4.50	4.01	3.72	3.29	3.06	2.61	2.12	6	300	0.75	0.81	0.87	0.84	0.92	0.88	0.89	0.92	0.93	0.97	0.96	0.96	0.93	0.92	0.86	0.87	0.86	0.90	0.77	0.77
7	1050	5.99	7.31	6.87	7.80	7.45	8.24	8.29	8.34	8.48	8.57	8.31	7.67	7.40	6.80	6.12	5.84	5.21	4.66	3.74	3.94	7	150	0.76	1.09	0.72	1.02	0.89	0.93	0.92	0.90	0.90	0.90	0.88	0.87	0.90	0.90	0.85	0.87	0.84	0.87	0.91	1.03
8	1200	7.27	11.37	7.85	7.26	8.41	8.19	8.36	8.54	8.93	8.97	8.87	8.61	7.94	7.75	7.29	6.41	6.31	5.19	4.79	5.46	8	150	-0.12	0.55	0.77	0.59	0.55	0.52	0.49	0.48	0.44	0.47	0.45	0.50	0.50	0.53	0.59	0.49	0.63	0.79	0.57	0.68

(c) MAAD 3

G1/G3	TEMPERATURE (°C)	G3=1200 Gy				PH=5 hrs@155 C																G2/G3	TEMPERATURE (°C)	G3=1200 Gy				PH=5 hrs@155 C															
SET A	DOSE (Gy)	200	210	220	230	240	250	260	270	280	290	300	310	320	330	340	350	360	370	380	390	SET A	DOSE (Gy)	200	210	220	230	240	250	260	270	280	290	300	310	320	330	340	350	360	370	380	390
1	300	1.08	1.27	4.07	6.72	7.39	6.44	5.82	6.05	5.54	5.28	5.13	4.59	4.33	4.11	3.56	3.26	2.94	2.59	2.37	2.17	1	2400	-1.33	1.37	2.73	3.36	3.87	3.29	2.89	2.80	2.61	2.41	2.27	1.99	1.85	1.85	1.70	1.72	1.68	1.57	1.67	1.54
2	600	3.04	13.00	7.92	7.44	6.91	6.29	5.73	5.90	5.56	5.35	5.04	4.98	4.42	4.15	3.89	3.27	2.90	2.87	2.51	2.68	2	2100	0.53	-2.15	1.28	1.85	2.39	2.11	1.99	1.99	1.80	1.72	1.61	1.65	1.58	1.61	1.64	1.58	1.53	1.66	1.49	1.71
3	900	0.08	20.90	4.66	8.84	4.82	5.58	5.46	5.56	5.17	4.75	4.84	4.48	4.38	4.13	3.83	3.51	3.13	2.98	2.63	2.36	3	1800	-1.15	-1.30	-4.30	-0.78	1.95	2.50	2.32	2.23	2.20	1.99	1.95	1.83	1.71	1.60	1.55	1.55	1.46	1.48	1.37	1.32
4	1200	9.88	8.45	9.07	7.58	6.75	6.52	6.88	6.53	6.26	6.22	6.00	5.67	5.24	4.89	4.11	3.81	3.41	3.25	3.00	2.53	4	1500	-0.02	0.59	1.70	1.34	1.43	1.51	1.59	1.53	1.49	1.51	1.45	1.45	1.43	1.42	1.32	1.36	1.29	1.33	1.37	1.20
5	1500	5.45	9.02	4.17	7.22	6.52	5.99	6.56	6.08	6.36	6.11	5.93	5.38	5.26	4.74	4.20	3.81	3.52	3.08	2.87	2.52	5	1200	7.23	10.38	2.55	2.19	1.84	1.51	1.64	1.42	1.49	1.35	1.32	1.19	1.20	1.19	1.22	1.20	1.14	1.06	1.04	0.90
6	1800	-0.24	8.48	13.33	23.07	12.06	10.36	10.96	10.39	9.44	7.85	7.36	6.46	5.64	5.07	4.41	3.95	3.49	3.12	2.81	2.59	6	900	0.82	3.91	1.02	1.49	1.46	1.56	1.40	1.63	1.50	1.30	1.27	1.20	1.11	1.07	1.00	0.97	0.94	0.91	0.86	1.02
7	2100	-1.52	-0.38	5.28	6.09	4.76	7.28	6.61	7.00	6.04	6.09	5.75	5.51	5.31	4.78	4.40	4.02	3.70	3.49	3.13	2.72	7	600	0.15	-0.24	-0.37	0.76	0.91	1.12	1.06	1.08	0.94	0.95	0.90	0.84	0.85	0.79	0.78	0.79	0.75	0.81	0.82	0.79
8	2400	-9.94	30.32	9.81	10.48	8.30	7.51	7.45	7.08	6.90	6.71	6.43	5.92	5.65	5.28	4.72	4.33	3.97	3.63	3.67	3.34	8	300	-1.18	4.32	0.99	0.68	0.55	0.48	0.49	0.51	0.53	0.47	0.48	0.45	0.46	0.47	0.48	0.46	0.45	0.47	0.53	0.53
SET B																						SET B																					
1	300	4.66	2.96	4.17	2.83	2.86	3.03	2.92	3.00	3.10	3.29	3.23	3.03	2.82	2.45	2.15	1.82	1.60	1.42	1.29	1.17	1	2400	2.35	2.24	2.17	1.75	1.73	1.89	1.79	1.82	1.75	1.81	1.76	1.66	1.61	1.52	1.45	1.34	1.32	1.26	1.30	1.30
2	600	2.24	8.68	9.50	9.38	10.42	8.00	8.11	7.74	6.85	6.52	6.11	5.20	4.61	4.18	3.68	3.31	2.87	2.69	2.20	2.00	2	2100	-0.82	-2.92	1.79	1.78	2.37	2.07	2.20	2.30	2.12	2.07	1.97	1.76	1.69	1.60	1.53	1.52	1.48	1.50	1.38	1.43
3	900	3.08	3.05	3.52	3.67	3.89	3.81	3.55	3.76	3.67	3.57	3.53	3.53	3.54	3.42	3.32	2.86	2.66	2.48	2.16	1.94	3	1800	1.75	2.08	1.48	1.93	1.82	1.67	1.56	1.63	1.50	1.39	1.33	1.30	1.33	1.34	1.38	1.31	1.32	1.34	1.15	1.13
4	1200	-22.00	13.33	3.46	2.91	3.22	3.55	3.38	3.32	3.26	3.21	3.52	4.02	4.32	4.45	4.16	3.91	3.49	3.18	2.90	2.38	4	1500	-9.89	12.44	1.45	1.15	0.99	1.10	1.11	1.02	0.98	0.95	0.99	1.12	1.23	1.29	1.27	1.36	1.29	1.29	1.30	1.15
5	1500	-0.20	1.01	1.75	1.79	1.88	1.93	1.72	2.00	2.09	2.37	2.70	2.88	2.99	3.08	3.00	2.78	2.63	2.50	2.30	2.05	5	1200	-0.57	-0.71	1.68	1.47	1.81	1.86	1.74	1.75	1.80	1.84	1.98	2.00	1.89	1.96	1.88	1.84	1.78	1.85	1.77	1.68
6	1800	0.91	-2.99	6.21	3.57	3.98	3.81	4.20	4.50	4.37	4.06	4.14	4.10	3.85	3.76	3.67	3.22	3.09	2.90	2.44	2.29	6	900	-0.24	0.21	0.13	0.21	0.20	0.58	0.74	0.66	0.69	0.74	0.80	0.86	0.86	0.91	1.00	1.04	1.06	1.07	0.92	0.97
7	2100	4.05	4.74	4.82	5.95	6.91	7.04	6.56	7.09	6.77	6.83	6.21	5.92	5.71	5.23	4.89	4.36	3.90	3.49	3.42	3.02	7	600	0.15	-0.01	0.36	0.52	0.48	0.76	0.78	0.89	0.80	0.81	0.76	0.76	0.78	0.78	0.71	0.71	0.65	0.73	0.62	0.67
8	2400	-4.32	-38.93	9.06	10.23	8.78	8.75	8.53	8.19	7.38	6.83	6.51	5.69	5.13	4.64	4.21	3.66	3.56	3.31	2.86	2.61	8	300	1.13	1.71	0.81	0.32	0.67	0.56	0.68	0.63	0.56	0.52	0.52	0.51	0.48	0.47	0.50	0.42	0.49	0.51	0.54	0.64

Table C4.6 (a)-(c) MAAD-TL runs 1-3: G1/G2 and G2/G3 10°C ratio data used to construct Figure 4.22. Full G1-G4 1°C and 10°C datasets can be found on the CD-R

(d) MAAD 4

G1/G3	TEMPERATURE (°C)	G3=600 Gy	PH=16 hrs@135 C	DISC CENTRED																	G2/G3	TEMPERATURE (°C)	G3=600 Gy	PH=16 hrs@135 C																	
SET A	DOSE (Gy)	200	210	220	230	240	250	260	270	280	290	300	310	320	330	340	350	360	370	380	390	SET A	DOSE (Gy)	200	210	220	230	240	250	260	270	280	290	300	310	320	330	340	350	360	370	380	390
1	150	4.40	1.95	1.76	1.73	1.88	2.07	2.09	2.14	2.45	2.55	2.66	2.70	2.82	2.93	2.72	2.60	2.38	2.03	1.62	1.36	1	1200	4.10	0.38	0.32	0.53	0.49	0.74	0.71	0.84	0.96	1.15	1.30	1.48	1.61	1.82	1.78	1.83	1.68	1.66	1.53	1.62
2	300	3.00	3.55	2.59	3.09	3.24	3.23	3.34	3.21	3.23	3.14	3.01	2.75	2.53	2.30	2.19	1.93	1.67	1.55	1.05	0.95	2	1050	1.81	1.59	1.30	1.59	1.58	1.57	1.60	1.54	1.54	1.43	1.32	1.16	1.06	0.97	0.98	0.98	0.86	0.91	0.81	0.84
3	450	12.06	4.81	5.63	4.19	4.30	4.10	4.04	3.69	3.49	3.39	3.44	3.45	3.32	3.39	3.29	2.92	2.76	2.79	2.60	1.74	3	900	3.84	1.47	1.68	1.32	1.35	1.41	1.48	1.44	1.41	1.43	1.46	1.42	1.36	1.45	1.44	1.49	1.45	1.73	2.01	1.80
4	600	12.00	3.40	-15.04	2.90	3.72	3.23	3.49	3.41	3.36	3.45	3.31	3.31	3.48	3.31	3.30	3.07	2.91	2.58	2.30	1.92	4	750	-0.71	0.69	-3.43	0.48	0.83	0.68	0.73	0.80	0.94	1.07	1.11	1.22	1.31	1.35	1.40	1.35	1.42	1.36	1.31	1.31
5	750	5.42	7.30	4.78	5.30	5.46	5.38	4.65	4.51	3.82	3.83	3.46	3.32	3.11	2.86	2.47	2.20	1.91	1.77	1.48	1.00	5	600	0.98	1.04	0.81	0.89	0.92	0.98	0.88	0.89	0.80	0.81	0.73	0.77	0.72	0.73	0.69	0.70	0.67	0.61	0.61	0.35
6	900	2.02	2.77	3.65	4.13	4.62	4.55	4.65	4.05	4.21	3.89	3.85	3.70	3.67	3.57	3.40	3.20	2.66	2.30	2.45	1.75	6	450	0.30	0.44	0.51	0.54	0.52	0.60	0.66	0.68	0.72	0.71	0.77	0.75	0.79	0.76	0.81	0.84	0.77	0.77	0.99	0.87
7	1050	5.09	6.08	5.13	4.67	4.42	4.34	3.88	3.79	3.43	3.47	3.45	3.48	3.59	3.49	3.40	2.96	2.85	2.55	2.05	1.49	7	300	0.40	0.41	0.49	0.45	0.44	0.47	0.48	0.55	0.58	0.60	0.65	0.68	0.74	0.72	0.73	0.73	0.72	0.77	0.54	0.52
8	1200	22.71	5.13	5.47	6.03	5.40	5.08	5.07	4.56	4.20	4.09	3.91	3.85	3.69	3.78	3.65	3.49	2.73	3.08	2.16	1.96	8	150	3.35	0.44	0.19	0.32	0.31	0.27	0.30	0.32	0.37	0.39	0.38	0.39	0.38	0.44	0.44	0.46	0.46	0.43	0.40	0.61
SET B																						SET B																				
1	150	2.63	2.86	3.24	2.83	3.13	3.18	2.95	2.97	3.08	3.06	3.08	3.03	3.04	2.93	2.71	2.57	2.23	1.94	1.76	1.79	1	1200	1.49	1.13	1.78	1.62	1.78	1.74	1.59	1.65	1.75	1.64	1.65	1.55	1.56	1.54	1.58	1.58	1.50	1.48	1.49	1.45
2	300	1.69	1.70	2.03	1.88	1.77	1.89	1.75	1.84	1.80	1.75	1.68	1.64	1.54	1.39	1.27	1.12	0.93	0.71	0.64	0.55	2	1050	0.19	0.71	0.60	0.75	0.66	0.67	0.62	0.66	0.63	0.60	0.59	0.58	0.52	0.51	0.49	0.46	0.43	0.42	0.46	0.45
3	450	4.22	6.25	3.63	3.75	4.23	4.16	4.02	4.20	4.12	4.43	4.42	4.54	4.37	4.09	4.00	3.63	3.80	2.67	2.54	1.61	3	900	1.44	1.85	1.05	1.08	1.04	1.22	1.18	1.36	1.27	1.50	1.54	1.51	1.53	1.59	1.47	1.53	1.92	1.34	1.45	1.26
4	600	3.00	4.14	3.80	4.46	4.01	4.49	4.35	3.93	4.04	4.10	4.07	4.02	3.75	3.58	3.62	3.34	2.71	2.70	2.41	1.42	4	750	0.62	1.17	0.99	1.10	0.95	1.18	1.15	1.13	1.18	1.25	1.24	1.23	1.16	1.18	1.34	1.28	1.21	1.32	1.32	0.87
5	750	1.35	1.41	1.77	1.85	2.09	2.40	2.63	2.62	2.85	3.00	3.00	3.17	2.99	2.83	2.63	2.40	2.29	2.05	2.09	2.12	5	600	0.43	0.51	0.75	0.67	0.65	0.71	0.70	0.70	0.76	0.76	0.68	0.69	0.68	0.69	0.64	0.70	0.68	0.67	0.68	1.05
6	900	0.69	0.83	0.82	0.75	0.76	0.71	0.65	0.56	0.46	0.39	0.30	0.24	0.21	0.18	0.16	0.13	0.10	0.09	0.06	0.05	6	450	1.20	1.45	1.47	1.40	1.55	1.56	1.53	1.45	1.35	1.26	1.03	0.90	0.86	0.79	0.78	0.71	0.64	0.66	0.62	0.59
7	1050	4.85	4.05	3.66	3.43	3.31	3.13	2.93	2.82	2.64	2.57	2.52	2.48	2.26	2.29	2.11	1.87	1.69	1.53	1.21	0.95	7	300	0.25	0.41	0.41	0.31	0.31	0.33	0.32	0.34	0.35	0.34	0.33	0.33	0.31	0.35	0.33	0.32	0.24	0.31	0.26	0.29
8	1200	11.08	2.72	3.95	7.96	4.14	4.53	4.95	5.04	5.02	4.62	4.76	4.95	4.56	4.85	4.41	4.30	3.61	3.25	3.29	2.31	8	150	1.08	0.18	0.21	0.47	0.29	0.19	0.23	0.27	0.30	0.28	0.34	0.36	0.37	0.39	0.36	0.42	0.44	0.37	0.45	0.28

(e) MAAD 5

G1/G3	TEMPERATURE (°C)	G3=600 Gy	PH=5 hrs@155 C	DISC CENTRED																	G2/G3	TEMPERATURE (°C)	G3=600 Gy	PH=16 hrs@135 C																	
SET A	DOSE (Gy)	200	210	220	230	240	250	260	270	280	290	300	310	320	330	340	350	360	370	380	390	SET A	DOSE (Gy)	200	210	220	230	240	250	260	270	280	290	300	310	320	330	340	350	360	370	380	390
1	300	2.40	0.57	5.11	3.17	3.37	3.84	4.08	3.97	4.63	5.12	5.10	5.33	4.83	4.56	4.40	3.74	3.74	2.97	2.49	3.38	1	2400	1.44	1.46	4.34	1.95	2.24	2.44	2.40	2.31	2.48	2.54	2.45	2.63	2.54	2.57	2.76	2.64	2.65	2.35	2.06	2.91
2	600	1.47	0.83	1.26	8.33	4.45	3.32	4.38	4.33	4.78	4.84	4.87	5.58	5.32	5.55	5.27	5.39	4.68	4.68	3.89	3.04	2	2100	1.21	1.45	1.33	3.15	2.22	2.16	2.54	2.30	2.49	2.41	2.31	2.51	2.35	2.39	2.23	2.52	2.34	2.60	2.39	1.93
3	900	0.60	2.45	7.67	7.63	11.39	8.49	8.93	9.48	8.93	8.46	7.88	7.79	7.54	6.72	6.33	5.80	5.51	5.03	4.29	4.47	3	1800	0.37	0.49	1.71	1.38	2.98	2.29	2.22	2.40	2.30	2.24	2.18	2.29	2.37	2.25	2.30	2.31	2.51	2.60	2.10	2.78
4	1200	1.38	2.47	2.85	8.08	13.55	8.46	8.06	8.85	8.43	8.45	8.55	8.03	7.52	7.02	6.28	5.90	4.98	4.23	3.91	4.36	4	1500	0.51	1.18	2.50	1.56	4.73	2.87	2.91	2.92	2.68	2.47	2.36	2.17	2.11	2.07	2.05	2.11	1.79	1.63	1.40	1.46
5	1500	1.10	2.00	2.48	8.98	24.17	12.35	15.09	8.87	11.55	8.94	9.22	7.43	7.15	6.68	6.62	5.50	5.23	4.51	3.97	3.39	5	1200	0.77	1.61	0.41	0.96	5.42	3.03	2.95	2.04	2.68	1.97	2.22	1.82	1.83	1.85	1.95	1.82	1.85	1.78	1.59	1.60
6	1800	2.18	5.19	10.05	8.39	5.84	6.62	7.12	6.95	7.41	7.66	7.57	7.50	7.43	6.61	6.28	5.85	5.16	5.11	4.58	3.68	6	900	0.65	1.36	1.30	0.52	0.95	1.09	1.16	1.19	1.22	1.33	1.28	1.32	1.42	1.36	1.33	1.48	1.44	1.48	1.72	1.47
7	2100	1.80	10.73	11.34	23.50	16.52	7.58	7.94	8.32	8.60	8.02	8.54	8.55	8.17	7.52	6.78	6.42	6.17	5.16	4.46	4.22	7	600	1.04	1.91	0.90	1.17	1.41	0.82	0.86	0.90	1.02	0.98	1.05	1.10	1.12	1.16	1.13	1.11	1.26	1.16	1.19	1.27
8	2400	5.44	1.60	4.06	12.29	4.42	7.23	8.33	6.39	6.13	6.54	6.95	7.07	7.07	6.90	6.80	6.65	5.87	5.26	4.79	4.71	8	300	1.44	0.66	0.45	1.92	0.46	0.64	1.08	0.76	0.77	0.81	0.80	0.83	0.79	0.81	0.77	0.81	0.83	0.86	0.68	0.77
SET B																						SET B																				
1	600	1.19	2.97	4.05	3.58	3.24	4.33	4.35	4.24	4.46	4.85	5.32	5.42	5.58	5.41	5.17	4.69	4.65	4.18	3.73	3.46	1	4800	1.68	1.94	1.49	3.33	2.75	4.30	4.25	3.97	4.03	3.95	3.98	3.89	3.84	3.85	3.92	3.74	4.04	4.20	4.13	3.80
2	1200	2.38	1.65	5.53	8.00	3.18	3.88	3.92	4.48	4.77	4.98	5.41	6.17	6.14	6.30	6.32	5.50	5.14	4.61	4.13	3.57	2	4200	2.12	1.23	4.59	6.37	2.72	3.42	3.29	3.56	3.61	3.51	3.42	3.56	3.45	3.56	3.70	3.50	3.49	3.42	3.25	3.12
3	1800	1.84	5.47	10.36	7.70	6.92	7.52	8.69	8.64	8.14	8.12	8.41	8.23	7.90	7.21	6.36	5.72	5.34	4.63	4.10	3.30	3	3600	0.26	3.31	4.53	3.23	2.93	3.58	3.72	3.84	3.38	3.24	3.40	3.44	3.55	3.55	3.44	3.41	3.31	3.21	2.87	2.55
4	2400	4.62	6.91	12.00	12.92	10.27	9.29	9.06	8.65	8.82	8.27	8.08	7.82	7.23	6.42	5.82	5.50	4.50	3.98	3.46	4.07	4	3000	1.05	2.56	5.55	6.38	4.58	4.54	4.27	3.80	3.74	3.46	3.30	3.16	2.93	2.78	2.73	2.70	2.36	2.13	2.03	2.51
5	3000	1.34	1.68	3.04	7.72	18.35	10.07	10.05	12.25	9.41	9.70	9.04	8.79	8.83	8.46	7.35	7.00	6.65	5.70	5.65	5.00	5	2400	0.95	0.76	1.09	2.83	6.20	3.49	3.57	3.96	3.08	3.12	2.94	2.88	2.75	2.82	2.69	2.68	2.83	2.51	2.69	2.46
6	3600	1.83	1.37	3.35	10.53	19.71	6.97	7.46	7.82	7.89	8.03	8.29	8.94	8.47	8.64	8.12	7.42	6.43	6.85	5.93	5.19	6	1800	1.28	1.11	0.88	3.03	2.29	2.01	1.83	1.89	2.03	2.07	2.14	2.42	2.32	2.44	2.48	2.36	2.26	2.64	2.67	2.31
7	4200	1.84	1.96	5.24	14.91	19.51	7.63	8.10	7.60	7.97	7.70	7.63	7.75	7.27	7.01	6.75	6.66	6.17	6.01	5.42	4.81	7	1200	0.82	0.44	1.70	5.45	6.89	2.58	2.83	2.66	2.69	2.47	2.32	2.17	1.91	1.86	1.81	1.83	1.78	1.75	1.78	1.76
8	4800	1.27	1.47	1.56	1.31	2.01	3.59	2.91	2.54	2.85	3.74	4.50	5.09	6.09	6.80	6.86	7.77	7.73	7.66	6.73	6.12	8	600	1.16	0.97	1.00	0.29	0.73	0.74	0.74	0.67	0.70	0.80	0.93	0.98	1.08	1.12	1.13	1.24	1.23	1.37	1.27	1.32

Table C4.6 (d)-(e) MAAD-TL runs 4-5: G1/G2 and G2/G3 10°C ratio data used to construct Figure 4.22. Full G1-G4 1°C and 10°C datasets can be found on the CD-R

SUTL551: UNCORRECTED REGENERATION GROWTH CURVE: DISCS 1-8 MEAN + STD ERROR

DOSE (Gy)	200-210		210-220		220-230		230-240		240-250	
0	0.0	0.0	0.0	0.0	0.0	0.0	0.0	0.0	0.0	0.0
500	42.0	6.9	47.9	5.0	98.1	9.9	202.9	21.6	390.0	29.9
1000	51.8	7.2	102.5	9.9	180.8	26.7	395.8	44.6	702.0	72.3
1500	91.6	14.2	153.3	16.9	260.5	20.3	500.4	42.3	938.8	88.1
2000	123.0	17.0	210.9	24.1	397.0	58.5	739.8	95.0	1366.8	160.8
2500	122.5	18.8	241.9	30.2	451.5	60.2	835.1	111.7	1492.0	166.4
3000	129.5	33.2	259.6	66.2	444.5	128.5	826.0	217.5	1562.3	403.0
4000	197.9	16.0	319.4	35.6	562.3	69.4	1011.3	129.1	1899.5	202.8
5000	140.8	15.1	282.4	36.7	474.9	61.3	917.3	124.3	1765.1	229.8
6000	180.0	29.5	341.2	53.2	600.0	100.1	1129.4	185.3	2109.4	308.5
N	77.5	10.9	124.3	16.6	313.9	33.6	605.5	68.2	1283.3	116.8

DOSE (Gy)	250-260		260-270		270-280		280-290		290-300	
0	0.0	0.0	0.0	0.0	0.0	0.0	0.0	0.0	0.0	0.0
500	744.0	74.0	1242.6	119.8	1893.4	155.1	2694.9	235.5	3403.6	273.2
1000	1274.3	125.6	2139.9	201.7	3235.3	281.0	4509.9	376.2	5636.6	458.4
1500	1713.9	141.7	2936.8	208.5	4491.8	325.8	6235.4	375.8	7790.9	451.3
2000	2388.9	262.6	3960.8	378.2	6006.8	487.2	8209.3	615.8	9965.1	692.9
2500	2595.8	241.1	4210.8	300.7	6313.1	388.5	8497.3	485.1	10427.8	537.9
3000	2808.4	667.2	4506.4	934.8	6678.4	1291.6	9056.5	1531.6	11001.3	1960.4
4000	3356.0	332.9	5373.9	460.7	7895.8	570.9	10503.9	662.1	12564.1	745.1
5000	3223.4	365.6	5394.8	559.4	8111.3	737.5	10917.8	885.9	13481.0	933.1
6000	3907.8	472.1	6280.2	619.2	9339.8	695.6	12534.6	856.8	15234.6	997.9
N	2387.1	227.5	4178.9	356.1	6804.9	517.1	9993.1	720.8	13101.5	832.3

DOSE (Gy)	300-310		310-320		320-330		330-340		340-350	
0	0.0	0.0	0.0	0.0	0.0	0.0	0.0	0.0	0.0	0.0
500	3838.1	290.0	4094.4	320.1	4032.9	293.5	3836.5	293.8	3666.5	274.2
1000	6354.8	487.3	6622.6	516.7	6551.6	470.3	6313.5	420.6	6000.3	398.5
1500	8880.9	470.9	9327.6	546.9	9272.8	524.0	8997.5	504.0	8388.3	456.4
2000	11249.4	742.5	11682.0	782.7	11672.1	779.2	11280.5	720.5	10708.6	674.7
2500	11564.6	594.3	12147.0	601.0	12377.6	650.4	11948.8	594.5	11288.3	531.9
3000	12440.0	2240.3	13194.6	2300.0	13672.3	2513.5	13559.5	2602.5	13129.6	2524.1
4000	14026.5	849.8	14806.4	930.0	15232.1	880.2	14949.0	841.3	14454.3	809.3
5000	15266.0	932.4	16417.8	969.1	16888.9	992.5	16890.6	1045.1	16554.3	1002.7
6000	17270.2	1188.2	18360.4	1351.5	18953.2	1365.8	19117.4	1427.6	18577.4	1284.1
N	15435.3	887.2	16528.1	973.0	16101.9	990.1	14786.3	959.7	12907.8	864.3

DOSE (Gy)	350-360		360-370		370-380		380-390		390-400	
0	0.0	0.0	0.0	0.0	0.0	0.0	0.0	0.0	0.0	0.0
500	3252.5	224.8	2857.9	226.9	2437.1	209.8	1970.6	206.5	1590.5	131.9
1000	5331.3	307.7	4565.0	276.0	3824.4	204.9	3022.6	194.4	2483.3	188.1
1500	7534.5	437.2	6353.5	408.0	5331.8	410.9	4465.1	330.2	3516.9	328.0
2000	9688.0	651.6	8429.6	681.5	6988.8	644.9	5757.3	553.6	4537.0	424.0
2500	10271.0	502.6	8752.4	492.3	7158.6	465.7	5787.5	402.6	4499.9	321.1
3000	12110.1	2300.2	10572.5	2251.7	8835.6	2106.8	6897.4	1708.0	5378.6	1190.7
4000	13144.8	678.7	11231.1	635.5	8985.0	532.2	7201.9	447.7	5469.5	364.2
5000	15316.3	932.7	13179.1	873.6	10907.6	949.5	8706.9	963.1	6901.4	732.6
6000	17518.8	1180.5	15258.6	1240.2	12495.8	1249.4	9719.2	1082.0	7370.8	958.4
N	11070.6	737.5	9307.5	619.8	7688.5	482.5	6375.5	403.6	4997.3	356.6

Table C4.7(a) Uncorrected SAR-TL 200-400°C 10°C for data the Óþoli Tephra (SUTL 551) data used to construct Figure 4.23. Shaded area corresponds to the glow curve peak positions and stable temperature plateau. Full 1°C and 10°C data and individual regression fitting analysis can be found in the enclosed CD-R.

SUTL551: DOSE CORRECTED REGENERATION GROWTH CURVE: DISCS 1-8 MEAN + STD ERROR

DOSE (Gy)	200-210		210-220		220-230		230-240		240-250	
0	0.0	0.0	0.0	0.0	0.0	0.0	0.0	0.0	0.0	0.0
500	2.1	0.5	2.3	0.4	6.0	1.6	8.1	2.3	8.2	2.3
1000	3.1	0.7	2.9	0.6	5.3	1.0	5.8	1.1	5.9	0.5
1500	2.2	0.4	9.4	4.0	7.6	1.3	11.5	2.4	8.4	0.9
2000	3.0	0.5	4.5	0.5	6.7	0.8	7.4	1.2	8.5	0.9
2500	4.1	2.5	6.0	2.5	7.0	3.7	9.6	3.3	9.4	1.7
3000	4.3	0.8	7.0	2.1	7.8	1.1	8.6	1.3	9.7	0.7
4000	5.5	0.9	7.3	0.9	8.8	1.1	11.9	1.2	13.2	1.6
5000	7.1	1.9	12.2	3.0	8.0	1.2	10.6	1.0	12.2	1.5
6000	5.8	2.3	29.8	15.2	10.6	1.8	14.6	1.6	16.2	2.4
N	7.2	1.4	12.0	3.5	34.1	13.7	17.8	3.0	36.0	9.4

DOSE (Gy)	250-260		260-270		270-280		280-290		290-300	
0	0.0	0.0	0.0	0.0	0.0	0.0	0.0	0.0	0.0	0.0
500	7.0	1.7	5.3	0.7	4.8	0.7	4.2	0.1	4.2	0.2
1000	6.6	0.5	7.5	0.7	6.5	0.2	6.6	0.3	6.3	0.3
1500	9.2	0.8	9.3	0.4	9.2	0.5	8.9	0.5	8.4	0.4
2000	9.0	0.6	9.2	0.8	9.6	0.7	9.6	1.0	9.2	0.9
2500	10.2	2.1	10.4	2.1	9.5	1.0	9.5	1.2	9.1	0.9
3000	10.3	0.7	10.6	0.9	10.0	0.5	9.9	0.4	9.6	0.5
4000	14.0	0.9	14.0	0.8	13.5	0.5	13.3	0.6	12.6	0.5
5000	12.5	0.9	13.3	1.4	12.1	1.0	11.5	0.9	11.2	1.1
6000	13.8	0.9	15.3	0.9	14.5	1.3	14.3	1.0	13.7	1.0
N	27.2	6.3	24.3	2.8	20.8	2.0	19.8	1.6	19.3	1.4

DOSE (Gy)	300-310		310-320		320-330		330-340		340-350	
0	0.0	0.0	0.0	0.0	0.0	0.0	0.0	0.0	0.0	0.0
500	4.2	0.2	4.3	0.3	4.5	0.6	4.6	0.6	4.7	0.8
1000	6.1	0.3	6.1	0.3	6.1	0.3	5.7	0.3	6.0	0.5
1500	8.3	0.4	8.2	0.4	8.0	0.4	8.8	0.4	8.5	0.4
2000	9.0	0.8	8.8	0.6	8.5	0.6	9.0	0.6	8.5	0.5
2500	8.8	1.2	8.6	1.3	8.7	1.2	8.6	1.4	8.8	1.7
3000	9.3	0.5	9.7	0.5	10.1	0.6	10.2	0.5	10.3	0.4
4000	12.2	0.6	12.2	0.4	12.2	0.5	12.6	0.5	13.3	0.9
5000	11.3	0.9	11.3	0.8	11.9	0.7	13.0	0.6	15.8	1.1
6000	12.8	0.7	12.9	0.6	13.7	0.4	16.1	1.7	18.9	2.9
N	18.7	1.1	18.6	1.7	19.1	2.3	18.7	2.0	18.1	2.4

DOSE (Gy)	350-360		360-370		370-380		380-390		390-400	
0	0.0	0.0	0.0	0.0	0.0	0.0	0.0	0.0	0.0	0.0
500	5.0	0.8	3.9	0.4	3.5	0.3	3.7	0.4	3.6	0.8
1000	6.4	0.8	5.6	0.5	5.1	0.3	5.0	0.6	6.6	1.4
1500	8.1	0.4	8.1	0.5	7.8	0.6	5.8	0.5	5.3	0.6
2000	8.9	0.8	7.9	0.6	7.5	0.8	6.0	0.7	5.5	0.6
2500	8.4	1.3	8.5	2.2	7.3	1.3	7.4	3.5	5.3	2.3
3000	10.7	0.4	11.1	1.1	11.1	1.1	10.9	2.6	6.7	1.1
4000	12.5	1.1	11.5	0.8	10.1	1.5	11.1	2.4	7.6	1.4
5000	16.2	1.3	15.4	1.5	14.6	1.8	16.3	3.6	12.2	2.1
6000	22.4	5.4	19.3	2.3	15.5	2.4	13.1	3.6	14.8	6.0
N	18.3	3.5	12.7	1.6	14.6	2.1	13.0	1.4	12.5	1.7

Table C4.7(b) Test dose corrected SAR-TL 200-400°C 10°C data for the Óþoli Tephra (SUTL 551) data used to construct Figure 4.23. Shaded area corresponds to the glow curve peak positions and stable temperature plateau. Full 1°C and 10°C data and individual regression fitting analysis can be found in the enclosed CD-R.

PIG7: UNCORRECTED REGENERATION GROWTH CURVE: DISCS 1-8 MEAN + STD ERROR

DOSE (Gy)	200-210		210-220		220-230		230-240		240-250	
0	0.0	0.0	0.0	0.0	0.0	0.0	0.0	0.0	0.0	0.0
50	42.9	7.8	35.5	4.6	45.4	7.5	69.9	10.7	137.3	16.8
75	46.6	6.1	45.5	3.8	38.1	5.9	102.5	10.3	180.4	26.7
100	36.3	5.7	36.9	3.7	58.8	8.6	108.1	15.6	221.0	27.3
125	50.6	5.8	60.0	11.8	91.9	12.4	165.6	27.7	359.9	51.8
150	32.9	3.9	41.6	7.0	89.0	13.0	215.1	23.3	434.9	44.0
200	56.4	31.8	70.1	24.1	110.6	50.6	239.9	90.6	510.3	138.5
300	64.3	7.4	75.4	6.9	175.3	15.7	430.8	50.4	952.6	86.3
-	0.0	0.0	0.0	0.0	0.0	0.0	0.0	0.0	0.0	0.0
-	0.0	0.0	0.0	0.0	0.0	0.0	0.0	0.0	0.0	0.0
N	28.6	2.4	33.0	2.0	68.0	11.0	165.1	16.3	454.4	46.7

DOSE (Gy)	250-260		260-270		270-280		280-290		290-300	
0	0.0	0.0	0.0	0.0	0.0	0.0	0.0	0.0	0.0	0.0
50	292.6	38.5	584.6	72.1	1086.5	126.8	1843.8	169.2	2710.6	201.7
75	356.9	39.4	723.3	88.6	1338.4	131.9	2394.8	236.9	3735.3	300.7
100	517.5	63.5	1032.9	95.8	1988.6	186.4	3457.5	276.7	5324.5	330.5
125	758.5	94.2	1568.0	186.4	2916.1	327.3	4987.1	487.5	7435.0	581.3
150	936.4	113.7	1966.8	208.3	3704.4	392.8	6306.6	580.8	9300.5	711.7
200	1125.8	308.4	2326.4	612.2	4397.5	1071.5	7657.6	1674.2	11718.0	1951.2
300	2048.1	189.7	4102.1	337.5	7692.8	576.2	12901.1	814.3	18747.4	890.3
-	0.0	0.0	0.0	0.0	0.0	0.0	0.0	0.0	0.0	0.0
-	0.0	0.0	0.0	0.0	0.0	0.0	0.0	0.0	0.0	0.0
N	1075.1	110.0	2262.4	229.3	4316.1	401.6	7245.9	563.2	10410.9	574.6

DOSE (Gy)	300-310		310-320		320-330		330-340		340-350	
0	0.0	0.0	0.0	0.0	0.0	0.0	0.0	0.0	0.0	0.0
50	3499.8	175.3	3819.3	246.3	3664.9	441.5	3170.9	552.5	2433.4	497.2
75	5012.4	311.6	5755.0	214.1	5637.6	248.3	4980.3	415.3	4173.5	634.3
100	7251.4	319.7	8328.0	343.7	8140.1	565.0	7082.4	712.2	5492.3	629.8
125	9561.9	477.7	10568.6	349.4	10207.1	733.8	8742.9	1043.3	6778.3	976.2
150	11669.9	619.4	12448.3	279.7	11637.8	383.5	9821.8	808.3	7716.6	1054.9
200	15234.6	1993.2	17308.3	1798.8	16611.3	2190.4	14196.0	2683.0	10878.6	2311.3
300	23186.1	946.9	24174.0	1271.3	21918.5	1600.4	17522.5	1461.2	12927.3	1218.9
-	0.0	0.0	0.0	0.0	0.0	0.0	0.0	0.0	0.0	0.0
-	0.0	0.0	0.0	0.0	0.0	0.0	0.0	0.0	0.0	0.0
N	12723.3	366.7	12877.4	556.1	11442.5	948.7	8964.9	1017.9	6487.0	811.8

DOSE (Gy)	350-360		360-370		370-380		380-390		390-400	
0	0.0	0.0	0.0	0.0	0.0	0.0	0.0	0.0	0.0	0.0
50	1764.0	282.5	1230.5	187.1	844.4	133.5	739.4	78.1	620.8	97.9
75	3308.8	733.3	2564.5	659.6	1771.3	430.6	1213.1	242.5	852.4	143.8
100	3835.9	421.8	2757.0	260.7	2040.1	174.9	1425.8	151.3	985.8	85.5
125	4724.0	692.2	3462.8	444.1	2505.3	275.1	1746.9	171.1	1212.9	114.2
150	5863.9	1178.6	4481.4	1096.5	3291.6	768.3	2435.9	500.2	1931.9	239.2
200	7786.6	1862.9	5510.8	1337.3	4110.8	689.8	3032.3	462.2	2268.1	486.6
300	9316.6	905.7	6722.0	613.2	5004.3	363.7	3849.3	235.5	3010.9	214.9
-	0.0	0.0	0.0	0.0	0.0	0.0	0.0	0.0	0.0	0.0
-	0.0	0.0	0.0	0.0	0.0	0.0	0.0	0.0	0.0	0.0
N	4496.9	586.4	3281.3	388.8	2561.9	251.7	1936.5	166.5	1486.3	149.3

Table C4.8(a) Uncorrected SAR-TL 200-400°C 10°C data for the Þórsmórk Ignimbrite (ÞIG 7) data used to construct Figure 4.24. Shaded area corresponds to the glow curve peak positions and stable temperature plateau. Full 1°C and 10°C data and regression fitting analysis can be found in the enclosed CD-R.

ÞIG 7: DOSE CORRECTED REGENERATION GROWTH CURVE: DISCS 1-8 MEAN + STD ERROR

DOSE (Gy)	200-210		210-220		220-230		230-240		240-250	
0	0.00	0.00	0.00	0.00	0.00	0.00	0.00	0.00	0.00	0.00
50	1.17	0.23	0.99	0.17	1.32	0.31	1.46	0.29	1.53	0.21
75	3.73	1.49	1.32	0.25	0.92	0.20	1.96	0.29	2.58	0.35
100	1.72	0.42	1.20	0.19	1.84	0.57	2.44	0.45	2.32	0.17
125	1.87	0.33	2.87	0.47	5.27	2.21	4.42	0.74	4.87	0.65
150	0.97	0.61	1.11	0.74	2.45	1.50	4.36	2.61	4.34	0.92
200	1.78	0.31	2.38	0.64	5.89	3.07	7.06	1.48	7.36	1.45
300	2.64	0.60	2.71	0.52	4.50	0.59	7.76	1.21	14.51	3.93
-	0.00	0.00	0.00	0.00	0.00	0.00	0.00	0.00	0.00	0.00
-	0.00	0.00	0.00	0.00	0.00	0.00	0.00	0.00	0.00	0.00
N	1.17	0.18	1.08	0.22	2.14	0.39	3.85	0.66	8.29	1.32

DOSE (Gy)	250-260		260-270		270-280		280-290		290-300	
0	0.00	0.00	0.00	0.00	0.00	0.00	0.00	0.00	0.00	0.00
50	2.14	0.26	2.02	0.20	2.04	0.16	2.06	0.15	1.97	0.11
75	2.40	0.21	2.20	0.20	2.20	0.15	2.25	0.14	2.41	0.13
100	3.19	0.34	3.37	0.24	3.12	0.17	3.16	0.15	3.32	0.13
125	4.19	0.32	4.47	0.39	4.19	0.26	4.20	0.25	4.08	0.23
150	5.78	1.66	5.38	0.36	5.68	0.83	5.53	0.67	5.31	0.50
200	7.11	0.88	7.13	0.78	7.28	0.54	6.86	0.43	6.81	0.37
300	11.19	0.58	11.29	1.29	10.55	0.66	10.97	1.20	10.42	0.94
-	0.00	0.00	0.00	0.00	0.00	0.00	0.00	0.00	0.00	0.00
-	0.00	0.00	0.00	0.00	0.00	0.00	0.00	0.00	0.00	0.00
N	9.91	0.89	9.26	0.92	9.33	0.81	8.85	0.72	7.87	0.40

DOSE (Gy)	300-310		310-320		320-330		330-340		340-350	
0	0.00	0.00	0.00	0.00	0.00	0.00	0.00	0.00	0.00	0.00
50	1.85	0.07	1.71	0.04	1.58	0.05	1.58	0.08	1.54	0.14
75	2.50	0.10	2.61	0.06	2.69	0.08	2.73	0.08	2.80	0.16
100	3.30	0.08	3.38	0.06	3.41	0.11	3.20	0.10	3.17	0.18
125	4.06	0.19	3.93	0.14	4.01	0.16	4.05	0.17	3.93	0.16
150	5.00	0.54	4.89	0.40	4.59	0.52	4.45	0.64	4.34	0.65
200	6.48	0.29	6.15	0.16	5.87	0.18	5.66	0.26	5.35	0.33
300	9.61	0.84	8.55	0.48	7.71	0.46	7.43	0.40	6.68	0.31
-	0.00	0.00	0.00	0.00	0.00	0.00	0.00	0.00	0.00	0.00
-	0.00	0.00	0.00	0.00	0.00	0.00	0.00	0.00	0.00	0.00
N	7.33	0.34	6.41	0.28	5.98	0.40	5.36	0.41	5.34	0.59

DOSE (Gy)	350-360		360-370		370-380		380-390		390-400	
0	0.00	0.00	0.00	0.00	0.00	0.00	0.00	0.00	0.00	0.00
50	1.56	0.11	1.46	0.11	1.44	0.28	1.34	0.16	2.59	1.01
75	2.81	0.16	3.10	0.24	2.33	0.38	2.50	0.48	1.67	0.37
100	3.06	0.25	3.08	0.23	3.69	0.48	2.49	0.40	5.34	2.50
125	3.92	0.24	4.65	0.39	4.16	0.27	4.36	0.66	2.10	0.29
150	4.06	0.72	4.31	0.93	4.58	1.68	3.68	1.67	4.65	3.80
200	5.38	0.45	5.13	0.49	5.75	0.29	4.89	0.51	7.55	1.48
300	6.51	0.29	6.69	0.40	7.04	0.97	5.49	0.39	4.60	0.72
-	0.00	0.00	0.00	0.00	0.00	0.00	0.00	0.00	0.00	0.00
-	0.00	0.00	0.00	0.00	0.00	0.00	0.00	0.00	0.00	0.00
N	5.07	0.66	5.92	0.59	5.51	0.58	5.31	0.67	4.77	0.85

Table C4.8(b) Test dose corrected SAR-TL 200-400°C 10°C ratio data for the Þórsmórk Ignimbrite (ÞIG 7) data used to construct Figure 4.24. Shaded area corresponds to the glow curve peak positions and stable temperature plateau. Full 1°C and 10°C data and regression fitting analysis can be found in the enclosed CD-R.

Tephra deposit Location	Sample ID	Distance to source (km)	Grain size statistics Mean ± 1σ (μm)	Median (μm)	Mode (μm)	Fractional percentages Clay <4 μm	Silt 4-62 μm	Sand 62-500 μm	>Sand >500 μm
Óþoli Tephra, NW Iceland									
Skagafjall, Section B	SUTL 551	?	68.75 ± 110.50	44.27	50.22	4.80	60.50	34.30	0.40
	SUTL 552	?	70.07 ± 109.80	39.92	55.13	11.90	53.40	34.50	0.20
Skagafjall, Section C	SUTL 558	?	91.45 ± 68.54	80.20	96.49	2.93	33.97	63.07	0.03
Hjallanes Tephra, NW Iceland									
Skagafjall, Section A	SUTL 513	?	81.27 ± 47.21	75.47	80.47	1.67	33.23	65.10	0.00
Öræfi 1362, SE Iceland									
Sandfellsheidi	ÖR 1	9	266.50 ± 346.80	127.00	140.10	3.75	30.15	60.70	5.40
Skalafell	ÖR 2	55	109.10 ± 151.80	66.27	140.10	4.34	43.76	51.30	0.60
Fossdalur	ÖR 3	85	69.35 ± 72.54	50.79	72.94	5.48	52.42	42.06	0.04
Askja 1875, N & E Iceland									
NE crater	ASK 5	0.5	347.10 ± 425.20	171.90	153.80	2.41	21.79	66.00	9.80
Fiskidalur	ASK 10	55	358.60 ± 440.30	162.40	140.10	2.63	24.77	61.70	10.90
Arnorsstadamuli	ASK 11	74	183.60 ± 298.70	75.39	72.94	4.21	37.99	54.10	3.70
Þörsmörk Ignimbrite, Þörsmörk, S Iceland									
Site 1	ÞIG 1b	20	286.10 ± 387.70	111.60	356.10	4.99	33.81	54.10	7.10
Site 7	ÞIG 7	18	314.10 ± 437.30	105.20	60.52	3.70	34.50	52.00	9.80

Table C5.1 Grain size data for Icelandic tephra deposits whose thermoluminescence characteristics were examined during the course of this study.

Notes: Samples were analysed by SJR using a Coutler Partical Size Analyser LS230 equipped with a fluid module and PIDS (Polarisation Intensity Differential Scatter) attachment - at the Department of Geography, University of Edinburgh. This machine uses a 5 mW, 750 nm laser beam and 126 detectors placed at a range of angles up 35° to the laser beam, measuring particle sizes from 0.4 μm - 2 mm. Samples were concentrated into a 'just-saturated' paste and mixed thoroughly before analysis and loaded into the counter vessel of known volume containing 1 % Calgon solution until obscuration values of 45-55 % and PIDS values of 8-12 % were obtained. Background readings were undertaken for each run. Samples were run continuously with offsets automatically measured every hour and detectors aligned every two hours; sample run time = 900 seconds; grain size parameters were modelled using the Fraunhofer model; sand/silt/ clay *etc.* divisions are as defined by Wentworth (1922). Interpolation of the LS 2230 data output was undertaken using v. 3.01 of the Coulter LS Control software, with further statistical analysis undertaken in Excel (v. 97), xlstat and Sigmaplot (v. 4). All data are mean ± 1s of 2 sets of 5 runs, except for ÞIG 1b and ÞIG 7 where there was insufficient sample for duplicate runs, SUTL 552 which is an average of 4 sets of 4 runs and SUTL 558 which is and average of 4 sets of 5 runs. SUTL 558 was used as a pseudo-control sample and run at the start, middle and end of analyses above. Grain size data for SUTL 558 presented here compares well with that obtained by Sigurvinsson (1983). ÞIG 1b and ÞIG 7 are the only two stratigraphically constrained unaltered ash fall deposits found in the Þörsmörk region. Samples from other ÞIG sites are from pumice shards, which are prone to disintegration, and slope ash deposits, which are prone to weathering, do not reflect accurate particle size characteristics that can be used for source-sample distance analysis.

Appendix D
Background to Discussion

D1: Glaciolacustrine Environments: Review & Case Studies

The following short review places the Skagafjall sedimentary record in context. It identifies general problems associated with establishing the glacial origin of sedimentary deposits and establishing periodicities of deposition. Using case studies that are particularly relevant to the interpretation of the Skagafjall deposits, it examines the depositional environments and characteristics of glaciolacustrine deposition at the margins of regional ice sheets.

Stratigraphic records from glaciolacustrine environments are excellent archives of rapid climate change because ice dammed lakes can preserve long, continuous and high resolution evidence of annual to sub-annual fluctuations sediment input at glacier margin (Karrow and Calkin, 1985; Leonard, 1986; Ashley, 1995; Lowe and Walker, 1997). Detailed chronostratigraphy, provided by incremental, palaeomagnetic, biostratigraphic, isotopic and/or tephrochronological dating techniques, is essential for accurate palaeoenvironmental reconstructions (De Greer, 1912; Cato, 1985; Gilbert and Shaw, 1981; Rose and Menzies, 1995).

D1.1 Contemporary glaciolacustrine environments

Understanding sedimentary processes in contemporary glacial lakes in alpine and arctic regions assists the interpretation of the palaeo-glaciolacustrine environments as they provide information on temporal and spatial variations in the rate and environment of deposition, lithological composition and organic content. Contemporary glaciolacustrine environments are classified according to the relative position of the ice margin (*e.g.* Ashley, 1988; Ashley, 1995: Table 13.1, p. 418). In summary, the rate and style of sedimentation is determined by the proximity of the lake to the glacier and the internal thermal and density structure of the lake as well as its chemical and biological composition (Eyles *et al.*, 1990; Ashley, 1995). The position of the meltwater inflow, lake basin geometry, the type and quantity of ice-rafting and the longevity and extent of winter ice cover are also important (Hambrey, 1994; Bennett and Glasser, 1996). In the ice-proximal environment outwash streams form glaciolacustrine deltas at inlets. In deeper, more distal parts of the lake finely laminated, rhythmic deposits form by suspension settling. Mass flow diamictons are common near the lake margins. Diamicton deposits formed by glacier overriding ice-rafting can occur in all parts of the lake, but the latter are more common near the lake outlet (McManus and Duck, 1988).

D1.2 Palaeo-glaciolacustrine environments

Although questioned in the mid-seventies and early eighties, ice-dammed lakes and catastrophic lake drainage (jökulhlaups) are most commonly associated with active deglaciation (Bennett *et al.*, 1998: p.

41 for list of relevant references). The sedimentary characteristics of modern analogues are commonly extrapolated into the past in accordance with Walther's Law (Middleton, 1973). This states that 'spatially contiguous lithofacies environments occur across the surface of the Earth and produce the same vertical succession of lithofacies units' (Hart, 1992; p. 120). Palaeo-ice dammed lake deposits have been used in combination with geomorphological and other sedimentological evidence to calculate relative rates of local glacial activity and their relationship to wider climatic influences (Eyles and Eyles, 1983; Menzies, 1996). For example, Leonard (1986) suggested that increased sedimentation rates in Hector Lake, Alberta were related to periods increased fluvial reworking during periods of ice recession for up to a century after ice maxima. Sediments from glacier-fed lakes provide good field constraints for glacial modelling exercises because maximum ice extents, direction of ice movement, sediment supply source and mode of deposition can often be inferred from them (*e.g.* Dowdeswell and Sharp, 1986; Benn, 1995).

Establishing the genesis of sedimentary deposits in former glacial environments is often problematic because similar lithofacies assemblages form in a wide variety of environments (Gravenor *et al.*, 1984; Owen, 1994; Ashley, 1995; Benn, 1995; Woodworth-Lynas, 1996; Ó Cofaigh and Dowdeswell, 2001, for summary tables of distinguishing criteria).). A list of distinguishing criteria for glaciomarine/glaciolacustrine and glaciotectonic deposits can be found in Hart and Roberts (1994) and Bennett and Hambrey (1996, p. 311). Distinguishing between glaciomarine and glaciolacustrine deposits is complex (Table D1.1; Ó Cofaigh and Dowdeswell, 2000). The presence of *in-situ* marine macro- and microfossil, bioturbation are thought to be diagnostic characteristics of glaciomarine environments (Dowdeswell and Scourse, 1990; Bennett and Glasser, 1996), but they are not always present and, often, general environmental setting is the key factor (Dowdeswell *et al.*, 2000).

D1.3 Characteristic deposits of ice-dammed lakes I: Rhythmites

Rhythmic sedimentary deposits form in glaciomarine or glaciolacustrine environments. Dropstones and finely graded stratigraphic sequences of laminated clay/silt and sand are representative of either depositional environment. A combination of basal ice scours or ridges, well preserved till and/or resedimented deposits are potentially diagnostic glaciolacustrine features (Eyles and Clark, 1988; Woodworth-Lynas, 1995). These are rarely preserved, however, because, unless dammed by a regionally stable ice-sheet, marginal glacial lakes are ephemeral with, at most, a decadal lifespan (Ashley, 1995).

Problems of equifinality are have been encountered in glaciolacustrine environments when attempting to establish the origin and annual nature of rhythmite deposits (Ashley, 1995; Table D1.1). Hart (1992) suggested the use of a 'rhythmite index'[43] to quantify the distinction between varved[44] and

[43] The rhythmite index is based on the relationship between the thickest layers and the mean distribution of the thickness layer

[44] Rhythmite couplets that reflect an annual depositional cycle are called varves.

turbidity current deposits of a non-annual nature, which often have a similar appearance in the field. Varves are common in many distal glaciolacustrine environments (*e.g.* Strömberg, 1985; Leonard, 1986). Classic varve couplets consist of a silt layer, which fines upwards and is deposited from summer underflow and a clay layer, which is massive, has a sharp upper contact and is deposited from suspension settling in the autumn and winter when surface ice suppresses wind shear and surface mixing (Ludlam, 1979; Benn and Evans, 1998). The internal structure of rhythmite beds is also indicative of regional climate variability. The progression from highly laminated to massive rhythmites has been linked to a reduction in sedimentation rates associated with initial retreat and/or stagnation to glacier stabilisation in increasingly warmer conditions (Lemmen, *et al.*, 1987). Stratigraphically discontinuous varved deposits from ice-marginal palaeolakes across Sweden have been linked and used to calibrate the radiocarbon time scale in the pre-dendrochronology era (Wohlfarth, 1996).

Glaciomarine	Glaciolacustrine
Settling from overflows/underflows	*Interflow/overflow deposition*
Thickness: 0.2-1 cm	< 1cm
Couplets consist of basal coarse-grained (fine sand-silt) lamina gradiationally overlain by silt-clay lamina	Silt laminae are massive and structureless
	Clay laminae show normal grading
Fine-grained laminae consistently thicker than basal coarse laminae	Sharp contacts between fine and coarse layers
Traction current structure absent within couplets	Laminae thin in down-lake direction; thickness may vary laterally across lake in response to Coriolis effect
Rhythmite may be interstratified with mass flow deposits and sandy turbidites (most common in ice proximal settings)	
Laminae thin with distance from ice-margin	Absence of flocculation during deposition results in greater sorting of the coarser layer compared to glaciomarine rhythmites
Marine micro- and macrofauna may be present	*Underflow and overflow/interflow deposition*
	Thickness: cm to m
	Lower delta foreslope: coarse layer consists of ripple-laminated sand or stacked units of normally graded sand and coarse silt. Coarse layer is massive or graded and has a sharp basal contact and is draped sharply by silty clay or clay layer
	Centre of lake basin: coarse layer comprises of parallel laminated silts with occasional units of rippled sand or graded microlaminae; overall, draped by clay
	Relative thickness of summer and winter layers varies according to the proximal/distal location in lake basin
	Clay layers can maintain a relatively uniform thickness across the lake basin

Table D1.1 Criteria for differentiating between glaciolacustrine and glaciomarine rhythmite deposits (modified from Ó Cofaigh and Dowdeswell, 2001).

D1.4 Characteristic deposits of ice-dammed lakes II: Diamictons

The introduction of the non-genetic term diamicton by Flint (1970) removed the implication of glacial origin that was associated with the term till. Distinguishing between different types of diamicton remains in formerly glaciated environments is difficult. Advancing ice, turbidity currents, slumping, mass movement, ice-rafting and post depositional alteration processes can all produce deposits with similar characteristics (*e.g.* Hart *et al.*, 1990; Eyles, 1987; Hart, 1992; Owen, 1994). Facies associations and, in particular, the nature of the contacts between units and fabric and /or microfabric

analysis have been used to successfully distinguish glacial and non glacial diamictons (*e.g.* Ashley, 1988, 1995; Dowdeswell and Sharp, 1986; Owen, 1994; Menzies, 1996; Benn, 1995).

Lithofacies assemblages and associations are commonly used to determine sedimentary origins in glacial environments. Differentiating between glaciomarine/glaciolacustrine or 'ice-rafted' diamictons and sub-glacial or glaciotectonic diamictons deposited by advancing ice is important. The former can be related periods of ice advance or stagnation calving at the ice-front or lateral margins while the later is usually associated with periods of climatic deterioration (Benn and Evans, 1998). Sub-glacial glaciotectonic deformation occurs predominantly in deformable sediments that are most common in lowland areas and sea beds. Deformation in upland areas can occur where lodgement till forms a deformable base layer (Hart and Roberts, 1994). The origin and climate regime of diamicton deposits can be ambiguous. Therefore, the relationship to, and the characteristics of adjacent rhythmite beds is often the most critical indicator of the direction of climate change.

D1.5 Pertinent Case Studies

The following case studies of the interpretation of facies associations in glaciolacustrine environments are particularly relevant to new interpretations of the Skagafjall sedimentary sequence.

(a) Scarborough Bluffs, Toronto, Canada

Eyles and Eyles (1983) based their 'ice-rafting and turbidity current' diamicton model on the sequence of glacial deposits preserved at Scarborough Bluffs, on the shores of Lake Ontario in the eastern suburbs of Toronto (Eyles, 1983; Fig. 6.1). The sequence of inter-bedded diamictons, deltaic sands and laminated silts and mud deposits dates back to the penultimate (Saalian-Warthe[45]) glacial maximum *ca.* 150-130 ka. The deposits were mostly formed at the regionally fluctuating margins of the advancing Laurentide ice sheet. Traditionally, the *ca.* 50 ka Sunnybrook 'Till' was thought to have been deposited from a series of multiple ice advances as the main ice sheet became grounded in the Scarborough area Lake Ontario area. The concentration of diamictons in topographic lows and the transitional nature of the rhythmite bed-diamicton contact led Eyles and Eyles (1983) to conclude that deposition had occurred from ice rafts as the advancing ice calved directly into present-day Lake Ontario.

(b) Trimingham, Norfolk, UK

The glacial sediments at Trimingham, Norfolk (England) have attracted similar controversy (Eyles *et al.*, 1989; Hart and Boulton, 1991; Hart, 1992). The main stratigraphic features are the Happisburgh and Walcott Diamictons. These bracket a series of laminated and massive ice-dammed or ice marginal deposits (the Trimingham Member) and are associated with fluctuations of the Anglian ice-sheet between *ca.* 480-430 ka. Eyles *et al.*, (1989) suggested the upper, Walcott Diamicton was a

[45] The NW European nomenclature for glacial-interglacial periods is used for consistency with other parts of this thesis. The Saalian-Warthe glaciation is equivalent to mid-late Illinoian in the North American stratigraphic nomenclature and oxygen isotope stage 6 (0.13-0.19 Ma) (see Lowe and Walker, 1997, Table 1.1, p. 11 for details).

glaciomarine deposit formed in a similar manner to the Sunnybrook 'Till'. Alternatively, Hart (1992) interpreted both diamictons as predominantly sub-glacially derived. The presence of graded lamination in the upper part of the Happisburgh Diamicton and rhythmic deposits immediately above this unit marks the transition from sub-glacial to glaciolacustrine deposition. The reestablishment of varved sedimentation after a period of shallow water facies deposition (*i.e.*marl-rich sediments and aeolian and/or beach sands) and structural deformation of upper laminated clay beds of the Trimingham Member was cited as evidence for a re-advancing ice-sheet and the subglacial deposition of the Walcott Diamicton (Hart, 1992).

References

ADAMIEC, G., & AITKEN, M. J. (1998). Dose-rate conversion factors: new data. *Ancient TL*, **16**(2), 37-50.

ADKINS J. F., BOYLE E. A., KEIGWIN L., & CORTIJO E. (1997). Variability of the North Atlantic thermohaline circulation during the last interglacial period. *Nature* **390**, 154-156.

AHLMAN, H. W. (1937). Vatnajökull in relation to other present day Iceland glaciers. *Geografiska Annaler*, **19**, 212-229.

AITCHISON, J. (1986). The statistical analysis of compositional data. *Journal of the Royal Statistical Society B*, **44**, 139-177.

AITKEN, M. J. (1979). Interlaboratory calibration of alpha and beta sources. *TLS*, **60**, 443-447.

AITKEN, M. J. (1985). *Thermoluminescence Dating*. Academic Press, London. pp. 359.

AITKEN, M. J. (1998). *An introduction to optical dating. The Dating of Quaternary Sediments by the Use of Photon-stimulated Luminescence*. Oxford University Press, Oxford. pp. 270.

AITKEN, M. J., & BOWMAN, S. G. E. (1975). Thermoluminescence dating: assessment of alpha particle contribution. *Archaeometry*, **17**, 132-138.

ALBERTSSON, K. J. (1976). *K/Ar ages of Pliocene-Pleistocene Glaciations with Special Reference to the Tjörnes Sequence, Northern Iceland*. Unpublished PhD Thesis, University of Cambridge.

ALBERTSSON, K. J. (1981). On Tertiary tillites in Iceland. In *Earth: Pre-Pleistocene glacial record.* Hambrey, H. J., & Harland, W. B. (Eds.). Cambridge University Press. p. 563-565.

ALBERTSSON, K. J., & EIRÍKSSON, J (1988). K/Ar ages of rocks from the Flatey borehole in the offshore Skjalfandi basin, North Iceland. *Jökull*, **38**, 527-529.

ALLEN, C. C. (1980). Icelandic subglacial volcanism: Thermal and physical studies. *Journal of Geology*, **88**, 108-117.

ALLEN, J. R. L. (1985). Wrinkle marks: an inter-tidal sedimentary structure due to aseismic sediment loading. *Sedimentary Geology*, **41**, 75-95.

ALLEY, R. B., & KOCI, B. R. (1993). Recent warming in central Greenland? *Annals of Glaciology*, **14**, 6-8.

ALLOWAY, B., NEALL, V. E., & VUCETICH, C. G. (1995). Late Quaternary (post 28 ka BP) tephrostratigraphy of northeast and central Taranaki, New-Zealand. *Journal of The Royal Society of New Zealand*, **25**(4), 385-458.

AMMANN, B. & LOTTER, A. F. (1989). Late-Glacial radiocarbon- and palynostratigraphy on the Swiss Plateau. *Boreas*, **18**, 109-126.

ANDREWS, J. T. (MANUSCRIPT). Marine sediments studies of the Iceland shelf. Palaeoceanography and land/ice sheet/ocean interactions.

ANDREWS, J. T., BOND, G. C., JENNINGS, A. E., KERWIN, M, KIRBY, M., MACLEAN, B., MANLEY, W., &, MILLER, G. H. (1995). A Heinrich-like event, H-0 (DC-0): sources for detrital carbonate in the North Atlantic during the Younger Dryas chronozone. *Palaeoceanography*, **10**, 943-952. (cited in Bond *et al.*, 2001).

ANDREWS, J. T., HARDARDÓTTIR, J., HELGADÓTTIR, G., JENNINGS, A., GEIRSDÓTTIR, A., SVEINBJORNSDÓTTIR, A. E., SCHOOLFIELD, S., KRISTJANSDÓTTIR, G. B., SMITH, L. M., THÓRS, K. & SYVITSKI, J. P. M. (2000). The N and W Iceland shelf: insights into the Last Glacial Maximum ice extent and deglaciation based on acoustic stratigraphy and basal radiocarbon AMS dates. *Quaternary Science Reviews*, **19**, 619-631.

ASHLEY, G. M. (1975). Rhythmic sedimentation in glacial lake Hitchcock, Massachusetts-Connecticut. In: Topling, A. V., & MacDonald, B. C. (Eds.). *Glaciofluvial and Glaciolacustrine Sedimentation*. Society of Economic Palaeontology and Mineralology, Special Publication, **23**, 304-320. (cited in Sigurvinsson, 1983).

ASHLEY, G. M. (1988). Classification of glaciolacustrine environments. In: Goldthwait, R. P., & Matsch, C. L. (Eds.). *Genetic Classification of Glaciogenic Deposits*. A. A. Balkema, Rotterdam. p. 243-260.

ASHLEY, G. M. (1995). Glaciolacustrine environments. In Menzies, J. (Ed): *Glacial Environments Volume 1: Modern Glacial Environments.* Butterworth Hiennneman, Oxford. p. 417-444.

AUSTIN, W. E. N., BARD, E., HUNT, J. B., KROON R. & PEACOCK J. D. (1995). The ^{14}C age of the Icelandic Vedde Ash: Implications for Younger Dryas marine reservoir age corrections. *Radiocarbon* **37**, 53-62.

AUSTIN, W. E. N., &, KROON, D. (1996). Late glacial sedimentology, forminifera and stable isotope stratigraphy of Hebridean Continental Shelf, Northwest Scotland. In: Andrews, J. T., Austin W.E.N., Bergsten, H. & Jennings, A. E. (Eds), *Late Quaternary Palaeoceanography of the North Atlantic Margins,* Geological Society Special Publication No. 111, p. 187-213.

BALESCU, S., LAMOTHE, M., LAUTRIDOU, J-P. (1997). Luminescence evidence for two Middle Pleistocene interglacial events at Tourville, northwestern France. *Boreas*, **26**, 61-72.

BARD, E. FAIRBANKS, R. ARNOLD, M., MAURICE, P., DUPRAT, J., MOYES, J., DUPLESSY, J. –C. (1989). Sea level estimates during the last deglaciation based on $\delta^{18}O$ and accelerator mass spectrometry ^{14}C ages measured in *Globigerina bulloides. Quaternary Research*, **31**, 381-391.

BARD, E., ARNOLD, M., FAIRBANKS, R. G., & HAMELIN, B. (1993). ^{230}Th-^{234}U and ^{14}C ages obtained by mass spectrometry on corals. *Radiocarbon*, **35**, 191-199.

BARD, E., ARNOLD, M., MANGERUD, J., PATERNE, M., LABEYRIE, L., DUPRAT, J., MELIERES, M.-A., SONSTEGAARD E., &, DUPLESSY J.-C. (1994). The North Atlantic atmosphere-sea surface ^{14}C gradient during the Younger Dryas climatic event. *Earth and Planetary Science Letters* **126**, 275-287.

BARD, E., HAMELIN, B., ARNOLD, M., MONTAGGIONI, L., CAGIOCH, G., FAURE, G., & ROUGERIE, F. (1996). Deglacial sea-level record form Tahiti corals and the timing of global meltwater discharge. *Nature* **382**, 241-244.

BARLOW, L. K., ROGERS, J. C., SERREZE, M. C., & BARRY, R. G. (1997). Aspects of climate variability in the North Atlantic sector: Discussion and relation to the Greenland Ice Sheet Project 2 high resolution isotopic signal. *Journal of Geophysical Research* **102 (C12)**, 26,333-26,344.

BAXTER, M. J. (1994). *Exploratory Multivariate Analysis in Archaeology*. Edinburgh University Press, Edinburgh. pp. 307.

BAXTER, M. J. (1998). Detecting multivariate outliers in compositional artefact data. *Archaeometry*, **41**(2), 321-338.

BAXTER, M. J. (1999). On multivariate normality of data arising from lead isotope fields. *Journal of Archaeological Science*, **26**(1), 117-124.

BECKER, B. (1993). An 11,000-year German Oak and Pine dendrochronology for radiocarbon calibration. *Radiocarbon*, **35**, 201-213.

BÉGET, J., MASON, O., & ANDERSON, P. (1992). Age, extent and climatic significance of the *ca.* 3400 BP Aniakchak tephra, western Alaska. *The Holocene*, **2**, 51-56.

BELL, W. T. (1979a). TL dating: radiation dose rate data. *Archaeometry*, **21**, 243.

BELL, W. T. (1979b). Attenuation factors for the absorbed radiation dose in quartz grains for luminescence dating. *Ancient TL*, **8**, 2-13.

BELL, W. T. (1980). Alpha dose attenuation in quartz grains for thermoluminescence dating. *Ancient TL*, **12**, 4-8.

BENDER, M., SOWERS, T., DICKSON, M. –L., ORCHARDO, J., GROOTES, P., MAYEWSKI, P. A., & MEESE, D. A. (1993). Climate correlations between Greenland and Antarctica during the past 100,000 years. *Nature*, **372**, 663-666.

BENN, D. I. (1995). Fabric signature of subglacial till deformation, Breiðamerjökull, Iceland. *Sedimentology*, **42**, 735-747.

BENN, D. I., & EVANS, D. J. A. (1998). *Glaciers and Glaciation*. Arnold/John Wiley & Sons, London. pp. 734.

BENNETT, K. D., BOREHAM, S., SHARP, M. J. & SWITSUR, V. R. (1992). Holocene history of environment, vegetation and human settlement on Catta Ness, Lunnasting, Shetland. *Journal of Ecology* 80, 241-273.

BENNETT, M. R., & GLASSER, N. F. (1996). *Glacial Geology: Ice Sheets and Landforms*. John Wiley and Sons. pp. 364.

BENNETT, M. R., HAMBREY, M. J., HUDDART, D., GLASSER, N. F., & CRAWFORD, K. (1998). The ice-dammed lakes of Ossian Sarsfjellet (Svalbard): their geomorphology and significance. *Boreas*, **27**, 43.

BENSON, L. V., BURDETT, J., LUND, S., KASHGARIAN, M., & MENSING, S. (1997a) Nearly synchronous climate change in the Northern Hemisphere during the last glacial termination. *Nature*, **388**, 263-265.

BENSON, L. V., SMOOT, J. P., KASHGARIAN, M., SARNA-WOJCICKI, A., & BURDETT, J. W.(1997b). Radiocarbon ages and environments of deposition of the Wono and Trego Hot Springs tephra layers in the Pyramid Lake Subbasin, Nevada. *Quaternary Research*, **47**, 251-260.

BERGER, G. W. & HUNTLEY, D. J. (1983). Dating volcanic ash by thermoluminescence. *PACT Journal*, **9**, 581-592.

BERGER, G. W. (1988a). Dating Quaternary events by luminescence. *Geological Society of America Special Paper*, **227**, 13-50.

BERGER, G. W. (1988b). TL dating studies of tephra, loess and lacustrine sediments. *Quaternary Science Reviews*, **7**(3/4), 295-303.

BERGER, G. W. (1990). Regression and error analysis for a saturating-exponential-plus-linear model. *Ancient TL*, **8**, 23-25.

BERGER, G. W. (1991). The use of glass for dating volcanic ash by thermoluminescence. *Journal of Geophysical Research*, **96**, 19,705-19720.

BERGER, G. W. (1992). Dating volcanic ash by use of thermoluminescence. *Geology*, **20**, 11-14.

BERGER, G. W. (1994). Thermoluminescence dating of sediments older than ~100 ka. *Quaternary Science Reviews*, **13**, 445-456.

BERGER, G. W. (1995). Progress in luminescence dating methods for Quaternary sediments. In: *Dating Methods for Quaternary Deposits*. Rutter, N. W. & Catto, N. R. (Eds.). Geological Association of Canada. p. 81-104.

BERGER, G. W., & HUNTLEY, D. J. (1983). Dating volcanic ash by thermoluminescence. *PACT Journal*, **9**, 581-592.

BERGER, G. W., & EYLES, N. (1994). Thermoluminescence chronology of the Toronto-area Quaternary sediments and implications for extent of the midcontinent ice sheet(s). *Geology*, **22**, 31-34.

BERGER, G. W., & HUNTLEY D. J. (1994). Tests for optically stimulated luminescence from tephra glass. *Quaternary Geochronology (Quaternary Science Reviews)*, **13**, 509-511.

BERGER, G. W., PILLANS, B. J., & PALMER, A. S. (1992). Dating loess up to 800 ka by thermoluminescence. *Geology*, **20**, 403-406.

BERGER, G. W., WESTGATE, J. A., & PREECE, S. J. (1996). Age of Sheep Creek tephra (Pleistocene) in Central Alaska from thermoluminescence dating of bracketing loess. *Quaternary Research* **45**, 263-270.

BERGER, G. W., & NEILL, P. A. (1999). Photon-stimulated-luminescence (PSL) dating tests of glass-rich volcanic ash. In: *9th International Conference on Luminescence and Electron Spin Resonance Dating (LED 99), Book of Abstracts.* Rome 6-10 September, 1999. p. 138.

BERGER, G. W., ROWLANDS, A. P., & NEILL, P. A. (1999). Luminescence emission spectra from glass-rich fractions of volcanic ash. In: *9th International Conference on Luminescence and Electron Spin Resonance Dating (LED 99), Book of Abstracts.* Rome 6-10 September, 1999. p. 139.

BETTINALLI, C., & FERRARESSO, G. (1968). Thermoluminescence in vitreous sodium silicate. *Journal of Chemistry & Physics*, **44**(6), 2262-2265.

BIERMANN, P., & TURNER, J. (1995). ^{10}Be and ^{26}Al evidence for exceptionally low rates of Australian bedrock erosion and the likely existence of pre-Pleistocene landscapes. *Quaternary Research,* **44**, 378-382.

BIGAZZI, G., & GALBRAITH, R. F. (1999). Point-counting technique for fission-track dating of tephra glass shards, and its relative standard error. *Quaternary Research*, **51**, 67-73.

BINGHAM, R. (1999). *Modelling ice-sheet dynamics in response to climatic changes in southern Iceland.* Unpublished MRes. Thesis, University of Edinburgh.

BINGHAM, R., HULTON, N., & DUGMORE, A. J. (2000). Modelling ice-sheet dynamics in response to climatic changes in southern Iceland. In: *Iceland 2000 – Modern Processes and Past Environments. Conference Abstracts.* April 27th-29th 2000. p. 15.

BINGHAM, R., HULTON, N. R. J., & DUGMORE, A. J. D. (SUBMITTED). Modelling the southern extent of the last Icelandic ice-sheet *ca.* 20 ka BP. *Submitted to Journal of Quaternary Science.*

BIRKS, H. J. B., & LOTTER, A. F. (1994). The impact of the Laacher See volcano (11,000 yr BP) on terrestrial vegetation and diatoms. *Journal of Palaeolimnology*, **11**, 313-322.

BIRKS, H. H., GULLIKSEN, S., HAFLIDASON, H., MANGERUD, J., & POSSNERT, G. (1996). New radiocarbon dates for the Vedde Ash and the Saksunarvatn Ash from Norway. *Quaternary Research*, **45**, 119-127.

BJÖRCK, S., INGÓLFSSON, O., HAFLIDASON, H., HALLSDÓTTIR, M., & ANDERSON, N. J. (1992). Lake Torfadalsvatn: a high resolution record of the North Atlantic Ash Zone I and the last glacial-interglacial environmental changes in Iceland. *Boreas*, **21**, 15-22.

BJÖRCK S., RUNDGREN M., INGÓLFSSON Ó., & FUNDER S. (1997). The Preboreal oscillation around the Nordic seas: terrestrial and lacustrine deposits. In: *Late Weichselian and early Holocene changes of vegetation, climate and sea level on the Skagi Peninsula, northern Iceland. Lundqua Thesis*, **40**, 1-17.

BJÖRCK, S., WALKER M. J. C., CWYNAR L. C., JOHNSEN S., KNUDSEN K. L., LOWE J. J., WOHLFARTH B. & INTIMATE MEMBERS. (1998). An event stratigraphy for the Last Termination in the North Atlantic region based on the Greenland ice-core records: a proposal by the INTIMATE group. *Journal of Quaternary Science*, **13** (4), 283-292.

BJÖRCK, J., & WASTEGÅRD, S. (1999). Climate oscillations and tephrochronology in eastern middle Sweden during the last glacial-interglacial transition. *Journal of Quaternary Science*, **14**(5), 399-410.

BLACK, T. M., SHANE, P. A. R., WESTGATE, J. A., & FROGGATT, P. C. (1996). Chronological and palaeomagnetic constraints on widespread welded ignimbrites of the Taupo volcanic zone. *Bulletin of Volcanology*, **58**, 226-238.

BLACKFORD, J. J., EDWARDS, K. J., DUGMORE, A. J., COOK, G. T., & BUCKLAND, P. C. (1992). Icelandic volcanic ash and the mid-Holocene Scots Pine (*Pinus sylvestris*) pollen decline in northern Scotland. *The Holocene*, **2**(3), 260-266.

BLOEMENDAL, J., & DEMONOCAL, P. (1989). Evidence for a change in periodicity of tropical climate cycles at 2.4 Myr from whole core magnetic susceptibility measurements. *Nature*, **342**, 897-900.

BLOEMENDAL J., LIU X.M. & ROLPH T.C. (1994). Correlation of the magnetic susceptibility stratigraphy of the Chinese loess and the marine oxygen isotope record: chronological and palaeoclimatic implications. *Earth and Planetary Science Letters*, **131**,371-380.

BOELLSTORFF, J. D. (1978). North American Pleistocene stage reconsidered in the light of probable Pliocene-Pleistocene continental glaciation. *Science*, **202**, 305-307.

BOND, G. C. & LOTTI, R. (1995). Iceberg discharges into the North Atlantic Ocean during the last glaciation. *Science*, **267**, 1005-1010.

BOND, G. C., HEINRICH, H., BROECKER, W. S., LABEYRIE, L., MCMANUS J., ANDREWS J., HUON S., JANTSCHIK, R., CLASEN S., SIMET C., TEDESCO, K., KLAS M., BONANI, G., & IVY S. (1992). Evidence for massive discharges of icebergs into the North Atlantic during the last glacial period. *Nature*, **360**, 245-249.

BOND, G. C., BROECKER, W. S., JOHNSEN, S., MCMANUS J., LABEYRIE, L., JOUZEL, J., & BONANI, G. (1993). Correlations between climate records from North Atlantic sediments and the Greenland Ice Cores. *Nature*, **365**, 143-147.

BOND, G., MANDEVILLE, C., & HOFFMAN, S. (2001). Were rhyolitic glasses in the Vedde Ash and in North Atlantic Ash Zone 1 produced by the same volcanic eruption. *Quaternary Science Reviews*, **20**(3), 1189-1199.

BONDE, A. MURRAY, A., & FRIEDRICH, W. L. (2000). Santorini: Luminescence dating of a volcanic province using quartz. *Quaternary Science Reviews*, **20**(5-9), 789-793.

BORCHARDT, G. A., ARUSCAVAGE, J., & MILLARD, H. T. (1972). Correlation of the Bishop Ash, a Pleistocene marker bed, using instrumental neutron activation analysis. *Journal of Sedimentary Petrology* **42**(2), 301-306.

BOTT, M. H. P. (1985). Plate tectonic evolution of the Icelandic transverse ridge and adjacent regions. *Journal of Geophysical Research*, **90** (B12), 9953-9960.

BOULTON, G. S., JARVIS, J., & THORS, K. (1988). Dispersal of glacially derived sediment over part of the continental shelf of South Iceland and the geometry of the resultant sediment bodies. *Marine Geology*, **83**, 193-223.

BOULTON, G. S., & CLARK, C. D. (1990). The Laurentide Ice Sheet through the last glacial cycle: drift lineations as a key to the dynamic behaviour of former ice sheets. *Transactions of the Royal Society of Edinburgh, Earth Sciences,* **81**, 327-347.

BOURDON, B., ZINDLER, A. & WÖRNER, G. (1994). Evolution of the Laacher See magma chamber. Evidence from SIMS and TIMS measurements of U-Th disequilibria in minerals and glasses. *Earth and Planetary Science Letters* **126**, 75-90.

BOYGLE, J. (1995). *Tephra in lake sediments: an unambiguous geochronological marker?* Unpublished PhD Thesis. University of Edinburgh.

BOYLE, E. A. (2000). Is ocean thermohaline circulation linked to abrupt stadial/inter-stadial transitions. *Quaternary Science Reviews*, **19**, 255-272.

BOYNTON, W. V. (1984). Geochemistry of the rare earth elements: meteorite studies. In Henderson, P. (Ed.). *Rare Earth Element Geochemistry*. Elsevier Science, p. 63-114.

BRADWELL, T. (2000). Annual moraines and summer temperatures, Lambatungnajökull, Iceland. In: *Iceland 2000 – Modern Processes and Past Environments. Conference Abstracts.* April 27th-29th 2000. p. 23-24.

BRADWELL, T. (2001). *Glacier fluctuations lichenometry and climatic change in Iceland.* Unpublished PhD Thesis. University of Edinburgh. pp. 355.

BRAMLETTE, M. N, &, BRADLEY, W. H. (1941). Geology and biology of North Atlantic deep sea cores between Newfoundland and Ireland I. Lithology and geologic interpretation. *US Geological Survey Professional Paper*, **109-A**, 1-34. (cited in Bond *et al.*, 2001).

BRIGHAM-GRETTE, J., & CARTER, L. D. (1992). Pliocene marine transgressions of the North Alaska-circum Arctic correlations and palaeoclimatic interpretations. *Arctic*, **45** (1), 16-33.

BRINGHAM-GRETTE, J., CARTER, L. D., MARINCOVICH, L., BROUWERS, E., & HOPKINS, D. M. (1994). Warm Pliocene high sea-level records from Arctic Alaska and possible implications for Antarctic ice volume 2.8-2.2 Ma. In: *ISGS Open-File Report*, **94-588**. Web-accessed report: (USGS Open-File Report 94-588) (http://geochange.er.usgs.gov/pub/PRISM/OFR_94-588/04_Brigham-Grette.html)

BRODZIKOWSKI, K., & HALUSZCZAK, A. (1987). Flame structures and associated deformations in Quaternary glaciolacustrine and glaciodeltaic deposits: examples from central Poland. In Jones, M. E., & Preston, R. M. F. (Eds). *Deformation of Sediments and Sedimentary Rocks.* Geological Society Special Publication No. 29, pp. 279-286.

BROECKER, W. (1997). Future directions of palaeoclimate research. *Quaternary Science Reviews,* **16**, 821-825.

BROECKER, W. S., & DENTON, G. H. (1989). The role of ocean-atmosphere reorganisations in glacial cycles. *Geochimica et Cosmochimica Acta*, **53**, 2465-2501.

BROOK, E. J. (1993). *Surface Exposure Geochronology Using Cosmogenic Nuclides: Applications in Antarctic Glacial Geology.* Unpublished PhD Thesis. Massachusetts Institute of Technology & Woods Hole Oceanographic Institute. WHOI Document, **93-50**, pp. 273.

BROWN, F. H., SARNA-WOJCICKI, A. M., MEYER, C. S., & HAILEAB, B. (1992). Correlation of Pliocene and Pleistocene tephra layers between the Turkana basin of East Africa and the Gulf of Aden. *Quaternary International*, **13/14**, 55-67.

BUCKLAND, P. C. & DUGMORE A. J. (1991). 'If this a refugium, why are my feet so bloody cold? The origins of the Icelandic biota in the light of recent research. In *Environmental Change in Iceland: Past and Present.* J.K. Maizels and C. Caseldine (Eds). Kluwer, Dordrecht. p. 107-126.

BUNTING, M. J. (1994). Vegetation history of Orkney, Scotland: Pollen records from two small basins in West Mainland. *New Phytologist*, **128**, 771-792.

BURCHART, J., DAKOWSKI, M. & GALAZAKA, J. (1975). A technique to determine high fission-track densities. *Bull. Acad. Polon. Sciences, Sér. Sci. Terre*, **23**, 1-7.

BURTON, K. W., LING, H-F., O'NIONS, R. K. (1997). Closure of the central American Isthmus and its effect on deep-water formation in the North Atlantic. *Nature* 386, 382-384.

CARMICHEAL, I. S. E., TURNER, F. J., VERHOOGEN, J. (1974). *Igneous Petrology*. McGraw-Hill Book Co., New York. pp. 739.

CARSON, R. J., SPENCE, W. H., & BIRDSEYE, R. U. (1976). Late Pleistocene tephra layers in the western Puget Lowland, Washington. *Geological Society of America, Abstracts with Programs*, **8**, 358.

CARSWELL, D. A. (1983). The volcanic rocks of the Sólheimajökull area, southern Iceland. *Jökull*, **33**, 61-71.

CAS, R. A. F., & WRIGHT, J. V. (1987). *Volcanic Successions: Modern and Ancient. A Geological Approach to processes, products and successions.* Allen and Unwin, London, pp. 528.

CASELDINE, C., HATTON, J., HUBER U., CHIVERRELL R., & WOOLLEY, N. (1998). Assessing the impact of volcanic activity on mid-Holocene climate in Ireland: the need for replicate data. *The Holocene*, **8**(1), 105-111.

CATO, I. (1985). The definitive connection of the Swedish geochronological time scale with the present, and the new date of the zero year in Döviken, northern Sweden. *Boreas*, **14**, 117-122.

CHALMERS, J. A., LARSEN, L. M., PEDERSEN, A. K. (1995). Widespread Palaeocene volcanism around the northern North Atlantic and Labrador Sea: evidence for a large, hot, early plume head. *Journal of the Geological Society, London*, **152**, 965-969.

CHAWLA, S., DHIR, R. P., SINGHVI, A. K. (1992). Thermoluminescence chronology of sand profiles in the Thar desert and their implications . *Quaternary Science Reviews*, **11**, 25-32.

CHAWLA, S., RAO, T. K. G, SINGHVI, A. K. (1998). Quartz thermoluminescence: dose and dose rate effects and their implications. *Radiation Measurements*, **29**, 53-63.

CHEN, Y-G., WU, W-H., LIU, T-K., CHEN, C-H. (1999). Finding a Holocene volcano by thermoluminescence age determination of the Xenolith. In: *9th International Conference on Luminescence and Electron Spin Resonance Dating (LED 99), Book of Abstracts.* Rome 6-10 September, 1999. p. 285.

CHESNER, C. A., ROSE, W. I., DEINO, A., DRAKE, R., & WESTGATE, J. A. (1991). Eruptive history of Earth's largest Quaternary caldera (Toba, Indonesia) clarified. *Geology*, **19**, 200-203.

CHIAVARI, C., MARTINI, M., SIBILIA, E., & VANDINI, M. (2000). Thermoluminescence (TL) characterisation and dating feasibility of ancient glass mosaic. *Quaternary Science Reviews*, **20**, 967-972.

CIVETTA, L., D'ANTONIO, M., ORSI, G., TILTON, G. R. (1998). The geochemistry of volcanic rocks from Pantelleria island, Sicily channel: Petrogenesis and characteristics of the mantle source region. *Journal of Petrology*, **39**(8), 1453-1491.

CLARK, P. A., & TEMPLER, R. H. (1988). Dating thermoluminescence samples which exhibit anomalous fading. *Nuclear Tracks and Radiation Measurements*, **14**(1/2), 139-141.

CLARKE, M. L., & RENDELL, H. M. (1997). Infra-red stimulated spectra of alkali feldpsars. *Radiation Measurements*, **27**, 221-236.

CLARKE, M. L., RENDELL, H. M., & WINTLE, A. G. (1999). Quality assurance in luminescence dating. *Geomorphology*, **29**, 173-185.

CLAUSEN, H. B., HAMMER, C. U., HVIDBERG, C. S., DAHL-JENSEN, D., & STEFFENSEN, J. P. (1997). A comparison of volcanic records over the past 4000 years from the Greenland Ice Core Project and Dye 3 Greenland ice cores. *Journal of Geophysical Research*, **102**(C12), 26,707-26,723.

CLIFT, P. D. & FITTON, J. G. (1998). Trace and rare earth element chemistry of volcanic ashes from sites 918 and 919: Implications for Icelandic volcanism. *Proceedings of the Ocean Drilling Program, Scientific Results*, **152**, 67-83.

COLMAN, S. M., PIERCE, K. L., & BIRKELAND, P. W. (1987). Suggested terminology for Quaternary dating methods. *Quaternary Research*, **28**, 314-319.

CONNELL, A. (1846). Analysis of volcanic dust which fell in the Orkney Islands on 2nd September 1845. *The New Edinburgh Philosophical Journal*, **40**(80), 217-219.

COX, K. G., BELL, J. D., & PANKHURST, R. J. (1979). *The interpretation of igneous rocks*. George, Allen, & Unwin, London.

CRONIN, T. M. (1991). Pliocene shallow water palaeoceanography of the North Atlantic ocean based on marine ostracods. *Quaternary Science Reviews*, **10**, 175-188.

CROWLEY, T. J. (1993). Use and Misuse of the Geologic "Analogs" Concept. In: Eddy, J. A., & Oeschger, H. (Eds.). *Global Changes in the Perspective of the Past*. John Wiley and Sons, New York. p. 18-27.

CURRY, W. B., & MILLER, K. G. (1989). Oxygen and carbon isotopic variation in Pliocene benthic foraminifers of the equatorial Atlantic. *Proceedings of the Ocean Drilling Program, Scientific Results*, **108**, 157-166.

DAHL, E. (1992). Nunatakkteori. IV. Hvor fantes isfrie områder og hva slags planter kunne leve på dem? *Blyttia*, **50**, 23-35; (In Danish - English Abstract).

DAHL-JENSEN, D., MOSEGAARD, K., GUNDESTRUP, N., CLOW, D., JOHNSEN, S. J., HANSEN, A. W., & BALLING, N. (1998). Past temperatures directly from the Greenland ice sheet. *Science*, **282**, 268-271.

DALGLEISH, A. N., BOULTON, G. S., & RENSHAW, E. (2000). The ice age cycle and the deglaciations: an application of non-linear regression modelling. *Quaternary Science Reviews*, **19**, 687-697.

DALRYMPLE, G. B. (1967). Potassium-argon ages of recent rhyolites of the Mono and Inyo Craters, California. *Earth and Planetary Science Letters*, **3**, 289-298.

DANIELS, F., BOYD, C. A., & SAUNDERS, D. F. (1953). Thermoluminescence as a research tool. *Science*, **117**, 343-349.

DANSGAARD W., WHITE J. W. C., & JOHNSON S. C. (1989). The abrupt termination of the Younger Dryas climatic event. *Nature*, **339**, 532-533.

DANSGAARD, W., JOHNSEN, S. J., CLAUSEN , H. B., DAHL-JENSEN, D., GUNDESTRUP, N. S., HAMMER C. U., HVIDBERG, C. S., STEFFENSEN, J. P., SVEINBJORNSDOTTIR, A. E., JOUZEL J. (1993). Evidence for general instability of past climate from a 250-kyr ice-core record. *Nature*, **364**, 218-220.

DARBYSHIRE, A., WHITE, R. S., & PREISTLEY, K. F. (2000). Structure of the crust and uppermost mantle of Iceland from a combined seismic and gravity study. *Earth and Planetary Science Letters*, **181**, 409-428.

DAVIES, S. M., TURNEY, C. S. M., & LOWE, J. J. (2001). Identification and significance of a visible basalt-rich Vedde Ash layer in a Late-glacial sequence on the Isle of Skye, Inner Hebrides, Scotland. *Journal of Quaternary Science*, **16**(2), 99-104.

DE GEER, G. (1912). A geochronology of the last 12,000 years. *Eleventh International Geological Congress* (1910), Stockholm, **1**, 241-253.

DE JONG, J. (1988). Climatic variability during the past 3 Ma, as indicated by vegetational evolution in northwest Europe and with emphasis on data from The Netherlands. *Philosophical Transactions of the Royal Society, London*, **B318**, 603-617.

DING, Z. L., RUTTER, N., & LIU, T. (1993). Pedostratigraphy of Chinese loess deposits and climatic cycles in the last 2.5 Myr. *Cantena*, **20**, 73-91.

DONN, W., & NINKOVICH, D. (1980). Rate of Cenozoic explosive volcanism in the North Atlantic inferred from deep sea cores. *Journal of Geophysical Research*, **85(B10)**, 5455-5460.

DORÉ, A. G. (1992). The base Tertiary surface of southern Norway and the northern North Sea. *Norsk Geologisk Tidsskrift*, **72**, 259-265.

DOWDESWELL J. A. & SHARP M. J. (1986). Characterisation of pebble fabrics in modern terrestrial glaciogenic sediments. *Sedimentology*, **33**, 699 - 710.

DOWDESWELL, J. A., & SCOURSE, J. D. (1990). *Glacimarine environments: Processes and Sediments*. Geological Society Special Publication, no. 53.

DOWDESWELL, J. A., WHITTINGTON, R. J., JENNINGS, A. E., ANDREWS, J. T., MACKENSEN, A., &, MARIENFELD, P. (2000). An origin for laminated glaciomarine sediments through sea-ice build up and suppressed iceberg rafting. *Sedimentology*, **47**, 557-576.

DOWSETT, H. J., & CRONIN, T. M. (1990). High eustatic sea-level during the Middle Pliocene: evidence from the southeastern U.S. Atlantic Coastal Plain. *Geology*, **18**, 435-438.

DOWSETT, H. J., & POORE, R. Z. (1991). Pliocene sea surface temperatures of the North Atlantic at 3.0 Ma. *Quaternary Science Reviews*, **10**, 189-204.

DOWSETT, H. J., BARRON, J. A., POORE, R. Z., THOMPSON, R. S., CRONIN, T. M., ISHMAN, S. E., &, WILLARD, D. A. (1994). In: *ISGS Open-File Report*, **94-588**. Web-accessed report: (USGS Open-File Report 94-588) (http://geochange.er.usgs.gov/pub/PRISM/OFR_94-588/04_Brigham-Grette.html).

DRUITT, T. H. (1997). Pyroclastic density currents. In: Gilbert, J. S., & Sparks, R. S. J. (Eds.). *The Physics of Explosive Volcanic Eruptions*. Geological Society of London, Special Publication, **145**, 145-182.

DU, Z. J., & FOUGLER, G. R. (1999). The crustal structure beneath the northwest fjords, Iceland, from receiver functions and surface waves. *Geophysical Journal International*, **139**, 419-432.

DUGMORE, A. J. (1989). Tephrochronological studies of Holocene glacier fluctuations in south Iceland. In *Glacier fluctuations and climatic change*. Oerlemans, J., (Ed), Kluwer Academic Publishers. p. 37-55.

DUGMORE, A.J., & MAIZELS, J. K. (1985). A date with tephra. *Geographical Magazine* **57**, 532-538.

DUGMORE, A. J., & SUGDEN, D. E. (1991). Do the anomalous fluctuations of Solheimajökull reflect ice-divide migration. *Boreas*, **20**, 105-113.

DUGMORE, A. J., SHORE, J. S., COOK, G. T., NEWTON, A. J., EDWARDS, K. J., & LARSEN, G. (1995a). The radiocarbon dating of Icelandic tephra layers in Britain and Ireland. *Radiocarbon*, **37**(2), 286-295.

DUGMORE, A. J., LARSEN, G, & NEWTON, A. J. (1995b). Seven tephra isochrones in Scotland. *The Holocene*, **5**(3), 257-266.

DUGMORE, A. J., NEWTON, A. J., EDWARDS, K. J., LARSEN, G., BLACKFORD, J.J. & COOK, G. T. (1996). Long-distance marker horizons from small-scale eruptions: British tephra deposits from AD 1510 eruption of Hekla, Iceland. *Journal of Quaternary Science*, **11**(6), 511-516.

DUGMORE, A. J., LARSEN, G. & NEWTON, A. J. (1999). Geochemistry of historical-age silicic tephras in Iceland. *The Holocene*, **9**(4), 463-471.

DUGMORE, A. J., NEWTON, A. J., LARSEN, G., & COOK, G. T. (2000). Tephrochronology, environmental change and the Norse Settlement of Iceland. *Environmental Archaeology*, **5**, 21-34.

DUGMORE, A. J., & MCCULLOCH, R. D. (SUBMITTED). Precipitation and the pattern of ultra long-distance tephra deposition: The Hekla 1947 AD eruption in Finland. *Journal of Quaternary Science*.

DULLER, G. A. T. (1991). Equivalent dose determination using single aliquots. *Nuclear Tracks & Radiation Measurements*, **18**, 371-378.

DULLER, G. A. T. (1994). Luminescence dating of sediments using single aliquots: new procedures. *Quaternary Science Reviews*, **13**, 149-156.

DULLER, G. A. T. (1995). Luminescence dating using single aliquots: methods and applications. *Radiation Measurements*, **24**, 217-226.

DUMITRU, T. A. (2000). Fission-track Geochronology. In Noller, J. S., Sowers, J. M., & Lettis, W. R. (Eds.). *Quaternary Geochronology Methods and Applications*. American Geophysical Union Reference Shelf 4. p.131-156.

EASTERBROOK, D. J. (1988). Palaeomagnetism of Quaternary deposits. *Geological Society of America: Special Paper*, **227**, 111-120.

EASTERBROOK, D. J., BRIGGS, N. D., WESTGATE, J. A., & GORTON, M. P. (1981). Age of the Salmon Springs Glaciation in Washington. *Geology*, **9**, 87-93.

EDEN, D. E., &, FROGGATT P. C. (1996). A 6500 year old history of tephra deposition recorded in the sediments of Lake Tutira, North Island, New Zealand. *Quaternary International*, **34-36**, 55-64.

EDEN, D. E., & FROGGATT, P. C. (1988). Identification and stratigraphic significance of distal Aokautere Ash in three loess cores from eastern South Island, New Zealand. In: *Loess: Its*

Distribution, Geology and Soils., Eden, D. N. & Furkert, R. J. (Eds.). Balkema, Rotterdam, p. 47-58.

EDWARDS, M. B. (1986). Glacial environments. In *Sedimentary Environments and Facies (2nd Edition).* H.G. Reading (Ed.). Blackwell Scientific Publishers. p. 445-470.

EDWARDS, L. E., MUDIE, P. J., &, DE VERNAL, A. (1991). Pliocene palaeoclimatic reconstruction using dinoflagellate cysts: comparison of methods. *Quaternary Science Reviews*, **10**, 259-274.

EGLOFF, J., & JOHNSON, G. L. (1979). Erosional and depositional structures of southwest Iceland insular margin: thirteen geophysical profiles. In: Watkins, J. S., Montadert, L., & Dickerson, P. W. (Eds.). *Geological and Geophysical Investigations of Continental Margins.* Tulsa, Oklahoma: AAPG, p. 43-63. (cited in Ingólfsson and Norðdahl, 2001).

EILER, J. M., GRONVÖLD, K., & KITCHEN, N. (2000). Oxygen isotope evidence for the origin of chemical variations in lavas from the Theistareykir volcano in Iceland's northern volcanic zone. *Earth and Planetary Science Letters*, **184**, 269-286.

EINARSSON, T. (1986). Tephrochronology. In Berglund, B. E. (Ed): *Handbook of Holocene Palaeoecology and Palaeohydrology*. John Wiley and Sons. p. 329-342.

EINARSSON, Þ. (1968). *Jarðfræði. Saga bergs og lands.* Mal og menning (Geology of Iceland), Reykjavík. pp. 335.

EINARSSON, Þ. (1991). *Geology of Iceland.* Mal og menning, Reykjavík. pp. 335.

EINARSSON, Þ ., & ALBERTSSON, K. J. (1988). The glacial history of Iceland during the last 3 million years. *Philosophical Transactions of the Royal Society of London*, **318**, 637-644.

EIRÍKSSON, J. (1981). Tjörnes, North Iceland: A bibliographical review of the geological research history. *Jökull*, **30**, 1-20.

EIRÍKSSON, J. (1985). Facies analysis of the Breidavik Group sediments on Tjörnes. *Acta Naturalia Islandica*, **31**, pp. 53.

EIRÍKSSON, J., & GEIRSDÓTTIR, A. (1991). A record of Pliocene and Pleistocene glaciations and climatic changes in the North Atlantic based on variations in volcanic and sedimentary facies in Iceland. *Marine Geology*, **101**, 147-159.

EIRÍKSSON, J., GUDMUNÐSSON, A., KRISTJÁNSSON, L., & GUNNARSSON, K. (1990). Palaeomagnetism of the Pliocene-Pleistocene sediments and lava flows on Tjörnes and Flatey, North Iceland. *Boreas*, **19**, 39-55.

EIRÍKSSON, J., KNUDSEN, K. L., HAFLIDASON, H., & HEINEMEIER, J. (2000a). Chronology of late Holocene climatic events in the northern North Atlantic based on AMS ^{14}C dates and tephra markers from the volcano Hekla, Iceland. *Journal of Quaternary Science*, **15**(6), 573-580.

EIRÍKSSON, J., KNUDSEN, K. L., HAFLIDASON, H., & HENRIKSEN, P. (2000b). Late-glacial and Holocene palaeoceanography of the North Icelandic shelf. *Journal of Quaternary Science*, **15**(1), 23-42.

ELLIOT, S. (1998). *The Physics and Chemistry of Solids.* John Wiley and Sons, Chichester, pp.770.

EMBLETON, C., & KING, C. A. M. (1975). *Glacial geomorphology.* Edward Arnold, London. pp. 892.

EVERITT, B. (1993). *Cluster Analysis.* Edward Arnold, London. pp. 170.

EYLES, C. H., & EYLES, N. (1983). Sedimentation in a large lake, a reinterpretation of the late Pleistocene stratigraphy at Scarborough Bluffs, Ontario, Canada. *Geology*, **11**, 146-152.

EYLES, N. (1983). *Glacial Geology, a Landsystems Approach.* In Eyles, N. (Ed.) *Glacial Geology.* Pergamon, Oxford, p. 1-18.

EYLES, N. (1987). Late Pleistocene debris flow deposits in glacial lakes in British Columbia and Alaska. *Sedimentary Petrology*, **53**, 33-71.

EYLES, N. (1996). Passive margin uplift around the North Atlantic region and its role in Northern Hemisphere late Cenozoic glaciation. *Geology*, **24**(2), 103-106.

EYLES, N., & CLARK, B. M. (1988). Storm dominated deltas and ice scouring in a Late Pleistocene glacial lake. *Geological Society of America Bulletin*, **100**, 793-809.

EYLES, N., EYLES, C. H., & MCCABE, A. M. (1989). Sedimentation in an ice-contact sub-aqueous setting: the mid-Pleistocene 'North Sea Drifts' of Norfolk, UK. *Quaternary Science Reviews*, **8**, 57-74.

EYLES, N., MULLINS, H. T., & HINE, A. C. (1990). Thick and fast: sedimentation in a Pleistocene fjord lake of British Columbia. *Geology*, **18**, 1153-1157.

EYTHORSSON, J. (1935). On the variations of glaciers in Iceland. *Geographiska Annualer*, **17**, 121-137.

FAIRBANKS, R. G. (1989). A 17,000 year glacio-eustatic sea level record: influence of glacial melting rates on Younger Dryas event and deep-ocean circulation. *Nature*, **342**, 637-642.

FIACCO, R. J., THÓRDARSON, T., GERMANI, M. S., SELF, S., PALAIS, J. M., WHITLOW, S., & GROOTES, P. M. (1994). Atmospheric aerosol loading and transport due to the 1783-84 Laki eruption in Iceland interpreted from ash particles and acidity in the GISP II ice core. *Quaternary Research*, **42**, 231-240.

FILLON, R. H., MILLER, G. H., & ANDREWS, J. T. (1981). Terrigenous sand in Labrador Sea hemipelagic sediments and paleoglacial events on Baffin Island over the last 100,000 years. *Boreas*, **10**, 107-124.

FISHER, R. V. (1961). Proposed classification of volcaniclastic sediments and rocks. *Geological Society of America Bulletin*, **72**, 1409-1414.

FISHER, R. V. (1966). Rocks composed of volcanic fragments. *Earth Science Reviews*, **1**, 287-298.

FISHER, R. V., & SCHMINCKE, H.-U. (1982). *Pyroclastic rocks*. Springer-Verlag, Berlin.

FITCH, F. J., HOOKER, P. J., & MILLER, J. A. (1976). ^{40}Ar-^{39}Ar dating of the KBS Tuff in Koobi Fora Formation, East Rudolf, Kenya. *Nature*, **263**, 740-743.

FLEISCHER, R. L., & HART, H. R. (1972). Fission-track dating: techniques and problems. In: *Calibration of Hominoid Evolution*. Bishop, W. W., Miller, J. A., & Cole, S. (Eds.). Scottish Academic Press, Edinburgh. p. 135-170.

FLEISCHER, R. L., & PRICE, P. B. (1964). Glass dating by fission fragment tracks. *Journal of Geophysical Research*, **69**, 331-339.

FLEISCHER, R. L., PRICE, P.B., & WALKER, R. M. (1965). Effects of temperature, pressure and ionisation on the formation and stability of fission tracks in minerals and glasses. *Journal of Geophysical Research*, **70**, 1497-1502.

FLEISCHER, R. L., PRICE, P. B. & WALKER, R. M. (1975). *Nuclear Tracks in Solids: Principles and Applications*. Berkeley, University of California Press.

FLINT, R. F. (1970). *Glacial and Quaternary Geology*. John Wiley, New York.

FLINT, R. F., SANDERS, J. E., & RODGERS, J. (1960). Diamictite: A substitute term for symmictite. *Bulletin of the Geological Society of America*, **71**, 1809-1810.

FORMAN, S. L. & MILLER, G.H. (1984). Time-dependent soil morphologies and pedogenic processes on raised beaches, Boggerhalvoya, Spitsbergen, Svalbard Archipelago. *Arctic and Alpine Research*, **16**, 381-394.

FORMAN, S. L., PIERSON, J., LEPPER, K. (2000). Luminescence Geochronology. In Stratton Noller, J., Sowers, J. M., Lettis, W. R. (Eds.): *Quaternary Geochronology: Methods and Applications*, p. 157-176.

FRANCIS, P.W., O'CALLAGHAN, L., KETZCHMAR, G. A., THORPE, R. S., SPARKS, R. S. J., PAGE R. N., DE BARRIO, R. E., GILLOU, G., & GONZALEZ, O. E. (1983). The Cerro Galan ignimbrite. *Nature*, **301**, 51-53.

FREUNDT, A., WILSON, C. J. N., & CAREY, S. N. (2000). Ignimbrites and block-and-ash flow deposits. In *Encyclopedia of volcanoes*. Sigurdsson, H. (Ed.). Academic Press. San Diego. p. 581-589.

FRIDLEIFSSON, G. O. (1995). Miocene Glaciation in SE Iceland. In Hroarsson, B., Jonsson, D., & Jonsson, J. (Eds.). *Eyjar I eldhafi*. Jonsson, J. Honorary Volume, p. 77-85. (cited in Sæmundsson, 2000)

FRIÐRIKSSON, S. (1962). Um aðflutning íslenku flórunnar. *Náttúrufrædingurinn*, 32, 175-189. (cited in Lárusson, 1983)

FROGGATT, P. C. (1992). Standardisation of the chemical analyses of tephra deposits: Report of the ICCT working group. *Quaternary International*, **13/14**, 93-96.

FROGGATT, P. C., NELSON, C. S., CARTER, L., GRIGGS, G., & BLACK, K. P. (1986). An exceptionally large late Quaternary silicic eruption from New Zealand. *Nature*, **319**, 578-582.

FROGGATT, P. C., & LOWE, D. J. (1990). A review of the late Quaternary silicic and some other tephra formations from New Zealand: their stratigraphy, nomenclature, distribution, volume and age New Zealand. *Journal of Geology and Geophysics*, **33**, 89-109.

FRONVAL, T., JANSEN E., BLOEMENDAL, J., & JOHNSEN S. (1995). Ocean evidence for the coherent fluctuations in the Fennoscandian and Laurentide ice sheets on millenial timescales. *Nature*, **374**, 443-446.

FURMAN, T., FREY, F., & PARK, K. –H., (1995). The scale and source heterogeneity beneath the Eastern neovolcanic zone. *Journal of Geological Society*, **152**, 997-1002.

GANSECKI, C. A. , MAHOOD, G. A., & MCWILLIAMS, M. O. (1996). $^{40}Ar/^{39}Ar$ geochronology of rhyolites erupted following the collapse of the Yellowstone caldera, Yellowstone Plateau volcanic field: implications for crustal contamination. *Earth and Planetary Science Letters*, **142**, 91-107.

GANSECKI, C. A. , MAHOOD, G. A., & MCWILLIAMS, M. (1998). New ages for the climatic eruptions at Yellowstone. Single-crystal $^{40}Ar/^{39}Ar$ dating identifies contamination. *Geology*, **26**, 343-346

GARY, M., MCAFEE, R. JR., &WOLF, C. L. (Eds.) (1976). *Glossary of Geology*. American Geological Institute, Washington D. C. pp. 805.

GEIRSDÓTTIR, A. (1988). *Sedimentologic Analysis of Diamictites and Implications for Late Cenozoic Glaciations in Western Iceland.* Unpublished PhD thesis, University of Colorado, Boulder; (cited and summarised in Geirsdóttir, 1991).

GEIRSDÓTTIR, A. (1991). Diamictites of late Pliocene age in western Iceland. *Jökull*, **40**, 3-25.

GEIRSDÓTTIR, A., & EIRÍKSSON, J. (1994). Growth of an intermittent ice sheet in Iceland during the Late Pliocene and Pleistocene. *Quaternary Research*, **42**, 115-130.

GELTING, P. (1934). Studies on the vascular plants of East-Greenland between Franz Josef fjord and Dove Bay. *Meddelser om Grönland*, **101**, 281-312. (cited in Lárusson, 1983).

GIBBARD, P. L., & WEST , R. G. (2000). Quaternary chronostratigraphy: the nomenclature of terrestrial sequences. *Boreas*, **29**, 329-336.

GIBBONS, A. (1997). Doubts over spectacular dates. *Science*, **278**, 220-222.

GILBERT, R., & SHAW, J. (1981). Sedimentation in proglacial Sunwapta Lake, Alberta. *Canadian Journal of Earth Sciences*, **18**, 81-93.

GJESSING, J. (1967). Norway's paleic surface. *Norsk Geogr. Tidsskr.*, **21**(2), 69-132. (cited in Kleman and Stroeven, 1997).

GLASSER, N. F., & HALL, A. M (1997). Calculating Quaternary glacial erosion rates in Northeast Scotland. *Geomorphology*, **20**, 29-48.

GÖKSU, H. Y. REGULLA, D. F., VOGENAUER , A., & WIESER, A. (1988). Dose dependent TL fading of obsidians. *Nuclear Track and Radiation Measurements*, **14**, 143-147.

GOW, A. J., & WILLIAMSON, T. (1971). Volcanic ash in the Antarctic Ice Sheet and its possible climatic implications. *Earth and Planetary Science Letters*, **13**, 210-218.

GRAVENOR, C. P., VON BRUNN, V., & DREIMANIS, A. (1984). Nature and classification of waterlain glaciogenic sediments exemplified by Pleistocene, Late Palaeozoic and Late Precambrian deposits. *Earth Science Reviews*, **20**, 105-166.

GRÖNVOLD, K. (1972). *Structural and petrological studies in the Kerlingafjöll region, Central Iceland.* Unpublished PhD Thesis, University of Oxford.

GRÖNVOLD, K., ÓSKARSSON, N., JOHNSEN, S. J., CLAUSEN, H. B., HAMMER, C. U., BOND, G., & BARD, E. (1995). Ash layers from Iceland in the Greenland GRIP ice core correlated with oceanic and land sediments. *Earth and Planetary Science Letters*, **135**, 149-155.

GROUSSET, F. E., PUJOL, C., LABEYRIE, L., AUFFRET, G., BOELAERT, A. (2000). Were the North Atlantic Heinrich events triggered by the behaviour of the European ice sheets? *Geology*, **28**, 123-126.

GUDMUNÐSSON, Á. (1986). Mechanical aspects of postglacial volcanism and tectonics of the Reykjanes Peninsula, Southwest Iceland. *Journal of Geophysical Research*, **91**, 12,711-12,721.

GUDMUNÐSSON, Á. (1989). *Jarðfræði við áformaðar jarðangaleiðir á norðanverðum Vestfjörðum (Vestfirðir Tunnel Report).* OS-89014/VOD-02 B. Órkustofnun. Iceland. pp. 17.

GUDMUNÐSSON, Á. (1995). Ocean-ridge discontinuites in Iceland. *Journal of Geological Society of London*, **152**, 1011-1015.

GUDMUNÐSSON, Á. (2000). Dynamics of volcanic systems in Iceland: example of tectonism and volcanism at juxtaposed hotspots and midocean ridge system. *Annual Reviews of Earth and Planetary Sciences*, **28**, 107-140.

GUDMUNÐSSON, Á., BERGERAT, F., & ANGELIER, J. (1996). Off-rift and rift zone palaeostress in Northwest Iceland. *Tectonophysics*, **255**, 211-228.

GUDMUNÐSSON, Á. T. (1996). *Volcanoes in Iceland: 10,000 Years of Volcanic History*. Vaka-Helgafell, Reykjavík. pp. 136.

GUDMUNÐSSON, H. (1997). A review of the Holocene environmental history of Iceland. *Quaternary Science Reviews*, **16**, 81-92.

GUINIER, A. (1984). *The Structure of Matter*. Edward Arnold, London, pp. 230.

HADJAS, I., ZOLITSCHKA, B., IVY-OCHS, S. D., BEER, J., BONANI, G. LEROY, S. A. G., NEGENDANK, J. W., RAMRATH, M., & SUTER, M. (1995). AMS radiocarbon dating of annually laminated sediments from Lake Holzmaar, Germany. *Quaternary Science Reviews*, **14**, 137-143.

HAFLIDASON, H., SERJUP, H. P., & KLITGAARD-KRISTENSEN, D. (1996). Quantification of the ^{14}C difference between terrestrial and marine environments during the Younger Dryas and the Holocene period in the North Atlantic region. *American Geophysical Union, Fall Meeting*, San Francisco, 15-19 December; (abstract). (cited in Haflidason *et al.*, 2000).

HAFLIDASON, H., SERJUP, H. P., KRISTENSEN, D. K., EIRÍKSSON, J., & KNUDSEN, K. L. (1998). Reservoir age estimate for the Norwegian-Greenland Sea for the late-glacial and Holocene time period. *6th International Conference on Palaeoceanography*, Lisbon, 22-28th August; (abstract). (cited in Haflidason *et al.*, 2000).

HAFLIDASON, H., EIRÍKSSON, J., & VAN KREVELD, S. (2000). The tephrochronology of Iceland and the North Atlantic region during the Middle and Late Quaternary: a review. *Journal of Quaternary Science*, **15**(1), 3-22.

HAJDAS, I., IVY-OCHS, S.D., BONANI, G., LOTTER, A. F., ZOLITSCHKA, B., & SCHLUCHTER, C. (1995a). Radiocarbon age of the Laacher-See-Tephra - 11,230+/-40 BP. *Radiocarbon*, **37**(2), 149-154.

HALL, A. (1987). *Igneous petrology*. Longman Scientific and Technical, Harlow. pp. 573.

HALL, A. M., & SUGDEN, D. E. (1987). Limited modification of mid-latitude landscapes by ice sheets: the case of north-east Scotland. *Earth Surface Processes and Landforms*, **12**, 531-542.

HALLET, D. J., MATTHEWS, R. W., & FOIT, F. F. (2001). Mid-Holocene Glacier Peak and Mount St. Helens We Tephra layers detected in lake sediments from southern British Columbia using high-resolution techniques. *Quaternary Research*, **55**, 284-292.

HALLSDÓTTIR, M. (1987). Pollen analytical studies of human influence on vegetation in relation to the Landnám tephra layer in southwest Iceland. LUNDQUA Thesis, **18**, pp. 45.

HAMBREY, M. J. (1994). *Glacial Environments*. UCL Press, London. pp. 364.

HAMMER, C. U. (1980). Traces of Icelandic eruptions in the Greenland Ice Sheet. *Jökull*, **34**, 51-65.

HANNA, G. C., WESTCOTT, C. H., LEMMEL, H. D., LEONARD, B. R., STORY, J. S., & ATTREE, P. M. (1969). Revision of values for the 2200m/s neutron constants for four fissile nuclides. *Atomic Energy Review*, **7**(4), 3-92.

HANNESDÓTTIR, L. (1976). Vestfjarðavirkjanir. Glàmusvæði. Jarðfræði stíflustæða og vatnafræði. Órkustofnun, Reykjavík, OS-ROD-7636, 1-19. (cited, summarised and translated in Lárusson, 1983).

HANSEN, L., FUNDER, S., MURRAY, A. S., MEJDAHL, V. (1999). Luminescence dating of the last Weichselian Glacier advance in East Greenland. *Quaternary Geochronology*, **18**, 179-190.

HANSOM, J. D., & BRIGGS D. J. (1991). Sea-level change in Vestfirðir, North West Iceland. In *Environmental Change in Iceland: Past and Present*. J. K. Maizels and C. Caseldine (Eds.). Kluwer Academic Publishers, p. 79-91.

HAQ, B. U., HARDENBOL, J., & VAIL, P. R. (1987). Chronology of the fluctuating sea levels since the Triassic. *Science*, **235**, 1156-1157.

HARALDSSON, H. (1981). The Markarfljót sandur area, southern Iceland: sedimentological, petrological and stratigraphical studies. *Straiae*, **15**, Uppsala, pp. 65.

HARDS, V. L. (1985). *The evolution of the Snæfell Volcanic centre, eastern Iceland.* Unpublished PhD Thesis, University of Durham.

HART, J. K. (1992). Sedimentary environments associated with Glacial Lake Trimingham, Norfolk, UK. *Boreas*, **21**, 119-136.

HART, J. K., & BOULTON, G. S. (1991). The inter-relation of glaciotectonic and glaciodepositional processes within the glacial environment. *Quaternary Science Reviews*, **10**, 335-350.

HART, J. K., & ROBERTS, D. H. (1994). Criteria to distinguish between subglacial glaciotectonic and glaciomarine sedimentation, I. Deformation styles and sedimentology. *Sedimentary Geology*, **91**, 191-213.

HART, J. K., HINDMARSH, R. C. A., & BOULTON, G. S. (1990). Different styles of subglacial glaciotectonic deformation in the context of the Anglian ice sheet. *Earth Surface Processes and Landforms*, **15**, 227-242.

HELGASON, J., & DUNCAN, R. (1992). Skaftafell: lava stratigraphy, magnetic polarity and K-Ar dating. *Geoscience Society of Iceland: Abstract Volume*, p. 45. (cited in Sæmundsson, 2000).

HILDRETH, W., & MAHOOD, G. (1985). Correlation of ash-flow tuffs. *Geological Society of America Bulletin*, **96**, 968-974.

HILGEN, F. J. (1991). Astronomical calibration of Gauss to Matayama sapropels in the Mediterranean and implications for the Geomagnetic Polarity Time Scale. *Earth and Planetary Science Letters*, **104**, 226-244.

HJARTSSON, Á. (1989). The ages of the Fossvogur layers and the Álftanes end-moraines, SW Iceland. *Jökull*, **39**, 21-31.

HJARTSSON, Á., & INGÓLFSSON, Ó. (1988). Preboreal glaciation of southeastern Iceland. *Jökull*, **38**, 1-16.

HJARTARSON, A., & HAFSTAD, T. H. H. (1997). *Svidinhornahraun, bedrock mapping*. Órkustofnun Report no. **OS-97016**. (cited in Sæmundsson, 2000).

HJORT C., INGÓLFSSON Ó., & NORÐDAHL H. (1986). Late Quaternary Geology and glacial history of Hornstranðir, Northwest Iceland: A reconnaissance study. *Jökull*, **35**, 9-28.

HODDER, A. P. W., DE LANGE, P. J. & LOWE, D. J. (1991). Dissolution and depletion of ferromagnesian minerals from Holocene tephra layers in an acid bog, New Zealand, and implications for tephra correlation. *Journal of Quaternary Science*, **6**(3), 195-208.

HOPPE, G. (1968). Grímsey and the maximum extent of the last glaciation of Iceland. *Geografiska Annaler* **50A**, 16-24.

HOPPE, G. (1982). The extent of the last inland ice-sheet of Iceland. *Jökull*, **32**, 3-11.

HORN, P., MÜLLER-SOHNIUS, D., STORZER, D., & ZÖLLER, L. (1993). ^{40}K-^{40}Ar, fission-track and thermoluminescence ages of Quaternary volcanic tuffs and their bearing on Acheulian artifacts from Bori, Kukdi Valley, Pune district, India. *Zeitschrift der Deutschen Geologishchen Gesellschaft*, **144**, 326-329.

HOUGHTON, B. F., WILSON, C. J. N., MCWILLIAMS, M. D., LANPHERE, M. A., WEAVER, S. D., BRIGGS, R. M., &, PRINGLE, M. S. (1995). Chronology and dynamics of a large silicic magmatic system: Central Taupo Volcanic Zone, New Zealand. *Geology*, **23**, 13-16.

HOWARD, W. R. (1997). A warm future in the past. *Nature*, **388**, 418-419.

HU, Q., SMITH, P., EVENSEN, N. M., YORK, D. (1996). Lasing into the Holocene: extending the 40Ar-39Ar laser probe method into the ^{14}C age range. *Earth & Planetary Science Letters,* **123**, 331-336.

HUBBARD, A. M., SUGDEN, D. E., NORÐDAHL, H., PETURSSON, H., & DUGMORE, A. J. (MANUSCRIPT). Modelling glacial decay and meltwater production in Iceland 23-10 ka.

HUGHEN, K. A., OVERPECK J. T., PETERSON L. C., & TRUMBONE S. (1997). Rapid climate change in the tropical Atlantic region during the last deglaciation. *Nature*, **380**, 51-54.

HUGHEN, K. A., OVERPECK, J. T., LEHMAN, S. J., KASHGARIAN, M., SOUTHON, J., PETERSON, L. C., ALLEY, R., & SIGMAN, D. M. (1998). Deglacial changes in ocean circulation from an extended radiocarbon calibration. *Nature*, **391**, 65-68.

HULTON, N. J., SUGDEN, D. E., PAYNE, A. J., & CLAPPERTON, C. M. (1994). Glacier modelling and the climate of Patagonia during the Last Glacial Maximum. *Quaternary Research*, **42**, 1-19.

HUNT, J. B., & HILL, P. G. (1993). Tephra geochemistry: a discussion of some persistent analytical problems. *The Holocene*, **3**(3), 271-278.

HUNT, J. B., & HILL, P. G. (1996). An inter-laboratory comparison of the electron probe microanalysis of glass geochemistry. *Quaternary International*, **34-36**, 229-241.

HUNT, J. B., & HILL, P. G. (2001). Tephrological implications of beam size – sample-size effects in electron microprobe analysis of glass shards. *Journal of Quaternary Science*, **16**(2), 105-117.

HUNTLEY, D. J., GODFREY-SMITH, D. I., & THEWALT, M. L. W. (1985). Optical dating of sediment. *Nature*, **313**, 105-107.

HUNTLEY, D. J., HUTTON, J. T., & PRESCOTT, J. R. (1993). Optical dating using inclusions within quartz grains. *Geology*, **21**, 1087-090.

HUNTLEY, D. J., HUTTON, J. T., & PRESCOTT, J. R. (1994). Further luminescence dates from the dune sequence in the southeast of South Australia. *Quaternary Science Reviews*, **13**, 201-207.

HUNTLEY, D. J., & PRESCOTT, J. R. (2001). Improved methodology and new thermoluminescence ages for the dune sequence in south-east South Australia. *Quaternary Science Reviews*, **20**, 687-699.

HURFORD, A. J. (1992). Fission Track Dating. In Smart, P. L. and Frances P. D. (Eds): *Quaternary dating methods - a users guide*: *Quaternary Research Association Technical Guide no. 4*. Quaternary Research Association, London. p. 84-107.

HURFORD, A. J. (1999). Zeta: the ultimate solution to fission-track analysis calibration or just an interim measure. In Van den Haute, P., & deCorte, F. (Eds.). *Advances in fission-track geochronology: A selection of papers presented at the International Workshop on Fission-Track Dating, Ghent, Belgium, 1996*. Kluwer Academic Publishers, Dordrecht. p.19-32.

HURFORD, A. J., & GREEN, P. F. (1983). The zeta calibration of fission-track dating. *Isotope Geoscience*, **1**, 285-317.

HURFORD, A. J., & HAMMERSCHMIDT, K. (1985). $^{40}Ar/^{39}Ar$ and K-Ar dating of the Bishop and Fish Canyon tuffs: calibration ages for fission-track dating standards. *Chemical Geology*, **58**, 23-32.

HURFORD, A. J., GLEADOW, A. J. W., & NAESER, C. W. (1976). Fission-track dating of pumice from the KBS Tuff, East Rudolf, Kenya. *Nature*, **263**, 738-740.

IMBRIE, J., BERGER, A., BOYLE, E.A., CLEMENS, S. C., DUFFY, A., HOWARD, W. R., KUKLA, G., KUTZBACH, J., MARTINSON, D. G., MCINTYRE, A., MIX, A. C., MOLFINO, B., MORLEY, J. J., PETERSON, L. C., PISIAS, N. G., PRELL, W. L., RAYMO, M. E., SHACKLETON, N. J., & TOGGWEILER, J. R. (1993). On the structure and origin of major glaciation cycles. 2. The 100,000-year cycle. *Palaeoceanography*, **8**, 699-735.

IMSLAND, P (1978). *The Petrology of Iceland: Some General Remarks*. Nordic Volcanological Institute Report 7808, p. 26.

INGÓLFSSON, Ó. (1987). *Investigation of the Late Weichselian glacial history of the lower Borgarfjörður region, western Iceland*. LUNDQUA thesis, **19**, Department of Quaternary Geology, University of Lund.

INGÓLFSSON, Ó. (1991). A review of the late Weichselian and early Holocene glacial and environmental history of Iceland. In Caseldine, C. J., & Maizels, J. (Eds.). *Environmental Changes in Iceland. Past and Present*. Kluwer, Dordrecht. p. 13-29.

INGÓLFSSON, Ó., & NORÐDAHL, H. (1994). A review of the environmental history of Iceland, 13,000-9000 yr BP. *Journal of Quaternary Science*, **9**(2), 147-150.

INGÓLFSSON, Ó., NORDDAHL, H. & HAFLIDASON, H. (1995). Rapid isostatic rebound in south-western Iceland at the end of the last glaciation. *Boreas*, **24**(3), 245-259.

INGÓLFSSON, O., & NORÐDAHL, H. (2001). High relative sea level during the Bolling Interstadial in western Iceland: a reflection of ice-sheet collapse and extremely rapid glacial unloading. *Arctic, Antarctic, and Alpine Research*, **33**(2), 231-243.

IPCC (INTER-GOVERNMENTAL PANEL ON CLIMATE CHANGE) (1995). *Climate Change 1995: Impacts, Adaptations and Mitigation of Climate Change*: Scientific-Technical Analyses. Watson, R.T., Zinyowera, M.C., and Moss, R.H., (Eds.), Cambridge University Press, Cambridge, pp. 879.

IPCC (INTER-GOVERNMENTAL PANEL ON CLIMATE CHANGE) (2001). *Climate Change 2001: I – The Scientific Basis.* Cambridge University Press. (Information obtained from www.cambridge.org/climatechange)

IRVINE, T. N., & BARAGAR, W. R. A. (1971). A guide to the chemical classification of common volcanic rocks. *Canadian Journal of Earth Sciences*, **8**, 523-548.

ITO, G., SHEN, Y., HIRTH, G., & WOLFE, C. J. (1999). Mantle flow, melting and dehydration of the Iceland mantle plume. *Earth and Planetary Science Letters*, **165**(1), 81-96.

JAFFEY, A. H., FLYNN, K. F., GLENDENIN, L. E., BEMTLEY, W. C., & ESSLING, A. M. (1971). Precision measurements of the half-lives and specific activities of ^{235}U and ^{238}U. *Physical Review*, **C4**, 1889-1906.

JAIN, A. K. & DUBES, R. C. (1988). *Algorithms for clustering data.* Prentice Hall, New Jersey. pp. 320.

JAKOBSSON, S. P. (1972). Chemistry and distribution pattern of Recent basaltic rocks in Iceland. *Lithos*, **5**, 365-386.

JAKOBSSON, S. P. (1979). Outline of the petrology of Iceland. *Jökull*, **29**, 57-73.

JANSEN, E., & SJØHOLM, J. (1991). Reconstruction of glaciation over the past 6 Myr from ice-borne deposits in the Norwegian Sea. *Nature*, **349**, 600-603.

JAPSEN, P., & CHALMERS, J. A. (2000). Neogene uplift and tectonics around the North Atlantic: overview. *Global and Planetary Change*, **24**, 165-173. (Web accessed version of journal www.elsevier.com/locate/gloplacha)

JARVIS, K. E., GRAY, A. L., & HOUK, R. S. (1992). *Handbook of Inductively Coupled Plasma Mass Spectrometry*. Blackie, Glasgow. pp. 380.

JENNINGS, A., SYVITSKI, J., GERSON, L., GRÖNVOLD, K., GEIRSDÓTTIR, A., HARDARDÓTTIR, A., ANDREWS, J., & HAGEN, S. (2000). Chronology and palaeoenvironments during the Late Weichselian deglaciation of the SW Iceland shelf. *Boreas*, **29**, 167-183.

JÓHANNESSON, H. (1975). *Structure and petrochemistry of the Rekjadalur central volcano and the surrounding areas, midwest Iceland.* Unpublished Ph.D. Thesis, Durham University. pp. 273.

JÓHANNESSON, H., FLORES, R. M., & JÓNSSON, J. (1981). A short account of the Holocene tephrochronology of the Snæfellsjökull central volcano, western Iceland. *Jökull*, **31**, 23-30.

JÓHANNESSON, H., & SÆMUNDSSON, K. (1989). *Geological map of Iceland. 1:500,000.* Museum of Natural History and the Iceland Geodetic Survey. Reykjavík.

JÓHANNESSON, H., & SÆMUNDSSON, K. (1998). *Geological map of Iceland. 1:500,000. Tectonics.* Icelandic Institute of Natural History, Reykjavík (1st Edition).

JÓHANSEN, J. (1975). Pollen diagrams from the Shetland and Faroe Islands. *New Phytologist*, **75**, 369-387.

JOHN, B. S. (1974). Northwest Iceland reconnaissance 1973 (Durham University Vestfirðir Project). *Dept. of Geography, University of Durham Special Publication,* pp. 54.

JOHN, B. S. (1975). Durham University Vestfirðir Project 1975. *Dept. of Geography, University of Durham Special Publication.*

JOHN, B. S., & SUGDEN, D. E. (1962). The morphology of Kaldalon, a recently deglaciated valley in Iceland. *Geographiska Annualer*, **44**, 347-365.

JOHNSEN, S. J., DAHL-JANSEN, D., GUNDESTRUP, STEFFENSEN, J. P., CLAUSEN, MILLER, H., MASSON-DELMOTTE, V., SVEINBJORNSDOTTIR, A. E., & WHITE, J. (2001). Oxygen isotope and palaeotemperature records from six Greenland ice-core stations: Camp Century, Dye-3, GRIP, GISP2, Renland and NorthGRIP. *Journal of Quaternary Science*, **16**(4), 299-307.

JOHNSON, N. M., & MCGEE, V. E. (1983). Magnetic polarity stratigraphy: stochastic properties of data, sampling problems and the evolution of interpretations. *Journal of Geophysical Research*, **88**, 1213-1221.

JOLLIFE, I. T. (1986). *Principal Components Analysis.* Springer-Verlag, New York. pp. 271.

JONES, J. G. (1966). Intraglacial volcanoes of south-west Iceland and their significance in the interpretation of the form of marine basaltic volcanoes. *Nature*, **212**, 586-588.

JONES, J. G. (1969). Intraglacial volcanoes of the Largarvatn region, Southwest Iceland, I. *Journal of the Geological Society of London*, **124**, 197-211.

JONES, J. G. (1970). Intraglacial volcanoes of the Largarvatn region, Southwest Iceland, II. *The Journal of Geology*, **78**, 127-143.

JONES, R. L., & KEEN, D. H. (1993). *Pleistocene Environments in the British Isles*. Chapman and Hall, London.

JØRGENSEN, K. A. (1980). The Þórsmörk Ignimbrite: An unusual comenditic pyroclastic flow from southern Iceland. *Journal of Volcanology and Geothermal Research*, **8**, 7-22.

JØRGENSEN, K. A. (1981). The eruption of Þórsmörk Ignimbrite, south Iceland. *Nordic Volcanological Institute, Reykjavik*, **Report no. 8103**.

JØRGENSEN, K. A. (1987). Mineralogy and petrology of alkaline granophyric xenoliths from the Þórsmörk Ignimbrite, southern Iceland. *Lithos*, **20**, 153-168.

JULL, M., & MCKENZIE, D. (1996). The effect of deglaciation on mantle melting beneath Iceland. *Journal of Geophysical Research,* **101**, 21,815-21,828.

KALDAL, I., & VÍKINGSSON, S. (1991). Early Holocene deglaciation in central Iceland. *Jökull*, **40**, 51-66.

KANEOKA, I. (1972). The effect of hydration on the ^{40}K-^{40}Ar ages of volcanic rocks. *Earth and Planetary Science Letters*, **14**, 216-220.

KARROW, P. F., & CALKIN, P. E. (1985). *Quaternary Evolution of the Great Lakes*. Geological Association of Canada: Special Publication, **30**, pp. 258.

KÄYHKÖ, J. (2000). Landscape processes in the Oldáðhraun region, north-eastern Iceland. In: *Iceland 2000 – Modern Processes and Past Environments. Conference Abstracts*. April 27th-29th 2000. p. 51-53.

KENNETT, J. P., & THUNNELL, R. C. (1975). Global increase in Quaternary explosive volcanism. *Science*, **187**, 497-503.

KIRKBRIDE, M. J., & DUGMORE, A. J. (2001). Timing and significance of mid-Holocene glacier advances in northern Iceland. *Journal of Quaternary Science*, **16**(2), 145-153.

KITAGAWA, H., & VAN DER PLICHT, J. (1998). Atmospheric radiocarbon calibration to 45,000 yr B. P.: Late glacial fluctuations and cosmogenic isotope production. *Science*, **279**, 1187-1190.

KIYAK, N., BULUR, E., & GUNESDOGDU, S. (1999). Thermoluminescent and spectrophotometric properties of gamma irradiated glass sheets. In: *9th International Conference on Luminescence and Electron Spin Resonance Dating (LED 99), Book of Abstracts.* Rome 6-10 September, 1999. p. 144.

KJARTANSSON, G. (1943). *Árnesingasaga Yfirlit og jarðsaga*. Árnesingafélagið, Rekjavik. pp. 250. (cited in Lárusson, 1983).

KJARTANSSON, G. (1969). Jarðfræðikort, 1:250,000. Blað 1. Norðvesturland. Menningarsjóður, Reykjavík. (cited and summarised in Lárusson, 1983).

KJÁRTSSON, G. (1970). Ur sögu berggrunns og landslags á Midsudurlandi. *Sudri*, **2**, 12-100. Reykjavík (cited in Haraldsson, 1981).

KLEMAN, J. (1994). Preservation of landforms under ice sheets and ice caps. *Geomorphology*, **9**, 19-32.

KLEMAN, J. & BORGSTRÖM, I. (1994). Glacial landforms indicative of a partly frozen bed. *Journal of Glaciology*, **40** (135), 255-264.

KLEMAN, J., & STROEVEN, A. P. (1997). Preglacial surface remnants and Quaternary glacial regimes in northwestern Sweden. *Geomorphology*, **19** (1-2), 35-54

KLEMAN, J., BORGSTRÖM, I., ROBERTSSON, A, -M., &, LILLIESKÖLD, M. (1992). Morphology and stratigraphy from several deglaciations in the Transtrand Mountains, western Sweden. *Journal of Quaternary Science*, **7**(1), 1-16.

KOÇ, N., JANSEN, E., AND HAFLIDASON, H. (1993). Palaeoceanographic reconstructions of surface ocean conditions in the Greenland, Iceland and Norwegian Seas through the last 14 Ka based on diatoms. *Quaternary Science Reviews*, **12**(2), 115-141.

KOÇ N., JANSEN E., HALD M., & LABEYRIE L. (1996). Late glacial-Holocene sea surface temperatures and gradients between the North Atlantic and the Norwegian Sea: implications for the Nordic heat pump. In Andrews J. T., Austin W.E.N., Bergsten H., Jennings A. E. (Eds). *Late*

Quaternary palaeoceanography of the North Atlantic margins. Geological Society Special Publication no. 11, pp. 177 - 185.

KOHN, B. P. (1979). Identification and significance of a late Pleistocene tephra in Canterbury district, South Island, New Zealand. *Quaternary Research*, **11**, 78-92.

KOHN, B. P., PILLANS, B., & MCGLONE, M. S. (1992). Zircon fission-track age for middle Pleistocene Rangitawa Tephra, New Zealand: stratigraphic and palaeoclimatic significance. *Palaeography, Palaeoclimatology, Palaeoecology*, **95**, 73-94.

KORENAGA, J., & KELEMEN, P. B. (2000). Major element heterogeneity in the mantle source of the North Atlantic igneous province. *Earth and Planetary Science Letters*, **184**, 251-268.

KOVACH, W. L. (1995). Multivariate data analysis. In Maddy, D. & Brew, J. S. (Eds.): *Statistical Modelling of Quaternary Science Data.* Quaternary Research Association Technical Guide no. 5, Cambridge, p. 1-38.

KRANTZ, D. E. (1991). A chronology of Pliocene sea-level fluctuations: the U.S. Middle Atlantic Coastal Plain record. *Quaternary Science Reviews*, **10**, 163-174.

KRISTJÁNSSON, L., FRIDLEIFSSON, I. B., WATKINS, N. D. (1980). Stratigraphy and palaeomagnetism of the Esja, Eyrarfjall and Akrafjall mountains, SW Iceland. *Journal of Geophysics*, **47**, 31-42.

KRISTJÁNSSON, L., PATZOLD, R., & PRESTON, J. (1975). The palaeomagnetism and geology of the Patreksfjörður -Árnarfjörður region of Northwest Iceland. *Tectonophysics*, **25**, 201-216.

KUKLA, G. (1989). Long continental records of climate - an introduction. *Palaeogeography, Palaeoclimatology, Palaeoecology*, **72**, 1-9.

KUKLA, G., & CILEK, V. (1996). Plio-Pleistocene megacycles: record of climate and tectonics. *Palaeogeography, Palaeoclimatology, Palaeoecology*, **120**, 171-194.

KUNO, H. (1966). Lateral variation of basalt magma types across continental margins and island arcs. *Bulletin of Volcanology*, **29**, 195-222.

KVAMME T., MANGERUD J., FURNES H., & RUDDIMAN W. F. (1989). Geochemistry of Pleistocene ash zones in cores from the North Atlantic. *Norsk Geologisk Tidsskrift*, **69**, 251-272.

KVASOV, D. D., & BLAZHCHISHIN, A. I. (1978). The key to sources of the Pliocene and Pleistocene glaciation is at the bottom of the Barents Sea. *Nature*, **273**, 138-140.

LACASSE, C., SIGURDSSON, H., JÓHANNESSON, H., PATERNÉ, M., & CAREY, S. (1995). Source of Ash Zone 1 in the North Atlantic. *Bulletin of Volcanology*, **57**, 18-32.

LACASSE, C., SIGURDSSON, H., CAREY, S., PATTERN, M., & GUICHARD, F. (1996). North-Atlantic deep-sea sedimentation of late Quaternary tephra from the Iceland hotspot. *Marine Geology* **129**(3-4), 207-235.

LACKSCHEWITZ, K. S., & WALLRABE-ADAMS, H-J. (1997). Composition and origin of volcanic ash zones in Late Quaternary sediments from the Reykjanes Ridge: evidence for ash fallout and ice-rafting. *Marine Geology*, **136**, 209-224.

LARSEN, E., & SEJRUP, H. P. (1987). Cave stratigraphy in western Norway: multiple Weichselian glaciations and interstadial vertebrate faunas. *Boreas*, **16**, 267-292.

LARSEN, G. (1981). Tephrochronology by microprobe analysis. In *Tephra Studies.* Self, S. & Sparks, R. S. J. (Eds.). D. Reidel Publishing Company. p. 95-102.

LARSEN, G. (1984). Recent volcanic history of the Veiðivötn area, Southern Iceland – an approach to volcanic risk assessment. *Journal of Volcanology and Geothermal Research*, **22**, 33-58.

LARSEN, G., & THÓRARINSSON, S. (1977). H4 and other acid tephra layers. *Jökull*, **27**, 28-46.

LARSEN, G., GUDMUNÐSSON, M. T. & BJÖRNSSON, H. (1998). Eight centuries of periodic volcanism at the centre of the Iceland hotspot revealed by glacier tephrostratigraphy. *Geology*, **26**(10), 943-946.

LARSEN, G., DUGMORE, A., & NEWTON, A. (1999). Geochemistry of historical-age silicic tephras in Iceland. *The Holocene*, **9**(4), 463-471.

LARSEN, G. [*ET AL.*,] (2000). Holocene volcanism in Iceland and tephrochronology as a tool in volcanology. In: *Iceland 2000 – Modern Processes and Past Environments. Conference Abstracts.* April 27th-29th 2000. p. 65-67.

LARSEN, G., NEWTON, A. J., DUGMORE, A. J., & VILMUNDARDÓTTIR, E. G. (2001). Geochemistry, dispersal, volumes and chronology of Holocene silicic tephra layers from the Katla volcanic system. *Journal of Quaternary Science*, **16**(2), 119-132.

LARSEN, H. C., SAUNDERS, A. D., CLIFT, P. D., BEGET, J., WEI, W., & SPEZZAFERRI, S. (1994). Seven million years of glaciation in Greenland. *Science*, **264**, 952-95.

LÁRUSSON, E. (1983). *Aspects of the glacial geomorphology of the Vestfirðir peninsula of northwest Iceland with particular reference to the Vestur-Isafjardarsysla region.* Unpublished PhD thesis, University of Durham. pp. 301.

LAWSON, C. A., NORD ,G. L., JNR., & CHAMPION, D. E. (1987). Fe-Ti oxide mineralogy and the origin of normal and reverse remnant magnetisation in dacitic pumice blocks from Mt. Shasta, California. *Physics of the Earth and Planetary Interiors*, **46**, 270-288.

LAWVER, L. A., & MILLER, R. D. (1994). Iceland hotspot track. *Geology*, **22**, 311-314.

LE BAS, M. J., LE MAITRE, R. W., STRECKEISEN, A., & ZANELLIN, B. (1986). A chemical classification of volcanic rocks based on the total alkali-silica diagram. *Journal of Petrology*, **27**, 745-750.

LE MAITRE, R. W. (1976). The chemical variability of some common igneous rocks. *Journal of Petrology*, **17**, 589-637.

LE MAITRE, R. W., BATEMAN, P., DUDEK, A. KELLER, J., LAMMEYRSE, L., LE BAS, M. J., SADINE, P. A., SCHMID, R., SORENSEN, H., STRECKEISEN, A., WOOLLEY, A. R., & ZANETTIN, B. (1989). *A Classification of Igneous Rocks and Glossary of Terms*. Blackwell, Oxford.

LEMMEN, D. S., GILBERT, R., SMOL, J. P., & HALL, R. I. (1987). Holocene sedimentation in glacial Tasikutaaq Lake, Baffin Island. *Canadian Journal of Earth Sciences*, **25**, 810-823.

LEONARD, E. M. (1986). Varve studies at Hector Lake, Alberta, Canada, and the relationship between glacial activity and sedimentation. *Quaternary Research*, **25**, 199-214.

LEROY, S., & DUPONT, L. (1994). Development of vegetation and continental aridity in northwestern Africa during the Late Pliocene: the pollen record of ODP Site 658. *Palaeogeography, Palaeoclimatology, Palaeoecology*, **109**, 295-316.

LI, S-H., & YIN, G-M. (2000). Luminescence dating of young volcanic activities in China. *Quaternary Science Reviews*, **20**(5-9), 865-868.

LIAN, O. B., & SHANE, P. A. (2000). Optical dating of paleosols bracketing the widespread Rotoehu tephra, North Island, New Zealand. *Quaternary Science Reviews*, **19**, 1649-1662.

LINDROTH, C. H. (1931). Die Insektenfauna und ihre Probleme. *Zoologiska Bidrag från Uppsala*, **13**, 105-599. (Translated in Lárusson, 1983)

LOBELLO, PH., FERAUD, G., HALL, C. M., YORK, D., LAVINA, P., & BERNAT, M. (1987). ^{40}Ar-^{39}Ar step-heating and laser fusion dating of Quaternary Pumice from Neschers, Massif Central, France: the defeat of xenocrystic contamination. *Chemical Geology (Isotope Geosciences Section)*, **66**, 61-71.

LONG, D., BENT, A., HARLAND, R., GREGROY, D. M., GRAHAM, D.K., & MORTON, A. C. (1986). Late Quaternary palaeontology, sedimentology and geochemistry of a Vibrocore from the Witch Ground Basin, central North Sea. *Marine Geology*, **73**, 109-123.

LONSDALE, P., & BATIZA, R. (1980). Hyaloclastite and lava flows on young seamounts. *Geological Society of America Bulletin*, **91**, 545-554.

LOTTER, A. F., & BIRKS, H. J. B. (1993). The impact of the Laacher See Tephra on terrestrial and aquatic ecosystems in the Black Forest, southern Germany. *Journal of Quaternary Science*, **8**, 263-276.

LOWE, D. J. (1988). Late Quaternary volcanism in New Zealand: towards an integrated record using distal airfall tephras in lakes and bogs. *Journal of Quaternary Science*, **3**(2), 111-120.

LOWE, D. J., & DE LANGE, W. P. (1998). Tephrochronologie et co-existence Hommes-Volcans. Tephrochronology, Man and Volcanoes). In *INQUA COTAV/UISPP31 Inter Congress Symposium Abstracts*. Brives-Charensac, France, 24-29 August 1998. p. 153-159.

LOWE, D. J., MCFADGEN, B. G., HIGHAM, T. F. G., HOGG, A. G., FROGGATT, P. C. & NAIRN, I. A. (1997). Radiocarbon age of the Kaharoa Tephra, a key marker for late Holocene stratigraphy and archaeology in New Zealand. *The Holocene*, **8**, 487-495.

LOWE J. J., & TURNEY C. S. M. (1997). Vedde Ash discovered in a small lake basin on the Scottish mainland. *Journal of the Geological Society*, **154**, 605-612.

LOWE, J. J., & WALKER, M. J. C. (1997). *Reconstructing Quaternary Environments*. Longman, London. pp. 446.

LOWE, J. J., HOEK, W. Z., INTIMATE GROUP MEMBERS (2001). Inter-regional correlation of palaeoclimatic records for the Last Glacial-Interglacial Transition: a protocol for improve precision recommended by the INTIMATE project group. *Quaternary Science Reviews*, **20**, 1175-1187.

LUDLAM, S. (1979). Rhythmite deposition in lake in the NE USA. In Schlüchter, Ch. (Ed.): *Moraines and Varves: Origin, Genesis and Classification. Proceedings of an INQUA symposium on genesis and lithology of Quaternary deposits*. A. A. Balkema, Rotterdam, p. 295-302.

MACDONALD, R., SPARKS, R. S. J., SIGURDSSON, H., MATTEY, D. P., MCGARVIE, D. W. & SMITH, R. L. (1987). The 1875 eruption of Askja volcano, Iceland: combined fractional crystallisation and selective contamination in the generation rhyolitic magma. *Mineralogical Magazine*, **51**, 183-202.

MANKINEN, E. A. & DAIRYMPLE, G. B. (1979). Revised geomagnetic polarity time-scale for the interval 0-5 Myrs. B. P. *Journal of Geophysical Research*, **84**, 615-626.

MANGERUD, J., LIE, S. E., FURNES, H., KRISTIANSEN, I.L., & LOMO, L. (1984). A Younger Dryas ash bed in western Norway and its possible correlations with tephra in cores from the Norwegian Sea and the North Atlantic. *Quaternary Research*, **21**, 85-104.

MANGERUD, J., FURNES, H., & JOHANSEN, J. (1986). A 9,000 year old ash bed on the Faroe Islands. *Quaternary Research*, **26**, 262-265.

MARCHANT, D. R., DENTON, G. H., SWISHER, C. C., &, POTTER, N. (1996). Late Cenozoic Antarctic palaeoclimate reconstructed from volcanic ashes in the Dry Valleys region of southern Victoria Land. *Geological Society of America Bulletin*, **108**, 181-194.

MASLIN, M. A., & BERGER, A. (1997). A European view of the future of palaeoclimate research. *Journal of Quaternary Science Reviews*, (On-line comment article) **no. 376**, p. 501-504.

MCDOUGALL, I. (1979). The present status of the geomagnetic polarity timescale. In *The Earth: Its Origin, Structure and Evolution*. McElhinny, M. W. (Ed). Academic Press, New York.

MCDOUGALL, I. (1995). Potassium-argon dating in the Pleistocene. In: *Dating Methods for Quaternary Deposits*. Rutter, N. W. & Catto, N. R. (Eds.). Geological Association of Canada. p. 1-15.

MCDOUGALL, I., & WENSINK, H. (1966). Palaeomagnetism and geochronology of the Plio-Pleistocene lavas in Iceland. *Earth and Planetary Science Letters*, **1**, 232-236.

MCDOUGALL, I., & HARRISON, T. M. (1988). *Geochronology and Thermochronology by the ^{40}Ar-^{39}Ar Method*. Oxford University Press.

MCDOUGALL, I., WATKINS, N. D., & KRISTJÁNSSON, L. (1976). Geochronology and palaeomagnetism of Miocene-Pliocene lava sequence at Bessastaða, eastern Iceland. *American Journal of Science*, **276**, 1078-1095.

MCDOUGALL, I. SÆMUNDSSON, K., JÓHANNESSON, H., WATKINS, N. D. (1977). Extension of the geomagnetic polarity time scale to 6.5 Ma.: K-Ar dating, geological and palaeomagnetic study of a 3500 m lava succession in western Iceland. *Bulletin of the Geological Society of America*, **88**, 1-15.

MCDOUGALL, I., KRISTJANSSON, L., & SÆMUNDSSON, K. (1984). Magnetostratigraphy and geochronology of Northwest Iceland. *Journal of Geophysical Research*, **89**, 7029-7060.

MCGARVIE, D. W. (1984). Torfajökull: A volcano dominated by magma mixing. *Geology* **12**, 685-688.

MCGARVIE, D. W. (1998). Evolution of Torfajökull. *Quaternary Volcanism Meeting: Book of Abstracts*, Cambridge University.

MCGARVIE, D. W. (2000). Torfajökull – the world's most active rhyolite volcano. In: *Iceland 2000 – Modern Processes and Past Environments. Conference Abstracts*. Keele University, April 27th-29th 2000. p. 71-73.

McGarvie, D. W., MacDonald, R., Pinkerton, H. & Smith, R. L. (1990). Petrogenetic evolution of the Torfajökull volcanic complex, Iceland II. The role of magma mixing. *Journal of Petrology*, **31**(2), 461-481.

McKeever, S. W. S. (1983). Dating meteorite falls using thermoluminescence. *PACT*, **9**(2), 321-333.

McKeever, S. W. S. (1985). *Thermoluminescence of solids*. Cambridge University Press. pp. 312.

McKeever, S. W. S., Larsen, A. N., Botter-Jensen, L., & Mejdahl, V. (1997). OSL sensitivity changes during single aliquot procedures: computer simulations. *Radiation Measurements*, **27**, 75-82.

McManus, J. F., & Duck, R. W. (1988). Localised enhanced sedimentation from icebergs in a proglacial lake in Bridskal, Norway. *Geographiksa Annaler*, **70A**, 215-233.

Meier, P. S., Sigurdsson, H., & Schilling, J. -G. (1985). Petrological and geochemical variations along Iceland's neovolcanic zones. *Journal of Geophysical Research*, **90** (B12), 10,043-10,073.

Mejdahl, V. (1979). Thermoluminescence dating: beta dose attenuation in quartz grains. *Archaeometry*, **21**, 61-73.

Mejdahl, V. & Botter-Jensen, L. (1994). Luminescence dating of archaeological materials using a new technique based on single aliquot measurements. *Quaternary Geochronology*, **13**, 551-554.

Mejdahl, V. & Christiansen, H. H. (1994). Procedures used for luminescence dating of sediments. *Quaternary Geochronology*, **13**, 403-406.

Menzies, J. (1996). Past glacial environments. In: Menzies J. (Ed.). *Glacial Environments Volume 2: Past Glacial Environments.* Butterworth-Hienneman, Oxford. p. 1-14.

Merkt J., Muller H., Knabe W., Muller P., &, Weiser T. (1993). The early Holocene Saksunarvatn tephra found in lake sediments in NW Germany. *Boreas*, **22**, 93-100.

Meyer, P. S., Sigurdsson, H. & Schilling, J-G. (1985). Petrological and geochemical variations along Iceland's neovolcanic zones. *Journal of Geophysical Research*, **90**, (B12), 10,043-10,072.

Middleton, G. V. (1973). Johannes Walther's Law of Correlation of Facies. *Bulletin of the Geological Society of America*, **84**, 879-988.

Miller, D. S. & Wagner, G. A. (1981). Fission-track ages applied to obsidian artifacts from South America using the plateau-annealing and track-size-age-correction techniques. *Nuclear Tracks*, **5**, 147-155.

Miller, G. H. (1982). Quaternary depositional events in Western Spitsbergen, Norway. Amino-acid stratigraphy and glacial history. *Arctic and Alpine Research,* **14**, 321-340.

Milne, J. D. G. (1973). Mount Curl Tephra, a 230,000 year-old marker bed in New Zealand and its implications for Quaternary chronology. *New Zealand Journal of Geology and Geophysics*, **16**, 519-532.

Mishra, S., & Venkatesan, T. R., Rajaguru, S. N., & Somayajulu, B. L. K. (1995). Earliest Acheulian industry from peninsular India. *Current Anthropology*, **36**, 847-851.

Mohn, H. (1877). Askeregnen den 29de-30te Marts 1875 (the tephra fall on 29-30 March 1875). *Vidensk. Selsk. Forhandlinger 1877*, **10**, 1-12.

Molspin (2001). *Minispin – Portable Rock Magnetometer.* http://www.molspin.com/mspintxt.htm. (accessed on 11/2/01).

Moorbath, S., Sigurdsson, H., Goodwin, R. (1968).K-Ar ages of oldest exposed rocks in Iceland. *Earth and Planetary Science Letters*, **4**, 197-205.

Moore, C. L. (1991). The distal terrestrial record of explosive rhyolitic volcanism - an example from Auckland, New-Zealand Sedimentary. *Geology*, **74**(1-4), 25-38.

Moore, J. G. (1976). Mechanism of formation of pillow lava. *American Scientist*, **63**, 269-277. (cited in Allen, 1980).

Morgan, W. J. (1981). Hotspot tracks and the opening of the Atlantic and Indian Oceans. In *The sea, &: The Oceanic Lithosphere*. Emiliani, C. (Ed). John Wiley and Sons, New York.

Mørk, M. E. (1984). Magma mixing in the post-glacial Veiðivötn fissure eruption, south-east Iceland - a microprobe study of mineral and glass variations. *Lithos*, **17**(1), 55-75.

MORLEY, J. J., & DWORETZKY, B. A. (1991). Evolving Pliocene-Pleistocene climate: a North Pacific perspective. *Quaternary Science Reviews*, **10**, 225-237.

MORTON, A. C., HITCHEN, K., RITCHIE, J. D., HINE, H. M., WHITEHOUSE, M., & CARTER, S. (1995). Late Cretaceous basalts form Rosmary Bank, Northern Rockall Trough. *Journal of the Geological Society of London*, **152**, 947-952.

MUDIE, P. J., DE VERNAL, A., &, HEAD, M. J. (1990). Neogene to Recent palynostratigraphy of the circum-Arctic basins: results of ODP leg 104, Norwegian Sea, Leg, 105, Baffin Bay and DSDP Site 611, Irminger Sea. In: *Proceedings of the International Workshop on Geological History of the Polar Oceans*. NATO ASI Series C, Reidel, Dordrecht. pp. 609-628. (cited in Edwards *et al.*, 1991).

MULLER, P., & SCHVOERVER, M. (1990). Factors affecting the viability of thermoluminescence dating of glass. *Archaeometry*, **35**(2), 299-304.

MUNYIKAWA, K. (2000). Cosmic ray contribution to environmental dose rates with varying overburden thickness. *Ancient TL*, **18**, 27-34.

MURRAY, A. S. (1996). Developments in optically stimulated luminescence and photo-transferred thermoluminescence dating of young sediments: Application to a 2000-year sequence of flood deposits. *Geochimica et Cosmochimica Acta*, **60**, 565-576.

MURRAY, A. S., & ROBERTS, R. G. (1998). Measurement of the equivalent dose in quartz using a regenerative-dose single aliquot protocol. *Radiation Measurements*, **29**(5), 503-515.

MURRAY, A. S., & MEJDAHL, V. (1999). Comparison of the regenerative-dose single-aliquot and multiple-aliquot (SARA) protocols using heated quartz from archaeological sites. *Quaternary Geochronology*, **18**, 223-229.

MUTTER, J. C., & ZEHNDER, C. M. (1988). Deep crustal structure and magmatic processes: the inception of seafloor spreading in the Norwegian-Greenland Sea. In Morton, A. C., Parson, L. M. (Eds.): *Early Tertiary Volcanism and the Opening of the NE Atlantic*. Geological Society Special Publication, **39**, 35-48.

NADIN, P. A., KUSZNIR, N. J., & TOTH, J. (1995). Transient regional uplift in the Early Tertiary of the northern North Sea and the development of the Iceland plume. *Journal of the Geological Society of London*, **152**, 953-958.

NAESER, C. W., & NAESER, N. D. (1988). Fission track dating of Quaternary events. *Geological Society of America: Special Paper*, **227**, 1-11.

NAESER, C. W., IZETT, G. A., & WILCOX, R. E. (1973). Zircon fission-track ages of Pearette family ash beds in Meads County, Kansas. *Geology*, **1**, 187-189.

NAESER, C. W., HURFORD, A. J., & GLEADOW, A. O. W. (1977). Fission-track dating of the pumice from the KBS Tuff, East Rudolf, Kenya. Reply to Wagner, G. W. *Nature*, **649**.

NAESER, C. W., IZETT, G. A. & OBRADOVICH, J. D. (1980). Fission-track and K-Ar ages of Natural Glasses. *US Geological Survey Bulletin*, **1489**.

NAISH, T., KAMP, P. J. J., ALLOWAY, B. V., PILLANS, B., WILSON, G. S., & WESTGATE, J. A. (1996). Integrated tephrochronology and magnetostratigraphy for cyclothermic marine strata, Wanganui Basin: implications for the Pliocene-Pleistocene boundary in New Zealand. *Quaternary International*, **34-36**, 29-48.

NAKADA, M., & YOKOSE, H. (1992). Ice age as a trigger of active Quaternary volcanism and tectonism. *Tectonophysics*, **212**, 321-329.

NAMBI, K. S. V., & AITKEN, M. J. (1986). Annual dose conversion factors for TL and ESR. *Archaeometry*, **28**, 202-205.

NEJSE, A. & DAHL, S. O. (1990). Autochthonous block fields in southern Norway: implications for the geometry, thickness and isostatic loading of the Late Weichselian Scandinavian ice sheet. *Journal of Quaternary Science*, **5**, 225-234.

NESJE, A., & WHILLANS, I. M. (1994). Erosion of Sognefjord, Norway. *Geomorphology*, 9, 33-45.

NESJE, A., DAHL, S. O., ANDA, E., &, RYE, N. (1988). Blockfields in southern Norway: significance for the Late Weichselian ice-sheet. *Norsk Geologisk Tidsskrift*, **68**, 149-169.

NESJE, A., DAHL, S. O., VALEN, V., &, OVSTEDAL, J. (1992). Quaternary erosion in the Sognefjord drainage basin, western Norway. *Geomorphology*, **5**, 511-520.

NEWNHAM, R. M., LOWE, D. J., MCGLONE, M. S., WILMSHURST, J. M. & HIGHAM, T. F. G. (1998). The Kaharoa Tephra as a critical datum for earliest human impact in Northern New Zealand. *Journal of Archaeological Science,* **25**, 533-544.

NEWTON, A. J. (1999). *Ocean Transported Pumice in the North Atlantic.* Unpublished PhD Thesis, University of Edinburgh. pp. 394.

NOLLER, J. S., SOWERS, J. M., COLMAN, S. M., & PIERCE, K. L. (2000). Introduction to Quaternary Geochronology. In Stratton, J. S., Sowers, J. M., Lettis, W. R. (Eds.): *Quaternary Geochronology Methods and Applications.* American Geophysical Union, Washington, DC. p. 582.

NORÐDAHL, H. (1981). A prediction of minimum age for Weichselian maximum glaciation in North Iceland. *Boreas*, **10**, 471-476.

NORÐDAHL, H. (1991). Late Weichselian and Early Holocene deglaciation history of Iceland. *Jökull*, **40**, 27-50.

NORÐDAHL, H., & HAFLIDASON, H. (1992). The Skógar Tephra, a Younger Dryas marker in North Iceland. *Boreas*, **21**, 23-41.

NORÐDAHL, H., & HJORT, C. (1993). Lateglacial raised beaches and glacier recession in the Þistilfjörður – Bakkaflói area, northeast Iceland. *Jökull*, **43**, 33-43.

NORÐDAHL, H., & EINARSSON, T. (1988). Late Weichselian deglaciation and sea-level changes in east and southeast Iceland. *Náttúrufræðingurinn,* **58**(2), 59-80.

NVI (2000). NORDIC VOLCANOLOGICAL INSTITUTE (www.nordvol.hi.is/askja.html). Visited 28/2/00.

Ó COFAIGH, C., & DOWDESWELL, J. A. (2001). Laminated sediments in glacimarine environments: diagnostic criteria for their interpretation. *Quaternary Science Reviews*, **20**, 1411-1436.

OESCHGER, F., & LANGWAY, C. C. JR. (Eds). *The Environmental Record in Glaciers and Ice Sheets.* John Wiley and Sons, Chichester and New York.

ÓLAFSDÖTTIR, Þ. (1975). Jökulgarður á sjávarbotni út af Breiðafirði (A moraine ridge on the Iceland shelf west of Breiðafjördur). *Náttúrufræðingurinn*, **45**, 31-36.

ÓSKARSSON, N. SIGVALDASSON, G., & STEINTHORSSON, S. (1982). A dynamic model of rift-zone petrogenesis and the regional petrology of Iceland. *Journal of Petrology*, **23**, 28-74.

ÓSKARSSON, N., STEINTHORSSON, S., & SIGVALDASSON, G. E. (1985). Iceland geochemical anomaly: Origin, volcanotectonics, chemical fractionation and isotope evolution of the crust. *Journal of Geophysical Research*, **90** (B12), 10,011-10,025.

OWEN, L. A. (1994). Glacial and non-glacial diamictons in the Karakoram Mountains and Western Himalayas. In: Warren, W. P., & Croot, D. G. (Eds.). *The Formation and Deformation of Glacial Deposits.* A. A. Balkema, Rotterdam. p. 9-28.

PALAIS, J. M., GERMANI, M. S., & ZIELINSKI, G. A. (1992). Inter-hemispheric transport of volcanic ash from a 1259 AD volcanic eruption to the Greenland and Antarctic Ice sheets. *Geophysical Research Letters* **19**, 801-804.

PÁLMASON, G., JÓNSSON, J. TÓMASSON, J., & JÓNSSON, I. (1965). Djúpborun í Vestmannaeyjum, *Raforkumálastjóri*, **43**. Reykjavík. (cited in Haraldsson, 1981).

PATIENCE, A. J., & KROON, D. (1991). Oxygen isotope chronostratigraphy. In Smart, P. L., & Frances, P. D. (Eds.): *Quaternary Dating Methods – A Users Guide.* Quaternary Research Association: Technical Guide No. 4.

PEACOCK, J. D. & CORNISH, R. (1989). *Glen Roy area.* Cambridge: Quaternary Research Association Field Guide.

PEARSON, G. W. & STUVIER, M. (1993). High-precision bi-decadal calibration of the radiocarbon time scale. *Radiocarbon*, **35**, 25-33.

PEARSON, K. (1901). On lines and places of closest fit to a system of points in space. *Philosophical Magazine*, **2**, 557-572.

PECCERILLO, R. & TAYLOR, S. R. (1976). Geochemistry of Eocene calc-alkaline volcanic rocks from the Kastamonu area, northern Turkey. *Contributions to Mineralogy & Petrology*, **58**, 63-81.

PERKINS, M. E., BROWN, F. H., NASH, W. P., MCINTOSH, W., & WILLIAMS, S. K. (1998). Sequence, age and source of silicic fallout tuffs in middle to late Miocene basins of the northern Basin and Range province. *Geological Society of America Bulletin*, **110**, 344-360.

PÉTURSSON, H. G. (1991). The Weichselian glacial history of the West Mekrakkaslétta, Northeastern Iceland. In Caseldine, C. J., & Maizels, J. (Eds.): *Environmental Changes in Iceland*. Kluwer, Dordrecht. p. 49-65.

PFLAUMANN, U., & VOELKER, A. (2000). Potential links between surging ice sheets, circulation changes, and the Dansgaard-Oeschger cycles in the Irminger Sea, 60-18 ka. *Palaeoceanography*, **15**, 425-442.

PILCHER, J. R., HALL, V. A., & MCCORMAC, F. G. (1995). Dates of Holocene Icelandic volcanic eruptions from tephra layers in Irish peats. *The Holocene*, **5**(1), 103-110.

PILLANS, B. J. (1992). New Zealand Quaternary stratigraphy: an overview. *Quaternary Science Reviews*, **10**, 405-418.

PILLANS, B. J., MCGLONE, M. S., PALMER, A. S., MILDENHALL, D., ALLOWAY, B. V., & BERGER, G. W. (1993). The Last Glacial Maximum in central and southern North Island, New Zealand: a palaeoenvironmental reconstruction using the Kawakawa Tephra as a chronostratigraphic marker. *Palaeography, Palaeoclimatology, Palaeoecology*, **101**, 283-304.

PILLANS, B. J., ROBERTS, A. P., WILSON, G. S., ABBOTT, S. T., & ALLOWAY, B. V. (1994). Magnetostratigraphic, lithostratigraphic and tephrostratigraphic constraints on lower and middle Pleistocene sea-level changes, Wanganui Basin, New-Zealand. *Earth and Planetary Science Letters*, **121**(1-2), 81-98.

PILLANS, B. J., KOHN, B. P., BERGER, G., FROGGATT, P., DULLER, G., ALLOWAY, B., & HESSE, P. (1996). Multi-dating comparison for mid-Pleistocene Rangitawa tephra, New Zealand. *Quaternary Science Reviews*, **15**, 641-653.PIRIOU, B. (1999). Luminescence of the Fe^{3+} and Mn^{2+} in the acid volcanic glasses. *EUG Journal Conference Abstracts, Strasbourg*.

PJETRUSS, H. (1900). The glacial palagonite formation of Iceland. *Scottish Geographical Magazine*, **16**, 265-293.

PORTER, S. C., & AN, Z. (1995). Correlation between climate events in the North Atlantic and China during the last glaciation. *Nature*, **375**, 305-308.

POTTS, P. J. (1987). *A Handbook of Silicate Rock Analysis*. Blackie, London. pp. 622.

PREECE, S. J., WESTGATE, J. A., STEMPER, B. A., & PÉWÉ, T. L. (1999). Tephrochronology of late Cenozoic loess at Fairbanks, central Alaska. *Geological Society of America Bulletin*, **111**(1), 71-90.

PRESCOTT, J. R. & FOX, P. J. (1990). Dating quartz sediments using the 325°C peak: new spectral data. *Ancient TL*, **11**(1), 27-30.

PRESCOTT, J. R., & HUTTON, J. T. (1988). Cosmic ray and gamma dosimetry for TL and ESR. *Nuclear Tracks and Radiation Measurements*, **14**, 223-227.

PRESCOTT, J. R., & HUTTON, J. T. (1993). Cosmic ray contributions to dose rates for luminescence and ESR dating: large depths and long-term time variations. *Radiation Measurements*, **23**, 497-500.

PRESCOTT, J. R. & ROBERTSON, G. B. (1997). Sediment dating by luminescence: A review. *Radiation Measurements*, **27**(5/6), 893-922.

PRESTVIK, T. (1979). Petrology of hybrid intermediate and silicic rocks from Öræfajökull, southeast Iceland. *Geologiska Foreningens i Stockholm Forhandlinger*, **101**, 299-308.

PRICE, P. B., & WALKER, R. M. (1963). Fossil tracks of charged particles in mica and the age of minerals. *Journal of Geophysical Research*, **68**, 4847-4862.

PRINGLE, M. S., STAUDIGEL, H., & GEE, J. (1991). Jasper Seamount: Seven million years of volcanism. *Geology*, **19**, 364-368.

PRINGLE, M. S., MCWILLIAMS, M., HOUGHTON, B. F., LANPHERE, M. A., & WILSON, C. J. N. (1992). $^{40}Ar/^{39}Ar$ dating of Quaternary feldspar: Examples from the Taupo Volcanic Zone, New Zealand. *Geology*, **20**, 531-534.

PYLE, D. M. (1995). Assessment of minimum volume of tephra fall deposits. *Journal of Volcanology and Geothermal Research*, **69**, 379-382.

RAM, M., & GAYLEY, R. I. (1991). Long range transport of volcanic ash to the Greenland ice sheet. *Nature*, **349**, 401-404.

RAM, M., DONARUMMO, J. & SHERIDAN, M. (1996). Volcanic ash from Icelandic ~57,300 yr BP eruption found in GISP2 (Greenland) ice core. *Geophysical Research Letters*, **23**(22), 3167-3169.

RAMPINO M. R., &, SELF, S. (1982). Historic eruptions of Tambora (1815), Krakatau (1883) and Agung (1963), their stratospheric aerosols and climatic impact. *Quaternary Research*, **18**, 127-143.

RASMUSSEN, T. L., TJEERD, C.E., VAN WEERING, & LABEYRIE, L. (1997). Climatic instability, ice sheets and ocean dynamics at high northern latitudes during the last glacial period (58-0ka BP). *Quaternary Science Reviews*, **16**, 71-80.

RAYMO, M.E., RUDDIMAN, W.F., BACKMAN, J., CLEMENT, B.M. & MARTINSON, D.G. (1989). Late Pliocene variation in Northern Hemisphere ice sheets and North Atlantic deep-water circulation. *Palaeoceanography*, **4**(4), 413-446.

REA, B. R., WHALLEY, W. B., EVANS, D. J., GORDON, J. E., & MCDOUGALL, D. A. (1998). Plateau Icefields: Geomorphology and Dynamics. *Quaternary Proceedings*, **6**, 35-54.

REED, S. J. B. (1996). *Electron Microprobe Analysis and Scanning Electron Microscopy in Geology*. Cambridge University Press, Cambridge.

RENDELL, H. M., & TOWNSEND, P. D. (1988). Thermoluminescence dating of a 10 m loess profile in Pakistan. *Quaternary Science Reviews*, **7**, 251-255.

RENDELL, H. M., STEER, D. C., & TOWNSEND, P. D. (1985). The emission spectra of TL from obsidian. *Nuclear Tracks and Radiation Measurements*, **10**, 591-600.

RENNE, P. R. (2000). K-Ar and $^{40}Ar/^{39}Ar$ Dating. In Stratton-Noller, J. S., Sowers, J. M., & Lettis, W. R. (Eds.): *Quaternary Geochronology Methods and Applications*. American Geophysical Union Reference Shelf 4.

RICHARDS, D. A., & SMART, P. L. (1991). Potassium-argon and argon-argon dating. In *Quaternary dating methods - a users guide: Quaternary Research Association Technical Guide no. 4.* Smart, P. L. and Frances P. D. (Eds). Quaternary Research Association, London. p. 37-44.

RICHARDS, M. A., DUNCAN, R. A., & COUTILLOT, V. E. (1989). Flood basalts and hot-spot tracks: plume heads and tails. *Science*, **246**, 103-107.

RICHARDSON, S. (1998). *Deglaciation and shoreline displacement adjacent to a spreading ridge, NE Iceland*. Unpublished PhD Thesis, Royal Holloway, University of London. pp. 408.

RICHARDSON, S. (2000). Late Quaternary deglaciation and relative sea-level changes in north-east Iceland. In: *Iceland 2000 – Modern Processes and Past Environments. Conference Abstracts.* April 27th-29th 2000. p. 85.

RICKWOOD, P. C. (1989). Boundary lines within petrologic diagrams which use oxides of major and minor elements. *Lithos*, **22**, 247-263.

RITTMAN, A. (1962). *Volcanoes and their activity*. John Wiley & Sons, New York. pp. 305.

ROBERTS, J. H., GOLD, R., & ARMANI, R. J. (1968). Spontaneous fission decay-constant of ^{238}U. *Physical Review*, **174**, 1482-1484.

ROBERTS, R. G., SPOONER, N. A., & QUESTIAUX, D. G. (1993). Cautions on the use of extended duration preheats in the optical dating of quartz. *Ancient TL*, **11**, 47-56.

ROBERTS, R. G., SPOONER, N. A., & QUESTIAUX, D. G. (1994). Palaeodose underestimates caused by extended duration preheats in the optical dating of quartz. *Radiation Measurements*, **23**, 647-653.

ROBERTS, S. J. (1997). *Lateglacial Tephra Deposits of Scotland*. Unpublished MSc. Dissertation, Royal Holloway, University of London. pp. 207.

ROBERTS, S. J., TURNEY, C. S. M., & LOWE, J. J. (1998). Icelandic tephra in Late-glacial sediments of Scotland (14 - 9,000 ^{14}C BP). *Fróðskaparrit*, **46**, 335-339.

ROBERTS, S. J., SANDERSON, D. C. W., DUGMORE, A. J., SIGURVINSSON, J. R. (1999). Mid-Pleistocene thermoluminescence ages for the Óþoli Tephra, NW Iceland. *LED 99: 9th International Conference on Luminescence and Electron Spin Resonance Dating*, p. 196. Rome, Sept. 6th-10th 1999.

ROBERTS, S. J., SANDERSON, D. C. W., EVEREST, J. D. & SIGURVINSSON, J. R. (2000). First TL evidence for Mid-Pleistocene glacial activity in Iceland? *Iceland 2000: Past Processes and Environments Conference Abstracts*. Keele, April 27th-29th 2000.

ROLLINSON, H. (1993). *Using Geochemical data: Evaluation, Presentation, Interpretation*. Longman, Harlow, pp. 352.

ROSE, J., & MENZIES, J. (1996). Glacial stratigraphy. In: Menzies J. (Ed.). *Glacial Environments Volume 2: Past Glacial Environments*. Butterworth-Hienneman, Oxford. p. 253-284.

ROSE, W. I., & CHESNER, C. A. (1990). World-wide dispersal of ash and gases from Earth's largest known eruption - Toba, Sumatra, 75 ka. *Global and Planetary Change*, **89**(3), 269-275.

RUDDIMAN, W. F., & GLOVER L. K. (1972). Vertical mixing of ice-rafted volcanic ash in North Atlantic sediments. *Geological Society of America Bulletin*, **83**, 2817-2836.

RUDDIMAN, W. F., RAYMO, M. E., MARTINSON, D. G., CLEMENT, B. M., & BACKMAN, J. (1989). Pleistocene evolution: Northern Hemisphere ice sheets and North Atlantic Ocean. *Palaeoceanography*, **4**(4), 353-412.

RUNDGREN, M., & INGÓLFSSON Ó. (1997). Plant survival in Iceland during periods of glaciation. *Lundqua Thesis*, **40**, IV, 1-13.

RUNDGREN, M., INGÓLFSSON Ó., BJÖRCK, S., JIANG, H., & HAFLIDASON, H. (1997). Dynamic sea level change during the last deglaciation of northern Iceland. *Boreas*, **26**, 201-215

SÆMUNDSSON, K. (1979). Outline of the Geology of Iceland. *Jökull*, **29**, 7-28.

SÆMUNDSSON, K. (2000). Cold climate and glacial vestiges in Iceland. In: *Iceland 2000 – Modern Processes and Past Environments. Conference Abstracts*. April 27th-29th 2000. p. 71-73.

SÆMUNDSSON, K., & NOLL, H. (1974). K/Ar dates of rocks from Húsafell, western Iceland and the development of the Húsafell Central Volcano. *Jökull*, **24**, 40-57.

SÆMUNDSSON, Þ. (1994). The deglaciation history of the Hófsardalur valley, Northeast Iceland. In: Warren & Croot (Eds.). *Formation and deformation of Glacial Deposits*. A. A. Balkema, Rotterdam, 173-187.

SÆMUNDSSON, Þ. (1995). *Deglaciation and shoreline displacement in Vopnafjörður, northeastern Iceland*. LUNDQUA Thesis, **33**, Department of Quaternary Geology, University of Lund, pp. 78.

SALTZMAN, B. (1995). Paleoclimatic Modelling. In: Hect, A. D. (Ed.). *Palaeoclimate Analysis and Modelling*. John Wiley and Sons, New York. pp. 341-391.

SANDERSON, D. C. W. (1982). *The thermoluminescence of archaeological glass*. MPhil Thesis, University of Bradford.

SANDERSON, D. C. W. (1986). *Thermoluminescence dating of Scottish vitrified forts*. PhD Thesis, Paisley College of Technology.

SANDERSON, D. C. W. (1988). Thick source beta counting (TSBC): a rapid method for measuring beta dose-rates. *Nuclear Tracks and Radiation Measurements*, **14** (1/2), 203-207.

SANDERSON, D., WARREN S. E. & HUNTER, J. R. (1983). The TL properties of archaeological glass. *PACT Journal*, **9**, 287-298.

SANDHU, A. S., & WESTGATE, J. A. (1995). The correlation between reduction in fission-track diameter and areal density in volcanic glass shards and its application in dating tephra beds. *Earth and Planetary Science Letters*, **131**, 289-299.

SANDHU, A. S., WESTGATE, J. A., & ALLOWAY, B. V. (1993). Optimising the isothermal plateau fission track dating method for volcanic glass shards. *Nuclear Tracks and Radiation Measurements*, **21** (4), 479-488.

SANDHU, A. S., WESTGATE, J. A., & PREECE, S. J. (1999). Thermal stability of fission-tracks in natural and synthetic glasses: An assessment of compositional effects. *Radiation Measurements*, **31**, 665-668.

SANZELLE, S., PILLEYRE, TH., MIALLIER, D., FAIN, J., & GANZAWA, Y. (2001). Thermoluminescence dating of a tephra deposit of the 'Toya' volcano (Hokkaido, Japan). *IAEA/INISAN Abstracts*, **32**(5): 5010.

SARNA-WOJCICKI, A. (2000). Tephrochronology. In Stratton-Noller, J., Sowers, J. M., Lettis, W. R. (Eds.): *Quaternary Geochronology: Methods and Applications*.

SARNA-WOJCICKI, A. M., MEYER, C. E., BOWMAN, H. R., HALL, T. M., RUSSELL, P. C., WOODWARD, M. J., & SLATE, J. L. (1985). Correlation of the Rockland ash bed, a 400,000-year-old stratigraphic marker in the northern California and western Nevada, and implications for middle Pleistocene, paleogeography of Central California. *Quaternary Research*, **23**, 236-257.

SCHMID, R. (1981). Descriptive nomenclature and classification of pyroclastic deposits and fragments: Recommendations of the IUGS Subcommission on the Systematics of Igneous Rocks. *Geology*, **9**, 41-43.

SCOTT, E. M., & HARKNESS, D. D. (2000). What future for radiocarbon? *Radiocarbon*, **42**(1), 173-178.

SCOTT, E. M., & SANDERSON, D. C. W. (1988). Statistics and the additive dose method in TL dating. *Nuclear Tracks and Radiation Measurements*, **14**(1/2), 345-354.

SCOURSE, J. D. (2000). Editorial. *Journal of Quaternary Science*, **15**(1), 1.

SCOURSE, J. D., HALL, I. R., MCCAVE, I. N., YOUNG, J. R., SUGDON, C. (2000). The origin of Heinrich layers: evidence from H2 for European precursor events. *Earth & Planetary Science Letters*, **182**(2), 187-195.

SEJRUP, H. P., SJØHOLM, J., FURNES, H., BEYER, I., EIDE, L., JANSEN, E., & MANGERUD, J. (1989). Quaternary tephrochronology on the Iceland Plateau, north of Iceland. *Journal of Quaternary Science*, **4**, 109-114.

SEJRUP, H. P., AARSETH, I., HAFLIDASON, H., LØVLIE, R., BRATTEN, Å., TJØSTHEIM, G., FORSBERG, C. F., &, ELLINGSEN, K. I. (1995). Quaternary of the Norwegian Channel: Glaciation history and palaeocenography. *Norsk Geologisk Tidsskrift*, **75**, 65-87. (cited in Sejrup *et al.* 2000).

SEJRUP, H. P., LARSEN, E., LANDVIK, J., KING, E. L., HAFLIDASON, H., & NESJE, A. (2000). Quaternary glaciations in southern Fennoscandia: evidence from southwestern Norway and the northern North Sea region. *Quaternary Science Reviews*, **19**, 667-685.

SELLI, R., ACCORSI, C. A., BANDINI MAZZANTI, M., BERTOLANI, MARCHETTI, D., BIGAZZI, G., BONADONNA, F. P., BORSETTI, A. M., CATI, F., COLALONGO, M. L., D'ONOFRIO, S., LANDINI, W., MENESINI, E., MEZZETTI, R., PASINI, G., SAVELLI, C., & TAMPIERI, R. (1977). The Vrica section (Calabria, Italy). A potential Neogene/Quaternary boundary stratotype. *Giornale di Geologia* (2), **XLII**, fasc I, 181-204.

SEVERINGHAUS, J. P., SOWERS, T., BROOK, E. J., ALLEY, R. B., & BENDER, M. L. (1998). Timing of abrupt climate change at the end of the Younger Dryas interval from thermally fractionated gases in polar ice. *Nature*, **191**, 141-146.

SEWARD, D. (1975). Fission-track ages of some tephras from Cape Kidnappers, Hawke's Bay, New Zealand. *New Zealand Journal of Geology and Geophysics*, **19**, 9-20.

SEWARD, D. (1979). Comparison of zircon and glass fission-track ages from tephra horizons. *Geology*, **7**, 479-482.

SEWARD, D., & KOHN, B. (1997). New fission-track ages from New Zealand Quaternary tephra: an interlaboratory experiment and recommendations for the determination of young ages. *Chemical Geology*, **141**, 127-140.

SHACKLETON, N. J., BACKMAN, J., ZIMMERMAN, H., KENT, D. V., HALL, A., HOMRIGHAUSEN, R. HUDDLESTUN, P., KEENE, J. B., KALTENBACK, A. J., KRUMSIEK, K. A. O., MORTON, A. C., MURRAY, J. W., & WESTBERG-SMITH, J. (1984). Oxygen isotope calibration of the onset of ice-rafting in the DSDP site 552A: history of glaciation in the North Atlantic region. *Nature*, **307**, 620-633.

SHACKLETON, N. J., BERGER, A., PELTIER, W. R. (1990). An alternative astronomical timescale based on ODP Site 677. *Transactions of the Royal Society of Edinburgh: Earth Sciences*, **81**, 251-261.

SHANE, P. (2000). Tephrochronology: a New Zealand case study. *Earth and Planetary Science Letters*, **49**, 223-259.

SHANE, P. A. R., &, FROGGATT, P. C. (1994). Discriminant function analysis of glass chemistry of New Zealand and North American tephra deposits. *Quaternary Research*, **41**, 70-81.

SHANE, P., FROGGATT, P., BLACK, T., & WESTGATE, J. (1995). Chronology of Pliocene and Quaternary bio-events and climatic events from fission-track ages on tephra beds, Wairarapa, New Zealand. *Earth and Planetary Science Letters*, **130**(1-4), 141-154.

SHANE, P., BLACK, T. M., ALLOWAY, B. V., & WESTGATE, J. A. (1996). Early to middle Pleistocene tephrochronology of the North Island, New Zealand.: implications for volcanism, tectonism and palaeoenvironments. *Geological Society of America Bulletin*, **108**, 915-925.

SHANE, P., BLACK, T. M., EGGINS, S., & WESTGATE, J. A. (1998). Late Miocene marine tephra beds: recorders of rhyolitic volcanism in North Island, New Zealand. *New Zealand Journal of Geology and Geophysics*, **41**, 165-178.

SHARP, M. (1984). Annual moraine ridges at Skalafellsjökull, south-east Iceland. *Journal of Glaciology*, **30**, 82-93.

SIGURDSSON, H. (1967). Dykes, fractures and folds in the plateau of western Iceland. *Rit Vísindafélags Islendinga*, **38**, 162-169.

SIGURDSSON, H. (1977). Generation of Icelandic rhyolites by melting of plagiogranites in the oceanic layer. *Nature*, **269**, 28.

SIGURDSSON, H. (1982). Utbreidsla islenskra gjoskulaga a botni Atlantshafs. Eldur er I Nordri. In *Eldur er í nordri*. Thorarainsdóttir, H., Óskarsson, O. H., Steinthorsson, S., & Einarsson. Th. (Eds.) Sögufélag, Reykjavík, pp. 119-127.

SIGURDSSSON, H (ED.) (2000). *Encyclopedia of volcanoes*. Academic Press, San Diego. pp. 1417.

SIGURDSSON, H. & SPARKS, R. S. J. (1978). Rifting episode in North Iceland in 1874-1875 and the eruptions of Askja and Sveinagja. *Bulletin of Volcanology*, **41**, 1-19.

SIGURDSSON, H., & LOEBNER, B. (1981). Deep sea record of Cenozoic explosive volcanism in the North Atlantic. In Self, S., & R. S. J. Sparks (Eds.): *Tephra Studies*. Reidel, Dordrecht. p. 289-316.

SIGURDSSON, H., & SPARKS, R. S. J. (1981). Petrology of rhyolitic and mixed magma ejecta from the 1875 eruption of Askja. *Journal of Petrology*, **22**, 41-84.

SIGURVINSSON, J. R. (1982). *Kvarter landmótun utnessins milli Dýrafjarðar og Önundarfjarðar*. Unpublished 4th year thesis, University of Iceland. pp. 87.

SIGURVINSSON, J. R. (1983). Weichselian glacial lake deposits in the Highlands of north-western Iceland. *Jökull*, **33**, 99-109.

SIGVALDASSON, G. E. (1968). Structure and products of subaquatic volcanoes in Iceland. *Contributions to Mineralogy and Petrology*, **18**, 1-16.

SIGVALDASSON, G. E., ANNERTZ, K. & NILSSON, M. (1992). Effect of glacier loading/deloading on volcanism: postglacial volcanic production rate of the Dyngjufjöll area, central Iceland. *Bulletin of Volcanology*, **54**, 385-392.

SINGHVI, A. K., SHARMA, Y. P., & AGRAWAL, D. P. (1982). Thermoluminescence dating of dune sands in Rajasthan, India. *Nature*, **295**, 313-315.

SISSONS, J. B. (1979). Catastrophic lake drainage in Glen Spean and the Great Glen, Scotland. Journal of *Geological Society of London*, **136**, 215-224.

SJØHOLM, J., SERJUP, H. P., AND FURNES, H. (1991). Quaternary volcanic ashes on the Iceland Plateau, southern Norwegian Sea. *Journal of Quaternary Science*, **6**, 159-173.

SMART, P. L. (1991a). *Quaternary dating methods - a users guide*: *Quaternary Research Association Technical Guide no. 4.* Quaternary Research Association, London. pp. 203.

SMART, P. L. (1991b). General Principles. In Smart, P. L. and Frances P. D. (Eds): *Quaternary dating methods - a users guide*: *Quaternary Research Association Technical Guide no. 4*. Quaternary Research Association, London. p. 1-15.

SMART, P. L. (1991c) Uranium series dating. In Smart, P. L. and Frances P. D. (Eds): *Quaternary dating methods - a users guide*: *Quaternary Research Association Technical Guide no. 4*. Quaternary Research Association, London. p. 45-83.

SMITH, D. G. W., & WESTGATE, J. A. (1969). Electron probe technique for characterising pyroclastic deposits. *Earth and Planetary Science Letters*, **5**, 313-319.

SMITH, D. J., & SANDERSON, D. C. W. (1999). Time resolved spectrometry of volcanic feldspars showing anomalous fading: the effect of pre-heating. In: *9th International Conference on Luminescence and Electron Spin Resonance Dating (LED 99), Book of Abstracts.* Rome 6-10 September, 1999. p. 120.

SMITH, D. J., & SANDERSON, D. C. W. (SUBMITTED). Fading and tunnelling in luminescence dating of volcanic feldspars.

SPARKS, R. S. J., WILSON, L., & SIGURDSSON, H. (1981). The pyroclastic deposits of the 1875 eruption of Askja, Iceland. *Philosophical Transactions of the Royal Society of London*, **299**, 241-273.

SPARKS, R. S. J., BURSIK, M. I., CAREY, S. N., GILBERT, J. S., GLAZE, L. S., SIGURDSSON, H., & WOODS, A. W. (1997). *Volcanic Plumes*. John Wiley and Sons, Chichester, pp. 574.

SPENCER, J. Q., CLAYTON, J. D., GEMMELL, & CLAPPERTON, C. M. (1999). Luminescence studies of glacial and pyroclastic deposits from Chile. In: *9th International Conference on Luminescence and Electron Spin Resonance Dating (LED 99), Book of Abstracts.* Rome 6-10 September, 1999. p. 275.

SPOONER, N. A. (1992). Optical dating: preliminary results on the anomalous fading of luminescence from feldspars. *Quaternary Science Reviews*, **11**, 139-145.

SPOONER, N. A. (1994). The anomalous fading of infrared-stimulated luminescence from feldspars. *Radiation Measurements*, **23**, 625-632.

SPOONER, N. A., & ALLSOP, A. (2000). The spatial variation of dose-rate from $^{90}Sr/^{90}Y$ beta sources for use in luminescence dating. *Radiation Measurements*, **32**, 49-55.

STAUDACHER, T. H., JESSBERGER, E. K., DOMINIK, B., KIRSTEN, T., & SCHAEFFER, O. A. (1982). $^{40}Ar/^{39}Ar$ ages of rocks and glasses from the Nördlinger Ries Crater and the temperature history of impact breccias. *Journal of Geophysics*, **51**, 1-11.

STECHER, O., CARLSON, R. W., & GUNNARSSON, B. (1999). Torfajökull: a radiogenic end-member of the Iceland Pb-isotopic array. *Earth and Planetary Science Letters*, **165**, 117-127.

STEEN-MCINTYRE, V. (1977). *A Manual for Tephrochronology*. Unpublished PhD thesis. Department of Anthropology, Colorado State University. pp. 167.

STEINDORSSON, S. (1962). On the age and immigration of the Icelandic flora. Rit Vísindafélags Íslendinga, **35**, 1-157.

STEINDORSSON, S. (1964). Um ísaldarplöntur. *Náttúrufrædingurinn*, **34**, 49-76.

STOCKER, T. F. (2000). Past and future reorganisations in the climate system. *Quaternary Science Reviews*, **19**, 201-319.

STOKES, S. (1994). The timing of OSL sensitivity changes in natural quartz. *Radiation Measurements*, **23**, 601-606.

STOKES, S. (1996). Pre-heats, palaeodoses and paradigms in the optical dating of quartz: some comments on Roberts *et al.* (1993). *Ancient TL*, **14**, 5-8.

STOKES, S. (1997). Dating of desert sequences. In Thomas, D. S. G. (Ed): *Arid Zone Geomorphology: Process, Form and Change in Drylands*. John Wiley & Sons Ltd. pp. 607-637.

STOKES, S. (1999). Luminescence dating applications in geomorphological research. *Geomorphology*, **29**, 153-171.

STOKES, S. & LOWE, D. J. (1988). Discriminant function analysis of Late Quaternary tephras from five volcanoes in New Zealand using glass shard major element chemistry. *Quaternary Research*, **30**, 270-283.

STOKES, S., THOMAS, D.S.G., & WASHINGTON, R. (1997). Multiple episodes of aridity in southern Africa since the last interglacial period. *Nature*, **388**, 154-158.

STORZER, D., & WAGNER, G. A. (1969). Correction of thermally lowered fission-track ages of tektites. *Earth and Planetary Science Letters*, **5**, 463-468.

STÖTTER, J., WASTL, M., CASELDINE, C., & HABERLE, T. (1999). Holocene palaeoclimate reconstruction in northern Iceland: approaches and results. *Quaternary Science Reviews*, **18**, 457-474.

STRATTON-NOLLER, J., SOWERS, J. M., & LETTIS, W. R. (2000). *Quaternary Geochronology: Methods and Applications*. American Geophysical Union Reference Shelf 4. pp. 582.

STRÖMBERG, B. (1985). New varve measurements in Vöstergotland, Sweden. *Boreas*, **14**, 111-115.

STUIVER, M., & SUESS, H. E. (1966). On the relationship between radiocarbon dates and true sample ages. *Radiocarbon*, **8**, 534-540.

STUIVER, M., & REIMER, P. J. (1993). Extended ^{14}C database and revised CALIB 3.0 ^{14}C age calibration program. *Radiocarbon*, **35**, 215-230.

SUC, J. -P, BERTINI, A., LEROY, S. A. G. & SUBALLYOVA, D. (1997). Towards lowering of the Pliocene/Pleistocene boundary to the Gauss-Matuyama Reversal. *Quaternary International*, **40**, 37-42.

SUGDEN, D. E. (1968). The selectivity of glacial erosion in the Cairngorm Mountains, Scotland. *Transactions of the Institute of British Geographers Special Publication*, **45**, 79-92.

SUGDEN, D. E. (1974). Landscapes of glacial erosion in Greenland and their relationship to ice, topographic and bedrock conditions. *Institute of British Geographers Special Publication*, **7**, 177-195.

SUGDEN, D. E., & JOHN, B. S. (1976). *Glaciers and Landscapes*. Edward Arnold, London, pp. 376.

SUGDEN, D. E., & WATTS, S. H. (1977). Tors, felsenmeer, and glaciation in northern Cumberland Peninsula, Baffin Island. *Canadian Journal of Earth Sciences*, **14**(12), 2817-2823.

SUGGATE, R. P. (1991). Late Pliocene and Quaternary Glaciations of New Zealand. *Quaternary Science Reviews*, **9**, 175-197.

SUMMERFIELD, M. A., STUART, F. M., COCKBURN, H. A. P., SUGDEN, D. E., DENTON, G. H., DUNAI, T., MARCHANT, D. R. (1999). Long-term rates of denudation in the Dry Valleys, Transantarctic Mountains, southern Victoria Land, Antarctica based on *in-situ*-produced ^{21}Ne. *Geomorphology*, **27**, 113-129.

SWEATMAN T.R., & LONG J.V.P. (1969). Quantitative electron microprobe analysis of rock forming minerals. *Journal of Petrology*, **7**, 332 - 379.

SYVITSKI, J. P., JENNINGS, A., & ANDREWS, J. T. (1999). High resolution seismic evidence for multiple glaciations across the southwest Iceland shelf. *Arctic, Antarctic, and Alpine Research*, **31**, 50-57.

TAKAMIYA, H., & NISHIMURA, S. (1986). Thermoluminescence ages of some volcaniclastic materials. *Nuclear Tracks and Radiation Measurements*, **11**, 251-257.

TAYLOR, R. E., STUVIER, M., & REIMER, P. J. (1996). Development and extension of the calibration of the radiocarbon time scale: Archaeological applications. *Quaternary Science Reviews*, **15**(7), 655-668.

TAYLOR, S. R., & MCLENNAN, S. M. (1985). *The Continental Crust: Its Composition and Evolution*. Blackwell Scientific Publishers, Oxford.

TEMPLER, R. H. (1986). The localised transition model of anomalous fading. *Radiation Protection Dosimetry*, **17**, 493-497.

TER BRAAK, C. J. F., & SMILAUER, P. (1998). *CANOCO Reference Manual and User's Guide for Canoco for Windows; Software for Canonical Community Ordination (version 4)*. Microcomputer Power, Ithaca, New York.

THOMPSON, R. (1991). Palaeomagnetic dating. In *Quaternary Dating Methods - A Users Guide. Technical Guide No. 4*. Smart, P. L. & Francis, P. D. (Eds.). Quaternary Research Association. p. 177-194.

THÓRARINSSON, S. (1937). The main geological and topographical features of Iceland. *Geografiska Annaler*, **19**, 161-175.

THÓRARINSSON, S. (1943). Oscillations of the Icelandic glaciers in the last 250 years. *Geographiska Annualer*, **25**, 1-54.

THÓRARINSSON, S. (1944). Tepfrokronologiska studier på Island. *Geografisker Analer*, p.1-203 (English summary, p. 204-217).

THÓRARINSSON, S. (1958). The Öræfajökull eruption of 1362. *Acta Naturalia Islandica*, **2**(2), 1-99.

THÓRARINSSON, S. (1963). *Askja on fire*. Álmenna Bókafélagid, Reykjavík.

THÓRARINSSON, S. (1967). The eruptions of Hekla in historical times - a tephrochronological study. In *The Eruption of Hekla 1947-1948: Volume 1*. Einarsson, T., Kjartansson, G., Thórarinsson, S. (Eds.). Societas Scientiarum Islandica: Reykjavík. pp. 170.

THÓRARINSSON, S. (1969). Ignimbrít í Þörsmórk. (Ignimbrite in Þörsmórk; partly in English) *Náttúrufræðingurinn*, **39**, 139-155.

THÓRARINSSON, S. (1974). The terms tephra and tephrochronology. In Westgate, J. A. & Gold, C. M. (Eds.). *World Bibliography and Index of Quaternary Tephrochronology*. INQUA/UNESCO, Edmonton. p. 17-19.

THÓRARINSSON, S. (1980). Road log for excursions for 1980: Tephra Studies Workshop in Iceland. *Tephra Studies as a Tool in Quaternary Research: Proceedings of the NATO Advanced Study Institute*. Laugarvatn and Reykjavík, Iceland. p. 18-29.

THÓRARINSSON, S. (1981). The application of tephrochronology in Iceland. In *Tephra Studies*. Self, S. & Sparks, R. S. J. (Eds). D. Reidel Publishing Company. p. 109-134.

THÓRARINSSON, S., & SÆMUNDSSON, K. (1979). Volcanic activity in historical time. *Jökull*, **29**, 29-32

THORGRÍMSSON, S. (1976). *Vestfjarðavirkjanir. Ísafjarðardjúp. Frumkönnun à byggingarefum og jarðfraeði*. Orkustofnun, Reykjavík, **OS-ROD-7630**, 1-8. (translated in Lárusson, 1983).

THORODDSEN, TH. (1892a). Islands Jökler i Fortid og Nutid. *Geografisk Tidsskrift*, **11**, 111-146. (cited in Hjort *et al.*, 1986).

THORODDSEN, TH. (1892b). Postglacial marine aflejringer, kystterrasjer og strandlinjer i Island. *Geografisk Tidsskrift*, **11**, 209-225. (cited in Lárusson, 1983).

THORODDSEN, TH. (1901). Islandske fjorde og bugter. *Geografisk tidskrift*, **16**, 58-82. (cited in Lárusson, 1983).

THORODDSEN, TH. (1902). Þættir úr jarðfræði Íslands. *Andvari*, **27**, 127-176. (cited in Lárusson, 1983; Hjort *et al.*, 1986).

THORODDSEN, TH. (1906). Island: *Grundriss der Geographie und Geologie*. Petermanns Mitt., Erganzungsh, 152 und 153. pp. 358. (cited in Hjort *et al.* 1986).

THORPE, R., & BROWN, G. (1985). *The Field Description of Igneous Rocks*. Geological Society fo London Handbook Series. Open University Press, pp. 154.

THORS, K. (1974). *(I) Sediments of the Vestfírðir Shelf, NW Iceland. (II). Geology of the Ulfarfell Area, SW Iceland.* Unpublished PhD thesis, University of Manchester. pp. 167.

THORS, K. & HELGADÓTTIR, G. (1999). Seismic reflection profiles from Isafjardardup, Jökulfirðir and Dupall, NW Iceland. *Geological Society of America Abstracts*, **31**(7), A74.

THUNNELL, R. C., & MORTON, P. G. (1995). Glacial climatic instability in the northeast Pacific Ocean. *Nature*, **376**, 504-506.

TIEDEMANN, R., SARNTHEIN, M., & STEIN, R. (1989). Climatic changes in the western Sahara: Aeolo-marine sediment record of the last 8 million years (Sites 657-661). *Proceedings of the Ocean Drilling Program: Scientific Results*, **108**, 241-261.

TÓMASSON, J. (1967). Minerological and petrological classification of Icelandic tephra-layers. In *The Eruption of Hekla 1947-1948: Volume 1*. Einarsson, T., Kjartansson, G., Thórarinsson, S. (Eds.). Societas Scientiarum Islandica: Reykjavík. p. 171-183.

TRYGGVASSON, T., JONSSON, J. (1958). *Geological map of the Reykjavik area.* Atvinnudeild Háskólans and Skrifstofa bæjarverkfræðings, Reykjavík.

TUCKER, M. (1982). *The Field Description of Sedimentary Rocks*. Geological Society of London Handbook Series. Open University Press, Buckingham, pp. 112.

TUCKER, M. (1991). *Sedimentary Petrology*. Blackwell Scientific Publications, London, pp. 260.

TURNEY, C. S. M. (1998). Extraction of rhyolitic component of Vedde microtephra from minerogenic lake sediments. *Journal of Palaeolimnology*, **19**, 199-206.

TURNEY, C. S. M., HARKNESS, D. D. & LOWE, J. J. (1997). The use of micro-tephra horizons to correlate lake sediment successions in Scotland. *Journal of Quaternary Science*, **12**(6), 525-531.

TURNEY, C. S. M., HARKNESS, D. D., LOWE, J. J. (1998). Carbon isotope variations and chronology of the Last Glacial Interglacial Transition (14-9 ka BP). *Radiocarbon*, **40**, 873-881.

TURNEY, C. S. M., COOPE, G. R., HARKNESS, D. D., LOWE, J. J., & WALKER, M. J. C. (2000). Implications for the dating of Wisconsinian (Weichselian) late-glacial event of systematic radiocarbon age differences between terrestrial plant macrofossils from a site in SW Ireland. *Quaternary Research*, **53**(1), 114-121.

TURNEY, C. S. M., LOWE, J. J., WASTEGÅRD, S., COOPER, R., & ROBERTS, S. J. (2001). The development of a tephrochronological framework for the last glacial-Holocene transition in

NW Europe. In Juvigné, E., & Raynal, J. –P. (Eds.): *Tephras: Chronologie, Archeologie, les Dossiers de l'Archeo-Logis no.1*. CDERAD editeur – 43150 Goudet. pp. 101-109.

VAN DEN BOGAARD, P., (1995). $^{40}Ar/^{39}Ar$ ages of sanidine phenocrysts from the Laacher See Tephra (12,900 yr BP): chronostratigraphic and petrological significance. *Earth and Planetary Science Letters*, **133**, 163-174.

VAN DEN BOGAARD, P., & SCHMINCKE, H, -U. (1985). Laacher See Tephra. A widespread isochronous Late Quaternary Tephra in central and northern Europe. *Geological Society of America Bulletin*, **96**, 1554-1571.

VAN DEN BOGAARD, P., HALL, C. M., SCHMINCKE, H.-U., & YORK, D. (1989). Precise single-grain ^{40}Ar-^{39}Ar dating of a cold to warm climate transition in Central Europe. *Nature*, **342**, 523-525.

VARMA, M. N., & CARRIVEAU, G. W. (1975). A precise alpha source calibration for thermoluminescence dating. *TLS*, **56**, 415-418.

VILMUNDARDÓTTIR, E. (1972). *Skýrsla um jardfræðirannsóknir við Jökulsá í Fjótsdal sumarið 1970*. Órkustofnun, Reykjavík. pp. 26. (cited in Lárusson, 1983).

VISOCEKAS, R. (1985). Tunnelling radiative combination in labradorite: its association with anomalous fading of thermoluminescence. *Radiation Measurements*, **10**, 521-529.

VOELKER, A.H.L., SARNTHEIN, M., GROOTES, P. M., ERLENKEUSER, H., LAJ, C., MAZAUD, A., NADEAU, M.-J., & SCHEIDER, M. (1998). Correlation of marine ^{14}C ages from the Nordic Seas with the GISP2 isotope record: Implications for ^{14}C calibration beyond 25 ka BP. *Radiocarbon*, **40**, 517-534.

WAGNER, G., & VAN DEN HAUTE, P. (1992). *Fission Track Dating*. Kluiver Academic Press.

WALKER, G. P. L. (1962). Tertiary welded tuffs in eastern Iceland. *Journal of the Geological Society of London*, **119**, 29-63.

WALKER, G. P. L. (1973). Explosive volcanic eruptions - a new classification scheme. *Geol. Rundsch.*, **62**, 431-446. (cited in Wright and Walker, 1980)

WALKER, M. J. C., BJÖRCK, S., LOWE, J. J., CWYNAR, L. C., JOHNSEN, S., KNUDSEN, K. –L., WOHLFARTH, B., INTIMATE GROUP. (1999). Isotopic 'events' in the GRIP ice core: a stratotype for the Late Pleistocene. *Quaternary Science Reviews*, **18**, 1143-1150.

WARD, S. (1988). *The thermoluminescence of glass slices and their potential as radiation dosimeters in the 0-160 kGy range*. Unpublished B.Sc. Thesis, Department of Physics and Applied Physics, University of Strathclyde. pp. 30.

WASHBURN, A. L. (1956). Classification of patterned ground and review of suggested origins. *Geological Society of America Bulletin*, **67**, 823-865 (cited in Gary *et al.*, 1976).

WASTEGÅRD, S., BJÖRCK, S., POSSNERT, G., & WOHLFARTH, B. (1998). Evidence for occurrence of Vedde Ash in Sweden: Radiocarbon and calendar age estimates. *Journal of Quaternary Science*, **13**(3), 271-274.

WASTEGÅRD, S., TURNEY, C. S. M., LOWE, J. J., & ROBERTS, S. J. (2000a). New discoveries of the Vedde Ash in southern Sweden and Scotland. *Boreas*, **29**, 72-78.

WASTEGÅRD, S., WOHLFARTH, B., SUBETTO, D. A., & SAPELKO, T. V. (2000b). Extending the known distribution of Younger Dryas Vedde Ash into north-western Russia. *Journal of Quaternary Science*, **15**(6), 581-586.

WASTEGÅRD, S., BJÖRCK, S., GRAUERT, M., HANNON, G. E. (2001). The Mjauvotn tephra and other Holocene tephra horizons from the Faroe Islands: a link between the Icelandic source region, the Nordic Seas, and the European continent. *The Holocene*, **11**(1), 101-109.

WATKINS, N. D., & WALKER, G. P. L. (1977). Magnetostratigraphy of eastern Iceland. *American Journal of Science*, **277**, 513-584.

WELTON, J. E. (1984). *SEM Petrology Atlas*. The American Association of Petroleum Geologists methods in exploration series no. 4. Tulsa, Oklahoma, USA. pp. 237.

WENSINK, H. (1964). Palaeomagnetic stratigraphy of younger basalts and intercalated Plio-Pleistocene tillites in Iceland. *Geologische Rundschau*, **54**, 364-384.

WERNER, R., WALLRABE-ADAMS, H-J., LACASSE, C., SCHMINCKE, H-U., & THEIDE, J. (1996). Distribution, chemical composition, and sources of Oligocene to Miocene volcanic ashes from

sites 907, 908, and 913. In: Theide, J., Myhre, A. M., Firth, J. V., Johnson, G. L., & Ruddiman, W. F. (Eds.). *Proceedings of the Ocean Drilling Program, Scientific Results*, **151**, 333-350.

WESTGATE, J. A. (1988). Isothermal plateau fission-track age of the Late Pleistocene Old Crow Tephra, Alaska. *Geophysical Research Letters*, **15**(4), 376-379.

WESTGATE, J. A. (1989). Isothermal plateau fission-track ages of hydrated glass shards from silicic tephra beds. *Earth and Planetary Science Letters*, **95**, 226-234.

WESTGATE, J. A., & FULTON, R. J. (1975). Tephrostratigraphy of Olympia Interglacial Sediments in South Central British Columbia, Canada. *Canadian Journal of Earth Science*, **12**, 489-502.

WESTGATE, J. A. & BRIGGS, N. D. (1980). Dating methods of Pleistocene deposits and their problems; Tephrochronology and fission track dating. *Geoscience Canada*, **7**, 3-10.

WESTGATE, J. A. & GORTON, M. P. (1981). Correlation techniques in tephra studies. In: Self, S. & Sparks, R. S. J. (Eds.). *Tephra Studies*. Reidel, Dordrecht. p. 73-94.

WESTGATE, J. A., & NAESER, N. D. (1995). Tephrochronology and fission-track dating. In: *Dating Methods for Quaternary Deposits*. Rutter, N. W. & Catto, N. R. (Eds.). Geological Association of Canada. p. 15-28.

WESTGATE, J. A., EASTERBROOK, D. J., NAESER, N. D., & CARSON, R. J. (1987). Lake Tapps Tephra: An early Pleistocene stratigraphic marker in the Puget Lowland, Washington. *Quaternary Research*, **28**, 340-355.

WESTGATE, J. A., STEMPER, B. A. & PÉWÉ, T. L. (1990). A 3 m.y. record of Pliocene-Pleistocene loess in interior Alaska. *Geology*, **18**, 858-861.

WESTGATE, J. A., WALTER, R. C., NAESER, N. (EDS.) (1992). Tephrachronology: stratigraphic applications of tephra. *Quaternary International*, **13/14**, pp. 203.

WESTGATE, J. A., PERKINS, W. T., FUGE, R., PEARCE, N. J. G., & WINTLE, A. G. (1994). Trace-element analysis of volcanic glass shards by laser ablation inductively coupled plasma spectrometry: application to tephrochronological studies. *Applied Geochemistry*, **9**, 323-335.

WESTGATE, J., SANDHU, A., & SHANE, P. (1997). Fission Track Dating. In *Chronometric Dating in Archaeology*. Taylor and Aitken (Eds). Plenum Press. New York. p.127-158.

WESTGATE, J. A., SHANE, P. A. R., NICHOLAS, J. G., PERKINS, W. T., KORISETTAR, R., CHESNER, C. A., WILLIAMS, M. A. J., & ACHARYYA, S. K. (1998) All Toba tephra occurrences across Peninsular India belong to the 75,000 yr B. P. eruption. *Quaternary Research*, **50**, 107-112.

WHITTEN, D. G. A. & BROOKS, J. R. V. (1972). *Dictionary of Geology*. Penguin Books, London.

WHITTINGTON, G., FALLICK, A. E., & EDWARDS, K. J. (1996). Stable oxygen isotope and pollen record from eastern Scotland and a consideration of Late-glacial and early Holocene climate change for Europe. *Journal of Quaternary Science*, **11**(4), 327-340.

WILLIAMS, M., DUNKERLEY, D., DE DECKKER, P., KERSHAW, P., & CHAPPELL, J. (1998). *Quaternary Environments*. Arnold. London. pp. 329.

WILLIAMS, D. F., PECK, J., KARABANOV, E. B., PROKOPENKO, A. A., KRAVCHINSKY, V., KING, J., & KUZMIN, M. I. (1997). Lake Baikal record of continental climate response to orbital insolation during the past 5 Ma. *Science*, **278**, 1114-1116.

WILSON, C. J. N., & WALKER, G. P. L. (1981). Violence in pyroclastic flow eruptions. In: S. Shelf and R. S. J. Sparks (Eds.). *Tephra Studies*. Reidel, Dordrecht, p. 441-448.

WINKLER, H. G. F. (1938). Zur Entstehung der isländischen fjorde (dargestellt am Skalmarfjord der NW Halbinsel Íslands). *Zeitschrift für Geomorphology*, **10**, 255-263.

WINTLE, A. (1973). Anomalous fading of thermoluminescence in mineral samples. *Nature*, **245**, 143-144.

WINTLE, A. (1977). Detailed study of a thermoluminescent mineral exhibiting anomalous fading. *Journal of Luminescence*, **15**, 385-393.

WINTLE, A. (1978). Anomalous fading. *PACT*, **2**, 240-243.

WINTLE, A. (1991). Luminescence Dating. In Smart, P. L. and Frances P. D. (Eds): *Quaternary dating methods - a users guide*: *Quaternary Research Association Technical Guide no. 4*. Quaternary Research Association, London. p. 108-127.

WINTLE, A. (1997). Luminescence dating: laboratory procedures and protocols. *Radiation Measurements*, **27**(5/6), 769-817.

WINTLE, A., & MURRAY, A. S. (1997). The relationship between quartz thermoluminescence, and optically stimulated luminescence. *Radiation Measurements*, **27**, 611-624.

WINTLE, A., & MURRAY, A. S. (1998). Towards development of a preheat procedure for OSL dating of quartz. *Radiation Measurements*, **29**, 81-94.

WOHLFARTH, B. (1996). The chronology of the Last Termination: a review of high-resolution terrestrial stratigraphies. *Quaternary Science Reviews,* **15**, 267-284.

WOLFE, C. J., BJARNASON, I. T., VANDECAR, J. C., SOLOMON, S. C. (1997). Seismic structure of the Iceland mantle plume. *Nature*, **385**, 245-247.

WOODWORTH-LYNAS, C. M. T. (1996). Ice scour as an indicator of glaciolacustrine environments. In: Menzies J. (Ed.). *Glacial Environments Volume 2: Past Glacial Environments.* Butterworth-Hienneman, Oxford. p. 161-211.

WRIGHT, J. V., & WALKER, G. P. L. (1981). Eruption transport and deposition of ignimbrite: a case study from Mexico. *Journal of Volcanology and Geothermal Research*, **9**, 111-131.

WRIGHT, J. V., SMITH, A. L., & SELF, S. (1980). A working terminology of pyroclastic deposits. *Journal of Volcanology and Geothermal Research*, **8**, 315-336.

WRIGHT, J. V., SELF, S., & FISHER, R. V. (1981a). Towards a facies model for ignimbrite-forming eruptions. In Self, S. & Sparks, R. S. J. (Eds): *Tephra Studies*. D. Reidel Publishing Company. p. 433-439.

WRIGHT, J. V., SMITH, A. L., & SELF, S. (1981b). A terminology for pyroclastic deposits In Self, S., & Sparks, R. S. J. (Eds.): *Tephra Studies*. Reidel, Dordrecht. p. 457-463.

XRAL (2001). Geochemical Exploration and Research Analysis: 2001 Schedule of Fees and Services.

YORK, D., HALL, C. M., YANASE, Y., HANES, J. A., & KENYON, W. J. (1981). ^{40}Ar-^{39}Ar dating of terrestrial minerals with a continuous laser. *Geophysical Research Letters*, **8**, 1136-1138.

ZANDER, A., DULLER, G. A. T., & WINTLE, A. G. (2000). Multiple and single aliquot luminescence dating techniques applied to quartz extracted from Middle and Upper Weichselian loess, Zemechy, Czech Republic. *Journal of Quaternary Science*, **15**(1), 51-60.

ZIELINSKI, G. (1995). Stratospheric loading and optical depth estimates of explosive volcanism over the last 2100 years derived from the Greenland Ice Sheet Project 2 ice core. *Journal of Geophysical Research*, **100**(D10), p. 20, 937-20,955.

ZIELINSKI, G. (2000). Use of paleo-records in determining variability within the volcanism-climate system. *Quaternary Science Reviews*, **19**, 417-438.

ZIELINSKI, G. A., MAYEWSKI, P. A., MEEKER, L. D., WHITLOW, S., TWICKLER, M. S., MORRISON, M., MEESE, D., ALLEY, R. B., &, GOW, A. J. (1994). Record of volcanism since 7000 B. C. from the GISP2 Greenland ice core and implications for the volcano-climate system. *Science*, **264**, 948-952.

ZIELINSKI, G. A., GERMANI, M. S., LARSEN, G., BAILLIE, M.G.L., WHITLOW, S., TWICKER, M. S., & TAYLOR, K. (1995). Evidence of the Eldgjá (Iceland) eruption in the GISP2 Greenland ice core: relationship to eruption processes and climatic conditions in the tenth century. *The Holocene*, **5**(2), 129-140.

ZIELINSKI, G. A., MAYEWSKI, P. A., MEEKER, D., WHITLOW, S., & TWICKLER, M. S. (1996). A 110,000-yr record of explosive volcanism from the GISP2 (Greenland) ice core. *Quaternary Research*, **45**, 109-118.

ZIELINSKI, G. A., MAYEWSKI, P. A., MEEKER, D., GRÖNVOLD, K., GERMAIN, M. S., WHITLOW, S., TWICKLER, M. S., & TAYLOR, K. (1997). Volcanic aerosol records and tephrochronology of the Summit, Greenland, ice cores. *Journal of Geophysical Research*, **102**, 26,625-26,640.

ZIMMERMAN, D. W. (1970). *The dependence of thermoluminescence on energy and type of ionising radiation and its significance for archaeologic age determination.* DPhil thesis, University of Oxford (cited in Spooner & Allsop, 2000).

ZIMMERMAN, D. W. (1971). Thermoluminescent dating using fine grains from pottery. *Archaeometry*, **13**, 29-52.

ZINK, A., & VISOCEKAS, R. (1997). Datability of sanidine feldspars using near infrared TL emission. *Radiation Measurements*, **27**, 251-262.